

AD-A068 806

ADVISORY GROUP FOR AEROSPACE RESEARCH AND DEVELOPMENT--ETC F/G 13/5  
BONDED JOINTS AND PREPARATION FOR BONDING.(U)  
MAR 79

UNCLASSIFIED

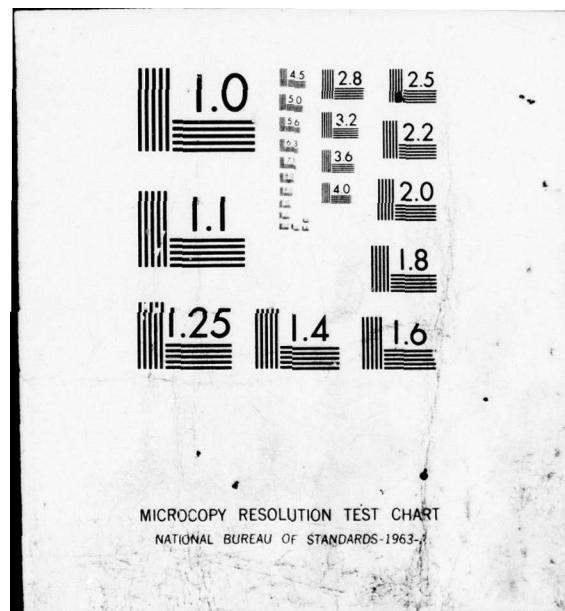
AGARD-LS-102

NL

1 OF 4  
AD  
A068806







AD A068806

DDC FILE COPY

AGARD-LS-102

# AGARD

ADVISORY GROUP FOR AEROSPACE RESEARCH & DEVELOPMENT

7 RUE ANCELLE 92200 NEUILLY SUR SEINE FRANCE

LEVEL

AGARD LECTURE SERIES No. 102

## Bonded Joints and Preparation for Bonding

**DISTRIBUTION STATEMENT A**  
Approved for public release;  
Distribution Unlimited

DDC  
MAY 22 1979  
A

NORTH ATLANTIC TREATY ORGANIZATION



DISTRIBUTION AND AVAILABILITY  
ON BACK COVER

79 05 18 081

1 14 AGARD-LS-102

NORTH ATLANTIC TREATY ORGANIZATION  
ADVISORY GROUP FOR AFROSPACE RESEARCH AND DEVELOPMENT ✓  
(ORGANISATION DU TRAITE DE L'ATLANTIQUE NORD)

11 Mar 79

12 317 P.

9  
AGARD Lecture Series No. 102

6  
BONDED JOINTS AND PREPARATION FOR BONDING.

DDC  
MAY 22 1979  
MULTIPLE  
A

DISTRIBUTION STATEMENT A  
Approved for public release;  
Distribution Unlimited

The material in this publication was assembled to support a Lecture Series under the sponsorship of the Structures and Materials Panel and the Consultant and Exchange Programme of AGARD presented on: 2-3 April 1979 in Oslo, Norway and 5-6 April 1979 in The Hague, The Netherlands.

Plans have been made to repeat this Lecture Series in the United States at Wright-Patterson Air Force Base, Dayton, Ohio on 16 and 17 October 1979.

400 043  
79 05 18 081 mt

## THE MISSION OF AGARD

The mission of AGARD is to bring together the leading personalities of the NATO nations in the fields of science and technology relating to aerospace for the following purposes:

- Exchanging of scientific and technical information;
- Continuously stimulating advances in the aerospace sciences relevant to strengthening the common defence posture;
- Improving the co-operation among member nations in aerospace research and development;
- Providing scientific and technical advice and assistance to the North Atlantic Military Committee in the field of aerospace research and development;
- Rendering scientific and technical assistance, as requested, to other NATO bodies and to member nations in connection with research and development problems in the aerospace field;
- Providing assistance to member nations for the purpose of increasing their scientific and technical potential;
- Recommending effective ways for the member nations to use their research and development capabilities for the common benefit of the NATO community.

The highest authority within AGARD is the National Delegates Board consisting of officially appointed senior representatives from each member nation. The mission of AGARD is carried out through the Panels which are composed of experts appointed by the National Delegates, the Consultant and Exchange Programme and the Aerospace Applications Studies Programme. The results of AGARD work are reported to the member nations and the NATO Authorities through the AGARD series of publications of which this is one.

Participation in AGARD activities is by invitation only and is normally limited to citizens of the NATO nations.

The content of this publication has been reproduced directly from material supplied by AGARD or the authors.

ADDITION BY	
DATE	DATE RECEIVED
DATE RECEIVED	DATE RECEIVED
INSTITUTION	
BY	
INSTITUTION/STATION/ADDRESS	
DATE	
DATE	

Published March 1979

Copyright © AGARD 1979  
All Rights Reserved

ISBN 92-835-1313-4



Printed by Technical Editing and Reproduction Ltd  
Harford House, 7-9 Charlotte St, London, W1P 1HD



## PREFACE

This Lecture Series has been organized on the initiative and under the sponsorship of the AGARD Structures and Materials Panel. Its timing is well chosen since, at the time of conception of these lectures, the aerospace community is at the onset of an era of large application of structures and materials that can be classified as "advanced structures".

It is typical of these structures that not only do they contain many new and non-metallic materials, but that the mechanical properties of these materials are based on complex physical and chemical phenomena and, also, that they are produced by intricate manufacturing processes. These are all new factors that make prediction of their long-term operational behaviour an entirely different matter than is the case for more conventional metal structures and materials.

In consideration of the important applications desired, many questions are raised as to whether knowledge of these materials and processes, as well as methods of quality control, is sufficient guarantee of long-term operational reliability and durability.

Adhesive bonding must be considered both as a precursor and as an important element of such advanced structures.

After more than thirty years of application in aircraft and spacecraft structures in rôles of various degrees of importance, adhesive bonded joints offer an important example of many aspects of these advanced structures. The experience gained with bonded joints must be regarded as an important asset in the field of advanced structures. On the other hand, many aspects of adhesive bonding still have to be studied in detail in order that its rôle of growing importance can be fulfilled successfully.

May this Lecture Series offer an effective contribution towards this goal.

Ce cycle de Conférences a été organisé sur l'initiative, et sous l'égide du Panel des Structures et Matériaux de l'AGARD. Il vient en temps opportun, car au moment de l'élaboration de ces conférences, la communauté aérospatiale aborde une ère d'application, sur une vaste échelle, de structures et matériaux que l'on peut qualifier d'"avancés".

Ce qui caractérise ces structures, c'est non seulement leur composition qui fait appel à de nombreux matériaux nouveaux et non métalliques, mais aussi le fait que ces matériaux présentent des propriétés mécaniques basées sur des phénomènes physiques et chimiques complexes et que leurs procédés de fabrication sont fort compliqués. Tous ces facteurs nouveaux font que la prédiction de leur comportement opérationnel à long terme diffère totalement de celle relative aux structures et matériaux métalliques classiques.

En raison de l'importance des applications désirées, se pose la question de savoir si les connaissances actuelles relatives à ces matériaux et procédés, ainsi que les méthodes existantes de contrôle de qualité, constituent une garantie suffisante de fiabilité opérationnelle et de résistance à long terme.

Les joints adhésifs peuvent être considérés à la fois comme une innovation et comme un élément important de ces structures avancées.

Après plus de trente ans d'application dans les structures d'aéronefs et de vaisseaux spatiaux, dans des rôles d'importance diverse, les joints collés adhésifs offrent un exemple spectaculaire de multiples facettes de ces structures avancées. L'expérience acquise en matière de joints collés peut être considérée comme un atout important dans le domaine des structures avancées. Toutefois nombreux sont les aspects de ce procédé qui exigent encore la conduite d'études détaillées pour que soit rempli avec succès le rôle grandissant qu'est appelée à jouer la liaison adhésive.

ROBERT J. SCHLIEKELMANN  
Lecture Series Director

## LIST OF SPEAKERS

Lecture Series Director: Ir. R.J.Schliekelmann  
Fokker-VFW Technological Centre  
P.O. Box 7600  
1117 AJ Schiphol  
The Netherlands

Dr Ing. W.Brockmann  
Fraunhofer-Gesellschaft  
Institut für Angewandte Materialforschung  
Lesumer Heerstrasse 36  
2820 Bremen 77  
Germany (GFR)

Dr T.Kinloch  
Procurement Executive  
Ministry of Defence  
Propellants, Explosives and Rocket  
Motor Establishment (Waltham Abbey)  
Powdermill Lane  
Waltham Abbey, UK

Mr J.C.McMillan  
Chemical Technology Section  
Boeing Commercial Airplane Company  
P.O. Box 3707  
Seattle, Washington 98124  
USA

Dr J.Romanko  
General Dynamics  
Fort Worth Division  
Materials Research Laboratory  
P.O. Box 748  
Fort Worth, Texas 76101  
USA

Mr E.W.Thrall, Jr  
Douglas Aircraft Company  
3855 Lakewood Boulevard  
Long Beach, California 90846  
USA

Professor K.L. de Vries  
The University of Utah  
College of Engineering  
Department of Mechanical and  
Industrial Engineering  
Salt Lake City, Utah 84112  
USA



## CONTENTS

	Page
PREFACE	iii
LIST OF SPEAKERS	iv
	Reference
OPERATIONAL EXPERIENCE WITH ADHESIVE BONDED STRUCTURES by R.J.Schliekelmann	1
INTERFACIAL FRACTURE MECHANICAL ASPECTS OF ADHESIVE BONDED JOINTS by A.J.Kinloch	2
ANALYSIS AND DESIGN OF ADHESIVE BONDED JOINTS by K.L.De Vries and G.P.Anderson	3
BEHAVIOUR OF ADHESIVELY BONDED JOINTS UNDER CYCLIC LOADING by J.Romanko	4
FAILURES IN ADHESIVELY BONDED STRUCTURES by E.W.Thrall, Jr	5
THE NATURE OF ADHESION MECHANISMS AND THE INFLUENCE OF SURFACE TREATMENTS ON THE BEHAVIOUR OF BONDED JOINTS by W.Brockmann	6
SURFACE PREPARATION – THE KEY TO BONDMENT DURABILITY by J.C.McMillan	7
NON-DESTRUCTIVE TESTING OF ADHESIVE BONDED JOINTS by R.J.Schliekelmann	8
BIBLIOGRAPHY	B

# OPERATIONAL EXPERIENCE WITH ADHESIVE BONDED STRUCTURES

by  
Rob J. Schliekelmann  
Fokker-VFW Technological Centre  
Schiphol-Oost  
The Netherlands

## SUMMARY

A survey is given of the operational experience with adhesive bonded structures in military and civil aircraft. In view of the widely different qualifications of these experiences, from "highly favourable" through "very unfavourable", an introduction is given to the various problem areas that have caused service troubles and that will form the topic of discussion in more detail during this Lecture Series. The objective of which is to develop full understanding of the principle causes of possible failures and to define ways and means to achieve fully reliable bonded joints, that will play in the future an even more important rôle than to-day.

## 1 INTRODUCTION

Adhesive bonded joints have seen their first structural applications in production aircraft already during World War II. They were used for the solution of peculiar problems such as the reinforcement of a basically wooden wingstructure by means of adhesive bonded aluminium alloy spar caps or doubler plates. (Fig. 1 and 2). /1/ However, in all-metal production aircraft for military as well as civil purposes, the use of adhesive bonded joints came on a larger scale in the fifties and has been growing ever since.

The bonded structures used can be categorized as follows:

- Metal-to-metal
  - . locally reinforced by bonded doubler plates (Fig. 3).
  - . large area multiply laminated with or without staggering dimensions for achievement of cross sectional variations (Fig. 4).
  - . stringer-to-skin panel
  - . combination of the above (Fig. 5, 6) /2/
  - . bonded panel splices with or without mechanical fasteners (Fig. 7).
- Metal-to-low density core in "sandwich" structures /3/
  - . Initially with plastic foam and end-grain balsa wood core (fig. 8).
  - . Presently most frequently used with honeycomb core made from aluminium foil or glass resp. organic (Nomex<sup>®</sup>) fibres. /4/
  - . With or without bonded doubler reinforcements and profile type edgemembers and/or inserts for load introduction (Fig. 9).

Each of the above categories of adhesive bonded structures was adopted for one or more aspects that seemed during the design stage an asset for optimum operational characteristics of the aircraft under development.

The reasoning behind justification of the use of adhesive bonded structures of the various categories as mentioned, has seen considerable developments over the years. Some examples there off are the following:

- Skin panels with adhesive bonded stiffening profiles were originally mainly preferred over riveted panels of similar configuration for reason of their greatly enhanced local stability properties due to the continuously bonded stiffener flanges. This shows up in improved load carrying capacity under end-compression and/or shear loading and also fatigue life due to the elimination of a number of rivet holes that might be starting points of fatigue cracks. In recent years evidence has grown that in addition to the above mentioned advantages bonded stiffener panels and shear webs have very attractive fracture mechanical properties. Properties, that fulfil excellently the more recent demands coming forth from the requirements for "damage tolerant" structures. Not only the operational lifetime until the occurrence of the first crack is enhanced by replacing the mechanical fastening methods with adhesive bonding, but also the behaviour in the cracked state is improved considerably. This leads to slower crack-propagation rates and higher residual strength when cracks have grown to significant dimensions. Based on these properties the idea was born to bond not only the longitudinal stiffening profiles of load carrying skin panels but to apply adhesive bonding as well to the attachments between skinpanel and flanges of transverse frames, ribs and bulkheads. /5, 6, 7, 8, 9/
- The very attractive fracture mechanical properties have also greatly developed the appreciation of the importance of the merits of adhesive bonded doubler plate reinforcements and the multiply laminated metal concept for loadcarrying components. Again, the properties of the adhesive bonded variants have shown to be superior in comparison to those of a similar product machined from the solid by means of efficient numerically controlled milling machines or chemical milling. The fact that the rather low modulus of elasticity of the cured adhesive layer allows each bonded sheet to deform practically independantly, also when a crack of some nature has

formed, is the basis for the high fracture toughness and other mechanical properties of a composite metal laminate being similar to those favourable properties of a thin rolled sheet rather than the unfavourable ones of thick solid plate. /10/  
In the lecture of Mr. E.W. Thrall Jr., Technical Director of the U.S.A.F. Primary Adhesive Bonded Structure Technology (PABST) Program these aspects will be discussed in much more detail.

- Low density core sandwich structures have originally been adopted for their attractive strength/stiffness/weight aspects as a result of their ideal stabilization of the skin sheets.

Nowadays sandwich structures are also favoured by the designers for a number of other reasons such as:

- . Fulfilment of the growing demands for close dimensional tolerances on aerodynamic airfoils and related parts such as trailing edges of fixed and movable wing and tailplane components: ailerons, rudders, elevators, spoilers, flaps, airbrakes, tabs, slats, vanes, etc.
- . Attractive acoustical damping characteristics to be employed in and around engines and nacelles in order to fulfil the growing demands for noise reduction for both passengers and crew as well as the environment of runways from which the aircraft are operating.
- . Good endurance in high sound pressure areas leading to good sonic fatigue life. /11/

Summarizing can be said that the attractive aspects of using adhesive bonded metal aircraft structures always have been numerous and that they are still growing. For future structures, such as those using advanced composite materials adhesive bonding looks to be the only solution for many fastening problems between composites among themselves as well as metals.

Now adhesive bonding has been used on a growing scale during several decades the question has been raised whether the many initial optimistic promises have been fulfilled.

## 2 FAILURE MODES OF ADHESIVE BONDED JOINTS

An adhesive bonded joint must be considered as a chain consisting of a number of individual links, the weakest of which finally determines the strength of the total chain. These links are (Fig. 10):

- (a) the cohesion strength of the cured adhesive layer
- (b) the adhesion strength between the cured adhesive layer and the oxide layer on top of the substrates to be bonded
- (c) the cohesion strength of the oxide layers
- (d) the cohesion strength of the substrates underneath the oxide layers

In case adhesive primers are used additional links are:

- (e) the cohesion strength of each primer layer
- (f) the adhesion strength between each primer layer and the cured adhesive layer.

The failure of each link defines a distinct failure mode.

- Ad (a) Failure of the cured adhesive layer can take place by external loads exceeding its failing strength. This can take place by straight-forward overloading of a good quality adhesive layer, but also due to normal loading of a low strength adhesive layer. This low strength can be the result of several factors:
- Low manufacturing quality due to either/or insufficient curing - temperature, - duration or -pressure. Of these factors insufficient pressure is the most frequent problem. It can be the result of fitting or tooling difficulties during manufacture, leading to void or porous adhesive layers. Proper N.D.I. procedures are able to catch up with these anomalies as will be discussed by the author in a separate lecture in this series.
  - Deterioration of the mechanical properties of an originally sound adhesive layer due to fatigue and/or environmental influences such as temperature, humidity, solvents. Proper evaluation of the adhesive properties against the loading and environmental conditions to be expected is able to avoid this problem.

Phenomena of this nature will be discussed in the presentations of Prof. de Vries and Dr. Romanko.

- Ad (b) Failure of the adhesion between adhesive layer and the oxide surface can be the result of either insufficient adhesion right from the moment of manufacture or break-down of originally sound adhesion due to environmental influences, due to p.e. water penetration, leading to desorption of the adhesive. These phenomena will be discussed in detail by Dr. Kinloch and Dr. Brockmann during the following lectures.
- Ad (c) The cohesion strength of the oxide layer is originally the result of the surface treatment process such as carried out during manufacture. A correct choice of the kind of surface treatment as well as an effectively controlled process are of prime importance. During the lectures of Messrs. McMillan and Dr. Brockmann this subject will be dealt with in more detail. /16, 17/



- Ad (d) The cohesion properties of the substrates under the oxide layers can be below expectations due to manufacturing defects such as cracks, flaws in the metal or voids between clad layer and base metal. Operational problems, however, frequently occur due to corrosion of the base metal and/or clad layers underneath a perfectly, to the oxide adhering adhesive layer, taking away the foundation on which the bonded joint has been built. Failure of this type seldomly affects the bonded joint alone. Insufficient general surface protection in view of the environmental operational conditions lead to general structural deterioration that may lead, as a secondary effect, also to failure of the bonded joints due to loss of cohesion strength of the base metal under the adhesive.
- Ad (e) The cohesive strength of adhesive primer layers follows similar rules as the adhesive layer (ad a) itself and may have similar failure modes. In addition to that, weakening of primer layers can occur due to excessive local concentrations of pigment in the cured resin layer causing low strength zones. This can be the result of superfluous amounts of pigment or pigment particles of a too large size, respectively insufficient mixing prior to spray application. However, very strong adhesion between mobile resin molecules and a highly activated surface may cause decomposition of well mixed wet primer films immediately after application, leaving a pigment rich layer on top of the dried or cured primer layer, showing up in yellowish pigment that can be wiped off from the dry primer coat.
- Ad (f) The adhesion between primer and adhesive can be a problem only in case of precured primer layers on which the adhesive may not adhere due to contamination of the primer surface or low compatibility of the physical properties of cured primers and uncured adhesive resin.

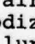
During discussion of the operational experiences with bonded structures the described failure modes (a) through (f) will be referred to as much as possible.

### 3 OPERATIONAL EXPERIENCE

In the following a report is presented about operational experiences with bonded structures of different types. The report is based on information that was obtained from both civil and military operating organizations that were addressed especially for this purpose with the request to supply as much as possible statistical data about operational experience with adhesive bonded structures. It is unfortunate that with some exceptions the response to those requests was generally quite limited. The reason for this was not explained in detail, but most probably must be based on the fact that no real statistical data of this nature had been accumulated.

In this lecture an attempt is made to present those data received from third parties, together with data found in open literature and directly accessible data from the author's Company in a systematic way in order that reliable conclusions may be drawn.

#### 3.1 Metal-to-metal bonded structures

- (a) Stringer-to-skin bonded panels have been used since 1946 to a large extent in European designed commercial transport aircraft both in skins of wings and fuselages. Most experience is based on the phenol-formaldehyde/vinyl formaldehyde adhesive systems. Only known problem areas are corrosion in bonded top hat stringer panels in lower fuselage bays where condensed water and "bilge" fluids were cause of general corrosion, starting from the porous adhesive spew at the bond edges leading to failures of type (d). This kind of failure is known only of panels with chromic-sulphuric acid etched surfaces. Of airliners using the same adhesive but surface treatment incorporating chromic acid anodizing and -stiffeners in the fuselage and top hat stiffeners in the wing no failures have been reported from a fleet of many hundreds of aircraft. One overhaul shop for this kind of aircraft reports on 1000 aircraft shopvisits no single case of bondline failure of this nature including stringer-to-skin panels of this and a related airliner type, including aircraft with ages of respectively 16.5; 17.5; 15 and 13 years, flight hours upto 31,500 hrs and 40,000 landings. High time aircraft of the same type did not show any problems after operation in Australia during periods upto 19 years, flight hours per individual aircraft upto 55,000 and flight numbers upto 56,000. It should be mentioned that all closed top hat bonded stringers, as used extensively in the wing- and tailplane skins of that aircraft type, had been thoroughly coated on the inside with phenolic adhesive resin that had been fully cured during the bonding operations of the panels.

Stringer-to-skin bonding was used in a military jet trainer aircraft using the same phenolic/vinyl adhesive in combination with only a chromic/sulphuric acid etch, so without anodizing. These panels, among else, were applied in split type trailing edge wing flaps that in opened condition came in close proximity of the runway. Statistics of a fleet of 20 aircraft operating from airfields, some of them close to the seacoast, indicate that the bonded components were perfectly sound after 10 years operation during which the aircraft remained long periods exposed to the weather in the open field. All (non-anodized) bonded components had been well painted after bonding with a waterrepellant paintprimer and, for exterior parts, an acrylic topcoat.

- (b) In last mentioned transport aircraft type extensive use has been made of multiply laminated wing and fuselage skin panels as well as wing spar caps. /15/ Statistics over 20 years of operation, representing some 8 million flights and 7.5 million flight hours show the following:

- . No failures in multiply phenolic/vinyl bonded skins or webs as used in combination with surface treatment including anodizing.
- . In 8 cases of oldest production aircraft after operation lives between 8 and 17,5 years type (d) defects were experienced in multiply spar caps leading to local delamination after corrosion of the bonded metal layers. There could be identified two distinct causes for these problems. The spar caps concerned were composed out of a number of sheet angles of equal cross section and corner radius. When the individual sheet angles are nested during the bonding process non-bonded cavities are formed in the corners between the layers. These cavities are entirely acceptable from a strength point of view. At the location where an inner metal ply stops the corner cavity of the ply can be open to the atmosphere and moisture may enter in case this location is exposed to weather. After many years this moisture may become the starting point of corrosion from the inside of the laminated spar cap in spite of the durable adhesive system and surface treatment processes used. (Fig. 11). The problem could be easily solved by sealing those entrances of these cavities that were particularly prone to atmospheric influences such as near aileron cut-outs in the wing trailing edges. Also extra precautions were taken in view of outside storage of aircraft without outer wings leaving the spar cap ends entirely accessible to rain. It had been recorded that at least in one of the 8 cases mentioned the aircraft concerned had been stored in the open with the outer wings disassembled waiting repair after some mechanical operational damage.

The other cause of difficulties with the spar caps concerned could be traced to a trimming operation that took place along the bonded edges after curing. That operation was required to bring the individual flanges of the bonded metal laminate to a smooth common edge. During that operation that was concluded by fine polishing all spar cap edges all cured adhesive as well as the anodic layers were removed (Fig. 12). It appeared that a single paint primer coat was insufficient to protect the metal edges against adverse environmental influences. Corrosion from the individual metal layers, from the edges inward, finally led to the type (d) failure of the adhesive bonded laminate. Some extra care to the protection of the mentioned vulnerable locations of the laminated metal spar caps solved the problem that remained limited so far to the number of aircraft mentioned.

One case of similar nature has been reported to have occurred on another aircraft type but with the same surface treatment and adhesive scheme (Fig. 13). In that case the edges of a reinforcement laminate of a tailplane skin panel had also been trimmed after bonding in order to allow for accurate fitting of a stabilizer leading edge. This resulted also in type (d) defects along one of the doublers after 3 years of operation. Attention to as much as possible avoidance of trimming of edges of bonded skin components at assembly and, if trimmed, attention to sufficient restoration of the corrosion protection schemes solved the problem.

Laminated fin spar caps of the before mentioned jet trainer aircraft had been bonded integrally with the web in the flat state and press formed into shape after bonding, simultaneously with the pressing of the flanged holes in the spar web. (Fig. 14). These components were chromic sulphuric acid etched only and painted with water repellent primer. Of the 20 aircraft on record no problems have been reported and components were found perfectly sound upon dismantling after withdrawal after 10 years of service.

- (c) Wing leading edge manoeuvring flaps of a fighter aircraft consisted of a rather thick skin supported by a conventional spar/rib structure. The thick skin sheet had been formed with a rather large leading edge radius after which a sharp radius aerodynamic sheet metal fairing had been bonded into a chemmilled rebate of the basic skin sheet. Simultaneously the fairing skin had been filled with a low density foaming resin. (Fig. 15). Of the fleet of some 100 aircraft on record all components (2 per a.c.) gave serious troubles within approx. 500 flight hours of operation. The bonded joints delaminated gradually under the aerodynamic loads after which corrosion starting from bond edges and countersunk fastener holes completed the disaster. Electron microscopical investigation revealed that chemical pretreatment of the bond surfaces of the related flap skin had been far from optimum. This, together with an epoxy-nitrile adhesive system of a rather low environmental stability led within a short time to a desorption of the adhesive and failure mode type (b) as well as subsequent serious corrosion. A prescribed repair method based on a room temperature curing adhesive system did not lead to any success. The mentioned insufficiency of the bond surface led within a short time to failure of a similar nature. The problem finally could be solved by means of a specially developed surface treatment method that yielded an optimum surface condition on the skin leading edge rebate. This chemical treatment had to be carried out on the complete mechanically assembled component without negative effects to the riveted and bolted joints (Fig. 16). So far the, in this way repaired, components have shown excellent performances. The combination of an optimum surface treatment with a modern modified epoxy adhesive system, having a proven better environmental resistance, including a corrosion resistant primer, apparently solved the problems satisfactorily.



- (d) The dome shaped rear fuselage pressure bulkhead of a commercial transport had been provided with a bonded doubler at the location of the attachment to the fuselage skin and a frame type reinforcement (Fig. 17). After about 10 years of operation it appeared that moisture from condensate, in spite of the presence of drainholes in adjacent structure would penetrate local porosities of the vinyl-phenolic adhesive layer and the non-anodized pressure bulkhead sheetmaterial would suffer from intergranular corrosion. In one case this led to cracking of the pressure dome and fatal explosive decompression followed by subsequent loss of the aircraft.
- (e) Access to the integral wing tanks of an aircraft type for naval purposes is given by elliptical doors in the top wing skins. The door consists of thick plate elliptical edge members containing the double fluid tight seals. Two skins are bonded on the heavy edge member in the central area supported by honeycomb core. The joints between edge members and skins had been realized by means of a polyamide epoxy adhesive system on etched-only surfaces. It appeared that on the greater part of the fleet the edge joints delaminated within an operational period of 3 years. As the main cause could be found that at locations of countersunk rivets and from unprotected edges water penetrated the moisture absorbing adhesive layer. This led to subsequent desorption and corrosion of the non-protected bondsurfaces and finally complete delamination. Laboratory tests showed the adhesive to be extremely sensitive to moisture absorption along edges. Negative results of this effect, could be avoided by including anodizing in the surface treatment process. However, use of a more moisture resistant adhesive would be preferable. (Fig. 18).
- (f) Bonded doubler plates, used on a large scale in fuselage panels of transport aircraft, were assembled with help of a roomtemperature curing epoxy adhesive film. Operational experience showed that in the adhesive concerned moisture was transported easily via the carrier (glass) cloth in the adhesive from bondedges and (countersunk) fastener holes to the bond interfaces. Desorption of the adhesive from the etched only adherend surfaces and subsequent serious corrosion were the results. After airline operation during in the order of 6 years extensive repairs are required.
- (g) The same adhesive and surface treatment system was applied in longitudinal joints of pressurized fuselages in combination with mechanical fasteners. Unfortunately also these joints suffered from similar service troubles as last mentioned doublers in the same operational life time.
- (h) Longitudinal fuselage joints of another aircraft model followed the same principles as described in last mentioned case e.g. to increase the fatigue life of the mechanically fastened joints by means of additional assembly bonding (Fig. 19). In this case, however, the roomtemperature curing adhesive was applied on a hot precured phenolic adhesive primer coat that had an optimally chromic-sulphuric acid etched and subsequently chromic acid anodized surface as a base. The adhesive was of the two-component roomtemperature curing epoxy resin nitrile rubber type. After some 10 years of operation with many flights also under the most, from a corrosion standpoint, adverse conditions no problems with these pressurized fuselage joints have been experienced. High time aircraft of this type with flying hours upto 25.000 and flights upto 42.500 had no problems. Interesting is the fact that the cold curing adhesive used by itself is known for its rather poor moisture sensitivity. It appeared possible to exploit other attractive features of this adhesive system thanks to a combination with the absolutely durable base formed by a precured phenolic primer on optimally etched and anodized surfaces.

### 3.2 Sandwich structures

- (a) Sandwich structures with adhesive bonded metal were initially used on production scale in aircraft of american manufacture in the early fifties. One of the earliest production projects was a naval attack aircraft in which considerable amounts of balsa core sandwich panels were used. Chromic-sulphuric etching was applied in combination with phenol-formaldehyde based adhesives. Operation of this aircraft, as far as known, has shown reasonable durability. The pickled-only skins showed after some time corrosion on insufficiently protected edges. The adhesion of the adhesive used showed good durability and the end-grain balsa core suffered only from limited moisture penetration. At that time it was already experienced that an effective paint scheme and thorough application of sealant on any open cavities and crevices was the best way to assure ample aircraft durability, in particular under maritime operational conditions.
- (b) The, rather excessive, density of endgrain balsa wood core led to the adoption of honeycomb type core materials in subsequent aircraft. Early operational experience showed that the honeycomb sandwich structures suffered at least from similar durability problems as defined in paragraph 3.1 for metal-to-metal bonded joints in addition to another even more serious one. After a rather short number of flights water started to accumulate in the honeycombcells, which, originally for reason of the use of volatile by-products releasing phenolic adhesives were made out of perforated foil. The presence of this water that, when sufficient in quantity, will burst the sandwich panel due to expansion when below freezing point, either on the ground or during flight, was caused by penetration of moisture into the cells at low altitude. This moisture is presumably sucked into the core due to slowly compensated residual lower airpressure shortly after landing. (Fig. 20). During high altitude flight the humidity would condense and freeze again. At landing new humidity would be accumulated and subsequently condensed when cooling again, etc. thus increasing the amount of water with each subsequent flight.



It was not only the risk of bursting the sandwich panel below freezing point, but also the increasing amounts of water affecting the durability of the interfaces between adhesive and skins, resp. core, that appeared to be the major factors causing service problems with bonded sandwich components. The mentioned problems would lead in even shorter periods of time to serious degradation of the bonds to aluminium alloy skins and core and subsequently to serious corrosion of skins and edgemembers and most serious of all, the aluminium alloy core that would, as a consequence, lose its strength and stiffness. The described problem showed itself as that serious that by the end of 1959 the Martin Company received a contract from the U.S. Bureau of Naval Weapons to make a thorough study of the waterentry problem of honeycomb structures. This study, under the direction of John P. Reese, evaluated the experiences and opinions of some 80 manufacturers, operating agencies and experts in the field and came to the following important conclusions: /12/

- All core materials must be of the non-perforated type in order to restrict transportation of humid air and water within the sandwich panel.
- Adhesive systems without volatile release are required. This led to the consequence that the durable, but polycondensating phenolic adhesive resins, had to be replaced by others such as those based on epoxy resins curing without by-products.
- The curing procedure must avoid entrapment of air and subsequent node bond failures (Fig. 21) to be achieved a.e. by a rigid control of the vacuum pressure during the cure cycle.
- All panel edges must be air- and fluid tight.
- Sealing of the panel edges must be guaranteed by boundary joints with high peel-strength and unsupported adhesive. The use of carrier cloth in the adhesive film, that would permit wicking of water along the fibres must be avoided.
- All trimmed edges of panels and drilled holes must be provided with adequate corrosion protective means.
- During operation damage due to sharp objects and paintstrippers must be avoided.

From the following it will appear that these basic rules that were clearly formulated in 1960 unfortunately have not enjoyed optimal follow-up in subsequent years and projects.

- (c) A large military transport aircraft (take off weight in the order of 144 tons) that came into fleet service from 1963 onwards contained over 250 honeycomb sandwich components in secondary and in several areas of primary structure. Bonded secondary structure is utilized in control surfaces (flap panels and trailing edges, spoiler panels, aileron servo tabs and trailing edges) wing-to-fuselage fairings, wing leading edges, main landing gear pod panels, pylon leading edges and wing trailing edge panels, petal doors, engine cowl doors and some frame members. Of primary structural nature were the aft pressure door, emergency escape hatches and nose wheel bay panels that form parts of the fuselage pressure vessel. /13/
- With the exception of some components with possible higher temperature exposure the majority of the components was of the normal service temperature class. The high temperature resistant components were bonded with 177°C (350°F) curing epoxy-phenolic adhesive with a glass fabric carrier. All other components were bonded with help of an unsupported polyamide-epoxy adhesive film curing at 121°C (250°F). All adherend surfaces were treated with the chromic-sulphuric acid process.
- During operation it appeared that the average life until replacement of a bonded panel was about 7 years. The maintenance costs of supporting these honeycomb sandwich components have been rather high. A replacement procurement in 1978 of honeycomb components amounted 9 million dollars. In addition, at depot level, honeycomb repair in 1977 approached 4,5 million dollars, excluding the manhours and materials expended at field level maintenance for daily support. As main causes for the unsatisfactory performance of these adhesive bonded components are mentioned:
- . The high environmental susceptibility of the used nylon-epoxy adhesive;
  - . Moisture penetration into the bondline at the face sheet/adhesive film interface resulting in adhesion failure, desorption of the adhesive by water and subsequent delamination and corrosion.
  - . Lastmentioned phenomena were aggravated by insufficient control of the etching process used, causing adhesion failures.
  - . Panel edges, cut-outs and fastener holes had not been adequately sealed on installation.

Safety of flight has not been in discussion with the mentioned secondary bonded structure. However, the assurance of the structural integrity of primary bonded structure on that aircraft has been also a major problem. This finally was the basis for the understandable, but for bonding experts painful, decision to replace the honeycomb sandwich aft pressure door with a riveted corrugated sheet metal door.

In recent years in replacement components improved surface treatment and modified epoxy adhesive systems in conjunction with corrosion inhibitive bonding primers have been introduced together with better corrosion resistant types of honeycomb core together with thorough application of moisture resistant polysulfide sealants.

- (d) The aircraft type for naval purposes as mentioned also in par. 3.1 e consisted for all load carrying skin panels of fuselage, wing and tailplanes out of honeycomb sandwich structure. Metal-to-metal bonds of edgemembers and doublers were for the greater part bonded with a similar polyamide-epoxy adhesive system as mentioned in 3.2 d. All remaining skin-to-core bonds were established with help of an asymmetric adhesive bonding

film having epoxy resin on the core side and a suitable phenolic resin on the metal side. All alclad sheet materials that covered the greater part of the aluminium parts of the sandwich structure were chromic/sulphuric acid etched only. All non-clad materials were acid etched plus chromic acid anodized. In view of the rather heavy loading of quite a number of the sandwich panels concerned, much attention was paid to the shear connections between the honeycomb core sections among themselves and also with the edge members.

For these joints a phenolic-epoxy intumescent resin film had been chosen. Initial manufacturing difficulties revealed that the pressure that the latter material would develop in closed cavities could be of such a high level that bond failures could be caused in the non-perforated honeycomb core. As result of this, that material was not used over the full height of the honeycomb core, allowing the rest of the cavities to be filled by less densely foamed material (Fig. 22). Furthermore at locations where core splices met perpendicularly with the edge member profiles vent holes were drilled. After several years of operation it appeared that the before mentioned water accumulation phenomenon occurred strongly in these panels. Moisture entered via insufficiently sealed ventholes and corner openings and penetrated the porous splice material along edgemember and further through core splices into the panels (Fig. 23). This caused in some cases very difficult or even not to repair damage due to core corrosion and sometimes skin delamination between the adhesive primer and the skin. The same phenomenon was augmented in some areas where the panel edge members for manufacturing reasons had been split into two separate angles and joined by riveting. In the latter case inadequate sealing of the joint allowed easy water penetration. In later aircraft the problem could be suppressed by paying more attention to sealing all possible leaking points and selecting a better and less porous core splice material. (Fig. 24).

- (e) The fighter aircraft as mentioned under par. 3.1 c carried a number of honeycomb sandwich components that caused operational problems of various nature.
- One aircraft lost the greater part of the rudder trailing edge after 494 flying hours during a flight at 7500 meters. The airplane landed safely. It was found that the failure most probably had started at a skin-to-core void of some 7.5 cm diameter. (Fig. 25).
  - One aircraft had the upper skin of the trailing edge flap torn off after 1027 flying hours (Fig. 26).  
The above two examples and a few of other sandwich components appeared to be on the total fleet of 100 aircraft isolated cases and no reoccurrence was reported after frequent thorough inspection of the skin-to-core bonds was introduced.
  - The same type developed delaminations in the sandwich fin leading edge of which one skin was torn off after 398 hours. Fleetwide inspection revealed a systematical problem in this component and 100 components had to be replaced. (Fig. 27).
  - A similar problem was suspected to be in a version of this aircraft with a fixed wing leading edge, entirely built as honeycomb sandwich structure. An holographic interference inspection revealed that the rather new component had a delamination covering more than 50% of the span of the component concerned (Fig. 28).

The problems mentioned on this aircraft type could be traced back to insufficiently controlled surface treatment and end-product inspection in combination with epoxy-nitrile rubber adhesive system with a clearly insufficient environmental stability that was demonstrated during accelerated laboratory tests (Fig. 16 d).

- (g) One of the problems with the manufacture of sandwich structures provided with enclosing edge-members is the interaction of the tolerances of the core thickness and the height of the edge-members. When the quality of the bonds between skins, core and flanges of edge-members must all simultaneously be of high cohesion quality the edge-member accuracy must be of a very high standard. One way out of this problems is to split the edge-member such that the flange height can be adjusted to the core thickness. (Fig. 24). The joint between the edgemember halves can be riveted with or without adhesive. Application of this design principle both in military as well as civil aircraft showed in operational use very rapidly to lead to waterentry into the core with subsequent deterioration of the whole component. Analysis showed that water penetrated via the rivetholes and the overlaps in the edgemember joints. The waterpenetration was furthermore stimulated by holes resulting from excessively deep drilling in the core prior to riveting. This problems was also mentioned under par. 3.2 d.
- (h) The experience with sandwich structures with entirely closed edgemembers such as those of which one face has a dished shape is just the opposite of the former case. Panels of that nature did not show any waterpenetration when used in the skin structures of the fin, rudder and tailplane of an aircraft type, it appeared that no waterentry was present after 8 to 10 years of operation under many different climatological circumstances. (Fig. 29 ).
- (i) There is one variety of the sandwich structures with closed edge members, such as described in paragraph(h), that has given very bad service experience. These are so-called sandwich panels with crushed edges. During manufacture the core for these panels is pressed into shape by the dished skin. In this way the honeycomb core in the region of the flanges is crushed. During the curing operation the crushed edges are bonded together by adhesive primer in which the core has been dipped previously. In practise it has shown that moisture can easily creep into the rather porous edges and also into



countersunk holes drilled in the crushed edges. Fig. 30 shows the principle of manufacture of crushed edge sandwich panels. Fig. 31 shows experienced corrosion problems around the crushed edges of such panels.

#### 4 GENERAL OPERATIONAL EXPERIENCE BY AIRLINE COMPANIES

In the scope of this study a questionnaire was sent to eight european and one american airline company. The replies in general were of more qualitative nature than quantitative. The one american airline company, who must be ranked as the largest jetairliner operator of the world, supplied quite detailed information about adhesive bonded structures, of a very large jet airliner fleet, that had to be repaired or rebuilt over a period of some 17 years. The author combined the supplied data with available literature data about the fleet development of the particular airline. It must be stated beforehand that the data concern exclusively honeycomb sandwich components. Service troubles of metal-to-metal components had not been reported quantitatively. The jet airliner fleet of this company developed in this period between 1960 and 1977 from 44 to 338 aircraft with a maximum number of 381 in 1971. A maximum of 6 different aircraft types of two different manufacturers was simultaneously in operation during this period of time. From the data about that fleet in the table given in figure 34, it can be seen that the average number of honeycomb sandwich components developed from 80 to 169 per aircraft. The company concerned gives most data on honeycomb sandwich components that had to be completely rebuilt by using undamaged salvaged parts and cured in an autoclave together with newly fabricated parts. On a total number of about 57.000 operational honeycomb sandwich components the percentage that is completely rebuilt each year has grown from 0,35 in 1967 to 2,37% in 1977. During that period of time the average aircraft life of the fleet has grown from 3,1 in 1967 to 9,4 in 1977. The percentage of honeycomb sandwich components that had to be completely rebuilt is only a fraction of those that had to be brought yearly into the shop for repair.

For three different types of aircraft during the period 1960 through 1974 a total of 5771 sandwich components were brought into the repair shop. Of this only 17% had to be rebuilt completely. However, this figure was per aircraft type quite different e.g. 9; 12 and 28%. The percentage that had to undergo major repairs using also autoclave curing was 1; 11 and 22% respectively with an average on the total fleet of the three types of 8%. Non-autoclave repairs were required for resp. 66; 71 and 80% (average 75%) of the total components that had to go to the shop for repair. Rough extrapolation to the total aircraft number of the fleet learns that the percentage of all honeycomb sandwich components in operation that have to visit the shop pro year for partial or complete repair had grown to the high figure of approximatedly 14%.

One of the european airlines with a jet airliner fleet in 1976 of 55 aircraft reported also about number of honeycomb sandwich components that had to be rebuilt completely. In the figures given here the newer generation of widebody aircraft was excluded. In the years 1975 through 1977 the average aircraft age grew from 7,7 to 8,3 years, which is somewhat less than the formerly discussed figure of 9.4 years in 1977. The number of completely rebuilt components average per aircraft was in 1976 of 0,8. This to be compared with 2,9 components per aircraft in 1976 for the american airline company. The difference might have been caused due to the different relative composition of both fleets regarding aircraft types and models. The european company reports average flight time until complete rebuilding of the components concerned of 26665 flying hours, with the highest 60847 and the lowest 718 flying hours. The age until rebuilding in calendar months was in average 68.6, with the highest 114 and the lowest 5 months. Further information given by the other airlines on bonded airframe components was qualitative only. It contained the general complaint about low durability and high repair and maintenance costs of the honeycomb sandwich components primarily. The second major complaint concerned doublers and skin overlaps that had been bonded with cold curing adhesives, as has been discussed earlier.

Another significant information was received concerning turbofan engine nacelle reverser panels. The engine nacelle concerned is used by a group of european airlines cooperatively. A number of 220 fan reverser halves were in operation during Jan. 1976 through Sept. 1978. During that period 67 halves were inspected and 27 of these found to have one or more bond-defects. (Fig. 32). The service lifes of these components were between 2645 and 17364 hours.

The tables and diagrams of figure 33 through 40 show more details about the analysis of the information received from the airlines. It should be kept in mind, however, that the accuracy of the figures is certainly not very high, but it is the best available to-date.

#### 5 CONCLUSION

From this study the following can be concluded:

- The general operational experience with honeycomb sandwich components is poor. There are however favourable exceptions.
- The operational experience with metal-to-metal varies widely from very poor to extremely good.
- The nature of the durability problems experienced is such that the causes of the failure are identifiable.

- There is no doubt that with the available know-how a better result could have been achieved.
- The following lectures will discuss the backgrounds of the failure experienced, giving a good base for the required considerable durability improvement of bonded structures.

## 6 REFERENCES

- /1/ Golf, W.E. "De Havilland Hornet", Aircraft Production Vol. 8 (1946) May, p. 211.
- /2/ van Beek, E. "Design Aspects of bonded structures" Bonded Aircraft Structures Conference, 1957, CIBA Ltd., Duxford England.
- /3/ Noton, B.R. "Bonded Composite Structures" Adhesion and Adhesives. Vol. 2, p. 345. Elsevier Publ. Comp. (1967).
- /4/ Ricard, G. "Flugzeugstrukturen in Honigwabenbauweise" Luftfahrttechnik VII (1961) Vol. 11, p. 192.
- /5/ MIL-STD-1530 "Aircraft Structural Integrity Program" Sept. 1972.
- /6/ MIL-A-83444 "Airplane Damage Tolerance Requirements.
- /7/ Schliekelmann, R.J. "Redux for Spars" Aeroplane (1952) Vol. 8, p. 216
- /8/ Rondeel, J.H. "Static and fatigue tests on Redux bonded built-up and solid light alloy sparbooms, Nat. Aerospacelab. N.L.R., Netherlands, Report M-1936 (1954)
- /9/ Rondeel, J.H. "Comparative fatigue tests on 2024 clad riveted and bonded stiffened panels", Nat. Aerospace Lab, N.L.R., Netherlands, Report S-411 (1952).
- /10/ Bijlmer, P.F.A. "Fracture toughness of multiply layer adhesive bonded aluminium alloy sheet" ICAS, Lisbon, Aug. 1978.
- /11/ Grimes, D.L., AGARD Report 181, 1958
- /12/ Reese, J.P. "Waterentry in honeycomb panels", The Martin Company, Baltimore, Report No. ER 11551, Nov. 1960.
- /13/ Griffin, L.D. "C-141A Service Experience , Materials and Processes". SAMPE Journal March/April 1978, p. 9.
- /14/ Kuperman, M., United Airlines San Francisco, "An airline view of composite airframe structure", 18th National SAMPE Symposium Volume 18, New Horizons in Materials and Processing, April 3, 1973, p. 7.
- /15/ Koetsier, J., Fokker-VFW Technological Centre, Schiphol, The Netherlands "Metal-to-metal bonded aircraft structures", 7th National SAMPE Conference, volume 7 Materials Review '75, October 14, 1975, p. 126.
- /16/ Bijlmer, P.F.A., Fokker-VFW Technological Centre, Schiphol, The Netherlands, "Adhesive bonding on anodized aluminium", Metal Finishing, April 1972, p. 30.
- /17/ Bijlmer, P.F.A., et. all., Fokker-VFW Technological Centre, Schiphol, The Netherlands, "The relation of surface condition after pretreatment to bondability of aluminium alloys", SAMPE Quarterly, October 1973.

## NOTE

1. In the above article no names of adhesive manufacturers, airline companies, type or model designations of aircraft or adhesives were mentioned. This had been done with the purpose not to disqualify any manufacturer or user.
2. It is well understood that this restriction in the information given withholds much detailed information that some categories of readers would have liked to receive. In view of the purpose of this publication the opinion was formed that in this way the trends could be demonstrated sufficiently clear.

## ACKNOWLEDGEMENTS

The information on operational experience could be published thanks to the kind cooperation of many operating organizations of which the names for obvious reasons remain undisclosed. Mrs. I. H hle-Meijer deserves credit for the realization of the manuscript.

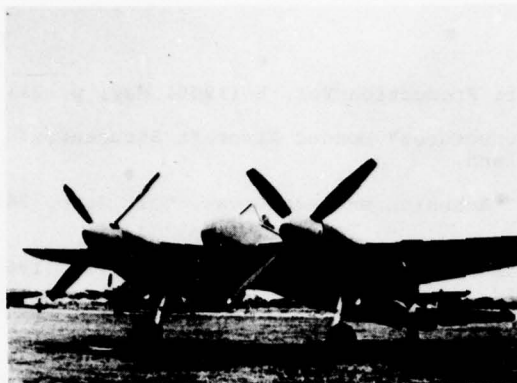


Fig. 1 De Havilland Hornet twin engined fighter aircraft built primarily as a wooden construction, but with locally bonded aluminium alloy reinforcements in the wing.



Fig. 2 Details of the wingstructure of the De Havilland Hornet. Note the light alloy lower spar boom (2) that has been adhesive bonded to the wooden structure (7). This was done via a ply of wood fineer (6) bonded on to the aluminium sparboom by means of a phenolic/vinylic adhesive.

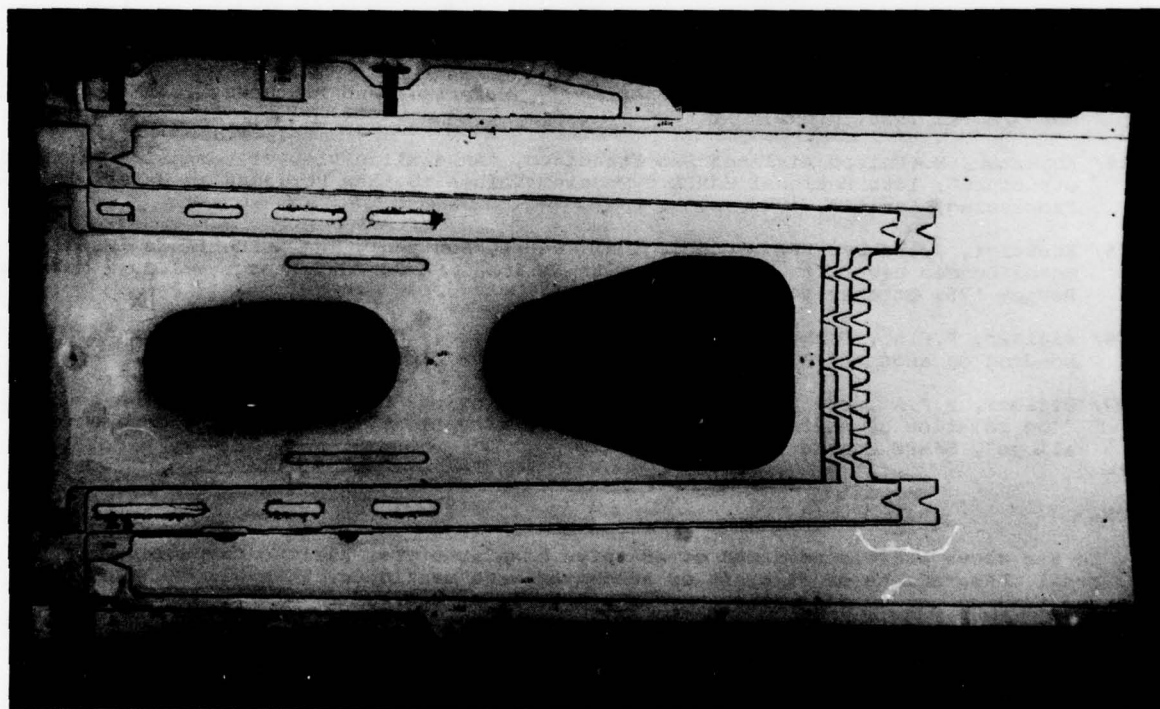


Fig. 3 Lower wing skin with multiply adhesive bonded doublers around large access openings.



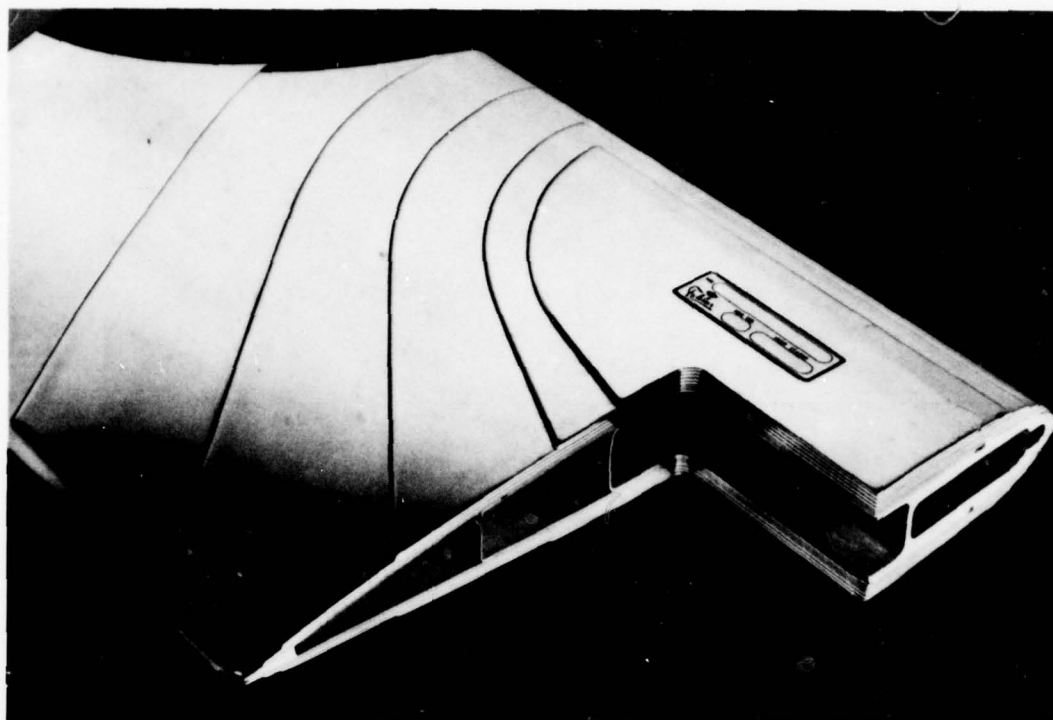


Fig. 4 Adhesive bonded multiply rootend reinforcement of metal helicopter (NH3 Colibri) rotorblade.



Fig. 5 Lower wing panel with adhesive bonded stringers and doubler-reinforcements around manhole openings.



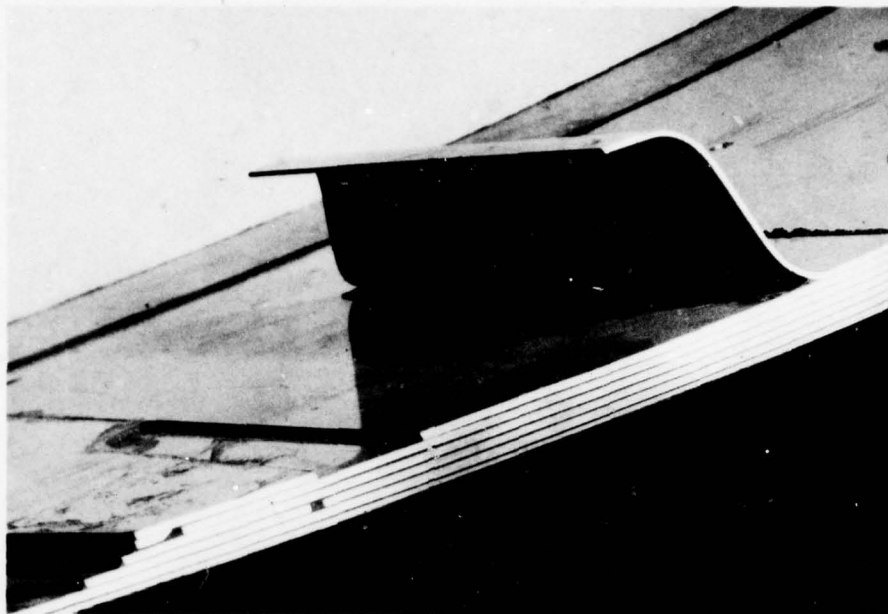


Fig. 6 Cross-section of rootend of multiply adhesive bonded lower wing skin (Fokker F27 "Friendship").

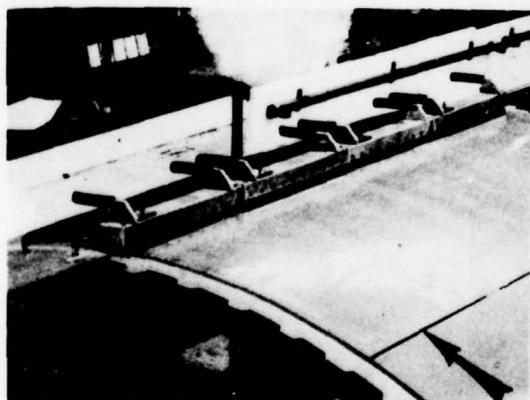


Fig. 7 Longitudinal joint in pressure cabine made by consecutive adhesive bonding and riveting. Bonding pressure is given by means of electromagnetic tools (Fokker F28 "Fellowship").

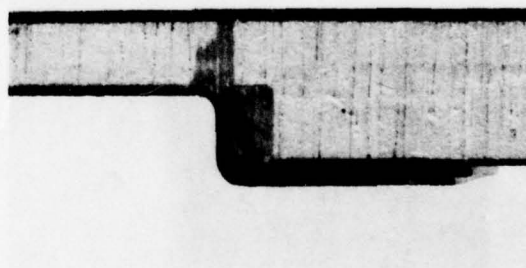


Fig. 8 Cross-section over balsa wood core sandwich floorpanel.

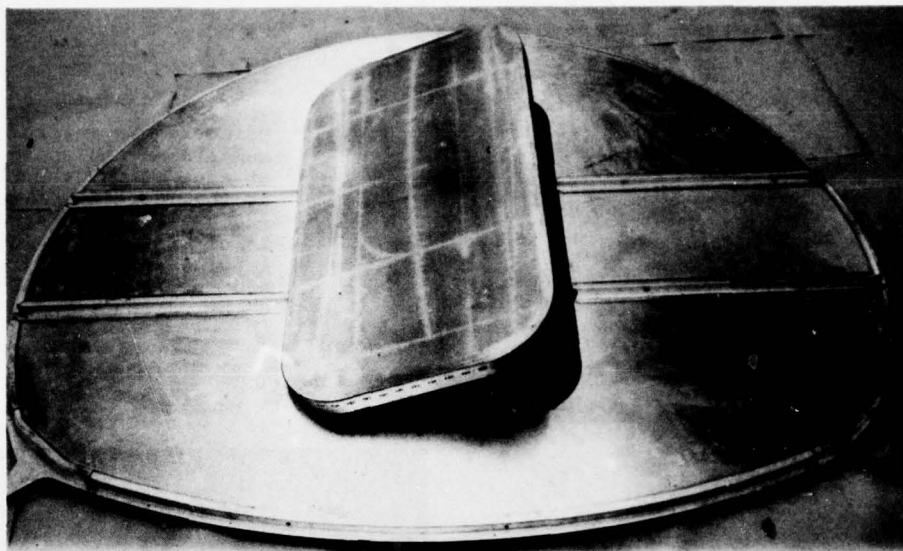


Fig. 9 Fuselage bulkhead entirely built as honeycomb core sandwich construction. Load introduction takes place primarily via bonded edge profiles.

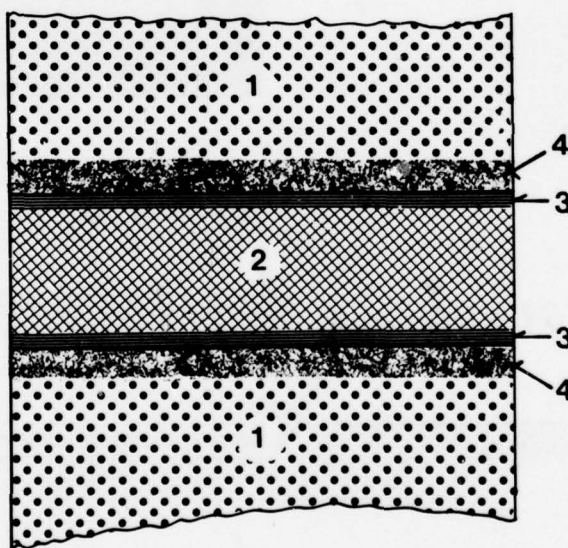


Fig. 10 Main elements of adhesive bonded metal joint.

1. Metal adherend
2. Cured adhesive resin layer
3. Primer layer (either precured on the adherend or predried and cocured with the adhesive layer)
4. Oxide layer on the adherend either single due to the chromic/sulphuric etching or double due to etching followed by anodizing.



Fig. 11 Moisture has entered multilaminated sparcap at edge of one sheetlayer at the location of corner radius. Moisture has spread in direction of arrows leading to surface corrosion and subsequent complete delamination.

Fig. 12 White arrows show how moisture penetrated gluelines of sparcaps that were left insufficiently protected after machining the edges of bonded laminate.

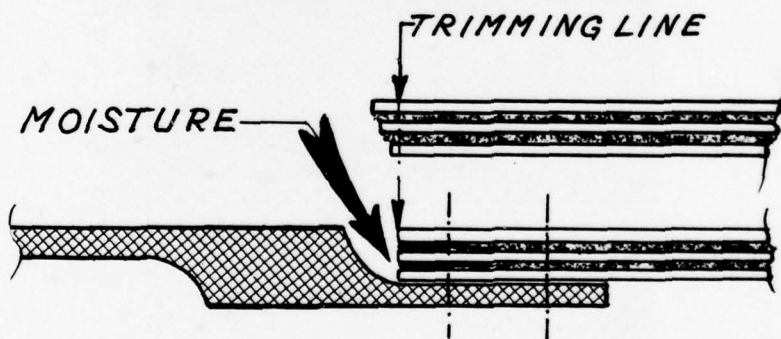


Fig. 13 Trimming of edges of adhesive bonded laminate requires extra care for corrosion protection in areas of severe humidity exposure.

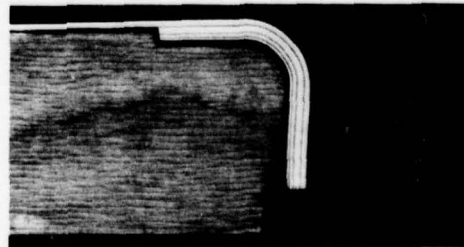
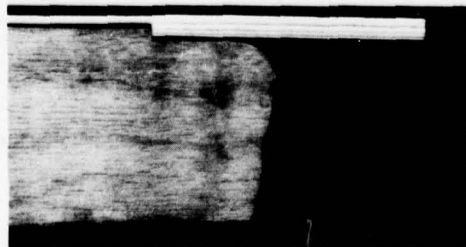


Fig. 14 Laminated fin sparcap for jet trainer had been bonded in flat state integrally with sparweb. Cap flanges were formed on rubber press after bonding cure cycle.

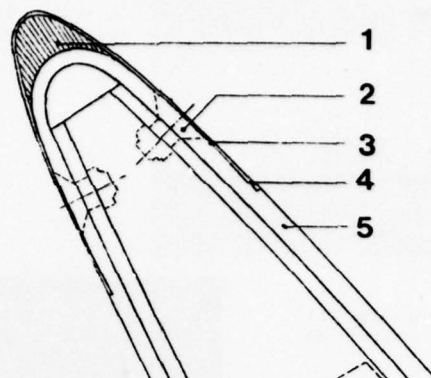
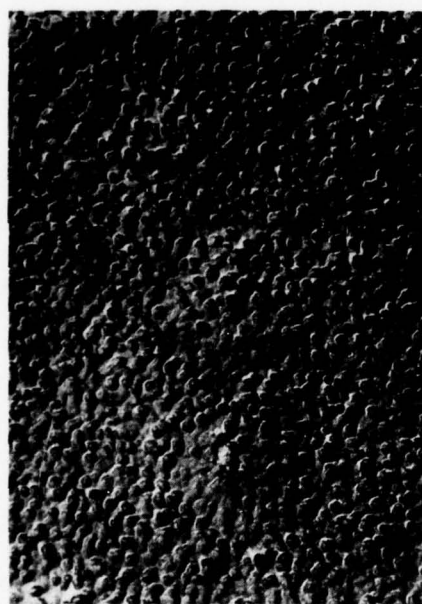


Fig. 15 Cross section over leading edge flap

1. Foaming adhesive
2. Steel countersunk bolt
3. Adhesive
4. Fairing sheet (7075-T6 clad)
5. Skin (7075-T6 bare) locally chemically milled



← Fig. 16 a

Bond surface showing the micro-etch pit oxide configuration indicative for optimal surface treatment.

Fig. 16 b →

Bond surface of rebate showing absence of micro-etch pits and scratch marks and contamination.





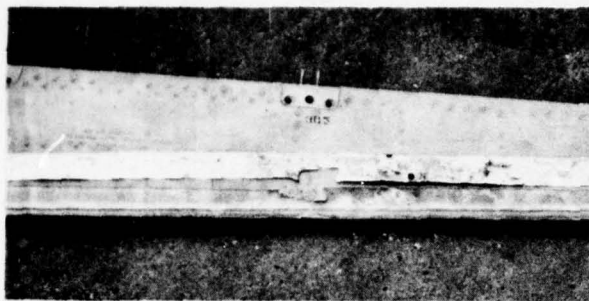


Fig. 16 c

Corroded leading edge bond with delaminated skin strip.

Fig. 16 d Salt spray test specimen with identical adhesive system as leading edge.

1. Reference
2. 30 days saltspray
3. 60 days saltspray
4. 90 days saltspray

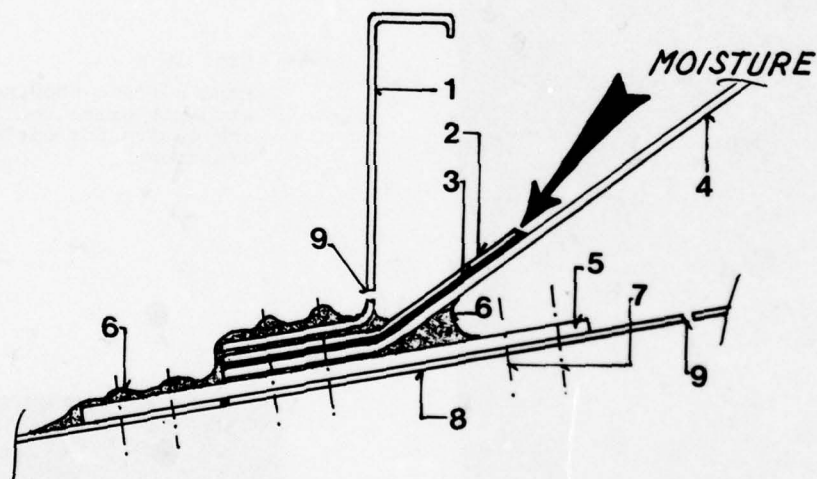


Fig. 17 Cross section of pressure bulkhead-skin joint

1. Frame
2. Doubler
3. Partly porous adhesive glue layer
4. Pressure bulkhead
5. Butt strap
6. Sealant
7. Rivets
8. Fuselage skin
9. Drain holes

Fig. 18 a Tank door with delaminated bonded edge joint.

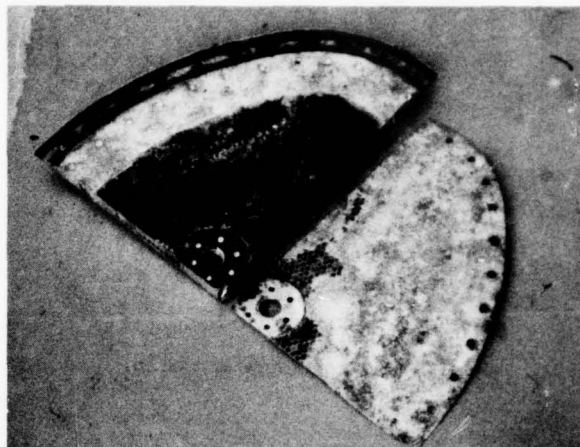
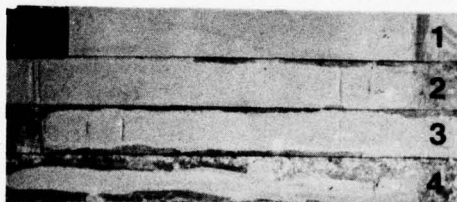


Fig. 18 b Saltspray specimen of the same adhesive system as used on the tank door.



1. reference
2. 30 days saltspray
3. 60 days saltspray
4. 90 days saltspray

Fig. 19 Longitudinal fuselage joint in the process of bonding. Roomtemperature curing two-component adhesive is applied on precured adhesive primer surface. Curing takes place with the clamping tools as shown in fig. 7.





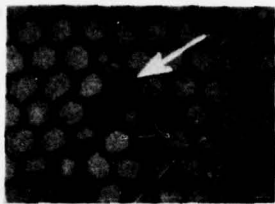


Fig. 20 Water filled honeycomb cells.

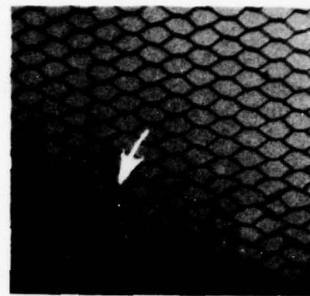


Fig. 21 Typical failure of the nodes of honeycomb cells due to wrong vacuum control during the autoclave cure cycle.

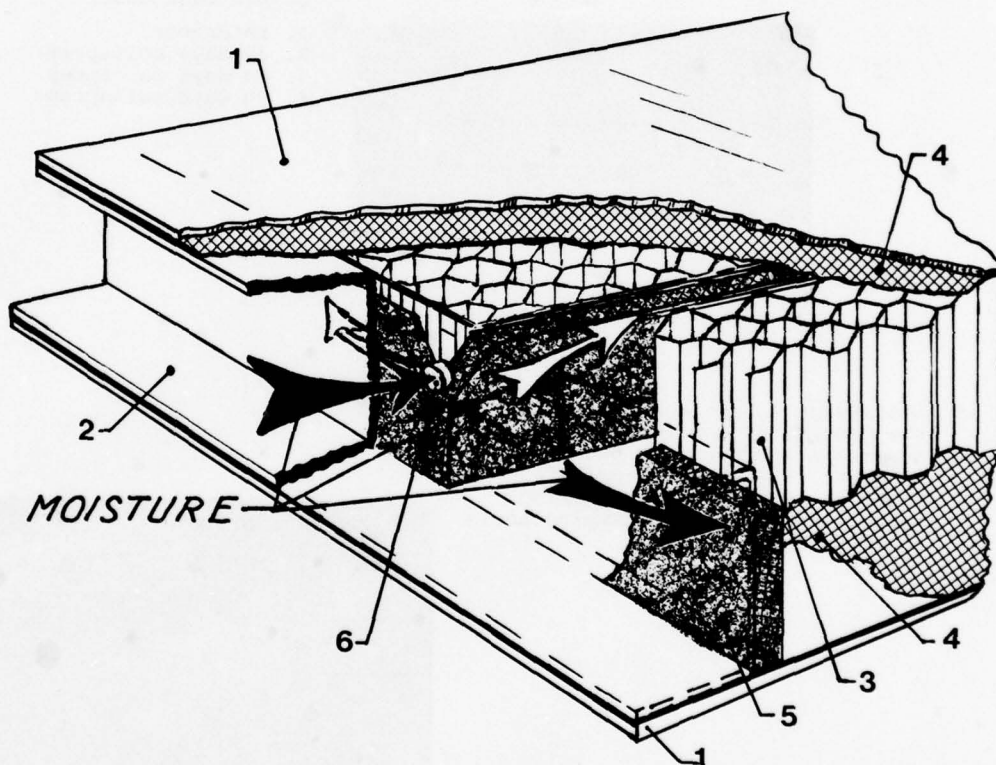


Fig. 22 Schematic illustration of moisture entry through open ventholes for vapour ventilation at location of intersecting core splices.

1. Skin
2. Edge member
3. Honeycomb core
4. Skin-to-core adhesive
5. Intumescent core splice adhesive
6. Venthole for ventilation of core splice adhesive vapours. Left open after bonding allowed moisture to pass through core splices and to spread through panel, causing extensive corrosion of core and skins as well as delamination.

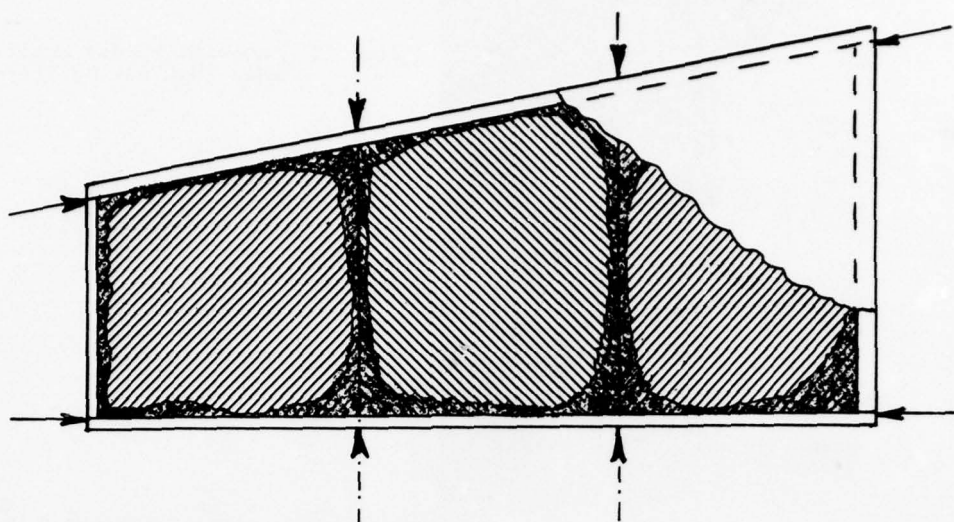


Fig. 23 Arrows indicate areas of core splice ventholes and openings between edge-members that can be starting points for moisture penetration and extensive damage to the whole panel, starting from core edges.

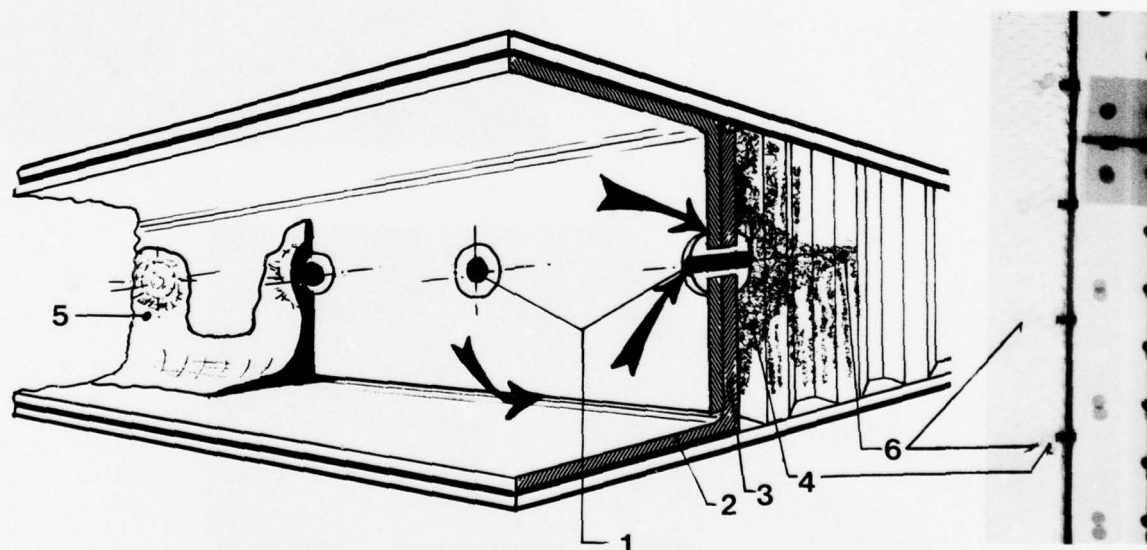


Fig. 24 Split edge members of sandwich panels are used for reasons of overcoming dimensional tolerance problems. They have the drawback of easy moisture penetration (indicated by arrows) along the blindrivets and profile edges. Moisture also easily spreads via damaged core at rivet locations.

1. Blind rivets
- 2, 3. Edge member profiles
4. Penetrated moisture and subsequent deterioration of core bonds and skins
5. Bead of sealant to be applied over joint edges of profiles and rivetheads
6. Damage area of core due to excessively deep drilling.

Note: Tightness of sandwich components has to be checked by hot water submersion test.



Fig. 25 Sandwich rudder trailing edge lost during flight.

Fig. 26 Upper skin of wing trailing edge was torn off after delamination at the adhesive bonded forward flange of the edge member due to desorption and subsequent corrosion of the adherends

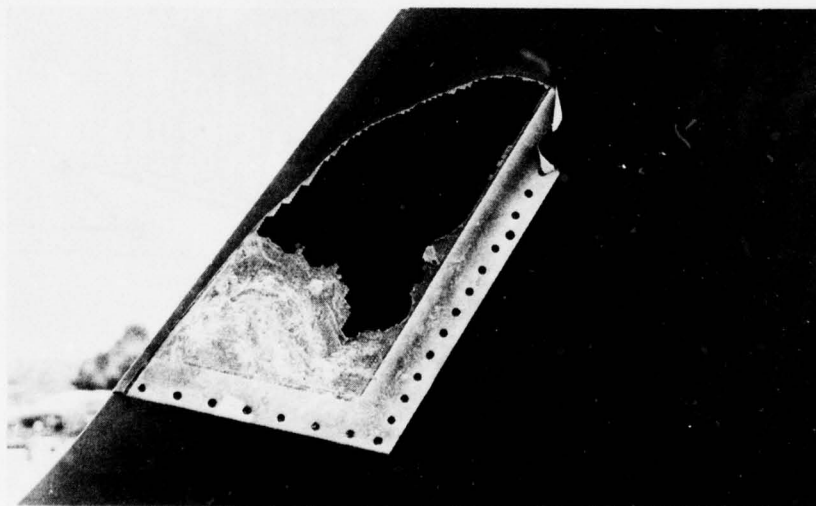
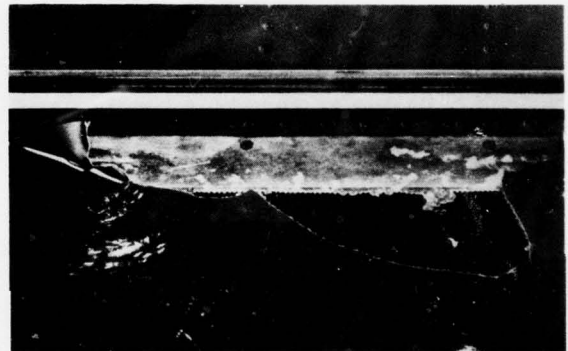


Fig. 27 Fin leading edge sandwich structure after loosing skin during flight.



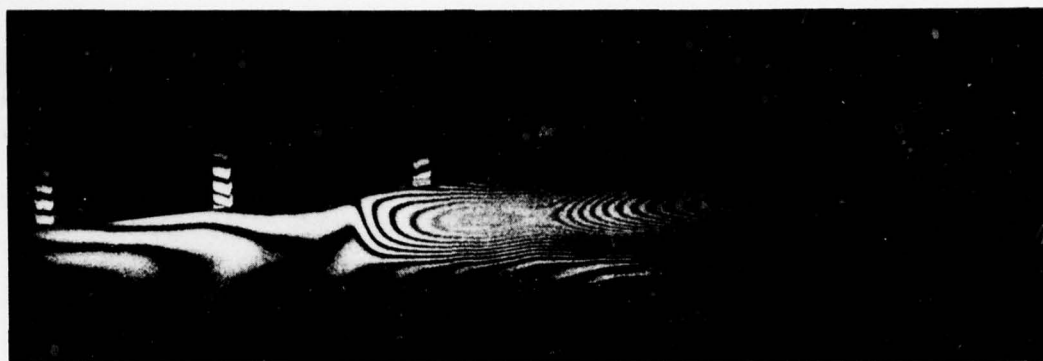


Fig. 28 Interference hologram of adhesive bonded sandwich wing leading edge. The right hand side shows to be completely void, which can be noticed from the closely spaced interference fringes.

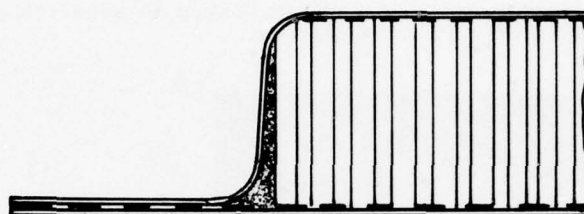


Fig. 29 Sandwich panel of which one skin is a pressformed component in which the edge members and the inner face are integrated.

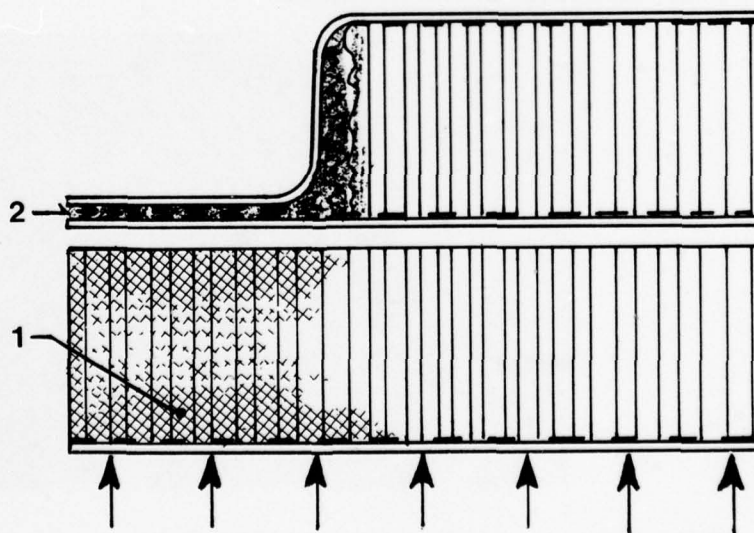


Fig. 30 Sequence of manufacture for crushed edge honeycomb panels.  
1. Honeycomb core edge dipped in adhesive primer.  
2. Crushed honeycomb core.

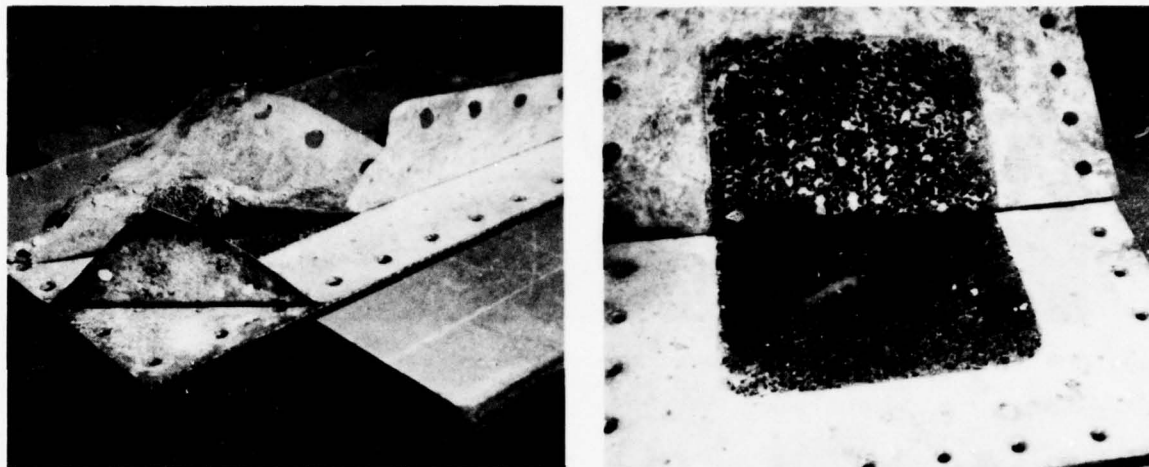
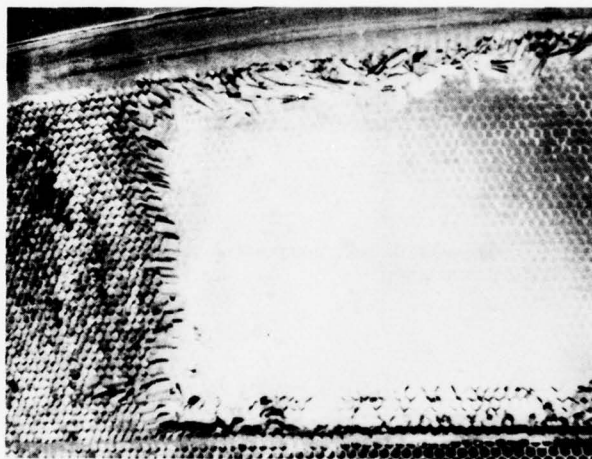


Fig. 31 Typical corrosion at edges of crushed honeycomb sandwich panels that occurs after a few years of airline operation.



← Fig. 32 a

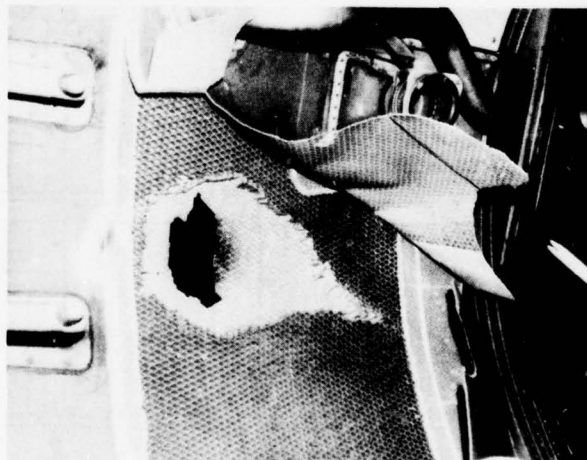


Fig. 32 b →

Fig. 32 Typical damage experience with honeycomb sandwich components from turbofan reversers.

- a. Corroded aluminium honeycomb core showing presence of important quantities of aluminium oxide.
- b. Completely blown-in innerskin resulting from ram airflow thru the perforated outerskin.

YEAR	A/C TYPE						FLEET TOTAL
	A	B	C	D	E	F	
1960	33	11	-	-	-	-	44
1962	36	29	-	-	-	-	65
1963	36	29	-	-	-	-	65
1966	55	29	69	-	-	-	153
1967	77	29	118	6	-	-	230
1968	99	29	143	44	-	-	315
1969	104	29	151	62	-	-	346
1970	114	29	150	75	-	-	368
1971	112	29	150	73	12	5	381
1972	112	-	150	69	14	18	363
1973	111	-	150	67	18	23	369
1974	111	-	150	67	18	30	376
1975	106	-	150	64	18	37	375
1976	100	-	150	59	18	37	364
1977	72	-	152	59	18	37	338

TABLE 33

Fleet composition of large airline company in the U.S. The aircraft types can be described as follows:

Type A and B: four engined jet aircraft.  
 Type C : three engined jet aircraft.  
 Type D : twin engined jet aircraft.  
 Type E and F: wide body airliners.

Note: these data are deducted from literature information.



YEAR	A/C FLEET *	HC COMP. IN SERVICE x	HC COMP. PER A/C x	HC COMP. REBUILT x	PERCENT. REBUILT
1960	44	3500	80	0	0
1961	+	4000	+	0	0
1962	+	4000	+	0	0
1963	65	4500	69	0	0
1964	+	8500	+	25	.29
1965	+	13500	+	25	.19
1966	153	19750	129	40	.20
1967	230	25750	113	90	.35
1968	315	38000	121	150	.39
1969	346	44500	129	200	.45
1970	368	49500	135	290	.59
1971	381	52500	138	375	.71
1972	363	54000	149	490	.91
1973	369	57000	155	625	1.10
1974	376	57000	152	725	1.27
1975	375	57000	152	860	1.51
1976	364	57000	157	1050	1.84
1977	338	57000	169	1350	2.37
*1978	+	57000	+	1500	2.63

\* ESTIMATE

+ UNKNOWN

\* FROM LITERATURE

x FROM AIRLINE

TABLE 34

Information regarding the amount of honeycomb components in service with the airline company as mentioned in table 33. It should be noted that the information about the fleet has been found in literature and the information on the amount of sandwich components rebuilt has been received from the airline company concerned. The figure on honeycomb components rebuilt concerns sandwich structures that were so far damaged that they had to be completely rebuilt in an adhesive bonding shop and hot-cured in autoclave.

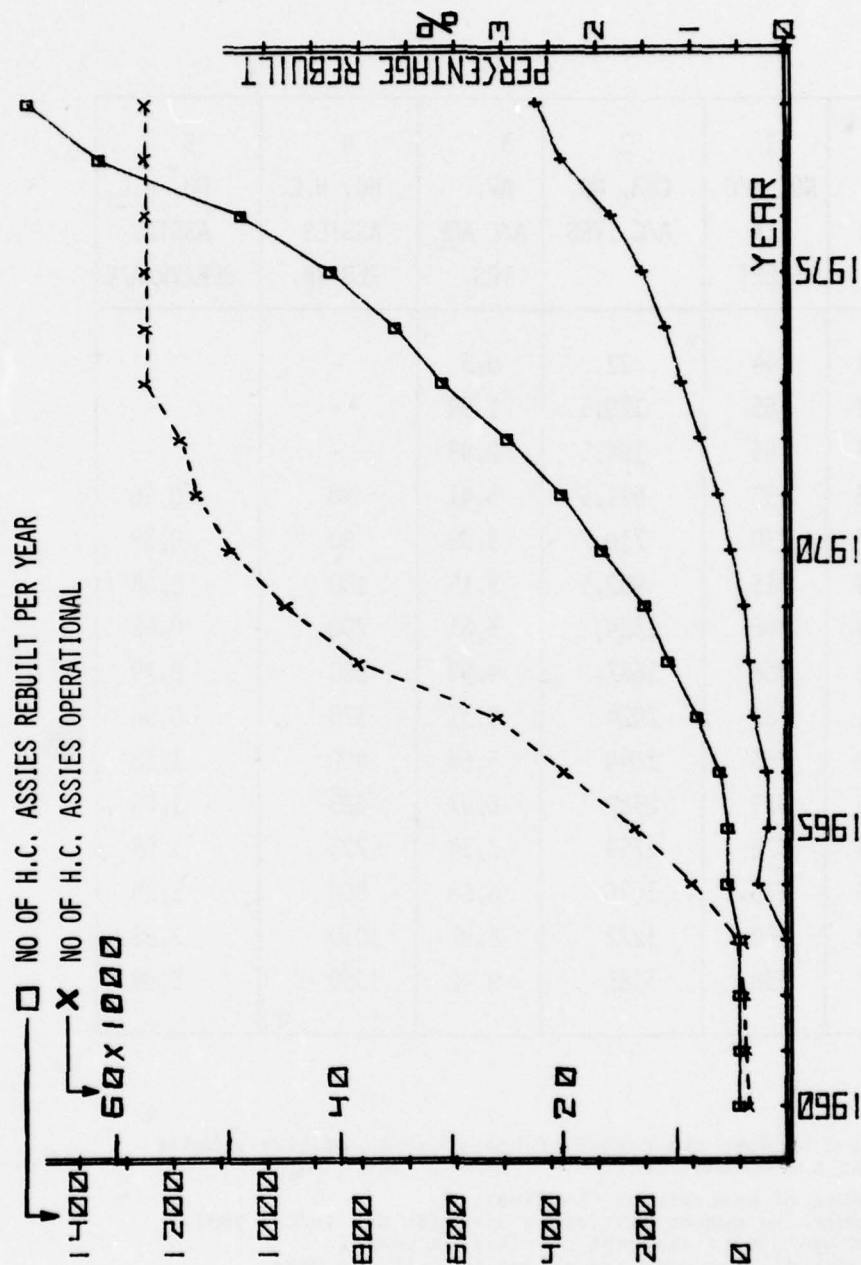


Fig. 35 The relation between the number of aircraft in the fleet, the number of operational honeycomb assemblies, the number of honeycomb assemblies to be rebuilt per year and the percentage of the number of honeycomb assemblies to be rebuilt per year of the total amount of operational honeycomb assemblies.

YEAR	1 NO. A/C IN FLEET	2 CUM. NO. A/C .YRS.	3 AV. A/C AGE YRS.	4 NO. H.C. ASSIES REB/YR.	5 NO. H.C. ASSIES REB/YR/A/C
1960	44	22	0,5	-	-
1962	65	129,5	1,99	-	-
1963	65	194,5	2,99	-	-
1966	153	521,5	3,41	40	0,26
1967	230	710,7	3,09	90	0,39
1968	315	992,5	3,15	150	0,48
1969	346	1324	3,83	200	0,58
1970	368	1687	4,58	290	0,79
1971	381	2024	5,31	375	0,98
1972	363	2044	5,63	490	1,35
1973	369	2387	6,47	625	1,69
1974	376	2759	7,34	725	1,93
1975	375	3026	8,06	860	2,29
1976	364	3272	8,99	1050	2,88
1977	338	3183	9,42	1350	3,99

Table 36 Relation between the number of honeycomb assemblies rebuilt and the age of the fleet.

- 1: Number of aircraft of the fleet.
- 2: Cumulative number aircraft x aircraft age (A/C . YRS).
- 3: Average age of aircraft in fleet in years.
- 4: Number of honeycomb assemblies rebuilt per year.
- 5: Number of honeycomb assemblies rebuilt per year per aircraft.



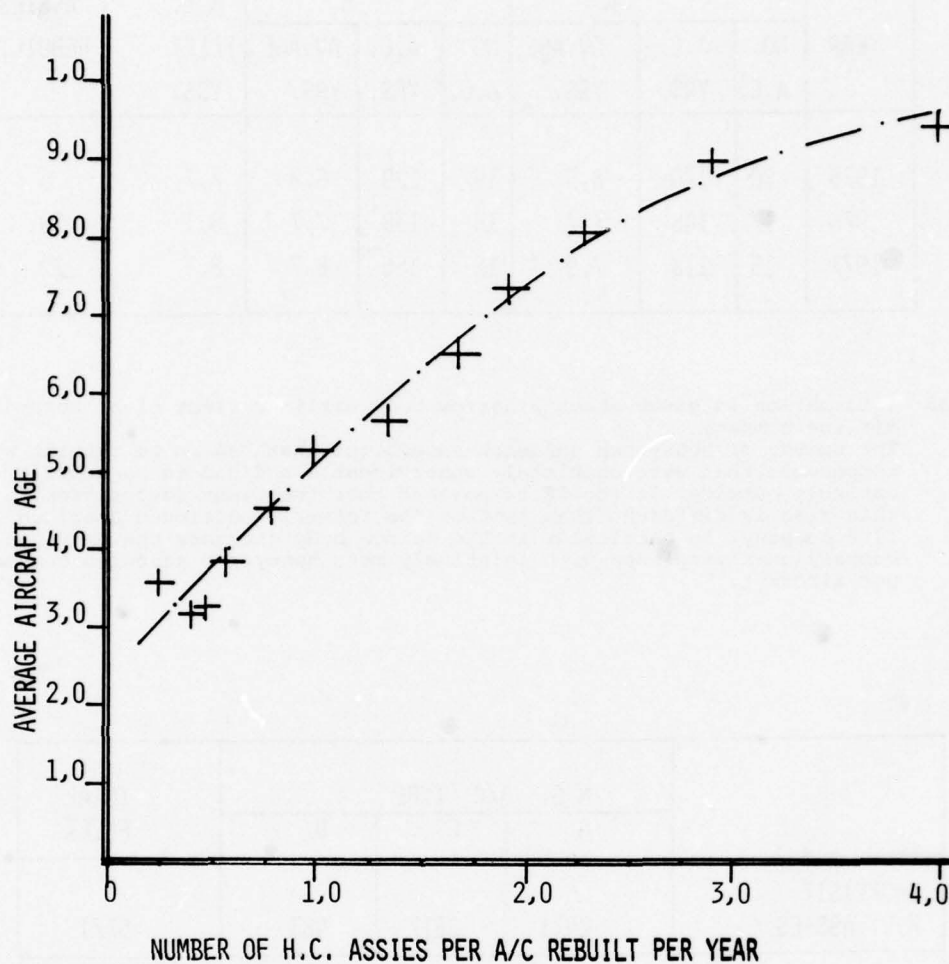


Fig. 37 Relation between number of honeycomb assemblies per aircraft that have to be rebuilt per year and the average fleet age. The influence of the changing fleet composition over the years has not been taken into account. The given curve therefore gives only a very rough trend.

YEAR	AIRCRAFT TYPE						AV. AGE N.B. FLEET YRS.	NO. H.C. ASSIES REBUILT
	A			B				
	NO. A.C.	A.C. YRS.	AV.AGE YRS.	NO. A.C.	A.C. YRS.	AV.AGE YRS.		
1975	20	170	8,5	19	129	6.8	7,7	5
1976	17	145	7,7	18	138	7,7	8,1	29
1977	15	118	7,9	18	156	8,7	8,3	22

Fig. 38 Information is given about a narrow body airliner fleet of a European airline company. The number of honeycomb sandwich assemblies that had to be rebuilt were components that were completely unserviceable and had to be rebuilt entirely outside. It should be noticed that the fleet composition in this case is different than that of the formerly mentioned American airline company. In particular in the narrow body category the American company uses airplanes with relatively more honeycomb sandwich components per aircraft.

	N.B. A/C TYPE			TOTAL FLEET
	A	C	D	
SHOPVISIT H.C. ASSIES	2471	2817	483	5771
REBUILT NO.	692	254	58	1004
" %	28	9	12	17
MAJOR REPAIRS NO.	25	310	106	441
" %	1	11	22	8
NON AUTOCLAVE REPAIR NO.	1754	2253	319	4326
" %	71	80	66	75

Fig. 39 Detailed information about the narrow body fleet of the before-mentioned American airline company. The number of shopvisits of the honeycomb assemblies is given over the years 1960 thru 1974. The shopvisits are divided in the number of honeycomb assemblies that had to be entirely rebuilt; those having to be repaired with help of an autoclave cure; and those who had to be locally repaired but did not require an autoclave cure.

## Appendix 40

In the following information is given that has been received from airline companies and that has not been given already in more detail either in the text, the tables or the diagrams.

### Airline 1

- . No cohesive failures.
- . Adhesive failure at interface is normal.
- . Causes of adhesive failure:
  - poor surface preparation by manufacturer.
  - moisture ingress causing corrosion of adherends.
- . Perforated honeycomb is to be avoided.
- . Honeycomb preferably chemically treated and/or dipped in primer.
- . Adhesive failure finally occurs with all adhesives.
- . Corrosion on doubler/skin joints.
- . Chemically or mechanically milled edges are preferred.
- . Bonded stringers in fuselages of closed type are to be avoided.
- . Non-metallic honeycomb to be dried before bonding.
- . Edges of panels have to be sealed.
- . Carrier in adhesives must be polyester and non-woven.
- . Cold bonded fuselage joints are source of trouble; difficult to repair.
- . Occasionally undercarriage doors and frame components have departed in flight.
- . "Battle" damage from collision with ground vehicles occurs frequently.
- . Speedy repairs while many parts are not interchangeable.

### Airline 2

- . Cold bonded joints in longitudinal skin lap joints, skin doublers, fail-safe straps and pressure bulkheads have frequent failures due to:
  - presence of voids
  - absence of corrosion inhibitor
  - absence of adhesive primer
  - moisture penetration
- . Hot bonded joints between doubler and skin failed only once.

### Airline 3

- . In 1977 44 control surface sandwich components were entirely rebuilt for reason of:
  - corrosion delamination
  - water in core
  - unsatisfactory cold bonding

### Airline 4

- . Wing/fuselage fairings show delamination after two years starting from bolt holes.
- . Flap panels delaminate after 4 to 6 years in 20.000 to 25.000 flying hours.

### Airline 5

- . In 20 months approximately 350 honeycomb panels and control surfaces as well as engine cowlings were completely rebuilt.
- . General experience is that life is about 5 years before failure.
- . However there are good exceptions upto 10 years without failure.
- . Main cause of trouble is moisture penetration.
- . Overloading due to missfit is a minor problem.

### Airline 6

- . Honeycomb sandwich forms really a problem in maintenance.
- . Sealing strength and durability is inadequate.

### Airline 7

- . Metal-to-metal bonded joints of phenolic/vinyl type on anodized surface performed well in maritime environments.

### Airline 8

- . Except for mechanical damage there is never cohesive failure, always interface failures starting at locations where the sealing has failed.
- . Starting points may be:
  - Tooling holes
  - Trailing- or leading edges
  - Rivet- or fastener holes
  - Broken sealing compounds or edge close-out material
- . Almost always the failures are of the corrosion/delamination type. On early parts perforated honeycomb core allowed rapid spreading of moisture.
- . Debond mechanism most frequently is alclad desolution.
- . Problems with non-primed surfaces of hot-bonded components occur after 20.000 thru 25.000 hours (7-9 years in service).



- . Components bonded with 120°C curing adhesive follow more quickly than those cured at 177°C.
- . Corrosion inhibiting primer is expected to give much improvement.
- . During the last 4 years the number of corroded bonded assemblies has increased almost exponentially.

#### Airline 9

Information concerns mainly fan engine thrust reverser components.

- . Of 67 components inspected in period Jan. 1976 - Sept. 1978, out of 220 in service, 27 failed.
- . These include the:
  - core structure with perforated outerskin and slotted core.
  - duct side walls with non-perforated skins.
  - translating cowls with non-perforated skins.
- . Core structure failed between service time of 4301 and 17364 flying hours.
- . Side wall structures failed between service time of 2645 and 16792 hours.
- . The core structure failed mainly due to overloading at high temperature.
- . The side walls failed due to corrosion often combined with high temperature loading.

'INTERFACIAL FRACTURE MECHANICAL ASPECTS OF ADHESIVE BONDED JOINTS'

A.J. Kinloch

Ministry of Defence (PE),  
 Propellants, Explosives and Rocket Motor Establishment  
 Waltham Abbey,  
 Essex,  
England

SUMMARY

A serious limitation frequently encountered in the use of structural adhesives is the deleterious effect moisture has upon the strength of a bonded component, especially when the component is also subjected to conditions of relatively high stress and temperature. It is generally agreed that while the locus of joint failure of well prepared joints is invariably by cohesive fracture in the adhesive layer, after environmental attack it is via failure in the interfacial regions of the joint. This interfacial locus of failure focuses attention on interfacial fracture mechanical considerations. The aim of this paper is to review mechanisms of environmental failure and consider techniques for estimating and increasing the service-lifetimes of bonded components. Particular emphasis is given to the contribution from the application of continuum fracture mechanics concepts to the study of environmental attack on adhesive joints.

1.0 INTRODUCTION

Adhesives are being increasingly used in structural engineering applications but a problem frequently encountered is that the mechanical properties of the bonded component may rapidly deteriorate upon exposure of the joint to its normal operating environment. Unfortunately for the adhesion scientist one of the most harmful environments for adhesive joints is water and this paper reviews mechanisms of failure, predictive techniques for estimating service-lifetimes and methods for increasing durability, with particular emphasis on the contribution from workers who have employed a continuum fracture mechanics approach to study environmental attack.

2.0 GENERAL OBSERVATIONS

It is of interest to distill from the many outdoor and accelerated laboratory trials some general observations on the parameters which influence joint durability and the mode of joint failure.

First, the obvious statement, namely that after exposure to hostile environments there have been observed unexpected, premature failures of bonded components or, alternatively upon subsequent testing of adhesive joints considerable reductions in their load-bearing capability have been recorded. The extent of the problem is illustrated in Figure 1 which shows the loss of strength of epoxy-polyamide/aluminium-alloy joints after exposure to a hot-wet tropical environment, while the hot-dry climate has little effect.

Second, while the locus of joint failure of well prepared joints is invariably by cohesive fracture in the adhesive layer, after environmental attack it is via apparent interfacial failure between the adhesive (or primer) and the substrate. This interfacial locus of failure means that interfacial fracture mechanical aspects of adhesive joints become of vital importance.

Third, the following parameters affect joint durability:-

- (a) Environment - the presence of an hostile environment is, of course, the essence of the problem and water, as discussed above, is undoubtedly the most harmful and most commonly encountered environment.
- (b) Adhesive type - it is well known that the older phenolic-based structural adhesives impart superior joint durability than the more modern epoxide-based adhesives (1,2,3). However, the latter type are now preferred on the basis of their lower cure-temperature/pressure requirements and generally superior peel strengths.
- (c) Substrate - joints to metallic substrates represent the main problem, ie steels, aluminium and titanium and their alloys. Joints to plastics, glass - and carbon-fibre reinforced plastic are far less susceptible to environmental attack; this is not to say that such joints do not ever suffer from environmental attack but when this does occur it is usually the substrate, eg the composite material, which is itself attacked more readily and rapidly than the adhesive or adhesive/substrate interface.
- (d) Substrate surface pretreatment - this is an extremely important parameter. To ensure initially strong joints it is usually sufficient to remove surface contamination, weak oxide layers, etc but to produce durable joints it is also necessary to form stable oxides which are "receptive" to the adhesive and, also, frequently to employ a specially developed primer. The effects of various surface pretreatments on the durabilities of epoxy/titanium (4) and epoxy/aluminium alloy (5) joints are shown in Figures 2 and 3 respectively and clearly demonstrates the importance of selecting an adequate pretreatment. The effectiveness of a pretreatment is often also dependent on the actual alloy type and manufacturing process employed.
- (e) Temperature - increasing the temperature increases the rate of strength loss.
- (f) Applied stress - the presence of an applied stress decreases the joint's service-life and this is illustrated in Figure 3.

(g) Joint design - since it is the interface region which is the failure site after environmental exposure a joint design which has a relatively high stress concentration at, or near, the interface will tend to reveal durability effects more readily, eg the Boeing wedge test (6) or peel test have greater sensitivities towards environmental attack than, say, the conventional lap joint.

The use of a continuum fracture mechanics approach to the study of environmental failure has contributed considerably to our understanding of the role of applied stress and the effects of joint design. Indeed, the fracture mechanics studies have directly led to the introduction, and now widespread use, of the Boeing wedge test to rank adhesives and surface pretreatments as to their environmental resistance.

### 3.0 MECHANISMS OF FAILURE

As stated above the locus of joint failure after environmental exposure is usually at, or very close to, the interface. Thus, while the adhesive, especially if moisture sensitive, may suffer some loss of modulus (7) and some loss of strength when tested at elevated temperatures near its glass transition temperature due to plasticisation by water, it is the interfacial regions on which our attentions must be focussed if the mechanisms are to be identified. Essentially two mechanisms, which are complementary rather than exclusive, have been proposed to account for the above observations: one examines the stability of the adhesive/metal oxide interface from a thermodynamic standpoint and the other considers the stability of the metal oxide.

#### 3.1 Interface Stability

##### 3.1.1 Thermodynamic considerations

Now the thermodynamic work of adhesion,  $W_A$ , required to separate unit area of two phases forming an interface may be related to the surface free energies by the Dupre equation. In the absence of chemisorption and interdiffusion the reversible work of adhesion,  $W_A$ , in an inert medium may be expressed by:-

$$W_A = \gamma_x + \gamma_y - \gamma_{xy} \quad \dots \dots \quad (1)$$

where  $\gamma_x$  and  $\gamma_y$  are the surface free energies of the two phases and  $\gamma_{xy}$  is the interfacial free energy. In the presence of a liquid (denoted by the suffix 'L'), the work of adhesion,  $W_{AL}$ , is:-

$$W_{AL} = \gamma_{xL} + \gamma_{yL} - \gamma_{xy} \quad \dots \dots \quad (2)$$

For a typical organic adhesive/metal oxide interface the work of adhesion,  $W_A$ , in an inert atmosphere, eg dry air, usually has a large positive value, indicating thermodynamic stability of the interface. However, in the presence of a liquid the thermodynamic work of adhesion,  $W_{AL}$ , may well have a negative value, indicating the interface is now unstable and will dissociate. Thus, calculation of the terms  $W_A$  and  $W_{AL}$  may enable the environmental stability of the interface to be predicted.

Some examples of values of  $W_A$  and  $W_{AL}$  are shown in Table 1 (8,9,10).

Interface	Work of adhesion	
	Inert medium, $W_A$ (mJ/m <sup>2</sup> )	In water, $W_{AL}$ (mJ/m <sup>2</sup> )
Epoxy/ferric-oxide	291	-255
Epoxy/silica	178	- 57
Epoxy/aluminium-oxide	232	-137
Epoxy/carbon-fibre-reinforced plastic	88 → 90	22 → 44

Notes: (a) Metal and c.f.r.p. surfaces prepared by grit-blasting.

(b) Values of surface free energies for c.f.r.p. were from Kaelble et. al. (11), and values of  $W_A$  and  $W_{AL}$  represent a range from a carbon-fibre rich to a resin-rich surface.

TABLE 1 Values of  $W_A$  and  $W_{AL}$  for various interfaces

The change from a positive to negative work of adhesion provides a driving force for the displacement of adhesive on the metal oxide or glass surface by water. It is therefore to be expected that if a joint is subjected to a humid environment there will be a progressive encroachment into the joint of debonded interface. This will have the effect of progressively reducing the joint strength and also of progressively changing the locus of failure from cohesive within the adhesive to interfacial between adhesive and substrate. This is exactly what has been observed in practice.

However, for the epoxy/c.f.r.p. interface both  $W_A$  and  $W_L$  are positive indicating greater stability of the epoxy/c.f.r.p. interface compared to those between epoxy and highly polar substrates such as glass and metal oxides. This stability is reflected in the locus of failure for c.f.r.p./epoxy/metal joints,



after environmental ageing, invariably being at the epoxy/metal interface or within the c.f.r.p. substrate.

This thermodynamic approach may also be employed to predict the stability of any interface in any liquid, providing chemisorption and interdiffusion across the interface are absent. Indeed, thermodynamic considerations predict that an epoxy/ferric-oxide interface will be stable in ethanol but dissociate in formamide and this has been experimentally confirmed (8).

Finally, it should be noted that the thermodynamics as stated in equations (1) and (2) take no account of interfacial adhesion forces arising from primary, chemical bonds or mechanical interlocking. Further, they provide no information on the expected service-life of joints upon being stressed in hostile environments. For this data the thermodynamic analysis needs to be combined with either a stress-biased activated rate theory, as developed by Zurkov and co-workers (12,13), and used in joint fracture studies by Levi et al (14), or a continuum fracture mechanics approach (Section 3.3) and such approaches should be considered as complementary rather than mutually exclusive!!

### 3.1.2 Locus of failure

Confirmation that the epoxy/mild-steel joints (ie the epoxy/ferric-oxide interface) did indeed fail exactly at the interface after environmental attack, as predicted, was obtained by employing modern surface analytical techniques such as Auger and X-ray photoelectron spectroscopy (15). The direct examination of surfaces and contaminants on them has recently become possible by the use of Auger electron and X-ray photoelectron spectroscopy (AES and XPS respectively). These two techniques are extremely useful in adhesion studies in that both enable the composition of the outer 1 to 5 atomic layers of the surface of a solid to be analysed. The basic technique in AES consists of bombardment of the surface with a beam of electrons in the range of 1-5 keV and analysis of the energies of the ejected electrons, which usually provides only an elemental analysis. In XPS, photoelectrons (and Auger electrons) are generated when the surface is flooded with soft X-rays; the photoelectrons have discrete binding energies whose values depend upon both the element and its state in the atomic matrix in the surface. Therefore it is possible to determine both the concentration and chemical state in the surface. The two techniques are in many ways complementary. AES gives good spatial resolution since a narrow (1-50  $\mu\text{m}$ ) electron beam is used while with XPS such spatial resolution cannot as yet be obtained, since it depends on X-ray photons to excite photoelectrons. The advantage of XPS is, however, that charging effects are minimised and surfaces of insulators can be more easily analysed. The usefulness of these techniques is illustrated by the results shown in Table 2 which are for the XPS analysis of carbon on mild-steel substrates (i) prior to bonding, (ii) after bonding and "dry" fracture and (iii) after bonding, exposure to a hot/wet environment and then fracture. To prevent the fresh, fracture surfaces being contaminated by atmospheric contaminants the fracture experiments were conducted inside the ultra-high vacuum system of the X-ray photoelectron spectrophotometer. As may be seen these results demonstrated convincingly that no significant amount of epoxy adhesive remained on the oxide after "wet" joint fracture and, since analysis of the adhesive showed no remains of oxide, the locus of failure for these joints after environmental attack was considered to be truly interfacial.

Sample	Chemical State			Comments
	Initially	After ion erosion of		
		50 Å	130 Å	
Substrate control, prior to bonding.	285.0 eV; 19.7%	284.8 eV; 8.5%	284.5 eV; 4.2%	Hydrocarbon contamination from atmosphere - disappears on ion erosion.
After "dry" joint fracture.	286.4 eV; 26.3%	284.0 eV; 20%	284.3 eV; 20.1%	Polymeric carbon which degrades on ion erosion. Indicates failure in adhesive.
After "wet" joint fracture.	284.7 eV; 2%	- -	- -	Negligible hydrocarbon contamination. Indicates failure at interface.

Note: (binding energy in electron volts; atomic percentage present)

TABLE 2 XPS analysis for carbon on mild-steel surfaces

### 3.1.3 Kinetics of failure

The work on the epoxy/mild-steel joints also provided an insight into the kinetics of the failure mechanism. From measuring the rate of interfacial debonding at different temperatures an activation energy for the displacement of adhesive by water of 32 kJ/mol was deduced. This value is similar to that for the diffusion of water through an epoxy resin, namely 16 to 38 kJ/mol as reported by other workers (17,18) and suggests that the rate of interface debonding is controlled by the availability of water at the interface which in turn is governed by diffusion of water probably through the adhesive. Now assuming Fickian and two-dimensional diffusion then the rate of water penetration into the adhesive may be calculated (19). For this particular adhesive the value of the diffusion constant at 60°C was approximately  $17 \times 10^{-9} \text{ cm}^2/\text{s}$  and employing this value the relations between water concentration and distance into adhesive, shown in Figure 4, were deduced. Since, at 60°C, the joints had lost almost all their original strength after a three months immersion in water, the attainment of the equilibrium, water-saturation concentration in the adhesive was obviously not necessary. On the other hand a critical, minimum water concentration in the adhesive would appear to be a requirement; below about 50% relative humidity storage these joints apparently suffered no environmental attack, even though of course the adhesive still adsorbed water up to an equilibrium concentration, although naturally of a lower value.

### 3.2 Oxide Stability

Noland (20) has reported that the oxide produced on aluminium alloys by a chromic-sulphuric etch is unstable in the presence of moisture and has postulated that the oxide changes to a weaker, gelatinous type which is hydrated and is "gelatinous-boehmite". His evidence for the change in oxide structure comes from X-ray photoelectron spectroscopy analysis of the oxide surface before and after ageing and Figure 5 shows that change in binding energy observed for the aluminium 2p peak position, indicating a change in oxide structure. Noland examined epoxy/aluminium-alloy joints after exposure to hot, humid conditions and reported that, although interfacial failure had visually occurred, in fact the locus of failure was in the weak, gelatinous-boehmite oxide layer.

As mentioned previously clad aluminium-alloys may present a particular problem and the reasons for this have been considered by Riel (16). With clad aluminium alloys the electrode potential is generally higher than the base alloy. This choice is deliberate in that the clad material is selected to be anodic with respect to the base alloy so that in a corrosive environment the cladding will be consumed, thus protecting the base alloy. This mechanism is very effective in protecting the structure from surface corrosion such as pitting and Figure 6 is a sketch showing how pitting penetration is restricted on clad aluminium, as compared to the same alloy without cladding. On the clad alloy pitting is less likely to occur due to the nature of the alloy and where pits do form and penetrate the clad surface, its anodic nature will cause the pit to grow laterally once the base alloy is reached; instead of penetrating into the base alloy. However, while this mechanism of corrosion inhibition may be effective for exposed aluminium-alloy structures, if one considers the mechanisms concerned whereby clad aluminium-alloy achieves its corrosion resistance then the clad layer is actually undesirable in the context of adhesive bonding. The sketch in Figure 7 shows how a galvanic cell may be established between cladding and substrate with the progressive destruction of the interfacial regions. Once this galvanic action starts, the acidity and oxygen concentration factors come into play and progressive delamination occurs. Bascom and Patrick (21) have commented that in general the attachment of the adhesive to a layer of metal which is anodic with respect to the rest of the metallic system is always undesirable from the standpoint of corrosion resistance. Also, chemical components in the adhesive may diffuse into the "electrolyte" area and, for example, if the adhesive is an amine-cured epoxy any unreacted amine diffusing into the region of corrosion could affect or even control the pH of the electrolyte solution. Indeed, certainly in the United States the trend is away from adhesive bonding to clad aluminium-alloys (4,22,34) but where unclad alloys are bonded and used in areas exposed to corrosive environments any non-bonded, exterior surfaces must be protected by appropriate means in order to limit surface corrosion.

### 3.3 Fracture Mechanics Approach

Continuum fracture mechanics is the study of the strength of a material which contains a flaw, usually considered as an elliptical crack. Two main, inter-relatable criteria for fracture are proposed. First, Irwin (23) found that the stress field around a crack could be uniquely defined by a parameter named the stress-intensity factor,  $K$ , and stated fracture occurs when the value of  $K$  exceeds some critical value  $K_c$ . Second, the energy criterion arising from Griffiths (24) and, later, Orowan's (25) work, which supposes that fracture occurs when sufficient energy is released (from the stress field) by growth of the crack to supply the requirements of the new fracture surfaces. The energy released comes from stored elastic or potential energy of the loading system and can, in principle, be calculated for any type of test piece. This approach, therefore, provides a measure of the energy required to extend a crack over unit area, and this is termed the fracture energy and is denoted by  $G_c$ . When plane-strain and a tensile opening-mode prevails it is denoted  $G_{Ic}$ .

The pioneering work in the application of continuum fracture mechanics to the failure of adhesive joints was undertaken by Mostovoy, Ripling and co-workers (26,27,28). They developed the tapered-double-cantilever-beam joint geometry, which is shown in Figure 8 and which is a constant-compliance geometry (this results in the adhesive fracture energy being independent of crack length) and thus well suited to environmental studies where crack velocity will be a function of the applied load and environment. They found that if a precracked specimen was loaded and placed in water then in the region of the interface near the original cohesive starter crack-tip, which is therefore strongly influenced by the stress field associated with the crack, interfacial debonding occurred. The new interfacial crack eventually propagated along the adhesive/metal-oxide interface and a typical relationship between the adhesive fracture energy,  $G_{Ic}$ , and resulting crack velocity,  $\dot{a}$ , is shown in Figure 9. As may be seen the value required to cause crack growth in an aqueous environment is much lower than that needed in a relatively dry environment. However, the measured adhesive fracture energies required for these crack growth rates are, of course, much higher than the values for the thermodynamic works of adhesion given in Table 1. This is because, under an applied load, mechanical strain-energy is available to assist environmental crack propagation and this is reflected in inelastic energy dissipative processes, eg plastic flow, occurring in regions of the adhesive around the crack tip. The values of  $W_A$  and  $W_{AL}$  do not allow for any such processes.

From data such as that shown in Figure 9 Mostovoy and Ripling concluded that there was a minimum value of  $G_{Ic}$ , denoted  $G_{Isc}$ , below which slow crack growth would not occur in aqueous environments and such a minimum value implies that there is a stress below which no environmental attack will occur. However, the evidence for such a proposition is conflicting. First, the time-scale over which the experiments were conducted for Figure 9, or in similar experiments on other adhesives (27), is insufficiently long to be able to state with confidence that a true minimum value of  $G_{Ic}$ , ie a  $G_{Isc}$  value, has been attained and plotting the data in the form of Figure 10, with a logarithmic  $G_{Ic}$  scale, clearly demonstrates this. Second, it is well established that joints under no externally applied stress\* may still suffer environmental attack

\* It is of interest to note that Cherry and Thomson (30,31) have recently also argued that the presence of stress is essential for environmental attack but consider that in the absence of an externally applied stress, internal shrinkage stresses provide the necessary strain-energy requirements. However, this hypothesis has yet to be proven, especially since (i) hot-cure adhesives will have the highest shrinkage stresses but generally result in the most durable joints and (ii) any shrinkage stresses will probably be rapidly diminished by stress relaxation processes in the adhesive, accelerated by plasticisation by water, and swelling stresses due to water adsorption.



(eg 1,2,3,8 etc). Thus, whether the presence of stress is essential for environmental attack to occur has yet to be firmly established but it is obvious that stresses, including applied, swelling (29) etc stresses, may accelerate the environmental decay mechanisms.

Kinloch, Gledhill and Dukes (9,32) have conducted static fatigue tests employing the tapered-double-cantilever-beam specimen which consisted of aluminium-alloy (grit-blasted surface pretreatment) bonded with a tertiary-amine cured epoxy resin. The value of the adhesive fracture energy,  $G_{Ic}$ , imposed and the resulting time taken for specimen fracture is shown in Figure 10 for two environments: 23°C and 56% relative humidity and 23°C and immersion in water. Considering first fracture in the former, drier environment, then the locus of joint failure was cohesive, in the centre of the adhesive layer and, as may be seen, there is a linear relationship between  $G_{Ic}$  and logarithmic time to fracture. Further, the time to fracture represents an incubation time; the original, naturally propagated, starter crack remained perfectly stationary up to the instant of fracture and it then propagated with a velocity of about 20 m/s; ie no relatively slow crack growth region was observed. From considering the crack to be modelled by an elastic-plastic material with a plastic zone at the crack tip it can be shown that there is a critical value of the plastic zone size at the crack tip at which fracture occurs. This gives a unique failure criterion for the fracture of these joints over eight decades of time. A value of 16  $\mu\text{m}$  for the critical plastic zone size was calculated for this particular adhesive (32,33).

The effect of immersion in water on the fracture behaviour of these joints is particularly interesting. The value of the thermodynamic work of adhesion,  $W_A$ , in a dry atmosphere is 232  $\text{mJ/m}^2$  (see Table 1), and being positive indicates stability of the interface, which is confirmed by the cohesive locus of joint failure observed above. However, when there is an adsorbed layer of water at the interface the thermodynamic work of adhesion,  $W_{A1}$ , has a negative value, -137  $\text{mJ/m}^2$ . This predicted instability of the interface is reflected by the locus of joint failure becoming interfacial in the presence of a water environment. Exceptions to this were, however, observed when the applied adhesive fracture energy was relatively high and the time to fracture short, about 300 seconds or less. Under such circumstances, water has insufficient time to diffuse and penetrate the interface prior to normal cohesive fracture occurring and thus the failure behaviour of the joints under these conditions resembled that of the dry fracture results.

However, apart from such exceptions, the mechanism of environmental failure appeared to be the penetration of water and the displacement of the epoxy/aluminium oxide interface as predicted from the thermodynamic considerations. Thus, as observed by Rippling and Mostovoy, in the region of the interface near the original cohesive starter crack, interfacial debonding occurred. However, in this case an incubation time was observed and no significant slow crack growth was recorded up to the instant of fracture when the crack propagated rapidly along the interface. Further, and more importantly, this environmental failure mechanism resulted in times to fracture, at a given value of  $G_{Ic}$ , about two decades shorter than those from fracture experiments conducted in the relatively dry environments. Finally in neither the low humidity nor the aqueous environments was there a discernible minimum value of  $G_{Ic}$ , below which failure did not occur.

The specimen geometry and test procedures used for the above experiments are too complex and costly for quality control use in industry and so two modifications have been devised and are shown in Figures 12 and 13 (34). Both are constant-displacement specimens rather than constant-load and thus caution must be exercised in interpreting the results since stress-relaxation may occur in the adhesive thereby diminishing the effective stress at the crack tip and lowering the observed crack growth rate. Indeed, crack tip blunting leading to a decrease in crack propagation rate, may be a problem with even the constant-load experiments (35) and may account for the often considerable scatter in the reported experimental data (eg 27). Further, the Boeing wedge test, Figure 13, does not lend itself to stress analysis because of non-linear bending displacements (36). However, the ease and speed of obtaining stressed, durability data make these specimens extremely valuable additions to the range of test techniques.

#### 4.0 INCREASING DURABILITY

Now the deleterious effect of water on the joint strength and post-failure corrosion of the substrate could be avoided if the integrity of the interfacial regions could be maintained. Thus, either water must be prevented from reaching the interface in sufficient concentration to cause damage or the intrinsic durability of the interface must be increased.

##### 4.1 Decreasing Water Permeation

All organic polymers are permeable to water and some values of permeability coefficients,  $P$ , and diffusion constants,  $D$ , for water through various polymers are given in Table 3 (10,37). As may be seen epoxy and phenolic materials are at the low end of the spectrum and whilst there is undoubtedly "room for improvement" the other properties of any adhesive, such as wetting/adhesion characteristics, processability, toughness, cost, etc must be balanced against the need for low values of  $P$  and  $D$ .

A second approach has been to use sealants (which are usually based upon organic polymers) to coat the edges of the exposed joint. However, while this will obviously slow down water penetration it is usually not possible to apply a thick enough layer to be very effective and has other disadvantages such as adding an extra operation and cost to the bonding process.



Polymer	Temp. (°C)	$P \times 10^9$ (a)	$D \times 10^9$ (cm <sup>2</sup> /s)
Vinylidene chloride/acrylonitrile copolymer	25	1.66	0.32
Polyisobutylene	30	7 → 22	-
Phenolic	25	166	0.2 → 10
Epoxy	25	10 → 40	2 → 8
Polyvinylchloride	30	15	16
Polymethylmethacrylate	50	250	130
Polyethylene (low-density)	25	9	230
Polystyrene	25	97	-
Polyvinylacetate	40	600	150

(a) in  $\frac{\text{cc S.t.p. cm}}{\text{cm}^2 \text{ s. cm Hg}}$

TABLE 3 Permeability coefficients (P) and diffusion constants (D) for water through polymers

#### 4.2 Increasing the Intrinsic Durability of the Interface

##### 4.2.1 Use of primers

It has been shown that the environmental resistance of joints consisting of mild-steel substrates bonded with a simple epoxy adhesive may be considerably increased by applying a  $\gamma$ -glycidoxypolytrimethoxy silane primer solution to the substrate prior to joint formation (38). Previous work (39) had shown that silane primer films are usually polymeric and essentially composed of a polysiloxane network and this was confirmed by using secondary ion mass spectroscopy (SIMS). With this technique ionized particles ejected from the surface by the action of an argon beam are mass analysed. As the current densities used in SIMS are low ( $\sim 10^{-10}$  A cm<sup>-2</sup>) the first one or two monolayers of the surface can be investigated. Either atoms or molecules can be ionized and thus details about the chemical state of atoms in a surface can be inferred. This technique also revealed the presence of Fe SiO<sup>+</sup> radicals from the primer-coated substrate surface (40). This is strong direct evidence for the formation of a chemical bond, probably -Fe-O-Si≡, between the metal oxide and polysiloxane primer. No such radicals were detected from several other silane coated surfaces where there was no improvement in joint durability. Thus only for the silane primer which resulted in improved joint durability was there any evidence for chemical, rather than purely secondary bonding, between the primer and metal oxide and it is postulated that it was the presence of these interfacial chemical bonds which were responsible for the greatly increased durability.

Further work, using Auger and X-ray photoelectron spectroscopy (15) has shown that although a silane primer often considerably increases joint durability, and the polysiloxane metal-oxide interface is resistant to water attack, the primer layer itself is now the weakest part of the joint and fracture may occur by cohesive failure of this layer. Thus, to increase joint durability further attention should be focussed on increasing the intrinsic strength of the silane-based primers commonly employed.

The silane primer also appears to be effective on grit-blasted aluminium alloy and Figure 14 shows the adhesive fracture energy,  $G_{IC}$ , versus time to fracture for epoxy/silane-primed, aluminium-alloy (9). Comparison with the previous results, shown in detail in Figure 11, clearly demonstrates that the presence of a silane at the interface maintains its integrity and forces the fracture to be cohesive in the adhesive and follow the failure behaviour of joints tested in the dry environment.

It would be of considerable interest if the contribution from interfacial primary, chemical bonds to the intrinsic stability of the interface could be quantified. However, without a detailed knowledge of the type of reactions, and their extent, occurring across the interface, it is at present impossible to calculate their contribution exactly. Nevertheless, an approximate indication may be obtained by taking the interfacial, chemical bond energy as 250 kJ/mol and assuming a coverage of 25 Å<sup>2</sup>/adsorbed site. This yields an intrinsic work of adhesion of +1650 mJ/m<sup>2</sup> and from energetic considerations, similar to those in Section 3.1.1, it would be unlikely that water would displace such a chemisorbed primer layer. More basic information on the interfacial forces and reaction mechanisms is required before more definitive calculations and predictions can be undertaken.

Finally, the presence of interfacial, covalent bonds may also explain why phenolic-based adhesives generally impart very good durability characteristics (41). The long-term, high-temperature cure conditions used with such resin systems (frequently in the presence of acid catalysts) leads to the evolution of water via condensation reactions. The reaction conditions required for this reaction are also precisely those that give the maximum probability of forming ether linkages between oxide surfaces and the resin. However, the existence of such an interface bond has still to be established and such a bond would be susceptible to hydrolysis in water because of its strongly ionic character. Thus the basic mechanisms for explaining the good durability associated with phenolic-based adhesives still remain unresolved.

Reinhart (42) has examined various primers and techniques for applying primers and, in particular, electro-priming. In this process a conductive tank is filled with a water suspension of the primer-resin system (approximately 10% solids by weight). A pre-cleaned metal substrate is suspended in the tank and made either anodic (positive electrode) or cathodic (negative electrode) depending on the charge contained by the resin particles. The film is initially formed on the part areas of highest current density, by migration of the charged resin particles under the influence of the applied voltage. Using this process Reinhart has studied the interesting possibility of forming the oxide layer on the metal substrate while, at the same time, depositing the polymeric polymer layer. Examination of the interfacial region of such a sample showed that the primer layer did indeed penetrate into the oxide and initial durability trials have been encouraging.

Reinhart has also studied the use of water soluble polymers such as phenol-formaldehyde, resorcinol-formaldehyde, urea-formaldehyde and their physical blends and copolymers, as well as the speciality types of water soluble epoxy resins, as potential candidates for improved primer formulations. The advantages of using water as the solvent in the formulation include its low cost, non-flammability, non-toxicity and non-polluting characteristics. The formulations evaluated have encompassed compositions including single-stage resoles as well as two-stage novolacs and cure of these latter primers was achieved by the addition of formalin, paraformaldehyde or polymeric curing agents. Various other additives were also required such as flow control, levelling and wetting agents, stabilisers, film tougheners and corrosion inhibiting materials. The water-based primers were applied directly to the pretreated metal substrates via dipping, spraying or brushing and the solids contents were adjusted by dilution with water to achieve the desired primer film thickness. The primers were normally dried and cured at room or elevated temperatures prior to adhesive application and bonding. Initial results from accelerated environmental trials are shown in Table 4 and, as may be seen, while the preliminary results from the water-soluble primers are not quite as good as those from a commercially available primer (non-water based), the durability achieved is definitely promising. Reinhart considered that a somewhat thinner and tougher primer film was required to perform satisfactorily in the lap-shear test.

Primer Formulation	Boeing Wedge Test; Crack growth (mm)		Lap-shear stress (MPa)			
	After 1 hour	After 24 hours	Unexposed		30 days/95% rh/49°C	
			23°C	82°C	23°C	82°C
Commercial Control	2.5	2.5	31.0	20.7	28.3	10.3
Resorcinol-formaldehyde based	2.5	5.1	26.4	13.0	8.5	2.6
Phenol-formaldehyde (Novolac) based	3.8	6.4	20.7	14.5	7.2	4.8
Phenol-formaldehyde (Resole) based	2.5	5.1	25.1	9.0	17.8	4.8

Notes: (a) Aluminium-alloy, chromic-sulphuric acid etched; modified-epoxy adhesive.

(b) Standard Boeing wedge test (see Figure 13), exposed to 95% rh; 49°C.

TABLE 4 Durability trials on water-based primers

#### 4.2.2 Oxide structure

Workers at Boeing (43,44) have developed a new surface treatment for aluminium-alloys based upon a phosphoric-acid anodizing method. This technique results in a much thicker, and more porous, oxide layer on the aluminium alloy, compared to a chromic-sulphuric acid etch and this may be seen from the diagrammatic representations in Figure 15. Further, X-ray photoelectron spectroscopy evidence, cited by Noland (20), shows that the oxide produced by this new method is more stable in the presence of hot/wet environments. The increases in joint durability which have been reported from using the phosphoric-acid anodizing technique are illustrated in Figure 16.

Bascom (45) has recently drawn attention to the point that penetration of adhesive resin molecules into these complex, porous microstructures would result in a resin/metal oxide composite interphase that may contribute significantly to joint durability, since failure through the oxide would involve plastic and viscoelastic deformations of ligaments of adhesive. Also in such a process mechanical interlocking may contribute significantly to the intrinsic adhesion and thus invalidate the thermodynamic work of adhesion as a sole criteria for interphase stability. Hence it appears that in certain instances the oxide must possess both a resistance to attack by water and the "correct" microstructure for maximum joint durability.

Workers at Fokker (46,47) have also examined the influence of various chemical pretreatments on the surface morphology and peel-strength of aluminium-alloys. They concluded that surfaces should be acid etched and then anodized, and for the highest peel strengths a chromic-sulphuric acid etch followed by anodizing in chromic acid gave the optimum results; etching in sulphuric acid alone gave inferior peel strengths. Transmission and scanning electron micrographs showed a relation between surface morphology and bondability and a fine etchpit structure within coarser etchpits gave the most desirable structure. They considered that low strengths were associated with either a weak oxide layer or a weakened aluminium surface.

These models of a resin/oxide inter phase at the adhesive/substrate boundary become even more complicated when a primer is also applied prior to bonding. The primer should wet and penetrate the porous oxide, inhibit any chemical changes in the oxide and exhibit energy dissipative mechanisms upon failure of the primer/oxide interphase region (45). Optimisation of oxide type and microstructure and primer composition is therefore an extremely complex procedure.

Indeed it is not, at present, really understood exactly which surface chemical and physical parameters are important for producing an oxide layer which will impart good environmental resistance to an adhesive joint. While the adhesion scientist may talk generally about requiring a contamination free, strong, stable, receptive, etc surface with the right morphology, the detailed parameters involved, their required values and how to logically obtain them are virtually unknown. Nevertheless it is to be hoped that by employing the new surface analytical techniques that are now available surfaces will be fully characterised and this information related to the subsequent environmental resistance of adhesive joints. Only via this type of approach will new improved adhesives, primers and surface pretreatments be rapidly developed.

## 5 MECHANICS OF ENVIRONMENTAL FAILURE

Having considered the various parameters involved in the environmental failure of structural adhesive joints the overall mechanics of the process may be identified.

The first stage is the accumulation of a critical concentration of water in the interfacial regions. The rate of attaining this critical concentration appears to be governed by the rate of water diffusion through the adhesive and this is obviously accelerated by temperature and, possibly, by stress. Also of interest is the fact that the new generation of rubber-modified epoxy adhesives achieve their high toughness partially through the formation of crazes (48). Obviously the presence of crazes would considerably increase the rate of diffusion. With some simple adhesive/substrate combinations the kinetics of the environmental failure mechanism are governed by the rate of water diffusion.

The second stage involves a loss in the integrity of the interfacial regions due to, depending upon the particular adhesive/substrate combination:-

- (i) The rupture of interfacial secondary bonds.
- (ii) Subtle changes occurring in the oxide structure, eg hydration, which causes a mechanical weakening of the oxide layer.
- (iii) Gross corrosion and delamination of a clad-layer on the metal substrate.
- (iv) Cohesive failure in a primer layer. The primer layer may have increased the intrinsic strength of the original adhesive/substrate interface, and hence joint durability, but may itself now be the "weakest link in the chain". For example, hydrolysis of a polysiloxane primer layer.

The rate of loss of strength of the interfacial regions will be faster if a stress is present, albeit an externally applied stress or internal stresses induced by adhesive shrinkage, incurred during cure, or by adhesive swelling due to water uptake. However, the presence of stress as a necessary requirement for environmental attack to occur has yet to be conclusively established but a primary or secondary bond will obviously be more susceptible to attack if stressed.

Third, for the joint to fracture or lose an appreciable amount of its original strength upon subsequent testing it is not usually necessary for the weakening of the interfacial regions to have proceeded completely through the joint. From basic fracture mechanics considerations only a relatively small "environmental crack" is required to have developed before a substantially decreased failure time, under a constant-load test, or a diminished joint strength is observed. From the Griffith equation the fracture stress is proportional to  $1/\sqrt{\text{crack length}}$  and thus a small increase in crack length has a considerable effect on fracture stress. Indeed with many joint geometries subjected to an imposed load and moisture catastrophic failure will occur when the environmental crack, which is growing by the mechanisms outlined above, attains a critical length. (This is analogous to a critical Griffith crack size in homogeneous materials.) However, on the positive side in this respect, plasticisation of the adhesive by water may diminish stresses by stress-relaxation and crack blunting mechanisms.

## 6.0 CONCLUSIONS

The main conclusions to be drawn are:-

- (1) Water is a particularly aggressive environment for adhesive joints and especially when the bonded component is also subjected to conditions of relatively high stress and temperature.
- (2) Environmental failure usually occurs at, or close to, the adhesive/substrate interface.
- (3) From studies of the interfacial fracture mechanical aspects, the following failure mechanisms have been identified:-
  - (a) Displacement of adhesive on the metal oxide by water and this can be predicted from thermodynamic considerations. The kinetics of this mechanism may be governed by the rate of diffusion of water through the adhesive to the interface.
  - (b) Loss of strength and failure of the oxide on the metal substrate due to subtle changes in the nature of the oxide.
  - (c) In special circumstances only, for example with clad aluminium-alloys or in a sea-water environment, is gross corrosion of the substrate a failure mechanism.



- (4) By combining thermodynamic, water diffusion and oxide structure information with a continuum fracture mechanics approach a general model for environmental failure can be postulated and may yield quantitative predictions as to expected service-lifetimes.
- (5) To increase environmental resistance either:-
- (a) Water must be prevented from reaching the interface in sufficient concentration, or
  - (b) Stable, receptive oxides must be formed and stronger interfacial forces must be forged which are resistant to rupture by water. It is argued that this approach has been the more successful to date and is more likely to yield the most significant improvements in the future.

## 7.0 REFERENCES

1. J.C. Bolger, 'Structural Adhesives for Metal Bonding', in 'Adhesion and Adhesives Vol 13', Ed. R.L. Patrick (Marcel Dekker, New York, 1973), page 1.
2. B.I. Buck and M.G.D. Hockney, 'Effect of Outdoor Exposure on Adhesive Bonded Joints' in 'Aspects of Adhesion - 7', Ed. K.W. Allen and D.J. Alner (Transcripta Books, London, 1973), page 242.
3. D.J. De Lollis and O. Montoya, 'Mode of Failure in Structural Adhesive Bonds', J. Appl. Polym. Sci., 11, 1967, 983.
4. J.L. Cotter, in 'Developments in Adhesives - 1', Ed. W.C. Wake, (Applied Science Publishers, London, 1977), page 1.
5. J.D. Minford, 'Comparison of Aluminium Joint Durability', J. Appl. Polym. Sci., Appl. Polym. Sympos., 32, 1977, 91.
6. J.A. Marceau, Y. Moji and J.C. McMillian, 'A Wedge Test for Evaluating Adhesive-Bonded Surface Durability', Adhesives Age, 20, (10), 1977, 28.
7. R.I. Butt and J.L. Cotter, 'The Effect of High Humidity on an Epoxy-Polyamide Adhesive', J. Adhesion, 8, 1976, 11.
8. R.L. Gledhill and A.J. Kinloch 'Environmental Failure of Structural Adhesive Joints', J. Adhesion, 6, 1974, 315.
9. A.J. Kinloch, W.A. Dukes and R.A. Gledhill 'Durability of Adhesive Joints' in 'Adh. Sci. and Technol', Ed. L.H. Lee, (Plenum Press, New York, 1975), page 597.
10. A.J. Kinloch, Unpublished work.
11. D.H. Kaelble, P.J. Dynes, L.W. Crane and L. Maus, 'Interfacial Mechanisms of Moisture Degradation in Graphite-Epoxy Composites', J. Adhesion, 7, 1974, 25.
12. S.N. Zhurkov and E.E. Tomashevsky, 'An Investigation of Fracture Process of Polymers by the E.S.R. Method' in 'Physical Basis of Yield & Fracture', (Institute of Physics, 1966), page 200.
13. S.W. Zhurkov and V.E. Korsukov, 'Atomic Mechanism of Fracture by Solid Polymers', J. Polym. Sci., Polym., Physics, 12, 1974, 385.
14. D.W. Levi, R.F. Wegman, M.C. Ross and E.A. Garnis, 'Use of Hot Water Ageing for Estimating Lifetimes of Adhesive Bonds to Aluminium', SAMPE Quarterly, 7, (3), 1971, 1.
15. M. Gettings, F.S. Baker and A.J. Kinloch, 'Use of AES and XPS to Study the Locus of Failure of Structural Adhesive Joints', J. Appl. Polym. Sci., 21, 1977, 2371.
16. F.J. Reil, 'Corrosive Delamination', SAMPE Journal, Aug/Sept, 1971, 16.
17. J. Bardeleben, 'Notes on the Diffusion of Water through Epoxy Resins', Kunststoffe, 53, 1963, 162.
18. J.A. Manson and E.H. Chiu, 'Penetration of Water in a Filled Epoxy Resin', J. Polym. Sci., C, 41, 1973, 95.
19. J. Crank, 'The Mathematics of Diffusion, (Oxford University Press, London, 1956).
20. J.S. Noland, 'Some Factors in Achieving Environmental Resistance in 120°C Structural Adhesives', in 'Adhes. Sci. and Technol', Ed. L.H. Lee, (Plenum Press, New York, 1975), page 413.
21. W.D. Bascom and R.L. Patrick, 'The Surface Chemistry of Bonding Metals with Polymer Adhesives', Adhesives Age, 17, (10), 1974, 25.

22. W.M. Scardino and J.A. Marceau, 'Comparative Stressed Durability of Adhesive Bonded Aluminium Alloy Joints', J. Appl. Polym. Sci., Appl. Polym. Sympos., 32, 1977, 51.
23. G.R. Irwin, 'Structural Aspects of Brittle Failure', Appl. Mater. Res., 3, (2), 1964, 65.
24. A.A. Griffiths, 'Phenomena of Rupture in Solids', Phil. Trans. Roy. Soc., A221, 1920, 163.
25. E. Orowan, 'Reports on Progress Physics', 12, 1948, 185.
26. E.J. Ripling, S. Mostovoy and R.L. Patrick, 'Measuring Fracture Toughness of Adhesive Joints', Mater. Res. Stds., 4, 1964, 129.
27. S. Mostovoy and E.J. Ripling, 'Influence of Water on Stress Corrosion Cracking of Epoxy Bonds', J. Appl. Polym. Sci., 13, 1969, 1083.
28. H.T. Corten, in 'Fracture Volume 7', Ed. H. Liebowitz, (Academic Press, New York, 1972), page 676.
29. Y. Weitsman, 'Stresses in Adhesive Joints due to Moisture and Temperature', J. Composite Mater., 11, 1977, 378.
30. B.W. Cherry and K.W. Thomson, 'Effect of Shrinkage Stresses on the Water Induced Failure of Epoxy/Aluminium Joints', in 'Adhesion - 1', Ed. K.W. Allen, (Applied Science Publishers, London, 1977), page 251.
31. B.W. Cherry and K.W. Thomson, 'Water Induced Interfacial Failure of Epoxy/Aluminium Joints', in 'Fracture Mechanics and Technology', (Sijthoff and Nordhoff, Netherlands, 1977), page 723.
32. R.A. Gledhill and A.J. Kinloch, 'Failure Criterion for the Fracture of Structural Adhesive Joints', Polymer, 17, 1976, 727.
33. R.A. Gledhill and A.J. Kinloch, 'Mechanics of Crack Growth in Epoxide Resins', Polym. Engng. Sci., 1978, to be published.
34. R.W. Shannon and E.W. Thrall, 'PABST Environmental Testing of Adhesive Bonded Joints', J. Appl. Polym. Sci., Appl. Polym. Sympos., 32, 1977, 131.
35. R.A. Gledhill, A.J. Kinloch, S. Yamini and R.J. Young, 'Relationship Between Mechanical Properties of and Crack Propagation in Epoxy Resin Adhesives', Polymer, 19, 1978, 575.
36. W.D. Bascom, S. Gadsomski and R.J. Jones, 'Stress Corrosion of Structural Bonds', Nat. SAMPE Tech. Conf., 2, 1977, 121.
37. J.A. Barrie, 'Water in Polymers', in 'Diffusion in Polymers', Ed. J. Crank and G.S. Park, (Academic Press, London, 1968), page 259.
38. W.A. Dukes and A.J. Kinloch, 'Preparation of Surfaces for Adhesive Bonding', Explosives Research and Development Establishment, 1976, TM 169.
39. W.D. Bascom, 'Structure of Silane Adhesion Promotor Films on Glass and Metal Surfaces', Macromols., 5, 1972, 792.
40. M. Gettings and A.J. Kinloch, 'Surface Analysis of Polysiloxane/Metal Oxide Interfaces', J. Mater. Sci., 12, 1977, 2511.
41. J.C. Bolger and A.S. Michaels, 'Molecular Structure and Electrostatic Interactions at Polymer-Solid Interfaces', in 'Interface Conversion for Polymer Coatings', Ed. P. Weiss and G.D. Cheever, (Elsevier, New York, 1968), page 3.
42. T.J. Reinhart, 'Novel Concepts for Priming Metallic Adherends for Structural Adhesive Bonding' in 'Adhesion - 2', Ed. K.W. Allen, (Applied Science, London, 1978), page 87.
43. J.C. McMillan and J.T. Quinlivan, 'Phosphoric-Acid Anodizing of Aluminium for Structural Adhesive Bonding', SAMPE Quarterly, 7, (3), 1976, 13.
44. A.W. Bethune, 'Durability of Bonded Aluminium Structure', SAMPE Journal, July, 1975, 4.
45. W.D. Bascom, J. Adhesion, to be published.
46. P.F.A. Bijlmer, 'Influence of Chemical Pretreatments on Surface Morphology and Bondability of Aluminium', J. Adhesion, 5, 1973, 319.

47. P.F.A. Bijlmer and R.J. Schliekelmann,

'Relation of Surface Condition after Pretreatment to Bondability of Aluminium Alloys', SAMPE Quarterly, 3, 1973, 13.

48. C.B. Bucknall,

'Toughened Plastics', (Applied Science, London, 1977), page 221.

#### 8.0 ACKNOWLEDGEMENTS

The author would like to thank Mr. M. Bergh (PERME) and Dr. J. Comyn (Leicester Polytechnic) for helpful discussions and assistance on the subject of water diffusion into epoxy resins.

"Copyright © Controller, HMSO, London, 1979"

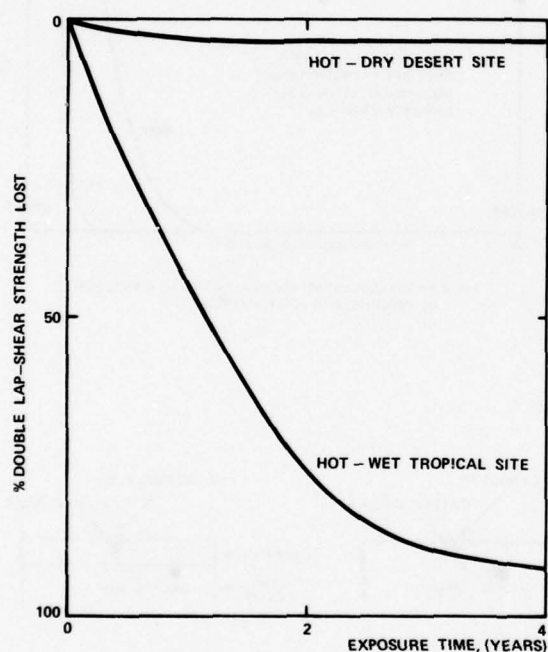


FIG. 1 EFFECT OF OUTDOOR WEATHERING ON THE STRENGTH OF EPOXY-POLYAMIDE/ALUMINIUM-ALLOY (CHROMIC-SULPHURIC ETCH SURFACE PRETREATMENT) JOINTS

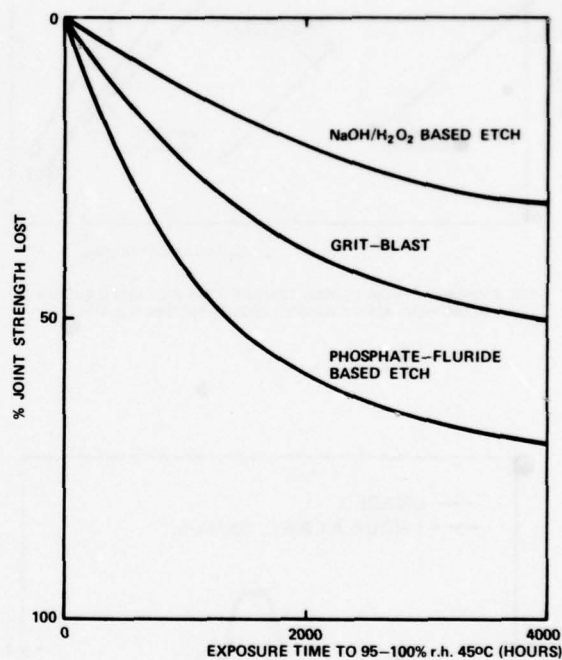


FIG. 2 EFFECT OF SUBSTRATE SURFACE PRETREATMENT ON THE DURABILITY OF EPOXY/TITANIUM JOINTS.



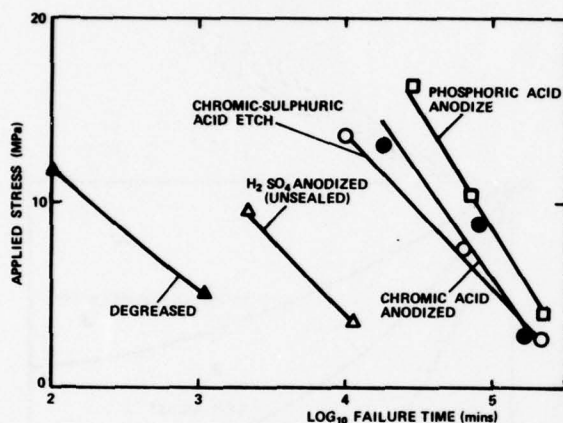


FIG. 3 APPLIED STRESS VERSUS FAILURE TIME FOR NITRILE-EPOXY/ALUMINIUM-ALLOY JOINTS EXPOSED TO 100% R.H, 52°C

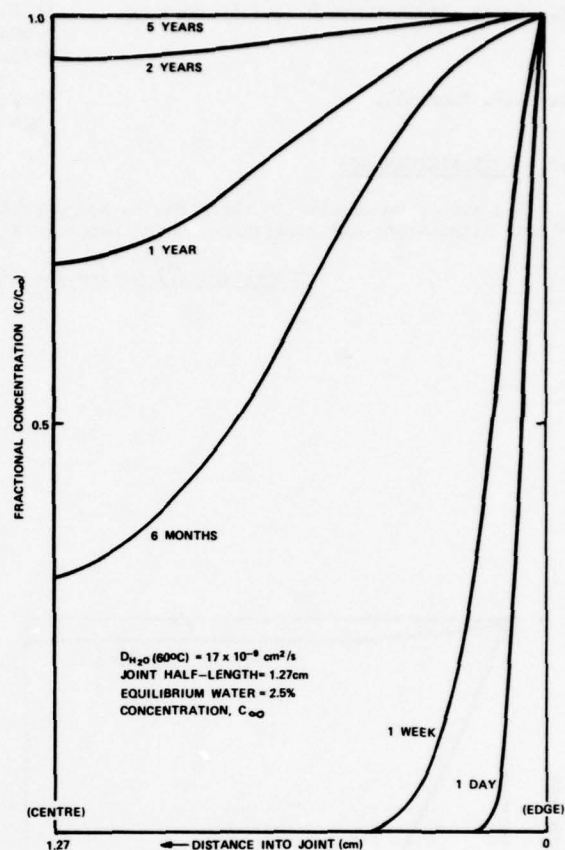


FIG. 4 WATER CONCENTRATION IN ADHESIVE AS A FUNCTION OF DISTANCE INTO JOINT AND TIME

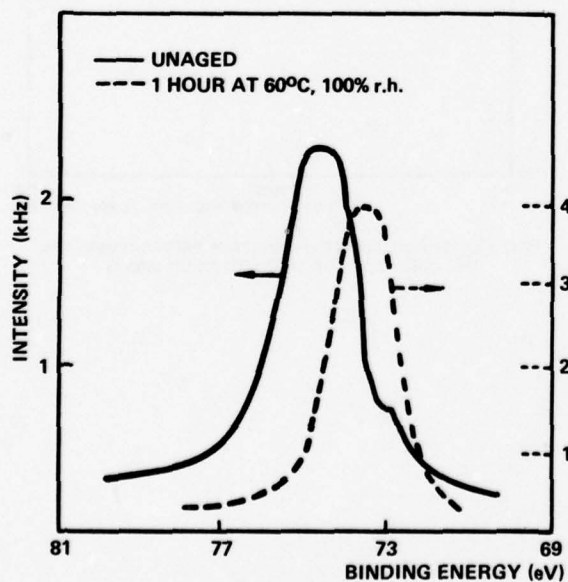


FIG. 5 XPS ANALYSIS OF CHROMIC-SULPHURIC ACID ETCHED ALUMINIUM-ALLOY SURFACE ( $Al_{2p}$ ) BEFORE AND AFTER AGEING.

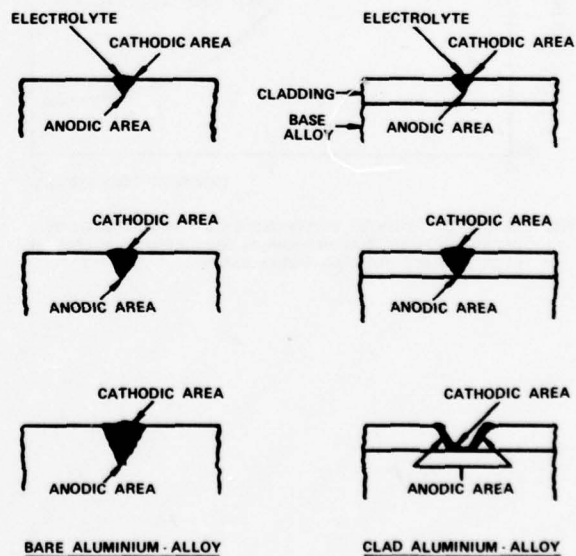


FIG. 6 PROGRESSIVE PITTING OF BARE AND CLAD ALUMINIUM-ALLOY IN A CORROSIVE ENVIRONMENT

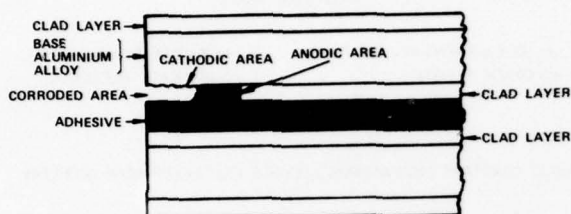


FIG. 7 CORROSIVE DELAMINATION OF ADHESIVE-BONDED CLAD ALUMINIUM-ALLOY

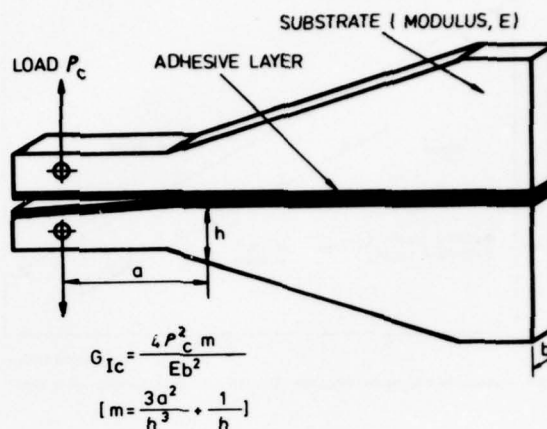


FIG. 8 TAPERED-DOUBLE-CANTILEVER-BEAM FRACTURE MECHANICS SPECIMEN.

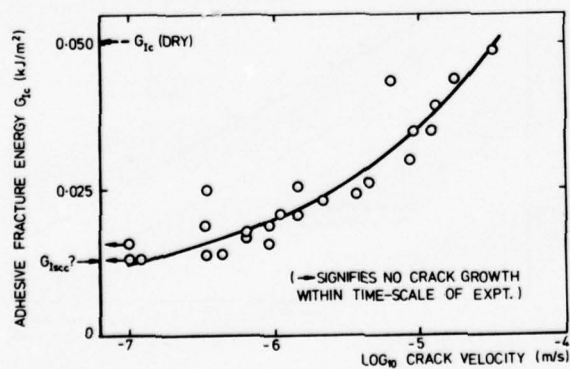


FIG. 9 ADHESIVE FRACTURE ENERGY VERSUS CRACK VELOCITY IN WATER FOR EPOXY-TETRAETHYLENEPENTAMINE CURED/ALUMINIUM-ALLOY JOINTS

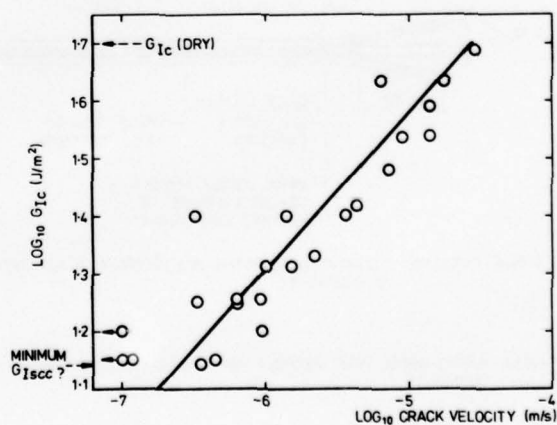


FIG. 10 EXISTENCE OF MINIMUM  $G_{Isc}$ ? DATA FROM FIGURE 9 REPLOTTED AS  $\log_{10} G_{Ic}$  VERSUS  $\log_{10}$  CRACK VELOCITY

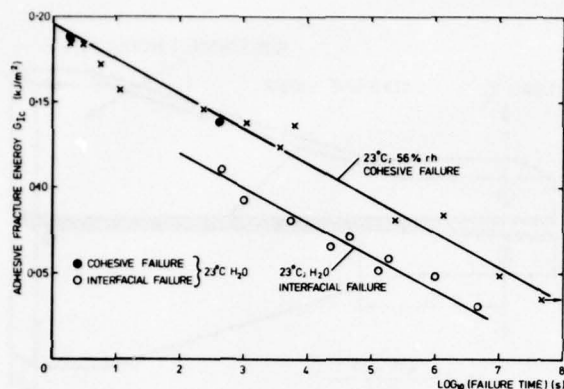
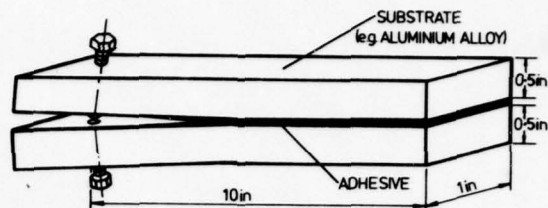


FIG. 11 ADHESIVE FRACTURE ENERGY VERSUS TIME TO FAILURE FOR EPOXY/ALUMINIUM-ALLOY JOINTS

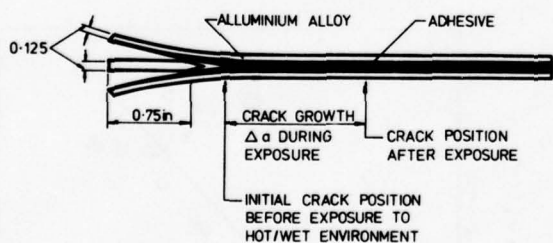


$$G_{Ic} = \frac{y^2 E h^3 [3(a+0.6h)^2 + h^2]}{16[(a+0.6h)^3 + ah^2]^2}$$

y = DISPLACEMENT AT LOAD POINT  
a = CRACK LENGTH

h = HEIGHT OF BEAM  
E = SUBSTRATE MODULUS

FIG. 12 CONSTANT DISPLACEMENT, DOUBLE CANTILEVER BEAM GEOMETRY



TYPICAL EXPOSURE: 1 HOUR AT 49°C; 100% rh Δa RECORDED IS MEASURE OF DURABILITY

FIG. 13 BOEING WEDGE-TEST SPECIMEN FOR RANKING ADHESIVE JOINT DURABILITY

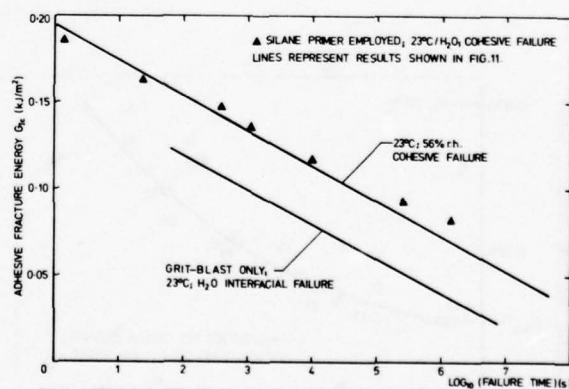


FIG. 14 IMPROVEMENT OBTAINED BY USE OF SILANE-PRIMER ON EPOXY/ALUMINIUM-ALLOY JOINTS



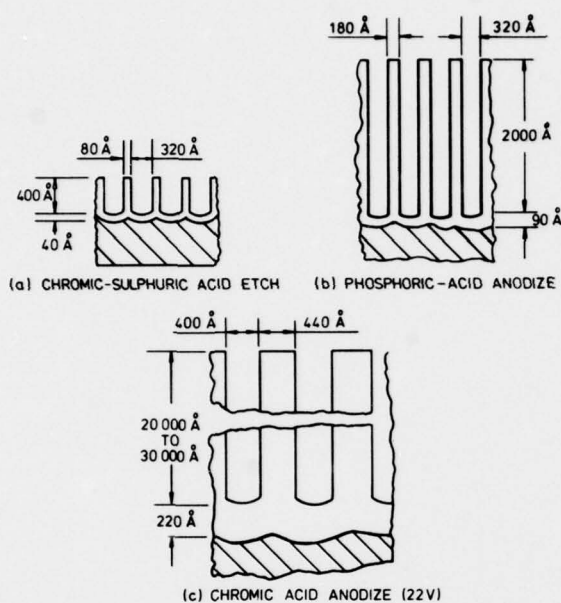


FIG. 15 OXIDE MORPHOLOGY ON ALUMINIUM ALLOY AFTER PRETREATMENT

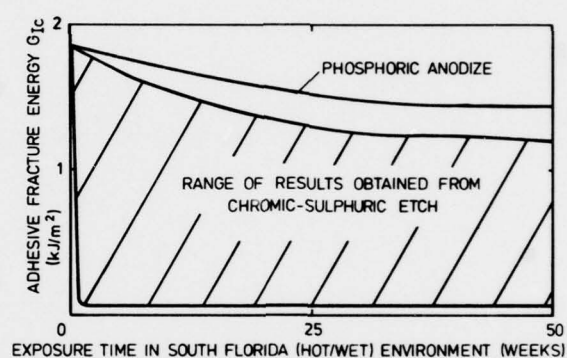


FIG. 16 EFFECT OF SUBSTRATE SURFACE PRETREATMENT ON THE DURABILITY OF EPOXY/ALUMINIUM-ALLOY JOINTS

## ANALYSIS AND DESIGN OF ADHESIVE-BONDED JOINTS

by  
K. L. DeVries\*  
G. P. Anderson\*\*

## ABSTRACT

The initial portion of this report contains a brief summary outline of the "standard" test methods that are in common usage. Many of these have been formalized by the American Society for Testing Materials (ASTM) through its Committee D-14 and their counterparts in other countries. These have the advantage of having elaborate, detailed testing and reporting procedures spelled out in published "Standards." One might therefore obtain accurate relative comparisons between adhesives produced and tested in different laboratories.

A short development of adhesive fracture mechanics is then presented. The use of fracture mechanics for cohesive systems is well established and has proven to be a very useful design tool. The adhesive fracture mechanics approach described in this presentation, in the opinion of the writers, holds the best potential to: (1) identify and/or design the best tests for evaluating a given adhesive, (2) define the best and most meaningful fundamental parameters by which adhesive might be characterized, and (3) make use of these parameters to design joints systematically and optimally and to predict their strength and performance.

Finally, a number of specific cases are treated. Several recent studies have demonstrated how the principles of fracture mechanics may be used to provide insight into specific problems. A variety of test geometries have been examined analytically or numerically. These along with several test methods and the type of useful parameters they yield are discussed. Analytical and numerical techniques have been developed to use these parameters to predict strength and optimize the design of adhesive joints. Specific examples of application in the aerospace, elastomer, medical, dental and other technologies are presented.

# SECTION I

## INTRODUCTION

Almost every engineering design requires that component members be connected. In meeting this requirement, the engineer may choose from several alternatives ranging from mechanical connectors such as nails, screws, or rivets, to welding. A serious disadvantage of mechanical connections is that they do not uniformly distribute the load, and hence almost always result in large local stresses. This problem can often be significantly reduced by adhesively joining the members. There are many structural advantages to be gained from using adhesive joints in engineering design ranging from the aerospace and machinery fields to the medical and dental fields. Recently, a great deal of research and development activity on adhesives has been initiated. Major questions that relate to the reliability of adhesives and that have tended to limit their even wider usage include:

1. By what test method (or methods) can the mechanical quality of an adhesive be best evaluated?
2. How do results obtained from a given test compare with results from other tests, perhaps made under very different conditions?
3. What do the results from the test mean in terms of the performance of the adhesive in an actual structure or other application? It would, for example, be useful if parameters obtained in (1) could be used to predict the strength of practical joint.

The strength or quality of an adhesive is perhaps its most important property. Tests are generally used to determine this property. Adhesive tests are used for various reasons, including:

1. To compare the mechanical properties of a group of adhesives.
2. A quality check for a "batch" of adhesives (e.g., is it still good, have its properties changed with age, etc.?).
3. To check the effectiveness of surface and/or other preparations.
4. A means to determine parameters that can be used in predicting performance in actual applications.

The first three of these might be classed as qualitative tests, and a variety of test methods might be applicable. Quantitative results as required for the fourth item are much more demanding. This aspect will be discussed in more detail later.

Testing is, of course, important in all aspects of material science and engineering, but in no area is it more important than in the adhesive field. The tests not only evaluate the (inherent) strength of the adhesive, but also the bonding technique, cleanliness of surfaces, effectiveness of surface treatments, etching of surfaces, application and distribution of the adhesive, and the curing cycles.

\*Professor, The University of Utah, Department of Mechanical and Industrial Engineering, MEB 3008, Salt Lake City, Utah 84112.

\*\*Scientist, Thiokol Corporation

## SECTION II

### STANDARD ADHESIVE TESTS

A great many test methods have been developed by government, industrial, society, and university investigators. The American Society for Testing Materials (ASTM), through its Committee D14 on adhesives, has been particularly active in this respect. This committee has a number of subcommittees carrying on a continuing effort to develop and standardize test methods, nomenclature, adhesive and adherend preparation procedures, etc. These test methods, as well as Federal Test Standards, are continually updated and revised. Finalized ASTM test methods are published in the ASTM Standards. It is not our intention here to review all these methods or even to reference them. The reader is referred to the ASTM Standards available in most technical libraries. There have also been a number of excellent reviews recently published.<sup>1, 2</sup> A brief description of a few of the tests should serve to illustrate the general approaches used for testing structural adhesives. These tests can be rather generally classified in three groups; i. e., tension, shear, and peel. Various ingenious investigators have adapted these configurations to study the effect of environment, temperature, and creep on bond strength.

#### TENSILE TESTS

Tensile tests are among the most common tests used for "evaluating adhesives." This is despite the fact that, where it is possible to use configurations that load the adhesive in other than a tensile mode, the experienced designer generally avoids loading adhesive joints in tension. Some of the reasons why one should endeavor to avoid testing in tension will become clear later on. Suffice it here to state that most structural materials have high tensile strengths compared to the tensile strength of structural adhesives. Such configurations in practice usually also allow for limited contact area. There are exceptions, however, where adhesives are used in tension; most notable perhaps are sandwich and honeycomb structures. Even here, however, during normal loading of such "skins," the adhesive is apt to be loaded in shear rather than tension. In fact, the honeycomb in the made-up plate is analogous to the shear web in a made-up I-beam. Its major roles during its usual loading modes are as a spacer and for the purpose of carrying the transverse shear often associated with bending. Internal pressurization or local buckling of the plate could, of course, expose the adhesive to a dominantly tensile stress state. This condition would be the exception, however. Despite these disadvantages, the tensile test is commonly used, and when inquiring about the strength of an adhesive the uninitiated is likely to inquire, "What is its tensile strength?" One of the reported advantages of the test is that it yields fundamental and uncomplicated tensile strain, modulus, and strength data. A closer look at the stress state induced in a tensile test of a thin layer of adhesive clearly indicates that the stress state is far from uncomplicated. M. L. Williams and his associates at California Institute of Technology proposed the exact same geometry to investigate the effect of tri-axial stress states on composite solid propellants.<sup>3</sup> They analyzed the configuration shown in Figure 1 (neglecting edge singularities), which they called the "poker chip" test, but which might just as well be viewed as an adhesive test. When the metal blocks were stiff compared to the "sandwich filling" or adhesive, and when this latter material had a Poisson's ratio of 1/2, they were able to obtain an analytical expression for the stress distribution in the poker chip. We should note here that these assumptions are approximately valid for many adhesives.

Their analysis showed that the stress was not uniformly distributed through the sample, as shown in Figure 2, except when the modulus of the adhesive matches that of the adherend. Rather they found that, in general, a difference in moduli results in shear stresses being transmitted across the interface, as shown in Figure 3. In fact, the material at the exact center (p) is in a state of pure hydrostatic tension for a sufficiently thin adhesive layer; i. e., having the same tensile stress in all directions. Equilibrium considerations, of course, dictate that the average stress across the face in the axial direction must be equal to  $P/A$ , where  $P$  is the applied load and  $A$  the cross sectional area. This is the stress that is normally given as the "adhesive tensile stress." The maximum stress across the interface may be much larger than the average. In practice, the problem often becomes even more complex when the thickness of the adhesive varies across the face, or the fixtures are not perfectly aligned in the tensile tester. Despite these drawbacks, one should be familiar with the standard tensile tests. They may provide useful comparisons and quality control values, and there is a great deal of data available from these tests. Standard tensile sample configuration and testing conditions have been proposed by various testing societies and other organizations. For example, ASTM D897 describes recommended standards for testing metal to metal adhesives in tension. ASTM D2094 and 2095 describe slightly different geometries (rod or bar configuration) that may be used with either metal or plastics. For samples that cannot readily be fashioned into these sample forms, the configurations described in ASTM C297, D1344, and in various textbooks might be useful.

#### SHEAR TESTS

Shear tests are very common because samples are simple to construct and closely duplicate the geometry and service conditions for many structural adhesives. Once again, the stress distribution is not uniform and, while it is often conventional to give the failure shear stress as the load divided by the bonding area, one should not lose sight of the fact that the maximum stress at the bondline may differ dramatically from the average. Furthermore, the stress in the adhesive often differs from pure shear. Depending on such factors as adhesive thickness, adherend stiffness, etc., the failure of the adhesive "shear" joint can be dominated by either shear or tension.

The most common shear test is the single lap shear test. ASTM D1002 describes what the book of standards calls the test for "shear properties of adhesion by tension loading (metal to metal)." Recommended thickness for the metals is  $1.62 \pm 0.125$  mm ( $0.064 \pm 0.005$  in.), the recommended length of overlap is  $12.7 \pm 0.25$  mm ( $0.5 \pm 0.1$  in.), and the recommended configuration is as illustrated in Figure 4. ASTM D3163 describes an almost identical test configuration (except for thickness) entitled, "Determining strength of adhesively bonded rigid plastic lap shear joints in shear by tension loading." One of the major problems in using small test specimens to predict failure of large adhesive structures, etc., is that of trying to duplicate all the service conditions in the small specimen. As noted above, adhesive extrusion may result in a thinner bond line. On the other hand, the adhesive properties may differ in the two cases. The authors are, for example, familiar with a case where a company undertook a very thoughtful, thorough, and well-planned adhesive evaluation program to select a suitable adhesive for a metal flooring application. After a number of



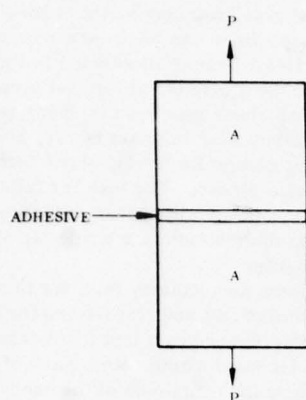


Figure 1. "Poker Chip" or Adhesive Tensile Test Configuration

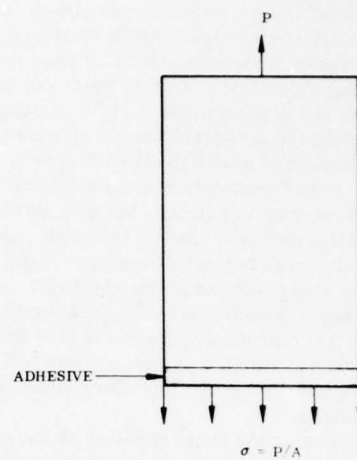


Figure 2. Stress Distribution in Tensile Adhesion Test With Adhesive and Adherend Moduli Equal  
(Note: Arrows on Adhesive Indicate Uniform Tensile Load)

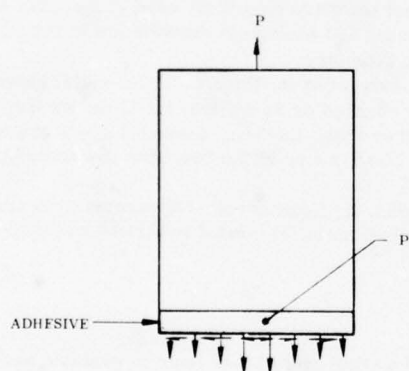


Figure 3. Stress Distribution in Tensile Adhesive Test With Adherend Modulus Greater Than Adhesion Modulus  
(Note: Arrows on Adhesive Indicate Nonuniform Tensile Load)

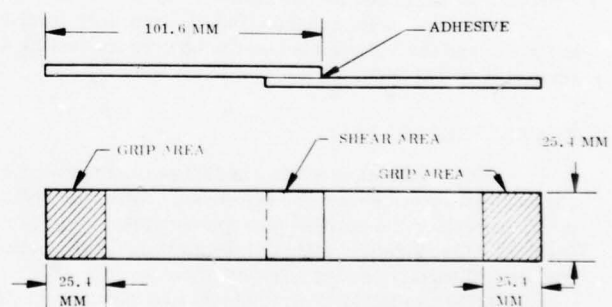


Figure 4. Single Lap Shear Test

failures, it was found that when the adhesive was mixed in large quantities, such as when used in service, it had markedly different properties from the properties when the adhesive was mixed in small quantities, such as for test sample preparation. This difference might be due to exothermic reactions, time span between mixing, spreading and cure, etc. This has led several investigators to propose conducting tests on portions of the actual structure. This might be accomplished by constructing samples from trim scraps or pieces rejected for other reasons. Several ingenious methods have been devised to help accomplish this task. ASTM D3165, for example, describes how a specimen can be prepared to determine the strength properties of adhesion in shear by tension loading of laminated assemblies. This is illustrated in Figure 5.

The double lap shear test (shown in Figure 6) has been favored by some over the single lap shear test because it reduces the cleavage and peel stresses. The distortion caused by loading a single lap shear specimen is shown in Figure 7. Even neglecting the secondary tensile stresses so produced, the stress distribution in the joint is very non-uniform. This is illustrated qualitatively in Figure 8. The stress usually listed in test results for lap shear tests is the average stress, even though this generally differs dramatically from the maximum stress. The load for failure depends not only on the amount of overlap, but also on the metal thickness (single lap), adhesive thickness, and other factors. Goland and Reissner<sup>4</sup> have made a thorough "classical" analysis of the stress distribution in a single lap shear joint. There have also been numerical analyses of such joints with the aid of a computer.<sup>5</sup>

Compression shear tests are also commonly used. ASTM D2182 describes sample geometry (similar to lap shear specimen) and the compression-shear-test apparatus. ASTM D1759 describes a similar test and test fixture for conducting shear block tests for quality control of glue bonds of scarf joints. ASTM D905 describes a test for determining the strength properties of adhesive bonds in shear by compression loading suitable for hard maple, etc. Each of these tests describes the construction of test fixtures that help align the samples and reduce the magnitude of the "nonshear" stresses at the interface.

Figure 8 illustrates the large stresses at the end of a lap shear specimen. For determining the shear modulus and strength of an adhesive, it would at times be convenient not to have these termini. ASTM E229 proposes accomplishing this task by determining the "shear strength and shear modulus" by torsional loading. With proper sample construction and alignment, the adhesive is subjected to a more homogeneous stress distribution in this configuration than with the lap shear specimens. The shear stress  $\tau$  is given approximately by the expression

$$\tau = \frac{Tr}{J}$$

where T is the applied torque, r the radius to a point, and J the polar moment of inertia of the adhesive cross section.

#### PEEL TESTS

Another form of tests that is in common usage is the peel test. Peel tests are commonly used to compare adhesives and as an inspection tool for adhesives. Once again it should be noted that the stress distribution is not simple and can depend on a number of the testing parameters, including specimen geometry.

In the ASTM D1876 peel resistance of adhesives test (T-peel test), two 0.032 in. thick 6 x 12 in. metal sheets are used, bonded over a 6 x 9 in. area (see Figure 9). This panel can then be sheared or sawed into 1 x 12 in. strips, which then serve as the test specimens, or it may be tested as one piece. In either case, the 3-in. unbonded areas are bent at right angles so that they can be gripped by standard tensile tester grips. The T shape of the resulting specimen is the source of the nickname for the test.

Other peel tests are the climbing drum test described in ASTM D1781, a "floating roller apparatus," as described in D3167, and the 180 deg peel test to be used for testing a flexible (stripping) material bonded to a rigid material as described in ASTM D903.

#### MISCELLANEOUS TESTS

ASTM, federal agencies, and other organizations have established a great many other tests to evaluate various characteristics and aspects of adhesives. Again we wish to emphasize that our brief descriptions here are in no way meant to replace the detailed test specifications found in the ASTM or other standards. Our purpose is rather to illustrate the wide variety of standard tests available and perhaps help direct the reader to the proper test(s). To this extent we will briefly catalog a few other tests:

D2718 and D2719 describe tests to measure adhesion in plywood in rolling shear and the strength of plywood in shear through the thickness.

D1877 suggests test methods for determining the permanence of adhesive-bonded joints in plywood under mold conditions.

D906 specifies tests to measure shear properties of adhesives in plywood-type construction by tensile loading (similar to D1002).

D1382 and D1383 describe tests for evaluating the susceptibility of dry adhesives to attack by roaches and laboratory rats, respectively.

D1174 describes similar methods for investigating the effect of bacterial contamination on permanence of adhesive preparations and bonds.

D2558 suggests tests to evaluate the peel strength of shoe sole-attaching adhesives.

D2559 provides tests for adhesives for structural laminated wood products for use under exterior exposure conditions.

D1184 describes a test to determine the flexural strength of adhesive bonded laminated assemblies.

C273 presents a shear test in the flat plane of flat sandwich constructions or sandwich cores.

Other ASTM procedures describe tests that can be conducted on the standard specimens described previously:

D3166 uses the D1002 specimen and a machine capable of applying cyclic loads to measure the fatigue properties of adhesives in shear by tension loading (metal to metal),

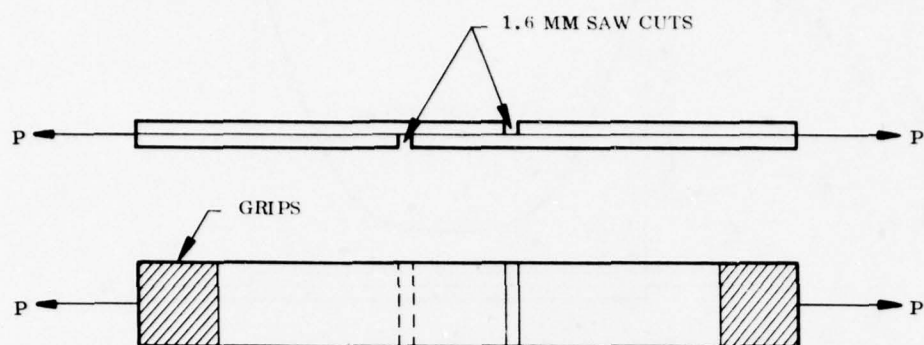


Figure 5. ASTM-D3165-23 Test Configuration

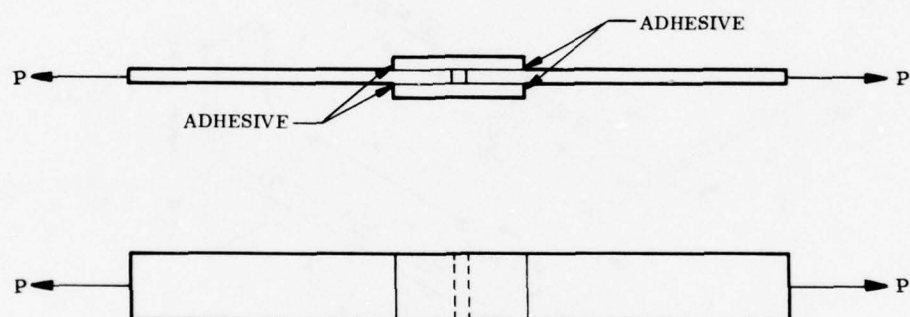


Figure 6. Double Lap Shear Test



Figure 7. Deformation of a Single Lap Shear Specimen



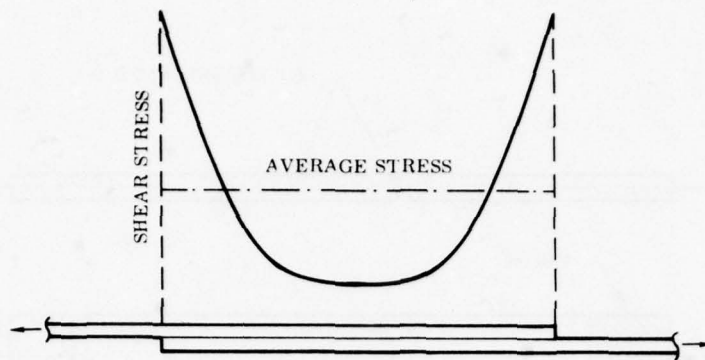


Figure 8. Shear Stresses in a Lap Shear Specimen

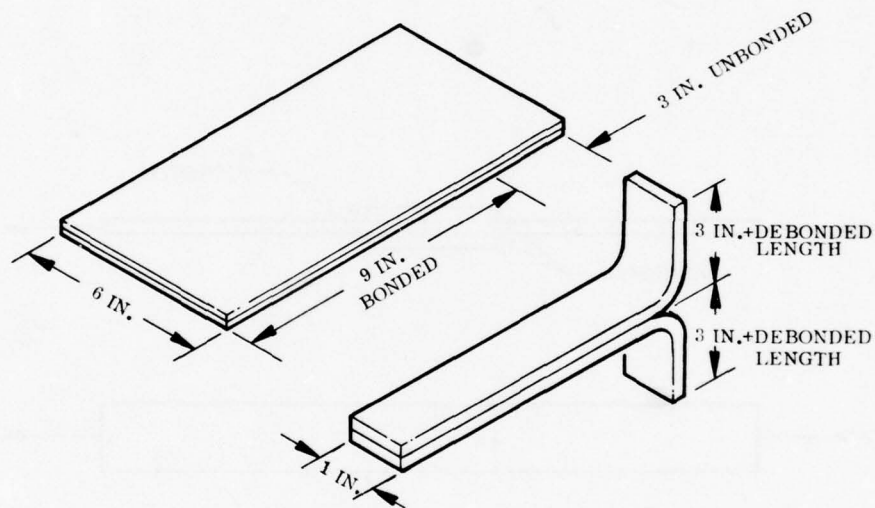
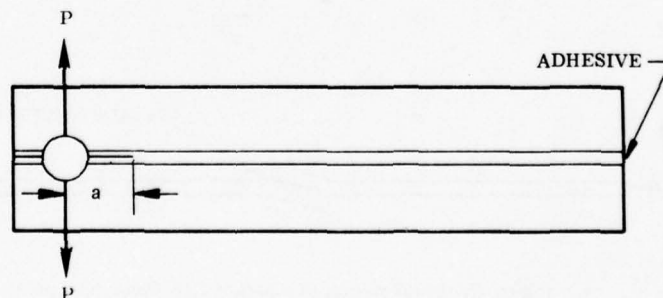


Figure 9. T Peel Test

Figure 10. Double Cantilever Beam Test  
(Fracture Toughness Specimen)

D1183 utilizes any of the specimens to determine the resistance of adhesives to cyclic laboratory aging conditions. D1828 provides for a similar investigation of the effect of atmospheric exposure of adhesive bonded joints and structures.

D2295 describes a tubular quartz lamp arrangement and thermocouple placement to investigate the strength properties of adhesives in shear by tension loading at elevated temperatures (metal to metal samples similar to D1002).

D2557 similarly describes techniques for determining strength properties of adhesives in shear by tension loading in the temperature range  $-267.8^{\circ}$  to  $-55^{\circ}$  C.

D1879 outlines standard techniques for using any specimen type to evaluate the effect of exposure of adhesive specimens to high-energy radiation ( $\gamma$ , electron, X-ray, etc.).

In a like manner, a number of different test specimens have been developed to make use of springs to apply sustained loads to measure creep or durability of joints. These include: D2293 and D2294 for determining properties of adhesives in shear by compression and tensile loading (metal to metal similar to D1002), D1780 for conducting creep tests of metal to metal adhesives, D2919 for determining durability of adhesive joints stressed by shear in tension loading, and D2918 for determining durability of adhesive joints stressed in peel.

There are standard tests for measuring properties other than strength of adhesives. These include: D1337 for determining the storage life of adhesives by consistency and bond strength, D1338 for measuring working life of liquid or paste adhesives by consistency and bond strength, D2739 for assessing volume resistivity of conductive adhesives, and D1916 for determining the resistance to penetration of adhesives. D2979 describes measurement of the pressure sensitive tack of adhesives using an inverted probe.

Standard surface treatments are described in such ASTM standards as D2093, preparation of surfaces of plastics prior to adhesive bonding; D2651, preparation of metal surfaces for adhesives bonding; and D2674, analysis of sulfochromate etch solution used in surface preparation of aluminum.

#### FRACTURE MECHANICS TEST METHODS

The fourth reason for performing bond tests, is "as a means of determining parameters that can be used in predicting performance of the bond in actual application," i.e., to obtain an absolute rather than a relative measure of bond strength. The principles of fracture mechanics can be employed for this purpose.

The subject of fracture mechanics and, in particular, its application to adhesive failure will be extensively discussed in a later section. It can be demonstrated that a wide variety of test methods may be used to obtain the parameters associated with fracture mechanics. In fact, in principle (with appropriate modifications), almost any test could be used. Nevertheless, there are certain geometries that particularly lend themselves to such analysis and experimental convenience. Ripling et al.<sup>6</sup> as well as Irwin<sup>7</sup> propose the use of double cantilever specimens, as shown in Figure 10. Analysis of the test results from such a specimen to obtain the fracture toughness  $G_C$  for the adhesive (to be defined in more detail later) is very straightforward. ASTM D1062 specifies a similar specimen for determination of the cleavage strength of adhesives. The D-14 committee is currently evaluating a tapered, precracked double-cantilever beam as a standard fracture mechanics specimen. A number of other sample geometries have been proposed as fracture mechanics samples. Some of these will be discussed in detail in later chapters.

### SECTION III FAILURE ANALYSIS AND FRACTURE MECHANICS

One might approach fracture from two distinctly different views: a macroscopic approach, or an atomic and molecular viewpoint. In the first, which has become very popular in engineering design, the material is viewed as a continuum (with perhaps mathematically introduced flaws), and some type of functional relationship is developed between failure and the stresses and/or strains in the material. In the molecular viewpoint, an attempt is made to establish a relationship between the applied loads and the forces resulting in the rupture of the molecular or atomic bonds. The accumulation of these ruptured bonds then leads to macroscopic material failure. Here we will concentrate primarily on the macroscopic approach.

It is important to realize that fracture of design components is characteristically approached in two ways by the analyst. Before recognition of the importance of inherent flaws in the material, he relied upon one of several average stress or strain criteria; e.g., maximum tensile stress, maximum principal strain, maximum octahedral stress, or others, depending usually on experimental evidence and experience. While the existence of microscopic or atomistic "holes" in material was recognized, it was generally assumed that their presence was of no design consequence, and, as long as material production control techniques were sufficiently reliable to produce microvoids of a small mean size with a low dispersion around the mean size, the use of an average stress or strain criterion was justified.

Hence, thinking of the material as a continuum, as in the case of a normal tensile specimen for example, the maximum tensile stresses measured in successive specimens of the same material were likely to be quite consistent. There is always some reasonably uniform distribution of small flaws present, whose size is related to the starting material and method of material fabrication; e.g., casting voids, filler surfaces, boundaries of spherulites, and boundaries of other phases. In general in "real materials" there will always be some distribution of flaws existing on some dimensional scale. The average tensile strength, therefore, reflects their presence, and the dispersion of strength data about the norm describes the uniformity of the flaw distribution. Because most standard materials are made under reasonably strict quality-control conditions, it is not surprising to find that some sort of consistent (average) stress or stress-functional criterion often may be used to predict failure.

Under more complicated conditions, such as the multiaxial stressing of a rotor disk, it is frequently customary to assume that the failure criterion is based on the octahedral shear stress ( $\tau_{oct}$ ) containing all three principal stresses and is defined as

$$\tau_{oct} = K \sqrt{(\sigma_1 - \sigma_2)^2 + (\sigma_2 - \sigma_3)^2 + (\sigma_3 - \sigma_1)^2} \quad (1)$$

Assuming this criterion applies, one predicts failure whenever a combination of principal stresses at any point in the part exceeds  $\tau_{oct}$ . And how is  $\tau_{oct}$  determined? If Equation (1) is a universal failure criterion, it must also apply to the failure of a simple uniaxial tensile specimen having stresses  $\sigma_1 = \sigma_{tens}$ , and  $\sigma_2 = \sigma_3 = 0$ . Thus, substituting into Equation (1), one finds that

$$\tau_{oct} = K \sqrt{2\sigma_{tens}^2} \quad (2)$$

so that upon solving for the desired constant K and resubstituting into Equation (1), one finds that failure is expected under a multiaxial principal stress combination whenever at some point in the body

$$\sqrt{(\sigma_1 - \sigma_2)^2 + (\sigma_2 - \sigma_3)^2 + (\sigma_3 - \sigma_1)^2} \geq \sqrt{2} \sigma_{tens} \quad (3)$$

In the more general average stress criterion case denoted as Region I in Figure 11, the failure criterion based upon average principal stresses would have the form

$$F(\sigma_1, \sigma_2, \sigma_3) \geq \sigma_{Fcr} \quad (4)$$

where F is some function of the principal stresses at a point in the material, and  $\sigma_{Fcr}$  is the value of F at failure.

On the other hand, there are conditions in which discrete flaws substantially larger than the uniform size distribution normally present can exist in the material. Such inherent flaws may arise from localized corrosive attack, improper fabrication, cyclic loading, or accidental surface nicks or cuts. Because they are discrete, usually relatively sharp, and larger than the surrounding voids, they can induce additional stress concentrations and provide loci of cohesive fracture initiation. Particularly if these inherent flaws are cracklike, ordinary elastic stress-concentration factors are essentially useless because theoretical results predict an infinite concentration factor multiplying the average stress in the vicinity. Thus, the local stress value will exceed the finite allowable stress experimentally measured for the base material containing only the reasonably uniform distribution on inherent voids. The strength degradation in such a situation is illustrated by Region II of Figure 11.

In a similar manner, the difficulty with many adhesive joints is that they also can possess very high stress concentrations at corners or along bond lines, and usually contain substantially larger than average internal flaws, frequently as the result of absorbing water or poor wetting of the interfaces. In any event, the flaw distribution becomes denser and/or of larger size than the average size for which an average tensile strength would be appropriate. Thus, the maximum permissible allowable stress for adhesive fracture is likewise decreased, phenomenologically similar to Region II behavior in cases of cohesive fracture.

Griffith<sup>8</sup> provided the first estimate of degradation as a function of the flaw size by considering the problem of a small, through, line crack in a thin sheet of brittle material. While theoretically the stress at the crack tips is (mathematically) infinite for an elastic body, thus giving rise to an infinite local stress at even small applied loadings--a degree of concentration for which Equation (4) is useless--Griffith avoided this problem by considering changes in strain energy in the sheet, which, as integration of the stress, remained finite. He proposed that cohesive fracture would commence at a critical applied stress,  $\sigma_{cr}$ , when the incremental loss of strain energy of deformation with increasing fracture area just equaled the work required to create new fracture surface. Hence, in his case, with the

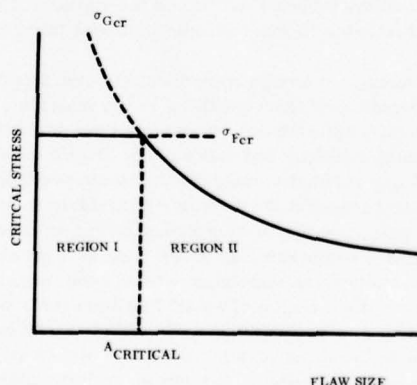


Figure 11. Dominant Behavior Regions Depending Upon Inherent Flaw Size, Region I Dominated By an Average Stress Criterion ( $\sigma = F(\sigma_1, \sigma_2, \sigma_3)$ ).

Region II Dominated by Energy Balance Criterion

$$\sigma_{Gcr} = k[E\gamma_c/a]^{1/2}$$



elastic strain energy of deformation (U) due to the presence of the crack of length  $2a$  being  $U = \pi a^2 \sigma_{cr}^2 / E$ , one would have fracture whenever

$$\frac{\delta}{\delta a} [\pi a^2 \sigma_{cr}^2 / E] \geq \frac{\delta}{\delta a} (4a \gamma_c) \quad (5)$$

where  $E$  is Young's modulus, and  $\gamma_c$  is the specific cohesive fracture energy density (in.-lb/in.<sup>2</sup>, or erg/cm<sup>2</sup>). That is to say, the strain energy of deformation lost as the crack extended was converted into the work to create the new fracture area. From Equation (5), the finite critical applied stress is determined (see Region II in Figure 11) as

$$\sigma_{cr} > \sqrt{\frac{2}{\pi} \frac{E \gamma_c}{a}} \quad (6)$$

In general, the dissipative processes which occur around the crack tip cause the fracture energy to exceed the surface free energy. Provided these processes are confined to a small region near the tip, the functional dependence of fracture stress on crack size of Equation (6) is retained.

The combination of the two criteria, one flaw insensitive (Region I) and the other dependent upon flaw size (Region II), thus permits the designer to select a maximum allowable design stress providing he knows, or determines by tests in the laboratory on precracked thin sheet tensile specimens with known crack size  $a$ , the critical crack size  $a_{cr}$  (Figure 11). This critical crack size is deduced by the intersection of normal, nominally unflawed, tensile data,  $\sigma_{Fcr}$  and initially precracked sheet data following the Griffith curve data,  $\sigma_{Gcr}$ . Once it is recognized that Equations (4) and (6) are not competing failure criteria, but instead are complementary, it is possible to approach the design against failure in a more direct manner.

The previous remarks, and Figure 11, were presented in the context of cohesive fracture. One can discuss a bonded joint in a similar way, say Material I in the upper half plane ( $y > 0$ ) and Material II in the lower half plane ( $y < 0$ ). Indeed as pointed out by Williams,<sup>9</sup> the mathematical analysis of this adhesive failure is the same. If the distribution of interfacial flaws along the interface ( $y = 0$ ) is statistically uniform, then it makes sense to use as a failure criterion some average stress,  $\sigma_{Fcr}$ , whereas if macroscopic size flaws,  $a_{cr}$ , are present, then some degradation of strength must be assessed (Figure 11) in an analogous manner as for cohesive separation,<sup>8</sup> e.g., with  $\gamma_c$  replaced by  $\gamma_a$ , the specific adhesive fracture energy.

The essential feature is that fracture, assuming the existence of inherent flaws of size  $a_{cr}$ , is proportional to the square root of two material properties: the tensile modulus ( $E$ ), and the specific fracture energy ( $\gamma_c$  or  $\gamma_a$ ). When no distinguishable predominant flaws are present, the failure responds (statistically) to a critical stress ( $\sigma_{Fcr}$ ).

For viscoelastic materials, the cohesive fracture energy,  $\gamma_c$  has been shown to depend upon load rate and test temperature.<sup>10</sup> However, the adhesive fracture energy,  $\gamma_a$ , is dependent on load rate and test temperature even for linear elastic materials.<sup>11</sup>

When the inherent flaw size is known or an initial debond of a given size is known to exist, the load carrying capability of the structure is determined by comparing the energy release rate of the structure (requirement) with the adhesive fracture energy value  $\gamma_a$  (capability). Those loads which cause the energy release rate to exceed the  $\gamma_a$  value will be sufficient to cause debond growth. The adhesive fracture energy values are determined by evaluating the energy release rate which has been determined to cause debond growth during laboratory testing of the particular adhesives and adherends of interest [i.e.,  $\gamma_a = \partial U / \partial A$  (evaluated at the debond load)]. Care must be taken in testing since the  $\gamma_a$  values are often influenced by load rate, loading mode and test temperature as well as physical parameters such as surface preparation, moisture present, etc.

In many cases debond initiates at bond edges. Since energy release rate is not defined at a bond edge except perhaps in terms of an inherent flaw size, a second approach is required. For such systems, the "requirement" can be defined in terms of stress intensity factors, and "capability" in terms of bond toughness (stress intensity factor at the debond load). This approach is discussed in further detail in Reference 11.

#### MICROSCOPIC FRACTURE PHENOMENA

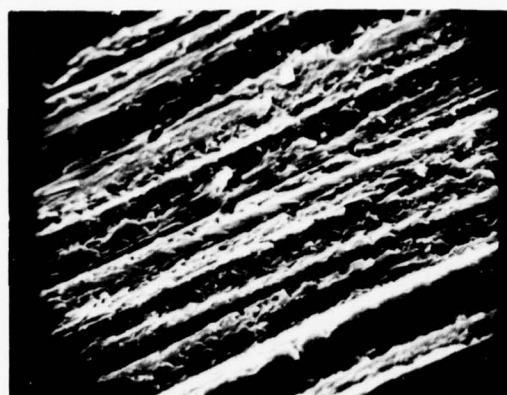
Turning now to a finer local scale to investigate fracture mechanisms which eventually lead to the macrofailure ones, it is fortunate that our ability is increasing to observe or deduce material behavior at increasingly small scales. The electron microscope, for example, has been most useful in both cohesive and adhesive fracture studies, including studies of teeth and dental materials. Some excellent reviews of some of these studies have recently appeared.<sup>12, 13</sup>

One example of some of the uses of the scanning electron microscope (SEM) at the University of Utah is the work of G. P. Anderson, et al. on the influence of loading direction upon the character of adhesive debonding.<sup>11, 14</sup> The specific adhesive fracture energy,  $\gamma_a$ , discussed earlier is deduced from adhesive fracture surfaces which have a topology affected by the mode (shear or tension) of applied loading that induced the separation. In fracture mechanics these modes are commonly designated as I, II, and III, respectively, identified with the forces at the crack tip tending toward normal separation, sliding shear, and rotational shear respectively.<sup>15</sup> Adhesive tests where the mode was varied showed an apparent dependence of  $\gamma_a$  on mode of loading. If the specific fracture energy is purely a measure of the energy required to separate molecular bonds on a unit surface, one would not expect it to be a function of loading mode. Except for the most brittle materials, however, the situation is not so simple; normally many factors such as the work of plastic deformation at the tip of the crack are lumped into  $\gamma$  along with the bond energy required to break bonds. In fact, for most systems these other factors appear to dominate the process; i.e., for many metals such as steel, Al, Cu, etc., and plastics such as PMMA, polystyrene, etc.,  $\gamma$  ranges from  $10^4$  to  $10^7$  ergs/cm<sup>2</sup>, while the energy required to rupture the number of bonds per square centimeter of a typical material would be approximately  $10^2$  to  $10^3$  ergs/cm<sup>2</sup>. When the energy per unit area,  $\gamma_a$ , is measured, it is common practice to associate this quantity with the projected fracture area on the fracture plane irrespective of actual surface topography. Hence the ratio of actual to projected fracture area introduces a perhaps artificial variation into the deduced value of the fracture energy, which might otherwise turn out to be more of a universal (time-temperature dependent) quantity, independent of mode of loading.

In studies conducted on adhesive debonds between polyurethane and polymethylmethacrylate,  $\gamma_a$  was found for Modes I, II, and III, respectively. Several different test methods were used to determine  $\gamma_a$ ; e.g., peel, blister, cone pull-out, and it was found that as long as the modes were similar,  $\gamma_a$  was similar. For this adhesive system the  $\gamma_a$ 's associated with Modes I, II, and III, respectively, varied approximately as 1:2:4.<sup>14</sup> Similar effects of mode have been noted for various structural adhesives by independent (and different) tests.<sup>16</sup> In fact for the systems studied, it was found that the  $\gamma_a$  associated with a mixed mode failure was reasonably predictable as a weighted average of the pure mode  $\gamma_a$ 's. The weighting factor for each mode was simply the percent of the strain energy density for the particular mode at the crack tip. In our studies this analysis was normally accomplished numerically with the aid of a computer.

We see, therefore, that for the designer trying to predict the strength of adhesive joints all that is required is a knowledge of the value(s)  $\gamma_a$  (perhaps in all three modes if all are present at the crack tip) plus a stress analysis from which the strain energy can be determined. In principle at least, and ignoring cost limitation, this latter calculation may generally be accomplished for even very complex geometries with the aid of recently developed computer techniques.<sup>11,17,18</sup> The authors have enjoyed some successful examples in using these techniques to investigate and evaluate the strength of bonds for various dental adhesives, barnacle cement, explosively welding plate, solid rocket propellant loading, etc.

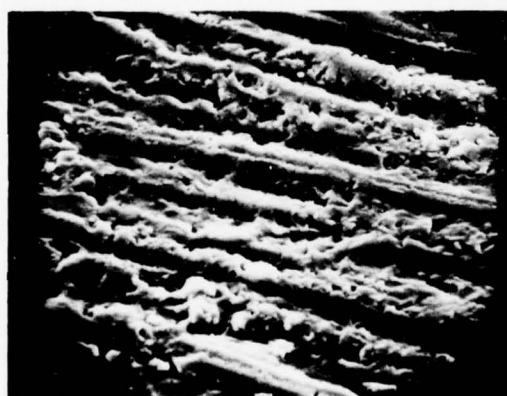
This leaves open, however, the fundamental question as to the reason for the mode dependence of  $\gamma_a$ . It is here that the SEM may be useful. Figure 12 shows electron micrographs of adhesive fracture surfaces of the polyurethane-PMMA system for the three modes. Qualitatively at least, these appear to indicate behavior consistent with above listed differences in  $\gamma_a$  for the three modes; i.e., the surface corresponding to Mode II is rougher and more "damaged" than that for Mode I. Likewise Mode III appears to be rougher, etc., than Mode II. It seems reasonable to assume that these greater surface damages represent more energy dissipation per unit area and hence larger values of  $\gamma_a$ .



a. Mode I (750 x)



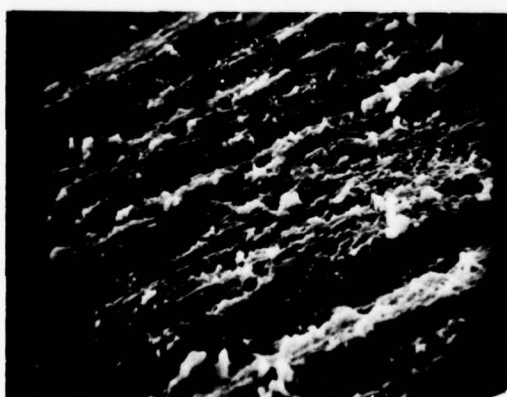
b. Mode I (2,800 x)



c. Mode II (750 x)



d. Mode II (2,800 x)



e. Mode III (750 x)



f. Mode III (2,800 x)

Figure 12. Electron Micrographs of Adhesive Fracture Surfaces  
Resulting From Various Loading Modes



# SECTION IV MATHEMATICAL ASPECTS - SINGULAR POINTS

Sharp corners in homogeneous materials have been recognized for many years as points from which fracture propagates. As demonstrated for two individual examples by Sneddon<sup>19</sup> in 1946 and later generalized by Williams,<sup>20</sup> linear elastic analyses of plane problems yielded series solutions for the stresses near a sharp notch in the form

$$\sigma_{ij} = \frac{K}{r^{1/2}} f(\theta) + O(r^{1/2}) + \dots \quad (7)$$

where  $r, \theta$  are polar coordinates with origin at the crack tip. For a general enclosed material angle of  $\beta$ , Equation (7) may be written

$$\sigma_{ij} = \frac{K}{r^\lambda} f(\theta) + \dots \quad (8)$$

where  $\lambda$  is a function of  $\beta$  as plotted in Figure 13a. For material angles less than  $\pi$ , no singular term is present ( $\lambda = 0$ ), while for material angles equal to  $2\pi$ , the square root of  $r$  singularity of Equation (7) is retained.

In many recent applications such as rocket motor grain retention systems and elastomeric bearings, multi-material bondlines must be considered. In these cases the stresses near the bondline terminus may be written

$$\sigma_{ij} = \frac{K}{r^\lambda} f\left[\theta, \left(\frac{\sin}{\cos}\right)(b \ln r)\right] + \dots \quad (9)$$

For plane problems in which one material is bonded at an angle  $\beta$  to a semi-infinite sheet of a second more rigid material<sup>21</sup> ( $E_1 = 0.001 E_2, \nu_1 = \nu_2 = 0.2$ ), values of  $\lambda$  and  $b$  are plotted as in Figure 13b. The function  $b$  in Equation (9) obviously depends upon material properties since for a homogeneous material,  $b$  is zero for all material angles. For the nonhomogeneous case, no singularity exists ( $\lambda = 0$ ) until a material angle of over 60 degrees is obtained. Thus fillet angles less than 60 degrees are advisable for such systems. For material angles greater than 210 degrees, a nonzero value of  $b$  is obtained. In addition to the mathematically infinite stresses at debond terminus which are characteristic of cohesive fractures, the analytical solutions now have an oscillatory character as the debond terminus is approached. The bounding singularity is still of the form  $r^{-\lambda}$ ; however, the signs of the stresses alternate between plus and minus for very small values of  $r$ .

As noted by several authors, the oscillations in the analytically determined stresses are not physically realistic. In fact, the analytically determined displacements on the two adjacent faces of the crack oscillate in a manner that would require the material on one side of the crack to intersect the material on the adjacent face in the crack tip vicinity. Thus one must conclude that the analytical solutions are not valid in this area. This phenomenon has not destroyed the usefulness of the analytical solution for predicting strength of the singularity near the crack tip or the stress intensity factor.

The largest value of  $r$  for which the sign change is noted ( $r = r_0$ ) depends upon material properties. For example the two semi-infinite sheet geometry shown in Figure 14 has bondline stresses of the form<sup>22</sup>

$$\tau_{xy} = \frac{2(1-\nu) Q e^{-\pi b}}{\pi (2ar)^{1/2}} \sin\left(b \ln \frac{r}{2a}\right) + \dots \quad (10)$$

$$\sigma_y = \frac{2(1-\nu) Q e^{-\pi b}}{\pi (2ar)^{1/2}} \cos\left(b \ln \frac{r}{2a}\right) + \dots \quad (11)$$

Thus as the point  $r = 0$  is approached, the first sign change takes place when

$$b \ln \frac{r_0}{2a} = -\pi/2 \quad (12)$$

The constant  $b$ , for plane strain conditions, simplifies to

$$b = \frac{1}{2\pi} \ln(3 - 4\nu_1) \quad (13)$$

when the modulus of Material 2 is much larger than that of Material 1, and Equation 12 reduces to

$$r_0/a = 2 e^{-\pi^2/\ln(3 - 4\nu_1)} \quad (14)$$

The character of the variation is given in Table I where, in particular, it may be noted that for an incompressible material  $r_0 = 0$ ; i.e., the stresses do not oscillate.

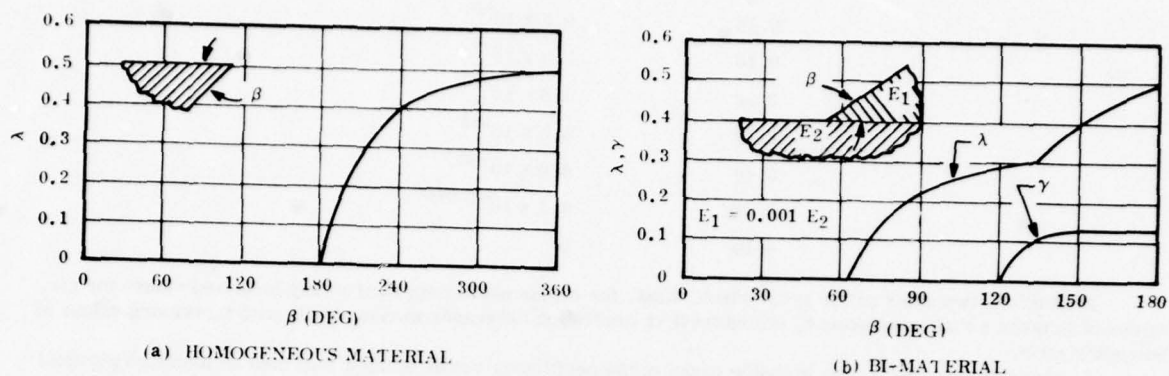


Figure 13. Singular Eigenvalues-Half Plane to Wedge

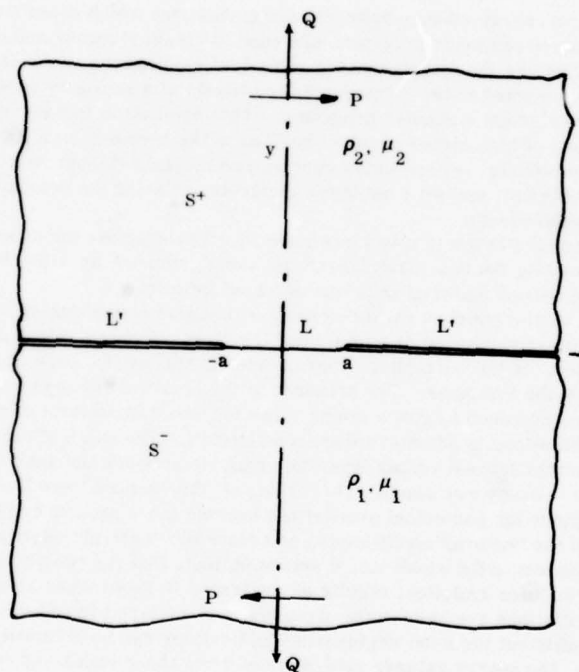


Figure 14. Two Semi-infinite Crack Geometry and Load Analyzed

TABLE I. POISSON'S RATIO VERSUS DISTANCE FROM CRACK TIP

$\nu$	$r_0/a$
0	$2.5 \times 10^{-4}$
0.10	$6.5 \times 10^{-5}$
0.20	$7.3 \times 10^{-6}$
0.30	$1.0 \times 10^{-7}$
0.40	$3.6 \times 10^{-13}$
0.48	$4.0 \times 10^{-56}$
0.499	$4.3 \times 10^{-1,040}$
0.50	0

In addition, two other points are evident: first, the stress oscillation is of a very localized nature for all values of Poisson's ratio; and second, the interval of oscillation decreases monotonically with increasing values of Poisson's ratio.

As stated by England<sup>23</sup> "the probable cause of the oscillatory result is the use of both an idealized physical model and the classical linear theory of elasticity." It would be interesting, if only from an academic viewpoint, to numerically analyze some problem of this type on a computer of sufficient size that the grid mesh in the crack tip vicinity was small enough to reproduce some of the analytically determined oscillations. If the analytical solutions are due only to the idealized physical model, one may be then able to show the true singularity behavior in this manner.

A second geometry pertinent to bond terminations is shown in Figure 15. The plot of  $\lambda$  in Figure 15 indicates that singular values are expected for all nonhomogeneous bond systems with the two quarter plane geometry. However, the order of the singularity is smaller than found in sharp notches. Thus, most nonfilleted bondlines in practice have singularity points, and the applicability of a strain or stress failure criterion may be questioned when linear elastic analyses are used.

#### NUMERICAL ASPECTS

Normally one relies on an energy balance approach for geometries which contain singular points. Since for complex geometries, finite element computer programs are used to obtain stresses and energy release rates, one questions the accuracy of these values for systems where analytical oscillations are observed.

Oscillations have also been noted in the stresses in the vicinity of a boundary condition discontinuity as calculated by the standard finite element computer programs. This oscillation is much more pronounced under the following conditions: (a) in areas of high stress gradient such as at the terminus of a fixed free boundary ( $E_1/E_2 \ll 1$ ), (b) for nearly incompressible materials, (c) for highly constrained systems (higher amplitude of oscillation for plane strain than for plane stress problems), and (d) compatible elements (relaxing the compatibility requirements normally reduces the magnitude of the oscillations).

An example of the stress oscillation is given in Figure 16. The analysis for these data was performed for a finite dimension sheet approximating the two-material infinite sheet geometry analyzed by Erdogan<sup>22</sup> as shown in Figure 14. The modulus of the second material ( $E_2$ ) was assumed infinite.

The computer program used a constant strain element with a grid consisting of 880 nodes. The width of the smallest element was 0.002 inch as compared to a total bond length of 2 inches. The height of the first row of elements above the crack tip is 0.001 inch. In the particular program used in this study, each quadrilateral element is divided into four triangular elements by the computer. The stresses at the centroid of each element are then calculated, and the four triangular stresses are averaged to give a single value for the quadrilateral element stress. Thus some degree of smoothing of the stress oscillations is automatically accomplished. The width of the smallest element is many orders of magnitude larger than the largest radius from the crack tip at which the analytically determined stresses oscillate ( $r_0 \sim 10^{-1,000}$  since  $\nu = 0.499$  was used). Therefore, all the "natural" oscillations occur within a very small portion of the first element. Since the numerical oscillations become more pronounced with high values of Poisson's ratio (the inverse being true of the "natural" oscillation), and since the "natural" oscillations all occur in a very small portion of the two elements adjacent to the crack tip, it seems unlikely that the two phenomena are related.

Comparisons of numerical and analytical results as presented in References 11 and 18 have demonstrated that even though rather severe oscillations are seen in the stresses at bi-material interfaces for the usual finite element formulations, stress values sufficient for most engineering applications can be obtained by suitable smoothing of the numerical values. In addition, the energy release rate obtained from these codes has compared favorably in all cases for which analytical and numerical results were compared.



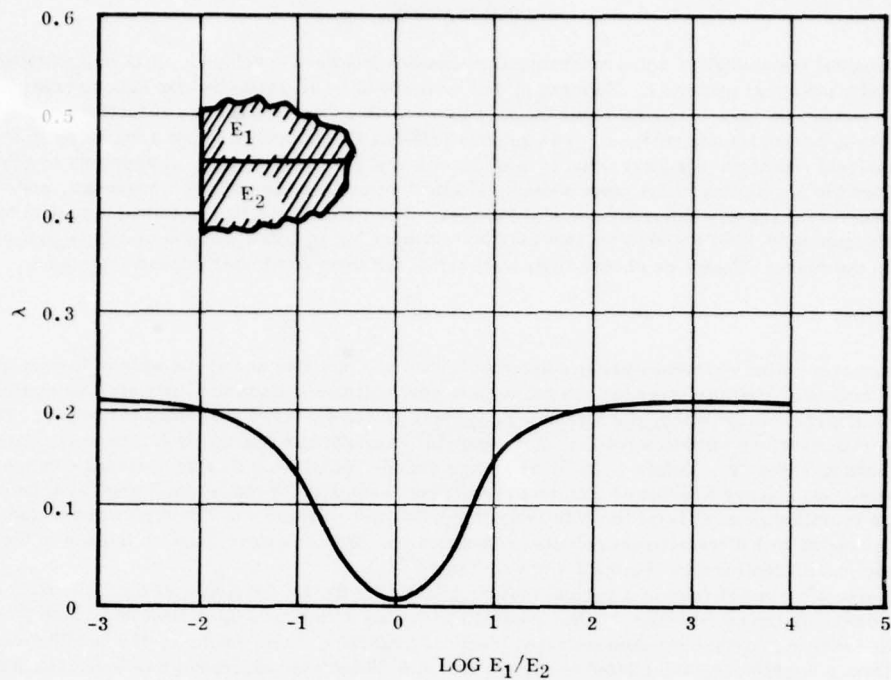
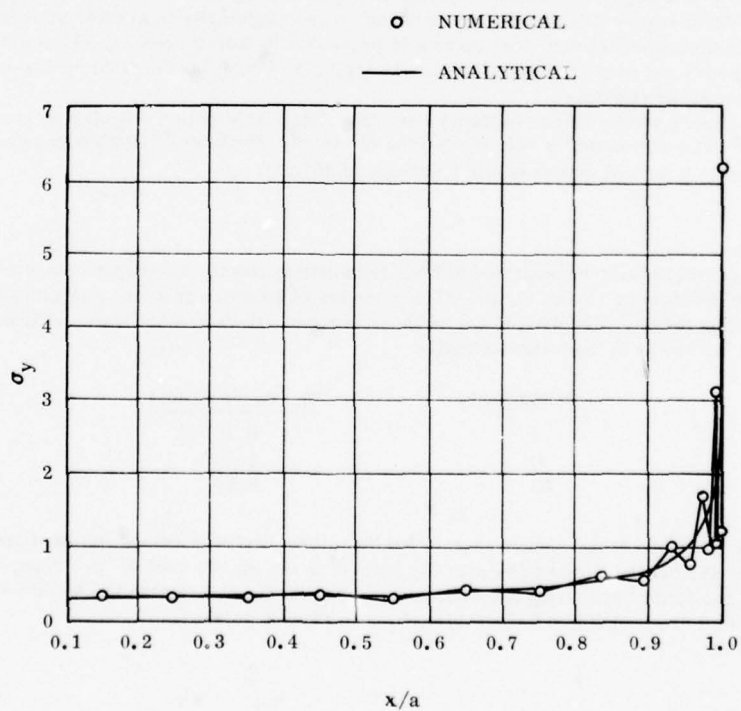


Figure 15. Singular Eigenvalues-Two Quarter Planes

Figure 16. Bondline Stresses Calculated Numerically and Analytically for  $\mu_2 = \infty$

## SECTION V APPLICATIONS

The fundamental framework of adhesive fracture mechanics has been developed. It is enlightening to apply these principles to specific practical problems. No attempt will be made to be all inclusive nor even to treat the problems analyzed in great detail. Rather, it is hoped that these problems will serve to show the versatility of the fracture mechanics approach to adhesive failure analysis. The authors feel that this approach is not a rigid, narrow set of rules for testing and analysis. Rather, it appears that it is more of a systematic philosophy of approach to adhesive problems that facilitates the acquisition of the most meaningful information from as simple, convenient, and straightforward a test as possible for the particular adhesive of interest. The information thus obtained may then be utilized for prediction of performance in other geometries that may be pertinent. It is hoped that the examples given might act as a stimulus to help the readers design or choose tests well suited for their particular adhesive systems.

### CONE TESTS

As shown above, infinite stresses are predicted at the tip of V notches and at the ends of bi-material interfaces for linear elastic analysis. Infinite stresses are not seen in real materials since the linearity assumption is violated as stresses become large. In practice, the stresses do become relatively large near singular points. These points are certainly potential fracture initiation points. For example, in applying a tensile load to two cylinders bonded with a butt joint as shown in Figure 17, Points 1, 3, 7, and 9 are singular points and therefore strong candidates for failure initiation. However, experience with poker chip test specimens demonstrates that Point 5 must also be considered as a potential failure initiation point at least for relatively thin bondlines. Systems of this type were tested<sup>14, 24</sup> using PMMA adherends bonded with a transparent polyurethane adhesive. Debonds were found to initiate in the high stress regions away from end discontinuities (Points 2 and 8 of Figure 17).

The butt joint is a special case of a conical test specimen (Figure 18) developed at the University of Utah for studying loading mode effects on fracture.<sup>11</sup> For conical specimens with cone angles from 5 through 90 degrees (butt joint), the bondline stress distributions demonstrated identical patterns. As an example, the bondline normal and shear stresses for a 5 degree cone are plotted in Figure 19. A 0.06 inch initial debond was built into these specimens. However, debond initiated in the high stress region away from the theoretical singular points (A and B of Figure 19). One could therefore assume that the higher (singular) stresses extend over such a small (plastic) region; they do not affect fracture. However it is conceivable that in an ideally elastic system, the energy release rate from a naturally existing flaw in a high stress region is greater than that from an initial debond in a low stress region. Thus even for ideal linear elastic materials, debonds could propagate from inherent flaws away from end induced singular points.

When the cone angle is reduced to zero (cylinder test), the stress pattern changes to that shown in Figure 20. The large normal stress at the bondline center is missing and debond propagated from the 0.06 inch initial debond region (Point A). Note from Figure 13b that the order of the stress singularity is greater at Point A than at Point B.

A more complete discussion of cone test results is presented in References 11, 24, and 25. However, the above brief discussion points out some of the difficulties in analysis of complex bondline systems. The weakest point in the system is not always obvious.

In cone test specimens where debond initiated away from bond termination singular points, the bondline normal stress was shown<sup>11, 25</sup> to be a reasonably reliable failure criterion. Solithane®\* PMMA cone test specimens of 5, 45, and 90 degrees all failed at a normal stress within 5 percent of 493 psi.

### LOADING MODE

In test specimens where failures occurred at bond termination points, an energy balance was used for failure criterion. As shown in References 11 and 14, the effective value of adhesive fracture energy ( $\gamma_a$ ) changes with direction of load application (loading mode). The magnitudes of these changes are very significant, at least for a PMMA-Solithane® bond system, as shown in the following table:

Loading Mode	$\gamma_a$ (in. lb/sq in.)
I	0.17
II	0.40
III	0.58

Although the  $\gamma_a$  data show large changes due to loading mode, the engineering implications are not as severe as one might suspect since the critical loads are generally related to the square root of  $\gamma_a$ . Thus, if the actual  $\gamma_a$  value is somewhere between the Mode I and Mode II values such as 40 percent higher than the Mode I value, a critical load predicted using the Mode I value would be conservative by less than 20 percent.

\*Transparent polyurethane manufactured by Thiokol Corporation.

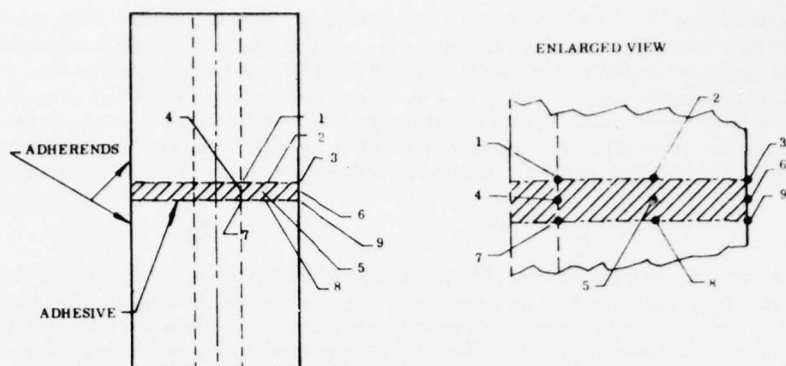


Figure 17. Potential Failure Initiation Points in a Butt Joint

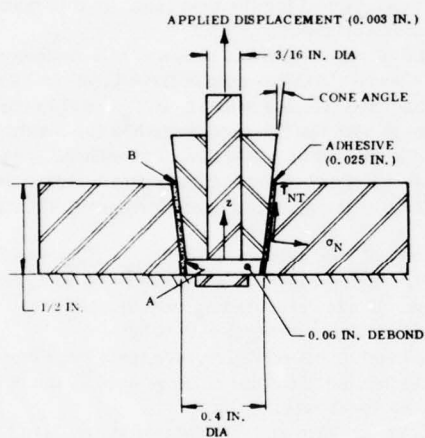


Figure 18. Cone Test Specimen

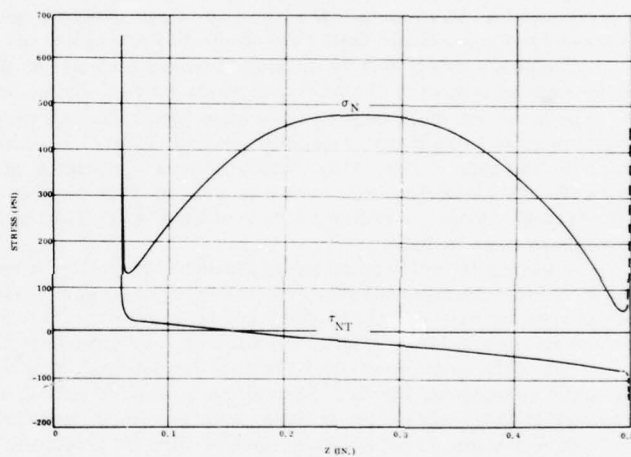


Figure 19. Normal and Shear Stress Components for 5 Degree Cone

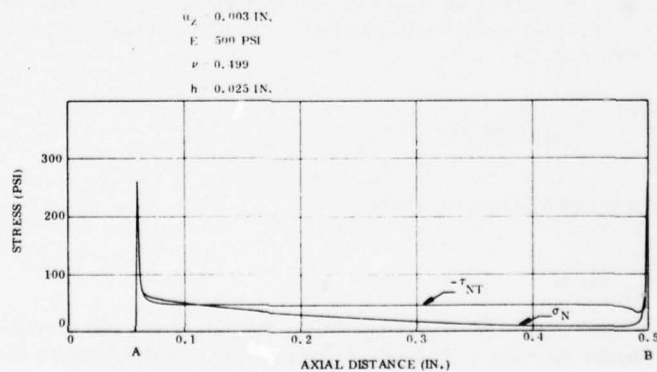


Figure 20. Normal and Shear Stress Components for 0 Degree Cone



## LOAD RATE AND TEMPERATURE

As shown in Reference 26,  $\gamma_a$  values are also rate and temperature dependent. Thus with the present state of the art, one must select laboratory tests for which temperature, loading rate, and loading mode duplicate as nearly as possible those in the bondline being analyzed. If there is difficulty in obtaining the desired load rate and/or temperature in the laboratory, it is possible to test specimens at a number of different load rates and temperatures. Then by applying a time-temperature shift of the resulting  $\gamma_a$  data in a manner similar to that used in obtaining relaxation modulus for viscoelastic materials, one can obtain a master  $\gamma_a$  versus log of reduced time, log (time/temperature shift factor), curve which may cover many decades of time. A thorough explanation of this procedure is given in Reference 11.

## CRITICAL LOAD

Substantial errors can be introduced in obtaining bond capability data by not measuring the load at which debond initiates (critical load,  $P_{cr}$ ). Most laboratory adhesion tests are completed at a constant rate of load application. This permits the load to increase while fracture or debond is propagating. In a constant displacement rate test, it is often not possible to look at a force-time trace and determine the force at which fracture propagation starts. Thus, the maximum load,  $P_{max}$ , instead of the load at fracture propagation,  $P_{cr}$ , is often used to calculate failure stresses. This may lead to considerable errors in predicting failure initiation loads.

The error in using  $P_{max}$  in place of  $P_{cr}$  may be nearly a factor of two as illustrated by References 11 and 27 using strip peel tests. Solithane<sup>®</sup> peel test specimens were constructed by casting a layer of Solithane<sup>®</sup> onto a sanded polymethylmethacrylate (PMMA) sheet (Figure 21). After cure (7 days) and mold removal, the Solithane<sup>®</sup> appears as a 2.5 mm thick sheet, 25 mm wide by 0.25 m long. The specimens were then mechanically debonded for a length of approximately 50 mm, and loaded at a constant displacement rate with the load applied perpendicular to the PMMA base plate. As the displacement was applied, the load at debond propagation and the maximum load were noted. As soon as the maximum load was reached, the load was removed and the specimen repositioned for the next test. In this manner, 18 data points were obtained before the debond had propagated the length of the specimen.

The displacement rate was changed between each test so that a total of nine rates was obtained in a random order (one to three tests at each of nine displacement rates). The Instron crosshead rate (XHS) ranges from 0.003 to 14 mm/sec. The data from these tests are plotted in Figure 22. Although the data exhibit some scatter, due in part to the small number of tests at each rate, their trend is clear; i.e., an increase in both the fracture force and the maximum force with load rate. The ratio of fracture force to maximum peel force is plotted as a function of crosshead speed in Figure 23. This ratio has little variation over the three decades of crosshead speed tested. These data indicate that, on the average, debond is initiated for a Solithane<sup>®</sup> to PMMA bondline at 54% of the maximum peel force over the range of crosshead rates tested.

In testing recently completed by Thiokol Corporation, a ratio of critical to maximum load ( $P_{cr}/P_{max}$ ) was found to be 0.91 for cylindrical adhesive fracture energy specimens (Figure 24). Solid propellant and liner were used in these tests and testing was conducted at 75° F and failure times of 1 to 3 minutes. Tests conducted on cylindrical cohesive fracture energy specimens (Figure 25) utilizing solid propellant showed a  $P_{cr}/P_{max}$  ratio of only 0.60.

One of the most promising techniques for detecting critical load in bond or cohesive fracture tests requires use of acoustic emission equipment. Several inert adhesive and cohesive test specimens typical of those used in the solid propulsion industry were recently tested while monitoring acoustic emission count rate.

Cohesive fracture energy cylinders (Figure 25) provided a very clear acoustic emission signal at fracture propagation; i.e., there was a clear correlation between visually observed fracture propagation and acoustic emission rate (Figure 26). We are presently in the process of applying acoustic emission techniques to adhesive systems.

## VISCOELASTICITY

There is presently no universally accepted method to obtain cohesive (or adhesive) fracture energy,  $\gamma_c$ , or critical stress intensity factor,  $K_{IC}$ , for viscoelastic materials. The earliest method<sup>28</sup> applied to solid propellant cohesive fracture involved finding an effective modulus value through use of a closed form energy release rate analysis for a spherical flaw in an incompressible viscoelastic material. The effective modulus for a constant applied displacement rate, as derived in Reference 28, is

$$E_{eff} = \frac{2}{t^2} \int_0^t \int_0^\xi E_{rel}(\tau) d\tau d\xi \quad (15)$$

A corresponding modulus for a constant pressure rate is

$$E_{eff}^{-1} = 2 \int_0^1 \xi D_{crp}(t\xi) d\xi \quad (16)$$

Several programs have been completed which demonstrate that this theory has provided satisfactory results for many applications.<sup>29, 30</sup> A similar approach is presently being used for adhesive fracture (i.e., the effective modulus from Equation 15 or 16 is applied to materials on both sides of the bondline).

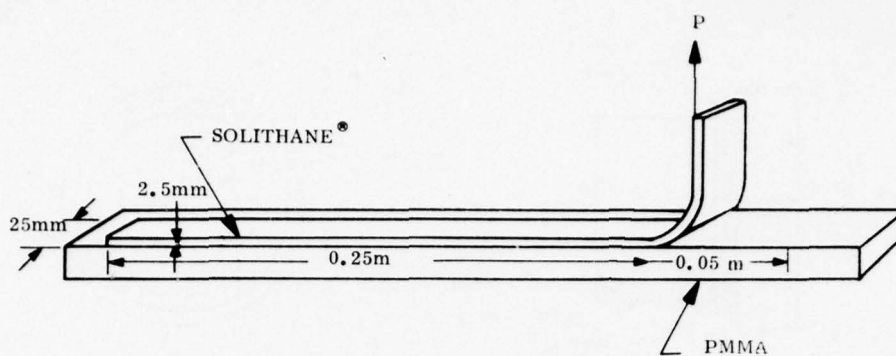


Figure 21. Peel Test Specimen

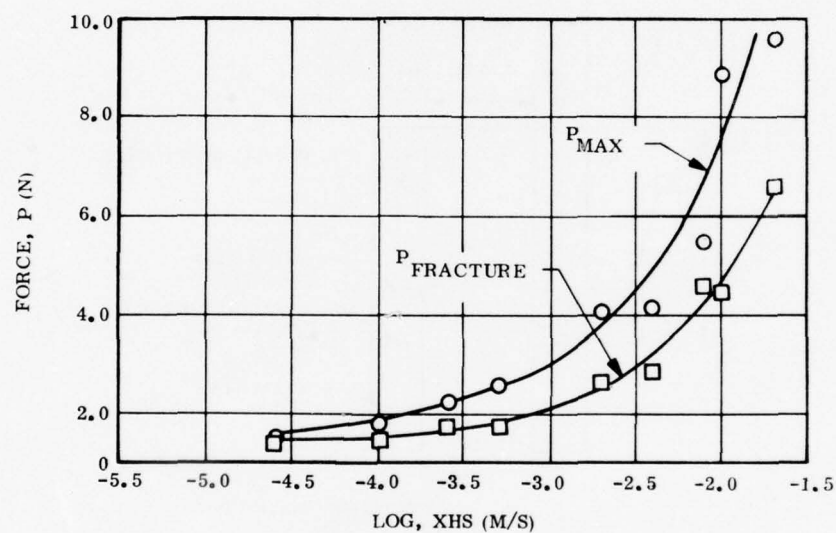


Figure 22. Rate Dependence of Solithane® to PMMA Peel Test (Constant Displacement Rate)

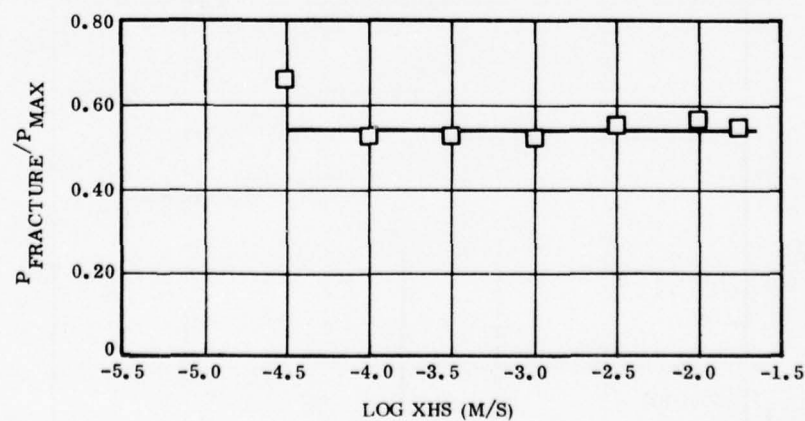


Figure 23. Ratio of Fracture Force to Maximum Force for Solithane® - PMMA Peel Test

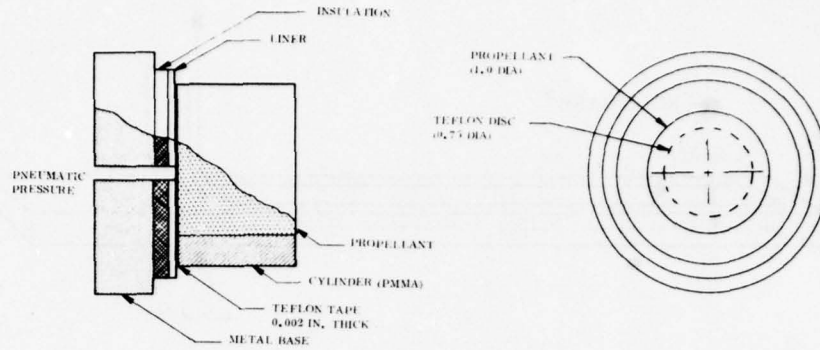


Figure 24. Cylindrical Adhesive Fracture Energy Test Specimen

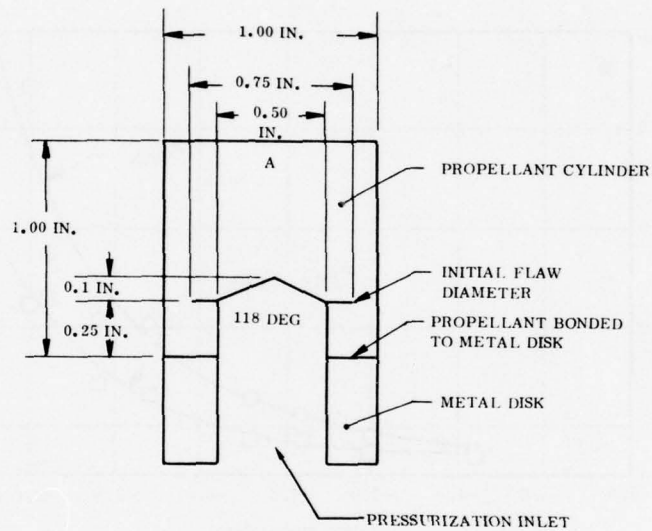


Figure 25. Cylindrical Cohesive Fracture Energy Specimen

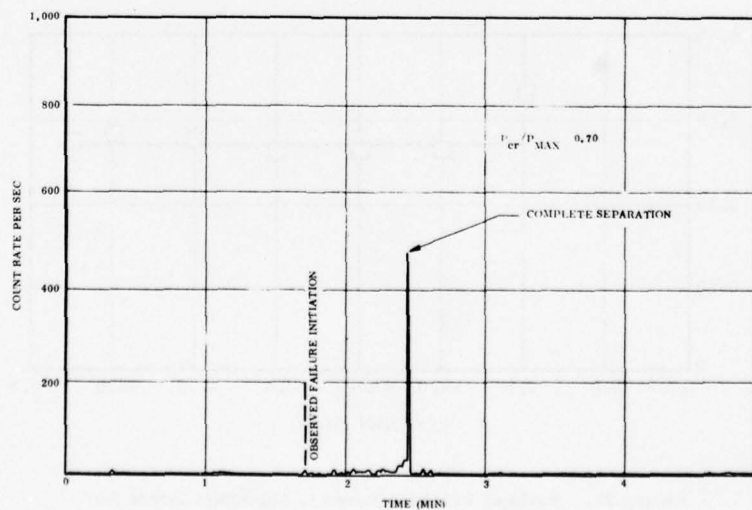


Figure 26. Acoustic Emission for Solithane Cohesive Fracture Energy Cylinder



The effective modulus approach as derived from the spherical flaw analogy is not mathematically precise.<sup>31</sup> However, it is fairly easy to apply and the successful correlation between laboratory testing and failure in large cohesive systems makes its application to adhesive systems fairly promising. Correlations between laboratory tests (solid propellant to liner debond) and bond failure in subscale rocket motors are presently being completed by the authors.

A second approach to cohesive viscoelastic fracture has been proposed by Schapery<sup>32</sup> and applied by Wang and Laheru<sup>33</sup> to solid propellant cohesive fracture. One advantage of Schapery's approach is that fracture rate as well as fracture initiation load can be determined. The authors are not aware of any application of this technique to adhesive fracture although the extension seems feasible.

#### TESTING DENTAL ADHESIVES

It is widely accepted that the availability of effective reliable adhesives for use in the oral environment could drastically change many aspects of dentistry. This has given rise to considerable activity directed toward dental adhesive development. A problem here is by what method can these adhesives best be tested and compared. Since these adhesives will generally be used under conditions where quality control will at best be difficult, it would also be helpful if the testing method could reveal what influence flaws or imperfections at the interface and changes in geometry might have on bond integrity. Fracture mechanics is suited to these purposes.

The tooth geometry does not readily lend itself to most standard test configurations. For example, the results of a variety of tensile tests that have been used to characterize dental adhesives have generally been characterized by very large scatter. This is at least in part due to difficulties in obtaining proper alignment of the tooth-adhesive structure.

A modification of the "blister test specimen"<sup>34</sup> has been proposed as a dental adhesive testing specimen that overcomes some of these problems.

A simplified blister test apparatus is shown in Figure 27. For this application, a tooth (or other material) is embedded in a rapidly curing plastic plug. The tooth serves as the lower substrate in the blister analysis. In this blister test, debonding is induced by a pressurized fluid. Water, saliva or other fluid is introduced through a small hole drilled through the plug and tooth. The pressure is then increased until debonding occurs. The modulus, flaw size, and the debonding pressure may then be used in an analysis to determine the adhesive fracture energy.

In setting, sanding, and drilling the hole, haste is of the essence. The structure of a tooth changes rapidly after extraction even if kept in vitro. One method that gave quite consistent results was to set the extracted tooth in a cuplike holder with a cold cure polymer that would set in less than 10 minutes. The hole was then quickly drilled and the surface sanded smooth with wet sandpaper (usually finishing with 50 grit). The sanding was done with a smooth fitting brass plug in place. This plug is left in place while the cement to be tested was cured. It was then removed to form the initial blister. A simple O-ring may serve as a mold for casting the material against the tooth.

Much of the fracture mechanics work presently being applied to the field of dentistry is being carried out at Dentsply International.<sup>35</sup> Researchers have applied adhesive fracture mechanics techniques to predict the bond strength between artificial acrylic teeth and various denture resins. The main purpose of this effort is to optimize dental restorative and prosthetic configurations. Adhesive fracture energy values were obtained using instrumented dynamic load impact tests. The tooth-denture base interfacial region was studied by cinematography and fractography. Failure loads at low and high strain rates and the interface morphology were determined by fracture surface analysis and related to the load-deflection curves obtained.

#### TESTING BARNACLE CEMENT

There are applications where it would be convenient to have adhesives that would adhere to a wet surface (dental oral applications being a notable example). Although technology has, to date, not completely solved the problem of adhesion to a wet surface, it has been pointed out that certain marine animals; e.g., barnacles and mussels, secrete natural adhesives that are capable of curing underwater and attaching the animal's shells, not only to moist but to completely submerged surfaces. Before extensive efforts are taken to synthesize the cement, it appeared wise to first ascertain its adhesive strength. Geometric problems make this a difficult task with most standard techniques, but the blister test readily lends itself to quantitative determination of the adhesive fracture energy of barnacle cements. Figure 28 is a schematic of the method used.<sup>36</sup> The barnacle is situated in the outer shell and on the base, which adheres to the substrate. The base itself is generally quite thin, from a few thousandths of an inch to 1/10 in. thick. The barnacle shell has a rather weak attachment to the base and can generally be pulled loose from the base before the base will pull free of the substrate. In the tests employed in these specimens, pressure is introduced to the bottom of the base through a hole in the substrate.

Various substrates were chosen upon which to "grow" the barnacles. The substrates were cut into plastic plates 12 x 12 in. in area, and 1/4 in. thick. Holes of various sizes were drilled in the plate in ordered arrays, and the sizes and locations of the holes were recorded for further reference. The holes then were filled with various waxes and solders. All the waxes and solders used melted at low temperatures (approximately 100°F), but were solid at the ocean temperatures (50° to 60°F) at which the fouling occurred. The surface was refinished so that the wax and the plate formed a smooth, flat surface.

The plates were transported to the paint laboratory at the San Francisco Bay Naval Shipyard. With the aid of Saryon and Linder at this laboratory, the panels were mounted in racks lowered over the side of a barge (see Figure 29). Fouling in these waters was rapid. The extra growth on the panels was removed at about two-week intervals, and all the barnacles and other deposits, with the exception of the ones almost centered over the wax or solder-filled holes, were scraped off.

After about three months, the barnacles had attained an average size between 1/2 and 3/4 in. in diameter. At intervals after this period, the plates were taken from the ocean and the barnacles were kept alive in an "instant ocean" saltwater aquarium until time to test them. For the tests, the wax was removed from the holes which were tapped to receive a tube connection. High pressure water was introduced to the bottom of the blister through this tube to uniformly load the debond cavity.

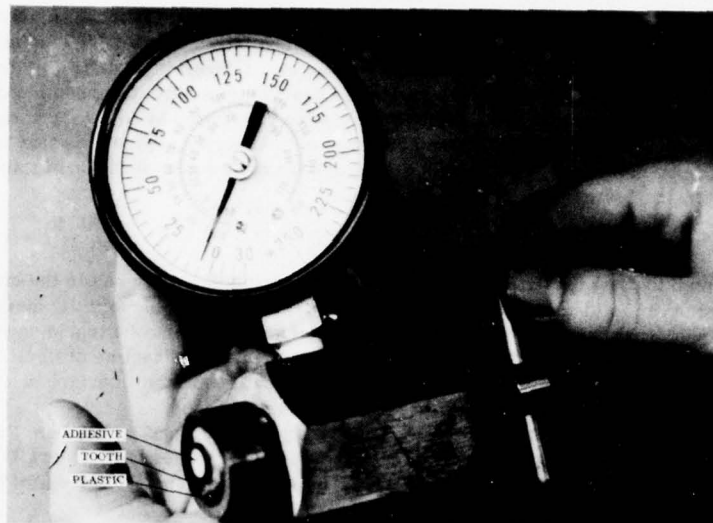


Figure 27. Blister Test for Dental Adhesives

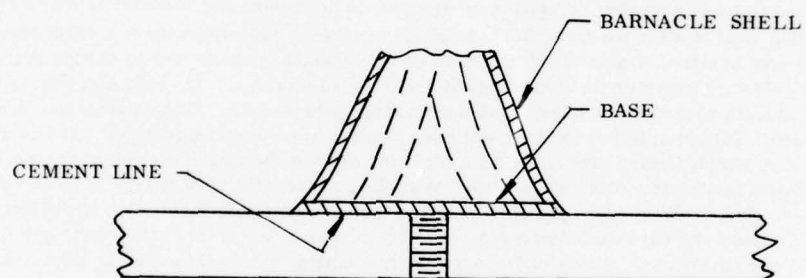


Figure 28. Experimental Arrangement for Determination of Adhesive Fracture Energy of Barnacle Cement

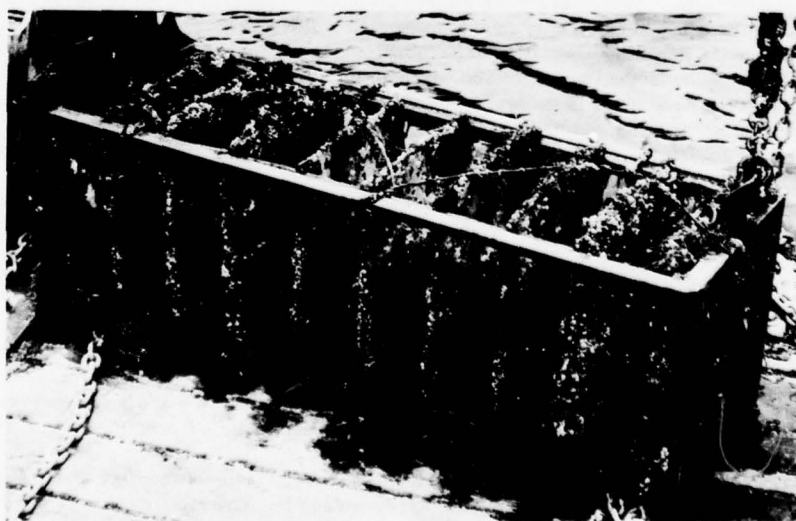


Figure 29. Panels After Several Weeks of Fouling

About 500 tests were conducted on barnacles by the procedure described above. As might be expected, the barnacles exhibited a much wider range of adhesive strengths than we have observed in experiments with commercial adhesives when adhesive application conditions could be more carefully controlled. It might be a reasonable conjecture, however, that the highest strengths of the natural adhesive observed would be comparable to a carefully prepared and applied synthetic barnacle cement. Although a number of the barnacles were loosely attached, the majority adhered quite strongly.

The value of  $\gamma_a$  determined was not high when compared to most structural adhesives ( $\gamma_a$  was one to two orders of magnitude less than some of the better structural epoxies tested), but it must be remembered that these were attached completely under water. Under similar conditions, most structural adhesives would have little if any strength at all. The synthesis of such a cement would likely yield an adhesive of moderate strength that could be attached completely under water. Such a material might have considerable technological value.

#### EXPLOSIVELY WELDED PLATES

While explosively welded plates are chemically and physically quite different from barnacles, there is at least one similarity. In determining their strength, neither readily lends itself to most adhesive test techniques, but each can be readily adapted to the "blister test." As a means of joining plates, explosive welding has some definite advantages: it is simple, requires very little surface preparation, can be used for a variety of materials, can be used to weld similar or dissimilar materials together, etc. In simplest terms, the test is conducted by using a sheet explosive to drive a plate onto the surface of a second plate. The plates are usually placed at a slight angle to each other and are usually submerged in water for the operation. The strength of the adhesive bond is a function of such parameters as amount of explosive, rate of combustion, angle between the plates, and surface conditions. Herein lies the major need to measure the adhesion between the plates: to optimize the welding conditions.

Through the courtesy of a colleague, Dr. A. A. Ezra, University of Denver, the authors obtained several explosively welded steel specimens. They were essentially thick cubes approximately one inch on a side to which had been explosively bonded on one side a thin steel sheet of one-tenth inch in thickness. After carefully tapping through the block perpendicular to the thin plate, pressurized oil was applied through the hole in an attempt to lift off the sheet in a blister experiment (see Figure 30). An adhesive fracture energy from less than 10 percent to approaching 90 percent of the cohesive fracture energy ("fracture toughness") of the steel was attained depending on the welding conditions. In a sense the ratio of  $\gamma_a/\gamma_c$  could be viewed as a weld efficiency. More details can be found in a report by DeVries, Luntz, and Williams.<sup>37</sup>

#### FATIGUE

Fatigue life of adhesive joints has been considered by several investigators, most notably Wang,<sup>38,39</sup> Gent,<sup>40</sup> Mostovoy and Rippling.<sup>41</sup> These investigators again demonstrate the usefulness of fracture mechanics in analyzing adhesive failure. The results of all these groups are interesting but too lengthy to extensively review here.

It is perhaps worthwhile, however, to briefly describe one of the tests and its results. Mostovoy, et al<sup>42</sup> have made use of a Tapered Double Cantilever Beam (TDCB) under cyclic loading to investigate crack growth. They report that the crack growth rate is related to the difference between the maximum and minimum energy release rate values  $\Delta G$  in the form

$$\frac{da}{dN} = A \Delta G^B$$

where the constants A and B are determined empirically. Values of A near  $2 \times 10^{-8}$  and of B near 6 are typical for various adhesives bonded to metal adherends when fracture rates are measured in inches per second, and when cycling is performed about a nominal value approaching half the maximum value.

Values of  $\Delta G$  for the adhesive fatigue threshold ( $G_{TH}$ ) are normally one to two orders of magnitude lower than the corresponding static values of  $\gamma_a$  ( $G_{1c}$ ).

These investigators also report that increased temperature lowers the fatigue resistance  $\Delta G$ . The shape of the  $da/dN$  curve does not change much with temperature; however, the growth rate generally increases with T.

There have been a variety of other studies in which fracture mechanics has been used to analyze adhesive failure. Among others are studies of: (1) stress mode dependence, (2) effect of adhesive bond thickness, (3) the role of fillers in adhesives, (4) the effect of plasticity and viscoelasticity in the adhesive and substrates, (5) thermal stresses, induced adhesive failure, and (6) chemical and environmental effects.

Many of these are reviewed in a recent book by the authors.<sup>11</sup> Hopefully, the few examples reviewed here will adequately serve to demonstrate the utility, versatility, and methodology of adhesive fracture mechanics. In conclusion, in each of these (and other) cases, it appears that fracture mechanics provides a systematic means of analyzing adhesive tests. Furthermore, it provides parameters and methodology that can be used to predict the strength for other geometries.

Portions of this work were supported by the National Science Foundation under Grant DMR 74-0271.



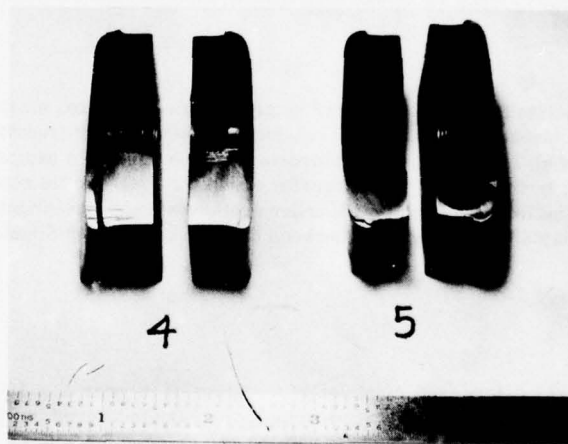
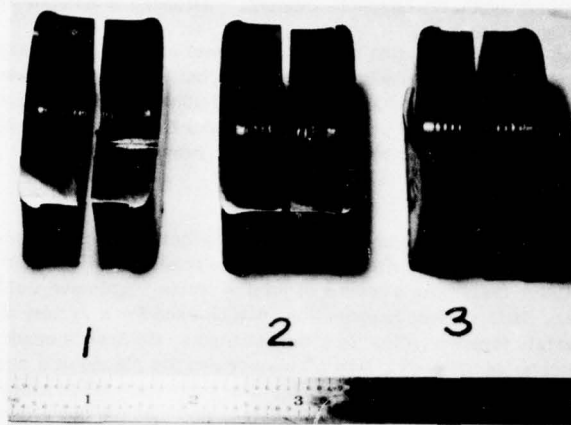


Figure 30. Blister Test Specimens for Explosive Weld Evaluation

# SECTION VI

## REFERENCES

1. Elliott, S. Y., "Techniques for Evaluation of Adhesives" in Handbook for Adhesive Bonding (C. V. Cagle, ed), McGraw-Hill Publishing Company, New York (1973).
2. Treatise on Adhesion and Adhesives, Vol I (R. L. Patrick, ed) Marcel Dekker, Inc, New York (1967).
3. Williams, M. L., Schapery, R. A., Zak, A., and Lindsey, G. H., "The Triaxial Tensile Behavior of Viscoelastic Materials," GALCIT Report SM63-6 (1963).
4. Goland, M., and Reissner, E., Journal of Applied Mechanics, Transactions of the ASME, 77, 17 (1944).
5. Wolley, G. R., and Carver, D. R., Journal of Aircraft 8 (10) (1971).
6. Ripling, E. J., Mostovoy, S., and Patrick, R. L., Material Research Studies 4 (1960) 129.
7. Irwin, G. R., in Treatise on Adhesion and Adhesives, Vol I (R. L. Patrick, ed) Marcel Dekker, Inc, New York (1967).
8. Griffith, A. A., Proceedings of 1st International Congress of Applied Mechanics, Delft, p 55 (1924).
9. Williams, M. L., Journal of Applied Polymer Science, 13:29-40 (1969).
10. Bennett, S. J., DeVries, K. L., and Williams, M. L., International Journal of Fracture, 10:33 (1974).
11. Anderson, G. P., Bennett, S. J., and DeVries, K. L., Analysis and Testing of Adhesive Bonds, Academic Press, New York (1977).
12. Murr, L. E., Electron Optical Application in Material Science, Material Science and Engineering Theories, McGraw-Hill, New York (1970).
13. Treatise of Adhesion and Adhesives (R. L. Patrick, ed) Marcel Dekker, Inc, New York, three volumes.
14. Anderson, G. P., DeVries, K. L., and Williams, M. L., "The Influence of Loading Direction Upon the Character of Adhesive Debonding," Journal of Colloid and Interface Sciences, Vol 47, No. 3 (1974).
15. Erdogan, F., and Sih, G. C., Journal of Basic Engineering, Transactions of the ASME, 519 (1963).
16. Chang, M. L., DeVries, K. L., and Williams, M. L., Experimental Mechanics, 14:89 (1974).
17. Anderson, G. P., Ruggles, V. L., and Stibor, G. S., International Journal of Fracture Mechanics, 7:63 (1971).
18. Anderson, G. P., DeVries, K. L., and Williams, M. L., "Finite Element in Adhesion Analyses," International Journal of Fracture, Vol 9, No. 4 (Dec 1973).
19. Sneddon, I. N., "The Distribution of Stress in the Neighborhood of a Crack in an Elastic Solid," Proceeding, Royal Society London, Vol A-187 (1946).
20. Williams, M. L., "On the Stress Distribution at the Base of a Stationary Crack," Transactions, American Society of Mechanical Engineers, Journal of Applied Mechanics (1957).
21. Hein, V. L., and Erdogan, F., "Stress Singularities in a Two-Material Wedge," International Journal of Fracture, 7 (1973), 317-330.
22. Erdogan, F., Journal of Applied Mechanics, 30 (1963) 232.
23. England, S. H., Journal of Applied Mechanics, 30 (1965) 400.
24. Anderson, G. P., "Applied Adhesive Fracture Mechanics," Ph.D Dissertation, Mechanical Engineering Department, University of Utah, Salt Lake City, Utah (1973).
25. Anderson, G. P., DeVries, K. L., and Williams, M. L., "Mixed Mode Stress Field Effect in Adhesive Fracture," International Journal of Fracture, Vol 10, No. 4 (Dec 1975).
26. Bennett, S. J., "Adhesive Fracture in Viscoelastic Materials," Ph.D Dissertation, Mechanical Engineering Department, University of Utah, Salt Lake City, Utah (1973).
27. Anderson, G. P., DeVries, K. L., and Williams, M. L., "The Peel Test in Experimental Adhesive Fracture Mechanics," Journal of the Society for Experimental Stress Analysis - Experimental Mechanics, Vol 16, No. 1 (1976).
28. Williams, M. L., International Journal of Fracture Mechanics, Vol 1, No. 4 (1966) 202.
29. AFRPL Report, "Predictive Techniques Program - Final Report," to be Published.
30. Anderson, G. P., and Stoker, J. N., "Fracture Prediction in High Solids Loaded Polymers," Presented at the 5th National Symposium on Fracture Mechanics, University of Illinois, 31 Aug 1971.
31. Nuismer, R. J., "On the Governing Equations for Quasi - Static Crack Growth in Linearly Viscoelastic Materials," Journal of Applied Mechanics, Sep 1974.
32. Schapery, R. A., "A Method for Predicting Crack Growth in Nonhomogeneous Viscoelastic Media," International Journal of Fracture, Vol 14, No. 3 (1978).
33. Wang, D. Y., and Laheru, K. L., "Poseidon C-3 Final Report, First Stage Propellant Grain Flaw Analysis," Hercules-Thiokol Report SA-015-A2A00HTJ-078, April 1978.
34. Williams, M. L., "The Continuum Interpretation for Fracture and Adhesion," Journal of Applied Polymer Science 13, 29-40 (1969).
35. Koblitz, F. F., "Mechanical Behavior of the Acrylic Tooth to Denture Base Band," Presented at the International Association for Dental Research (1976).
36. Despain, R. R., et al, Journal of Dental Research, Vol 52 (1973).
37. DeVries, K. L., Luntz, R. D., and Williams, M. L., Third International Conference on High Energy Forming, Vail, Colorado, June (1971).
38. Wang, D. Y., "Influence of Stress Distribution on Fatigue Strength of Adhesive Bonded Joints," Experimental Mechanics, June (1964).
39. Wang, D. Y., "The Effect of Stress Distribution on the Fatigue Behavior of Adhesive Bonded Joints," Air Force Materials Laboratory, Report ASD-TDR-63-93 (1963).
40. Gent, A. N., Lindley, P. B., and Thomas, A. G., Journal of Applied Polymer Science, 8 (1964) 455.
41. Mostovoy, S., and Ripling, E. J., "Final Report - Fracturing Characteristics of Adhesive Joints," Material Research Laboratory, Inc., Contract No. N00019-74-C-0274 (1975).
42. Mostovoy, S., and Ripling, E. J., Journal of Applied Polymer Science, 15, 641 (1971).

## BEHAVIOR OF ADHESIVELY BONDED JOINTS UNDER CYCLIC LOADING

by

John Romanko  
Senior Engineering Specialist  
Materials Research Laboratory  
General Dynamics  
Fort Worth Division  
Fort Worth, Texas 76101

### SUMMARY

This lecture will elucidate on the state of the art in determining the fundamental mechanisms of fatigue degradation in structural adhesive joints and in identifying the dominant fatigue mechanisms with the service environmental regimes, including cyclic mechanical load, temperature and humidity. The term "fatigue" as used here refers to cyclic loading and unloading in a broad sense and includes a range of combinations of duration of load applied and load removed as well as a range of loading rates or strain rates.

The scope involves an in-depth assessment of fatigue mechanisms and failure modes primarily in adhesively bonded metal/metal joints over the range of loads and environmental conditions experienced by modern high performance aircraft. The materials and processes considered are consistent with high-durability, adhesive-bonding technology. Interdisciplinary scientific methodologies are applied to establish the physical and mechanical property changes that occur during fatigue cycling.

Analytical and experimental stress analysis methods are described to quantitatively define the constitutive relations for the adhesive interlayer material in bonded joints and to describe the changes (and rate of changes) that occur during instrumented fatigue testing. Discussions of relevant methods of testing and interpretation of test results are given. Quantitative post-test examinations are used to verify the fatigue processes.

The adhesively bonded joints are analyzed to describe the stress/strain distributions developed within the adhesive interlayer by load/environmental fatigue conditions. The stress analysis involves a finite-element computer program called MARC with capabilities of large deflections and non-linear viscoelastic material behavior. Factors considered include cure and shrinkage stresses, expansion and contraction due to moisture absorption and desorption, time and temperature dependence of the constitutive relations, and their relation to measurable joint-response parameters. Iterative procedures between analysis and testing are considered.

Joints fatigued to various stages of joint life, including failure, are examined for degradation mechanisms using the technique of adherend etching with optical and SEM analyses of the remaining intact adhesive interlayer and XPS surface analysis of failed surfaces.

Measurements and observations are related, insofar as possible, to the damage processes and failure modes and the results are assessed with respect to the relevance of existing failure theories and criteria. Items covered include: nature of fatigue cracks and crack propagation; residual strength; influence of initial voids; flaws and/or cracks in adhesives or adherends.

The development of methodology for predicting the necessary service life of adhesively bonded joints is outlined.

### INTRODUCTION

Adhesive bonding of aerospace systems and components is increasing at a rapid pace. Substantial savings are possible with this joining technique in weight reduction and in manufacturing costs. Advantages over riveted or bolted structures also include facile joining of thin and contoured sheets and reduced stress concentration and galvanic corrosion. However, adhesive bonding has seen limited use as a bonding technique in the U.S.A. for primary structural elements in the past because of low reliability and limited durability of the joints. Now, with the advent of better metal-surface-preparation techniques and better adhesive materials, it is expected that eventually much improved fatigue life, improved fail-safe capability, and reduced manufacturing costs of airframes will finally be realized. Unfortunately, the usefulness of this joining technique, for primary structural elements, is presently impaired by the lack of understanding of the environmental effects of moisture and high temperature during fatigue loading.



In order to achieve some of the promises of this joining technique for primary structures, a thorough understanding is required of the fundamental mechanisms of fatigue degradation operative in structural adhesive joints in terms of the service environmental regimes, including cyclic mechanical load, temperature, and humidity.

The Air Force Materials Laboratory (AFML) W-P AFB, Ohio, is currently sponsoring a number of separate programs, each designed to provide solutions to various segments of the puzzle of the structural behavior of adhesively bonded systems. They fall under the general topics of analysis, failure mechanisms, design/failure criteria, design data, and test methods. Some of these include: Characterization of Surfaces Prior to Adhesive Bonding (F33615-75-R-5143), Fracture Mechanics Methodology for Structural Adhesive Bonds (F33615-75-R-5224); Structural Properties of Adhesives (F33615-75-R-5205), Cure Monitoring Techniques for Adhesive Bonding Processes (F33615-76-R-5170) and Improved Adhesive Bond Flaw Measurement Methods (F33615-75-R-5079).

Among these, a current program on Fatigue Behavior of Adhesively Bonded Joints (F33615-76-C-5220) (Ref. 1), conducted by General Dynamics Fort Worth Division, is one of the more ambitious technology programs which, when completed, will be an important element in contributing towards the development of accurate methods for predicting the service life of adhesively bonded joints.

Already, this innovative program, initiated in mid-1976, has generated important environmental behavior data on an advanced adhesive, FM-73M, and on model thick-adherend, single-lap shear joints fabricated therewith and subjected to a range of fatigue loads, temperature, and moisture environments representative of service conditions for modern high-performance aircraft. In an iterative procedure, this data is being coupled with a finite-element stress-analysis computer program developed at General Dynamics using a sophisticated (MARC) viscoelastic procedure to define and accurately predict the behavior of the instrumented bonded joints under the aforementioned in-service environmental conditions. Measurement of the complete load-deflection histories of neat adhesive coupons and bonded joints for combinations of environmental exposure and testing parameters and subsequent post-test examination of the adhesive interlayer, before, during and after failure using sophisticated analysis techniques are used to elucidate on the basic fatigue degradation mechanisms characterizing the joint failure.

Some of the questions this program intends to answer include: why low-cycle fatigue failure is detected in what appears to be a relatively short period of time; what is the relation between load intensity and fatigue life; and whether data generated on environmental testing under "accelerated" testing conditions are valid, and, if so, to what extent?

A program on "Structural Properties of Adhesives", recently completed by Vought Corporation (Refs. 2,3) has developed test procedures and instrumentation for generating rigorous engineering structural property data on adhesives.

Schjelderup of Douglas Aircraft Co. (Ref. 4) has conducted a series of cyclic fatigue tests on thick-adherend bonded joints as part of the PABST Environmental Program (Ref. 5) to obtain mechanical property data for FM-73M and to determine if a correlation between neat (cast) tension tests and thick-adherend shear tests could be established. A compilation of the mechanical property data, including load-deflection curves, are summarized in Reference 4 without analysis of the data.

Marceau and McMillan of the Boeing Commercial Airplane Co. (Ref. 6) have conducted some cyclic load testing of thick-adherend lap shear joints, reporting results on the effects of cyclic rate, stress level, environmental exposure, and loading mode on fracture path and specimen life with emphasis on fracture mechanics.

Combining the fatigue degradation mechanisms approach with the fracture mechanics approach should lead to a methodology for the prediction of fatigue life of bonded structures.

This lecture will be concerned primarily with a specific bonded-joint geometry, the thick-adherend, single-lap shear model joint (Ref. 7), and on the fatigue properties of such a joint as a function of various environmental exposure and testing parameters. In the interest of preserving the natural sequence of events, this lecture covers chronologically six main topic areas of interest, with the results obtained as of approximately August, 1978. These six interrelated experimental and analytical topics are:

- o Specimen Preparation - fabrication and environmental conditioning of model single lap shear joints, neat adhesive specimens, and moisture control specimens.
- o Adhesive Material Characterization - measurement of mechanical and physical properties necessary to define constitutive relations for the adhesive interlayer over a range of

temperatures and moisture contents.

- o Stress Analysis - use of finite-element techniques to describe the stress-strain distributions within the adhesive interlayer.

- o Model Joint Testing - measurement of static and dynamic mechanical response of model lap shear joints as a function of temperature, moisture content, load level, load rate, load duration, and frequency.

- o Post-Test Examination - use of NDE techniques, adherend etching and optical and scanning electron microscopy, and X-ray photoelectron spectroscopy techniques to characterize the physical, topographical, and chemical characteristics of specimens and failed surfaces.

- o Prediction of Fatigue Degradation Mechanisms - delineation and assessment of the observed degradation mechanisms and failure modes in terms of the individual and combined effects of environment, and prediction of service-induced degradation.

More emphasis will be extended in this lecture on the topics of joint fatigue testing, post-test examination, and model development since these relate more directly to this presentation on the behavior of bonded joints under cyclic loading.

## 1. SPECIMEN PREPARATION

### 1.1 Model Joint Specimens

The model joint specimen used for all fatigue testing is the thick-adherend, single-lap shear model joint shown in Figure 1 (Ref. 8). The one-quarter-inch-thick adherend material is bare aluminum alloy 7075-T651, which is alkaline cleaned, acid etched, and anodized using the phosphoric-acid (BAC-5555) process (Ref. 9). After oven drying following rinse, the anodized parts are coated with Bloomingdale BR-127 primer and cured according to recommended procedures for 60 minutes at 250°F (Ref. 10).

The adhesive is FM-73M, a 250°F -cure tape of nominal thickness, approximately 8 to 10 mils with a matte dacron carrier, manufactured by American Cyanamid, Havre de Grace, MD. PABST testing results (Ref. 11) have shown this carrier to be superior to the woven type.

One-quarter-inch-thick panels, approximately 7" x 16", are assembled with the primed aluminum and single-layer adhesive film and bonded according to recommended cure procedures for each adhesive (Ref. 12). The panels are saw cut on each side to form the one-half-inch overlap, and the 7" x 1" model joint specimens are cut from the panels, slotted, drilled for clevis holes, and individually identified.

### 1.2 NDE Ultrasonic Inspection

The 7" x 16" bonded panels and each finished test specimen are ultrasonically inspected in the overlap area for debonds, voids, bondline thickness, porosity, and saw cut edge damage. The inspection is accomplished using a computer automated ultrasonic inspection system operating in the through-transmission C-scan mode and records of each specimen are kept in a computer disk or tape for future correlation and clarification of mechanical test results.

### 1.3 Measurement of Bondline Thickness

An optical comparator (projection microscope) with 20X optics and a computer-automated ultrasonic inspection system operating in the pulse-echo mode with Fourier transform analysis (Ref. 13) are used for measurement of bondline thickness in the overlap area.

The optical technique also permits direct visual inspection of each model specimen along the edges for voids, porosity, and other bondline anomalies; this information can be correlated with the ultrasonic through-transmission C-scan data obtained on the parent uncut sandwich plate.

The ultrasonic Fourier analysis technique involves pulse-echo-signal convolution of the resonance frequency,  $\Delta f$ , using an analytical Fourier transform coded for a digital computer. If the velocity of sound,  $v$ , is known in the adhesive interlayer of thickness,  $t$ , the latter is determined from the relation,  $2t = v \Delta f$ . The agreement between the two bondline thickness measuring techniques is found to be very good.

#### 1.4 Adhesive Characterization Specimens

Thick laminates of the adhesive films, with and without scrim carrier, are made by bonding several layers of film together to a thickness of about 45 mils according to the recommended adhesive cure cycle. Laminating and bonding is accomplished between aluminum plates, coated with release agent, so that these adhesive specimens are subjected to the same bonding environment as the adhesive tape in the model bonded joints. Such thick laminate plates, but with integrally bonded aluminum end tabs, subsequently sliced in approximately one-quarter-inch widths (with 3" between end tabs), provide suitable tensile creep compliance and fatigue test specimens. Other laminated adhesive panels are cut to provide smaller specimens for thermal and moisture expansion measurements, among others.

#### 1.5 Moisture Control Specimens

Two types of moisture control specimens are fabricated: the first type consists of individually made neat adhesive specimens. The second type consists of a single film of adhesive bonded with 0.002" Al foil skins. Specimens of various sizes, including 0.5" x 1.0", are used to simulate the model joint lap area. During specimen conditioning, small slices are cut from edges to measure moisture content.

#### 1.6 Specimen Conditioning

The moisture conditioning of the so-called "wet" specimens, both neat adhesives and model joints, is achieved by storing them in an environmental chamber at 150°F/condensing (100% RH) humidity for suitable periods of time.

A moisture absorption model using a finite difference solution to Fick's Law of Diffusion has been developed to predict the concentration and distribution of moisture in resin systems. Comparison of predictions of this model with laboratory test results is good (Ref. 14).

#### 1.7 Moisture Diffusion in Bonded Joints

The diffusion coefficients determined for neat FM-73M (Ref. 15) are used in a calculation of the moisture distribution in the 1" x 0.5" overlap region of the bonded joints. The moisture diffusion parameters for FM-73M adhesive were determined to be

$$P_e = 2.17\% \text{ in } 100\% \text{ RH, and } D_{H_2O} = 1.84 \times 10^{-4} \text{ in}^2/\text{day}$$

The one dimensional solution for moisture distribution as a function of time,  $t$ , and position,  $x$ , in a body exposed on both sides (Ref. 16) is

$$\frac{P(x,t)}{P_e} = 1 - \frac{4}{\pi} \sum_{j=1}^{\infty} \left[ \frac{(-1)^{j-1}}{2j-1} \right] \exp \left[ -(2j-1)^2 kt \right] \cos \left[ (2j-1) \frac{\pi x}{2\delta} \right] \quad (\text{Equ. 1})$$

where  $P_e$  = equilibrium moisture content (saturation level)

$2\delta$  = total thickness

$k = D/(2\delta)^2$

$D$  = diffusion constant

If the moisture ingress from the 1.0" dimension can be neglected along the centerline, the bondline can be modeled as a wide plate with a thickness of 0.5". Equation 1 was programmed on a desk computer and the results obtained for FM-73M are shown in Figure 2. The small peaks near the center of the overlap are attributed to poor series convergence of the equation at very low concentrations. After one year, the FM-73M specimens will be nearly saturated throughout the entire interlayer.

## 2. MATERIALS CHARACTERIZATION

### 2.1 General Considerations

One of the basic needs in quantifying the fatigue behavior of any bonded joint is the development of an accurate analytical representation of the stress-strain distribution in the adhesive interlayer as a function of the applied loading force. Any suitable analytical representation contains terms representing characteristic mechanical (physical) properties of the adhesive interlayer material.

In the current formulation, the two main properties of interest are the tensile creep compliance,  $D(t)$ , and Poisson's ratio,  $\nu(t)$ , of the adhesive material. These are interrelated in the so-called constitutive relations of the material (Ref.17), and



may be time, temperature, and moisture dependent in general.

Other material properties of the adhesive that influence the determination of the stress-strain state therein include moisture absorption (expansion) and moisture desorption (contraction) characteristics; thermal expansion coefficient,  $\alpha_T$ , glass transition temperature,  $T_g$ , among others.

FM-73M adhesive is a modified epoxy with a matte dacron carrier so that the material is, strictly speaking, not homogeneous nor isotropic. However, because the carrier is a random matte, it is assumed that specimens laminated from these films are sufficiently isotropic so that characterization techniques developed for isotropic solids are sufficiently accurate. Results on time-dependence (or independence) are thus not violated by this assumption.

## 2.2 Static Tensile Tests

In order to establish the maximum load-carrying capacity of the tensile creep compliance specimens, constant-strain-rate tensile tests were conducted over a broad temperature range, at a strain rate of  $5 \times 10^{-4}$  1/sec, on an Instron machine with a Missimer environmental chamber (Ref. 18). The data obtained are summarized in Figure 3. Measured stress-strain histories for dry and wet FM-73M adhesive coupons at room temperature are shown in Figure 4.

## 2.3 Moisture Expansion

When an adhesive material absorbs moisture, a volumetric expansion takes place. When it loses moisture, a shrinkage occurs. Such dimensional changes can be a very important influence on the stress state in the adhesive layer of a bonded joint.

In order to characterize the moisture expansion characteristics of FM-73M, small coupons (1.0" x 0.5" x 0.035") were cut from laminated adhesive sheets. Two coupons of each adhesive were exposed to 140°F water immersion, 140°F 100% RH and 140° dry air. The coupons were periodically weighed, and measured in micrometer jigs. The moisture expansion data for FM-73M are presented in Figure 5.

## 2.4 Anomalous Moisture Absorption in FM-73M

Figure 6 records the anomalous moisture uptake of FM-73M exposed to 100% RH at various temperatures in the region of the glass transition temperature,  $T_g$ .

The anomalous weight gain behavior in the 100°C and 82°C specimens appears to be controlled by a mechanism different from simple diffusion. It has been suggested that this anomalous moisture behavior is consistent with the saturation-level vs temperature hysteresis curve shown in the inset in Figure 6.

## 2.5 Residual Stresses in Bonded Joints

Residual stresses in an adhesive layer can be determined experimentally and calculated using finite-element techniques. When the stress distributions are uniform through the layers, they can be experimentally determined by material removal and trepanation techniques, as discussed in Ref. 15.

## 2.6 Thermomechanical Tests

Thermal expansion coefficient  $\alpha_T$ , and glass transition temperature,  $T_g$ , were obtained for dry and wet FM-73M adhesives of dimensions 0.5" x 0.25" x 0.035" using a Perkin-Elmer TMA apparatus, a model TMS 1 Thermomechanical Analyzer.

The expansion-temperature plot for dry and wet FM-73M are shown in Figure 7, which reveals dynamic transitions at 220°F and 195°F for dry and wet FM-73M, respectively. A correlation analysis of the corresponding temperature derivatives (expansion coefficients) gives  $T_g$  at 150°F and 120°F, respectively.

## 2.7 Creep Compliance Measurements

A dead-weight-loading creep frame with an LVDT elongation measurement system was used for creep compliance measurements of the variously conditioned FM-73M adhesive specimens. From this data, creep compliance master curves can be constructed.

A series of creep compliance curves were obtained at 2000 psi for dry and wet FM-73M over a temperature range between -54°C and above  $T_g$ . The data for wet FM-73M are presented in Figure 8. The creep data on dry FM-73M indicate a strong change in creep behavior between 60° and 72°C. This is consistent with the placement of the second order

glass transition temperature at 65°C from the TMA tests. The creep data on wet FM-73M (Fig. 8) indicate the presence of  $T_2$  between 43 and 57°C. This range is consistent with the value of  $T_g$  obtained from TMA testing at 49°C.

The creep compliance curves at various temperatures are shifted in compliance and time to form creep compliance master curves from which the viscoelastic response of the materials to other load histories can be calculated. Specifically, the creep compliance master curves are used to predict relaxation and dynamic behavior of the adhesive specimens and eventually the same behavior for the bonded joints.

## 2.8 Time Dependence of Poisson's Ratio

The two characteristic functions selected to describe the adhesive mechanical properties are  $D(t)$  and  $\nu(t)$ . Thus it is important to establish the time dependence, if any, of  $\nu(t)$  of the adhesive FM-73M for various environmental conditions, including temperature and moisture content.

Combining some of the good ideas of Heflinger et al. (Ref. 19) and those of Jones (Refs. 20,21), with additional innovative modifications, including the use of retro-reflective paint (Ref. 22), a novel laser/optical configuration has been developed to measure  $\nu(t)$  of compliant materials of dimensions  $3 \frac{1}{8}'' \times \frac{3}{4}'' \times \frac{1}{16}''$  loaded in a modified four-point bending configuration (Ref. 23).

When the deformation produced by four-point bending is observed by double-exposure holographic interferometry, the recorded fringes represent contours of constant out-of-plane displacement (Refs. 24 and 25). The strip deforms into a state of anticlastic curvature, and the fringes produced are two conjugate sets of hyperbolae with the Poisson's ratio,  $\nu$ , of the material related to the smaller asymptotic angle,  $\alpha$ , between the hyperbolae by the equation:

$$\nu = \tan^2 \frac{1}{2} \alpha. \quad (\text{Equ. 2})$$

Within experimental error of measuring the angle  $\alpha$  (about 2%), the  $\nu$  value at room temperature for dry FM-73M is determined to be 0.320 and is found to be time-independent, at least over a period of 30 days. This is true whether the differential load  $\Delta L$  is applied externally to the specimen, or whether the natural creep in the material is allowed to provide the differential motion in the specimen between the double exposures. Measurements are being planned at other temperatures and for different moisture contents.

## 2.9 Fatigue Testing of Neat Adhesives

The fatigue response of dry and wet FM-73M adhesive tensile coupons was measured for sinusoidal tension-tension loading over a broad temperature range.

A fixture adapted to a servo-hydraulic testing machine applies a 0-100-lb amplitude sine wave through a load cell to the 3-ply laminated adhesive specimens. The load cell provides a feed-back signal to a servo-amplifier and the load output to an X-Y recorder. A function generator, capable of providing both sine and square-wave outputs, provides the command signal to the servo system.

Deflection measurements are taken with an induction proximity gage which has a range of 0.100 inches and is linear to 0.5%, with good long-term stability. The output voltages of the load and deflection measuring systems are fed to an X-Y recorder with an automatic presettable pen-down control, which allows recordings to be registered at only pre-determined intervals. A typical load,  $F$ , -deflection,  $\delta$ , curve for wet FM-73M adhesive is shown in Figure 9.

## 2.10 Optical and SEM Analysis of Neat Adhesives

Fractographic examination of surfaces of failed coupons of FM-73M adhesive in both dry and wet conditions under fatigue loading, and of wet material under fatigue and single cycle to failure (static) conditions show about the same fracture topography in the mainly porous regions of the bulk adhesive. There is no evidence to indicate any change in fracture mode in the porous areas due to moisture.

The solid epoxy (dense area) of the wet material shows quite a different fracture pattern, however, appearing featureless, suggesting that the separation occurred in an uncured state in a cleavage type fracture mode (Fig. 10). This difference in the fracture topography of the dense epoxy regions between wet and dry FM-73M is the only effect of the moisture noted to date.

Optical and Scanning Electron Microscope (SEM) examination of the wet specimen surface exposed after metallographic polishing shows that the dense epoxy is cracked

with the tip of the cracks extending just beyond the dense material (Fig. 11). Radiating from the crack is a strained zone in the material which scatters and reflects light, much like that of a crazed area. An SEM photomicrograph of one of the lower crack extensions beyond the dense epoxy at 5000 magnification reveals that the crack in the porous bulk material has been stretched open, while the crack in the dense epoxy is still tightly closed.

### 3. STRESS ANALYSIS

#### 3.1 Application to an Adhesively Bonded Joint

The problem of the stress analysis of an adhesively bonded single lap shear joint has been approached on a classical mechanics basis by Goland and Reissner (Ref. 26) and more recently by Hart-Smith (Ref. 27). The latter solution describes the thickness averaged shear-load-transfer distribution and peel-stress effects that need consideration in the design of such joints for load-carrying purposes. In the study of fatigue properties of joints, we address a different problem: that of the stresses in the adhesive and their distribution throughout the adhesive thickness. It is also of considerable interest to look at the effects of moisture ingress and cure stresses on the cyclic loading response of the joint. Such changes in the adhesive properties would be very difficult to account for by a closed form solution. It is only with a flexible, numerical system, such as a sophisticated finite-element package, that these real-life effects can be easily and accurately analyzed.

The application of advanced finite-element techniques to an adhesively bonded specimen not only results in a realistic stress analysis but also allows the introduction of point-by-point material variations, as will occur in the adhesive under the influence of different environments, including moisture, temperature, and cyclic loading. Utilization of incremental loading with finite-element techniques may allow evaluation of the effect of non-linear viscoelastic behavior of the adhesive.

A complete viscoelastic characterization of the adhesives allows the computation of the adhesive joint's deformational response to loading over the full range of environments. The initial instrumented response of the single lap shear specimens provides a verification of the stress analysis program.

As the joints are fatigue cycles, the properties of the interlayer change and adhesive possibly degrades. Because the relationship between adhesive properties and the model joint's deformational response are previously determined by the numerical stress analysis, any change of degradation in the adhesive's properties are revealed by the mechanical response of the bonded joint. In this manner, degradation of the adhesive under fatigue loading and environmental conditions can be continuously monitored during testing, and any fatigue failure mechanism concerning degradation of the adhesive under the influence of cyclic loading can be possibly identified and quantified.

#### 3.2 General

A computer code capable of viscoelastic and material nonlinear stress analysis has been selected to model the thick-adherend, single-lap shear bonded joint. It is the MARC finite-element program and is being accessed through CDC Cybernet Service, Dallas, TX. MARC is a general-purpose finite-element program designed for the linear and nonlinear analyses of structures in the static and dynamic regimes.

A detailed elastic stress analysis of the joint using the MARC program has been developed using linear-strain quad (plane strain) elements, 1000 lb. load, and 2 grids - 1 and 4 elements through adhesive thickness. The presence of a stress singularity has been verified, with a high peel-stress gradient at the corner. A representative peel stress distribution obtained with the MARC program is shown in Figure 12.

The viscoelastic stress analysis procedure in the MARC program and its applicability to the analysis of the bonded joint have also been studied. Basically, MARC uses a limited model in the finite-element solution applying the material response of 1 Voigt element and 1 elastic spring in series to approximate the viscoelastic response of a material. The ability of this limited model to accurately depict the adhesive interlayer response over a time range of a few days has been verified.

#### 3.3 Analysis for Water Absorption and Desorption-Induced Stresses

The stresses in the bonded joint created by the expansion of the adhesive due to moisture absorption will be calculated by the finite element method using the MARC computer program. In calculating these stresses, use will be made of experimentally measured changes in the material properties that occur in the adhesive as moisture is absorbed. These property changes in the water-saturated adhesive can be accounted for



by specifying appropriate material properties for those elements in the adhesive affected by the water. The expansion of the saturated adhesive will be applied to the appropriate elements by way of free expansions. The MARC program will then calculate the residual stresses which are created.

The MARC finite element program contains a solid-body heat-transfer capability. This procedure can be used to solve a basic diffusion problem. Using this routine the moisture diffusion and distribution can be calculated by solving an analogous heat-transfer problem. The moisture absorption into the adhesive from the exposed edges is analogous to the heat-flow problem with temperature increase comparable to increases in moisture content. After calculating a particular temperature distribution for the adhesive, these results can be input into the thermal stress analysis procedure. Then using an appropriate coefficient of thermal expansion, the resulting stress distribution can be calculated. This process will allow the calculation of residual stresses created by moisture content.

Adhesively bonded joints in aircraft will be exposed to moisture and temperature cycles from flight and weather. These effects may be an important addition to the fatigue behavior of adhesively bonded joints. It would be desirable to model such cyclic thermal and moisture effects using the MARC program.

### 3.4 Cure-Shrinkage Stresses

In an effort to determine the total residual stress distribution in the adhesive prior to any cyclic loading, the curing process must be analyzed. As the adhesive stiffens a certain amount of contraction occurs in the material. If the adhesive can be characterized with regard to the rate of stiffening, the resulting residual stresses can be calculated in a manner analogous to that for free thermal expansions.

Additional stresses are created in the adhesive as the joint is cooled from the cure temperature to the test temperature. Although this appears on the surface to be just a typical thermal stress problem, it is complicated by the fact that the adhesive material properties change with temperature. This problem can be analyzed, however, using the thermal stress analysis routine in the MARC program. MARC allows the specification of temperature dependence for material properties. The variation of material properties with temperature is input in MARC as a piecewise linear curve. Having defined the thermal response of the material, the thermal stress problem can be solved.

### 3.5 MARC Viscoelastic Analysis

The MARC program can be used for both linear and nonlinear forms of analysis. In the problem of the adhesive bonded joint where material time dependence is involved, a viscoelastic analysis is appropriate. The MARC program calculates the viscoelastic strain rate for any time increment by considering the response of a simple Voigt element (spring and dashpot in parallel). This makes the strain rate a function of material stress and Voigt strain. Although the user must define the dashpot coefficient and the spring constant for the Voigt element, this data is provided through a user supplied subroutine and may be dependent on stress, temperature, or other properties. This allows a representation of a nonlinear Voigt element.

### 3.6 Summary

The stress-strain distribution developed in the adhesive interlayer of the model joint by various load environmental test conditions is thus being characterized by a suitable finite-element stress analysis using the MARC computer program. Included in the analysis will be the effects of cure and shrinkage stresses during specimen preparation; expansion and contraction due to moisture absorption and desorption; effects of bending stresses and time and temperature dependence of the constitutive relations defining the adhesive interlayer, and their relation to the measurable joint response parameters. Procedures will be developed to effect nonlinear analysis.

Iterative procedures between stress analysis and instrumented joint and adhesive material testing will be used to correlate the analytical and experimental results.

## 4. CYCLIC TESTING OF BONDED JOINTS

### 4.1 Relevant Methods of Cyclic (Fatigue) Testing

A recently concluded program on "Structural Properties of Adhesives" (Ref. 3) assesses and develops the tests and test methodology required to generate rigorous engineering property data at low cost on structural adhesives. This data includes, as a minimum, complete shear and tensile stress-strain response of the adhesive in a variety of environments. In addition, consideration is given to developing Poisson's ratio data and to developing a test method for determining combined effects of tension and shear.

This program also considered developing techniques for generating additional adhesive property data necessary for understanding the structural response of bonded joints. This included response to cyclic loading, creep behavior, and relaxation data under a variety of load and environmental conditions. Finally, the program generated data on several adhesive systems, including FM-73M, to demonstrate the utility of the procedures developed.

A test procedure, "Preliminary Test Specification for Characterizing the Shear (Tension) Fatigue Stress-Strain Response of Structural Adhesives" was developed for the determination of the tensile and shear fatigue stress-strain response of adhesives for application in fatigue design of load-bearing bonded assemblies (Ref. 3).

The recommended practice covers the determination of the fatigue shear and tension stress-strain response of structural adhesives, for various strain ratios, temperatures, relative humidities and frequencies, with the adhesive restrained by relatively high modulus adherends in a thin bondline. It is intended to be used to develop the shear and tension stress-strain response of adhesives for design of metal adherend bonded structures. Properties obtained include apparent shear (tension) modulus, maximum strain vs. cycles to failure and the general shape of the fatigue stress-strain response curve. This method can be used to evaluate environmental effects of the adhesive's shear and tensile response for various environmental conditions.

During the course of the program, a parallel-plate capacitive measurement device was recommended for use in the measurement of adhesive deformation in a thick-adherend model joint, and for various strain rates. Design and fabrication of this adhesive deformation measurement device were subsequently completed and test results were conducted therewith by the end of the program, but not in time for use in the "fatigue behavior" program. The results are reported in Reference 3 entitled "Design and Fabrication of the Adhesive Measurement Device".

#### 4.2 Fatigue Testing Equipment

Tension-tension fatigue testing of adhesively bonded single lap shear joints are conducted at a stress ratio,  $R$ , of 0.1 in the Ametek servo-hydraulic fatigue test machine (see Figure 13) on a 3000-lb. full-scale range. Displacement of the test joint is measured by means of a strain gage system (compliance gage) clipped to grooves milled into the slotted edges of the bonded joint. Load-displacement ( $F$  vs.  $\delta$ ) curves are recorded on a Hewlett Packard Model HP 7004B X-Y plotter. From these curves it is possible to monitor the change in the "effective modulus" (slope) as well as the size of the hysteresis loop of each individual cycle, to evaluate the effects of temperature, moisture level, loading waveform, frequency, and stress level on fatigue characteristics of the adhesive interlayer of the bonded joint.

Testing temperatures of  $-65^{\circ}\text{F}$  to  $+140^{\circ}\text{F}$  for FM-73M are obtained through the use of special environmental chambers surrounding the region between the clevises of the Ametek fatigue machine. The low-temperature environment is obtained by blowing vaporized liquid nitrogen into a polystyrofoam enclosure surrounding the region between the loading fixtures.

Two thermocouples are used to monitor and control temperatures; one to monitor temperature inside the milled notch of the bonded joint and the other in the chamber enclosure to activate the temperature controller valve. The compliance gage used to measure displacements is wrapped in thermal insulation to reduce the effects of temperature fluctuation on the sensitive, component strain gages.

The elevated temperature tests are conducted in a special test chamber, with temperature maintained to  $+3^{\circ}\text{F}$  by means of a recirculating fan and a Honeywell proportional temperature controller regulating the electrical resistance heat.

#### 4.3 Monitoring of Loads and Deformation Measurement

One of the key elements of the fatigue testing program is the accurate measurement of the instrumented model joint test specimen response to the loads imposed under the different temperature/moisture environments and relating this to the adhesive material characteristics.

Vought Corporation's program on "Rigorous Property Measurements of Adhesively Bonded Joints" (Ref. 3) evaluated at least two extensometer techniques to measure deformation in the model joint: the linear variable differential transformer (LVDT) concept and the air gap capacitor concept, for both the static and cyclic loading cases.

Accurate measurement of the adhesive deformation is difficult unless one can attach a measurement device at the adhesive bondline. Such a system, based on the LVDT

principle and using a three point pick-up on each side of the specimen and attached with the adhesive-adherend interface has recently been proposed by Krieger of American Cyanamid for measurement of deflections under static loads (Ref. 28).

An air gap capacitor device has also been evaluated by Renton of Vought Corporation and has recently been checked out for use on thick-adherend single lap shear joint specimens for both the static and cyclic loading cases (Ref. 3).

The environmental effects (temperature, humidity), the long term stability, and the dynamic response of these two systems are as yet somewhat undetermined. The standard clip compliance gage is used in the fatigue behavior program which was well underway before Renton's work was completed.

The strain of the joint in shear is measured with a compliance "clip" gage, similar to those commonly used in crack opening displacement studies, placed in the saw-cut in the retaining rail grooves (See Figure 14). This gage provides a direct measurement of the response of the adhesive to the loading imposed on it by the adherends. It also provides a method for recording the hysteresis and permanent set of the joint. This method provides the information of a "zero-gage-length extensometer" (Ref. 7) but is more resistant to the testing environments and thus provides more reliable information.

A comparison of this compliance gage measurement of load-deflection history to the response predicted in the MARC finite element stress analysis provides a measure of the change of adhesive properties during cyclic loading. The MARC program has been shown to be very successful in predicting the displacements in FM-73M, thick adherend joints (Ref. 29).

#### 4.4 Fatigue Testing Matrix

An assessment of fatigue mechanisms and failure modes in metal-to-metal joints is being made over a range of loads and environmental conditions experienced by modern high performance aircraft. The fatigue loading is, for the most part, constant amplitude in order that the results might be integrated with those of the other programs with the intent of eventually deriving a form of "cumulative damage" model, or for developing a methodology for predicting service life and for establishing criteria for accelerated testing of bonded joints and structures.

The model joint test program outlined herein consists of fatigue tests under combinations of environments intended to isolate and determine the individual and combined effects of load level, load rate, frequency, duration, temperature, and moisture content. The matrix for the constant amplitude fatigue tests of the model joints is shown in Table 1. The test program is specifically structured to identify failure mechanisms and changes in mechanisms.

Table 1. Model Joint Constant-Amplitude Fatigue Cycling Matrix

		T <sub>1</sub> (-65°F)		T <sub>2</sub> (RT)			T <sub>3</sub> (140°F)		
Moisture	Dry	M <sub>1</sub>	M <sub>2</sub>	Dry	M <sub>1</sub>	M <sub>2</sub>	Dry	M <sub>1</sub>	M <sub>2</sub>
FM-73		10 <sup>-4</sup>		10 <sup>-4</sup>	10 <sup>-4</sup>			10 <sup>-4</sup>	
		10 <sup>-2</sup> ~A <sub>1</sub>		10 <sup>-2</sup> ~A <sub>1</sub>	10 <sup>-2</sup> ~A <sub>1</sub>			10 <sup>-2</sup> ~A <sub>1</sub>	
	10 <sup>-2</sup>	10 <sup>-2</sup> ~A <sub>2</sub>	10 <sup>-2</sup>	10 <sup>-2</sup> ~A <sub>2</sub>	10 <sup>-2</sup> ~A <sub>2</sub>	10 <sup>-2</sup>	10 <sup>-2</sup>	10 <sup>-2</sup> ~A <sub>2</sub>	10 <sup>-2</sup>
		10 <sup>-2</sup> ∩		10 <sup>-2</sup> ∩	10 <sup>-2</sup> ∩			10 <sup>-2</sup> ∩	
		3	3	3	3	3		3	3
	30	30		30	30		30	30	30

- NOTES:
- o 3 specimens per condition
  - o 10<sup>-4</sup>, 10<sup>-2</sup>, 3, 30 are anticipated cyclic frequencies
  - o ∩, ∩ are loading waveforms
  - o ~A<sub>1</sub>, ~A<sub>2</sub> are different constant amplitude sinusoids
  - o All loads sinusoidal unless otherwise indicated
  - o Based on the static creep results on adhesive material with primary emphasis on the more severe conditions.



#### 4.5 Fatigue Testing Results

Table 2 shows some typical results of the "matrix testing" on dry and wet FM-73M-bonded joints.

Table 2. Test Data Summary of Model Joint Fatigue Cycling for Various Environmental Parameters

Joint No.	Conditioning		Temp. OF	Freq. Hz.	Wave-form	Max. Stress Psi	Cycles to Fail	Type of Failure
	Time(Mo.)	Environ.						
52A-9		RT/Dry	-65	.17	~	7200	75	Coh
49A-8			-65	1	"	6000	5719	Coh/Adh
49A-9			-65	.17	"	6000	2434	Coh/Adh
37A-8			78	.17	⌋	4800	39	
8C-8			78	1	"	4800	2871	Coh/Adh
8C-9			-65	.17	"	7200	20	Coh/Adh
8C-10			-65	.17	"	6000	960	Coh/Adh
33A-4			+140	.17	~	4800	2	Coh
33A-5			+140	.17	"	4000	81	Coh
45A-10			+140	.017	"	4000	39	Coh
C9-4			+140	1	⌋	4000	319	Coh
29A-12			+140	1	"	4000	70	Coh
29A-11			+140	.17	"	4000	13	Coh
42A-4	5.5	150°F/ Condensing Humidity	78	.017	~	4200	3	Coh
29A-6	5.5		78	.017	"	4000	10	Coh
C1-5	6.5		-65	.017	"	6000	21	Coh
C1-1	6.5		-65	.17	"	6000	150	Coh
C1-3	6.5		-65	1.0	"	6000	1099	Coh

Typical F- $\delta$  curves for dry and wet FM-73M-bonded joints are shown in Figures 5 and 6, respectively. A large permanent set with fatigue cycles, with little change in the "effective modulus", is evident in the "wet" joint. Moisture appears to significantly lower the fatigue life of a model joint.

Figures 15 and 17 show the different effects of the square wave loading as compared with sinusoidal loading for FM-73M bonded joints at room temperature. Analysis of such load-deflection plots to failure obtained at various temperatures up to 140°F indicates that a logarithmic relationship exists between temperature and fatigue life. Preliminary results also indicate that fatigue life varies linearly with frequency (within the stress range studied), as shown in Figure 18.

Cyclic testing has been conducted at the lowest frequency attainable, viz., 0.006 cpm, for the first one or two cycles of loading and unloading at low stress levels and different environmental conditions. The analytical prediction of these histories by use of the MARC finite-element-analysis computer program of the model joint is currently being formulated. The analytical prediction of the response of an adhesive coupon has already been described (Ref. 30).

Measurements are currently being made of the various characteristics of the load-deflection histories of the model joints with the possibility of relating these to the fatigue mechanisms occurring in the joints. For example, the area enclosed by each loading and unloading loop, which can be approximated by an ellipse, represents the energy dissipated per cycle, and for true rheological (reversible) behavior can be expressed in terms of the appropriate real and imaginary parts of the dynamic modulus. Also, the total strain at the midpoint of each loop as a function of time or cycle can be calculated, along with the instantaneous slope of the major axis of the hysteresis loop as a function of time or cycle. Variation of this slope with number of cycles can possibly be related to non-reversible mechanisms occurring in the joint.

Conducting hysteresis experiments at very low stress levels, combined with those at the higher stress levels, may provide a method for comparing the reversible rheological behavior as compared with non-reversible damage (cracking) behavior of the model joints. It may even be possible to quantify the damage near the unbonding or delaminating edge of the model joint with the percent of area of debonding of the adhesive interlayers of the model joint after specified loading histories at different frequency, temperature, and moisture levels. These analysis techniques are all currently being evaluated.

#### 4.6 Nonlinear and Long-Time Fatigue Effects

Additional joint tests are planned to obtain data which, when applied with data to

be generated for the corresponding neat adhesives in the task on adhesive materials characterization, will permit direct evaluation of nonlinear behavior as well as long-time creep behavior of environmentally conditioned joints. In general, a number of competing degradation processes will be occurring in joints under fatigue that can be represented by different activation energies corresponding to the appropriate Arrhenius rate equations. If the fatigue experiment is conducted over a short time scale, the failure will be representative of only the short-lived processes. Possible important long-lived processes, which characterize the real world in so far as long-term damage effects are concerned, will be undetected. Thus, extrapolation of testing data obtained on a short-time scale in the laboratory toward the prediction of long-term effects, may not be too meaningful. A number of long-term tests are being conducted to measure these important long-lived processes. The duration of these long-term experiments will be of the order of a few weeks or even months, as compared with those conducted to date over periods of a few hours to a few days.

#### 4.7 Other Studies of Fatigue Testing of Bonded Joints

Some cyclic fatigue testing of model thick-adherend, single-lap shear specimens has been conducted by Marceau et al. (Ref. 6). The adherends are of 2024-T3 aluminum, anodized by the BAC-5555 process, and the adhesive is an unspecified 250°F-cure system. The adhesive interlayer appears to not have been cut out in the slotted areas (see Figure 24) and the bonded joints appear not to have been preconditioned prior to testing. One of the two specimen configurations used was the thick-adherend, single-lap shear specimen for combined Mode I (cleavage) loading and Mode II (forward shear) loading. The stressed durability of bonded joints under sustained loads versus cyclic loads was studied for controlled environments and different loading modes. In addition, the effect of loading frequency on durability performance was investigated.

Both sustained loads and cyclic loads were applied to the bonded joints. Sustained stress tests were conducted using stressing fixtures activated by compressing a helical spring in a tensile tester, with the entire fixture placed in a 140°F/condensing humidity chamber. Time to failure was recorded for specimens that failed, and residual shear strengths at room temperature were obtained for those that did not.

Cyclic loading tests at 0.8 cph and 10 cph were conducted using cantilevered beams weighted to produce the desired stress,  $f_{max}$ , on the joints. The test specimens were enclosed in a 140°F/condensing humidity chamber. The load cycle profile for 0.8 cph was 1 hour at  $f_{max}$  and 1/4 hour at zero load, a test cycle developed by Bell Helicopter Tektron (Ref. 8). The 10-cph profile was 4 minutes at  $f_{max}$  and 2 minutes at zero load. For both the 0.8-cph and 10-cph cycles, the cyclic load profile was trapezoidal. Cumulative cycles to failure were recorded for each specimen, or residual shear strengths at room temperature were determined for those that did not.

Cyclic loading tests at 1800 cycles per minute (cpm) were conducted using a Wiedemann Baldwin Model SF-1-U fatigue machine at a stress ratio,  $R$ , of 0.06. Again, the controlled test environments were obtained by encapsulating each specimen in a small environmental chamber. The load cycle profile was sinusoidal and cycles to failure were recorded.

In general, the results of the sustained and cyclic tests show the following:

Room temperature lap shear (static) strengths are typical for the adhesive system tested, with failure occurring in the center of bond. There were no failures of lap shear specimens under sustained stress in the 140°F/condensing humidity environment during the 9-month test period. The residual tensile shear strength was determined under laboratory ambient conditions. All "static" failure modes were 100% cohesive, i.e., center of bond.

There was a slight increase in the average residual shear strength for those specimens stressed at 1200 and 1500 psi for the 9 months as compared to the baseline controls, and a progressive decrease in residual strength for those specimens stressed at 900 and 600 psi. The averages show a systematic relationship between the high-stressed and low-stressed specimen values. The differences and systematic relationship appear statistically significant, but would have to be verified by more systematic testing. Why this relationship should exist is not known, but it could relate to changes in the rheological properties of the adhesive when subjected to long-term sustained stresses and moist environmental conditions.

Test results for the three different cyclic load frequencies and 140°F/condensing humidity are shown in Figures 19, 20, and 21. The 0.8-cph frequency is the most severe and the 1800-cpm frequency is the least severe in terms of damage per cycle. On the basis of hours to failure versus stress, it is difficult to predict which frequency would produce failures the earliest, except that at low stress levels, it most likely would be the 10- and 0.8-cph frequencies. Extrapolation of the 1800-cpm curve suggests many more hours to failure at low stress levels. From Figure 20 it appears that the

slow cyclic tests are more damaging to the bondlines.

The 1800-cpm tests were also conducted in four different environments. The general trend seems to be that elevated temperature shortens the specimen life and humid air has no effect at these cyclic rates. At these high cyclic rates, the water had little chance to affect the adhesive because of the short exposure times involved before failure occurred. Had the specimens been presoaked long enough to saturate the bondline, or had the cyclic rate been substantially slower, the results may have been different.

## 5. POST-TEST EXAMINATION

### 5.1 Optical and SEM Analyses of Failed Joints

One of the more direct techniques of studying fatigue failure mechanisms in bonded joints is the use of the optical microscope and the scanning electron microscope (SEM) to interrogate the nature and topography of the failed joint surfaces.

The different techniques of viewing with the optical microscope, including dark-field illumination, bright-field illumination, and viewing in transmitted light, are used to advantage in studying fatigue degradation in bonded joints.

Photomicrographs are obtained with a JEOL Model JSM-35 SEM operating at 20 kv. The specimen of failed surfaces are carefully cut with a wafering saw to approximately 1 x 1 cm<sup>2</sup> and fastened to SEM mounting pegs with adhesive-coated, conductive copper tape. To enhance conductivity, a thin (~200Å) film of Au/Pd alloy is vacuum evaporated onto the samples. Photomicrographs are generally taken with the samples inclined at some specified angle to the incident electron beam, usually about 20°.

Optical studies of failed surfaces of FM-73M-bonded joints, both dry and those conditioned to approximately 9 months at 150°F and condensing humidity show two quite similar general features of failure, but with some important differences.

One general feature consists of an apparent primarily adhesive failure zone emanating from the high-stress region of the overlap, the so-called load-transfer edge. An example of this feature for a failed dry joint is shown in Figure 22c, labeled "A" and "B". This "adhesively failed" region is variously referred to herein as the "slow-crack-growth" region or the "fatigue-failed" zone and constitutes the fingernail feature described by Marceau et al (Ref. 6). The "missing" material at the bottom portion of Figure 22c constitutes the "slow-failed zone" on the other (mate) adherend. These two "slow-failed" regions are labeled A and B, respectively, in Figure 23.

The second general feature of the failed joint surfaces consists of the primarily cohesive failure zone between the aforementioned two symmetric slow-failed regions. This "cohesively failed" zone is also referred to herein as the "fast crack" zone or the "statically failed" region and generally occurs along the scrim plane parallel to and midway between the two adherend-adhesive interface planes, labeled CC<sup>1</sup> in Figure 23.

These two distinct features of failed surfaces are much more pronounced in the dry joint. In the wet joints, the "slow growth" zone, although still recognizable, is smaller in extent, and, generally, appears interspersed with small cohesive failure zones (Fig. 22b).

The second main feature of the wet failed joint surface, viz., the fast-growth cohesive zone, extends over a correspondingly larger area of the overlap than for the dry joint. Some small adhesive failure regions are found to dot the primarily cohesive failure region (Fig. 22b). This same topography is evident in the dry joints fatigued at low frequency (0.17 Hz) and at high temperature (140°F) (e.g., Figure 22a).

Optical study of the fracture surface reveals that, as the stress is reduced, the size of the adhesive-interfacial delamination region increases. (Figures 22b and 22c). Correspondingly, the number of cycles to failure increases with decreasing load, as expected (Figures 22c and 22d).

The extent of the "slow crack growth" region also decreases with decreasing frequency of cycling. In the examples cited in Figure 22, the low cycle failures (at 0.17 Hz) exhibit only a very small "slow crack growth" region, with the joints appearing to fail almost entirely in the cohesive mode (Figures 22a and 22b).

The above-described dependence on cyclic frequency of the slow and fast crack growth regions has also been observed by Marceau et al. (Ref. 6). They observe both features in the fast cycle (30 Hz) specimens, but no evidence of its zone of slow crack propagation for the slow cycle (~1 cph) specimens and the sustained load specimens, as indicated in Figure 24.



SEM examination shows a mixture of adhesive-delamination and cohesive failure occurring in the fatigue-cracked zone in some cases (Figure 25). The statistically failed region consists of a cohesive matrix failure with tearing away from the randomly oriented reinforcing dacron fibers. There is a difference in the texture of the interfacial failure in the slow (fatigue) and fast (static) crack growth zones. The texture of the fast crack zone shows a large portion of tear failures that progress into the interior of the adhesive.

Extremely high magnification (10,000X) SEM examination of the fatigue surface formed by slow crack growth (Figure 26a) does not reveal any of the fatigue striations commonly found in metal fractures. This is also noted by Sutton (Ref. 31). However, it is possible that the thin sputtered-gold coating, vacuum-deposited uniformly on the non-conducting adhesive surface during sample preparation for SEM analysis, does not highlight fatigue striations in the same manner as does chromium-shadowing, used in transmission electron microscopy (TEM). Thus, fatigue striations may be present, but another technique would have to be developed to display them.

SEM analysis of the matrix material surrounding the reinforcing fibers in the cohesively failed region (Figures 26b and 26c) show many small nucleating dimples on the matrix surface and tear ridges adjacent (left side, Figure 26b) to the dacron fibers.

## 5.2 Direct Measurement of Crack Growth

Attempts to monitor adhesive-delamination crack growth optically during fatigue testing, as in da/dN measurements for metals, proved unsuccessful, even with a 45X Gaertner creep microscope. Since the bondline is loaded primarily in shear, the crack opens up very little, and it is difficult to discern the crack tip from the line formed by the junction of the adhesive and adherend. Use of red penetrant dye-check to accentuate the fatigue crack as it progresses also proved unsuccessful because of smearing.

## 5.3 Optical Analysis of Adhesive Interlayers after Adherend Removal by Etching

A relatively simple technique of studying fatigue damage mechanisms in bonded joints involves removal of the adherends after fatigue cycling in the following manner. A series of initially "identical" bonded joint specimens are cycled to progressively larger total number of cycles. The bonded joints are subsequently sacrificed to remove intact the corresponding adhesive interlayers. This is accomplished by adherend etching removal of the aluminum by concentrated, 12N, hydrochloric acid in the overlap area, leaving bare the corresponding adhesive interlayer, (Ref. 30). The intact adhesive interlayers contain a permanent record of the fatigue damage sustained during joint cycling and can be examined at leisure by any number of suitable analysis techniques to extract information on the fatigue degradation mechanisms.

This technique proves especially valuable in studies involving translucent adhesives, such as FM-73M, which can readily be studied optically by transmission microscopy to elucidate damage features on both the exposed surfaces and at various depths within the volume of the interlayer.

Use of microtoming techniques, common in the analysis of biological specimens, with and without negative staining (Ref. 32), can further enhance the usefulness of the technique in studying details of the internal damage effects.

The adherend etching technique thus reveals internal damage within the volume of the delamination zone. The translucence of the FM-73M adhesive interlayer reveals internal failure mechanisms by transmitted light. As shown in Figure 27, sub-surface cracks originate at the dacron reinforcing matte fibers initiating from the high-stress edge. The heaviest concentration is adjacent to the milled notch in the aluminum adherends. These internal cracks are not necessarily continuous, with some isolated cracks forming in advance of the coalesced internal crack front (Fig. 27b). Internal voids in the adhesive sometimes act as stress raisers causing cracks to form, whereas other voids had no effect (Figure 27c).

SEM examination of the interfacial-adhesive, surface delamination zone above the zone of internal cracking in the dry joint does not reveal any evidence of fracture topography directly relatable to the random internal cracking occurring below it. Apparently, the internal cracks weaken the interfacial bond and cause subsequent interfacial delamination to occur.

## 5.4 Effect of Cycling Duration and Humidity

Through sacrifice of a number of joints in a series of fatigue experiments maintaining constant conditions but varying the number of cycles, N, for example, the progression of the above-described internal volume damage initiating from the high-stress edges of

the overlap into the center of the joint can be permanently recorded and studied. In fact, the condition of the internal damaged region just before failure can be estimated from observation of the portion of the interlayer on the adjacent side of the slot to the failed region, where the stress fields are somewhat similar.

In two series involving dry and wet FM-73M model joints, transmission photographs graphically display the progress of the internal damage in the high-stress edges of the overlap (Regions A and A<sup>1</sup> in Figure 23) with increasing N values of 10,000, 15,000, and 20,000 cycles and at failure at 27,000 cycles.

Measurements of the average extent of the internal damaged region from the lap edge,  $\bar{\ell}$ , termed the advancing damage length, are plotted in Figure 28 against the respective N values. The curves, showing the dependence of advancing damages length on number of fatigue cycles for dry and wet joints have shapes reminiscent of the da/dN plots for fatigue crack propagation in metals. As indicated in Figure 28, the damage is greater for the wet joint than for the dry joint at the same number of cycles, N.

A distinction must be made here between the adhesive-delamination zone, which is pronounced in the dry specimens and characterized as the fingernail feature herein and by Marceau et al. (Ref. 6), and the internal cracking phenomena around the matte dacron scrim fibers within the central plane of the interlayer volume, quantified herein as the internal damage length,  $\bar{\ell}$ . Both originate at the load transfer edges and proceed toward the center of the overlap but apparently at different rates depending on whether the joint is initially dry or wet. Although these two dimensions appear to be approximately the same for the dry joint, the fingernail feature is of much smaller dimensions or extent when compared with the internal damage for the corresponding wet joint. The reasons for this are as yet unknown. Thus, when a measurement of "crack length" is made on the intact joint during fatigue cycling, as with a traveling microscope trained on the side of the overlap, the measurement is not necessarily of the internal cracking damage length,  $\bar{\ell}$ .

#### 5.5 Chemical Surface Analysis of Failed Joints

Scanning electron microscopy (SEM), X-ray energy dispersive spectrometry (XES), and X-ray photoelectron spectroscopy (XPS) are indispensable tools for the analysis of the nature, topography, and chemical and elemental structure of the surfaces of failed joints. With these techniques, it is possible to examine surface effects and surface phenomena in great detail.

Detailed physical and chemical surface characterization of failed adhesively bonded joints, guided by qualitative fracture mechanics theory, constitutes a semi-empirical method to elucidate adhesive bonding phenomena.

An XPS spectrometer measures the kinetic energy of the X-ray ejected electrons from the parent atom or molecule and produces a spectral plot of the electron intensities at binding energies in the 0 to 1-keV range. Qualitative identification of the atoms associated with observed binding energies is obtained from tables listing the multiple binding energies for each atom. In addition to the elemental composition of the sample, the XPS spectra display chemical shifts, giving the chemical state of the atoms and molecular-structure information. Furthermore, when an ion gun is used to sputter off surface layers of the sample, XPS spectra can be obtained as a function of depth into the sample, yielding elemental and chemical depth distributions.

In one recent adhesive bonding program involving a series of experimental polyimides (Ref. 33), surface analysis by SEM/XES has shown effects on fracture surfaces of adhesive formulation, process, and test variables. In a companion study on various fluoropolymer joints (Ref. 34), the results are explained in terms of the elastic modulus and fracture work in the failure zone. XPS analysis shows a small amount of fluorocarbon transfer to the adhesive. The combination of SEM and XPS shows cohesive failure in two different fluoropolymer formulations, with one separating closer to the interface and with relatively little deformation.

Interpretation and correlation of joint testing and SEM/XES results are shown to be facilitated by reference to qualitative fracture mechanics theory. This approach identifies: inherent flaws, viscoelastic and plastic deformation, crazing and crack propagation, and interfacial failure as the main factors contributing to overall strength. Changes in parameters of adhesive formulation processing, and joint testing alter the proportions of each of these failure mechanisms. Results from SEM combined with XES suggest that, in some cases, useful estimates of the thickness of residual adhesive layers may be made.

In another study (Ref. 35), SEM of the fracture surface of a simple epoxy resin (Epikote 828) revealed important variations in fracture surface features as a function

of differing amounts of curing agent, in this case diaminodiphenyl-methane.

Failed surfaces of the dry and wet FM-73M model joints, adhesive interlayers obtained after adherend etching, and neat adhesive specimens were analyzed at Vought Corporation with a PHI Model 548 XPS unit (Ref. 29). The XPS spectra display the ever-present O 1s, N 1s, and C 1s peaks (see, e.g., References 23 and 35).

Both the unspattered and spattered spectra of FM-73M adhesive interlayer display Cl peaks, probably due to the HCl etchant. In addition, the spattered adhesive interlayer spectrum (Fig. 29) shows Al peaks, which high-resolution analysis reveals the oxide of aluminum rather than metallic aluminum. This is tentatively attributed to a portion of the oxide layer produced on the Al adherend during the phosphoric-acid anodize treatment. Evidently, some of this oxide remains on the adhesive interlayer after the adherend etching process (Ref. 37).

## 6. MODEL DEVELOPMENT

### 6.1 Introduction

The strength of a joint is usually defined in terms of its load-carrying capability. It depends, in turn, on the geometry of the joint and the local stresses induced in the bondline as a result of the applied mechanical loads, whatever their origins may be. (Ref. 38)

### 6.2 Bulk Effects

Stresses set up in the adhesive interlayer may arise from a number of different mechanisms: from adhesive curing kinetics and resultant adhesive shrinkage; from expansion and contraction of the adhesive interlayer due to moisture absorption and desorption, respectively; from temperature differentials between the metal adherends and the predominantly dielectric adhesive; from chemical reactions that could occur between absorbed moisture and the adhesive; from swelling in water of resins containing imbedded crystals of various ionic and non-ionic substances (see, e.g., Ref. 39); and from temperature excursions in the adhesive occurring during fatigue cycling. On the basis of the foregoing, it is apparent that two important general considerations must be accounted for in studying fatigue degradation in adhesively bonded joints. First, the rheological properties of the adhesive material per se, must be delineated as a function of the important ambient environmental parameters, including temperature, humidity, and cyclic loading. Second, the distribution of stress in a bonded joint must be computed and analyzed in conjunction with the ambient environments in order to predict the onset of joint failure.

One of the difficulties in determining moisture degradation of adhesively bonded joints arises from geometry effects, only a small portion, namely the ends and sides, of the adhesive material of a joint is exposed directly to moisture which upon plasticization might inhibit further moisture ingress. Another complicating factor is the parabolic stress distribution along the lap length in, for example, lap-shear specimens upon plane stress loading, as predicted by the well-known Goland and Reissner derivation (Ref. 26). This gives rise to the most severe stresses at the ends of the joint so that the center portion of the adhesive contributes very little to the total load carrying capacity of the joint. Unless these high stresses are relieved, e.g. by plastic deformation, local brittle fracture of the adhesive can occur. A crack once started at the joint end propagates rapidly and can result in brittle failure of the entire joint at a relatively low average-stress level below the strength of the adhesive unless plastic or viscoelastic response to these shearing stresses is available. On the other hand, if such response to shearing stress is too efficient, the joint will fail at a relatively low load level from the accumulated shearing deformation itself.

### 6.3 Interfacial Effects

In a discussion of the importance of the rheological properties of the bulk adhesive interlayer in the determination of fatigue degradation mechanisms, mention should also be made of the role of interfacial effects. Certainly in the "static" loading studies of Gledhill and Kinloch (Ref. 40), the data strongly suggest that the loss in joint strength of a mild-steel butt joint cemented with a simple epoxy after immersion in water results from the adverse affect of water on the interface, or interphase, rather than on the bulk properties of the adhesive. Their experiments involved strength measurements of butt joints and of the bulk "neat" adhesive itself over a large range of moisture uptake (up to 2500 hours of immersion time) and over a wide range of temperatures (up to and exceeding the glass transition temperature,  $T_g$ , of the adhesive).

Pre-failure and post-failure analysis of the surfaces were conducted by electron probe microanalysis, X-ray diffraction, and by scanning electron microscopy for



identification of chemical corrosion products and for locus of failure details. Their studies show that water ingress in a joint results in an absorbed water layer at the interface, which changes the interfacial thermodynamic work of adhesion from a positive value to a negative value ("spontaneous debonding"), and this provides the driving force for the displacement of the adhesive on the metal oxide surface resulting in joint-strength degradation. Their data indicate that if a joint is subjected to a humid environment, there is a progressive encroachment into the joint of this debonded interface that has the effect of progressively reducing the joint strength and also of progressively changing the locus of failure from cohesive within the dry adhesive region to interfacial between the "wet" adhesive areas and the substrate. The rate of this debonding is controlled by the availability of water at the interface, which is governed by the diffusion of water (with activation energy  $\sim 32\text{ kJ/mole}$ ) through the adhesive. The rate of interfacial debonding is greatly increased above  $T_g$ , and possible chemical degradation of the adhesive occurs at this high temperature. Corrosion is also shown to occur in the debonded substrate region as the initial ferric oxide ( $\text{Fe}_2\text{O}_3$ ) is converted to magnetic iron oxide ( $\text{Fe}_3\text{O}_4$ ) in the presence of water.

A work-of-adhesion model has been modified at General Dynamics to predict the relative environmental stability of an adhesively bonded system in any liquid, including water, and in air. This is described in detail in Reference 41. Defined in the three-phase model are: a locus (straight line) of effective bond coordinates in the wettability diagram on which the bond stability is unchanged; regions on either side thereof where the interfacial bond is more stable and less stable, respectively, upon water immersion; a locus (circle) of liquids for which the bond stability is the same; and a locus (circle) encompassing the adhesive bond coordinated within which the liquid immersant will cause spontaneous debonding of the joint. This model predicts environmental stability criteria described by a current fracture mechanics model of moisture stability of adhesively bonded systems (see, for example Ref. 42) and additional criteria.

In another study involving the application of a combination of static stress and solvolysis to tapered double cantilever beam (TDCB) specimens containing a precrack, it was shown experimentally that true interfacial failure is possible (Ref. 43). Furthermore, it was shown that while rapid cracking of the epoxide bond of the TDCB specimen results in center of bond failure, slow crack extension in a humid environment, or liquid water, can take place at the interface.

Whereas this interfacial effect may be operative in the static loading case in the predominantly Mode I loading examples of the butt joint and stress-solvolytic cracking study cited above, it is not possible to generalize its importance in the cyclic loading case in the predominantly Mode II loading example of the model lap shear joint.

Two excellent review articles on various aspects of environmental failure of structural adhesive joints are presented by Wake (Ref. 44) and Kinloch (Ref. 45).

#### 6.4 Fatigue Degradation Mechanisms

Adhesives fail in fatigue. They do so, in analogy with more well-studied metals, because of a cycle-by-cycle accumulation of damage resulting from repeated non-elastic strain. This non-elastic strain is influenced by frequency of loading, temperature, humidity, and time (viscoelastic) effects. After a sufficient number of stress (strain) applications, numerous micro-cracks form, grow incrementally, and eventually propagate in an unstable manner, resulting in specimen failure. Fatigue failure is, therefore, an important consideration in the design of structural bonded components.

An important goal of the program on fatigue behavior of adhesively bonded joints is the development of a model to describe the fundamental mechanisms of fatigue degradation and to identify the dominant failure mechanisms of structural adhesive joints in aircraft service environmental regions. To accomplish this, the results of all six tasks, experimental and analytical, are being effectively integrated to identify the separate effects of the individual environmental parameters, including temperature, moisture, and cyclic loading, and also, if possible, to identify the synergistic effects of combinations thereof.

The results of researchers studying damage mechanisms in other adhesive systems and bonded joints are being surveyed for comparison. For example, the damage mechanisms proposed by Sutton (Ref. 31) for an epoxy are not unlike those found for FM-73M. Photomicrographs of the fatigue fracture surface in Sutton's adhesive tensile coupons reveal no observable fatigue striations but show a rough hackle, whose features are roughly one or two orders of magnitude larger than the average growth per cycle. This lack of fatigue striations was noted in unfailed FM-73M joints in the "fatigue behavior" program (Ref. 30). The rough surface hackle is also characteristic of failed surfaces of FM-73M observed in the current program. In addition, the presence of cleavage-like or branch cracking mechanisms (river markings) in failed epoxy recorded by Sutton and others have been

observed in the "fatigue behavior" program.

The two different fracture modes observed by Marceau et al. (Ref. 6), one type in fast cyclic tests (30 cps) and the other type in the slower cyclic rate tests and in the sustained load tests, have also been observed in the "fatigue behavior" program. In the former case, a fingernail-fatigue-type pattern initiates in the bondline at the load transfer edges, then slowly propagates adhesively towards the center of the overlap with fatigue cycling, after which the failure mode changes and ultimate fracture occurs cohesively and instantaneously over the remainder of the joint. In the latter case (slow cyclic and static tests), the fracture is virtually entirely in the center of the bond in the cohesive mode. Figure 24 shows the two fracture modes observed for fast and slow cycling. Figure 23 herein shows schematically the fracture mode for fast cycling.

An example of the fast cyclic case in FM-73M model joints is reported in Reference 30. In the example cited therein, variation with cyclic frequency of the penetration length of the adhesive mode of failure initiating from the bondline at the load transfer edges was reported. This penetration length varied approximately inversely with the cyclic frequency.

The following explanation of the observed failure modes in thick-adherend model joints with FM-73M adhesive as a function of various environmental conditioning and testing parameters is advanced at this time: No matter what environmental conditioning or environmental testing conditions the bonded joint experiences, a main feature of damage in the interlayer is the initiation of small internal cracks around the individual matte fibers of the dacron scrim layer starting from the high-stress edge of the overlap and progressing towards the center of the joint along the matte scrim plane. With fatigue cycling, more fibers become the centers of these small internal cracks which coalesce to form larger internal cracks propagating into the center of the joint along the matte scrim plane, thus weakening the joint. The following different situations occur:

#### Dry FM-73M Joint, Room-Temperature Case

In addition to the scrim plane cracking phenomenon occurring during fatigue cycling, the high peel and shear stresses operative along the overlap edge are probably instrumental in the initiation of the delamination which propagates along the adhesive-adherend interface, probably along the aluminum-oxide-primer interphase, giving the fingernail feature described earlier. As this interface cracking proceeds, a point is reached when the competing cracking in the scrim plane has weakened the material sufficiently so that a change in mode to cohesive failure occurs along the scrim plane.

This interfacial delamination increases with decreasing fatigue load level and increases with increasing fatigue frequency. In the low-frequency limit, i.e., the static loading case, this interfacial delamination is almost non-existent so that static cohesive failure occurs along practically the entire scrim plane.

#### Wet FM-73M Joint

Even in the 9-month-environmentally conditioned specimens, the FM-73M adhesive interlayer is plasticized to a high degree with even the driest (central) section of the overlap at approximately 80% of saturation (See Figure 2). During the course of this 9-month conditioning (at 150°F, condensing humidity), it is even possible that moisture has ingressed along the matte-dacron-fiber, modified-epoxy-resin interface starting at the high-stress overlap edge enough to weaken the structure along and close to this overlap edge (cf Wake's wicking phenomenon, Ref. 44). Thus, no matter what the environmental testing parameters are, the joint fails almost entirely in the cohesive mode along the plasticized fiber-resin plane. That this wicking phenomenon is occurring is supported by the following observation:

Removal of the adhesive interlayer by the adherend etching technique of a 21-month-moisture-conditioned specimen reveals optical capacity of the fiber-epoxy interface similar to that observed by Wake (Ref. 44) signifying a refractive index change arising from moisture ingression at this interface. At this moisture level, the specimen is almost completely saturated (See Figure 2).

Model development of fatigue degradation mechanisms in bonded joints continues. In the interim, the following conclusions can be drawn.

#### 6.5 Interim Conclusions

FM-73M adhesive material displays time- and temperature-dependent behavior. FM-73M absorbs water in an anomalous manner, with approximately 3% saturation at 60°C (140°F) and 12% saturation at 100°C (212°F). Moisture plasticizes FM-73M and lowers T<sub>g</sub> approximately 40°F with less than 30% neat strength reduction. The Poisson's ratio at

room temperature of dry FM-73M appears to be time-independent over a one month period.

Many similarities are being noted between neat adhesive and bonded joint fatigue behavior; e.g., displaying lower stiffness at high temperature and load-deflection hysteresis losses varying with temperature, moisture and loading frequency, and wave shape. The bonded joints have their own non-uniform stress distributions and, since the first approximation analyses have assumed linear behavior, care must be exercised in making "correlations" at this time. The adherend etched joints reveal "crazed" or "cracked" regions that verify the approximate analytical stress distributions, and these damaged regions precede and accompany the contiguous cracks. The measured joint compliance change is due in part to crazing and crack growth which constitutes irreversible damage. Certainly one major mechanism of fatigue damage is crack growth whose growth rate is sensitive to temperature, moisture, loading frequency, and wave shape.

#### 6.6 Phenomenological Model

An approach to development of a phenomenological model of cumulative damage to relate, where possible, the observed cyclic fatigue degradation effects, dominant fatigue mechanisms with the service environmental regimes, including cyclic mechanical load, temperature and humidity, is currently being considered.

One form of the phenomenological model could be based on the approach proposed by Halpin et al. (Ref. 47), which involves a representation of accelerated aging effects occurring in combined environments, i.e., the cumulative damage effects of mechanical (M), thermal (T), or environmental (C = chemical or corrosion) stresses, where M is static or cyclic, in the form

$$\phi = \exp (-Kt^b/a_t a_M a_C) \quad (\text{Equ. 3})$$

where

$\phi$  = cumulative degradation function  
 $t$  = exposure time  
 $K$  = a system constant  
 $a_t, a_M, a_C$  = time shift factors relating to respective thermal, mechanical, or chemical effects  
 $b$  = a time exponent

Ultimately it is intended, if possible, to relate the cumulative damage index in terms of the spectral fatigue loading i.e., in terms of the series of individual load spectra consisting of a range of constant amplitudes at the various (cyclic) frequencies. If such a cumulative damage procedure is developed for spectral fatigue, failure criteria can be developed for real environmental loading conditions.

#### REFERENCES

1. Contract F33615-76-C-5220, "Fatigue Behavior of Adhesively Bonded Joints", sponsored by USAF AFML/MBC Wright-Patterson AFB, Ohio 45433, and conducted by General Dynamics' Fort Worth Division, July 1976 - March 1980.
2. Contract F33615-76-C-5224, "Structural Properties of Adhesives", sponsored by USAF AFML/MBC Wright-Patterson AFB, Ohio 45433, and conducted by Vought Corporation, Advanced Technology Center, Inc., Dallas, Texas, May 1976 - May 1978.
3. Renton, W. J., Structural Properties of Adhesives, Vol. 1, Final Technical Report, AFML-TR-78-127, Wright-Patterson AFB, Ohio, December 1978.
4. Schjelderup, H. C., A Compilation of Mechanical Property Data FM-73, Task 610 and Part of 609, Douglas Aircraft Co., McDonnell Douglas Corp. Data Report No. MDC-J6074, 28 September 1977.
5. Contract F33615-75-C-3016, "Primary Adhesively Bonded Structure Technology (PABST)", sponsored by USAF AFFDL/Wright-Patterson AFB, Ohio 45433, and conducted by Douglas Aircraft Co., McDonnell Douglas Corp., Long Beach, California, March 1975 - December 1978.
6. Marceau, J. A., McMillan, J. C., and Scardino, W. M., "Cyclic Testing of Adhesive Bonds", 22nd National SAMPE Symposium, San Diego, California, 26-28 April 1977.
7. Frazier, T. B., "A Computer Assisted Thick Adherend Test to Characterize the Mechanical Properties of Adhesives," SAMPE Tech. Conf. Series, 16, 1970, 71-88.



8. Frazier, T. B., and Lajoie, A. D., Durability of Adhesive Bonded Joints, Technical Report AFML TR-74-26, March 1974.
9. Boeing Process Specification, BAC 5555, "Phosphoric Acid Anodizing of Aluminum for Structural Bonding", Rev. B, Jan. 28, 1975.
10. Douglas Aircraft Co., McDonnell Douglas Corp., Long Beach, California, "PABST Alert Technical Bulletin", October 31, 1975.
11. Douglas Aircraft Co., McDonnell Douglas Corp., Long Beach, California, "PABST Technical Bulletin No. 1", March 28, 1975.
12. FM 73 Adhesive Film, Data Bulletin BPT 20B, Cyanamid Bloomingdale Aerospace Products, Havre de Grace, Maryland 21078.
13. Chang, F. H., Flynn, P. L., Gordon, D. E., and Bell, J. R., Determination of Adhesive Bondline Quality by Ultrasonic Techniques, General Dynamics' Fort Worth Division Report ERR-FW-1664, December 1975.
14. Life Assurance of Composite Structures, Vol. 1 Moisture Effects, General Dynamics' Fort Worth Division Report AFML-TR-75-51, May 1975.
15. Quarterly Progress Report No. 5 (1 July to 30 September, 1977), Fatigue Behavior of Adhesively Bonded Joints, General Dynamics' Fort Worth Division Report FZM-6697, October 1977.
16. Carter, H. G., and Kibler, K. G., "Rapid Moisture-Characterization of Composites and Possible Screening Applications", J. Comp. Mtls., 10, 1976, 355-370.
17. Heer, E. and Chen, J. C., "Finite Element Formulation for Linear Thermoviscoelastic Materials", JPL Technical Report, 1 June 1969, 32-1381.
18. Quarterly Progress Report No. 2 (2 October to 31 December 1976), Fatigue Behavior of Adhesively Bonded Joints, General Dynamics' Fort Worth Division Report FZM-6633, January 1977.
19. Heflinger, L. O., Wuerker, R. F., and Spetzler, H., "Thermal Expansion Coefficient Measurement of Diffusely Reflecting Samples by Holographic Interferometry", Rev. Sci. Instr., 44, 1973, 629-633.
20. Jones, R., "Strain Distribution and Elastic-Constant Measurement Using Holographic and Speckle-Pattern Interferometry", J. Strain Anal., 9, 1974, 4-9.
21. Jones, R., and Bijl, D., "A Holographic Interferometric Study of the End Effects Associated with the Four-Point Bending Technique for Measuring Poisson's Ratio", J. Phys. E: Sci. Instr., 7, 1974, 357-358.
22. Fagan, W. F., and Waddell, P., "The Non-Stroboscopic Visualization of Vibrational Patterns by Real-Time/Time Averaged Hologram Interferometry", Proc. Symp. Eng. Appl. Holography, SPIE Publ., 1972.
23. Quarterly Progress Report No. 4 (1 April to 30 June 1977), Fatigue Behavior of Adhesively Bonded Joints, General Dynamics' Fort Worth Division Report FZM-6679, July 1977.
24. Yamaguchi, I. and Saito, H., "Application of Holographic Interferometry to the Measurement of Poisson's Ratio", Jap. J. Appl. Phys. 8, 1969, 768-71.
25. Bijl, D., and Jones, R., "On Tri-Hologram Interferometry and the Measurement of Elastic Anisotropies Using an Adapted Form of Cornu's Technique", Proc. Int. Symp. Holography Applications de l' Holographie (Laboratoire de Physique General et Optique, Universite' de Besanson), 1970.
26. Goland, M., and Reissner, E., "The Stresses in Cemented Joints," J. Appl. Mech. 11, 1944, A17-A27.
27. Hart-Smith, L. C., Adhesive-Bonded Single-Lap Joints, NASA CR-11236, January 1973.
28. Krieger, R. B., Jr., "Stiffness Characteristics of Structural Adhesives for Stress Analysis in Hostile Environment", American Cyanamid Company Bloomingdale Plant, Havre de Grace, Maryland, presented at Albuquerque, N.M., SAMPE Meeting, October 1975.

AD-A068 806

ADVISORY GROUP FOR AEROSPACE RESEARCH AND DEVELOPMENT--ETC F/G 13/5  
BONDED JOINTS AND PREPARATION FOR BONDING.(U)  
MAR 79

UNCLASSIFIED

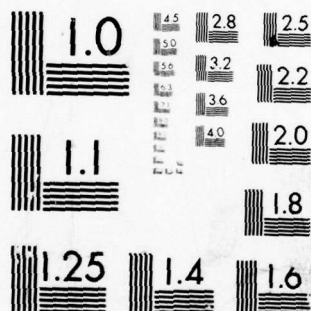
AGARD-LS-102

NL

2 OF 4

AD  
AO 88806





MICROCOPY RESOLUTION TEST CHART  
NATIONAL BUREAU OF STANDARDS-1963-A



29. Quarterly Progress Report No. 8 (1 April to 30 June 1978) "Fatigue Behavior of Adhesively Bonded Joints", General Dynamics' Fort Worth Division Report, FZM-6773, July 1978.
30. Quarterly Progress Report No. 6 (1 October to 31 December, 1977), Fatigue Behavior of Adhesively Bonded Joints, General Dynamics' Fort Worth Division Report FZM-6717, January 1978.
31. Sutton, S. A., "Fatigue Crack Propagation in An Epoxy Polymer", Engng. Fract. Mech. 6, 1974, 587-595.
32. Urry, D. W., "SEM and EPM in Biomedical Research", Research/Development, August 1976, 25-34.
33. Dwight, D. W., Counts, M. E., and Wightman, J. P., "Surface Analysis and Adhesive Bonding. II. Polyimides", Recent Advances in Colloid and Surface Science, M. Kerker, editor, Academic Press, 1977.
34. Dwight, D. W., "Surface Analysis and Adhesive Bonding, I. Fluoropolymers", J. Colloid and Interface Sci., 1977.
35. Selby, K. and Miller, L. E., "Fracture Toughness and Mechanical Behavior of an Epoxy Resin," J. Mat. Sci., 10, 1975, 12-24.
36. Romanko, J., Environmental Stability of Adhesively Bonded Systems, General Dynamics' Fort Worth Division Report ERR-FW-1650, 28 November 1975.
37. Romanko, J., "Surface Analysis of Failed Adhesively Bonded Joints", Southwest Electron Spectroscopy User's Conference, University of Texas, Austin, Texas, 2 June 1978.
38. Sharpe, L. H., "The Interphase in Adhesion," Aspects of Adhesion, 7, Transcripta Books (London), 1973, 139-151.
39. Fedors, R. F., "A New Mechanism of Failure in Polymers," Polymer Letters Edition 12, 1974, 81-84.
40. Gledhill, R. A., and Kinloch, A. J., "Environmental Failure of Structural Adhesive Joints," J. Adhesion, 6, 1974, 315-330.
41. Romanko, J., Environmental Stability of Adhesively Bonded Systems, General Dynamics' Fort Worth Division Report, ERR-FW-1650, 28 November 1975.
42. Kaelble, D. H., "A Relationship Between the Fracture Mechanics and Surface Energetics Failure Criteria," J. Appl. Polymer Sci., 18, 1974, 1869-1889.
43. Patrick, R. L., Brown, J. A., Verhoeven, L. E., Ripling, E. J., and Mostovoy, S., "Stress-Solvolytic Failure of an Adhesive Bond," J. Adhesion, 1, 1969, 136-141.
44. Wake, W. C., "Moisture and Adhesion-A Review," Aspects of Adhesion 7, Transcripta Books (London), 1973, 232-241.
45. Kinlock, A. J., "Environmental Failure of Structural Adhesive Joints - A Literature Survey," ERDE TN 95, August 1973.
46. Quarterly Progress Report No. 7 (1 January to 31 March, 1978), Fatigue Behavior of Adhesively Bonded Joints, General Dynamics' Fort Worth Division Report, FZM-6735, April 1978.
47. Halpin, J. C., and Polley, H. W., "Observations on the Fracture of Viscoelastic Bodeis," J. Composite Materials, 1, 1967, 64.

#### ACKNOWLEDGEMENTS

Much of the work was sponsored by Air Force Systems Command, Air Force Materials Laboratory, Wright-Patterson Air Force Base, OH, under Contract F33615-76-C-5220, "Fatigue Behavior of Adhesively Bonded Joints". The author especially wishes to acknowledge the interest and guidance of Dr. W. B. Jones, Jr., AFML/MBC project engineer on this program and consultant Dr. W. G. Knauss of California Institute of Technology. Many scientists of Materials and Structures Technology, General Dynamics' Fort Worth Division, contributed to the efforts reported herein, including Messrs. R. S. Chambers, R. L. Jones, F. C. Nordquist, J. D. Reynolds, R. H. McDaniel and Dr. P. L. Flynn.

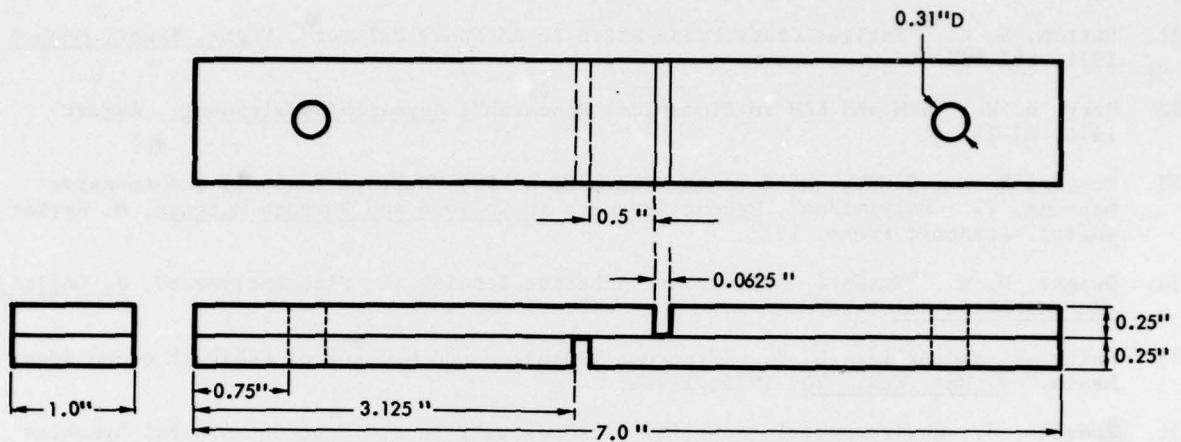


Fig. 1 Model Thick-Adherend Single Lap Shear Specimen

$$D_{H2O} = 1.84 \times 10^{-4} \text{ in}^2/\text{day}, \quad P_e = 2.2\%$$

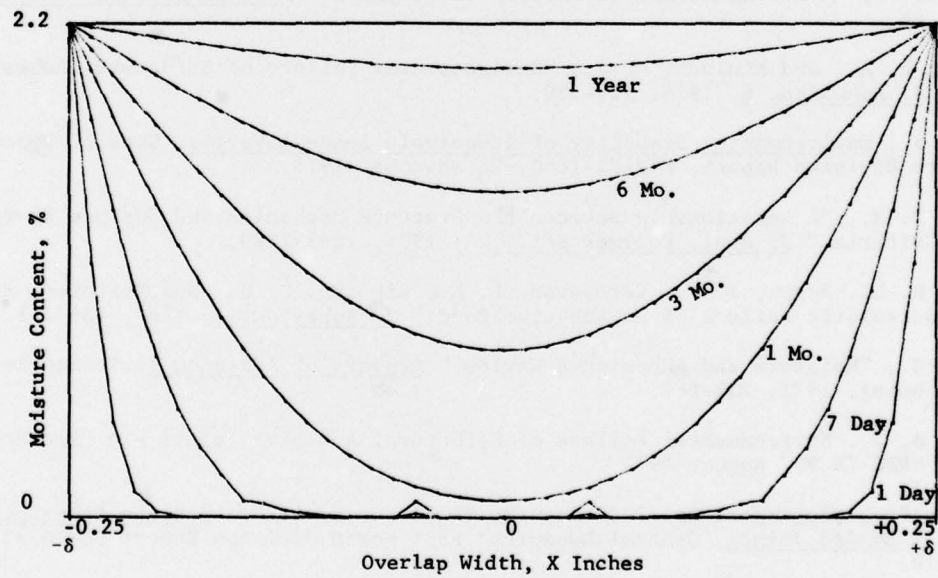


Fig. 2 Moisture Distribution in FM-73M Adhesive Exposed to 100% RH at 60°C.

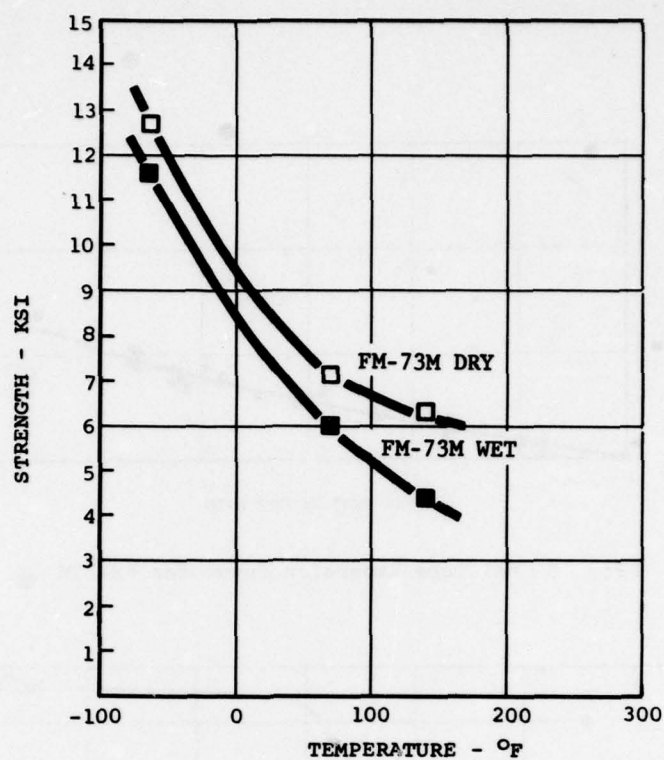


Fig. 3 Strength-Temperature Histories for Dry and Wet FM-73M

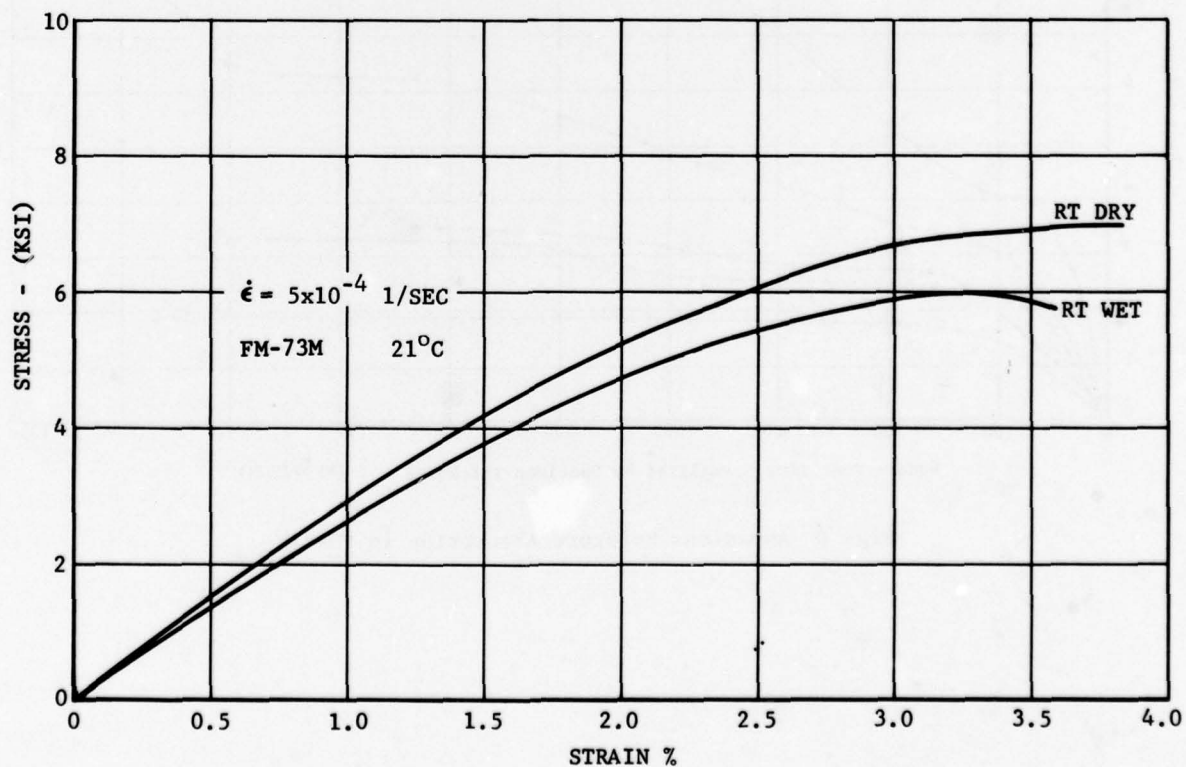


Fig. 4 Tensile Stress-Strain Histories for Dry and Wet FM-73M



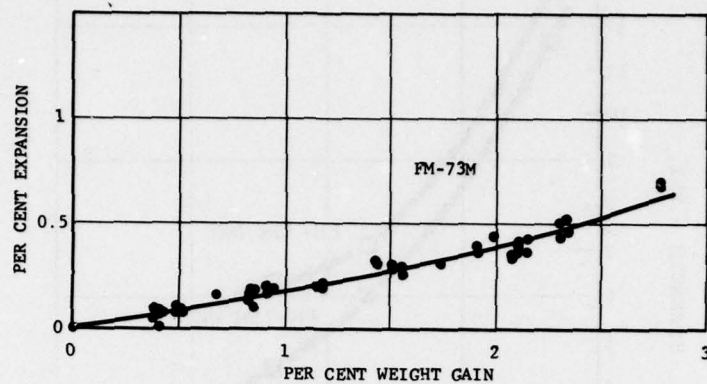


Fig. 5 Moisture Expansion Curve for FM-73M

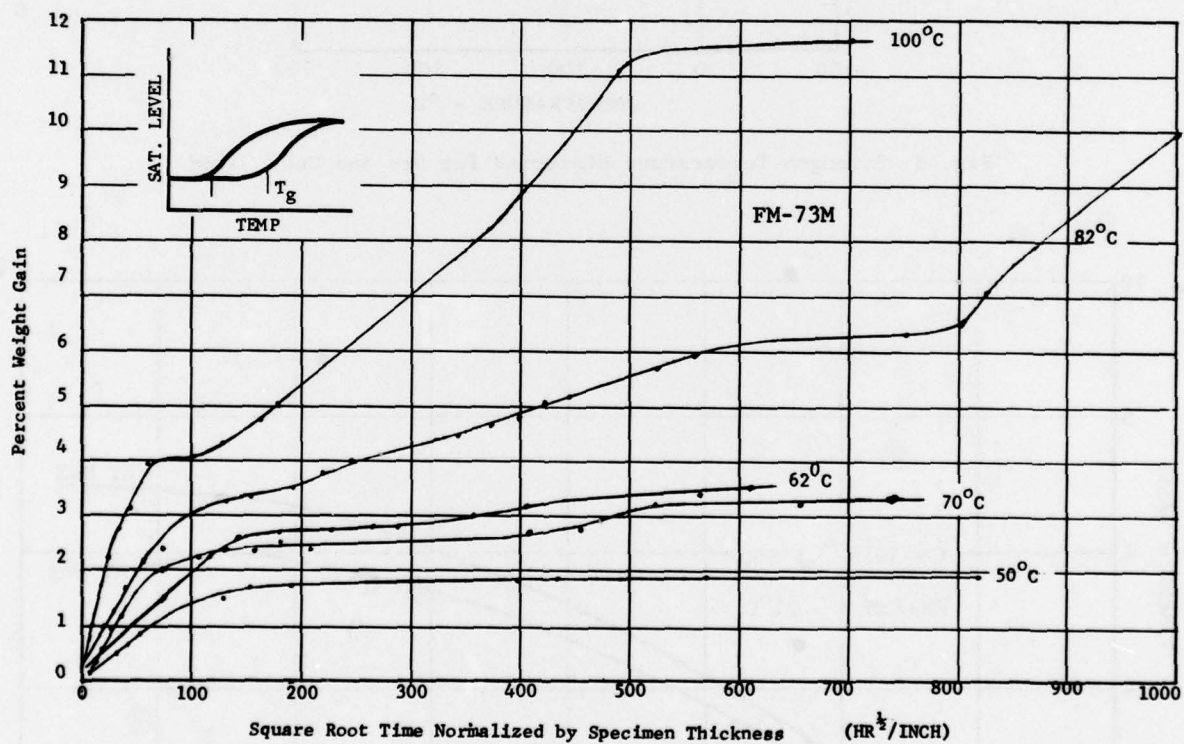


Fig. 6 Anomalous Moisture Absorption in FM-73M

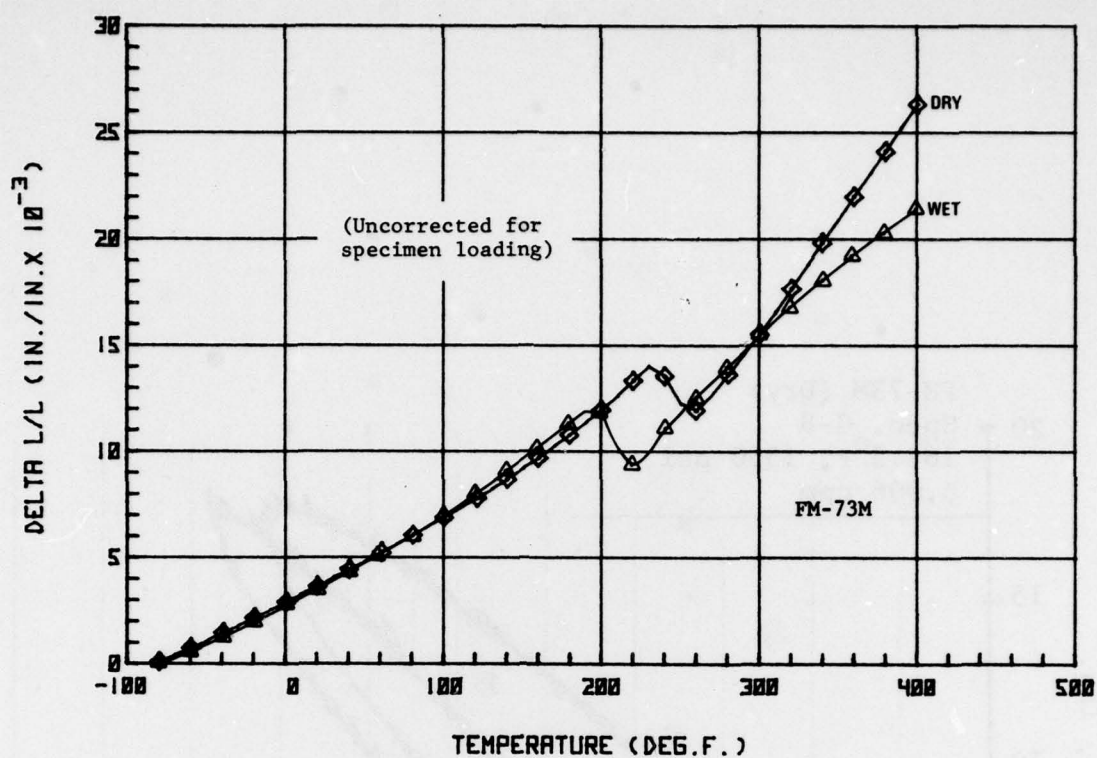


Fig. 7 Expansion-Temperature Curves for Dry and Wet FM-73M

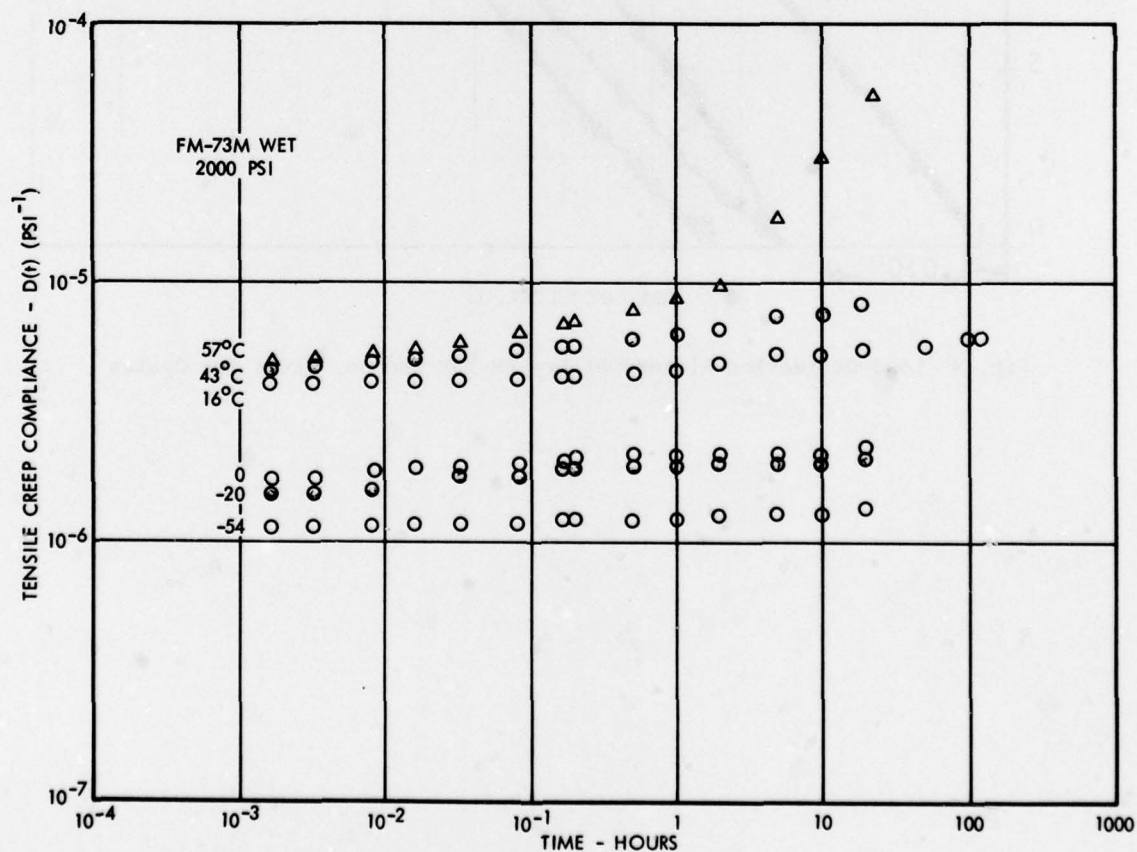


Fig. 8 Tensile Creep Compliance for Wet FM-73M at Various Temperatures

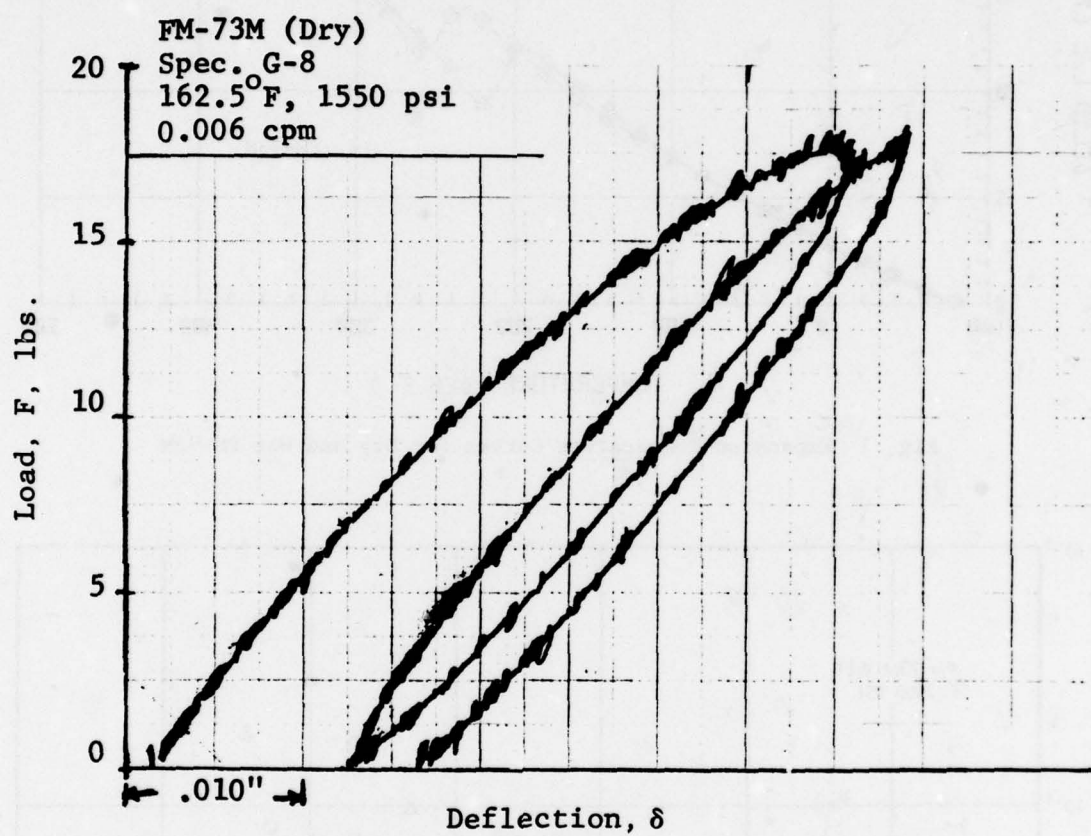
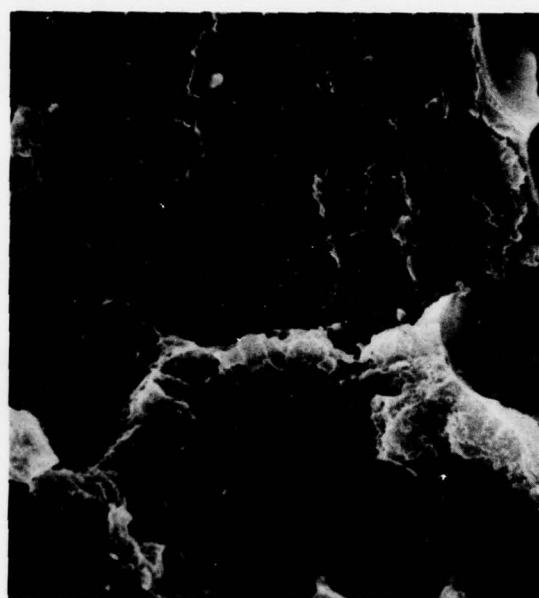


Fig. 9 Load-Deflection History of Dry FM-73M Coupon, First Two Cycles





a. Fatigue - FM-73M - Dry 1000X  
Specimen I-7



b. Fatigue - FM-73M - Wet 1000X  
Specimen B-8



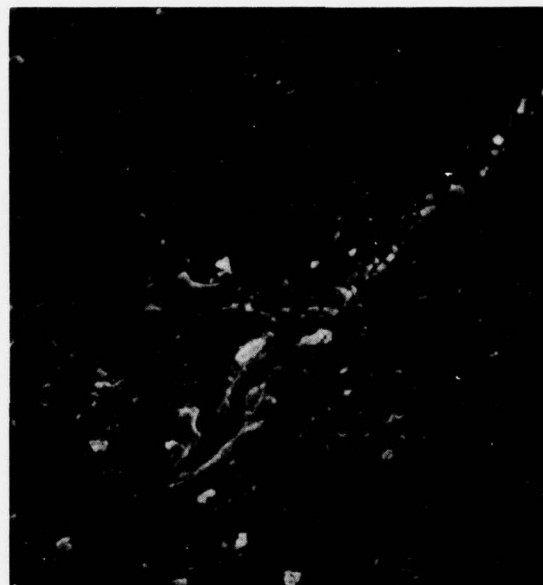
c. Static - FM-73M - Wet  
Specimen B-7

1500X

Fig. 10 SEM Fractography of Failed Dry and Wet FM-73M Coupons  
Showing Similarity of Matrix Structures



a. SEM - Same Area As Sketch c. 500X



b. SEM 5000X  
Higher Magnification Of Crack  
Tip

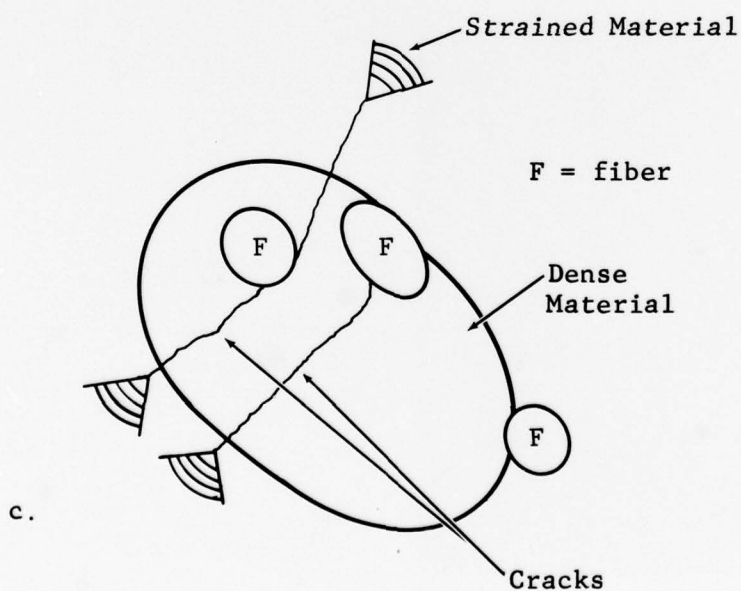


Fig. 11 Photomicrographs of Secondary Cracks in Polished Cross  
Coupon Section of Fatigue-Failed Wet FM-73M

$E = 300,000 \text{ psi}$       Cure and Thermal Shrinkage = 0

$\nu = 0.320$

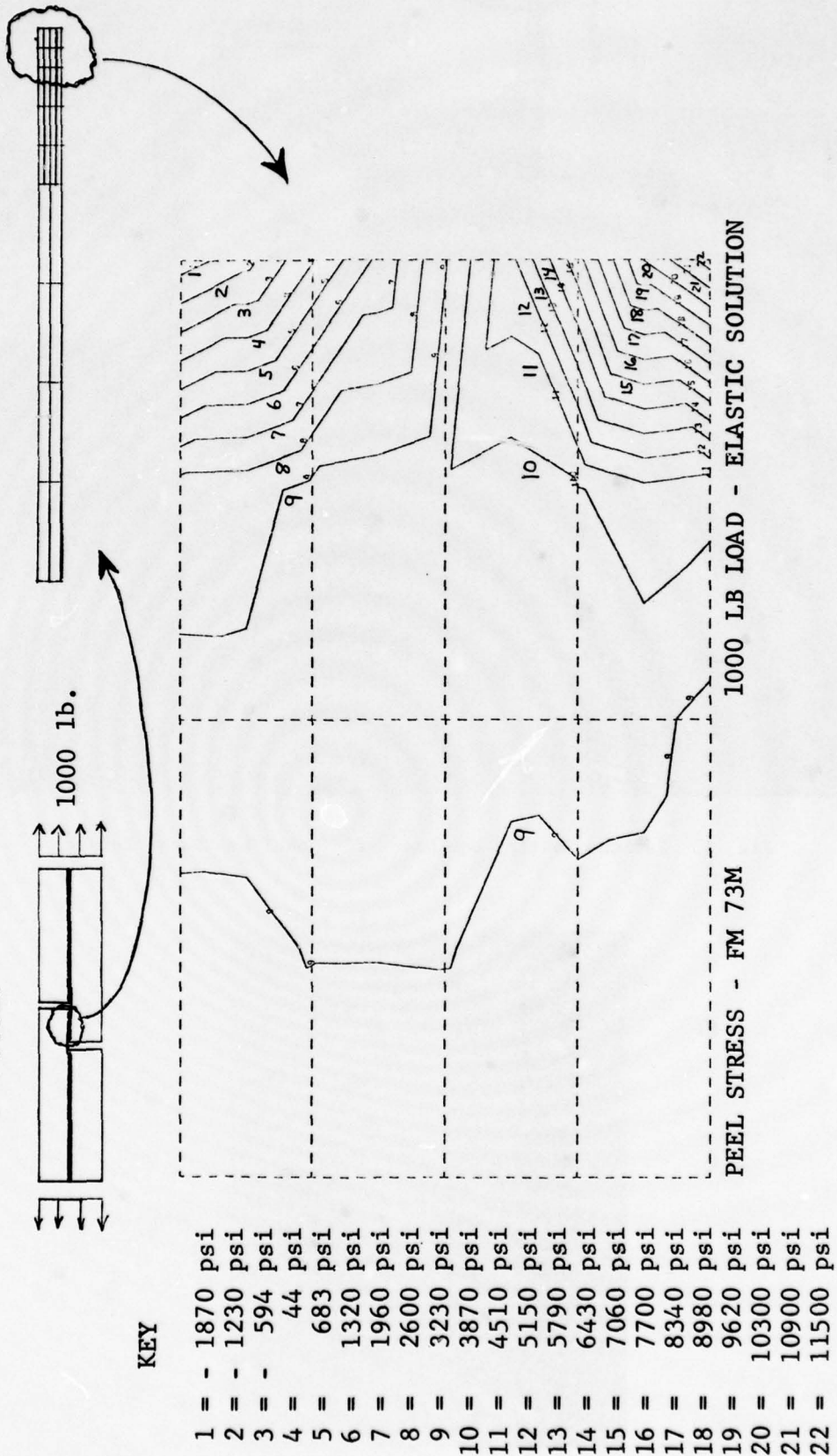


Fig. 12 A Representative Peel Stress Distribution in Adhesive Interlayer



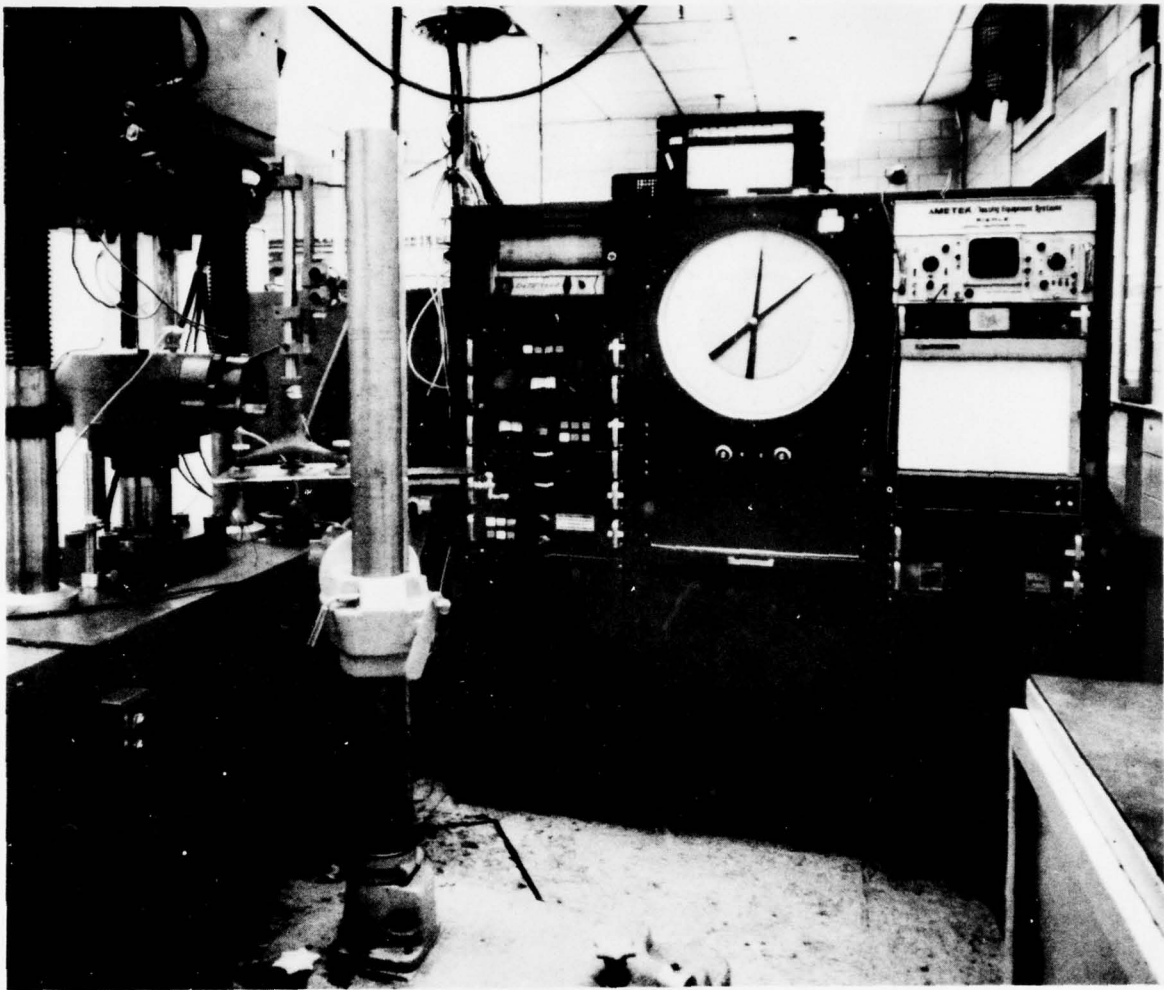


Fig. 13 Fatigue Testing Equipment for Model Lap Shear Joints

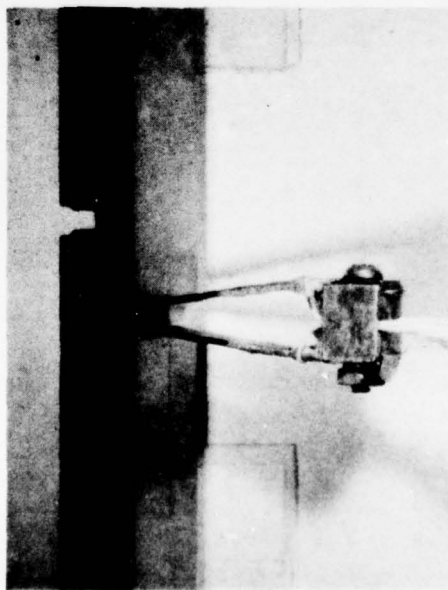


Fig. 14 Instrumented Model Bonded Joint

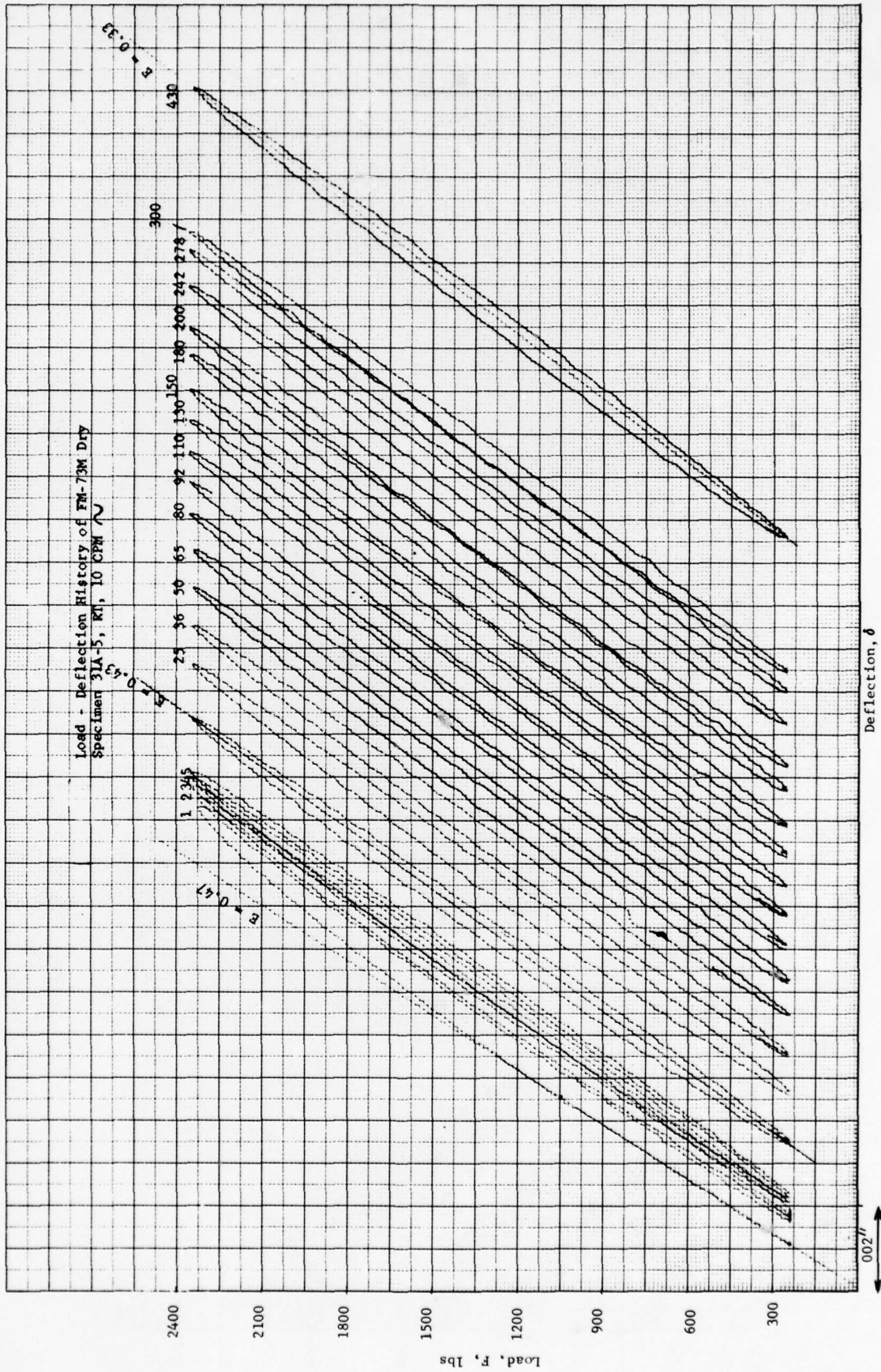


Fig. 15 Room Temperature Load-Deflection History of Dry FM-73M Model Joint

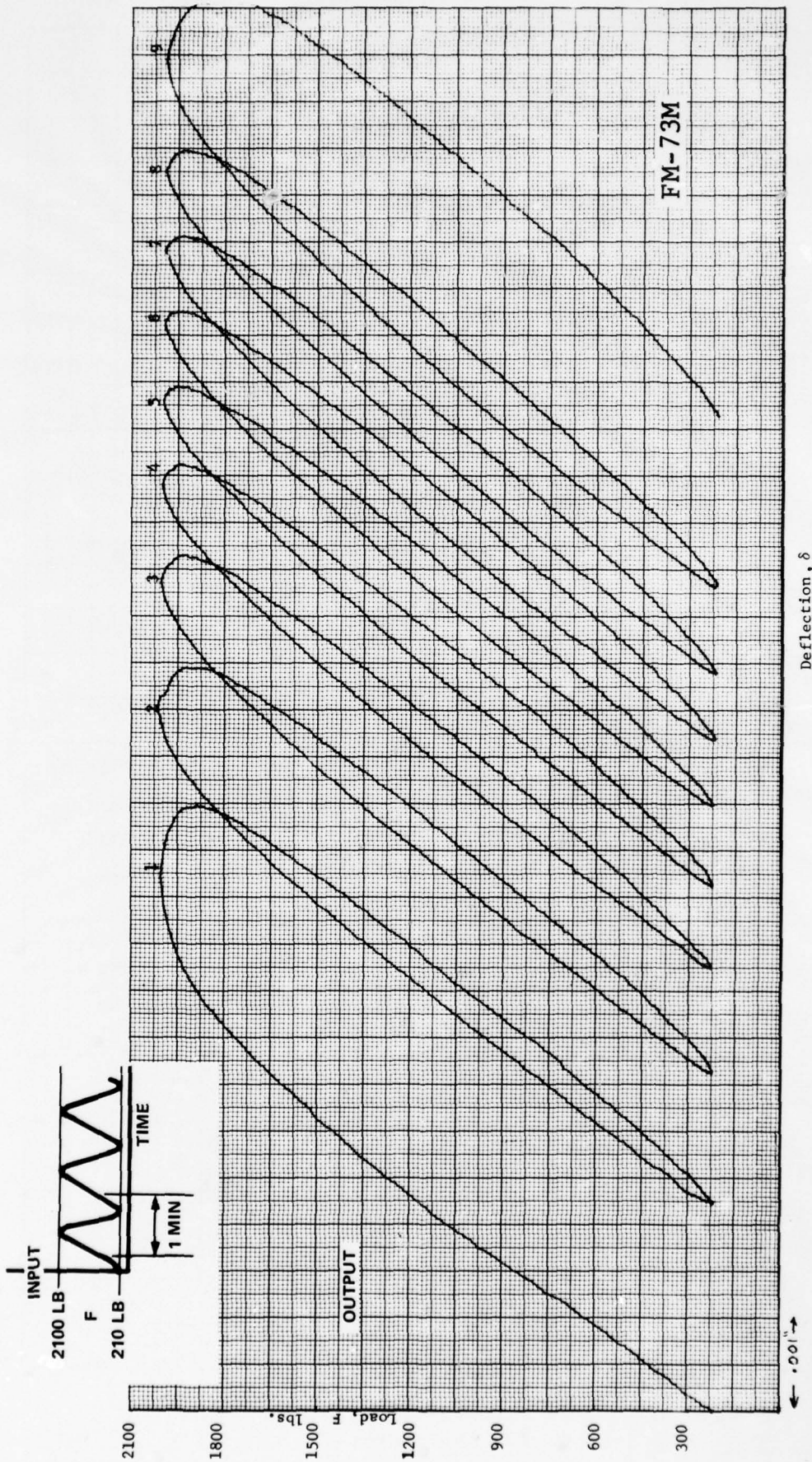


Fig. 16 Room Temperature Load-Deflection History of Wet FM-73M Model Joint



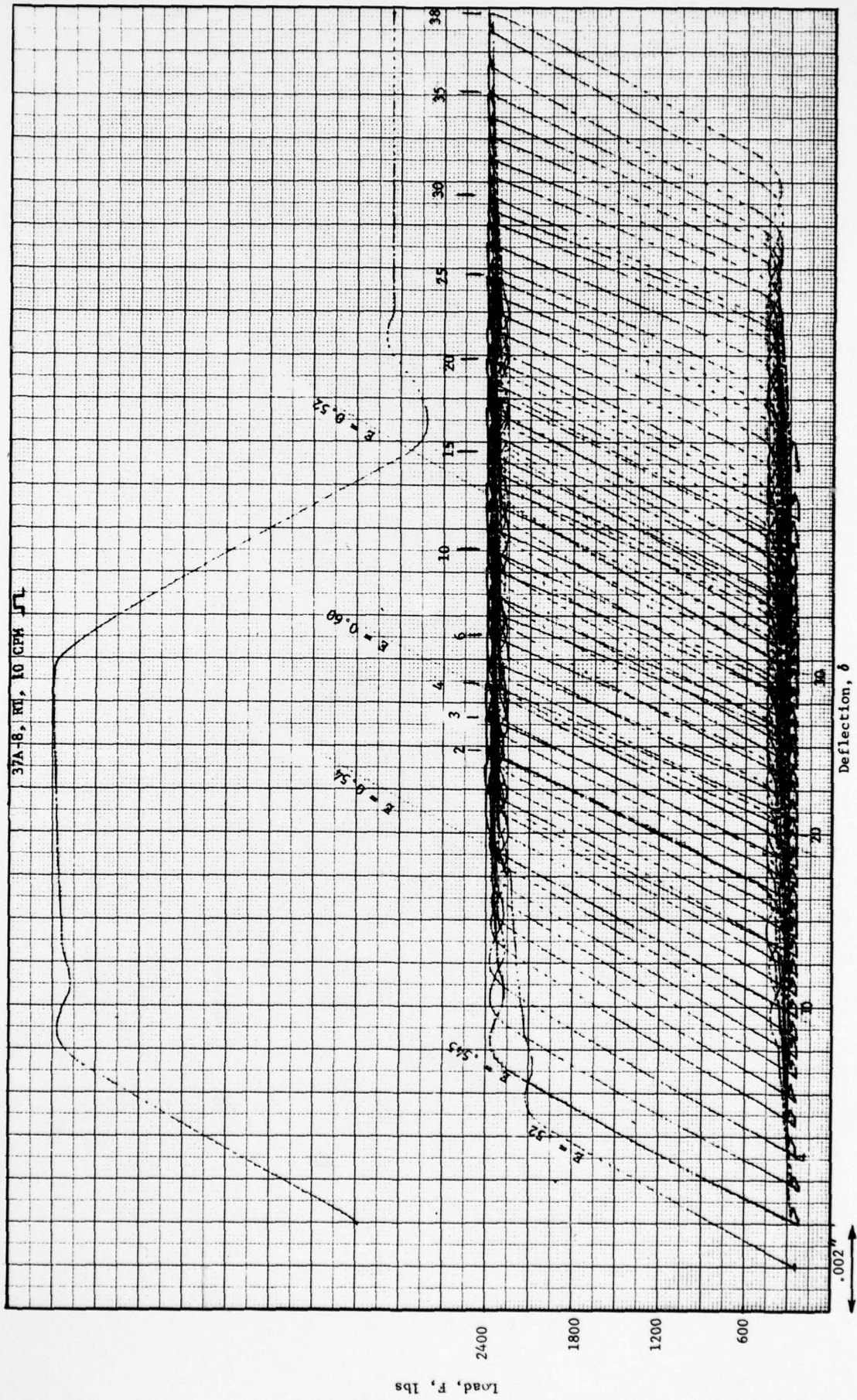


Fig. 17 Load-Deflection History of Dry FM-73M Model Joint (Square Wave Loading)

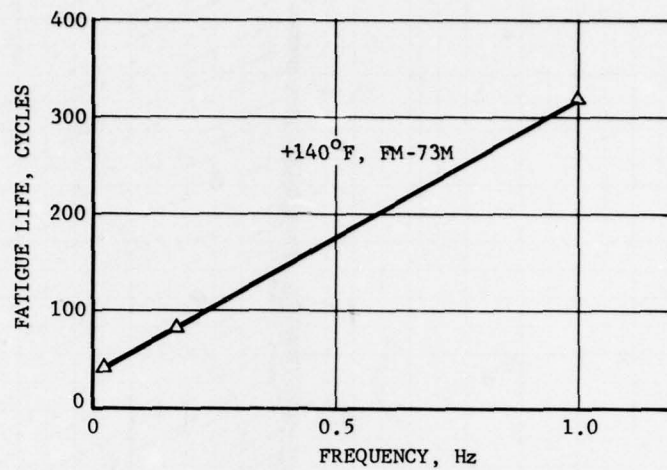


Fig. 18 Fatigue Life Dependence on Cyclic Frequency of Bonded Joints

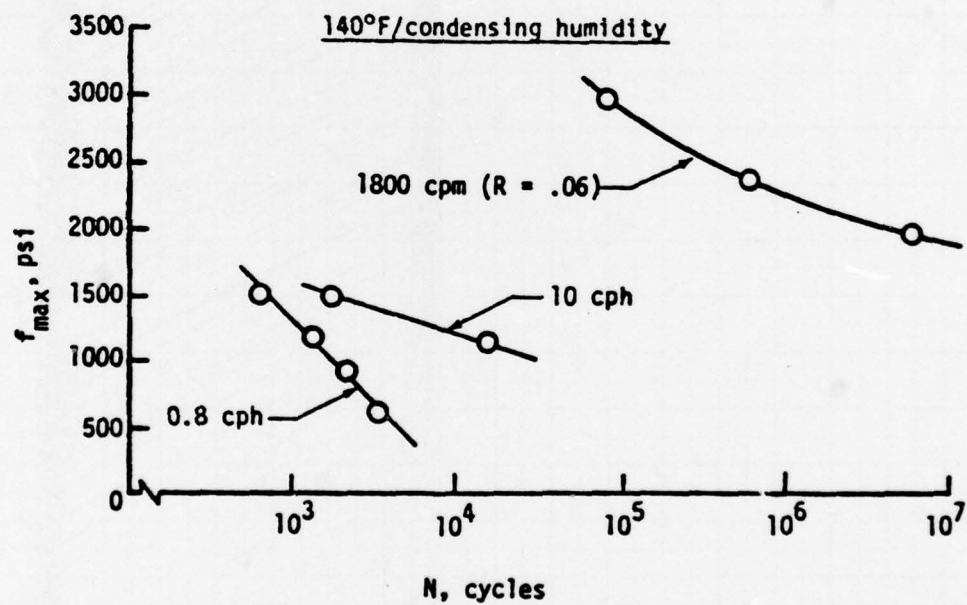


Fig. 19 Cycles to Failure Comparisons of Slow and Fast Cyclic Loading of Model Joints  
(From Ref. 6)

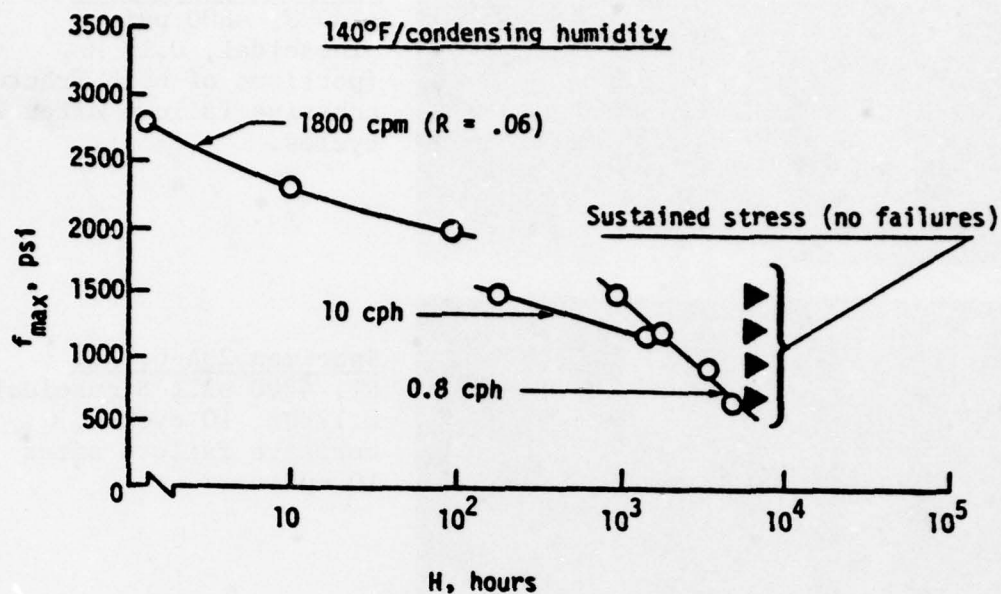


Fig. 20 Hours to Failure Comparisons of Slow and Fast Cyclic Loading of Model Joints (From Ref. 6).

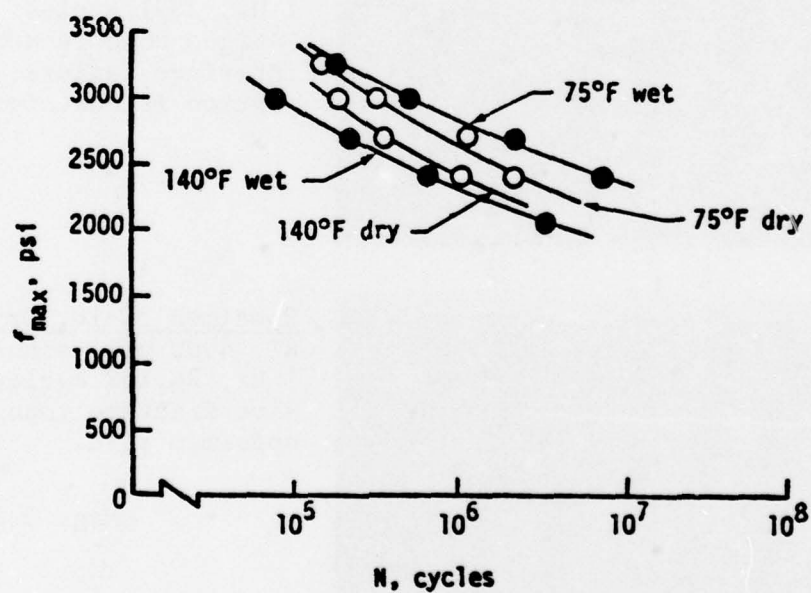
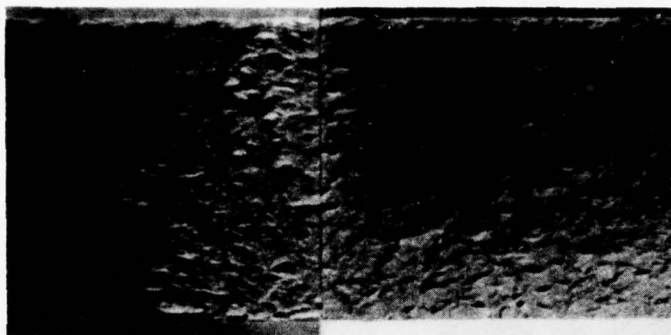


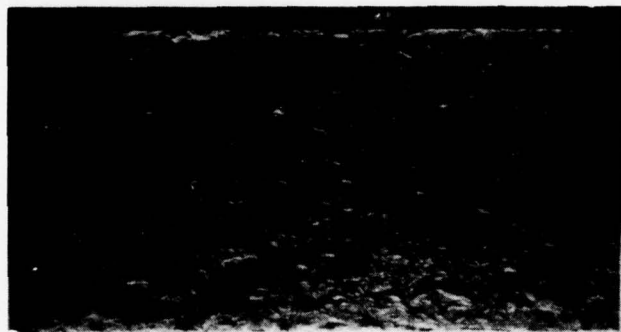
Fig. 21 Environmental Effects on Cycles to Failure at Model Joints at 30 Hz (From Ref. 6).





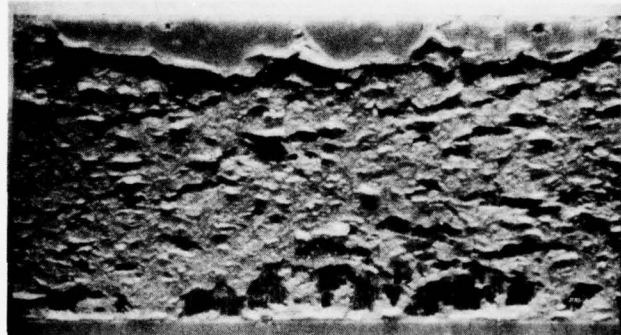
Specimen 33A-4, Dry  
+140°F, 4800 psi,  
sinusoidal, 0.17 Hz,  
(portions of both fractures),  
cohesive failure after 2  
cycles.

a.



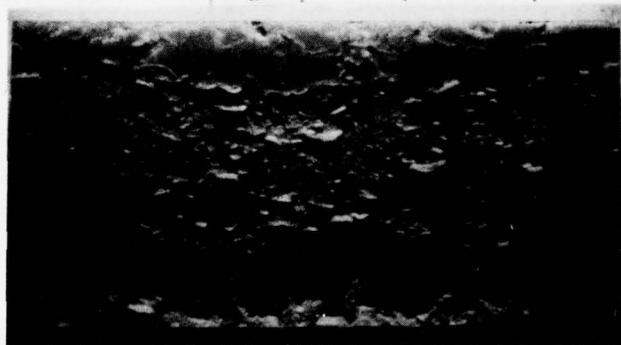
Specimen 29A-6, Wet  
RT, 4000 psi, Sinusoidal  
0.17 Hz, 10 cycles,  
cohesive failure after  
10 cycles.

b.



Specimen 8C-8, Dry  
RT, 4800 psi, square,  
1 Hz, 2871 cycles.  
Fatigue zone is adhesive,  
interface failure. Static  
portion is cohesive.

c.



Specimen 3C-10, Dry  
RT, 4000 psi, sinusoidal,  
1 Hz, 24,182 cycles.  
Same fracture topography as  
specimen 8C-8.

Mag. 3.8X

d.

Fig. 22 Appearance of Fracture Surfaces of Fatigue-Failed FM-73M Model Joints, Different Testing Conditions

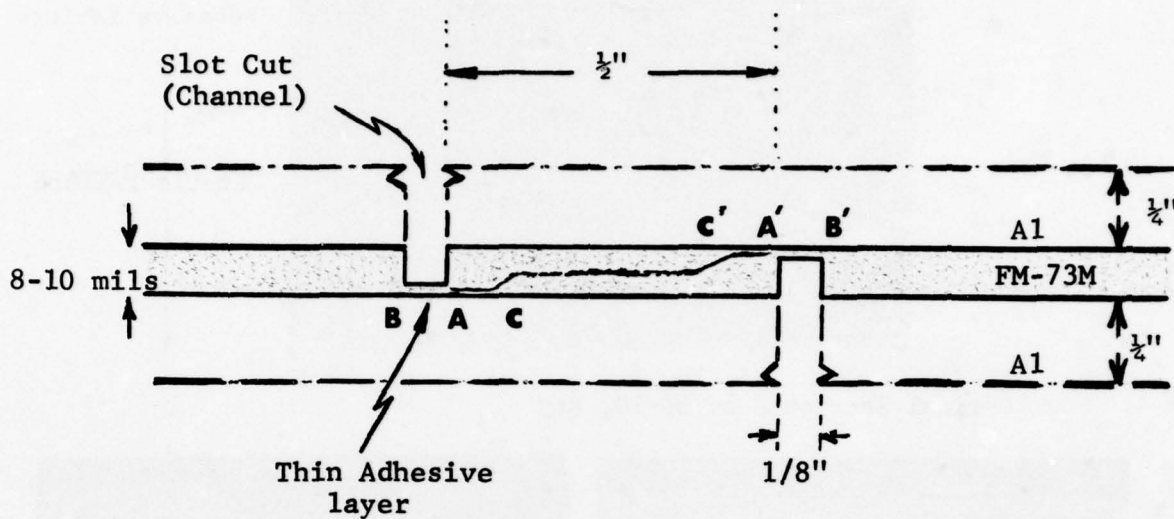


Fig. 23 Side View of Overlap Region, FM-73M Model Joint (Schematic)

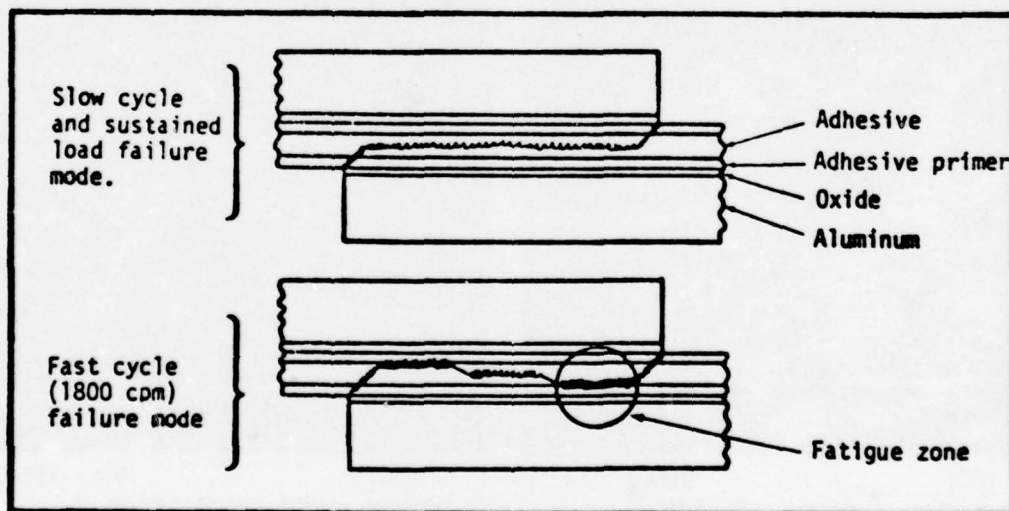
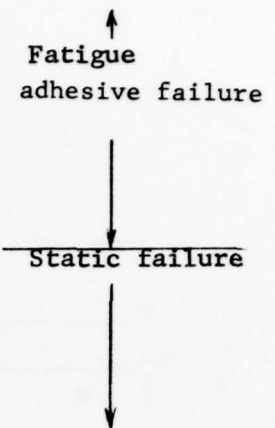
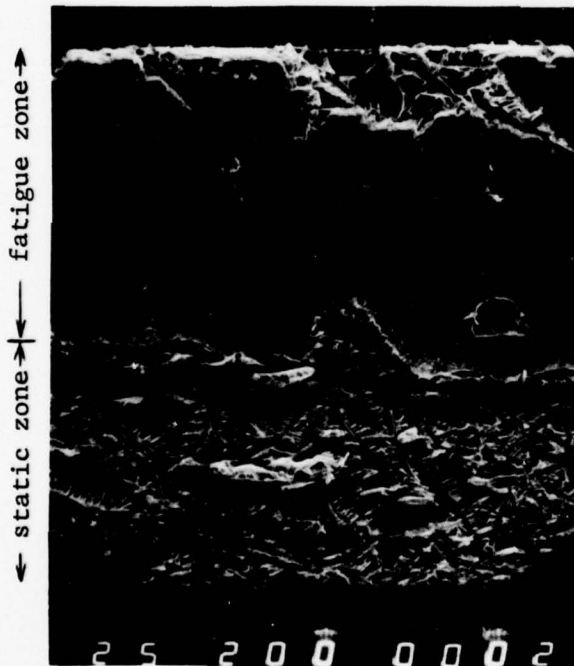


Fig. 24 Failure Mode Characteristics of Model Joints (From Ref. 6).



Mag. 15X

a. Optical Section A of 3C-10, Dry



SEM

Mag. 20X

b. Section B of 3C-10, Dry



SEM

Mag. 100X

c. Enlargement of Section B

Fig. 25 Optical and SEM Photos of Sections of Fatigue-Failed FM-73M Model Joint





Mag. 10000X

a. Zone of slow fatigue crack growth. Typical fatigue striations are not evident. Microcracks are present at debonded interface with aluminum joint.

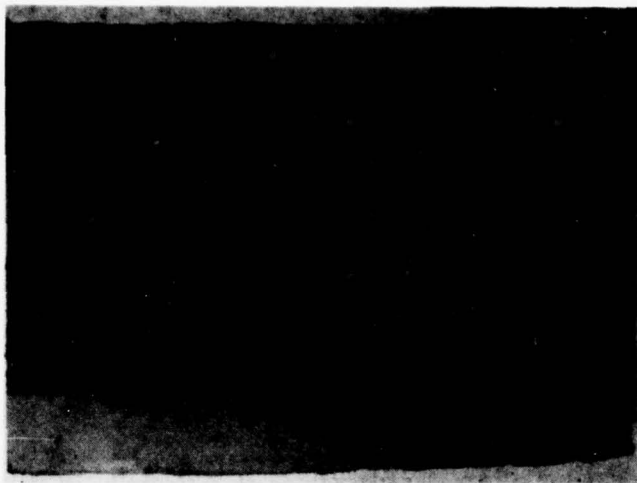
Mag. 1000X

b. Statically failed adhesive at scrim cloth fiber interface.

Mag. 1000X

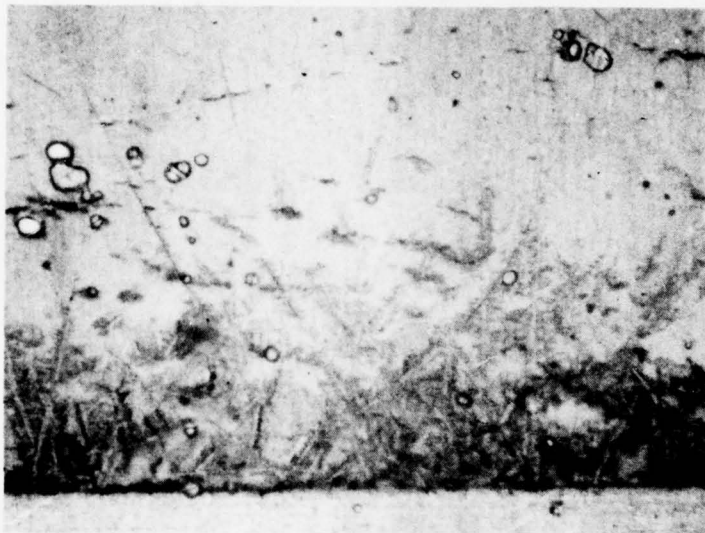
c. Scrim cloth fiber pulled loose from adhesive matrix. Note nucleating failure dimples on adhesive failure surface.

Fig. 26 SEM Photomicrographs of Fatigue-Failed FM-73M Model Joint



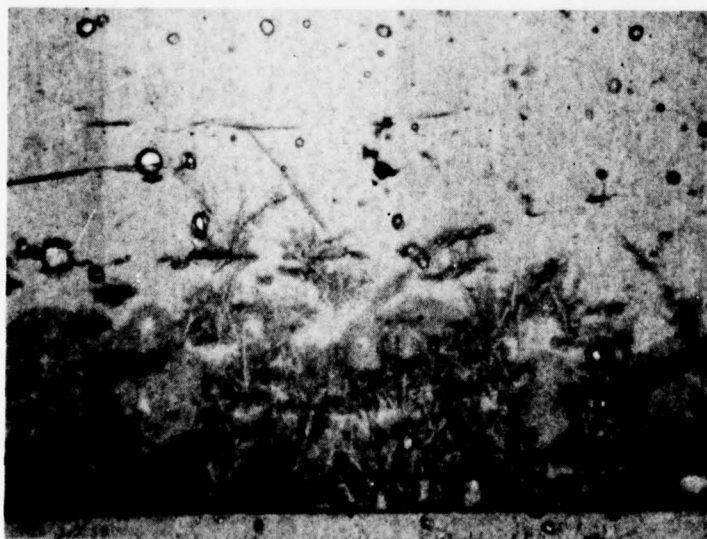
- a. Internal fatigue cracks can be seen originating at notches milled into aluminum adherends.

Mag. 3.8X



- b. Enlargement of a. showing cracks starting along scrim cloth fibers. Note that some cracks formed in advance of coalesced internal crack front.

Mag. 15X



- c. Same as b.; Note that some voids acted as stress risers causing cracks to form whereas other voids had no effect.

Mag. 15X

Fig. 27 Transmitted Light Photographs of FM-73M Adhesive Interlayer

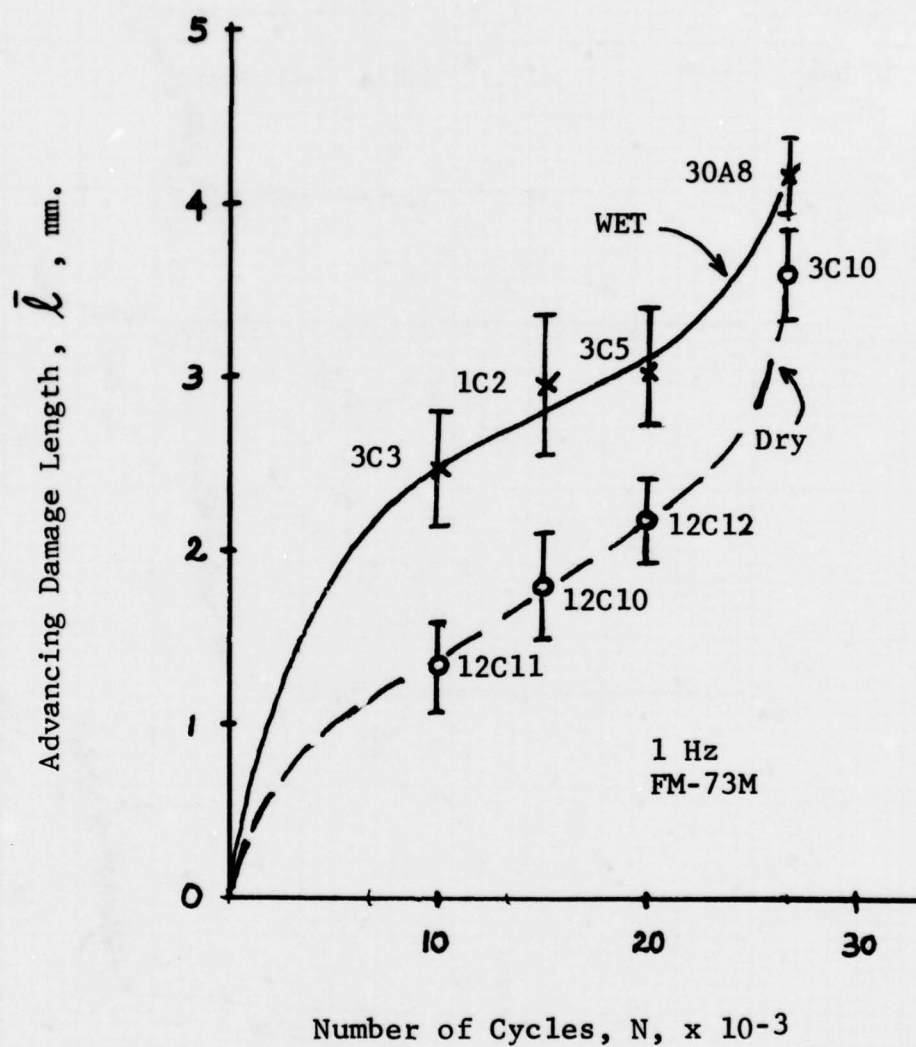


Fig. 28 Dependence of Advancing Damage Length on Number of Cycles for Dry and Wet FM-73M Model Joints



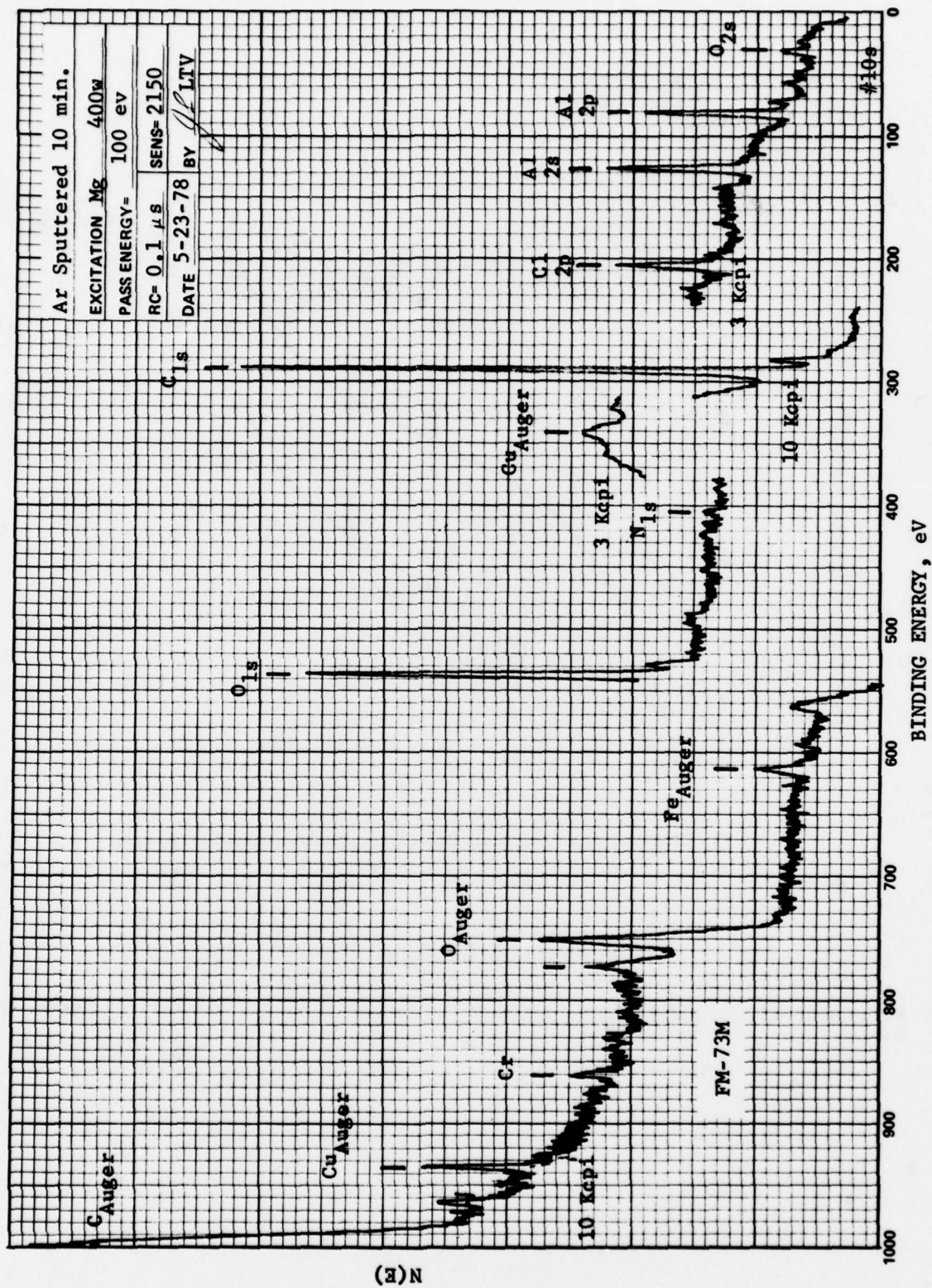


Fig. 29 ESCA Spectrum of Sputtered FM-73M Adhesive Interlayer

## FAILURES IN ADHESIVELY BONDED STRUCTURES

by

Edward W. Thrall, Jr.  
Program Manager — PABST

Douglas Aircraft Company, McDonnell Douglas Corporation  
Long Beach, California 90846

When planning to introduce bonded joints into a primary structure, the designer must have confidence in the structural reliability of this type of joint. The Primary Adhesively Bonded Structure Technology (PABST) program was undertaken to validate the bonded joint with tests and analyses. This paper presents the program structural tests conducted to compare the strength of bonded joints to the classical riveted design. The tests were conducted to determine allowables for static, fatigue, and damage tolerance (crack growth). Also presented are the analytical methods for predicting the bond line strength characteristics. The analyses were found to match the test results.

### THE PABST PROGRAM — AN OVERVIEW

#### Initial Goals and Scope of the Program

In 1972, some 70 participants assembled for a manufacturing cost reduction study at an Air Force-sponsored conference. They represented key management and technical specialists from 25 industrial firms and several Air Force organizations. One recommendation made was to "reduce the number of detail parts and fasteners in a selected fuselage panel by fabricating a large bonded structural panel. This concept should be clearly applicable to large transport/bomber fuselage."<sup>(1)</sup>

It should be noted that there are essentially no primary aircraft structures of U.S. design in commercial service today which rely on an adhesive to carry or transfer 100 percent of the local structural loads. Many so-called secondary structures are joined with adhesives (honeycomb sandwich and doublers) but in many cases, rivets are also installed through the metal-to-metal joints. It is well known that this combination joint has superior fatigue strength (life) when compared with rivets alone. In Europe, several primary structures have been joined by using an *adhesively bonded joint*; for example, the Fokker F-27 and F-28 (1955), the DeHavilland Comet (1949), and Hawker-Siddeley Trident IIIB, all using Redux as the adhesive (Figure 1). Both wing and fuselage longerons were bonded to their respective adjacent skins but no panel splices rely on the adhesive strength for 100 percent of load transfer.

A follow-on Air Force seminar on low-cost manufacturing and design was held in May 1973.<sup>(2)</sup> At this meeting, it was concluded that the limitations in the utilization of the bonding process for primary structures are:

1. Lack of confidence
  - a. Fundamental information
  - b. Strength data
  - c. Service data
  - d. No established success criteria
2. Adhesive needs.

Because of these limitations, 12 general bonding program areas were recommended, including the following:

1. Correlate defect size, shape, and location to structural strength.
2. Conduct a detailed study of moisture effect on adhesives and methods to improve properties.
3. Relate surface chemistry studies to manufacturing processes for surface preparation.
4. Establish stress analysis procedures adapted to adhesive bonded structures.
5. Develop repair procedures and a general repair manual.

A sample of the day-to-day experience of bond failures in service is shown in Figure 2. The figure illustrates a piece of trailing-edge structure where a doubler is bonded to the skin to protect against acoustic fatigue. The part was in service 7 years and was held together only by the rivets shown when removed from the aircraft.

The Air Force initiated an advanced development program (ADP) to investigate the possibility of achieving significant improvements in cost, weight reduction, integrity, and durability of primary fuselage structure by the application of adhesively bonded joints. The ADP procedure is a low-risk method of utilizing high-risk advanced technologies so that future aircraft systems can gain the benefits. Another important facet of the ADP concept is the use of a real-world baseline to enhance the technological transition and achieve near-term payoff potential. Major advancements in surface treatment and adhesive technology in the early 1970s showed that the new 250°F cure adhesive systems have greatly increased durability. The timing of the program coincided with the development of the Air Force Advanced Medium STOL Transport (AMST). Therefore, this fuselage structure merited attention since the emerging Air Force system has a stringent design-to-cost requirement.

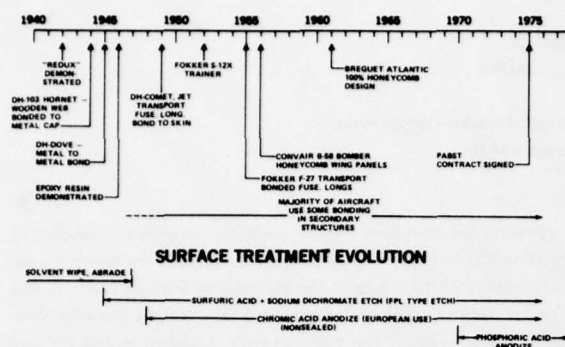


FIGURE 1. BONDED AIRCRAFT STRUCTURAL EVOLUTION

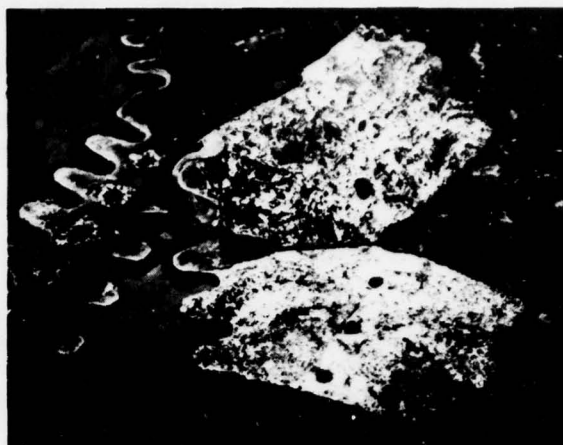


FIGURE 2. CORRODED BONDED JOINT

On 18 February 1975, the Air Force awarded Douglas Aircraft Company a \$18.4 million contract for the PABST program. The objective of the PABST program is to demonstrate and validate that applications of adhesive bonding to primary structure can reach a goal of 20-percent cost saving and a concurrent 15-percent weight reduction when compared to existing fabrication techniques. In addition, significant improvements should be attained in structural integrity and durability. Because Douglas has the contract, the fuselage shape and detail loads of its AMST candidate, the YC-15, are used as the baseline for the bonded test demonstrator (Figure 3).

The PABST program is a multidisciplinary approach to the validation of bonding primary structure. Much more information is available than can be given in the allotted time. Also, the preceding AGARD papers cover some of the subjects investigated in the PABST program. Accordingly, this paper presents information on only one subject, failures in adhesively bonded structures. A short summary of the PABST program and significant results will be presented in the next section of this report.

#### Surface Treatment Evaluation

In the first 18 months of the program, surface treatments, adhesives, nondestructive inspection, and structural arrangements were investigated and many structural tests were performed. For surface preparation or processing evaluation, the PABST program investigated chromic acid anodize (Bell Helicopter Company, Specification BPS FW4352, Rev. G) and phosphoric acid anodize (Boeing Company Specification BAC 5555), and compared them against the sulfuric acid, sodium dichromate etch (FPL) (Boeing Company Specification BAC-5514) which was to act as a baseline control treatment. The primary test for bond surface treatment durability was the wedge crack propagation test. This test, originally proposed by A. W. Bethune in 1975, is shown in Figure 4.<sup>(3)</sup> Test matrices were developed for each surface treatment to identify concentration, voltage, temperature, and time limits in a solution. Wedge crack specimens were made from two 6- by 6-inch plates which were processed (including priming), bonded, and sawed into five 1-inch-wide strips or specimens. Each strip was wedged apart for 1 inch with a 1/8-inch-thick wedge which failed the adhesive locally in tension. The crack end was marked after one hour after one hour at room temperature and the specimen was then placed in a cabinet at 140°F and 95- to 100-percent relative humidity for one hour, removed, and the crack growth noted. The part was then completely separated so the failure mode could be evaluated.



FIGURE 3. PRIMARY ADHESIVELY BONDED STRUCTURE TECHNOLOGY

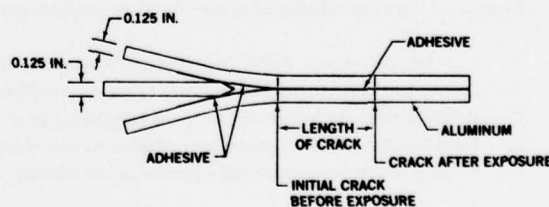


FIGURE 4. WEDGE CRACK SPECIMEN

For the comparisons of surface treatments, all processes after anodizing were the same. Adhesive primer (American Cyanamid BR-127) was applied within 2 hours after anodizing. The primer thickness was 0.0002 inch. It was air-dried for 30 minutes and cured for 60 minutes at 255° ± 5°F. One layer of adhesive was used (FM-73, 0.045 pound per square foot, with mat carrier). This adhesive was cured in an autoclave at 245° ± 5°F for 90 minutes at 40 psi. The heat-up rate was kept within the limits of 3° to 6°F per minute. Pressure was maintained during cooldown until 150°F was reached. The aluminum used in all tests was nonclad 7075-T6.

From the results of these comparative tests, phosphoric acid anodize was selected because no adhesive failures occurred within the full range of the test matrix. The other processes had adhesive failure except when the test matrix conditions were held to close



tolerances that were not considered practical in a production environment. To date on the PABST program, over 10,000 phosphoric acid anodized wedge crack specimens have been prepared in a production environment, and all had cohesive failures when tested.

The PABST program has determined that an anodized surface can be contaminated by handling with white cotton gloves, neutral kraft paper and, of course, bare hands before the primer is applied and cured. Accordingly, in the PABST program, no handling was allowed after the cleaning process started through anodizing, inspection, and the primer application until the primer was fully cured. Then, white gloves and neutral kraft paper were carefully used to move and keep parts clean until the bonding operation was finished.

A long-term outdoor wedge crack test program followed the short-term tests. The 2000 and 7000 series aluminum alloys, clad and nonclad, were compared. The results to date, shown in Figure 5, clearly indicate that aluminum-clad 7075-T6 does not have any durability at all. If other aluminum alloys are to be bonded, then long-duration tests may be run to determine acceptability.

#### Adhesive Selection

The PABST program called for an adhesive system to be selected for the full-scale demonstration component. Four candidate adhesive systems of the latest environment-resistant, 250°F cure, modified epoxy adhesives and their primers were furnished to the program in 1975. These were: (1) American Cyanamid, FM-73/BR-127 Mat Carrier; (2) Hysol Division, The Dexter Corporation, EA9628/9202 Woven Carrier; (3) 3M Company, AF55/3950 Woven Carrier; and (4) Narmco Material, Inc., M1133/6740 Woven Carrier.

The first battery of PABST tests were process-type tests conducted with classical materials such as static lap shear and peel. While these tests tend to show some environmental effects or sensitivities, they yield little information on which to base a material selection for durability. Lap shear tests, as called for in FED SPEC MMM-A-132, yield comparable data (Figure 6). T-peel strength tests show quite dramatically the effect of the carriers (Figure 7). The failure modes on these tests were all cohesive, as desired. As shown in subsequent long-term durability tests, however, material selection based on static peel or lap shear performance would have been incorrect.

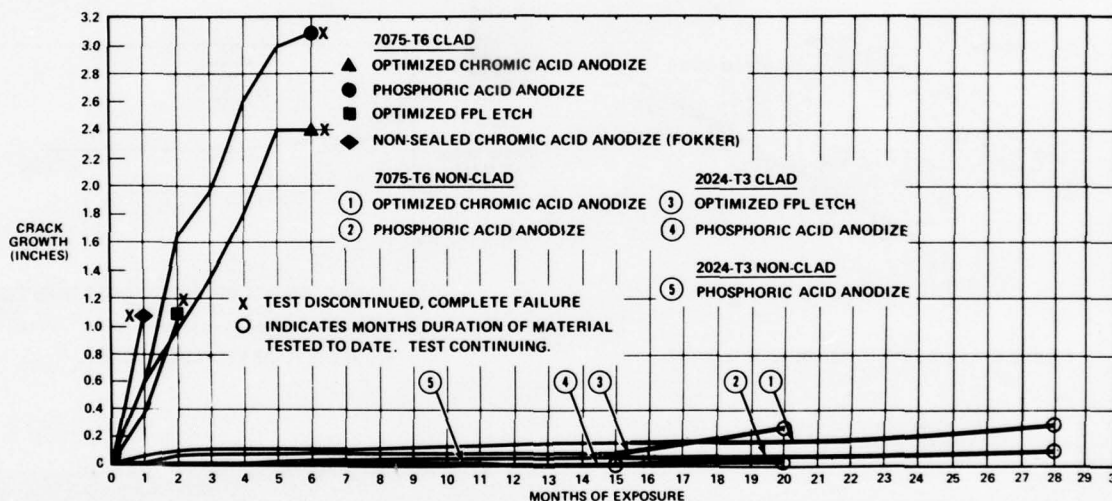


FIGURE 5. BEACH EXPOSURE TEST

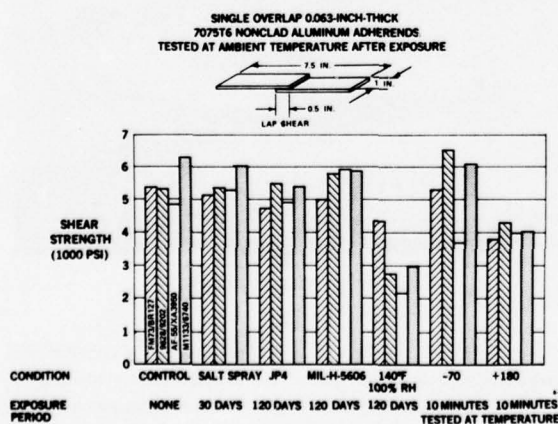


FIGURE 6. LAP SHEAR TEST

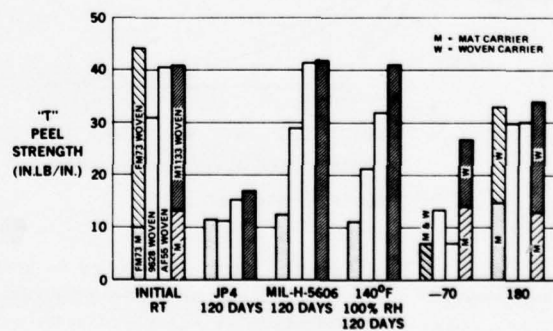


FIGURE 7. "T" PEEL TEST

The PABST program has made extensive use of the Raab specimen (Figure 8). These specimens are unique in that 2.75 inches of faying surface bond line are exposed for a shear area of 0.2 square inch. The moisture intrusion is therefore maximized when the specimen is compared to a normal production lap joint. Care must be taken in manufacture to reduce the scatter of the test results.

Environmental stress rupture and sustained load testing of the Raab specimen were conducted with the four adhesive systems. Exposure was at 140°F, 100-percent relative humidity at sustained loads of 2050-, 1750-, and 1450-psi average shear stress. These tests showed discrimination between adhesive materials, indicating FM-73 was the best performer (Figures 9 and 10). The failure modes were mostly cohesive, but moisture did penetrate the woven carrier joints and cause corrosion pits. However, it cannot yet be said that a pass/fail criterion can be determined by this test alone. FM-73 adhesive had the longest life from the test, but it cannot be categorically determined that this system would have the durability required for primary structure application. For example, the Raab specimens made with Redux, a system with 25 years of successful experience in F-27 aircraft, performed poorly in this test. More comparative tests must be run to find the most representative type of durability test. Because of the eccentricities that exist in the Raab specimen, Douglas has designed, built, and started testing a double overlap environmental shear (DOES) specimen (Figure 8).

#### Structural Evaluation

The PABST program design phase started with an all-out search for fuselage structural arrangements that would be most amenable to bonding. To make the design realistic, the Air Force directed that the AMST be used as a baseline. Since Douglas had won the contract, this meant that YC-15 fuselage dimensions and detail design loadings would be used. The fuselage is 216 inches in diameter, pressurized to a maximum of 7.15 psi, and capable of carrying a large assortment of Army trucks, tanks, and palletized payloads. Besides the normal static strength requirements, the structure must satisfy the fatigue, damage tolerance, and fail-safe requirements of the Air Force specifications.

The large diameter and relatively short length of the fuselage (Figure 11) results in most structure being critical for cyclic effects of the cabin pressure (once each flight) and, alternatively, the landing loads on the fatigue and fail-safe requirements rather than the static strength. This fact eliminated the potential weight saving from use of bonding. Other aircraft structural configurations could expect weight savings up to approximately 25 percent.

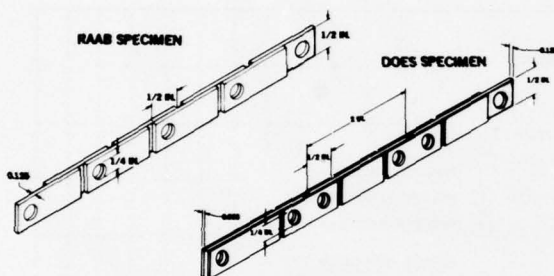


FIGURE 8. ENVIRONMENTAL SHEAR SPECIMENS

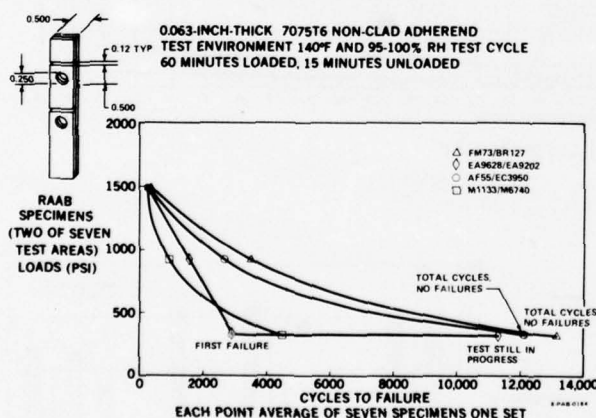


FIGURE 10. RAAB CYCLIC TEST

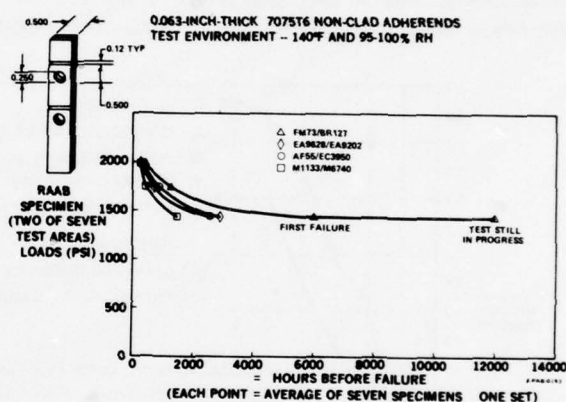


FIGURE 9. RAAB SUSTAINED LOAD



FIGURE 11. YC-15 AIRCRAFT

Three basic structural arrangements were selected for in-depth cost analysis. One configuration was essentially the conventional design arrangement used for riveted structures and identified as an internally stiffened structure. The second configuration is identical to the first, except the longitudinal stiffeners are placed on the outside of the skin which is ideal structurally. This arrangement eliminates frame cutouts for the longerons and the resulting stress concentrations. The major drawback, outside of appearance, is the added drag. The third configuration is a honeycomb sandwich design. With this type of skin stiffening, many frames are removed and no longerons are required. A large reduction in part count is achieved with this arrangement. To maintain the same weight and strength capability as the two other designs, very light face sheets are required. This is not practical since the thin, 0.025-inch skins are easily subject to damage from foreign objects and associated costly repairs. It was determined that the frequency of repairs would be higher than for the conventionally stiffened heavier-skin designs.

At the PABST program review by the Air Force team on 16-20 August 1976, Douglas recommended the structural arrangement shown in Figure 12. The area above the floor is of conventional structure using bonded internal longerons across the top and vertical frames on the sides. As indicated, longerons were eliminated on the sides because of low load levels and tear stopper (flat) strips added for fail-safe requirements. The external longerons are used below the floor and will present a challenge to the bond shop because members are bonded to both sides of the fuselage skin. Attempts to date have shown it is difficult to get proper bonding pressure at the intersections.

During the initial design study phase, it became apparent that several quick tests should be run to see if any "show stoppers" existed in bonded designs. Failure to get an allowable equivalent to riveted structure could defeat the program. The first series of tests was conducted to simulate the pressure load between the fuselage skin and the supporting frames. The cabin pressure can be resisted by the fuselage skin. However, load distributing frames which attach to the skin will not expand under cabin pressure and therefore the fuselage skin has a tendency to pull away or impart a tension load between the skin and the frames. It was decided to make small specimens to represent the tension load effects produced from cabin pressurization. For the proposed bonded design, the frame caps would be bonded to the fuselage skin. Figure 13 illustrates the specimen used and the resulting tension load capabilities of the joint. The specimen was designed with a rigid support which acted as a spreader bar and limited skin deflection to that calculated for the aircraft structure under cabin pressure.

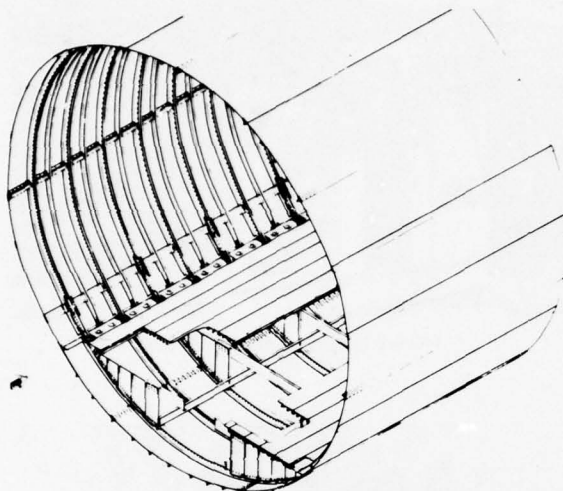
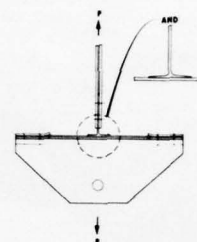


FIGURE 12. FULL-SCALE DEMONSTRATION COMPONENT



SKIN	ADHESIVE	PRIMER	FAILURE LOAD				DESIGN LOAD
			TEST TEMP				
			-50 - 5°F	R.T.	140 - 5°F	-50°F	
0.090 7075 T6	FM 73	BR 127	1740 LB				249 LB
0.040 7075 T6	FM 73	BR 127	1595 LB				389 LB
0.090 7075 T6	AF 55	XA 3950			4000 LB		249 LB
0.090 7075 T6	M 1133	BR 127	2170 LB				249 LB
0.090 7075 T6	AF 55	XA 3950	5810 LB	5050 LB	5075 LB		249 LB
0.090 7075 T6	M 1133	BR 127	2640 LB	4650 LB			249 LB
0.040 7075 T6	AF 55	XA 3950	1670 LB	3700 LB	4220 LB		389 LB
0.040 7075 T6	M 1133	BR 127	2105 LB	3275 LB	3358 LB		389 LB

FIGURE 13. TENSION TEE TEST

## STRUCTURAL JUSTIFICATION TESTS

### Static Shear Panel Tests

Again, recognizing that an adhesive joint is weak in peel, it was considered necessary to make some shear panels to determine the strength characteristics of bonded longerons resisting the intrusion of severe skin shear wrinkles. The shear panels were built with the proper fuselage radius of 108 inches. Table 1 shows the list of various panels tested and the resulting loads. Since 0.090-inch skin thickness was the heaviest anticipated at this time in the design and because the shear wrinkles would be the heaviest, a riveted design was built to compare with a bonded design, each with the same stiffener and frame spacing. A photograph of the shear jig is shown in Figure 14.

The detailed results of some of the shear panel tests are presented in the following section.

**Static Test, Riveted Shear Panel** — This test was conducted to determine the static ultimate allowable shear for a representative riveted construction for the baseline YC-15.




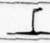
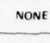
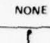
Panel Radius: 108 inches, test conducted at room temperature  
 Skin: 0.090-inch-thick 7075-T6  
 Longerons: 12 inches on center, area 0.332 sq in., Z-section  
 Frame: 24 inches on center, area 0.808 sq in., L-section  
 Rivets: 1.19 inches on center, 3/16-inch diameter.

The specimen is installed in the picture frame jig shown in Figures 15 and 16. The onset of diagonal tension wrinkling occurred at a test load of 36,000 pounds. The panel was loaded up to a value of 77,000 pounds with no evidence of permanent set. The deflection of the panel was 0.59 inch at this load. The first rivets failed at a load of 101,000 pounds at the junction of the middle frame and the first longeron in from the edge of the panel (see Figure 17). The panel would carry no more load after 129,000 pounds was reached. Figures 18 and 19 show the final failed condition of the panel. The effective panel height is 58.19 inches, resulting in a shear stress of 24,632 psi.



TABLE 1  
SHEAR STATIC TEST PANEL RESULTS

PRIMER BR127

SKIN 7075T6	LONGERON	ADHESIVE	TEST TEMP	TEST SHEAR (KSI)	DESIGN SHEAR (KSI)	ANALYSIS FAILURE PREDICTION (KSI)
0.04		FM73	-50°F	19.8	13.0	18.3
0.09		RIVETED	R.T.	24.6	20.0	21.8
0.09		FM73	R.T.	26.5	20.0	21.8
0.04		M1133	-50°F	27.5	13.0	18.3
0.04		M1133	140°F	25.3	13.0	18.3
0.09	NONE	FM73	140°F	19.6	20.0	10.6
0.09*	NONE	FM73	140°F	23.8	20.0	12.6
0.0434		FM73	140°F	30.7	13.0	23.3

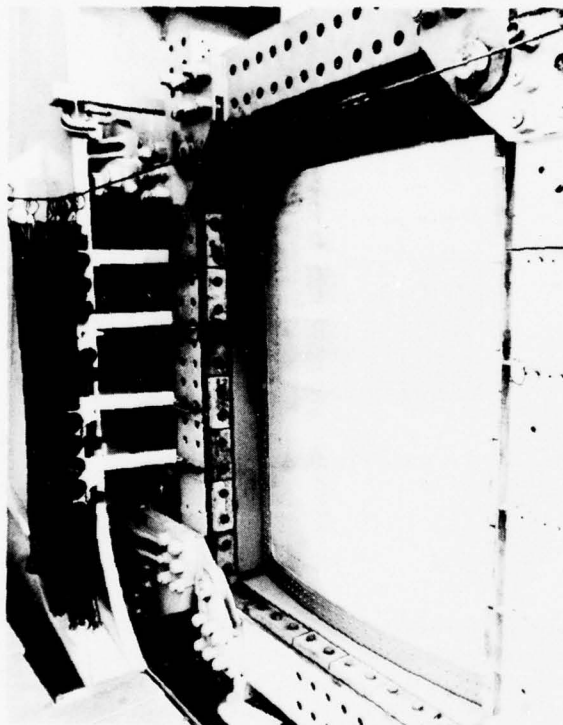
\*12 IN. FRAME  
SPACING\*\*48 IN. FRAME  
SPACING

FIGURE 15. PRETEST SPECIMEN INSTALLATION

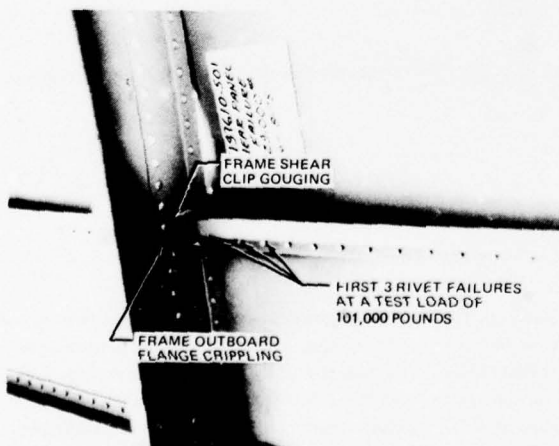


FIGURE 17. TEST FAILURES, RIVET PANEL - BACK VIEW

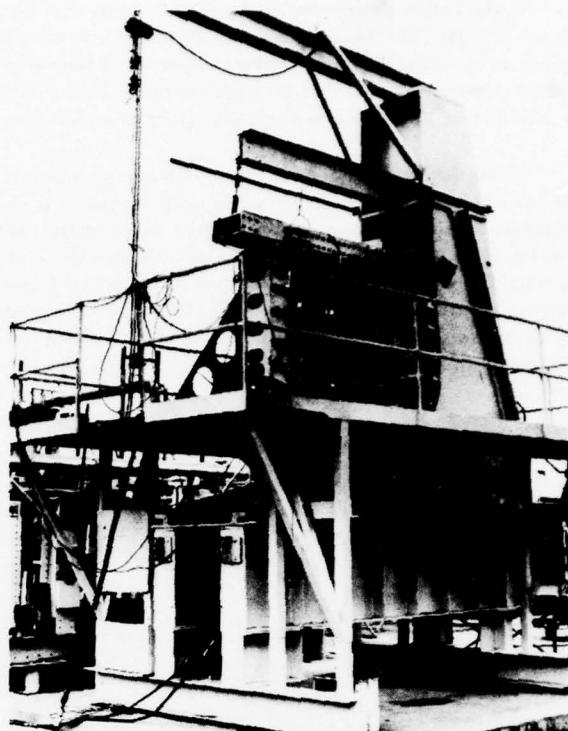


FIGURE 14. SHEAR JIG TEST SETUP



FIGURE 16. PRETEST SPECIMEN INSTALLATION

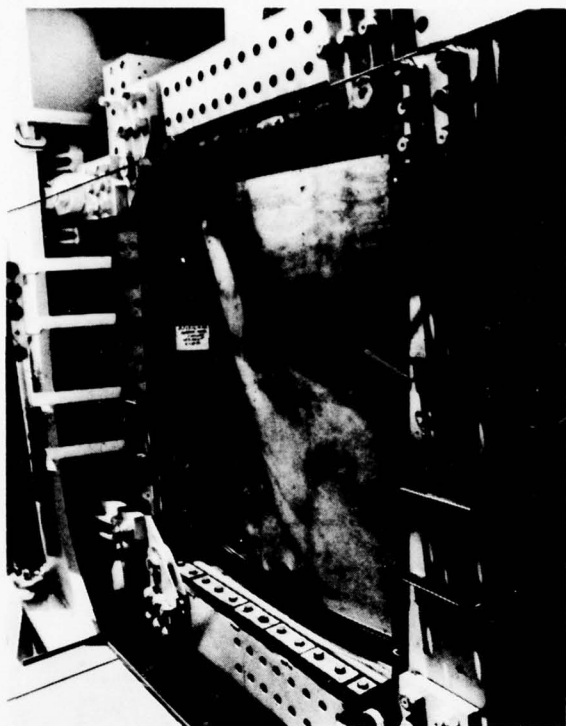


FIGURE 18. TEST FAILURES, RIVET PANEL - FRONT VIEW



FIGURE 19. TEST FAILURE OUTBOARD FLANGE CRIPPLING

**Static Test, Bonded Shear Panel** - This test was conducted to get a comparative static ultimate allowable shear for a shear panel with bonded stiffeners and frame attaching T-section. The panel was installed in the jig described above.

Panel Radius: 108 inches, test conducted at room temperature  
 Skin: 0.090-inch-thick 7075-T6  
 Longerons: 12 inches on center, area 0.298 sq in., I-section  
 Frame: 24 inches on center, area 0.808 sq in., T-section  
 Bonding: surface treatment phosphoric acid anodize, BR-127 adhesive primer and FM-73 adhesive, 0.045 pound per sq ft, mat carrier

The panel is shown installed in the jig in Figure 20. The onset of the diagonal tension wrinkling occurred at a test load of 38,000 pounds. It was not possible to identify specific failures prior to the final maximum load application. Final failure occurred at 138,500 pounds at the junction of the middle frame (F2) and the center of the west longeron (L2) (see Figure 21). Bond failure of the frame-to-skin shear clip appears to have resulted as a consequence of the frame and longeron flange crippling, all associated with the frame-to-longeron clip rivet failure (see Figure 22). The resulting shear stress at failure was 23,800 psi.

From these tests, it is apparent that the bonded panel, which was designed to the same criteria as the riveted panel, also carried the same load at the point of failure and that the yield point was perhaps a little higher.

**Static Test, Bonded Shear Panel** - The preceding test evaluated the bonding of heavy skin and stiffeners. The second bonded panel examines the other extreme, or the minimum thickness that would be used on the airplane. For the skin material, 7475-T651 was selected because of its high tensile strength. The test was also run at an elevated temperature where the adhesive would have reduced properties. The panel was installed and tested in the same jig used for the other panels.

Panel Radius: 108 inches, test temperature was 140°F  
 Skin: 0.0434-inch-thick 7475-T651 (chem-milled to thickness shown)  
 Longerons: 13 inches on center, area 0.228 sq in., bulb T-section  
 (This was an externally stiffened shear panel with these longerons on the outside of the skin, as shown in Figure 23.)  
 Frame: 24 inches on center, area 0.623 sq in., T-section  
 Bonding: surface treatment phosphoric acid anodize, BR-127 adhesive primer and FM-73 adhesive, 0.045 pound per sq ft, mat carrier

Because the panel was tested at elevated temperature, the shroud prevented the panel from being observed under load and therefore the exact yield point of the structure and the onset of diagonal tension wrinkles were not observed. The panel was loaded to 38,300 pounds or 658 pounds per inch, with no evidence of permanent set. The failing load was 77,400 pounds, or 1,330 pounds per inch. This converts to a shear stress of 30,648 psi. Figure 24 shows the frame failure, Figure 25 shows the shear wrinkle as it affects the external longerons, and Figures 26 and 27 show the longeron failures. The diagonal tension wrinkle across the panel was quite severe, and it was

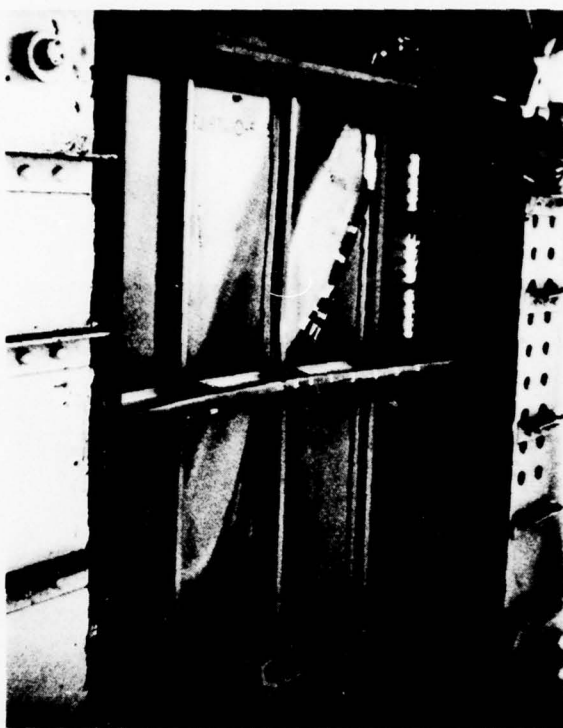


FIGURE 20. BONDED SHEAR PANEL FAILURE - BACK VIEW

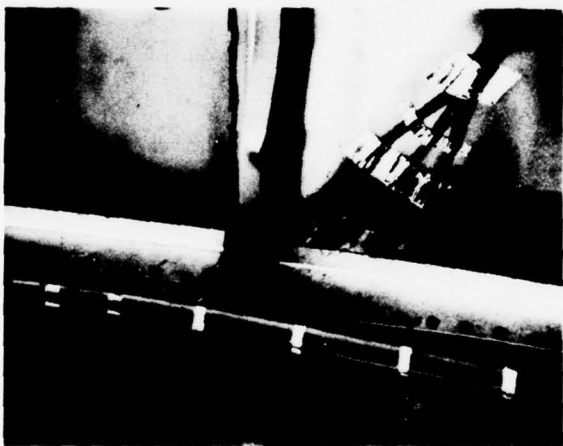


FIGURE 22. BONDED SHEAR PANEL LOCAL FAILURE

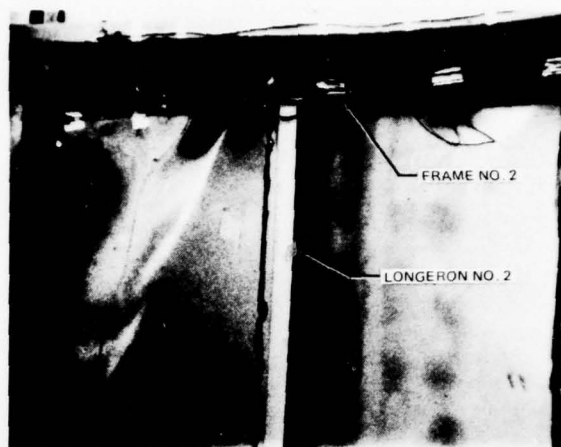


FIGURE 21. BONDED SHEAR PANEL FAILURE DETAIL

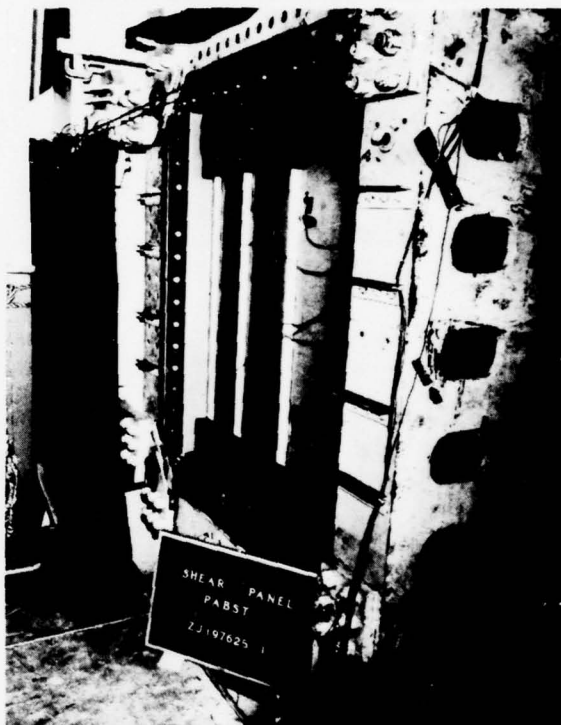


FIGURE 23. STATIC SHEAR TEST SETUP

interesting to note that the adhesive held (Figure 26) and failed the outside leg of the longeron. Some disbonding occurred during the failure on the other stiffener (see Figure 27). It appears that higher shear stresses could be obtained with increased frame strength and longeron area. The adhesive does not appear to be limiting the strength of the shear panel. The following data present specific properties of the adhesive used in the panel.

	Ambient (lb)	180°F (lb)
Lap shear test results	5476	3583
0.063-inch-thick 7075-T6 bare 0.5-inch overlap	5370	3846
	5185	3795
	5075	3872
	4870	3767
Average	5195	3772

T peel test results at 180°F = 15 pounds per inch width  
(0.032-inch-thick 2024T3 bare) at ambient temperature = 10.5 pounds per inch width

Singer butt tension tests at ambient temperature - 4000 psi

Tee specimens, failing load at ambient temperature - 1635 and 1625 pounds

Nondestructive inspection with the Fokker Bondtester found no flaws in the bonded assembly.



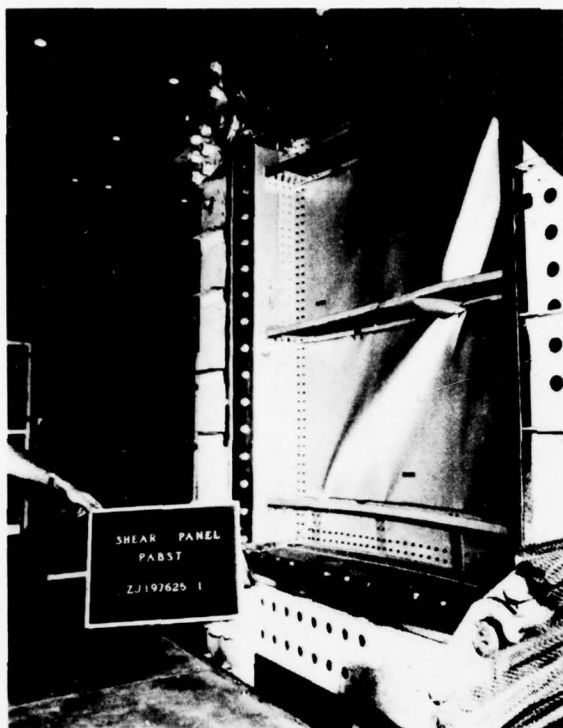


FIGURE 24. SHEAR TEST FAILURE - BACK VIEW

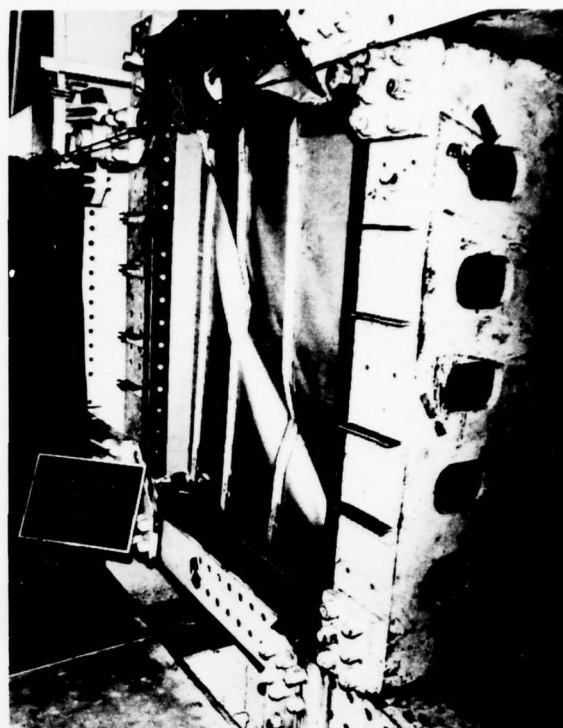


FIGURE 25. SHEAR TEST FAILURE - FRONT VIEW



FIGURE 26. SHEAR TEST FAILURE DETAIL



FIGURE 27. SHEAR TEST FAILURE DETAIL

**Static Test, Bonded Honeycomb Shear Panel** — A honeycomb configured shear panel was built using 0.020-inch-thick, 2024-T3 face sheets and honeycomb core of 0.800-inch thickness, 1/4 by 0.0015 inch, 5056 aluminum, 3.4 pounds per cubic foot, Grade B (corrosion-resistant). This panel was tested at room temperature and loaded until the panel would accept no more load, only increased deflection. The maximum load level achieved was 99,200 pounds or 1,700 pounds per inch. This is equivalent to a shear stress of 42,600 psi, which is the shear strength of the 2024-T3 material used. The permanent set in the panel at the end of the test was 2 inches, with no visible deformation within the panel. The same surface treatment and adhesive used in the preceding bonded panels were used to bond this panel.

### Shear-Compression/Tension Interaction Tests

In addition to testing the bonded panels in pure shear, it was thought advisable to examine the effects of combined shear and compression plus shear and tension. Five panels were built using the 108-inch-radius, 7475-T651 nonclad aluminum skin, all bonded after phosphoric acid anodize and BR-127 primer with FM-73 adhesive (mat carrier) 0.060 pound per square foot. All tests were conducted at the elevated temperature of 140°F. Four panels were made with 0.050-inch-thick skin and two panels had internal stiffeners 15 inches on center and frames spaced at 24 inches (Figure 28). The other two panels were externally stiffened with the same 15.5-inch longeron spacing and 24-inch frame spacing. The fifth panel was made using 0.090-inch-thick skin with no longerons and with frame spacing at 12 inches. This panel would represent the sides of the fuselage section to be built and tested.

The shear jig used for the previous tests was modified to add corrugated steel panels which run in the longitudinal direction of the panel plus added linkage at each corner. This allowed the application of tension or compression loads which represent fuselage bending loads to the shear panel and minimized the rigidity of the jig in resisting the load (see Figure 29).

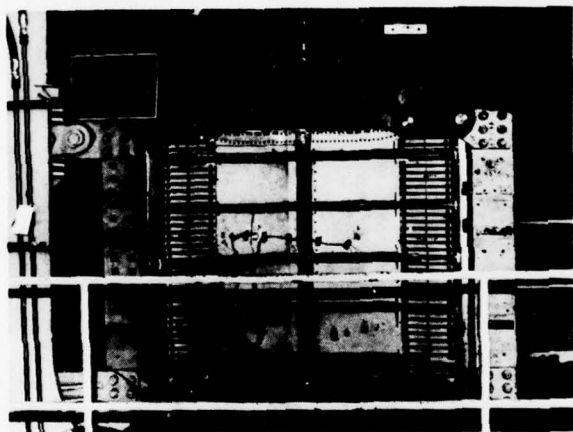


FIGURE 28. SHEAR INTERACTION PANEL

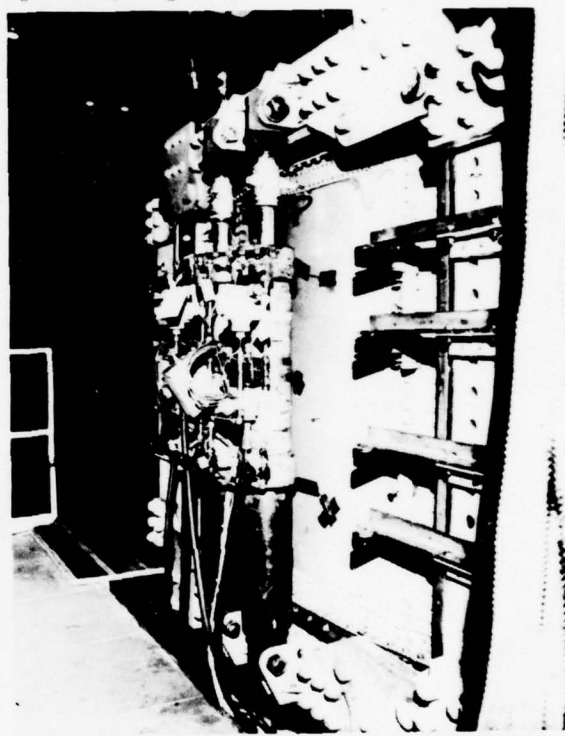


FIGURE 29. SHEAR AND COMPRESSION/TENSION TEST SETUP

In order to obtain as much data as possible from each of the five test panels, each test was conducted through a series of combined tension and compression plus shear. The first series started at approximately 90 percent of the calculated strength. For each test, the shear load was applied first, followed by the compression or tension load. The results of the five tests are shown in Figures 30 through 34. In each test, the panels were taken to failure. Figures 35 through 37 show photographs of the shear-compression final failure. The nondestructive inspection report for this shear-compression interaction panel is shown in Figure 38. Evaluation of the panel was made with the Fokker Bondtester, Model 70. The Bondtester detected:

1. One 3/4- by 2-1/2-inch and one 3/8- by 1-1/2-inch area of low bond strength, north side of the panel, beneath the center of the frame
2. One 1-1/4- by 2-1/4-inch area of low bond strength beneath the outside longeron
3. One 1-3/4- by 2-1/2-inch area of low bond strength beneath the center longeron adjacent to the center frame.

The assembly was accepted for test with no corrections.

It is evident that no bond failures resulted from the low strength indications from the Fokker Bondtester. The final failures of the shear-tension external longeron specimen are shown in Figures 39 through 41. It is interesting to note that on the concave side of the panel, the frame shear tee failed and the bonded portion stayed intact with the severely buckled skin. However, on the convex side, the central bulb tee was completely disbonded by the final failure. The shear-compression panel failure for the internally stiffened design is shown in Figures 42 through 45. Some disbonding occurred on the center longeron and center frame where the major buckle intersected. The shear-tension failure in the internally stiffened panel is found in Figures 46 through 48. The failure of the 0.090-inch-thick shear-compression panel with closely spaced frames and no longerons is shown in Figures 49 through 51. Again, metal failures predominated in this panel.

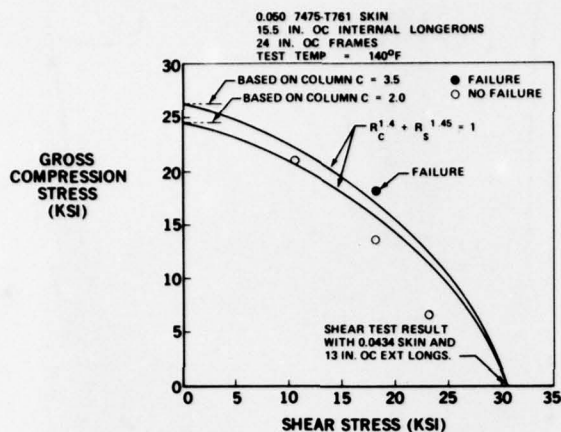


FIGURE 30. SHEAR-COMPRESSION ALLOWABLES

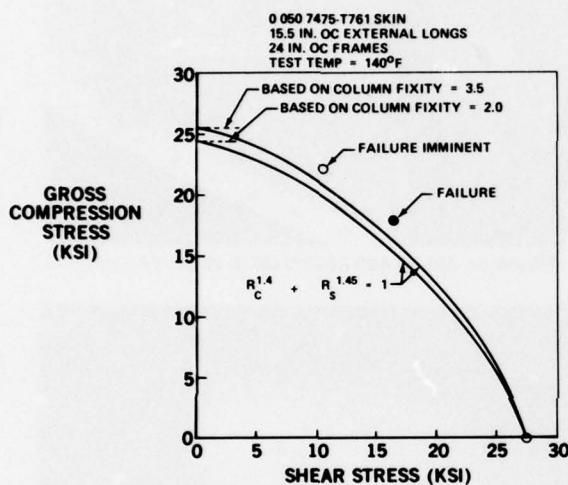


FIGURE 32. SHEAR-COMPRESSION ALLOWABLES

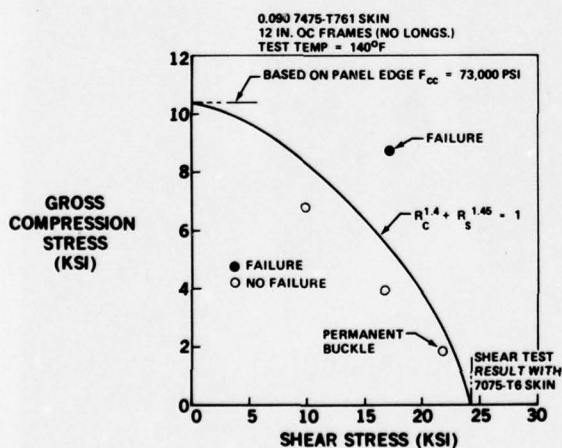


FIGURE 34. SHEAR-COMPRESSION ALLOWABLES

#### Frame Bending Test

The next test was conducted to examine the effect of frame bending on the internally stiffened design concept where the outer flange is in compression. This test was run at room temperature. The specimen consisted of three short frame segments bonded to the skin as shown in Figure 52. There are three longerons bonded on the skin also. The frames were each loaded as simple beams with a pair of symmetrical vertical loads to provide pure bending with no shear over the central test section. The load was applied so that the skin was in compression, which is the most critical direction of frame bending for static strength. The central frame (No. 2), having more effective skin working with its section properties, was the stiffest of the three frames. The test jig whiffing provided equal deflections in all frames, thus ensuring that the initial failure occurred in the central frame (No. 2). The specimen was loaded by a single hydraulic jack to apply approximately the same deflection to the three frames (see Figure 53).

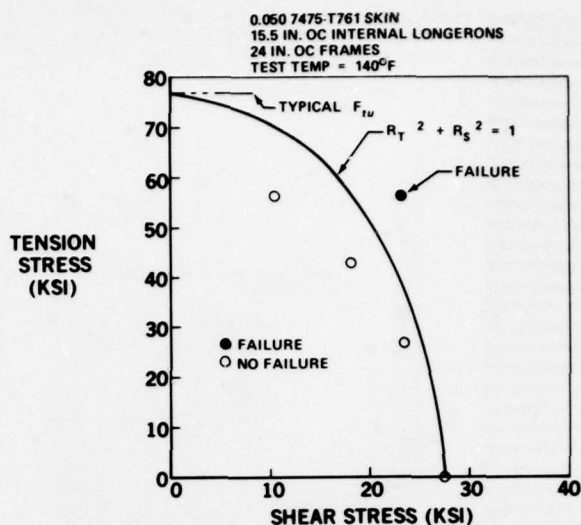


FIGURE 31. SHEAR-TENSION ALLOWABLES

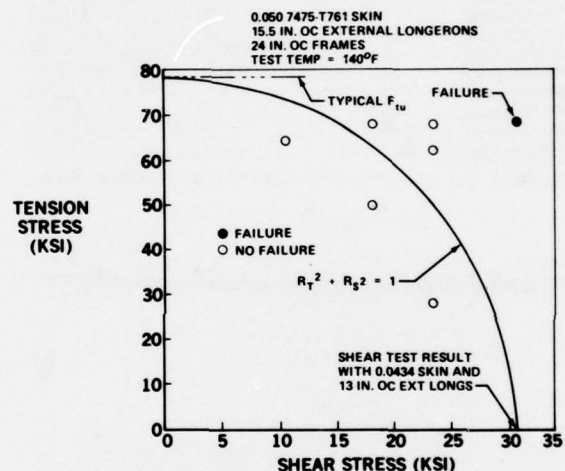


FIGURE 33. SHEAR-TENSION ALLOWABLES

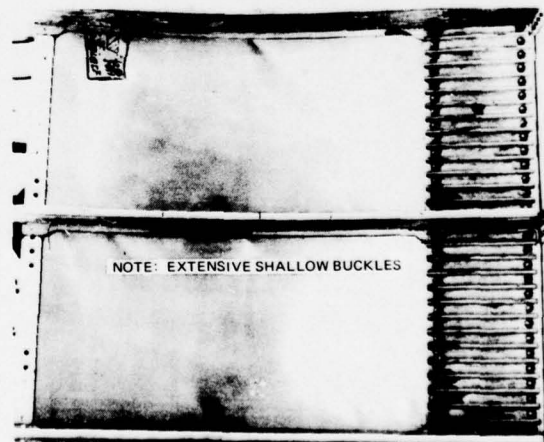


FIGURE 35. SHEAR AND COMPRESSION FAILURE - BACK VIEW



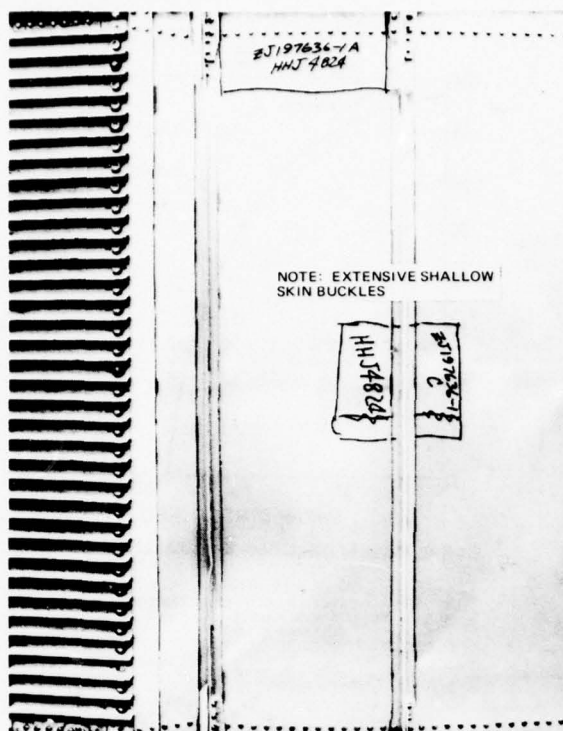


FIGURE 36. SHEAR AND COMPRESSION FAILURE - FRONT VIEW

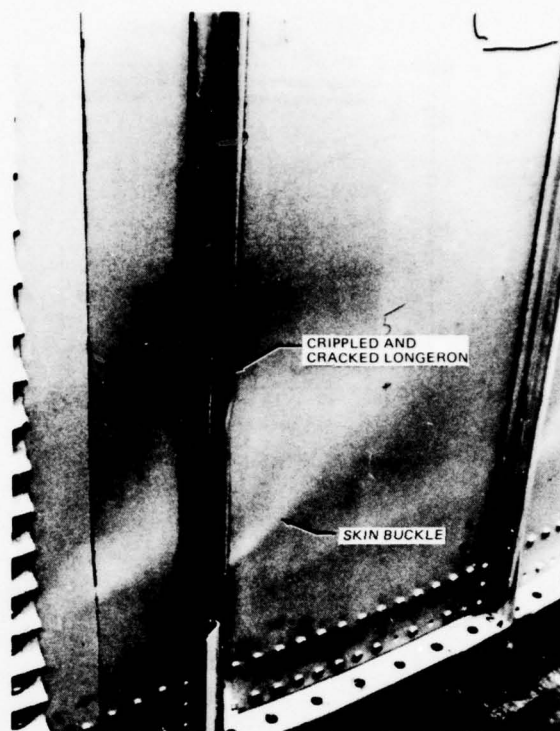


FIGURE 37. SHEAR AND COMPRESSION LOCAL FAILURE

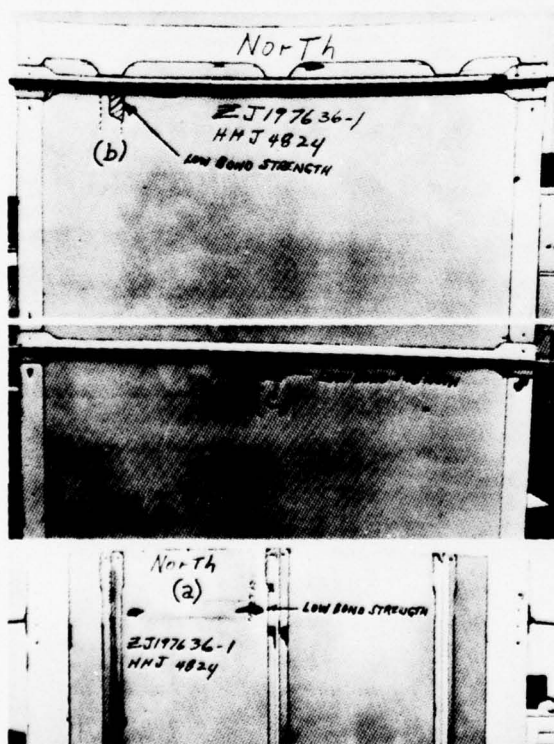


FIGURE 38. FOKKER BONDTESTER RESULTS FOR SHEAR-COMPRESSION PANEL

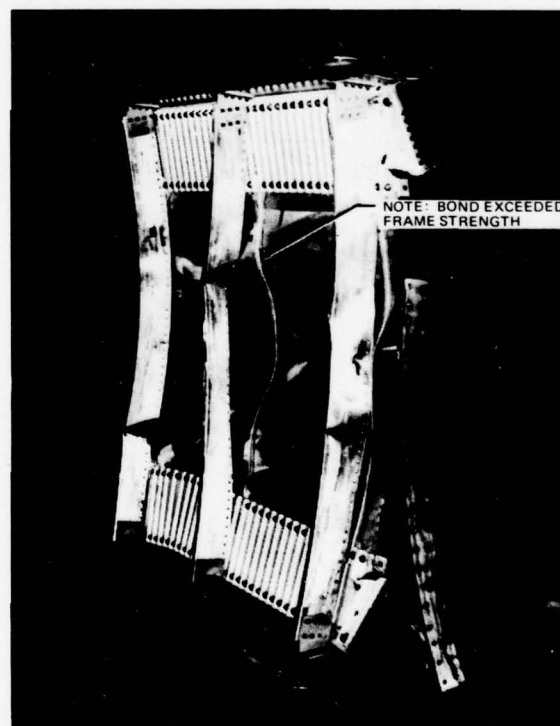


FIGURE 39. SHEAR AND TENSION FAILURE - BACK VIEW

The initial failure was observed to originate in the bond, over 1 inch long, starting at the edge of the central frame shear clip (Figures 54 and 55). A few seconds later, at the same test load, the remaining bond delaminated as shown in Figures 56 and 57. This was followed immediately by the remaining failures in frames and skin-to-frame shear clip disbond.

#### Mechanical Joints Fatigue Tests

Due to the large diameter and length of the full-scale demonstration component, it was necessary to join the bonded panels together with mechanical fasteners. It takes seven panels joined together to complete the full circumference of the 108-inch-radius fuselage. These longitudinal splices can have a single lap or be double-lapped. The top centerline joint, which was the last joint to be made, is a

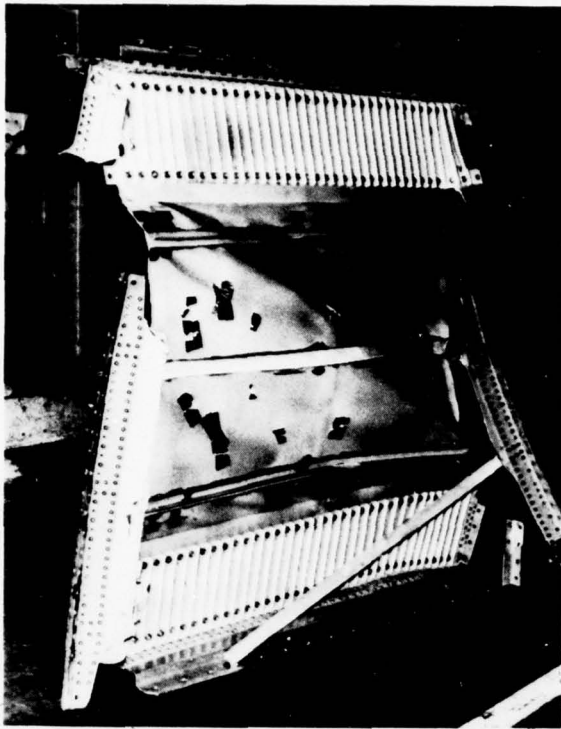


FIGURE 40. SHEAR AND TENSION FAILURE - FRONT VIEW

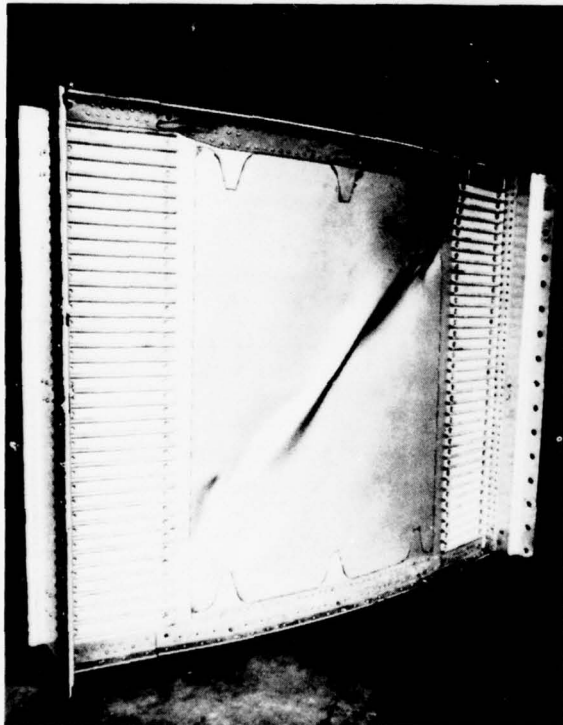


FIGURE 42. SHEAR AND COMPRESSION FAILURE - FRONT VIEW

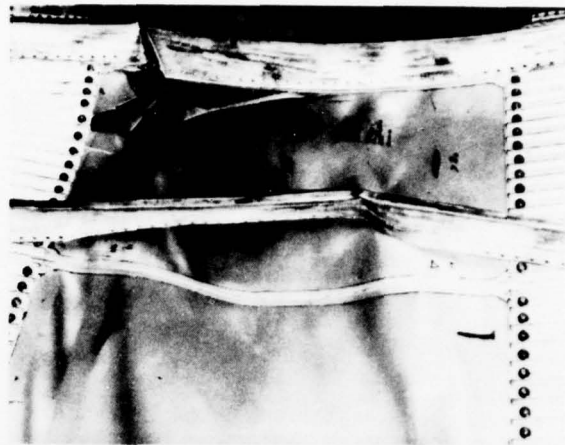


FIGURE 41. SHEAR AND TENSION RIB FAILURE

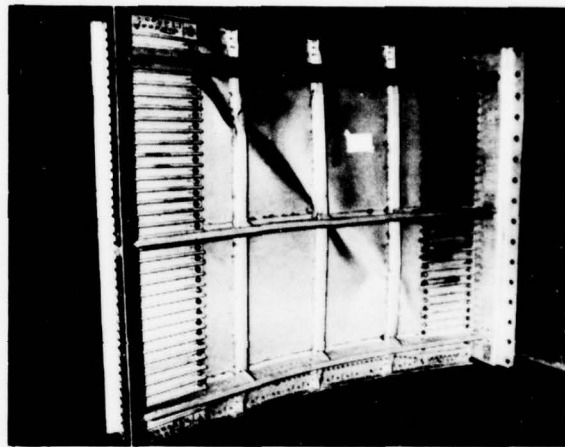


FIGURE 43. SHEAR AND COMPRESSION FAILURE - BACK VIEW

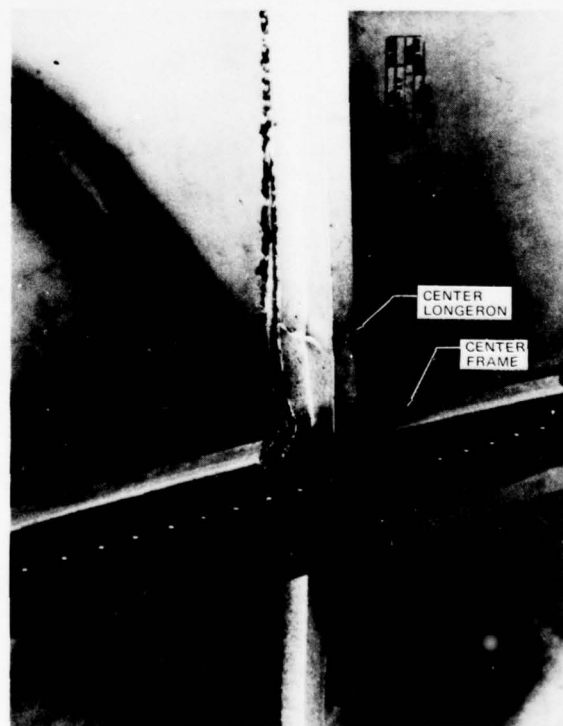


FIGURE 44. SHEAR AND COMPRESSION FAILURE DETAIL

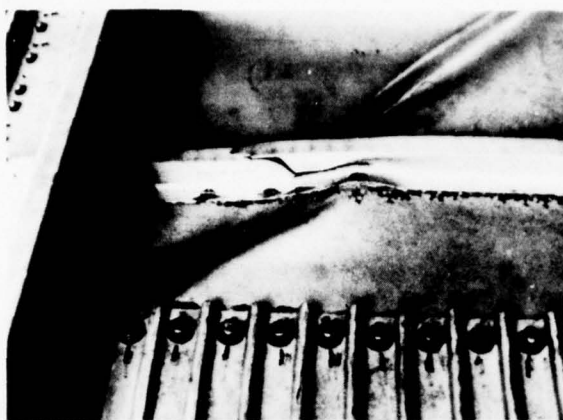


FIGURE 45. SHEAR AND COMPRESSION LONGERON FAILURE



FIGURE 47. SHEAR-TENSION FAILURE - BACK VIEW

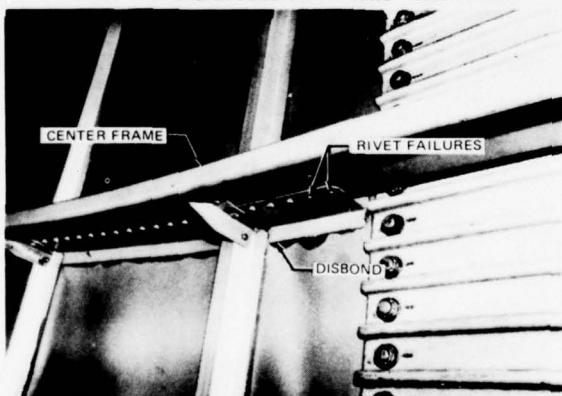


FIGURE 48. SHEAR-TENSION RIVET FAILURE

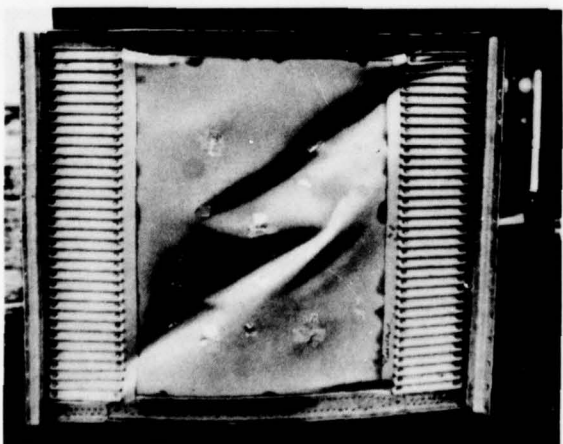


FIGURE 50. SHEAR AND COMPRESSION FAILURE

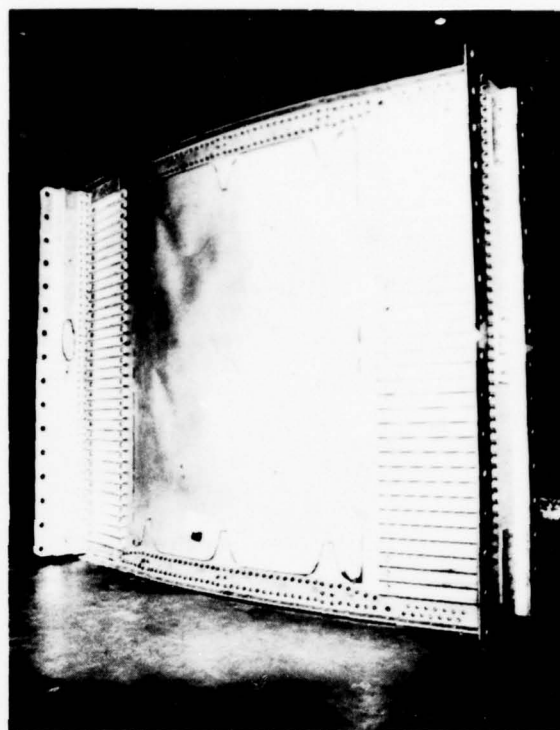


FIGURE 46. SHEAR-TENSION FAILURE - FRONT VIEW

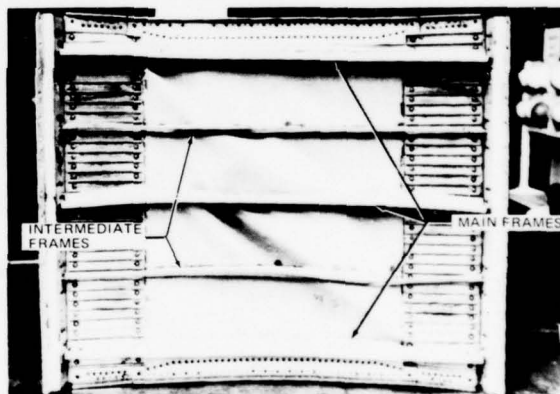


FIGURE 49. SHEAR AND COMPRESSION FAILURE - BACK VIEW

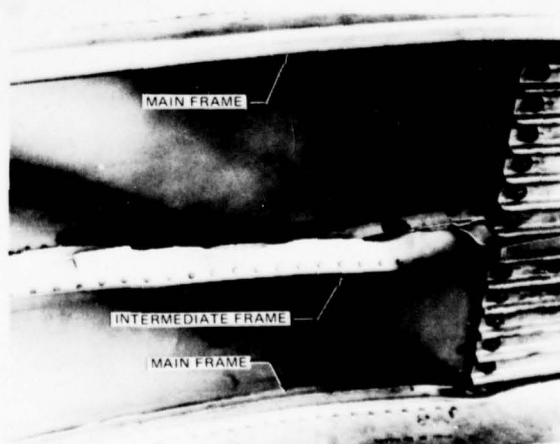


FIGURE 51. SHEAR AND COMPRESSION FRAME FAILURE



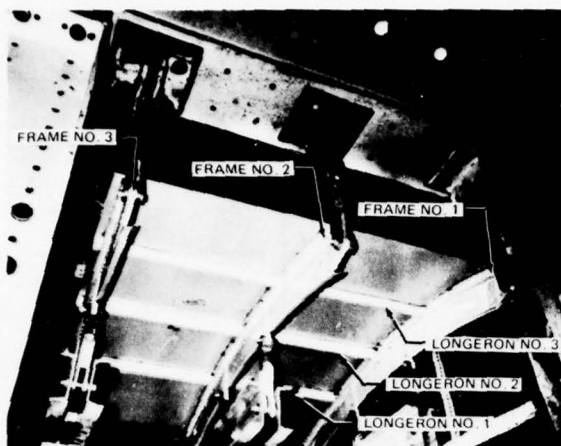


FIGURE 52. FRAME BENDING TEST SETUP

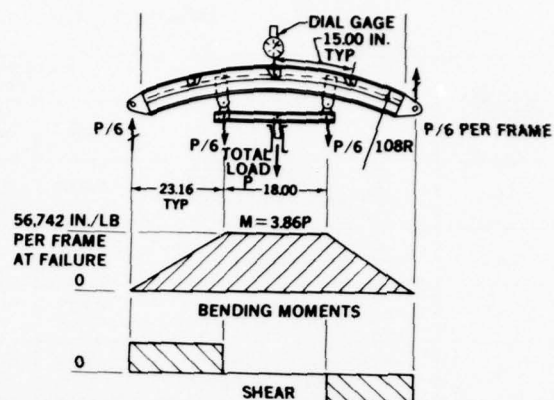


FIGURE 53. FRAME BENDING TEST

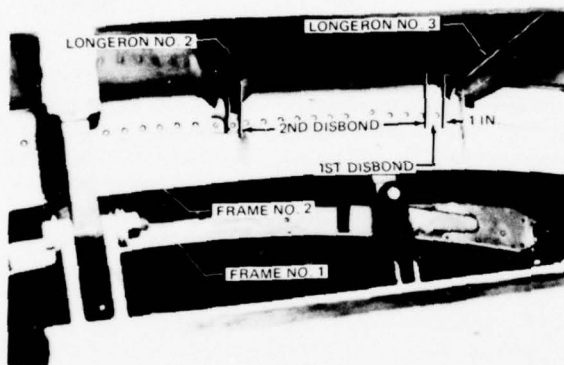


FIGURE 54. FRAME BENDING TEST FAILURE, DISBOND

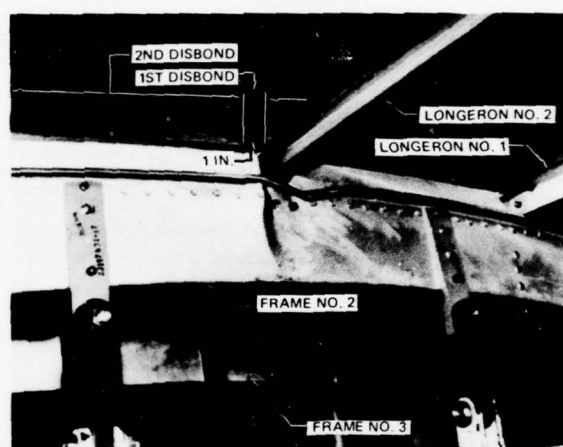


FIGURE 55. FRAME BENDING TEST, FRAME FAILURE

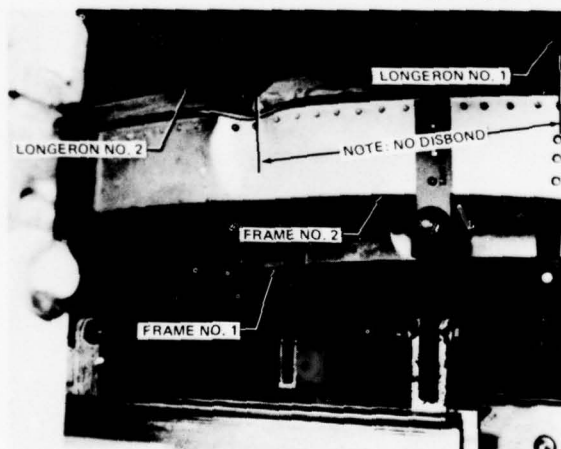


FIGURE 56. FRAME BENDING TEST, FRAME BUCKLE

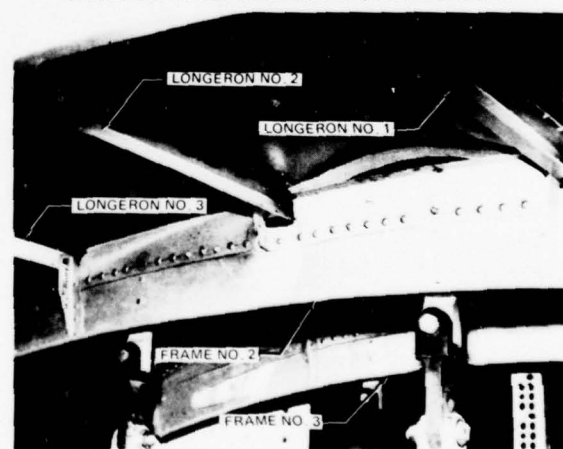


FIGURE 57. FRAME BENDING TEST, FRAME TEE DISBOND

double-overlap splice (see specimen No. 1 in Table 2). The other longitudinal splices used on the full-scale demonstration component are single overlap. Since several designs were created, each was tested (see Table 2). The cross hatch layer shown in the joint cross sections is a sealant, PR 1431G (MIL-S-81733). On one test panel joint, a curing adhesive was tried at room temperature. This adhesive was discarded because of its short pot life, which made it impractical to apply to faying surfaces and then join pieces before the adhesive had set.

#### FAIL-SAFE REQUIREMENTS AND EVALUATION TESTS

##### Specifications and PABST Requirements

The fail-safety of aircraft fuselages is strongly influenced by the manner in which skin cracks. Cracks appear in all structure, grow, and, with proper structural design and manufacture, are retarded, turned, or arrested by surrounding skin-stiffening members.



and crack arrest member (if present) failed. For the first requirement, at least the skin crack adjacent to a frame (or splice), where high stresses are induced from frame bending and pressure, shall be considered. All cracks considered shall be assumed to propagate in both directions.

For honeycomb structure, the longitudinal skin crack shall be in the face sheet on the side opposite the stiffening members. For foreign object damage, both face sheets and the core are cracked through a common plane.

Circumferential Cracks – The structure shall be able to withstand (1) a two-bay crack with the center longeron (or splice) intact, and (2) a 15-inch-long foreign object damage crack with the longeron (or splice) and crack arrest member (if present) failed. All flaws shall propagate in both directions.

Figure 58 presents a chart of the damage tolerance analysis.

The damage tolerance criterion for adhesive bonded joints was established as follows:

The analytical damage tolerance assessment shall be confined to residual strength estimates. The analyses shall assume the presence of flaws in the bond placed in the most unfavorable location and orientation with respect to applied stress and material properties. The experimental investigation shall be limited to distinguishing between flaws which grow and those which do not. Thermal and humidity effects shall be accounted for.

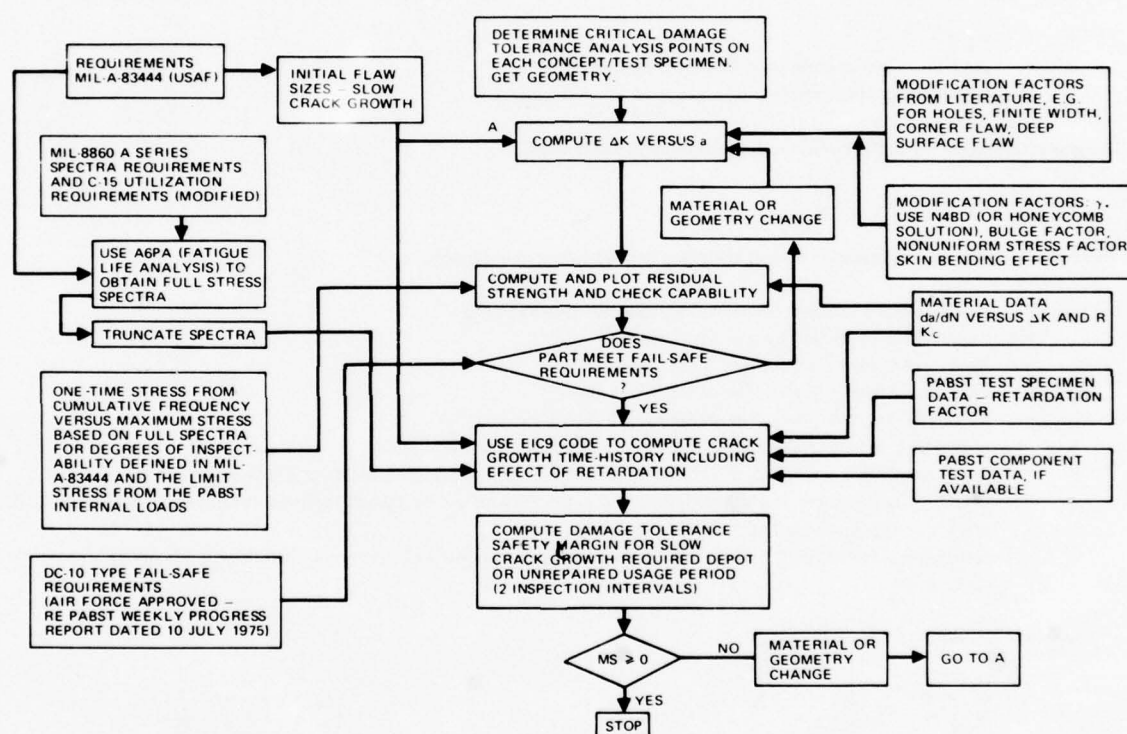


FIGURE 58. DAMAGE TOLERANCE ANALYSIS FOR METAL STRUCTURE

Entire panels or parts which are improperly processed (i.e., parts with global damage) shall be rejected. Parts with local contamination or flaws shall be reworked to a quality in which the flaws shall not grow to unacceptable sizes within two airframe lifetimes.

Initial Flaw Sizes – An initial flaw shall be assumed to exist in each and every bond in its most critical location, including those highly stressed areas resulting from variable bond line thickness. The size of the flaw shall be the greater of (1) the minimum detectable size for the nondestructive inspection technique used on the bond, or (2) the smallest flaw remaining after a larger flaw has been repaired. Each flaw shall be analyzed for residual strength independently of all other flaws, either in the bond or metal. Initial flaws shall be located so there is no interaction between them.

Bond Inspectability – The detail design shall minimize the use of uninspectable bonds and, wherever practical, shall be such as to force the first evidence of failure into a visible or easily inspected area. Techniques such as staggering the ends of the overlaps shall be used to facilitate inspection of the bonds. Each uninspectable bond shall be limited in extent to a subcritical size.

Flaw Growth in Bonds – Flaws in bonds induced in service shall not grow from initial sizes defined above to critical size within two airframe lifetimes. All flaws large enough to grow in service shall be repaired prior to delivery of the aircraft to preclude corrosion. In addition, bonds which contain subcritical flaws in areas subject to corrosion shall be sealed to provide environmental resistance.



**Fail-Safe Capability** – The fail-safe capability of the bonded structure shall be demonstrated by test and/or analysis. The structure shall be capable of withstanding (1) limit load with each of the following two-bay disbond configurations:

- (a) a two-bay disbond in only one side of a double-lap splice,
- (b) a two-bay disbond in a single-sided bonded splice,
- (c) a two-bay longeron-to-skin disbond, and
- (d) a two-bay shear-clip-to-skin or crack-arrest-member-to-skin disbond,

and (2) the maximum average internal member load occurring in 20 lifetimes, but less than limit load, for impact or the foreign object damage specified as:

- (a) a 15-inch disbond on both sides of a splice, and
- (b) a 15-inch-long foreign object damage skin crack with both the center frame (or splice) and the crack arrest member failed or with both the longeron (or splice) and crack arrest member failed as applicable.

**Damage Tolerance Analysis Methods (Metals)** – The crack growth and residual strength analyses of the metallic structure were based on classical linear-elastic fracture mechanics in which the model consists of a symmetric crack growing from a through-the-thickness flaw in an infinite sheet. A basic assumption made is that the local stress conditions at the crack tip are defined by the local stress intensity  $K$ , where:

$$\begin{aligned} K &= \sigma \sqrt{\pi a} \\ \sigma &= \text{gross area stress remote from the crack tip (psi)} \\ a &= \text{half-crack length (inches)} \end{aligned}$$

The general equation for stiffened thin-walled structure of finite size is

$$K = \sigma \sqrt{\pi a} \beta_1 \beta_2 \dots \beta_N$$

where the  $\beta_N$  terms are modification factors including the following, as applicable:

- $F (a/r)$  = Bowie correction for symmetric or asymmetric cracks at holes
- $\lambda_1$  = Finite width correction for eccentric cracks<sup>(4)</sup>
- $\lambda_2$  = Finite width correction for single edge cracks<sup>(4)</sup>
- $a_b$  = Liu back surface correction factor for corner flaws<sup>(5)</sup>
- $M_k$  = Kobayashi factor for deep surface discontinuities<sup>(6)</sup>
- $\gamma$  = Swift factor accounting for the effect of stiffening on a cracking sheet<sup>(7)</sup>
- $B$  = Correction factor accounting for the effect of bulging on a cracking curved sheet due to pressure<sup>(8)</sup>
- $\xi$  = Effect of nonuniform stress distribution from the pressurized uncracked stiffened cylinder on a longitudinal skin crack. See Figures 59 and 60.
- $F$  = Knockdown factor for the effect of the skin bending stress on a circumferential crack near a frame in a pressurized shell.

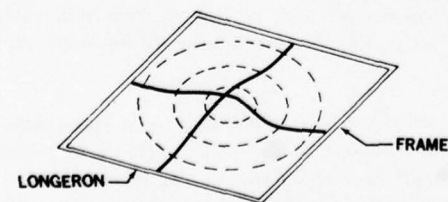
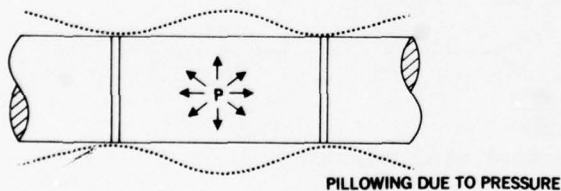


FIGURE 59. STRESS DISTRIBUTION IN A PRESSURIZED STIFFENED CYLINDER

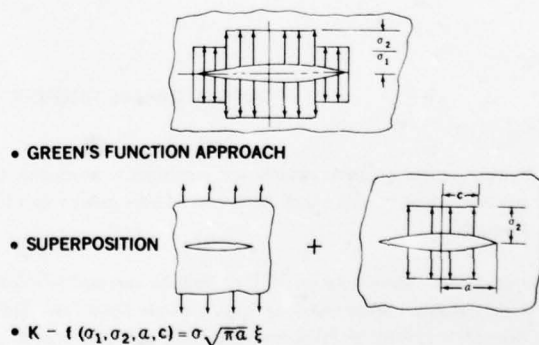


FIGURE 60. NONUNIFORM STRESS DISTRIBUTION FACTOR

The damage tolerance analyses were based on the Hart-Smith method of predicting the stress distribution in a pressurized stiffened cylinder (Figure 60). This method is more accurate than the classical solution since (1) the distortion under load included in shell buckling theory is accounted for, (2) the deflected shape is defined by nonoscillatory exponential decay functions, (3) the correct frame stresses are obtained by using the junction stresses between the skin and frame determined by the skin bending moments, and (4) the axial stiffener influence on the skin stresses is accounted for (through Poisson effects).

The crack growth time histories of the cracked structural members analyzed were calculated using a Douglas computer program that is an expanded version of the Air Force CRACKS program. Residual strength was calculated using critical stress intensity (i.e.,  $k_c$ ) data.

### Crack Growth Tests

**Flat Panels** — At the start of the PABST program, it was decided to make some crack growth tests to compare effects of bonded stiffeners versus riveted stiffeners and to verify the analyses. Two flat panel tests were run. One panel had a single central stiffener with a small flaw at a rivet hole and another had a similar total length crack in the skin under bonded stiffener joint (see Figure 61). The results seemed very favorable to the bonded configuration because it took 230,000 crack growth cycles to reach a 3-inch half-crack length versus 140,000 for the riveted design. Also, when testing a bonded specimen at 140°F where the adhesive had reduced shear strength, 275,000 cycles were required to reach 3-inch half-crack lengths. All panels were tested at a maximum basic skin stress of 14,000 psi.

The second set of panels built were wider and had two stiffeners and a central crack between them. The initial crack length was 0.25 inch and was allowed to grow to a full length of 14 inches. Figure 62 shows the crack growth history. Again, the bonded stiffener offered more retardation to the initial crack growth up to the time the crack reached the stiffener, and then the rate of crack growth across the stiffener and beyond was reduced. For the rivet stiffener, the last 1.5 inches of crack growth took approximately 1,000 cycles while the bonded stiffener configuration took 11,000 cycles to go the last 1.5 inches. The residual strength failing load of the bonded panel was 13.5 percent greater than for the riveted panel. Other flat, unpressurized bonded panels have had cracks grow straight across to the stiffeners and beyond, and fail-safe panels have demonstrated that fast fractures can be arrested by adjacent bonded stiffeners.

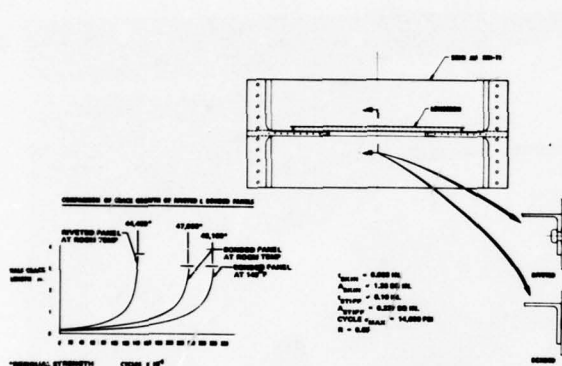


FIGURE 61. DAMAGE TOLERANCE TEST SPECIMEN

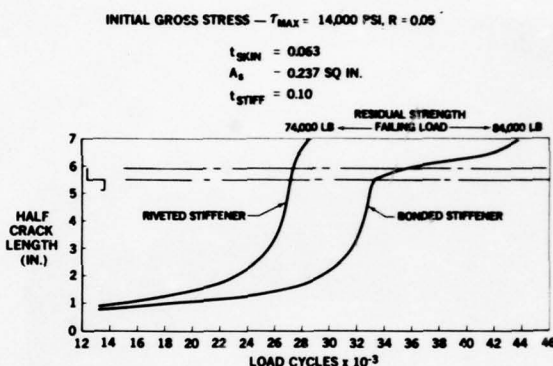


FIGURE 62. CRACK GROWTH COMPARISON TESTS

It was determined that the damage tolerance capability of the internal longeron structural concept to be used on the upper quadrant of a full-scale test article should be tested to verify the analytical methods. Two specimens were built. One was 84 inches wide and contained four representative frames, one longeron, and one longitudinal splice with longeron. The panel was 136 inches long and flat. Loads were applied to the short dimension and represented the cabin pressure. Two longitudinal sawcuts, 0.20 inch long, as called for in military specifications, were put in the panel, one adjacent to the center of the longeron and the other in the outer splice doubler, behind the longeron. The constant-amplitude cyclic stress was 17,800 psi at a stress ratio ( $R$ ) of 0.05. This is the hoop tension resulting from full cabin pressure. The cycle rate was approximately 1 Hz. The goal was to obtain two lifetimes (38,028 cycles) or failure, whichever occurred first. The flaw in the 0.050-inch-thick 7475-T761 skin started to propagate after 12,000 cycles and grew to a length of 2.78 inches at 36,803 cycles, when the panel failed. The flaw in the 0.040-inch-thick 7475-T761 doubler did not propagate during the entire test.

From experience on riveted design, the intersection of the longeron and the frame has been a critical area for crack initiation. At the intersection of the frames, which ran lengthwise on this test panel, and at each of the two representative longerons, there was a cutout in the frame shear tee. This is referred to by the designers as a "mouse hole." The mouse-hole detail for the longeron was different from the mouse hole for the longeron at the splice. The shear tee joggles up on the internal splice doubler but at the other longeron, the edge of the mouse-hole cutout in the shear tee terminates on the 0.050-inch-thick skin (Figure 63). During an inspection at 31,270 cycles, a 4.25-inch crack was discovered at one of the longeron mouse holes. After 35,070 cycles, four of the possible eight mouse-hole locations where shear tee stopped on the skin were cracked. The longest was 10.25 inches and the other three were 1.25, 2.29, and 2.51 inches. The panel was tested through 36,803 cycles when a complete panel failure occurred through three of the mouse-hole cracks. After the test, it was determined that all eight similar locations had developed fatigue cracks prior to the failure. Figure 64 shows the total layout of the panel and the location of the two sawcuts and the fatigue cracks at the mouse-hole cutout. It should be noted that the mouse-hole cutouts at the splice area developed no fatigue cracks. Figure 65 is a closeup of the failure nucleation points at three frame locations. Figure 66 shows the cracks which started at the fourth mouse-hole location but were not involved in total panel failure.

As a result of the failure in the first panel, engineering changes were incorporated in the second panel at the longeron mouse holes. The discontinuity at the shear tee cutouts was corrected by cold-bonding a short strap on the skin leg of the shear tee and the skin leg of the longeron (see Figure 67). Figure 68 shows the details of the panel. The panel is 108 inches wide with five frames, 144 inches long, one longeron, and a double-lap splice in the skin. A manufactured flaw, 0.290 inch long, was made at one side of the mousehole in the center frame. This duplicates the crack that developed in the preceding panel. The panel was cycled at the same stress level used for the previous panel, 17,800 psi and  $R = 0.05$ .



FIGURE 63. MOUSE HOLE CUTOUTS

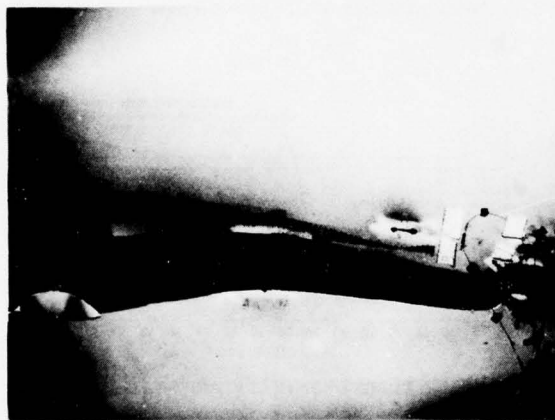


FIGURE 65. FAILURE NUCLEATIONS

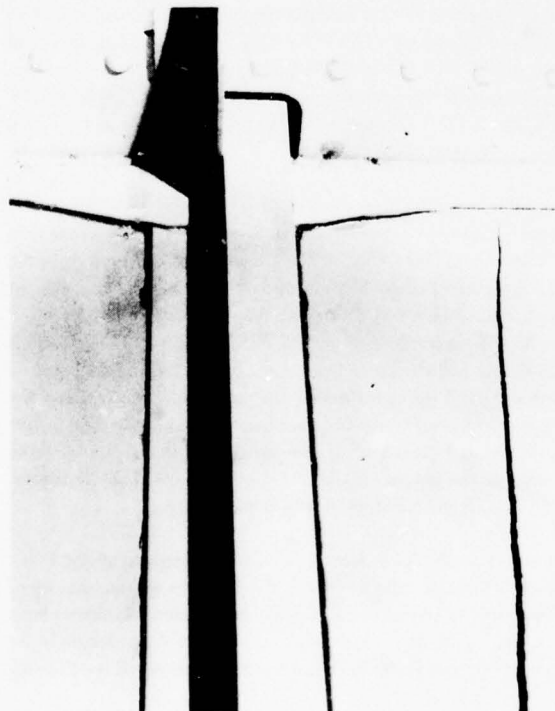


FIGURE 67. BONDED REPAIR DOUBLER

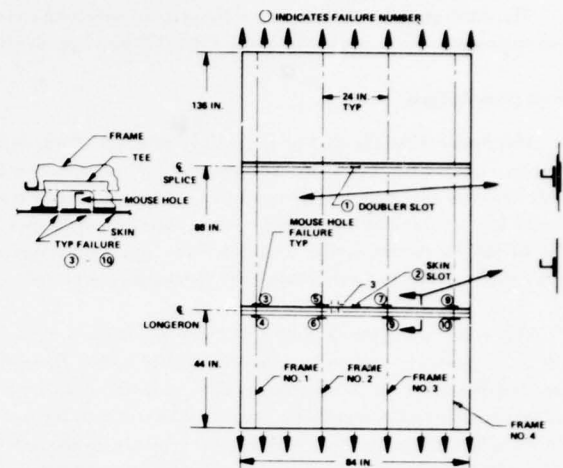


FIGURE 64. INTERNAL LONGERON TEST FAILURE LOCATIONS



FIGURE 66. MOUSE HOLE CRACK INITIATIONS

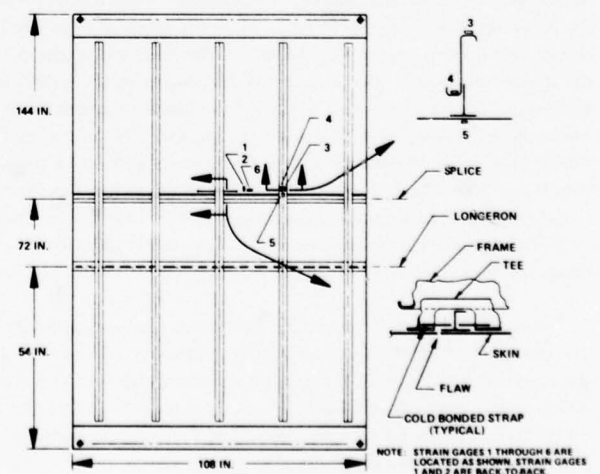


FIGURE 68. TEST SPECIMEN DETAILS



The panel was cycled until the total crack length was 15 inches. It took 37,208 cycles. This is the crack length needed to test for the foreign object damage criteria. The crack growth time history is shown in Figure 69. The center frame was sawed in two above the skin initial flaw since the center frame must be broken to test for the residual strength required for foreign object damage. The fail-safe load was calculated to be 153,770 pounds or 18,400 psi. This is the full cabin pressure load times a dynamic load factor. The load was applied at a rate of 15,000 pounds per minute. The crack fast-fractured to the two adjacent frames (47.50 inches) at a load of 151,617 pounds and self-arrested. The test results are listed in Table 3 and plotted in Figure 70. Figure 71 shows the 15-inch crack and Figure 72 shows the crack arrest point near the frame. Figure 73 shows the frame sawcut. This test was considered a success for the design.

**Pressurized Panels** — The next testing effort examined the concepts by subjecting them to biaxial stresses and then evaluating the fatigue life and damage tolerance capability of three bonded designs. These tests would verify that the structure was capable of sustaining two lifetimes (38,028 cycles) of limit pressure (the ground-air-ground cycle) and verify that the slow crack growth damage tolerance criteria of two additional lifetimes at limit pressure could be met. Further, the tests would verify the fail-safe criteria which required that the structure would be capable of withstanding limit cabin pressure with (1) a two-bay crack, and, separately, (2) a 15-inch crack from foreign object damage. The test specimen which would be representative of a panel from the side of a bonded YC-15 fuselage is shown in Figure 74. The overall dimensions are shown and the structural arrangements are detailed in Figure 75. All the frame members (shear tees) are bonded to the fuselage skin (0.05-inch 7475-T761) as well as the bonded splice and longeron No. 2, shown in Figure 75. Details of the structural components are shown in Figure 76. A transverse splice and a longitudinal mechanical splice are built into this panel for purposes of evaluating the fatigue life of this design.

Figure 77 is a photograph of the test fixture showing the vacuum box which is used to apply the effects of cabin pressure on the fuselage panel. Circumferential whiffle trees resist the pressure load while axial (longitudinal) jacks supply the other component of the cabin pressure load to place the panel in an equilibrium condition that is found on the aircraft. No shear loads are applied to this test panel. It was necessary to apply a vacuum of 8.6 psi in order to achieve circumferential resisting loads that would be felt when the airplane cabin was pressured to 7.15 psi. Figure 78 presents a photograph of the panel installed in the test fixture. The panels were cycle-tested at a rate of one pressure cycle each four seconds. The hydraulic axial load was synchronized with the vacuum pressure load. The panel successfully withstood 38,028 pressure cycles with no fatigue cracks being generated in the participating structure. Subsequent to this, six damage tolerance flaws were cut in the structure and identified as DT1 through DT6 in Figure 79.

TABLE 3  
CRACK GROWTH VERSUS LOAD

PERCENT OF LOAD	LOAD (LB)	CRACK LENGTH (IN.)		
		LEFT	RIGHT	TOTAL
0	0	8.08	6.98	15.06
10	15,377	8.08	6.98	15.06
20	30,754	8.08	6.98	15.06
30	46,131	8.08	6.98	15.06
40	61,508	8.08	6.98	15.06
50	76,885	8.08	6.98	15.06
60	92,262	8.08	6.98	15.06
70	107,639	8.08	6.98	15.06
80	123,016	8.10	7.05	15.15
90	138,393	8.30	7.25	15.55
98.6	151,617	23.60	23.90	47.50

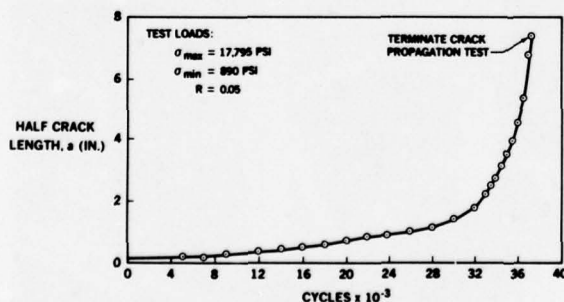


FIGURE 69. CRACK GROWTH TIME HISTORY



FIGURE 71. FAST-FRACTURE CRACK GROWTH

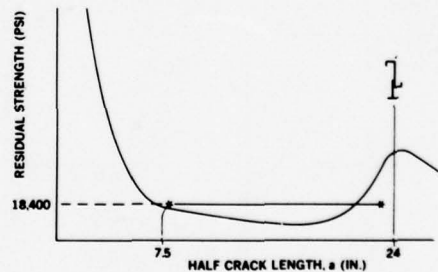


FIGURE 70. RESIDUAL STRENGTH FOR FOREIGN OBJECT DAMAGE



FIGURE 72. FAST-FRACTURE CRACK TERMINATION

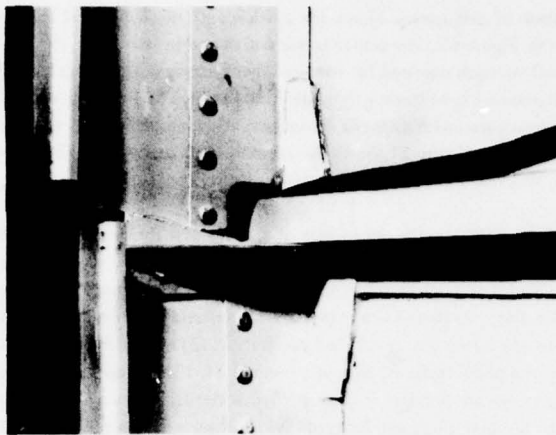


FIGURE 73. INITIAL FRAME SAWCUT

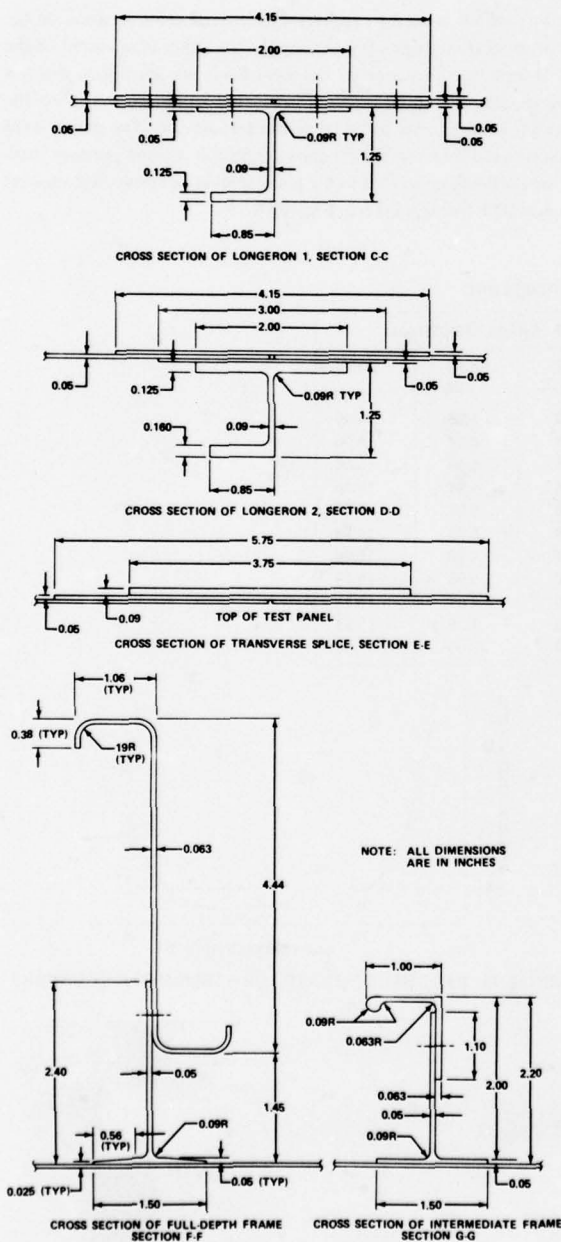


FIGURE 76. FRAME CROSS SECTIONS

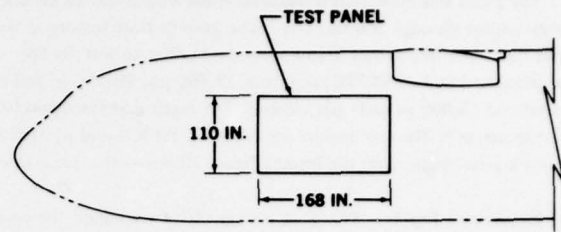


FIGURE 74. TEST PANEL SIZE IN RELATION TO YC-15 FUSELAGE

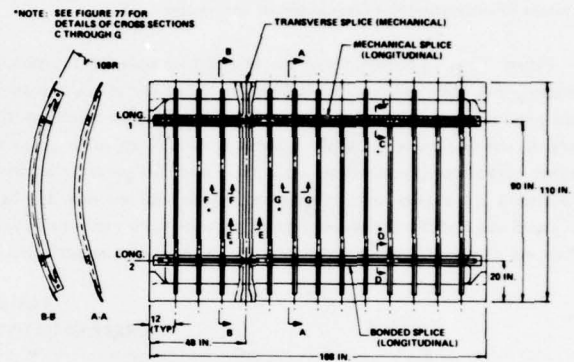


FIGURE 75. STRUCTURAL ARRANGEMENT OF TEST PANEL

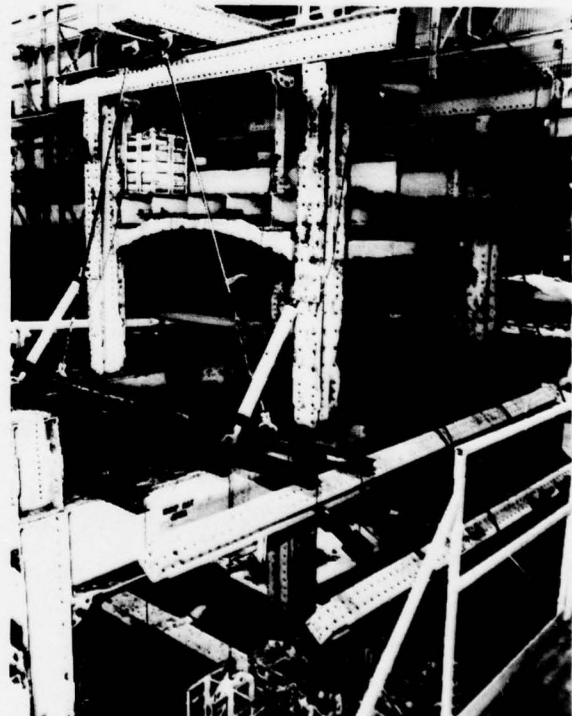


FIGURE 77. PRESSURE TEST SETUP

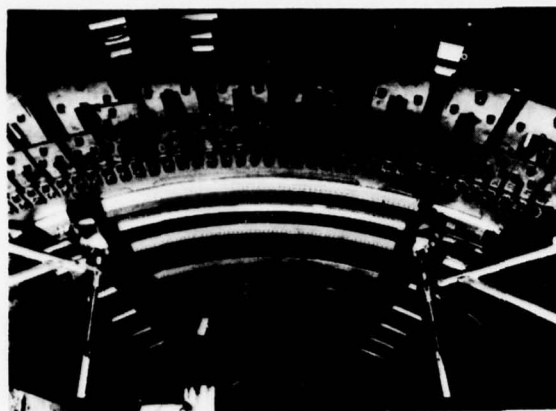


FIGURE 78. TEST PANEL INSTALLED IN PRESSURE JIG

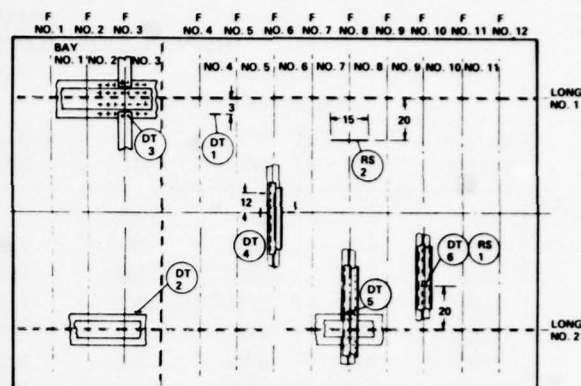


FIGURE 79. INITIAL FLAWS AND RESIDUAL STRENGTH SAWCUTS

In the figure,

- DT1 – Bay No. 4, an 0.25-inch slot in midbay along the panel centerline. The slot is in the longitudinal direction. The final 0.025-inch length of the slot at each tip was achieved by a modeling saw.
- DT2 – Bay No. 2, same as bay No. 4, except that the 0.025-inch slot is in the skin along with the longeron No. 2 bond line. The 0.025 inch at each tip was achieved with a modeling saw.
- DT3 – Frame between bays No. 2 and No. 3 at longeron No. 1 with a through-the-thickness flaw (0.05 inch) on one side of the fastener hole. The flaw was extended through all the thicknesses of the T-clip, skin, and doubler materials.
- DT4 – Bay No. 5, an 0.25-inch slot in the transverse (circumferential) direction along the T-clip bond line. The slot centerline coincides with the panel longitudinal centerline. The final 0.025 inch at each tip was achieved with a modeling saw.
- DT5 – Frame between bays No. 7 and No. 8 at the doubler bond line (longeron No. 2), an 0.25-inch slot in the skin, longitudinal direction. The final 0.025 inch at each tip was achieved with a modeling saw. Care was taken to avoid damage to the T-clip flange.
- DT6 – Frame between bays No. 9 and No. 10, same as DT5 except the slot is located 20 inches from the centerline of longeron No. 2.

The panel was again cycled for an additional 38,028 cycles (two lifetimes) at the limit pressure load. Constant surveillance was maintained of each of the damage tolerance flaws (DT1 through DT6). The crack growth is shown in Table 4. Other than the propagation of the damage tolerance flaws, no fatigue cracks were encountered in the participating structure.

The next phase of testing on this panel was to cut the fail-safe flaws and test for residual strength. Two flaws were planned for this test, but each was tested separately. The first fail-safe flaw, RS1, is a two-bay crack with the centerline frame intact. This was accomplished by extending the flaw, DT6, 18 inches centered on the centerline frame. This sawcut was sharpened by pressure-cycling the panel at 5 psi for 40 cycles. This produced a visible fatigue crack at each end of the sawcut. The fail-safe load was applied in the following manner: cabin pressure was increased from zero to the maximum 8.6 psi with the longitudinal load held at zero. After the full pressure was reached, the longitudinal load was increased to its maximum of 114,500 pounds. No flaw growth was noted on the application of the pressure loading alone, but as the longitudinal load was applied, the crack tips grew and turned 90 degrees to the sawcut direction. Total crack growth was 0.65 inch and occurred on the west side of the crack tip. No further failures were encountered with this crack length. The crack was increased 1 inch at each tip and sharpened by cycling to a pressure of 5 psi. Fail-safe load was applied in the same sequence as before and, again, the west side of the crack tip grew circumferentially at the end of the new crack tip. Again, the sawcut was increased to a full length of 22 inches and the fail-safe load applied as before.

During the application of the longitudinal load, the crack tips propagated to the adjacent frame shear tee bond lines and each turned circumferentially, but in opposite directions. The crack was successfully arrested by the bonded shear tees and the fail-safe load successfully carried. Figure 80 shows the crack pattern as developed by this fail-safe test. This flaw was patched with a riveted doubler and the second fail-safe flaw, RS2, was made. This was to represent the results of foreign object damage and was made by sawing through a frame in the skin longitudinally, as shown in Figure 79.

It was intended that the fail-safe load be applied in the same sequence as for RS1. However, at a pressure of 6.9 psi and no longitudinal load, the flaw propagated to the adjacent frames and disappeared into the frame tee flange glue lines. The loading sequence was changed to apply the pressure and longitudinal load simultaneously to the peak value, and hold the pressure and relax the longitudinal loads in steps. No further failure was encountered. Again, the fast fracture was resisted by the adjacent bonded joints, the test result was considered satisfactory, and the damage tolerance requirements were satisfied. The RS2 crack was patched with a riveted doubler.

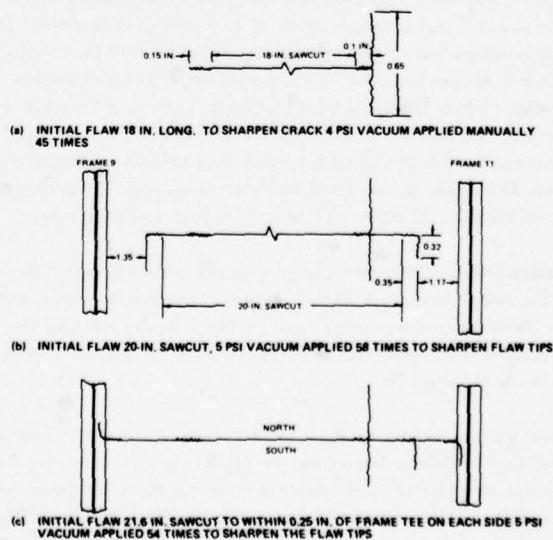


**TABLE 4**  
**DAMAGE TOLERANCE FLAW GROWTH TIME HISTORIES**

NO. OF* CYCLES	TOTAL CRACK LENGTH (IN.)			STRAIN GAGE READINGS (PSI)			CABIN PRESS. $\Delta P$ (PSI)
	DT1	DT2	DT4	STR GAGE NO. 11	STR GAGE NO. 12	STR GAGE NO. 16	
0	0.221	0.250	0.250				
9,000	0.221	0.270	0.250	12,483	9,739	17,390	8.894
12,000	0.328	0.270	0.500	11,805	8,938	17,081	8.679
14,825	0.328	0.270	0.540	11,990	9,061	16,895	8.679
18,000	0.410	0.280	0.720	12,298	9,493	16,957	8.691
24,000	0.450	0.280	0.850	11,681	8,692	16,895	8.631
28,000	0.510	0.280	1.15	11,866	8,815	16,772	8.571
29,000	0.560	0.330	1.25				
32,000	0.660	0.330	1.61				
34,000	0.670	0.430	1.93	12,914	8,912	17,673	8.667
38,030	0.91	0.50	1.95				
42,030			2.56				
44,530		0.65	2.80	11,281	9,031	16,957	8.613
47,530			3.05	10,849	9,697	16,338	8.649
49,530	1.58		3.20				
51,530			3.43	11,897	8,987	17,081	8.517
54,030	1.75		3.72				
57,465			4.21				
59,530	2.82	1.12**	4.63				
60,570	2.97		4.88				
62,405	3.17	1.22	5.44				
64,030	3.75	1.30	5.94	12,575	9,123	17,270	8.565
64,530	3.88	1.55	6.15				
66,030	4.41	1.55	7.1**				
70,130			8.6				
70,000			8.95				
70,530			9.43				
70,780			9.91				
71,030			10.40				
71,200			10.80	11,897	9,000	17,019	8.514
71,590			11.10				
74,480		2.30					
74,805		2.45		11,959	9,431	16,833	8.433

\*FROM START OF DAMAGE TOLERANCE TEST

\*\*CRACK HAD STOPPED AT A RIVET HOLE ON THE NORTH SIDE OF THE ORIGINAL SAWCUT



**FIGURE 80. FLAW CONFIGURATIONS FOR RESIDUAL STRENGTH TESTS**

After the residual strength tests, an additional 37,000 cycles, almost two lifetimes, were imposed on the specimen and still there were no fatigue failures. The specimen was therefore subjected to a total of almost six lifetimes without experiencing any fatigue failures in the participating structure.

The next panel built and tested was the honeycomb pressure panel, shown in Figures 81 and 82. The core was 1/4-inch hexagonal cell, 0.0015-inch foil thickness, 3.4 pounds per cubic foot, 5056 aluminum corrosion-resistant honeycomb. The face sheets were 2024-T3 bare aluminum; 0.020-inch-thick inner face sheet and 0.032-inch-thick outer face sheet with a core depth of 0.80 inch. The panel included four splices: bonded transverse, bonded longitudinal, mechanical transverse, and mechanical longitudinal. They are shown in Figure 83. The bonded splices were made up of an 0.020-inch-thick inner splice and an 0.032-inch-thick outer splice. The mechanical splices used an 0.040-inch-thick inner and outer splice. In addition to fasteners in the mechanical splices, bonding was used to improve the fatigue life. The inner and outer longitudinal splices and the inner transverse splice were cold-bonded with EA9309 adhesive, while the outer transverse splice was hot-bonded with FM-73 during the hot-bond cycle. A solid machined aluminum block was bonded between the face sheets in place of the honeycomb under all fasteners (see Figure 83). The panel also contained four frames and a crack stopper. The frame was made up of a frame tee extrusion bonded to the inner face sheet and an 0.063-inch-thick sheet metal J-section riveted to the frame tee (see Figure 84). A typical frame tee splice and crack stopper splice are also shown in Figure 84. Three of the four frames were stabilized with intercostals. Locations for these intercostals are shown in Figure 82.

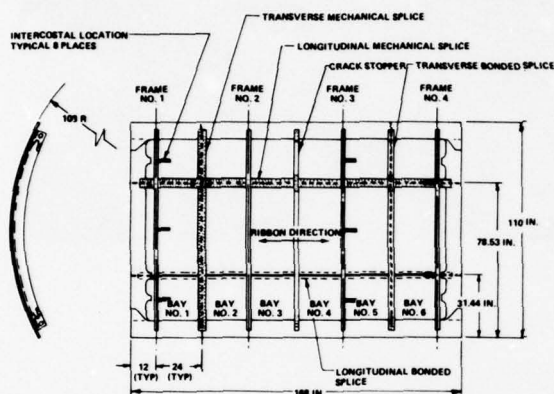


FIGURE 81. HONEYCOMB PRESSURE PANEL

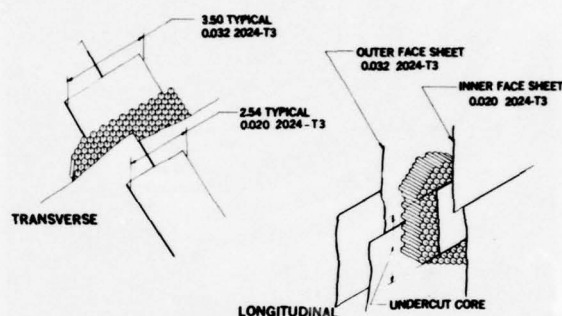


FIGURE 82. HONEYCOMB PRESSURE PANEL

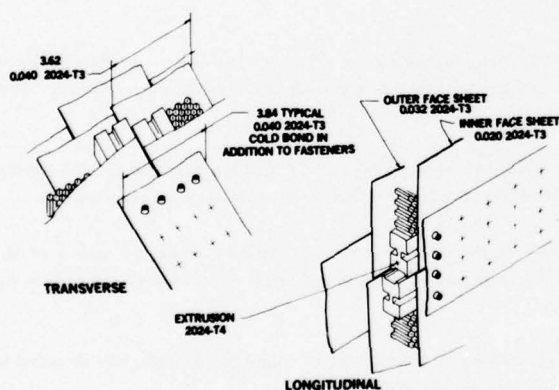


FIGURE 83. HONEYCOMB PANEL SPLICES

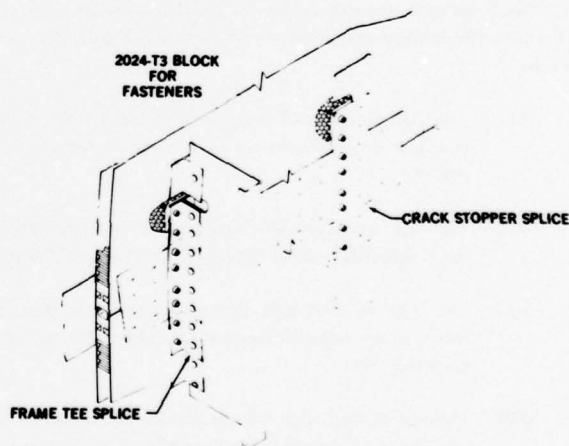


FIGURE 84. HONEYCOMB PANEL SPLICES

The fatigue test consisted of 38,028 load cycles. During this test there were no fatigue cracks generated in the participating structure. Later, after the damage tolerance flaws were introduced, an additional 21,640 cycles were applied. Other than the propagation of one of the damage tolerance flaws, again no fatigue cracks were encountered in the participating structure. The specimen was therefore subjected to a total of over three lifetimes of load without experiencing any fatigue failures.

The last panel to be built and tested in this jig is shown in Figure 85. The bonded assemblies are shown in Figure 86 during nondestructive inspection and the built-up panel is shown in Figure 87. The overall dimensions are the same as for the preceding panels, and therefore the same whiffle tree system could be used. The reason for building and testing this panel was to gain preliminary test information on the fatigue life of a panel with a representative cabin entrance door cutout. In previous airplane cycle tests, cracks have emanated from door cutout corners. The panel had bonded doublers around the door cutout. The panel also had a radial cross section with two radii. This was done in an effort to obtain frame bending from cabin pressure loads such as are found in the forward section of the YC-15 aircraft.

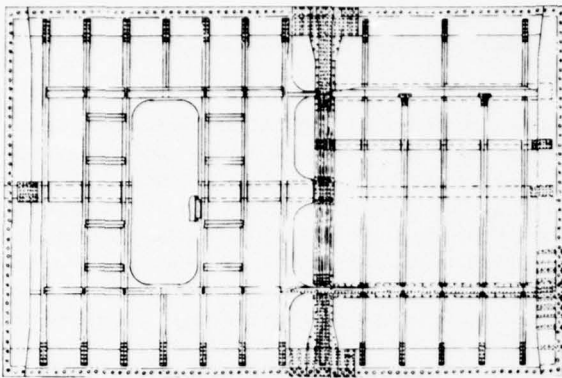


FIGURE 85. COMPOUND CURVE PANEL



FIGURE 87. COMPLETE PANEL ASSEMBLY

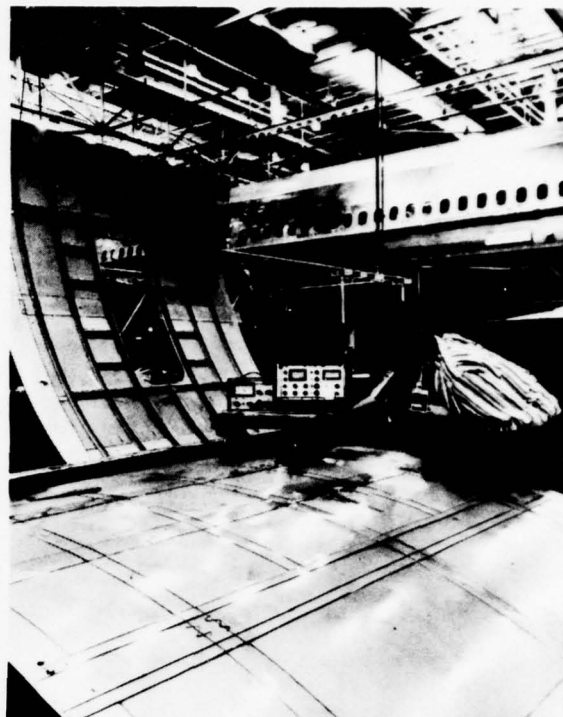


FIGURE 86. PANEL BOND ASSEMBLIES

Six flaws were introduced into the panel to monitor crack growth characteristics in typical full-scale development component nose structure. The locations of the flaws are shown in Figure 85 as well as their orientation. The reason each flaw was introduced is given below.

- DT1 – This flaw was located in the skin oriented at 45 degrees to the longitudinal axis of the panel. It was a corner flaw 0.05 inch in radius. Door corners are likely areas to develop fatigue cracks, and this flaw was designed to establish the efficacy of the cutout.
- DT2 – This flaw was located on the opposite corner and identical to DT1 in all respects except that it was oriented at 30 degrees to the longitudinal axis of the panel. Like DT1, DT2 was directed to evaluate the influence of orientation on crack growth.
- DT3 – This was an 0.05-inch through-the-thickness flaw located in the middle rivet hole between frames 3 and 4 of the mechanically fastened longitudinal splice. The sawcut was oriented parallel to the panel longitudinal axis; i.e., normal to the hoop direction.
- DT4 – This was an 0.25-inch through-the-thickness flaw in the skin located at and parallel to frame 3. This flaw was intended to evaluate crack growth in the circumferential direction in a wide-spaced longeron region.
- DT5 – This was an 0.25-inch through-the-thickness skin flaw oriented longitudinally, located midway between frames 3 and 4, halfway between the tear stopper and the bonded longitudinal splice.
- DT6 – This was an 0.25-inch through-the-thickness skin flaw, 6 inches below longeron No. 2 midway between the wide-spaced (24-inch) frames 3 and 5. The flaw orientation was longitudinal and was designed to investigate crack propagation characteristics in the lower quadrant of the full-scale development component below the floor line.

A requirement of the program was that adequate residual strength would be provided under conditions of: (1) a two-bay crack with the center stiffener intact, and (2) 15-inch foreign object damage with the center stiffener broken. Of these two, previous experience indicated that the foreign object damage case was more severe, and this was considered for test on this panel. There was also some concern that with metal yielding in a bonded splice, a general and catastrophic disbonding of the splice would occur.

These two requirements were accomplished in a single test. A 15-inch flaw was sawcut into the edge of the splice and across frame 5, as shown in Figure 85. This flaw was referred to as RS1. The test itself was the last item to be accomplished on this panel at the end of almost nine lifetimes of cyclic loads.



This panel demonstrated excellent structural integrity and was used far more than originally intended. The total test was 170,258 cycles or almost nine lifetimes. At the conclusion of the test, the panel was intact and available for further testing if desired.

Two lifetimes of fatigue testing were conducted from 0 to 38,025 cycles.

At the conclusion of two lifetimes (38,025 cycles), six damage tolerance flaws were sawcut into the panel. The locations and orientations of these flaws are shown in Figure 85. DT1 and DT2 were corner flaws 0.05 inch deep at the edge of the crew door cutout. The flaw DT3 was a through-the-thickness flaw at the edge of a rivet hole midway between frames 3 and 4. The flaw DT4 was an 0.25-inch through-the-thickness sawcut adjacent and parallel to frame 3 and 14 inches below longeron 1. The flaws DT5 and DT6 were longitudinal sawcuts 0.25 inch long and through-the-thickness. These two flaws grow under the influence of hoop loads.

Since no propagation was evident after 37,258 cycles, it was decided to increase the length of some of the damage tolerance flaws. DT2 was increased to 0.6 inch through both skin and doubler, and DT4, DT5, and DT6 were increased symmetrically to 2.0 inches. Cycling was resumed and the flaws were monitored periodically.

At this stage, the panel had experienced 2.5 lifetimes with the damage tolerance flaws present and had evidenced no growth. It was decided to further increase the sawcuts to induce the flaws to grow. DT1 was sawcut to 0.8-inch length through the inner skin only. DT4 was increased to 4.0 inches by sawcutting 2.0 inches on the north side only. DT5 and DT6 were increased to 4.0 inches by cutting one additional inch at each tip.

DT2, DT5, and DT6 showed growth during continued cycling. DT4 still showed no growth. Therefore, the length of DT4 was increased at 86,770 cycles to 6.0 inches by sawcutting an additional 2.0 inches on the north side only.

After testing to 90,320 cycles, the following results were obtained:

1. DT1 (Figure 88) showed no propagation in spite of the 0.8-inch cut in the skin. The bonded doubler inhibits any flaw growth in the skin.
2. DT2 (Figure 89) propagated into strain gage 0.35-inch from the sawcut tip.
3. DT3 showed no evidence of propagation during the entire test.
4. DT4 showed minimal propagation.
5. DT5 propagated into the frame tee bondlines on each tip (see Figures 90 to 92).
6. DT6 (Figures 93 and 94) showed evidence of flaw growth. It should be noted that the crack growth was askew to the sawcut (longitudinal) direction, indicating that there was some shear in the panel causing the principal stresses to be oriented at a small angle to the normal panel loading axes.

After 91,535 cycles, DT6 propagated rapidly after it had been extended to 6.0 inches. The flaw had propagated to the adjacent frames 24 inches apart. On approaching the frames, the crack had turned parallel to the frames after penetrating the bondlines. Disbonding occurred in the path of the crack subject to peel loads; it is shown in Figure 95 as hash marks. The crack and the associated disbond had become so large that it was difficult to maintain the vacuum over the panel.

Hot-bonded repairs were installed over DT5 and DT6. The intent was to demonstrate the durability of such repairs made under field conditions for at least two lifetimes. The repair of DT6 is shown in Figures 96 and 97. The repair of DT5 consisted of doubler bonded on the inner side. This doubler was jogged over the frame tee on one side. On the opposite side, it was flush with the frame tee. A second doubler was bonded over the frame.

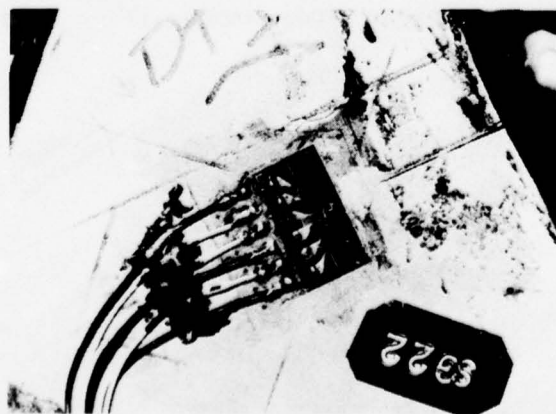


FIGURE 88. INITIAL SAWCUT DT1



FIGURE 89. DT2 CRACK GROWTH

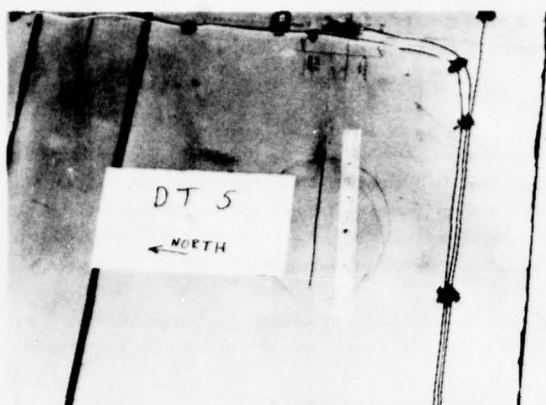


FIGURE 90. FRONT VIEW OF DT5 CRACK GROWTH

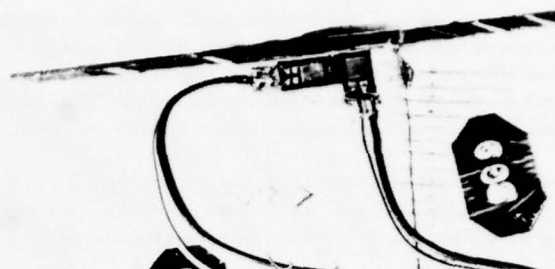


FIGURE 91. DT5 CRACK TIP - BACK VIEW

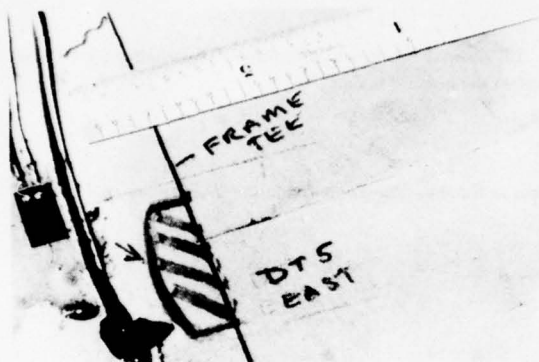


FIGURE 92. DT5 CRACK TIP - FRONT VIEW

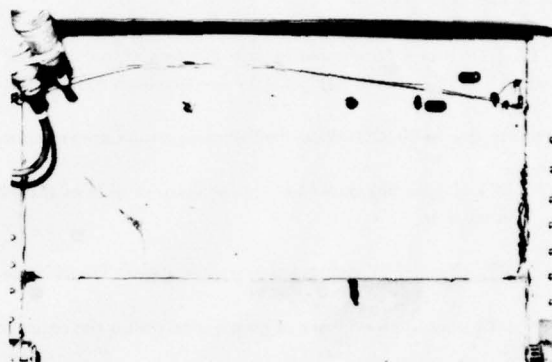


FIGURE 93. DT6 CRACK GROWTH



FIGURE 94. DT6 CRACK TIP

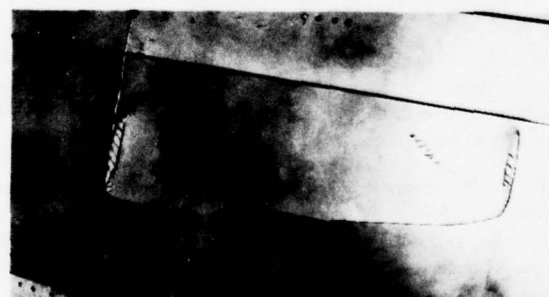


FIGURE 95. DT6 TOTAL CRACK GROWTH

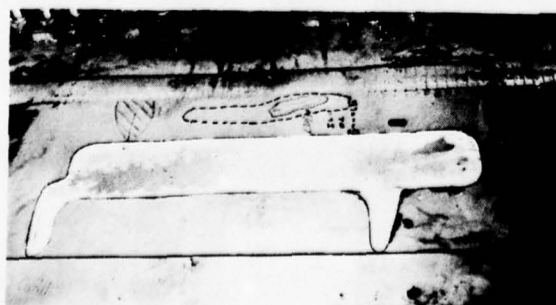


FIGURE 96. DT6 REPAIR - FRONT VIEW

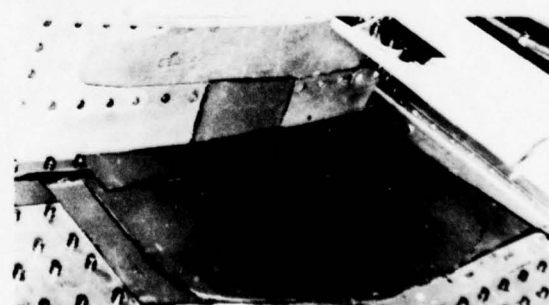


FIGURE 97. DT6 REPAIR - BACK VIEW

The tests were continued with the bonded repairs in place and successfully withstood the cycle loading of two lifetimes to bring the total panel cycle history to 170,258 pressurizations.

Let us review the results of crack growth tests presented. The flat panels were tested which had load or stress levels in the skin and stringer equal to those in the fuselage shell under pressure. Cracks grew and were retarded more as they passed across a bonded stiffener than when the stiffener was riveted on. However, the crack grew across the bonded joint. In these pressurized panel tests, where the axial skin stresses were the same on flat unpressurized panels, the cracks were truly arrested and kept within the bonded edges of the panel. With a crack opening as in Figure 95, the test air supply of 1600 cfm was able to develop only 3 psi due to the "window"-shaped failure. The normal test pressure is 7.15 psi.

The YC-15, with two air-conditioning packs, develops 100 cfm before both audible and visual warnings are displayed to the flight crew that cabin pressure is being lost. The result is that the window-shaped failure precludes pressurizing the aircraft. Past experience on pressurized, curved, riveted test panels has shown that cracks sometimes passed through the riveted stiffener joint and on other occasions, turned at right angles to crack along the riveted line (see Figure 98). Further test cycling commonly results in the crack working out of the riveted line and continuing in the same original direction until catastrophic failure occurs (see Figure 99). Due to the opening size, full cabin pressure was maintained during this test with the 1600-cfm air supply. In many flight aircraft where longitudinal skin cracks have developed, they pass across the riveted frames to lengths of 75 to 130 inches before they are visually detected.

In two kinds of tests conducted for crack growth information on bonded panels, a significant difference was noted. When testing in the tension-tension environment for crack growth with no pressure simulation, the only crack growth difference between the bonded and riveted designs was the increased retardation present as the crack progressed over the bonded stiffener. The crack grew across the bonded stiffener and continued until the test panel failed as with the riveted panels. As noted above for pressure tests, the crack growth performance of bonded panels is different than for riveted designs. This means that to get proper crack growth information for pressurized bonded fuselage structures, the test must be conducted with cabin pressure simulated. The differences in the crack growth pattern are due to the local skin pillowing stresses caused by cabin pressure (see Figure 100).

#### Crack Growth Analysis

It has long been known that structures with cracks or other flaws in them will fail at net area stresses well below their ultimate strength. There have been a number of catastrophic incidents as a consequence of these unexpected failures.



FIGURE 98. RIVETED, CURVED PANEL CRACK PROPAGATION AT A FRAME

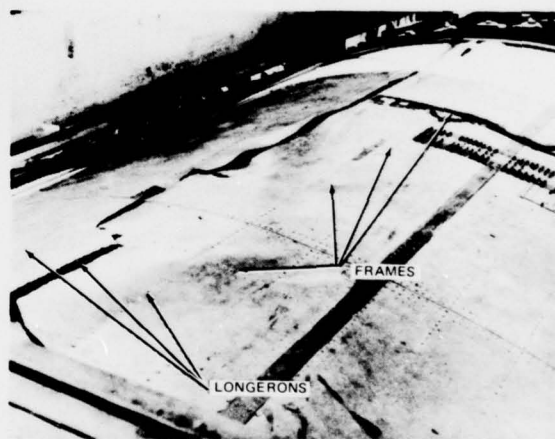


FIGURE 99. RIVETED CURVED PANEL CRACK PROPAGATION AFTER FAST FRACTURE

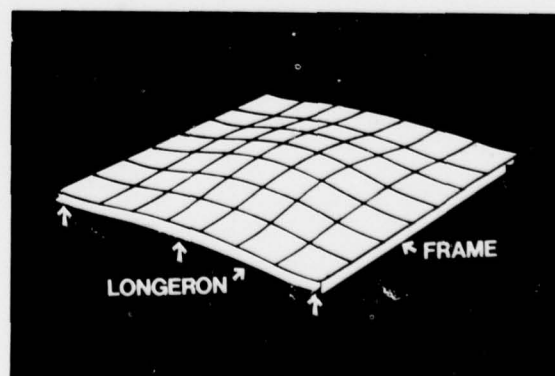


FIGURE 100. EFFECTS OF PRESSURE PILLOWING IN A STIFFENED CYLINDER



The example given in Figure 101 illustrates how the static strength of a part can be reduced by the presence of a fatigue crack. In the example, the residual strength predicted by fracture analysis on the right side of the figure is approximately half the strength shown on the left side. The figure is based on the net section ultimate strength, even though the net areas are the same in both cases.

In aircraft structural design, the ability to predict the rate of flaw propagation and the residual strength during the design stage would be invaluable. Linear-elastic fracture mechanics attempts to do just that with considerable success.

The damage tolerance analysis as applied to the PABST full-scale development component structure is shown in Figure 58. Each of the elements of the flow chart will be discussed in the following sections.

**Linear Elastic Fracture Mechanics** – The three modes of crack surface displacement are shown in Figure 102. The crack opening Mode I is the one generally encountered and the one for which most of the data are available. For this reason, the discussion will be confined to Mode I. The equations which govern the stress field ahead of a crack tip based on the coordinate system of Figure 103 are:

$$\begin{aligned} \sigma_x &= \frac{K}{\sqrt{2\pi r}} \cos \frac{\theta}{2} \left( 1 - \sin \frac{\theta}{2} \sin \frac{3\theta}{2} \right) \\ \sigma_y &= \frac{K}{\sqrt{2\pi r}} \cos \frac{\theta}{2} \left( 1 + \sin \frac{\theta}{2} \sin \frac{3\theta}{2} \right) \\ \tau_{xy} &= \frac{K}{\sqrt{2\pi r}} \sin \frac{\theta}{2} \cos \frac{\theta}{2} \cos \frac{3\theta}{2} \end{aligned} \quad (1)$$

where  $K$  is the stress intensity factor and is a function of the problem geometry and loading. For a crack in an infinite sheet (Figure 104), it can be shown that

$$K = \sigma \sqrt{\pi a} \quad (2)$$

and the stress field ahead of the crack is defined by Equation (1).

The stress intensity factor  $K$ , as defined in Equation (2), is fundamental to linear-elastic fracture mechanics. In practice, fracture problems are far more complex, and correction factors have been developed which cover most of the problems encountered in practical

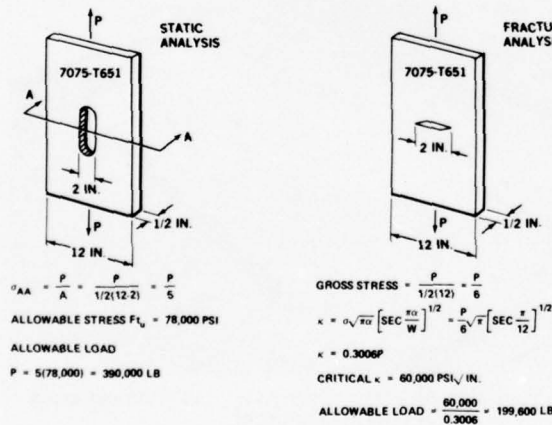


FIGURE 101. RESIDUAL STRENGTH CALCULATIONS

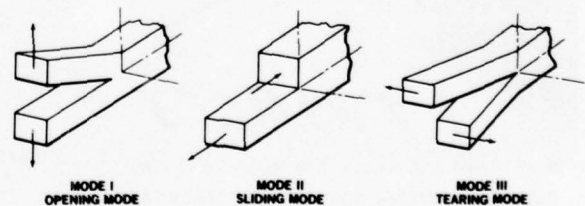


FIGURE 102. THE THREE MODES OF CRACK SURFACE DISPLACEMENT

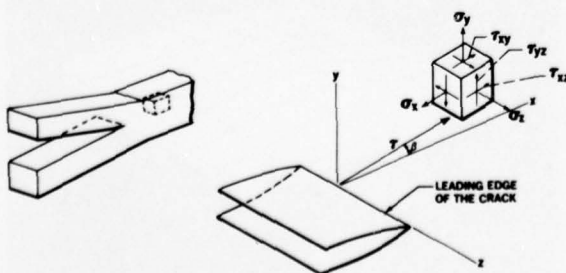


FIGURE 103. STRESS FIELD COORDINATE SYSTEM

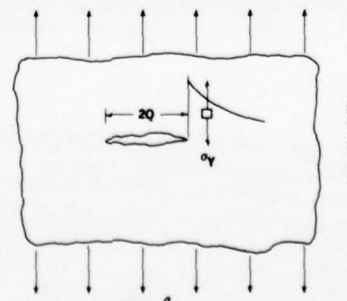


FIGURE 104. CRACK IN AN INFINITE SHEET

structures. Stress intensity factors for some of the typical airframe geometries are shown in Figure 105. For other cases, the reader is referred to the literature where solutions are given for many types of notches.

The expression for stress intensity factor may then be written as

$$K = \sigma \sqrt{\pi a} \beta_1 \beta_2 \beta_3 \dots \beta_n \quad (3)$$

where  $\beta_1, \beta_2, \dots, \beta_n$  are the correction factors due to various geometric configurations of the problem at hand.

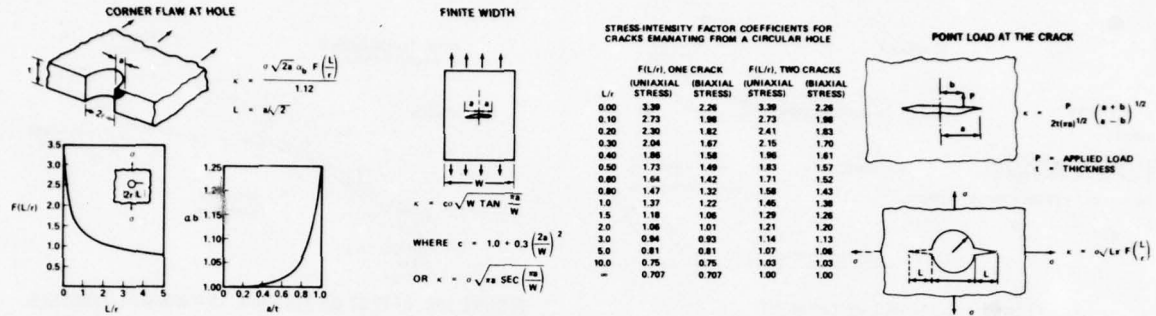


FIGURE 105. EXAMPLES OF STRESS INTENSITY FACTORS

In addition to the geometric correction factors, additional corrections to  $K$  are required. These are discussed below.

#### 1. Reinforcement Correction

Airframe structures are always stiffened and the effect is to lower the value of  $K$ . This effect must be taken into account. Methods have been developed at Douglas to calculate the stress intensity factor for basic damage types shown in Figure 106, using computerized closed-form solutions. These solutions basically involve the calculation of fastener loads by making the deflections in the cracked sheet compatible with deflections in the stiffener while accounting for stiffener bending and fastener flexibility. This is shown in Figure 107. The equations and their derivations are too cumbersome to be presented here. For detailed development of the analysis and the computer code, the reader is referred to the work of Tom Swift.<sup>(7)</sup> The program output yields the crack tip stress intensity factor as a function of crack length for the structure under consideration.

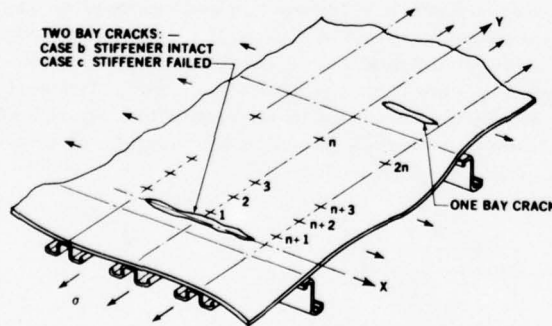


FIGURE 106. DAMAGE TYPES

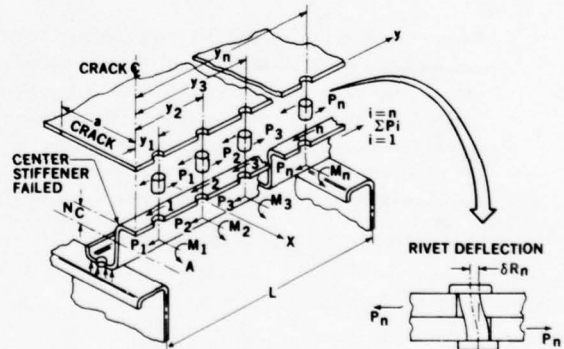


FIGURE 107. CENTER STIFFENER BENDING

$$\delta = d \frac{\tau}{G}$$

where

$\tau$  = adhesive shear stress

$G$  = adhesive shear modulus

These computer analyses were originally derived for mechanical fasteners for the PABST damage tolerance analysis. These programs were adapted for the adhesive bonds. The adhesive segment representation is as shown in Figure 108. Equation (5) represents the flexibility of the stiffener-to-skin attachment, which is the same as an equivalent rivet flexibility. A series of such elements along the length of the stiffener represents a continuous bond line.

## The flexibility of the adhesive element

$$\delta = \frac{d}{W\eta G} \quad (5)$$

## 2. Effect of Bulging Due to Internal Pressure

Longitudinal cracks under the influence of internal pressure will bulge as illustrated in Figure 109 and influence the crack tip stress intensity factor. As the crack approaches the stiffener (frame), the effect is to pinch off the bulging. Equation (6) is the bulge factor derived by Paul Kuhn.

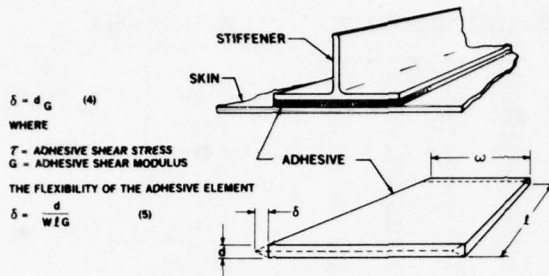


FIGURE 108. ADHESIVE SEGMENT

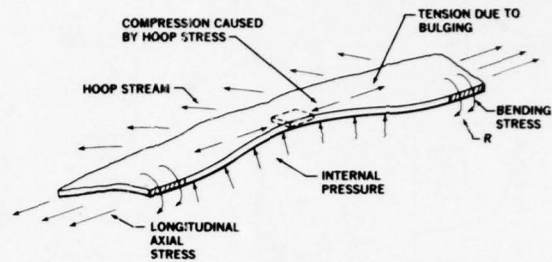


FIGURE 109. EFFECT OF BULGING AND BIAxIAL STRESSES

$$B = 1 + \frac{5a}{R} \quad (6)$$

where

$a$  = half-crack length

$R$  = radius of the shell

This expression is applicable while the crack is well away from either stiffener. As the crack approaches the stiffener, the value of  $B$  decays to unity. For convenience, the decay was assumed to be sinusoidal.

## 3. Effect of Biaxial Stress

When a load is applied normal to a crack, a compressive stress is induced parallel to it. This results in local buckling of the sheet and increased stress intensity factor. Application of a tensile stress parallel to the crack relieves this compression, thereby reducing the stress intensity factor. Biaxial stress field will also reduce the stress intensity due to bulging, as illustrated in Figure 110. This fact can be illustrated by taking a sheet of paper and cutting a transverse slit through the middle. Two people should face each other and simultaneously pull on the paper, one normal to the slit and the other parallel to it. No failure of the paper will occur, providing the slit is not too long. Now, let the person applying the load parallel to the slit release his hold. It will be noticed that the sheet of paper will tear into two pieces through the slit.

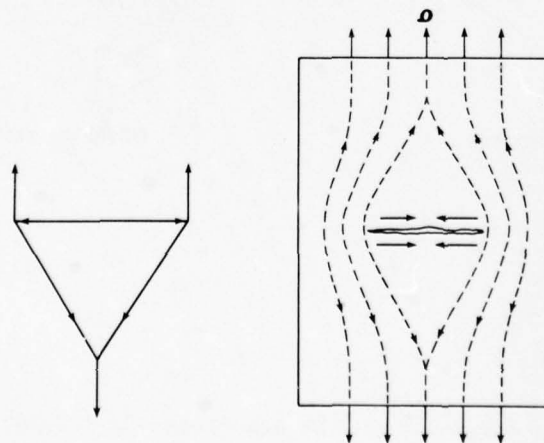


FIGURE 110. STRESS FIELD INDUCING COMPRESSION



#### 4. Bending Correction

The crack tip stress intensity factor under bending loads is less than that due to direct tension. The extreme fiber bending stress is divided by the nondimensional factor

$$F = \frac{\left\{ 4 \left[ \left( \frac{K_c}{\sqrt{\pi a}} \right)^2 - \sigma_T^2 \right] \right\}^{1/2}}{\left( \frac{K_c}{\sqrt{\pi a}} - \sigma_T \right)} \quad (7)$$

where

$K_c$  = critical stress intensity factor

$\sigma_T$  = the applied tensile stress

and the result is then added to the applied tensile stress for use in calculating the stress intensity factor.

#### 5. Pillowing Due to Internal Pressure

In stiffened pressurized shells, a skin bulging phenomenon (see Figure 100) is experienced. The restraint of the frames and longerons forces the skin to pinch in and induce bending stresses in the vicinity of the restraints. In the vicinity of the frame, the stress field is defined by the following equation:

$$\sigma_{\text{HOOP}} = \frac{\Delta \text{PR}}{h} - E \frac{\delta_o}{R} \frac{[\lambda_2 - e^{\lambda_1(X/R)} - \lambda_1 e^{-\lambda_2(X/R)}]}{(\lambda_2 - \lambda_1)} \quad (8)$$

and

$$\sigma_{\text{bending}}]_{\text{MAX}} = \pm \left[ \frac{Eh}{2(1-v^2)} \right]_s \frac{\delta_o}{R^2} (\lambda_1 \lambda_2 - v)$$

where

$$\delta_o = \frac{\left[ \frac{\Delta \text{PR}}{Eh} - \frac{\sqrt{\sigma_X}}{E} \right]_s R}{1 + \left[ \frac{2Eh^3}{12(1-v^2)R} \right]_s \frac{1}{(EA)_f} [\lambda_1 \lambda_2 (\lambda_1 + \lambda_2)]} \quad (9)$$

$$\lambda_1, \lambda_2 = \pm \left[ \left\{ (\phi - v\alpha) \pm \sqrt{(\phi - v\alpha)^2 - 4\alpha(1-v^2)} \right\} / 2\alpha \right]^{1/2}$$

$$\phi = \frac{\sigma_X]_s h(1-v^2)}{Eh}$$

$$\alpha = \frac{h^2}{12R^2}$$

$$\sigma_X]_{\text{SKIN}} = \sigma_L + v\sigma_r \frac{(A_{\text{str}}/A_s)}{(1 + A_{\text{str}}/A_s)}$$

$\Delta P$  = cabin pressure differential       $x$  = distance normal to the frame

The subscripts

$\sigma_r$  =  $\Delta \text{PR}/h$

$E$  = modulus of elasticity

$s$  = skin

$R$  = shell radius

$\sigma_L$  = longitudinal stress, algebraic sum of pressure and inertia stresses

$f$  = frame

$h$  = skin thickness

$v$  = Poissons ratio

For the case of the skin longeron combination

$$\sigma_{\text{bending}}]_{\text{MAX}} = \frac{Eh}{2(1-\nu^2)} \frac{\delta_g}{R^2} \xi_1 \xi_2 \quad (9)$$

where

$$\xi_1 \xi_2 = \pm \sqrt{\left\{ (\xi - \alpha) \pm \sqrt{[(\xi - \alpha)^2 - \phi \alpha (1 - \nu^2)]} \right\} / 2\alpha}$$

and

$\delta_g$  = Longeron deflection as a function of  $x$  solved iteratively by computer program.

$$\xi = \frac{\Delta PR(1 - \nu^2)}{Eh}$$

In the event of a longitudinal flaw, the most critical location would be midway between frames and adjacent longeron at the point of maximum skin bending. The flaw would propagate parallel to the longeron until it approached the adjacent frame. At the frame-longeron intersection, the membrane stresses are reduced considerably, causing the crack to turn into the relatively highly stressed region, which in this case would be skin bending parallel to the frame. The crack would have a tendency to turn through 90 degrees from its original direction and parallel to the frame.

#### 6. Variable Stress Correction Factor

Based on the above pillowowing analysis, it is apparent that the stress field varies along both the longeron and the frame. A crack propagating in a variable stress field will be sensitive to it, and this fact must be accounted for in the calculation of the stress intensity factor. The variable stress field (broken line) is represented by the two-step field as shown in Figure 111. The correction factor is shown in Equation (10).

$$\beta = \frac{\sigma_1 \sqrt{\pi a} + 2\sigma_2 \sqrt{\frac{a}{\pi}} \left[ \sin^{-1} \frac{c}{a} \right]}{\sigma \sqrt{\pi a}} \quad (10)$$

$$\sigma = \sigma_1 + \sigma_2$$

$$\beta = 1.0 \text{ for } a \leq c$$

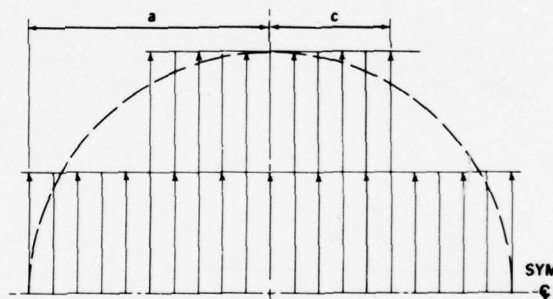


FIGURE 111. VARIABLE STRESS FIELD

Thus, a factor  $\beta$  can be calculated for all values of  $a > c$ . An expression can be derived for a continuously varying stress field, but for purposes of the PABST program, the two-step simulation was found to be adequate.

**Material Properties** — In addition to the normal material strength properties, two additional elements of data are required for fracture analysis: the critical stress intensity factor, and crack propagation data.

Concerning the critical stress intensity factor  $K_{Ic}$ , the state of stress has an effect on material fracture toughness. For thin sheets, a plane-stress state exists. The fracture is of the shear lip type. As the thickness increases, more and more of the section will experience a plane-strain condition and the fracture face is flat.

The relationship between fracture toughness and material thickness is shown in Figure 112. Fracture toughness  $K_{Ic}$  decreases as thickness increases, reaching a limiting value of  $K_{Ic}$ , the subscript I referring to the fracture Mode I (Figure 102). Fast fracture is experienced when the stress intensity factor in an element of structure achieves a value equal to or greater than  $K_{Ic}$ .

Regarding crack propagation data ( $da/dn$ ), a typical center cracked panel under constant-amplitude cyclic loading will yield a crack propagation curve. The rate of crack growth is the slope of the crack propagation curve. By test, a family of  $da/dn$  curves was developed as shown in Figure 113 for 2024-T3 for use in the PABST program crack growth analysis.

Because of irregularities in the  $da/dn$  curves of Figure 113 and variations in the R factor, it is important to represent the  $da/dn$  data accurately in order to predict crack growth with any degree of confidence. To overcome the shortcomings of the several available empirical equations, a tabular format was used to represent the  $da/dn$  data for computer analysis. This tabular format is coupled with an interpolation routine so that the  $da/dn$  values used in the crack growth analysis very accurately represent test data.

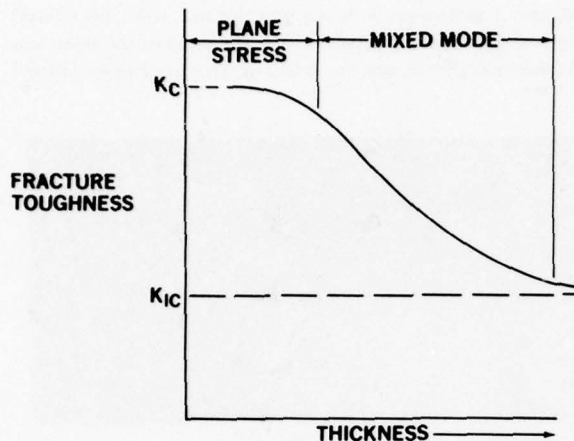


FIGURE 112. FRACTURE TOUGHNESS VERSUS THICKNESS

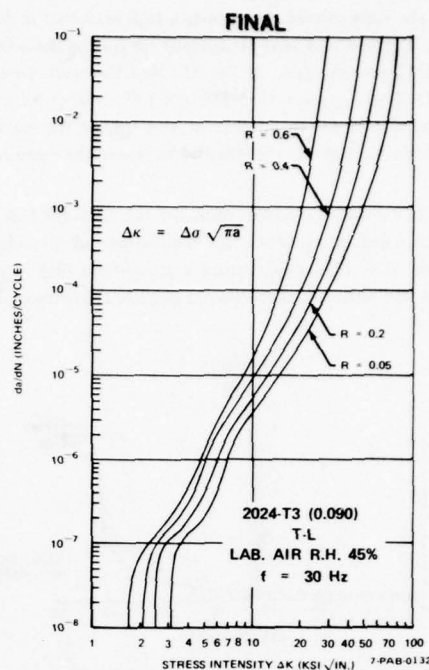


FIGURE 113. CRACK GROWTH RATE DATA FOR 2024-T3

**Crack Growth Retardation Model<sup>(9)</sup>** – The retardation model used in the PABST analysis is the Willenborg. The crack retardation results from the occasional high maximum stress which induces a yield zone at the crack and the associated compressive residual stress. The effect is to reduce the crack tip stress-intensity factor and lower the rate of crack propagation at all stresses lower than the occasional high stress.

Our experience has been that best crack growth correlation is obtained if only 80 percent of the Willenborg retardation is used.

**Crack Growth Analysis** – When considering a complete aircraft structure, a limited number of critical points are selected from stress analysis for the damage-tolerant crack growth analysis. Each critical point of the structure will experience a stress spectrum based on aircraft utilization. This spectrum can be represented by the data shown in Table 5. Then, the stress-intensity factor  $\Delta K$  [see Equation (3)] is calculated at points on the airplane. For the initial crack length defined in the damage tolerance criteria, the correction factor  $\beta$  is calculated as described above. For known values of  $\Delta K$ , a  $da/dN$  value is obtained from the tabular format from Figure 113. With this value of  $da/dN$  and the frequency at this value of  $\Delta\sigma$  from Table 5, an incremental value of  $\Delta a$  is calculated. This is then added to the initial value  $a_0$  to give a new crack length of

$$a = a_0 + \Delta a \quad (11)$$

TABLE 5  
ELEMENT STRESS SPECTRUM

CRITICAL POINT STRESS	STRESS RATIO	NO. OF CYCLES PER 1000 FLT HR
$\Delta\sigma_1$	$R_1$	$N_1$
$\Delta\sigma_2$	$R_2$	$N_2$
$\Delta\sigma_4$	$R_4$	$N_4$

This leads to a new value of stress-intensity factor. This integration procedure is accomplished on a computer program and continued until a failure occurs. The computer program is capable of cycle-by-cycle integration, a procedure which takes considerable computer time and is therefore very expensive. The analyst must exercise judgment in achieving optimum accuracy at minimum expense. A fast fracture will occur when the local stress increased by the stress-intensity factor equals the critical stress for the metal. A damage-tolerance requirement states that the panel will have sufficient residual strength to support limit loads after a crack has been allowed to propagate for the equivalent of two lifetimes of operation. This fact must be verified by analysis and checked during the crack growth tests.

**Test-Analysis Correlation** – During the PABST program, efforts to predict both the crack growth time histories under spectrum loading and residual strength under static loading met with considerable success. Examples of the successful prediction are given below.



One of the early curved panel tests setups is shown in Figure 78. The damage-tolerance flaws incorporated in the panel are shown in Figure 79. The test and analysis correlation for the flaws DT1 and DT2 is shown in Figure 114. The DT1 correlation is excellent. The analysis for DT2 was the same as for DT1 and the corrections used are as noted in the preceding paragraphs. The test indicates that the analysis for DT2 was conservative. The most likely area for error in the analysis was the calculations for the effect of bulging. Because DT2 was located adjacent to a longeron, one side of the crack was held flat while the other was permitted to bulge. It can be assumed from the test results that it is conservative to ignore the extra restraint. Figures 115 and 116 show the crack.

Figure 117 shows the correlation for the flaw DT4 in the same test, and after approximately 30,000 cycles the correlation was good. At this point, a repair was installed to permit a residual strength test of another crack. It was observed that under the residual strength loads, flaw DT4 experienced a stress field large enough to cause a crack opening in spite of the repair. When the repair was removed and test resumed, there was a significant slowing or retarding of the crack growth rate. For details of crack, see Figures 118 and 119.

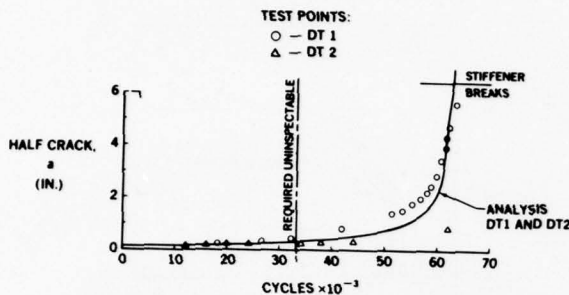


FIGURE 114. TEST-ANALYSIS CORRELATION



FIGURE 115. CRACK DT1

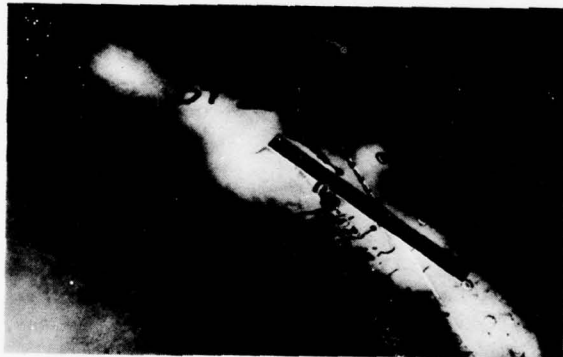


FIGURE 116. CRACK DT2

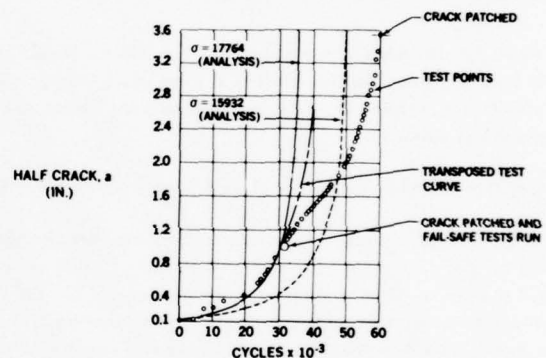


FIGURE 117. TEST ANALYSIS CORRELATION, FLAW DT4

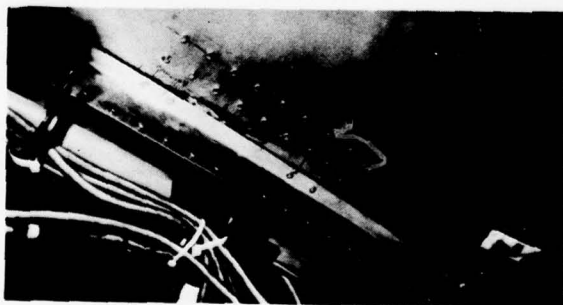


FIGURE 118. BACK VIEW OF CRACK DT4

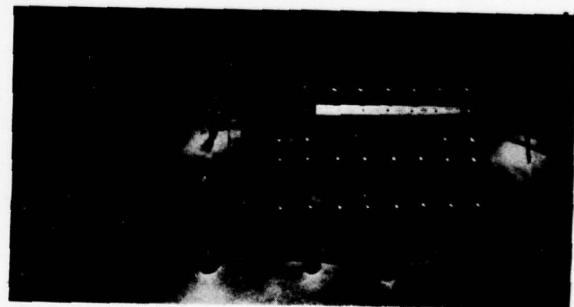


FIGURE 119. FRONT VIEW OF CRACK DT4

The results of a residual strength test of a large, flat panel under uniaxial stress are shown in Figure 120. The panel had a simulated 15-inch penetration from foreign object damage which included a severed center frame. Fast fracture was experienced as the load reached 18,400 lb/in.<sup>2</sup> and the crack was arrested when it achieved a half-length of 23 inches. The arrest occurred at a crack length somewhat longer than the predicted value, but the correlation is quite acceptable. The important fact is that the crack was arrested. Figure 121 shows the failure.

An interesting analysis of an early PABST test of a bonded panel was conducted. The analysis was done after the test, but the results are significant in that they were able to (1) calculate the failure load, (2) follow the sequence of events during the failure process, and (3) calculate stiffener (Z-section) stress and show yielding, thus accounting for permanent set in the stiffener of the failed specimen.

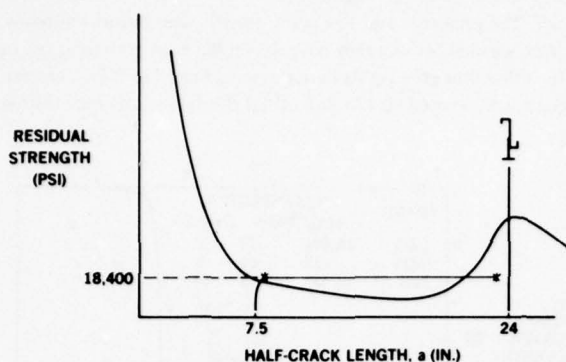


FIGURE 120. RESIDUAL STRENGTH DIAGRAM - FOREIGN OBJECT DAMAGE

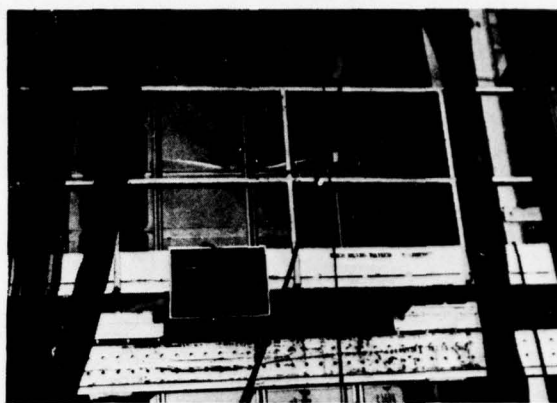


FIGURE 121. PANEL FAILURE - RESIDUAL STRENGTH TEST

The results of the analysis are given in Figure 122. With a 16.4-inch crack and no adhesive delamination in the panel as the load is increased to point A, fast delamination and arrest occur to point B. As load is increased further, additional adhesive delamination occurs along line BFH. Because of the crack, the load is transferred from the skin to the stiffener, the eccentricity of the load path causing stiffener bending and outer cap yielding. The stiffener yielding causes unloading of the adhesive. As the load is increased and delamination proceeds, the stiffener becomes less and less effective, thus increasing the stress intensity in the skin. The panel should fail at point H, the intersection of the allowable skin stress line and the adhesive delamination line, as it actually did.

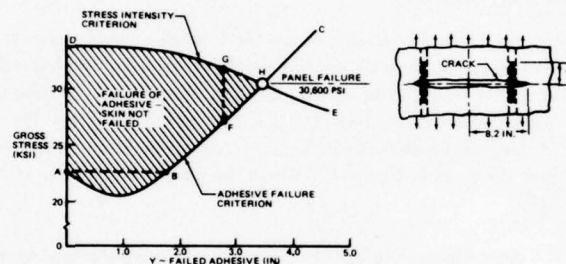


FIGURE 122. FAILURE PROPAGATION

Thus far, the correlation of analysis with tests on panels has been shown. The final proof of the analysis is the correlations achieved on the PABST full-scale demonstration component. Eighteen damage-tolerance flaws were sawcut in the full-scale development component, as shown in Figure 123. The flaws were 0.25-inch sawcuts, with finite radius tips. Crack growth time histories were to be

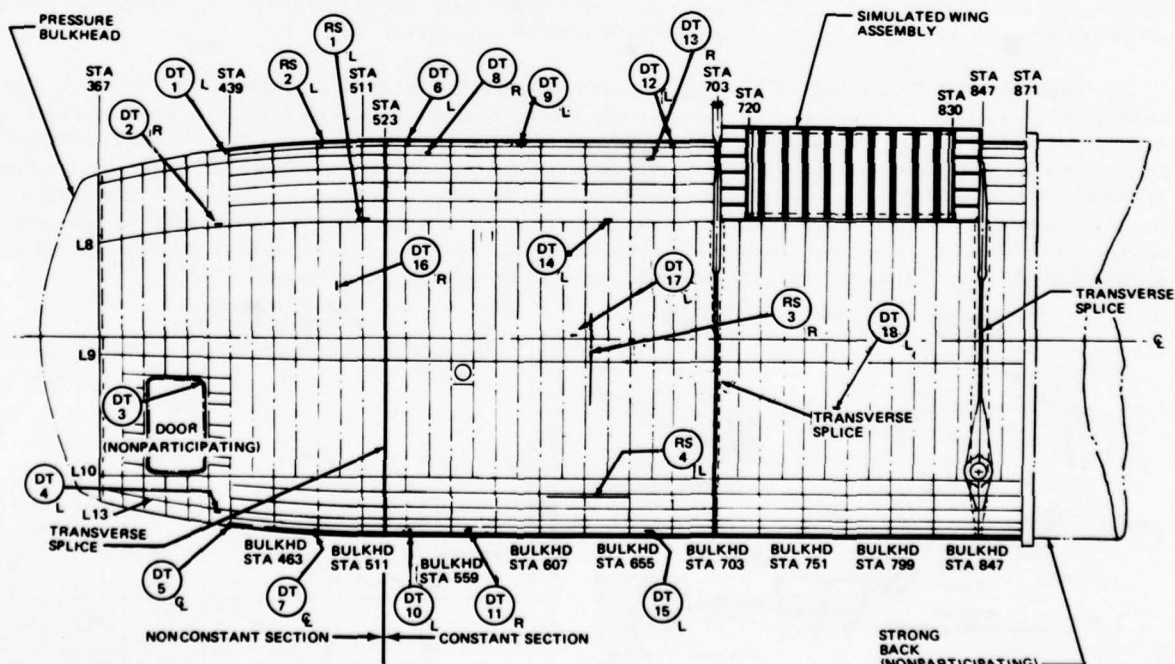


FIGURE 123. DAMAGE TOLERANCE AND RESIDUAL STRENGTH FLAWS

measured from the time that fatigue cracks nucleated at the sawcut tips. Only six of the 18 original sawcuts had nucleated fatigue crack as of December 1, 1978. The cracks started moving after 27,000 cycles. The predicted and test crack growth time histories for two, DT14 and DT17, are shown in Figures 124 and 125. These two flaws were selected because they have shown the most growth so far. In the case of DT14, the correlation is excellent and is representative of the other four growing flaws not covered here. For DT17, observe that at  $N = 0$ , the point at which the flaw was first observed to have nucleated, a equals 0.125-inch. If all the data points were shifted correspondingly to the right, the correlation would improve significantly.

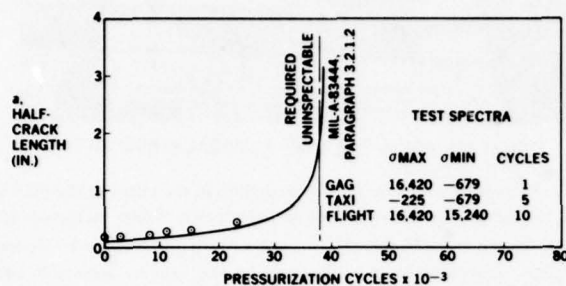


FIGURE 124. ANALYSIS - TEST CORRELATION DT14

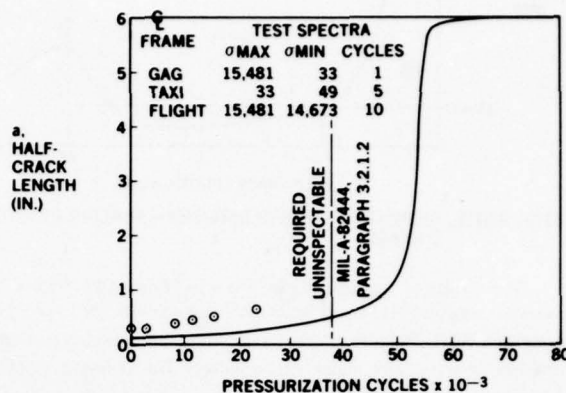


FIGURE 125. ANALYSIS - TEST CORRELATION DT17

### ENVIRONMENTAL TEST OF A STRUCTURAL PANEL

Originally, the environmental effects on the surface treatment and the bonded assembly were to be checked using small coupons. The bonded assemblies were not representative of a bonded joint that would be formed of the full-scale development component. They are usually characterized by a small overlap of the adherends. This would allow a more rapid intrusion of the environment than would be found in a structural joint. Also, the failure would always be in the glue line, not in the metal. The large, 42-foot, 216-inch-diameter fuselage section would be cycled in laboratory air, which is essentially no environment. Also, it would be tested at a fairly high cycle rate of one cabin pressurization or flight each 39 seconds. Figure 126 shows the dilemma of how to relate the full-scale test to the small specimen tests.

To solve the problem, two identical shear panels were built to represent a piece of the fuselage structure, as shown in Figure 126. The first panel was tested in laboratory air like the full-scale development component and had the same external load. The spectrum for the shear panel, shown in Figure 127, is a little more complex than the one used on the full-scale development component, which will be reviewed later. Since cabin pressure is the overriding stress component, one spectrum is equal to two flights or pressurizations and takes 60 seconds to apply. Figure 128 shows how the various loads are applied. All loading cylinders are driven by compressed air. A rotary cam actuates switches which operate solenoids which turn the air on and off for each load increment. By using compressed air instead of hydraulic oil pressure, it was possible to run the test continuously, seven days a week, unattended, which was a real cost-saving procedure. The panel successfully withstood 45,600 cycle spectrums (91,200 pressure cycles) or 4.8 lifetimes. No bondline flaws grew in size and only two of the four metal flaws showed slight growth. No metal fatigue failure developed.

The second shear panel was placed in the same jig, but with two changes. The laboratory air environment was changed to apply 140°F at 100-percent relative humidity when the flight was in the taxi mode, and the temperature was raised to ambient for low-level dash and then lowered to -50°F to represent the high-altitude flight case. The other major change over the previous test was the cycle rate. The time to complete one spectrum was 90 minutes. (The environmental equipment was able to change specimen temperature from +140°F to -50°F.) Figure 129 shows the complete spectrum and the relationships of loads and temperatures. The same number of ground and flight g-loads were applied to the specimen as were applied in the rapid cycle test. As of November 1, 1978, the specimen had 3540 spectra or 7080 flights, which is 37 percent of one lifetime. There has been no growth of the bondline or metal flaws to date. Figure 130 shows the vacuum box lifted to expose the shear panel, and Figure 131 shows the overall test setup.

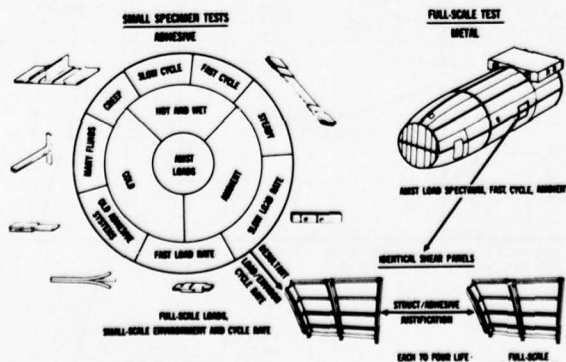


FIGURE 126. ENVIRONMENTAL JUSTIFICATION TESTS

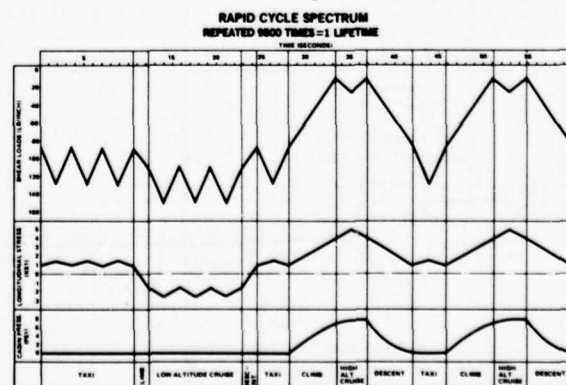


FIGURE 127. PABST INTERACTION FATIGUE TESTS



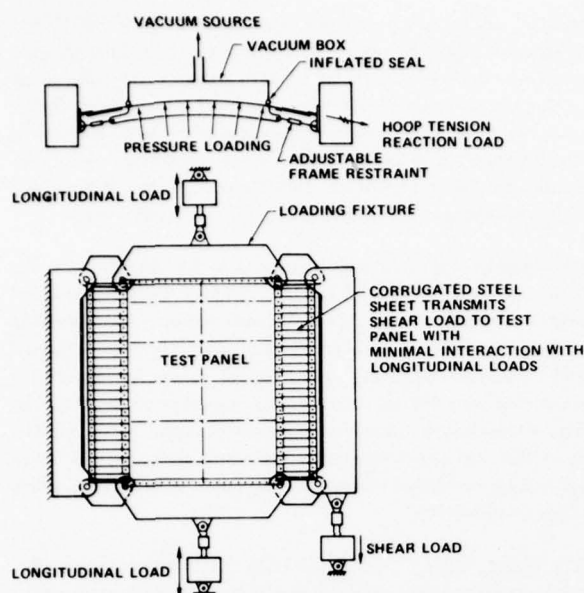


FIGURE 128. INTERACTION PANEL LOADING CONCEPTS

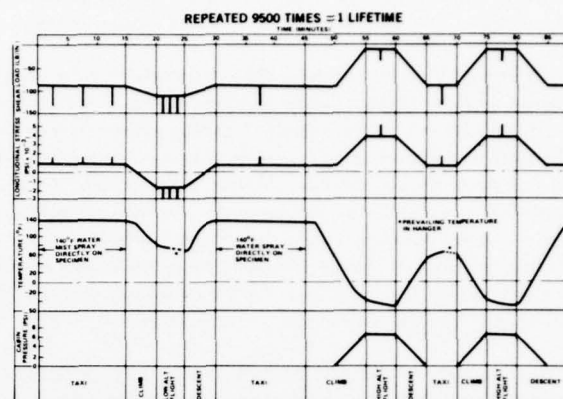


FIGURE 129. INTERACTION FATIGUE TEST SPECTRUM

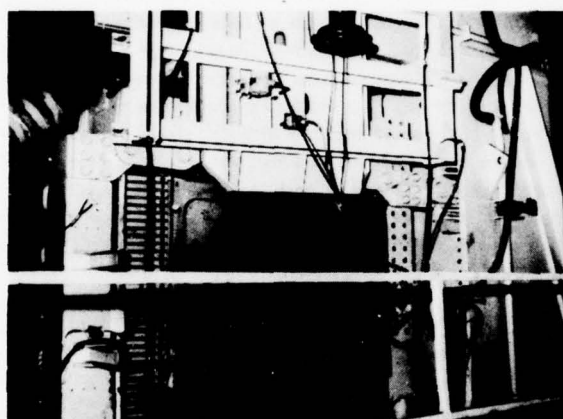


FIGURE 130. TEST PANEL, ENVIRONMENTAL JIG

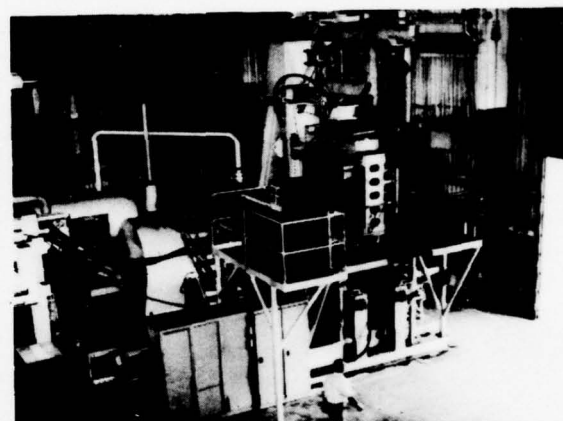


FIGURE 131. ENVIRONMENTAL TEST INSTALLATION

## EVALUATING THE ADHESIVELY BONDED JOINT

### Stiffness Characteristics of Structural Adhesives

As we consider the design requirements of a bonded joint and its subsequent analysis, the first thing required is an allowable. Ultimate shear allowables can be taken from lap shear specimens with thin or thick adherends, but neither will give us sufficient information. Adhesives that cure in the 250°F temperature range are very ductile. Consequently, it is most important to have an accurate stress-strain curve because the elastic and plastic characteristics are needed. Since temperature and moisture can affect the adhesive shear modulus of elasticity, separately or in combination, the test specimen must have a known pretreatment. The neat adhesive specimen is easy to make, subject to a desired environment, and easy to test as a dog bone specimen in tension in a standard testing machine. But, again, the properties measured from these tests are not like those seen in a bonded joint. With no adherend to restrain the adhesive, a change in cross section (Poisson's ratio) occurs. A short overlap shear specimen with a thick-adherend has the most uniform shear stress distribution and therefore is the better specimen (Figure 132). The main problems with the specimen are the very short gauge length of the adhesive, which is 0.002 to 0.005 inch long, and the difficulty in getting the specimen (adhesive) wet for environmental tests. To wet the specimen takes a long time, about 60 days of soaking in the humidity and temperature desired. Testing machines are not capable of measuring such small deflections; therefore, several special extensometers have been developed.

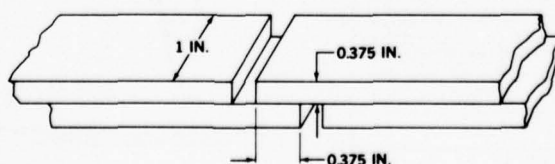


FIGURE 132. THICK ADHEREND LAP-SHEAR SPECIMEN

The KGR-1 extensometer was developed by Raymond B. Krieger, Jr., of the American Cyanamid Company, Havre de Grace, Maryland, to give the shear stress-strain curve for a glue line in a thick-adherend lap-shear specimen. The instrument straddles the glue line with two points in one adherend and one in the other. The system measures deflection by the principle of linear variable differential transformer. The core is made to move in a coil the same amount the glue line deforms in shear. The electric signal is converted into deflection of the glue after some corrections are made such as deflection of metal between gauge points which are 0.094 inch apart. There are several other specimen errors that must be checked and compensated for in order to get a good stress-strain curve. The instrument signal is amplified so that for one mil (0.001) movement of the glue line, the recorder pen will travel 2 inches on the chart. Therefore, you can read 0.0005 inch or less with a 7X glass. Krieger's thick adherend specimen has an 0.375-inch overlap (9.7 mm).

Another method of measuring shear deformations is by using the "napkin ring" adherend specimen. At the adhesive face, the adherends are right, circular, hollow cylinders, having a 3-inch outside diameter and a wall thickness of 0.125 inch. These two cylinder faces, which were anodized, are bonded together with one layer of adhesive. The cylinders are held parallel and concentric by a special jig for bonding. The loading mode is pure shear because no tensile forces are acting on the joint. In torsion tests, the strain is a function of the radial distance from the axis. The thin wall and large radius of the adherends eliminate possible errors. Again, to measure the deformation, a very sensitive extensometer is needed. A technique for measuring the micromechanical properties of the thin film adhesives was developed by employees of Singer-Kearfott.<sup>(10) to (12)</sup> The extensometer consists of two parallel copper plates, in close proximity, which are mounted straddling the adhesive bonded joint so that one capacitor plate is stationary along with the fixed adherend while the other plate moves as the second adherend rotates. A suitable circuit determines the capacitance of the system, which is a measure of the separation of the plates. Sensitivities of  $5 \times 10^{-7}$  inches are obtained.

Another shear deformation measuring device has been developed by Walter Althof.<sup>(13)</sup> It is similar to the KGR-1 instrument in that it has a coil and moving core and is attached to the adherends with three points. Good stress-strain measurements have been produced by this instrument. His thick-adherend specimens have a 5-mm overlap (0.2 inch).

Tables 6 and 7 show samples of the kind of data that are generated by the instruments. All data are for FM-73 adhesive on top of the BR-127 primer. Table 6 presents results of thin-adherend (0.063-inch) standard-lap (0.5-inch) shear specimens. Table 7 shows the lap shear results from the napkin ring test which has eliminated all tension loads from the bonded joint. The Table 7 values are 19 percent higher. Figure 133 is a plot of the shear stress-strain data, at room temperature (70°F or 23°C), obtained by three different instruments and specimens. The elastic modulus,  $G$ , varies from 40,000 to 86,000 psi. Figure 134 presents data from Althof<sup>(7)</sup> showing effects of test temperature, effects of test temperature after a 76-week soak at 122°F and 95 percent relative humidity, and the effect of varying the loading rate. Many more variables need to be investigated so that the designer can select the critical environmental condition. It has been found recently that greatly reduced shear modulus and ultimate shear values were obtained when an FM-73 adhesive film was exposed to moisture before cure, lap-shear specimen bonded, and then tested after the bonded specimen was soaked 60 days until saturated.

TABLE 6  
LAP SHEAR TESTS, FM-73, 74°F

BOND LINE THICKNESS (INCH)	OVERLAP AREA (SQ INCH)	FRACTURE STRESS (PSI)	COHESIVE FAILURE (%)
0.0030	1.056 ± 0.539	4500	100
0.0040	1.064 ± 0.559	4240	100
0.0040	1.042 ± 0.549	4475	100
0.0040	1.053 ± 0.536	4570	100
0.0045	1.021 ± 0.538	4620	100
AVERAGE		4480 ± 65	

TABLE 7  
NAPKIN RING SHEAR TESTS, FM-73, 74°F

BOND LINE THICKNESS (INCH)	MODULUS (PSI)	YIELD STRESS (PSI)	FRACTURE STRESS (PSI)	FRACTURE STRAIN (%)	COHESIVE FAILURE (%)
0.00451	88,720	650	5590	68.1	100
0.00454	77,700	350	5470	78.4	100
0.00459	93,180	590	5460	60.1	100
0.00478	73,100	510	4870	45.7	100
0.00504	86,890	390	5380	54.9	100
AVERAGE	83,920 ± 3700	498 ± 57	5350 ± 126	61.4 ± 5.6	

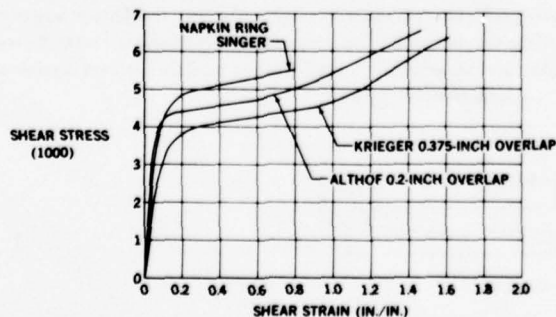


FIGURE 133. STRESS-STRAIN DIAGRAM, FM-73, 74°F

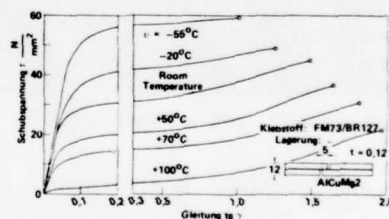


BILD 56: SCHUBSPANNUNGS-GLEITUNGS-DIAGRAMME FM 73, UNTERSCHIEDLICHE PRÜFTEMPERATUREN

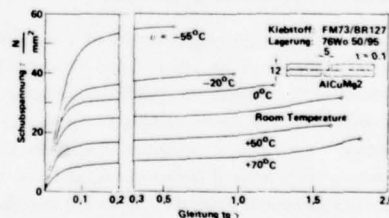


BILD 61: SCHUBSPANNUNGS-GLEITUNGS-DIAGRAMME FM 73, LAGERN BEI FEUCHTER WÄRME 50/95, PRÜFUNG BEI VERSCHIEDENEN TEMPERATUREN

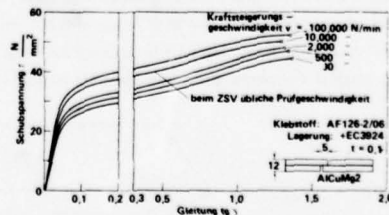


BILD 100: SCHUBSPANNUNGS-GLEITUNGS-KURVEN DES KLEBSTOFFS AF 126-2 BEI UNTERSCHIEDLICHEN PRÜFGESCHWINDIGKEITEN BEIM ZSV

FIGURE 134. DATA FROM W. ALTHOF TESTS

The Fokker-VFW Technological Center adopted the torsion pendulum test method for determination of the shear modulus  $G$  and the logarithmic decrement  $\Lambda$ . The instrument used is the Zwick Torsiomatic which is fully automatic. The following data are from Clevel.<sup>(14)</sup>

For calculation of  $G$  and  $\Lambda$ , the shear modulus and logarithmic decrement are calculated from a plotted curve. The logarithmic decrement  $\Lambda$  is defined as follows:

$$\Lambda = \ln \frac{A_n}{A_{n+1}} \quad (12)$$

where  $A_n$  and  $A_{n+1}$  are amplitudes of two consecutive oscillations.

The shear modulus of specimens with a rectangular section is calculated as follows:

$$G^1 = If^2 F_g F_d - S_e \quad (\text{Nmm}^{-2}) \quad (13)$$

where:

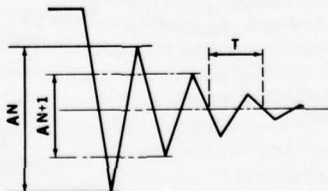
$$F_g = \frac{12\pi^2 l}{wt^3 (1 - 0.63 \frac{l}{w})} \quad (\text{mm}^3)$$

$$F_d = 1 + \frac{\Lambda^2}{4\pi^2} \quad (-)$$

$$S_e = \frac{mgw}{4t^3 (1 - 0.63 \frac{l}{w})} \quad (\text{Nmm}^{-2})$$

The signs used in above equations stand for:

$\Lambda$ = (natural) logarithmic decrement of the damped oscillation	$S_e$ = gravitational stiffness factor ( $\text{Nmm}^{-2}$ )
$A_n$ = amplitude of one oscillation (mm)	$m$ = mass of the oscillating suspension (g)
$A_{n+1}$ = amplitude of the next oscillation (mm)	$f$ = frequency of oscillation ( $\text{s}^{-1}$ )
$G^1$ = (elastic) shear modulus ( $\text{Nmm}^{-2}$ )	$w$ = width of specimen (mm)
$I$ = moment of inertia of all mass suspended to the specimen ( $\text{g/mm}^{-2}$ )	$t$ = thickness of specimen (mm)
$F_g$ = dimensional factor ( $\text{mm}^{-3}$ )	$l$ = length of specimen (mm)
$F_d$ = factor allowing for the influence of damping on frequency	$g$ = acceleration of gravity ( $\text{mms}^{-2}$ )



From a plotted curve (see example), the amplitudes  $A_n$  and  $A_{n+1}$  are measured. The logarithmic decrement can then be calculated. The other variable to be calculated is the frequency "f" of the curve (necessary to calculate  $G^1$ ):

$$f = \frac{V}{T} \quad (\text{s}^{-1}) \quad (14)$$

where

$V$  = film speed, adjustable ( $\text{mms}^{-1}$ )

$T$  = oscillation time of curve (mm)



Table 8 summarizes the FM-73 results for nine temperatures and seven exposures (-2 through -8).

**TABLE 8**  
**SHEAR MODULUS G IN Nmm<sup>-2</sup>**

NOTE: 1 Nmm<sup>-2</sup> = 145 PSI

°C	°F	-2	-4	-3	-5	-6	-7	-8
-60	-76	1341	1413	1450	1379	1481	1344	1351
-40	-40	1225	1234	1270	1225	1284	1227	1235
-20	-4	1106	1096	1133	1080	1130	1113	1119
0	+32	1023	996	1032	978	1029	1033	1039
+20	+68	951	906	940	895	940	960	966
+40	+104	876	807	835	805	848	888	895
+60	+140	773	701	692	715	751	817	827
+80	+176	656	581	563	559	574	732	740
+100	+212	426	336	282	255	237	486	492

See legend in Footnote.

#### Criteria and Analysis Methods

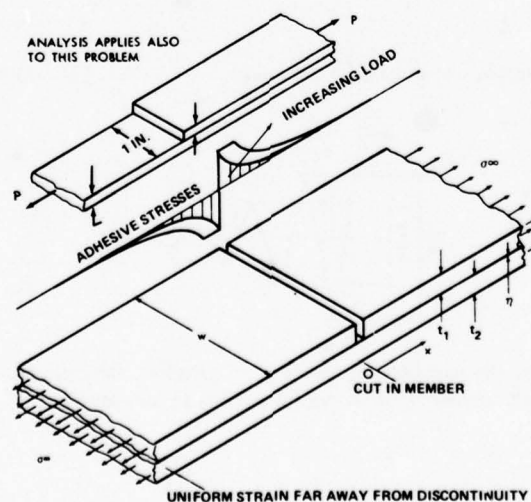
In well-designed adhesively bonded structures, it is most unusual for the weak link to be located in the adhesive rather than in the metal. (The one classical exception is the problem of environmental degradation of the bond-to-adherend interface, and this paper is not concerned with that aspect of bonding.) Any potential stress concentrations in the bonds for intact structure can be alleviated by careful detail design, employing such techniques as tapering, fingered doubles, additional bond area (where appropriate), and the like. However, in providing for bonded structures which may be damaged or broken in service, there is no place for finesse in relieving potential bond stress concentrations because the precise location of potential structural failure damage cannot be predicted. Therefore, the design must permit any metal elements to be broken at any location without causing the adhesive bond to fast-fracture catastrophically under fail-safe load levels.

Analysis methods are presented for adhesive bond stresses associated with structural splices and discontinuities such as broken members and stiffener runouts and the notching of one stiffener where two intersect. The solutions so derived can serve to establish acceptable combinations of stiffener spacing, sheet gage, stiffener area, bond width, and adhesive properties. The solutions presented are simple enough to be evaluated on a pocket calculator, yet show good agreement with experimental evidence.

The elastic-plastic adhesive analysis methods developed by Dr. L. J. Hart-Smith<sup>(15)(16)</sup> for adhesive-bonded joints form the basis of the analyses presented here. The analyses in this paper account for only the shear stresses in the adhesive. Peel stresses in the adhesive due to eccentricities in load paths are also important, whether associated with broken elements or not.

Figure 135 shows the geometry and nomenclature for the analysis of a bonded laminate with one member (identified by subscript 1) cut. The analysis applies equally if the other member is severed by interchanging the subscripts 1 and 2. Out-of-plane displacements are considered to be constrained to eliminate peel stresses in the adhesive and bending stresses in the adherends. The analysis is performed in terms of an equivalent thickness of each member per unit width of bond. The conditions of longitudinal force-equilibrium for a differential element  $dx$  within the joint are

$$\frac{dT_1}{dx} - \tau = 0, \quad \frac{dT_2}{dx} + \tau = 0 \quad (15)$$



**FIGURE 135. GEOMETRY AND NOMENCLATURE AT STRUCTURAL DISCONTINUITY**

Legend: (2) Tested after 7 days at R.H. lower than 10%  
(3) Ref. (2) plus 28 days in water at R.T.  
(4) Ref. (2) plus 7 days in water at R.T.  
(5) Ref. (2) plus 7 days at 60°C and about 100% R.H.

(6) Ref. (2) plus 28 days at 60°C and about 100% R.H.  
(7) Ref. (2) plus 7 days at 60°C and R.H. lower than 10%  
(8) Ref. (2) plus 28 days at 60°C and R.H. lower than 10%

where the subscripts 1 and 2 refer, respectively, to the cut (or terminated) and intact member. The stress-strain relations for the assumed elastic adherends yield

$$\frac{d\delta_1}{dx} = \frac{T_1}{E_1 t_1} + \alpha_1 \Delta T, \quad \frac{d\delta_2}{dx} = \frac{T_2}{E_2 t_2} + \alpha_2 \Delta T \quad (16)$$

As a first approximation, the adhesive shear strain is taken to be

$$\gamma = (\delta_1 - \delta_2)/\eta \quad (17)$$

Within the elastic adhesive region, more than  $d$  from the end of the discontinuous member, the adhesive shear stress is assumed to be

$$\tau = G\gamma = \frac{G}{\eta} (\delta_1 - \delta_2) = f(x) \quad (18)$$

while, throughout the plastic region adjacent to the end of the discontinuous member,

$$\tau = \tau_p = \text{constant} \quad (19)$$

This analysis covers both elastic and elastic-plastic situations by adjusting the adhesive characteristics. Eliminating  $\delta_1$  and  $\delta_2$  between Equations (17) and (16) produces

$$\frac{d\gamma}{dx} = \frac{1}{\eta} \left[ \frac{T_1}{E_1 t_1} - \frac{T_2}{E_2 t_2} \right] + \frac{(\alpha_1 - \alpha_2)\Delta T}{\eta} \quad (20)$$

The use of Equation (15) to eliminate  $T_1$  and  $T_2$  then yields the governing differential equation

$$\frac{d^2\gamma}{dx^2} = \frac{1}{\eta} \left[ \frac{1}{E_1 t_1} + \frac{1}{E_2 t_2} \right] \tau \quad (21)$$

Within the elastic region, this equation becomes

$$\frac{d^2\tau}{dx^2} - \lambda^2\tau = 0 \quad (22)$$

in which

$$\lambda^2 = \frac{G}{\eta} \left[ \frac{1}{E_1 t_1} + \frac{1}{E_2 t_2} \right] \quad (23)$$

Within the elastic zone, the solution of the differential Equation (22) is

$$\tau = \tau_p e^{-\lambda x}, \quad \gamma = \gamma_e e^{-\lambda x} \quad (24)$$

where the origin for the  $x$  coordinate is at the edge of the plastic adhesive zone, of width  $d$ . Within the plastic zone,

$$\gamma = \left[ \frac{\lambda^2 \tau_p}{2G} \right] \xi^2 + C \xi + (\gamma_e + \gamma_p) \quad (25)$$

At  $\xi = 0$  (at the discontinuity in member 1), from Equations (25) and (20),

$$\frac{d\gamma}{d\xi} = C = - \frac{T_2^0}{E_2 t_2 \eta} + \frac{(\alpha_1 - \alpha_2)\Delta T}{\eta} \quad (26)$$

in which the superscript 0 denotes the value at the discontinuity ( $\xi = 0$ ), so that, in the plastic zone,

$$\gamma = \left[ \frac{\lambda^2 \tau_p}{2G} \right] \xi^2 - \left[ \frac{T_2^0}{E_2 t_2 \eta} - \frac{(\alpha_1 - \alpha_2) \Delta T}{\eta} \right] \xi + (\gamma_e + \gamma_p) \quad (27)$$

Now, the integral of the bond stresses over the entire bond area is obviously equal to the load in the broken member at infinity ( $x = \chi = \infty$ ). Thus, from Equations (19) and (24),

$$T_1^\infty = \tau_p (d + 1/\lambda) \quad (28)$$

in which  $d$  is the extent of the plastic zone. It is assumed that, at station  $x = \infty$  far removed from the discontinuity in member 1, both members are strained identically so that, from Equation (16),

$$\frac{T_1^\infty}{E_1 t_1} + \alpha_1 \Delta T = \frac{T_2^\infty}{E_2 t_2} + \alpha_2 \Delta T \quad (29)$$

Overall force equilibrium requires that

$$T_2^0 = T_1^\infty + T_2^\infty \quad (30)$$

$$T_2^0 = T_1^\infty \left[ 1 + \frac{E_2 t_2}{E_1 t_1} \right] + E_2 t_2 (\alpha_1 - \alpha_2) \Delta T \quad (31)$$

The expression (27) at  $\xi = d$  has the form

$$\left[ \frac{\lambda^2 \tau_p}{2G} \right] d^2 - \left[ \frac{T_2^0}{E_2 t_2 \eta} - \frac{(\alpha_1 - \alpha_2) \Delta T}{\eta} \right] d + \gamma_p = 0 \quad (32)$$

since

$$\gamma = \gamma_e \text{ at } \xi = d \quad (33)$$

Now, from Equation (28),

$$d = \frac{T_1^\infty}{\tau_p} - \frac{1}{\lambda} \quad (34)$$

so that the unknown extent of plastic adhesive zone can be eliminated between Equations (32), (34) and (31). A quadratic expression in  $T_1^\infty$  then results. This is

$$\left[ \frac{\lambda^2 \tau_p}{2G} \right] \left[ \frac{T_1^\infty}{\tau_p} - \frac{1}{\lambda} \right]^2 - \left[ \frac{T_1^\infty}{E_2 t_2 \eta} \left[ 1 + \frac{E_2 t_2}{E_1 t_1} \right] \right] \left[ \frac{T_1^\infty}{\tau_p} - \frac{1}{\lambda} \right] + \gamma_p = 0 \quad (35)$$

whence

$$T_1^\infty = \sqrt{\frac{(\gamma_e/2 + \gamma_p) 2G \tau_p}{\lambda^2}} = \frac{\tau_p}{\lambda} \sqrt{1 + 2 \left( \frac{\gamma_p}{\gamma_e} \right)} \quad (36)$$

In terms of the load, at infinity, in the continuous member, Equation (36) is modified by Equations (33) and (34) to become



$$T_2^\infty = \frac{E_2 t_2}{E_1 t_1} \frac{\tau_p}{\lambda} \sqrt{1 + 2 \left( \frac{\gamma_e}{\gamma_p} \right)} + E_2 t_2 (\alpha_1 - \alpha_2) \Delta T \quad (37)$$

so that the total load at infinity is given by

$$T_2^0 = T_1^\infty + T_2^\infty = \left[ 1 + \frac{E_2 t_2}{E_1 t_1} \right] \frac{\tau_p}{\lambda} \sqrt{1 + 2 \left( \frac{\gamma_p}{\gamma_e} \right)} + E_2 t_2 (\alpha_1 - \alpha_2) \Delta T \quad (38)$$

The adhesive stress and strain distributions can be expressed once the extent  $d$  of the plastic zone is established. This is accomplished by eliminating  $T_1^\infty$  between Equations (28) and (36), leading to

$$d = \frac{l}{\lambda} \left[ \sqrt{1 + 2 \frac{\gamma_p}{\gamma_e}} - 1 \right] \quad (39)$$

Typical adhesive stress and strain distributions are illustrated in Figure 136. For load levels sufficiently low not to load the adhesive into the plastic state (i.e.,  $\gamma_p \equiv 0$  and  $\gamma_{\max} \leq \gamma_e$ ), Equation (39) predicts correctly that  $d = 0$ . In the expressions such as (36) to (38), for elastic loads, it is necessary to set  $\gamma_p \equiv 0$  and replace  $\tau_p$  by  $\tau_{\max} = G\gamma_{\max} \leq \tau_p$ .

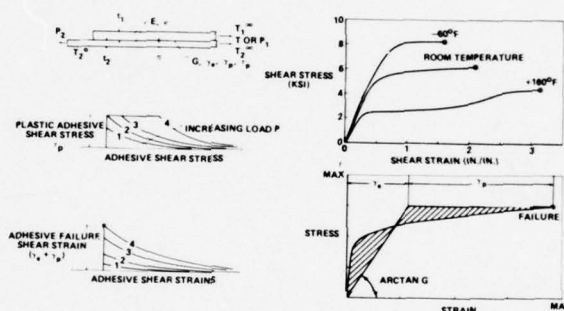


FIGURE 136. TYPICAL ADHESIVE STRESS AND STRAIN DISTRIBUTIONS

As in the case of adhesive-bonded double-lap joints, Equations (36) to (38) indicate that the strain energy in shear is the single necessary and sufficient characterization of the adhesive for this problem (provided that peel stresses and eccentricity effects are eliminated).

#### Example 1:

Consider the case of a doubler bonded on a skin and terminating as is shown in the upper sketch of Figure 135. Using a unit width and 2024-T3 bare sheet,

$$t_1 = t_2 = 0.063 \text{ inch}$$

$$\gamma_e = 0.117$$

$$p = 1 \text{ inch}$$

$$\gamma_p = 0.5$$

$$\eta = 0.002 \text{ inch}$$

$$G = 60,000 \text{ psi}$$

$$E = 10.5 \times 10^6 \text{ psi}$$

$$F_T = 47,000 \text{ psi}$$

$$\nu = 0.3$$

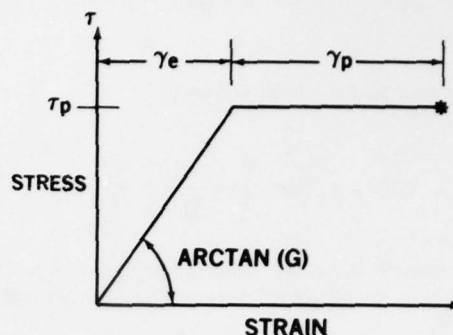
$$F_{TY} = 74,000 \text{ psi}$$

$$\tau_p = 7000 \text{ psi}$$

(adhesive properties are for a  $-50^\circ\text{F}$  condition). Adhesive properties are given in Table 9.

TABLE 9  
TYPICAL CHARACTERISTICS FOR 250°F CURING ADHESIVE

TEMPERATURE	P(PSI)	G(PSI)	$\gamma_e$	$\gamma_p$
R.T. (70°F)	5,000	50,000	0.1	1.0
-50°F	7,000	60,000	0.117	0.5
+160°F	2,500	40,000	0.063	1.5



Evaluating the residual strength of such a bonded panel makes it possible to identify the weak member, be it adhesive or the skin. Using Equations (23) and (36) to solve for

$$\lambda^2 = \frac{60,000}{0.002} \left[ \frac{1}{10.5 \times 10^6 \times 0.063} + \frac{1}{10.5 \times 10^6 \times 0.063} \right]$$

$$\lambda^2 = 90.70$$

$$\lambda = 9.52$$

$$T_1^\infty = T_2^\infty = \frac{7000}{9.52} \sqrt{1 + 2\left(\frac{0.5}{0.117}\right)} = 2272 \text{ pounds}$$

$$T_2^0 = T_1^0 + T_2^\infty = 4594 \text{ pounds}$$

then

$$\sigma^\infty = \frac{T_1^\infty}{A_{SKN}} = \frac{2272}{0.063} = 36,060 \text{ psi}$$

The analysis shows that the doubler would start to disbond if the sheet stress exceeded  $\sigma^\infty$  above. If the hot-day conditions had been used, then  $\sigma^\infty$  would equal 15,770 psi.

To determine the length of splice necessary to transfer one half the load from the single sheet,  $t_2$ , to the spliced doubler,  $t_1$ , solve the following equations.

The length of the plastic zone is determined from Equation (34)

$$d = \frac{T_1^\infty}{\tau_p} - \frac{1}{\lambda} = \frac{2272}{7000} - \frac{1}{9.52} = 0.221 \text{ inch}$$

The length of the elastic zone is determined from the Equation  $\ell_e = \frac{3}{\lambda}$

$$\ell_e = 0.315 \text{ inch}$$

Therefore, the total length of bond necessary to transfer load is

$$\ell = d + \ell_e = 0.221 + 0.315 = 0.546 \text{ inch}$$

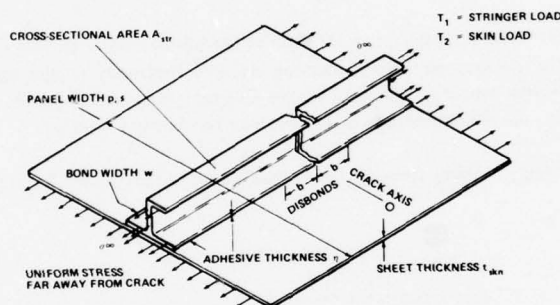
Examining  $\sigma^\infty$ , we see the stress in the doubler sheet away from the splice origin is 36,060 psi. This same stress exists in the basic sheet in the area where it is bonded to the doubler away from the splice origin. Therefore, the sheet stress at  $T_2^0$  at the bond edge ahead of the splice is 2 times 36,060 psi or 72,120 psi. Sheet will not fail because  $F_{TU}$  equals 74,000 psi. Since this exceeds the yield of the metal,  $F_{TY}$  equals 47,000 psi, some very small local yielding of the metal will occur at the leading edge of the adhesive.

**Example 2:**

Consider the case of a bonded stiffener and sheet combination in which the stiffener is cracked through and the sheet is intact. By neglecting the shear distortion in the sheet, the analysis presented can be used to approximate this condition. Evaluate the residual strength of such a bonded panel made from 2024-T3 bare sheet, in which

$$\begin{aligned}
 A_{str} &= 0.2 \text{ sq in.} & \tau_p &= 7000 \text{ psi} \\
 w &= 1.5 \text{ inch} & \gamma_e &= 0.117 \\
 p &= 12.0 \text{ inches} & \gamma_p &= 0.5 \\
 t_{skn} &= 0.063 \text{ inch} & A_{skn} &= pt_{skn} = 0.756 \text{ sq in.} \\
 \eta &= 0.002 \text{ inch} & G &= 60,000 \text{ psi} \\
 E &= 10.5 \times 10^6 \text{ psi} & F_{TY} &= 47,000 \text{ psi} \\
 \nu &= 0.3 & F_{TU} &= 74,000 \text{ psi}
 \end{aligned}$$

and identify the weak link, be it adhesive or the sheet. The terminology for this problem is identified in Figure 137. The equivalent thicknesses are



**FIGURE 137. SHEET BONDED TO CRACKED STIFFENER**

$$\begin{aligned}
 t_1 &= A_{str}/w \text{ and } t_2 = t_{skn}p/w \\
 &= 0.133 \text{ in.} \quad = 0.504 \text{ in.}
 \end{aligned} \tag{40}$$

Equations (36) (23) and (40) yield, for the cut stiffener,

$$\sigma^\infty = \frac{\sqrt{E} \sqrt{\tau_p (\gamma_e + 2\gamma_p)}}{\sqrt{\frac{A_{str}}{\eta w}} \sqrt{1 + \frac{A_{str}}{A_{skn}}}} \tag{41}$$

The numerical solution for the problem above is

$$\sigma^\infty = 31,222 \text{ psi, } \lambda = 5.21, T^\infty = 4151 \text{ pounds}$$

Strain compatibility away from the crack dictates that the sheet and stiffener have the same stress. The geometric influence is confined to the denominator, which should be minimized to maximize the residual strength of the structure for a given adhesive. Obviously, as long as the sheet is intact and the stiffener broken, minimizing the stiffener area maximizes the strength. However, this would lead to a deficient structure as far as restraining a sheet crack with an intact stiffener is concerned. Both cases must be considered in optimizing the geometric proportions. An increase in adhesive layer thickness will increase the value of  $\sigma^\infty$ .

For the above example, the initial failure would be by disbonding of the stiffener if the sheet or panel stress  $\sigma^\infty$  is raised above 31,222 psi. The initial disbond can be propagated only by an increase in applied load. As the disbond propagates, the sheet in line with the stiffener will be able to stretch significantly over the length of the disbond, and this will have the effect of relieving the tendency of the disbond to propagate further. As the skin elongates at the end of the stiffener, the load is redistributed so that in the intact skin, the skin carries a greater percent of total load and the stringer less, hence stopping the disbond action. A more refined analysis is needed to



identify the length of the disbond before the skin in line with the stiffener reaches a yield stress. Once the skin yields, the disbond propagates steadily toward the end of the stiffener as long as the skin stress (at the tip of the disbond) is maintained at the metal yield stress level.

From Equation (39), solve for the plastic zone length,

$$d = \frac{1}{5.21} \left( \sqrt{1 + 2 \left( \frac{0.5}{0.117} \right)} - 1 \right)$$

$$= 0.399 \text{ inch}$$

Using Equation (34) to solve for  $d$

$$d = \frac{4151}{7000} - \frac{1}{5.21} = 0.401 \text{ inch}$$

$$\ell_e = \frac{6}{\lambda} = 1.15 \text{ inches of the elastic zone}$$

Total length of load carrying bond is

$$\ell = 0.400 + 1.15 = 1.55 \text{ inches}$$

In the preceding analysis, Equation (41) predicts the onset of failure of the adhesive bond. However, in many instances, this will not be immediately catastrophic. The initial disbond can be self-arresting and will frequently require application of additional load to propagate further. This section analyzes that aspect of the problem and illustrates how such disbonds can alleviate the severity of the stress concentration in the adhesive due to the discontinuity in one of the members bonded together.

The stress in both the sheet and stiffener far away from the discontinuity is defined to be  $\sigma^\infty$ . Therefore, the total sheet load is

$$wT_2^\infty = \sigma^\infty t_{skn} p \quad (42)$$

while the stiffener load, which must be transferred through the bond, is

$$wT_1^\infty = \sigma^\infty A_{str} \quad (43)$$

where the load intensities  $T_1$  and  $T_2$  are expressed per unit width of bond.

Now, because of the additional load being transferred in and out of the sheet by the broken stiffener, the ends of the intact bond separate under load a displacement given by Equation (44), as the sheet distorts.\*

$$\Delta = \frac{2(3-v)(1+v)q}{4\pi E} \left[ \ell \ln \left( \frac{2b}{\ell} \right) - (2b + \ell) \ln \left( \frac{2b}{2b + \ell} \right) \right] \quad (44)$$

The extent  $\ell$  of the effective load transfer zone can be approximated by considering the adhesive to be fully plastic. Then overall equilibrium requires that

$$q\ell t_{skn} = \tau_p \ell w = \sigma^\infty A_{str} \quad (45)$$

so that, in Equation (44),

$$\ell = (\sigma^\infty A_{str})/(\tau_p w) \text{ and } q = \tau_p w/t_{skn} \text{ and } \Delta_1 = \Delta_2 \quad (46)$$

(If the load level is not sufficiently high to cause the adhesive to yield, the bond length  $\ell$  in Equation (46) should be increased by replacing  $\tau_p$  with the lesser value  $\tau_{max}$ .) The stretching of the sheet between the stiffener break and the intact adhesive follows from Equations (44) and (46).

$$\Delta_1 = \frac{(3-v)(1+v)}{4\pi E} \frac{\tau_p w}{t_{skn}} \left[ \ell \ln \left( \frac{2b}{\ell} \right) - (2b + \ell) \ln \left( \frac{2b}{2b + \ell} \right) \right] \quad (47)$$

\*It is assumed here that the associated displacements at the edges of the sheet are negligible, so a more precise analysis would be needed to cover sheet segments which are not much wider than the bond width.

If the load in the stiffener were to induce uniform stretching of the sheet over the same expanse, that lesser stretching would be

$$\Delta_2 = \frac{\sigma^\infty b}{E} \frac{A_{str}}{p t_{skn}} \quad (48)$$

The difference between Equations (47) and (48) may be looked upon as effective additional shear-strain capacity for the adhesive bond, which would be reflected in the boundary condition for  $\gamma_p$  in Equation (32). It follows, in turn, from Equation (41) that the increased stiffener load needed to cause propagation of the disbond can be approximated by adding to the adhesive bond displacement. That is,

$$\Delta_{effective} = \eta \left[ \frac{\gamma_c}{2} + \gamma_p \right] + \Delta_1 - \Delta_2 \quad (49)$$

Equation (41) is then modified with (45) to read

$$\sigma^\infty = \frac{\sqrt{E} \sqrt{2\tau_p \Delta_{effective}} w}{\sqrt{A_{str}} \sqrt{1 + \frac{A_{str}}{p t_{skn}}}} \quad (50)$$

From the preceding set of equations and the panel geometry set forth, the following answers result, assuming the presence of an 0.5-inch disbond (b).

$$\text{From Equation (41), } \sigma^\infty = 31,222 \text{ psi}$$

$$(46), \quad \ell = 0.595 \text{ inch}$$

$$q = 167,000 \text{ psi}$$

$$(47), \quad \Delta_1 = 0.0047 \text{ inch}$$

$$(48), \quad \Delta_2 = 0.00039 \text{ inch}$$

$$(49), \quad \Delta_{EFF} = 0.0054 \text{ inch}$$

$$(50), \quad \sigma^\infty = 68,653 \text{ psi}$$

As indicated above, the result of Equation (50) depends on (49) which used the  $\sigma^\infty$  from Equation (41). Since only one value of  $\sigma^\infty$  can exist, an iteration process must be utilized. In the above example, the final  $\sigma^\infty = 82,100$  psi.

Indeed, this stress is sufficient for gross yielding, so the initial disbond does not propagate far as the load builds up to complete sheet failure. Figure 138 shows the effect of a range of disbands on the critical strength for this example. It is evident that the sheet will yield prior to gross disbonding, as shown by the curve in Figure 138.

The sheet stress at the tip of the disbond is assumed to be constant over the length of the disbond and can be approximated by the maximum value, under the cracked stiffener, of

$$(\sigma_{skn})_{max} \approx \sigma^\infty + \frac{\tau_p \left(d + \frac{1}{\lambda}\right)}{t_{skn}} = \sigma^\infty \left[ 1 + \frac{A_{str}}{w t_{skn}} \right] = 97,300 \text{ psi} \quad (51)$$

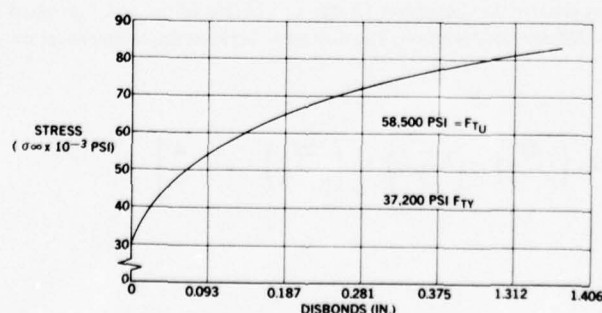


FIGURE 138. EFFECT OF DISBOND ON STRESS  $\sigma^\infty$

(This value is greater than the average value on that cross section. Even within the bond width  $w$ , the sheet stress may exceed this value [Equation (51)] because the load in the stiffener web and outer cap is not uniformly distributed across the full bond width but is concentrated near the web.) Once the sheet yields from the above stress and the load is sustained, the disbond will not propagate further because the sheet between the remaining intact bonds can stretch more than enough to accommodate the stress and strain concentrations in the bond without permitting any increase in them. The stress amplification defined by Equation (51) explains why a fatigue crack in the sheet would develop rapidly in association with any discontinuity in a stiffener, such as at the mouse holes in frames, to permit longerons to pass through.

The method presented in this section can be adapted to analyze the stresses in the metal and adhesive where a finite length of stiffener is absent, as at the mouse holes in frames (or frame/shear-tee combinations). The method is imprecise in such an application but, with sound engineering judgment of the input and output, a good qualitative assessment of such problems can be gained. A missing length of stiffener can be replaced mathematically by an initial disbond of the same length because the analysis assumes a constant stress across the entire stiffener cross section. The broken stiffener is unloaded for the extent of the disbond. While this would be a reasonable assumption for the outer portions of the stiffener flange bonded to the sheet, it is far from the truth near the stiffener web. The skin fatigue cracks induced at poorly detailed stiffener intersections or runouts start in line with the web, where the effective stiffener thickness per unit bond width is locally much greater than the average. Consequently, the key to applying the present analysis to such a problem is the choice of an effective stiffener thickness in line with the web of the stiffener. Usually, not all of the stiffener is notched, so some load remains in the continuous portion of the stiffener rather than passing through the bond to the sheet. Account must be taken of this alternative loadpath for some of the stress concentrations at the notch. Usually, the termination of the stiffener flange itself will not present a problem. At stiffener runouts, it is usually sufficient to cut back the web and any flange not adjacent to the sheet progressively over several inches. However, if the stiffener web is terminated too abruptly and has a large cross section, the application of ultimate loads will either cause the bond to fast fracture until enough of the sheet can stretch to relieve the stress concentrations in the bond or the sheet yields throughout the gap in the interrupted stiffener.

In either event, the corresponding fatigue stresses will induce fatigue cracks in the sheet in line with the cut in the stiffener web if no alternative loadpath is provided. Continuous crack stoppers between frames and skin, joggling of the frame shear tees (or outer flanges) over both longeron flanges in contact with the skin, and gussets joining the shear tees to the longerons are suitable techniques for eliminating the mouse-hole problem. The panel testing for the PABST program indicates that relatively little is needed in the way of alternate loadpath to prevent the initiation of such fatigue cracks at the mouse holes, but that such cracks will initiate and grow rapidly in the absence of any alternative loadpaths to reinforce the skin at the cutouts.

The next problem to be analyzed is identified in Figure 139, which also gives the terminology used in the analysis. The stretching of the sheet, which is concentrated near the stiffener, adds to the strain capability of the adhesive in relieving the critical bond conditions at the sheet crack. A uniform stiffener stress is assumed at each cross section, and the presence of any possible disbond is initially excluded from consideration. The key to the analysis is an approximation of the constraints of displacement compatibility, accounting for all the major effects.\*

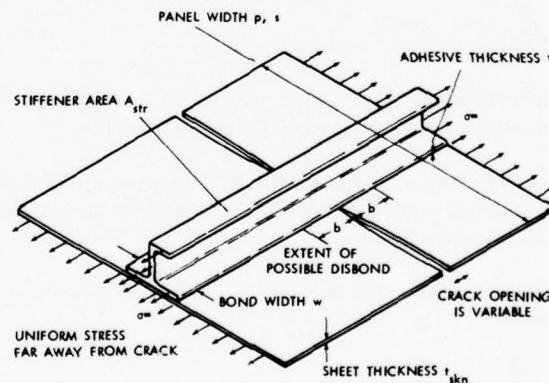


FIGURE 139. STIFFENER BONDED TO FULLY CRACKED SHEET

The sheet distortion can be approximated by Equations (A.22) and (A.25) of Smith<sup>(17)</sup> provided that the plate width  $p$  is reasonably large in comparison with the stiffener bond width  $w$ . The difference between displacements at the edge of the sheet and in the middle of the bond area is

$$\Delta = \frac{2}{\pi E} \left( \frac{\sigma_p}{w} \right) \left[ - \left( \frac{p+w}{2} \right) \ln \left( \frac{2d}{p+w} \right) + \left( \frac{p-w}{2} \right) \ln \left( \frac{2d}{p-w} \right) + w \ln \frac{d}{w} \right] \quad (52)$$

\*Mathematically, more rigorous elastic analyses are possible, but the results of such methods do not actually represent the critical conditions for typical structural adhesives.



This distortion must be independent of the arbitrary constant  $d$ , which can be verified by rearrangement of Equation (52) to the form

$$\Delta_3 = \frac{2}{\pi E} \left( \frac{\sigma^\infty p}{w} \right) \left[ \frac{p}{2} \ln \left( \frac{p+w}{p-w} \right) + \frac{w}{2} \ln \left( \frac{p+w}{2w} \right) + \frac{w}{2} \ln \left( \frac{p-w}{2w} \right) \right] = 0.184 \text{ inch} \quad (53)$$

this distortion can exceed the relative movement between the stiffener and cracked sheet across the adhesive layer, and must therefore be accounted for in any analyses of this problem.

Two distinct failure mechanisms must be assessed in turn. These are failure of the bond with the stiffener behaving elastically, and yielding of the stiffener before the adhesive is loaded to its entire capacity. However, in the second case, if the load is sustained at a level that causes the stiffener to yield, the bond will progressively (or perhaps catastrophically) fracture. The effects of progressive disbonding on this problem are addressed after the analysis of the initially intact bond case. The limiting displacement implicit in Equation (36) is now replaced by

$$\Delta_{\text{effective}} = \eta \left[ \frac{\gamma_e}{2} + \gamma_p \right] + \Delta_3 = 0.0011 + 0.184 = 0.185 \text{ inch} \quad (54)$$

so that the stress far away from the sheet crack, which is associated with critical conditions in the bond, becomes

$$\rho^\infty = \sqrt{\frac{2E\tau_p \Delta_{\text{effective}}}{\frac{pt_{\text{skn}}}{w} \left( 1 + \frac{pt_{\text{skn}}}{A_{\text{str}}} \right)}} = 106,247 \text{ psi} \quad (55)$$

The corresponding stiffener stress is

$$\sigma_{\text{str}}^0 = \sigma^\infty \left[ 1 + \frac{pt_{\text{skn}}}{A_{\text{str}}} \right] = 74,000 \text{ psi} \quad (56)$$

and, since  $A_{\text{str}}/(P t_{\text{skn}})$  is typically less than 0.5, this stress amplification factor may result in the stiffener developing its yield stress prior to the adhesive bond becoming critical.

Consider again the example in Figure 137, but with a complete sheet crack substituted for the complete stiffener crack. An iterative solution of Equations (55) and (54) is required, checking with Equation (56) to ascertain whether stiffener yield is more critical than disbonding. Accounting for the sheet distortion, the initial failure is predicted to be yielding of the stiffener [from Equation (56)] or a nominal sheet stress of  $\sigma^\infty = 15,481$  psi. If this distortion is neglected, however, the prediction is the disbond will not propagate until a sheet stress  $\sigma^\infty$  is in excess of 106,247 psi, so the bond would not be critical.

In the event that the stiffener is sufficiently stiff not to yield, a disbond will be initiated. It is appropriate now to determine whether an increase in load is needed to propagate the disbond or if the bond will fast fracture instantaneously over the length of the bonded assembly. The additional stretching of the sheet in line with the end of the bond will be diminished by any disbond. The amount of this reduction can be approximated by Equation (44) in conjunction with the above analysis. Figure 140 explains how the analyses in Smith<sup>(8)</sup> are used to represent this situation. Distributed loads are used to avoid the singularities associated with point loads. The distortion of Equation (53) in (b) of Figure 140 is reduced by an amount (c) in the figure, which is derived from Equation (44). The latter amount is

$$\Delta_4 = \frac{(3-\nu)(1+\nu)}{4\pi E} \left[ \frac{\tau_p w}{t_{\text{skn}}} \right] \left[ \ell \ln \left( \frac{2b}{\ell} \right) - (2b+\ell) \ln \left( \frac{2b}{2b+\ell} \right) \right] = 0.000028 \text{ inch} \quad (57)$$

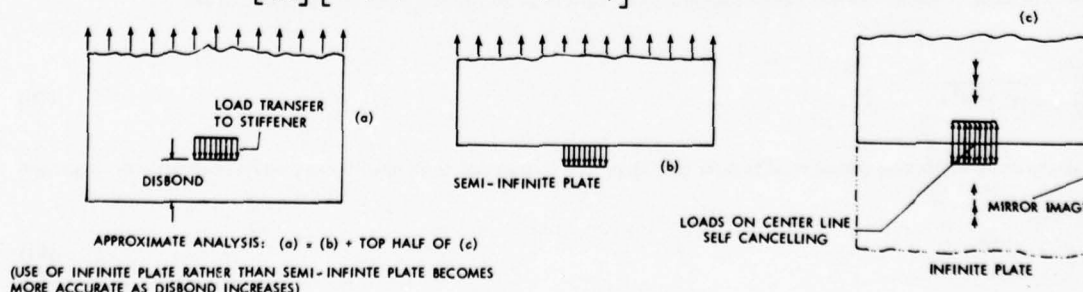


FIGURE 140. DISTORTIONS IN CRACKED SHEET

in which the extent  $\ell$  of the effective load zones in the adhesive is given as in Equation (45). Recalling that the sheet is cracked here instead of the stiffener, the value of  $\sigma^\infty$  equal to 15,481 psi should be used.

$$\ell = (\sigma^\infty A_{skn})/(\tau_p w) = (\sigma^\infty p t_{skn})/(\tau_p w) = 1.115 \text{ inches} \quad (58)$$

(Again, if the load level is not sufficient to cause the adhesive to yield, the bond length  $\ell$  in Equation (58) should be increased by replacing  $\tau_p$  by the lesser value  $\tau_{max}$ .) The effective displacement in Equation (54) is now replaced by

$$\Delta_{\text{effective}} = \eta \left[ \frac{\gamma_c}{2} + \gamma_p \right] + \Delta_3 - \Delta_4 = 0.0279 \text{ inch} \quad (59)$$

It is now obvious that, in this case, the influence of any disbond is to accelerate its propagation. This is in marked contrast to the situation in the preceding example with the stiffener cut rather than the sheet.

An assessment of a simultaneous solution of Equations (53) to (59) reveals that, for practically all geometries, the stiffener is more likely to yield than to disbond. The reason is that the in-plane skin distortions [Equation (56)] are so much greater than the bond displacements [Equation (57)] that the latter can usually be neglected. However, once such a disbond started, it would fast fracture along its entire length instantaneously. None of the other geometries analyzed in this paper indicate such a phenomenon — their disbands are self-arresting until some metal element is overloaded.

The explanation in the preceding paragraph explains some observations during the testing for the PABST program. Bonded stiffeners fell off some cracked panels. The stiffeners remained permanently bent after unloading. Everything happened too quickly during the test to establish the failure sequence. It now appears that the sequence of events was: (1) propagation of the sheet crack, which may or may not have been temporarily arrested, (2) an initial disbond which was probably arrested, (3) stiffener yielding which reduced the effectiveness of the stiffeners in holding the sheet crack closed, (4) propagation of the sheet crack across the full panel width and, finally, (5) complete failure of the bond on one or both sides of the sheet crack because of the very high stresses and strains in the stiffeners at the disbond fronts and the associated very low stresses and strains in the sheets within the extent of the disbands. When the stiffeners were completely unbonded on one side of the sheet crack and broken where the load was introduced into the stiffener at the end of the panel, there were disbands at least 2 inches long on the other side.

One of the test panels involved was a 36-inch-wide, 48-inch-long, 0.063-inch-thick sheet of 2024-T3 aluminum alloy with two longitudinal Z-stiffeners of 0.237-square-inch cross section 12 inches apart, and bonded over an 0.938-inch width. Failure occurred at a gross stress of 30,600 psi. Two other panels were 20-inch-wide, 48-inch-long, 0.063-inch-thick sheets of 2024-T3 aluminum alloy with a single Z-stiffener of the same cross section bonded down the middle of each panel. Failure of these panels occurred at gross stresses of 31,400 and 30,800 psi, respectively.

This same combination of a full-width crack not being arrested by bonded stiffeners which subsequently fell off after failing was also manifest in the testing of a PABST panel having a flush splice across its middle. The panel was 24 inches wide and 48 inches long, of 0.090-inch-thick 7075-T6 aluminum alloy. A tapered splice plate 0.125 inch thick (maximum) and 6.5 inches wide bonded the two sheet segments (24 inches square) together. Two stiffeners, of 0.237-square-inch cross section, were bonded 12 inches apart on the same side of the sheet as the splice plate and perpendicular to it. A small fatigue crack grew in the splice plate, in line with the sheet junction, located about halfway between a stiffener and the edge of the panel. This small crack, 0.7 inch long on the faying surface side (where the crack was concealed beneath the adhesive) and 0.3 inch long on the inner surface (where it was held shut and invisible by the bending stresses in the splice plate) fast-fractured across the entire panel width at a sheet stress of 24 ksi. Both stiffener bonds failed and then the stiffeners failed at their ends, where the load was introduced far away from the splice crack.

The analyses in preceding examples indicate that the sheet distortions permitted by a full-width sheet crack alleviate most problems associated with the bond between the stiffener and sheet until the load level is sufficient to cause the stiffener to fail. Such large beneficial distortions cannot occur if the crack in the sheet extends for less than the full width of the panel. Another potential failure mode is added — that of propagation of the sheet crack. This problem, which is analyzed below, is described in Figure 141.

An analysis in Swift<sup>(7)</sup> establishes that the opening of a sheet crack in an unstiffened panel can be expressed as

$$\delta = \frac{2\sigma^\infty}{E} \sqrt{(a^2 - y^2)} \quad (60)$$

where  $a$  is half the crack width. The critical condition for propagation of such a crack in an unstiffened panel is conventionally expressed in the form

$$\sigma_{\text{critical}} = K_c / \sqrt{\pi a} \quad (61)$$

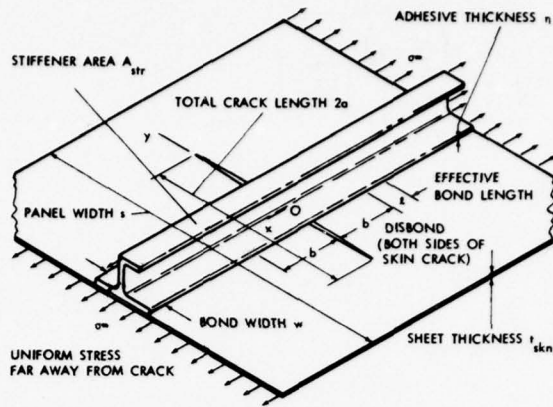


FIGURE 141. TWO-BAY CRACK RESTRAINED BY BONDED STIFFENER

Finite-width effects are customarily accounted for by a modification factor of the form

$$\sigma_{\text{critical}} = \frac{K_c}{\sqrt{\pi a \sec(\pi a/s)}} \quad (62)$$

for a centrally located crack of extent  $2a$  in a sheet of total width  $s$ . The present theories can be modified to account for this and other such effects in a straightforward manner.

The same provisions for sheet distortion which were developed in the form of Equations (53) and (57) for  $\Delta_3$  and  $\Delta_4$  are to be superimposed upon the basic crack-opening expression Equation (60) which, for a central stiffener, reduces to

$$\delta_0 = 2\sigma^\infty a/E \quad (63)$$

Since there is no displacement in the  $x$  direction at the crack tip, Equation (53) should be modified to read

$$\Delta_5 = \left[ \frac{\sigma_b^\infty 2a}{\pi E} \right] \left[ \frac{2a}{w} \ln \left( \frac{2a+w}{2a-w} \right) + \ln \left( \frac{2a+w}{2w} \right) + \ln \left( \frac{2a-w}{2w} \right) \right] \quad (64)$$

This distortion  $\Delta_5$  represents the amount by which the central crack opening  $\delta_0$  in Equation (63) reduces because of the bonded stiffener. If any disbond is present, this relief is reduced by the amount given in Equation (57)

$$\Delta_4 = \frac{(3-\nu)(1+\nu)}{4\pi E} \left[ \frac{\tau_p w}{t_{\text{skn}}} \right] \left[ \ell \ln \left( \frac{2b}{\ell} \right) - (2b+\ell) \ln \left( \frac{2b}{2b+\ell} \right) \right] \quad (65)$$

in which, as in Equation (61), the plastic zone of highly loaded adhesive adjacent to the crack (or disbond, as appropriate) extends a distance

$$\ell = (\sigma^\infty A_{\text{skn}})/(\tau_p w) = (\sigma^\infty 2at_{\text{skn}})/(\tau_p w) \quad (66)$$

The influence of any disbond is very considerable because, even though the disbond effectively stiffens the sheet ( $\Delta_5$  being reduced by  $\Delta_4$ ), it permits a length  $2b$  of the stiffener to stretch far more than the sheet because of the high stiffener stress in the vicinity of the crack. One anticipates that steadily increasing load levels would be needed to propagate the disbands in Figure 141.

In the application of displacement compatibility of this problem, the concern is with the load  $2at_{\text{skn}}\sigma^\infty$  in the sheet in line with the crack. Some of the load transfers through the adhesive bond to the stiffener and passes over the crack. The remainder remains in the sheet and is diverted around the crack tips. Accordingly, the analysis is separated into two parts. The sheet stress increments at  $x = \pm \infty$  are identified by  $\sigma_b^\infty$  and  $\sigma_c^\infty$ , respectively, to denote those increments passing through the bond and around the crack. The contribution of each is analyzed in turn.

For the load passing through the bond, the appropriate width of sheet to incorporate in  $\lambda$ , Equation (23), is the total crack width  $2a$  because Equation (16) shows how the analysis is formulated in terms of strains, which extend uniformly across the entire width. The load transferred by the bond is limited by the width  $2a$ , with the stress in the sheet beyond the crack passing straight on. Thus, if the influence of sheet distortion on  $\sigma_b^\infty$  is neglected, Equation (36) becomes



$$\sigma_b^\infty = \frac{\tau_p w}{\lambda 2at_{skn}} \sqrt{1 + 2\left(\frac{\gamma_p}{\gamma_e}\right)} = \sqrt{\frac{2E\tau_p \eta \left(\frac{\gamma_e}{2} + \gamma_p\right)}{\left[1 + \frac{2at_{skn}}{\Lambda_{str}}\right]}} \left[\frac{w}{2at_{skn}}\right] \quad (67)$$

and the corresponding stiffener stress is

$$\sigma_{str}^0 = \sigma_b^\infty \left[1 + \frac{2at_{skn}}{\Lambda_{str}}\right] \quad (68)$$

The total stiffener stress over the crack is then

$$\sigma_{str}^{tot} = \sigma_{str}^0 + \sigma_c^\infty \quad (69)$$

because the stress  $\sigma_c^\infty$  must be applied to the stiffener as well as to the sheet so as not to alter the relative motion between them which gave rise to the  $\sigma_b^\infty$  and  $\sigma_{str}^0$ .

The sheet stress  $\sigma_c^\infty$ , which passes around the crack, tries to induce a crack opening on one side of the crack centerline given by Equation (63) as

$$\delta_0 = 2\sigma_c^\infty a/E \quad (70)$$

This will be reduced by the resultant of  $\Delta_5 - \Delta_4$  given by Equations (64) and (65) with  $\sigma_b^\infty$  replacing  $\sigma^\infty$ . Likewise, the  $\sigma^\infty$  in Equation (66) refers here to  $\sigma_b^\infty$ . If there be any disbonds present, the stiffener between such disbonds will stretch an amount

$$\Delta_6 = b\sigma_{str}^{tot}/E \quad (71)$$

on each side of the crack.

Displacement compatibility then requires that

$$\Delta_6 + \eta(\gamma_{max}) = \delta_0 - \Delta_5 + \Delta_4 \quad (72)$$

The adhesive shear strain  $\gamma_{max}$  is used in place of the maximum allowable  $(\gamma_e + \gamma_p)$  because the sheet may crack or the stiffener may yield prior to the adhesive failing. Equation (72) can be reexpressed as

$$\eta(\gamma_{max}) + \frac{b\sigma_{str}^0}{E} + \Delta_5 - \Delta_4 = \frac{\sigma_c^\infty}{E} (2a - b) \quad (73)$$

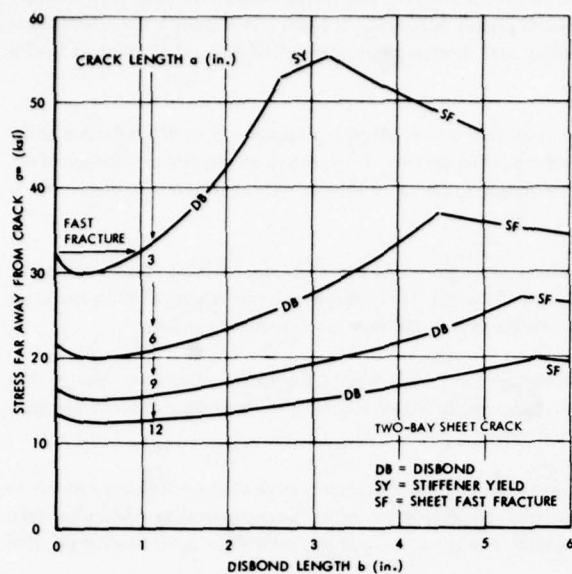
The left side of Equation (73) can be evaluated in terms of  $\sigma_b^\infty$ , while the right side is a function of  $\sigma_c^\infty$ . The method of analysis is to assume trial values of  $\gamma_{max}$ , from which  $\sigma_b^\infty$  can be determined in terms of Equation (67). The remaining stress  $\sigma_c^\infty$  follows from Equation (73). Concurrent checks are made to ensure that  $\sigma_{str}^{tot}$  does not exceed the stiffener yield stress and that  $\sigma_c^\infty$  is not sufficient to cause fast sheet fracture. In rare instances, a check on sheet yield is also needed. Equation (73) shows that a disbond on each side of the sheet crack which is longer than the crack itself is sufficient to nullify the crack-closing characteristics of the bonded stiffener.

At less than a critical condition, the load sharing between load being diverted around the crack tips and passing across the crack through the bonded stiffener can be assessed as follows. A value of  $\sigma_b^\infty$  is assumed and the associated value of  $\gamma_{max}$  established from Equation (67). The other stress  $\sigma_c^\infty$  then follows from Equation (73).

**Examples:** Figures 142 to 147 show the results of parametric analyses using the present solution for two-bay sheet cracks held closed by a bonded central stiffener.

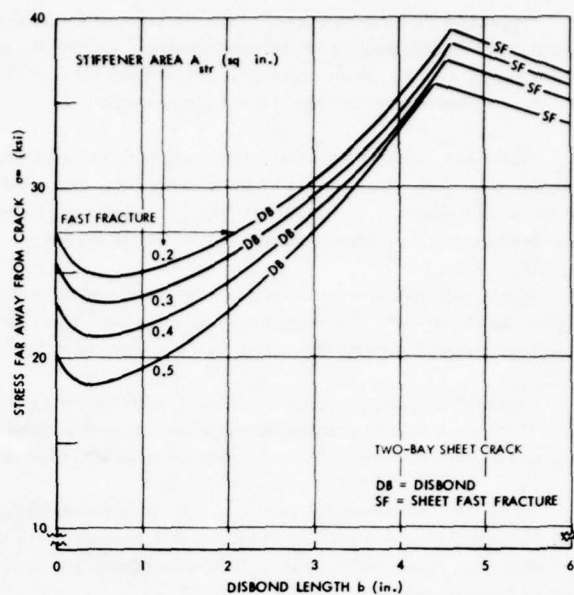
Figure 142 shows the influence of the length of the sheet crack on the panel stress at infinity as a function of the disbond length. Naturally, the longer the crack, the weaker the panel. The initial failure, in every case, is a disbond which is self-arresting after an initial failure. The application of greater loads results in stable propagation of the disbond. For the shorter sheet cracks, still greater loads cause the stiffener to yield once the disbond has spread far enough to reduce the effectiveness of the stiffener in holding the crack shut. For longer sheet cracks, the increase of load leads directly to fast fracture of the sheet. The same final failure mode also prevails for shorter cracks, once the stiffener has yielded.

Figure 142 can also be interpreted as a record of the growing disbond once the sheet starts to fast fracture. With a 6-inch total crack length, the disbond for sheet fracture is 3.2 inches long on each side of the crack. Once the crack grew to 12 inches, the panel strength dropped from 55 ksi to 37 ksi and the disbond grew to 4.5 inches. The disbond continued to grow as the crack propagated, reaching 6.5



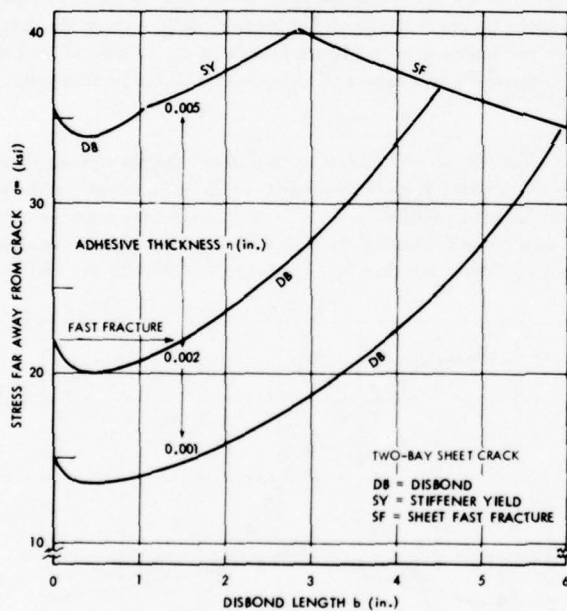
$t_{skn} = 0.063$  in.,  $A_{str} = 0.25$  sq in.,  $p = 12$  in.,  $s = 36$  in.,  $w = 1.5$  in.,  
 $\eta = 0.002$  in.,  $\tau_p = 5500$  psi,  $G = 60000$  psi,  $\gamma_p = 0.55$ ,  $E = 10.5 \times 10^6$  psi,  
 $K_c = 134$  ksi  $\sqrt{\text{in.}}$ ,  $F_{y str} = 75$  ksi,  $F_{y skn} = 65$  ksi

FIGURE 142. INFLUENCE OF CRACK LENGTH ON STRENGTH



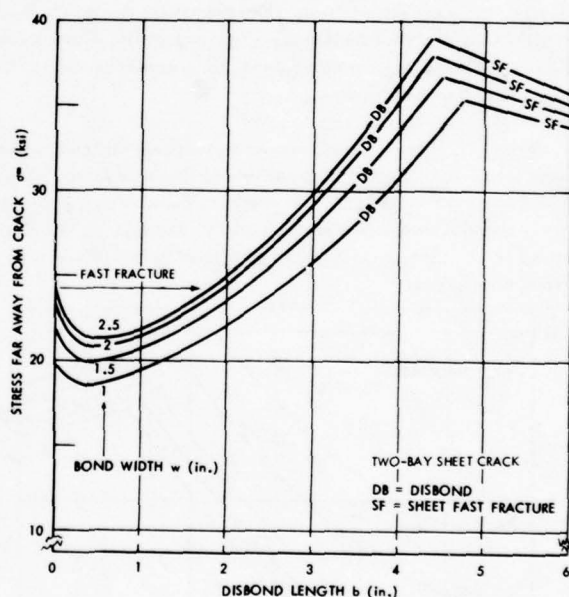
$t_{skn} = 0.063$  in.,  $2a = 12$  in.,  $p = 12$  in.,  $s = 36$  in.,  $w = 1.5$  in.,  
 $\eta = 0.002$  in.,  $\tau_p = 5500$  psi,  $G = 60000$  psi,  $\gamma_p = 0.55$ ,  $E = 10.5 \times 10^6$  psi,  
 $K_c = 134$  ksi  $\sqrt{\text{in.}}$ ,  $F_{y str} = 75$  ksi,  $F_{y skn} = 65$  ksi

FIGURE 143. INFLUENCE OF STIFFENER AREA ON STRENGTH



$t_{skn} = 0.063$  in.,  $A_{str} = 0.25$  sq in.,  $2a = 12$  in.,  $p = 12$  in.,  $s = 36$  in.,  
 $w = 1.5$  in.,  $\tau_p = 5500$  psi,  $G = 60000$  psi,  $\gamma_p = 0.55$ ,  $E = 10.5 \times 10^6$  psi,  
 $K_c = 134$  ksi  $\sqrt{\text{in.}}$ ,  $F_{y str} = 75$  ksi,  $F_{y skn} = 65$  ksi

FIGURE 144. INFLUENCE OF BOND THICKNESS ON STRENGTH



$t_{skn} = 0.063$  in.,  $2a = 12$  in.,  $A_{str} = 0.25$  sq in.,  $p = 12$  in.,  $s = 36$  in.,  
 $\eta = 0.002$  in.,  $\tau_p = 5500$  psi,  $G = 60000$  psi,  $\gamma_p = 0.55$ ,  $E = 10.5 \times 10^6$  psi,  
 $K_c = 134$  ksi  $\sqrt{\text{in.}}$ ,  $F_{y str} = 75$  ksi,  $F_{y skn} = 65$  ksi

FIGURE 145. INFLUENCE OF BOND WIDTH ON STRENGTH

inches once the crack grew to a total of 24 inches (12 inches on each side of the stiffener). Actually, if the load is maintained as the sheet fast fractures, the additional load must be carried in the stiffener, which will yield, causing even greater extents of disbonds for that grossly unstable condition than have been computed in Figure 142 for the onset of instability.

Figure 143 illustrates the effect of stiffener area. The greater the stiffener area, the more effective the stiffener is in keeping the crack tips closed, so the greater the panel strength. The failure sequence, as a function of disbond length, shares the above characteristics. An initial fracture of the bond at constant load is followed by stable progression of the disbond under increasing load until fast fracture of the sheet occurs. For the particular examples shown, there is no indication of stiffener yielding. However, the stiffener would yield prior to sheet fracture for small enough stiffeners.

Figure 144 shows the influence of the thickness of the adhesive between the stiffener and cracked sheet. The final sheet fracture characteristic is independent of the bond thickness, but the thinner bonds permit disbonding at lower panel stress levels. The thicker bonds permit yielding of the stiffener as a transition between disbonding and sheet fracture. The initial disbond at constant load is self-arresting and requires additional load to be propagated.

Figure 144 also shows qualitatively the effect of variations in any of the mechanical adhesive properties. Since the influence of the adhesive is uniquely characterized by the adhesive shear strain energy per unit bond area  $\eta \tau_p \left( \frac{1}{2} \gamma_e + \gamma_p \right)$ , proportionate changes in any of the shear modulus  $G$ , plastic shear stress  $\tau_p$ , or elastic or plastic shear strains  $\gamma_e$  and  $\gamma_p$  would have the same effect in Figure 144 as the corresponding proportionate change in adhesive thickness  $\eta$ .

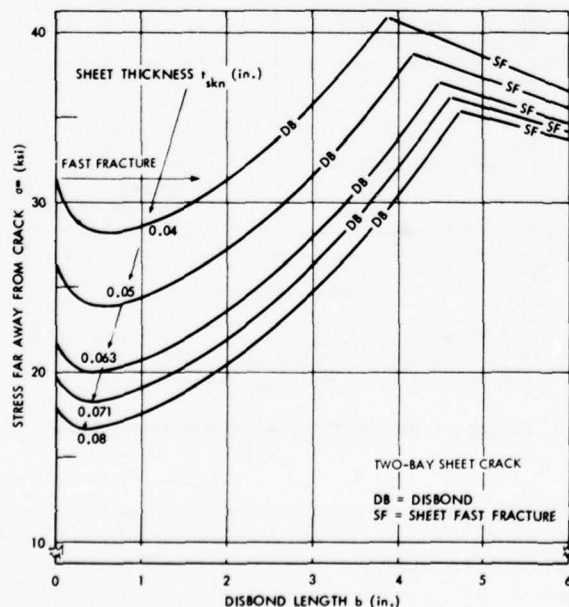
Figure 145 indicates the influence of the bond width for the stiffener, for a given cracked sheet and stiffener cross section. The greater the bond width, the lower the bond strains and hence the stronger the panel. This strength increase applies to both the sheet fast-fracture as well as to the disbonding. In some cases, the additional width can make a stiffener more prone to yielding.

Figure 146 depicts the influence of sheet thickness for a common stiffener and crack length. The thinner sheets are stronger than the thicker ones unless the stiffeners are reinforced for the latter. The characteristic failure sequence for increasing disbond lengths is repeated — initial fracture, arrest, stable disbond growth, and fast sheet fracture.

Figure 147 shows how the maximum adhesive shear strain decreases once the disbond is great enough to make stiffener yielding or fast fracture of the sheet crack more critical than propagation of the disbond. The figure also shows the corresponding relation between the total sheet stress, the strength of the cracked panel devoid of stiffening, and the portion of the total sheet load which is diverted around the crack tip.

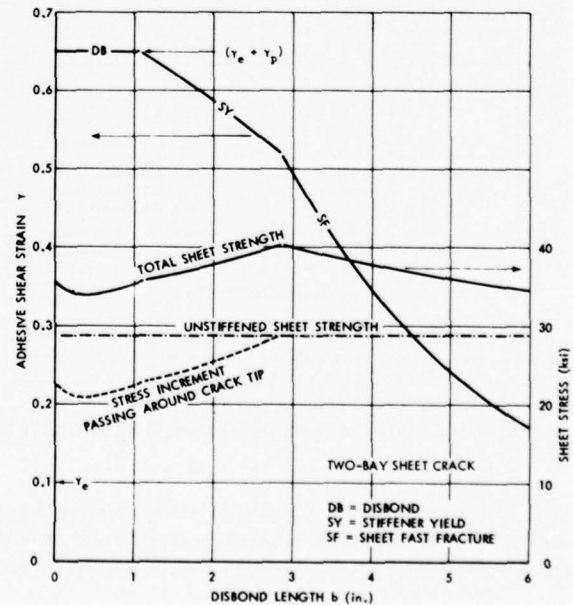
Since the initial dip in the strength versus disbond curve is so characteristic of these bonded stiffened panels with sheet cracks — and the same is found to be true in the next section for one-bay cracks as well as the two-bay cracks considered here — it is appropriate to further explain the phenomena. This is possible because the computer program was developed progressively, adding each distortion contribution, one at a time. With reference to the compatibility Equation (73), it can be stated that the contribution of stiffener stretching  $\Delta_6$  [Equation (71)] tends to alleviate the stress concentration at the tip of the bond and to increase the panel strength. Likewise, the sheet distortion  $\Delta_5$  [Equation (64)] due to the crack closing up under the bonded stiffener tends to increase the panel strength. Only the contribution  $\Delta_4$  [Equation (65)], which measures the tendency to nullify the benefits of  $\Delta_5$  because of the gap between the crack and the intact bond, has a weakening effect. This negative effect is eventually overpowered by the positive effects, giving rise to the observed dips.

When a sheet crack grows between two adjacent stiffeners in a panel, the crack growth is retarded as the crack approaches and grows slowly across the stiffener. The analysis methods presented here are not sensitive enough to account for the influence of a stiffener bonded beyond the crack tip. The crack tip must be trying to open up for the bonded stiffener to be able to exert any major force to keep it closed. Therefore, slow crack growth under fatigue loading is usually not terminated until after the crack has passed over all or part of the bonded crack stopper or stiffener. The analysis presented in this section therefore ignores that portion of any stiffener beyond the crack tip.



$2a = 12$  in.,  $A_{str} = 0.25$  sq in.,  $p = 12$  in.,  $s = 36$  in.,  $w = 1.5$  in.,  
 $\eta = 0.002$  in.,  $\tau_p = 5500$  psi,  $G = 60000$  psi,  $\gamma_p = 0.55$ ,  $E = 10.5 \times 10^6$  psi,  
 $K_c = 134$  ksi  $\sqrt{\text{in.}}$ ,  $F_{y str} = 75$  ksi,  $F_{y skn} = 65$  ksi

FIGURE 146. INFLUENCE OF SHEET THICKNESS ON STRENGTH



$t_{skn} = 0.063$  in.,  $A_{str} = 0.25$  sq in.,  $2a = 12$  in.,  $p = 12$  in.,  $s = 36$  in.,  
 $w = 1.5$  in.,  $\eta = 0.002$  in.,  $\tau_p = 5500$  psi,  $G = 60000$  psi,  $\gamma_p = 0.55$ ,  
 $E = 10.5 \times 10^6$  psi,  $K_c = 134$  ksi  $\sqrt{\text{in.}}$ ,  $F_{y str} = 75$  ksi,  $F_{y skn} = 65$  ksi

FIGURE 147. ADHESIVE SHEAR STRAIN VERSUS DISBOND LENGTH



The model for the problem being solved here is defined in Figure 148. The method of analysis follows that described in the previous example in that the various individual displacements and distortions are balanced to ensure compatibility. Treating the cracked sheet as being unstiffened, Equation (60) would indicate that, in line with the center of each stiffener, the crack would try to open up on each side an amount

$$\delta_0 = \frac{2\sigma_c^\infty}{E} \sqrt{a^2 - \left(\frac{p}{2}\right)^2} \quad (74)$$

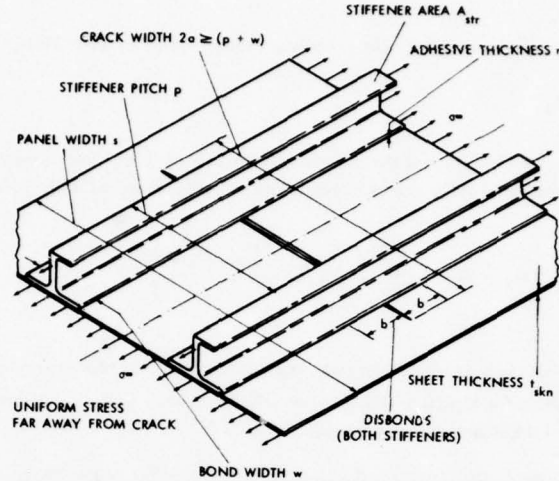


FIGURE 148. ONE-BAY SHEET CRACK RESTRAINED BY BONDED STIFFENERS

The critical sheet stress  $\sigma_c^\infty$  which must not be exceeded if the crack is not to propagate instantaneously is given in Equation (62). This opening will be resisted by the load in the stiffeners which will cause the sheet to distort an amount given by Equation (A.31) in Smith.<sup>(17)</sup> In eliminating the arbitrary constant  $d$  from that equation, the true zero displacement reference is taken at the crack tip. The correction factor is expressed by Smith<sup>(17)</sup> in Equation (A.27) on setting  $y = a - (p + w)/2$ . The resultant closing of the crack at the middle of the stiffeners is given by

$$\Delta_7 = \frac{q}{\pi E} \left[ 2w \ln \left( \frac{1}{w} \right) + (2p + w) \ln \left( \frac{1}{2p + w} \right) - (2p - w) \ln \left( \frac{1}{2p - w} \right) - (2a - p + w) \ln \left( \frac{1}{2a - p + w} \right) \right. \\ \left. - (2a + p + w) \ln \left( \frac{1}{2a + p + w} \right) + (2a - p - w) \ln \left( \frac{1}{2a - p - w} \right) + (2a + p - w) \ln \left( \frac{1}{2a + p - w} \right) \right] \quad (75)$$

The load intensity  $q$  in Equation (75) is given as in Equation (45) by

$$q = \sigma_b^\infty \frac{2a}{2w} \quad (76)$$

in which  $\sigma_b^\infty$  is the sheet stress at infinity which is amplified in the ratio  $A_{skn}/A_{str}$  as it is transferred through the bond to the stiffener. If there be any disbands present, this contraction is reduced by an amount derivable from Equation (A.62) in Smith<sup>(17)</sup> as

$$\Delta_8 = \frac{(3 - \nu)(1 + \nu)}{4\pi E} \left( \frac{\tau_p w}{t_{skn}} \right) \left[ \ell \ln \left( \frac{2b}{\ell} \right) - (2b + \ell) \ln \left( \frac{2b}{2b + \ell} \right) \right] \quad (77)$$

in which the effective adhesive zone extends a distance  $\ell$  given in Equation (66) as

$$\ell = (\sigma_b^\infty 2at_{skn}) / (2\tau_p w) \quad (78)$$

If the influence of sheet distortion on  $\sigma_b^\infty$  is neglected, the component of stress in the sheet away from the crack which passes through the bond is given by Equation (36) as

$$\sigma_b^\infty = \frac{\tau_p 2w}{\lambda 2at_{skn}} \sqrt{1 + 2 \frac{\gamma_p}{\gamma_e}} = \sqrt{\frac{2E\tau_p \eta \left( \frac{\gamma_e}{2} + \gamma_p \right)}{\left( 1 + \frac{2at_{skn}}{A_{str}} \right)}} \left[ \frac{2w}{2at_{skn}} \right] \quad (79)$$

and the corresponding stiffener stress is

$$\sigma_{str}^0 = \sigma_b^\infty \left[ 1 + \frac{2at_{skn}}{A_{str}} \right] \quad (80)$$

Over a disbond length  $b$  on each side of the sheet crack, the stiffener will stretch an amount  $\Delta_6$  given in Equation (71) as

$$\Delta_6 = b\sigma_{str}^{tot}/E = b(\sigma_{str}^0 + \sigma_c)/E \quad (81)$$

Exactly the same compatibility requirement as in the preceding example must be met. Thus,

$$\Delta_6 + \eta(\gamma_{max}) = \delta_0 - \Delta_7 + \Delta_8 \quad (82)$$

The adhesive shear strain  $\gamma_{max}$  may not exceed the maximum allowable ( $\gamma_e + \gamma_p$ ) but, if the failure should initiate in the sheet or stiffener,  $\gamma_{max}$  may not attain that full value. After rearrangement, Equation (82) is solved in the form

$$\eta(\gamma_{max}) + b \frac{\sigma_b^\infty}{E} \left( 1 + \frac{2at_{skn}}{A_{str}} \right) + \Delta_7 - \Delta_8 = \frac{\sigma_c^\infty}{E} \left( 2 \sqrt{a^2 - \left( \frac{P}{2} \right)^2} - b \right) \quad (83)$$

Again, it is evident that a disbond twice as long as the sheet crack is sufficient to nullify the effectiveness of the bonded stiffener as a crack arrester. The method of analysis for Equation (83) is to assume trial values of  $\gamma_{max}$ , deduce  $\sigma_c^\infty$  from this equation, and keep increasing  $\gamma_{max}$  until some element of the structure becomes critically loaded.

The analytical procedure for less-than-critical loads is the same as described at the end of the preceding example.

**Examples:** Figures 149 to 154 illustrate some parametric effects on the strength of bonded panels with a one-bay sheet crack extending slightly past bonded stiffeners. All solutions exhibit the same characteristic form as the disbond grows – the three phases, in order, are disbond, stiffener yield, and sheet fast fracture. The first two phases can be absent, depending on the geometry.

Figure 149 shows the influence of how far past the stiffener the crack has spread. As far as the sheet fracture is concerned, the longer the crack, the weaker the panel. The same sequence holds true for yielding of the stiffeners. However, with regard to the initial disbond, there may be a different phenomenon when the crack extends only immediately beyond the bonded stiffeners. Figure 149 shows little sensitivity of the disbond length to the crack size. This is because the stiffener yielding relieves the bond stresses and strains as long as the load is reduced while the sheet crack grows. Were the load maintained at the 37 ksi associated with the 6.76-inch semicrack length as the sheet crack grew, the stiffeners could stretch only as much as the opening of the sheet crack permitted, even though they were yielding. But once the crack has extended across the entire width of the panel (36 inches in this case), the overload stiffeners would stretch more and more until they fractured. In association with this last phase of failure for the stiffened panel, the disbond would try to grow along the entire length of the stiffener if the strain rate of the loading device were not too fast. The stiffener would then fall off the panel and break far away from the sheet crack.

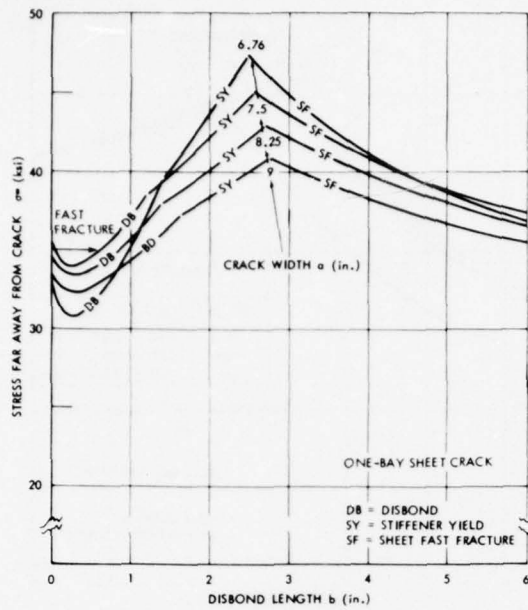
Figure 150 shows the influence of variations in the width of adhesive used to bond stiffeners of common area. The general tendency of the greater width increasing the strength is complicated by the occurrence of yielding of the stiffener at a stress less than that needed to fast-fracture the sheet. The reason for the change to stiffener yielding is that the greater bond width permits the stiffener to accept more load without breaking the bond.

Figure 151 shows how greater stiffener cross sections are effective in increasing the panel strength.

Figure 152 shows that finite sheet widths can effect significant reductions in panel strength, indicating the need to account for this factor in analyses.

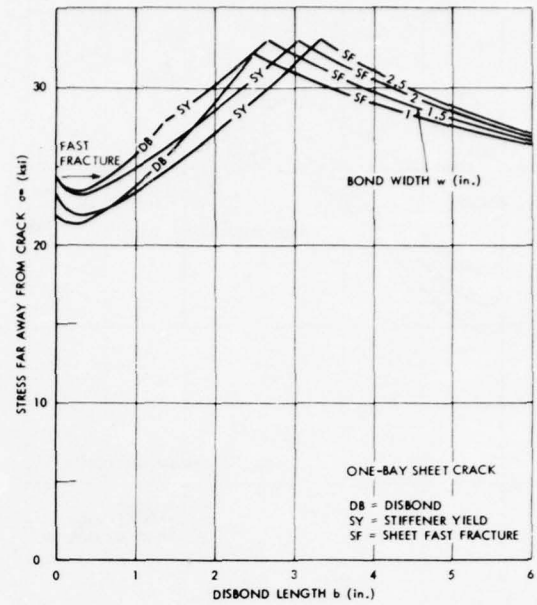
Figure 153 shows how, for a constant stiffener cross section, greater strengths are developed by the thinner, cracked sheet panels. The failure sequence is an initial disbond at constant load which is self-arresting, a stable propagation of the disbond under increasing load until the stiffener yields, and eventually, the sheet fast-fracture.

Figure 154 demonstrates that, while the fast-fracture and disbond characteristics can be affected significantly by change in adhesive properties with temperature (and therefore other environments as well), the overall effect on panel strength is slight. The reason for the relatively small changes is that the overall adhesive properties vary with temperature and moisture in such a way that the shear strain energy to failure changes little. As the temperature is reduced (or the adhesive dried out), the adhesives become stiffer and more brittle while, at higher temperatures or moisture content, the adhesives become softer and more ductile. The curves for room temperature and +140°F have adhesive characteristics so that the strain energy to failure of the adhesive in shear is practically identical. Consequently, those two failure characteristics in Figure 154 lie close together. The adhesive properties at -67°F were artificially modified by representing the adhesive as being more brittle than it really is in order to amplify the effects on the cracked stiffened sheet failure characteristic. This artificial adhesive had only about half the shear-strain energy when it was cold than the real adhesive had at room



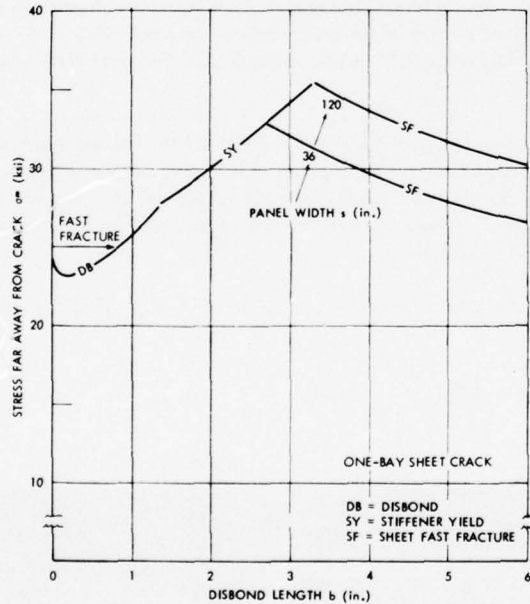
$t_{skn} = 0.063$  in.,  $A_{str} = 0.25$  sq in.,  $p = 12$  in.,  $s = 36$  in.,  $w = 1.5$  in.,  
 $\eta = 0.002$  in.,  $\tau_p = 5500$  psi,  $G = 60000$  psi,  $\nu_p = 0.55$ ,  $E = 10.5 \times 10^6$  psi,  
 $K_c = 134$  ksi  $\sqrt{\text{in.}}$ ,  $F_{y str} = 75$  ksi,  $F_{y skn} = 65$  ksi

FIGURE 149. INFLUENCE OF CRACK LENGTH ON STRENGTH



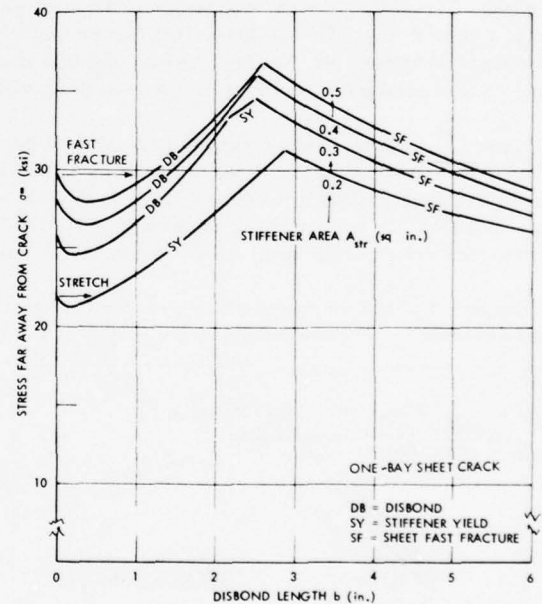
$t_{skn} = 0.063$  in.,  $2a = 16.5$  in.,  $A_{str} = 0.25$  sq in.,  $p = 12$  in.,  $s = 36$  in.,  
 $\eta = 0.002$  in.,  $\tau_p = 5500$  psi,  $G = 60000$  psi,  $\nu_p = 0.55$ ,  $E = 10.5 \times 10^6$  psi,  
 $K_c = 134$  ksi  $\sqrt{\text{in.}}$ ,  $F_{y str} = 75$  ksi,  $F_{y skn} = 65$  ksi

FIGURE 150. INFLUENCE OF BOND WIDTH ON STRENGTH



$t_{skn} = 0.063$  in.,  $2a = 16.5$  in.,  $A_{str} = 0.25$  sq in.,  $p = 12$  in.,  $w = 1.5$  in.,  
 $\eta = 0.002$  in.,  $\tau_p = 5500$  psi,  $G = 60000$  psi,  $\nu_p = 0.55$ ,  $E = 10.5 \times 10^6$  psi,  
 $K_c = 134$  ksi  $\sqrt{\text{in.}}$ ,  $F_{y str} = 75$  ksi,  $F_{y skn} = 65$  ksi

FIGURE 151. INFLUENCE OF STIFFENER AREA ON STRENGTH



$t_{skn} = 0.063$  in.,  $2a = 16.5$  in.,  $p = 12$  in.,  $s = 36$  in.,  $w = 1.5$  in.,  
 $\eta = 0.002$  in.,  $\tau_p = 5500$  psi,  $G = 60000$  psi,  $\nu_p = 0.55$ ,  $E = 10.5 \times 10^6$  psi,  
 $K_c = 134$  ksi  $\sqrt{\text{in.}}$ ,  $F_{y str} = 75$  ksi,  $F_{y skn} = 65$  ksi

FIGURE 152. INFLUENCE OF PANEL WIDTH ON STRENGTH

temperature and above. The reason why adhesive strain energy has so much more of an effect than the adhesive failure stress  $\tau_p$  or strain  $(\gamma_e + \gamma_p)$  is that the strain has a major effect on the load which the stiffener can carry without propagating a disbond while the stress represents only a small perturbation on the sheet distortion (provided that the crack tip is not too close to the bonded stiffener).

The results of an example problem, obtained from testing a stiffened center-crack panel at Douglas during the PABST development test program, provide a means of assessing the accuracy of the present analytical method. This test panel is discussed fully in Swift,<sup>(4)</sup> so only a brief description is presented here. The basic sheet was of 0.063-inch-thick 2024-T3 aluminum alloy (bare), 36 inches wide by 48 inches long, with the grain in the transverse direction. Two bonded Z-stiffeners of 7075-T6 aluminum alloy extrusion, having an area of 0.237 square inch and a bond contact width of 0.938 inch, were bonded longitudinally at a 12-inch pitch. A central crack was grown to 8.2 inches on one side and 7.2 inches on the other. The adhesive thickness varied between 0.001 inch under the web of the stiffener and 0.0025 inch at the free edge of the flange. The gross stress at failure was measured to be 30,600 psi.





## SYMBOLS

$A_{str}$	stiffener cross-sectional area	$\alpha_1, \alpha_2$	adherend (metal) coefficients of thermal expansion
$a$	half crack width	$\gamma$	adhesive shear strain
$b$	extent of disbond on each side of discontinuity	$\gamma_e, \gamma_p$	adhesive elastic and plastic shear strains
$C$	constant	$\Delta$	displacement (sheet distortion)
$d$	extent of adhesive plastic zone, adjacent to discontinuity	$\delta_1, \delta_2$	adherend displacements across bondline
$d$	distance from discontinuity to zero displacement reference	$\eta$	adhesive layer thickness
$E_1, E_2, E$	Young's modulus for adherends	$\lambda$	exponent of adhesive shear stress distribution
$e$	2.718281828, base of natural logarithms	$\pi$	3.141592654, Pi
$F_y$	yield stress	$\sigma_1, \sigma_2$	adherend stresses
$G$	adhesive shear modulus (elastic)	$\tau$	adhesive shear stress
$K_c$	fracture toughness coefficient for cracked sheet	$\tau_p$	adhesive plastic (maximum) shear stress
$\ell$	effective extent of adhesive load zone adjacent to discontinuity	Subscripts:	
$\ln$	natural logarithm	$b$	pertaining to bond
$P$	concentrated load	$c$	pertaining to crack in sheet
$p$	stiffener pitch	$r, \theta$	radial and circumferential coordinates (in appendices)
$q$	distributed load	$skn$	pertaining to sheet (skin)
$s$	panel width	$str$	pertaining to stiffener (stringer)
$T_1, T_2$	adherend loads per unit width	Superscripts:	
$\Delta T$	temperature differential ( $T_{operating} - T_{cure}$ )	$0$	identified with discontinuity
$t_1, t_2, t$	adherend effective thicknesses per unit bond width	$\infty$	identified with conditions far away from discontinuity
$t_{skn}$	thickness of sheet	$tot$	total
$w$	width of bond		
$x, y, \xi, \chi$	coordinates		

## Bondline Flaw Growth Under Slow-Cycle Loading

During the early stages of the PABST program, behavior of bondline flaws under cyclic loading was not understood. It was obvious that such flaws would be generated during processing and assembly of expensive components and panels, and it was a matter of concern to establish the behavior of these defects under realistic flight environments. The effects of defects program was undertaken with a view to answering these questions. Figure 157 shows the cycle rate.

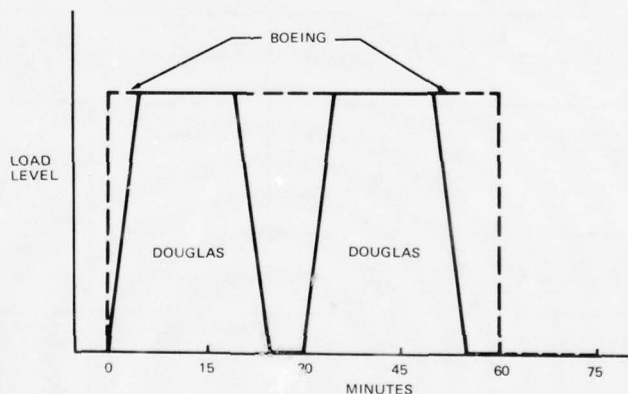


FIGURE 157. THE DOUGLAS AND BOEING LOAD CYCLE RATES

The geometric configurations of the test specimens are shown in Figure 158. The specimens that were flawed intentionally are identified in Table 10 by part number ZJ197660 or ZJ197664. Flaws in all other specimens listed in the table were accidentally introduced during manufacture.

The material of the specimens was 2024-T3 bare sheet with thicknesses varying from 0.04 to 0.08 inch. The ZJ197660 specimens, which were the primary effects of defects splice specimens, were 0.05 inch in thickness.

The specimens were phosphoric acid anodized, primed with the prescribed primer, and bonded using the specified adhesive. The bonding process was controlled within the tolerance limits specified by the adhesive manufacturer, except in those cases where the flaw required deviation from the optimum curing parameters. The environment for these tests was 140°F and 100-percent relative humidity.

The PABST internal pressure hoop load is 750 lb/in. Thus, the test load selected for the effects of defects program was 1500 pounds because the specimens are 2.0 inches in width. A few of the specimens were subjected to 3000 pounds but they all resulted in early metal failure (see Table 11). The 3000-pound specimens are indicated in Table 10. All other specimens with no load shown were loaded to 1500 pounds.

**TABLE 10**  
**BONDLINE FLAW TEST SUMMARY**

	TYPE OF FLAW	FLAW SIZE AT		FAILURE MODE OR COMMENT
		INITIAL INSPECTION	LAST INSPECTION	
FM-73	CONTAMINATION - BARE HAND WIPE OVER BONDED SURFACE (ZJ197660-503)	ALL FOUR SIDES ACCEPTABLE BOND STRENGTH	NO CHANGE FROM INITIAL INSPECTION	STILL IN TEST WITH 20,575 CYCLES
	LOW BONDING TEMPERATURE DURING CURE (ZJ197660-505)	ALL FOUR SIDES ACCEPTABLE BOND STRENGTH	NO CHANGE FROM INITIAL INSPECTION	STILL IN TEST WITH 20,575 CYCLES
	TOO SHORT TIME AT CURING TEMPERATURE (ZJ197660-507)	ALL FOUR SIDES ACCEPTABLE BOND STRENGTH	NO CHANGE FROM INITIAL INSPECTION	STILL IN TEST WITH 20,575 CYCLES
	POROSITY BY FOREIGN OBJECT INSERTION (ZJ197660-509)	SIDE A - ACCEPTABLE SIDE B - 50-PERCENT LOW BOND STRENGTH SIDE C - 20 PERCENT LACK OF BOND SIDE D - ACCEPTABLE FIGURE 159	NO CHANGE FROM INITIAL INSPECTION	STILL IN TEST WITH 20,575 CYCLES
	VOIDS - 0.25-IN. RADIUS SEMI-CIRCULAR IN SIDES B AND C (ZJ197660-515)	SIDE A - ACCEPTABLE SIDE B - 0.25-IN. RADIUS VOID UNEXPOSED BONDLINE SIDE C - 0.25-IN. RADIUS VOID EXPOSED BONDLINE SIDE D - ACCEPTABLE	NO CHANGE FROM INITIAL INSPECTION	STILL IN TEST WITH 18,030 CYCLES
	FRACTURED BONDLINE FULL WIDTH OF SPECIMEN, 0.25 IN. IN DEPTH (ZJ197660-521)	ALL FOUR SIDES FRACTURED FULL WIDTH OF SPECIMEN SIDE A - 3/8 IN. SIDE B - 1/8 IN. SIDE C - 3/8 IN. SIDE D - 9/16 IN.	FLAW GROWTH ON ALL FOUR SIDES - SEE FIGURE 160	STILL IN TEST WITH 20,670 CYCLES
	HONEYCOMB SPECIMEN FREE OF FLAWS (ZJ197661-501)	NONE	NONE	STILL IN TEST WITH 20,670 CYCLES
	HONEYCOMB SPECIMEN WITH SURFACE DINGS AND CRUSHED CORE (ZJ197661-503)	ONE DING SIDE A WITH CRUSHED CORE - CONFIRMED BY X-RAY	NONE	STILL IN TEST WITH 20,670 CYCLES
	LOW BOND STRENGTH (ZJ197614-513 NO. 3)	SIDE A - VERY LOW BOND STRENGTH PER FOKKER BONDTESTER	NO CHANGE IN THE FLAW CONFIGURATION	THE SPECIMEN FAILED AT THE END HOLE ON SIDE BD AT 18,194 CYCLES. METAL = 19 KSI
	VOID (ZJ197615-501 NO. 1) (BOEING CYCLE) 3000 LB	VOID ON SIDE A CONFIRMED BY C-SCAN AND FOKKER. POSSIBLE VOID SIDE B BY C-SCAN NOT CONFIRMED BY FOKKER	NO NONDESTRUCTIVE INSPECTION	4962 METAL FAILURE SIDE AC 6305 BOND FAILURE SIDE BD BOEING CYCLE 3000-LB LD $\sigma$ METAL = 45 KSI
	VOID AND LOW BOND STRENGTH (ZJ197615-501 NO. 6)	SIDE A - VOID SIDE B - VOID SIDES C AND D - LOW BOND STRENGTH	NO FLAW GROWTH SEE FIGURE 161 FOR FLAW CONFIGURATION	THE SPECIMEN NOW HAS 32,378 AND CYCLING
	VOID (ZJ197615-501 NO. 3) 3000 LB	SIDES A AND B VOIDS PER C-SCAN AND FOKKER	NO NONDESTRUCTIVE INSPECTION	12,039 CYCLES METAL FAILURE SIDE AC 12,279 CYCLES METAL FAILURE SIDE BD $\sigma$ METAL = 45 KSI
	VOIDS AND LOW TO VERY LOW BOND STRENGTH (ZJ197615-515 NO. 3) 3000 LB	SIDE A - 100 PERCENT VLBS SIDE B - 100 PERCENT LBS SIDE C - 100 PERCENT VLBS SIDE D - 15 PERCENT VOID AT BONDLINE EDGE 85 PERCENT VLBS	NO FLAW GROWTH IN THE BONDLINES	METAL FAILURE END BD AT 26,638 $\sigma$ METAL = 19 KSI
	VERY LOW BOND STRENGTH (ZJ197615-517 NO. 2) 3000 LB	FOKKER BONDTESTER INDICATED VERY LOW BOND STRENGTH ON SIDES A AND B	NO CHANGE IN BONDLINE FLAW DURING THE TEST	10,195 METAL FAILURE ON END AC 10,301 METAL FAILURE END BD $\sigma$ METAL = 45 KSI
	LOW BOND STRENGTH (ZJ197615-519 NO. 1) 3000 LB	SIDES A, B, C AND D LOW BOND STRENGTH BY FOKKER BONDTESTER	NO FLAW GROWTH	6480 METAL $\sigma$ METAL = 45 KSI



**TABLE 10**  
**BONDLINE FLAW TEST SUMMARY (Continued)**

	TYPE OF FLAW	FLAW SIZE AT		FAILURE MODE OR COMMENT
		INITIAL INSPECTION	LAST INSPECTION	
FM-73	LOW BOND STRENGTH (ZJ197615-519 NO. 2)	SIDES A, B, C AND D LOW BOND STRENGTH PER FOKKER BOND-TESTER	NO FLAW GROWTH SEE FIGURE 162	27,211 AND STILL CYCLING
	LOW BOND STRENGTH (ZJ197615-521 NO. 1) 3000 LB)	SIDES A, B, C AND D LOW BOND STRENGTH PER FOKKER BOND-TESTER	NO FLAW GROWTH	10,276 METAL FAILURE SIDE AC 12,728 METAL FAILURE SIDE BD $\sigma$ METAL = 45 KSI
	LOW BOND STRENGTH (ZJ197615-521 NO. 2)	SIDES A, B, C AND D LOW BOND STRENGTH PER FOKKER BOND-TESTER	NO FLAW GROWTH	23,889 METAL FAILURE $\sigma$ METAL = 22.5 KSI
	NONE - CONTROL SPECIMEN (ZJ197664-517)	ACCEPTABLE BOND FRAME "TEE" PEEL SPECIMEN	NO FLAW GROWTH	12,684 AND CYCLING
	CONTAMINATION - WIPE BONDING SURFACE WITH A BARE HAND (ZJ197664-521)	FRAME "TEE" PEEL SPECIMEN	NO FLAW GROWTH	12,684 AND CYCLING
	LOW BONDING TEMPERATURE DURING CURE CYCLE (ZJ197664-523)	FRAME "TEE" PEEL SPECIMEN	NO FLAW GROWTH	12,684 AND CYCLING
	SHORT CURE CYCLE AT CURE TEMPERATURE (ZJ197664-525)	FRAME "TEE" PEEL SPECIMEN	NO FLAW GROWTH	12,684 AND CYCLING
	POROSITY (ZJ197664-527)	SIDE A - 80 PERCENT POROUS SIDE B - 70 PERCENT POROUS FRAME "TEE" PEEL SPECIMEN	NO FLAW GROWTH FIGURE 163	12,684 AND CYCLING
	VOID (ZJ197664-529)	0.12-IN. RADIUS VOID AT SIDE B TOO SMALL TO DETECT BY FOKKER FRAME "TEE" SPECIMEN	NO FLAW GROWTH FIGURE 164	12,684 AND CYCLING
	FRACTURED BONDLIN (ZJ197664-531)	CORNER ON BONDLIN ON SIDE B FRACTURED FRAME "TEE" SPECIMEN	NO FLAW GROWTH FIGURE 165	12,684 AND CYCLING
EA9309	VOID (ZJ197664-533)	0.25-IN. SEMICIRCULAR VOID CENTERLINE SIDE B FRAME "TEE" SPECIMEN	NO FLAW GROWTH FIGURE 166	12,684 AND CYCLING
	EXCESSIVE TIME BETWEEN MIXING AND APPLICATION OF ADHESIVE (ZJ197660-1)	SIDES A, B, C AND D SHOW LOW BOND STRENGTH	FLAW GROWTH SIDE A - 60 PERCENT VLBS SIDE B - 10 PERCENT LACK OF BOND FIGURE 167	5873 BOND FAILURE ON SIDE AC 9227 BOND FAILURE ON SIDE BD
	CONTAMINATION - BARE HANDS WIPE OVER BONDING SURFACE BETWEEN ANODIZING AND PRIMING (ZJ197660-501)	ACCEPTABLE BONDS ON ALL FOUR SURFACES	FLAW GROWTH FIGURE 168 FOR DETAILS	8424 BOND FAILURE ON SIDE AC 16,086 BOND FAILURE ON SIDE BD
PL729	FRACTURE BONDLIN (ZJ197660-525)	SIDE A - 1/4-IN. FRACTURE FULL WIDTH SIDE D - 3/16-IN. FRACTURE FULL WIDTH	NO EVIDENCE OF FLAW GROWTH	4012 BOND FAILURE ON SIDE AC 4444 BOND FAILURE ON SIDE BD
	POROSITY ALONG EACH OF FOUR EDGES BY WIRE INSERTION (ZJ197660-513)	NO POROSITY DEVELOPED IN THE SPECIMEN	NO FLAW DEVELOPMENT OR GROWTH	20,575 AND CYCLING
	FRACTURED BONDLIN (ZJ197660-523)	SIDES A AND B SHOWED FRACTURE BONDLIN C-SCAN	FLAW GROWTH IN ALL FOUR BONDLIN FIGURE 169	BOND AND METAL FAILURE END B AT 11,545
	LOW BOND STRENGTH (ZJ197615-553 NO. 2)	SIDES A, B, C AND D LOW BOND STRENGTH	NO EVIDENCE OF FLAW GROWTH	17,546 METAL FAILURE END BD

**TABLE 10**  
**BONDLINE FLAW TEST SUMMARY (Concluded)**

	TYPE OF FLAW	FLAW SIZE AT		FAILURE MODE OR COMMENT
		INITIAL INSPECTION	LAST INSPECTION	
PL729	VOID (ZJ197660-517)	SEMICIRCULAR VOID 0.25-IN. RADIUS SIDE A - INSIDE SIDE B - EXPOSED EDGE	NO GROWTH	20,575 AND CYCLING
AF55	POROSITY BY FOREIGN OBJECT INSERTION (ZJ197660-511)	POROSITY ON ALL FOUR BONDLINES FIGURE 170	NO FLAW GROWTH	18,079 BOND FAILURE. FAILED SURFACE SHOWS EVIDENCE OF POROSITY BUT NO GROWTH
	VERY LOW BOND STRENGTH (ZJ197615-535 NO. 2)	VERY LOW BOND STRENGTH ON ALL FOUR BONDED SURFACES	NO FLAW GROWTH	28,867 AND CYCLING
	LOW BOND STRENGTH (ZJ197615-555 NO. 2)	ALL FOUR SIDES LOW BOND STRENGTH SIDE B - VERY LOW BOND STRENGTH APPROXIMATELY 1/2 IN. ALONG EXPOSED EDGE	NO FLAW GROWTH	17,187 BOND FAILURE ON SIDE BD
M1133	VOID (ZJ197615-511 NO. 1)	SIDE B - VOID FULL WIDTH C-SCAN NOT CONFIRMED BY FOKKER SIDE C - VOID FULL WIDTH C-SCAN AND FOKKER	NO EVIDENCE OF FLAW GROWTH	13,361 COHESIVE FAILURE OF BONDS B AND D
	VERY LOW BOND STRENGTH (ZJ197615-539 NO. 2)	SIDE C - VERY LOW BOND STRENGTH EXPOSED CORNER APPROXIMATELY 25 PERCENT BOND AREA	NO EVIDENCE OF FLAW GROWTH	28,867 AND CYCLING
	LOW BOND STRENGTH (ZJ197615-559 NO. 1)	SIDES A, B, C AND D LOW BOND STRENGTH	NO FLAW GROWTH	28,867 AND CYCLING
	LOW BOND STRENGTH (ZJ197615-563 NO. 1)	LOW BOND STRENGTH ALL FOUR SIDES	NO FLAW GROWTH	15,929 BOND FAILURE ON SIDE AC 20,091 BOND FAILURE ON SIDE BD
FM-73	VERY LOW BOND STRENGTH	VERY LOW BOND STRENGTH SIDE A - 80 PERCENT SURFACE SIDE B - 100 PERCENT SURFACE SIDE C - 100 PERCENT SURFACE SIDE D - 85 PERCENT SURFACE	FLAW GROWTH OBSERVED IN INSPECTIONS 1, 2 AND 3 FIGURE 171	TEST DISCONTINUED AT 19,017 CYCLES. SPECIMEN SPLIT LONGITUDINALLY IN HALF: HALF FOR STATIC TEST, HALF TO WPAFB
M1133	LOW BOND STRENGTH (ZJ197615-565 NO. 1)	LOW BOND STRENGTH ALL FOUR SIDES	NO FLAW GROWTH	30,143 AND CYCLING

The cycles to failure for the metal are well below what would be expected under ambient condition and a cycling rate of 30 Hz. It was therefore inferred that these early failures result from the adverse environment and slow cycling. Table 10 details all the specimens in the effects of defects program. There were 42 specimens subjected to 4,012 to 30,143 cycles. A summary of the specimens that have experienced either flaw growth or bondline failure is given in Table 12. In the case of FM73, only one bondline failure was experienced, and that was caused by the specimen being subjected to a cyclic load of 3000 pounds which is twice the PABST load intensity. Under normal PABST loads, two specimens experienced flaw growth, one of which is still under test with 20,670 cycles. The other specimen was removed from the test at 19,017 cycles without failure. Figures 159 through 171 show the flaws that are found in the specimens from start of test to date.

Two of the three room temperature cure adhesive EA9309 specimens tested failed in the bondline at relatively low number of cycles. The other three adhesive systems, PL729, AF55, and M1133, had failures in the bondlines under normal PABST loads (1500 pounds). The FM73 adhesive system clearly demonstrated its superiority in its resistance to flaw growth and failure when compared to the other adhesive systems tested. Further, many of the specimens exceeded 19,000 cycles, which represents one AMST flight lifetime.

Some analysis has been done on bond flaws. Figure 172 shows the results of an edge flaw in a splice. The exposed edge of the adhesive still has the same stress level as before and only the central trough is smaller. Figure 173 shows the effect of central disbond, and as would be expected, this has no effect on stress distribution. Figure 174 shows the effect of a flaw lying between the above two. This flaw can increase exposed bond stress level slightly. The type of double-lap splice shown with the 1.50-inch overlap is like that used on the PABST full-scale demonstration component.

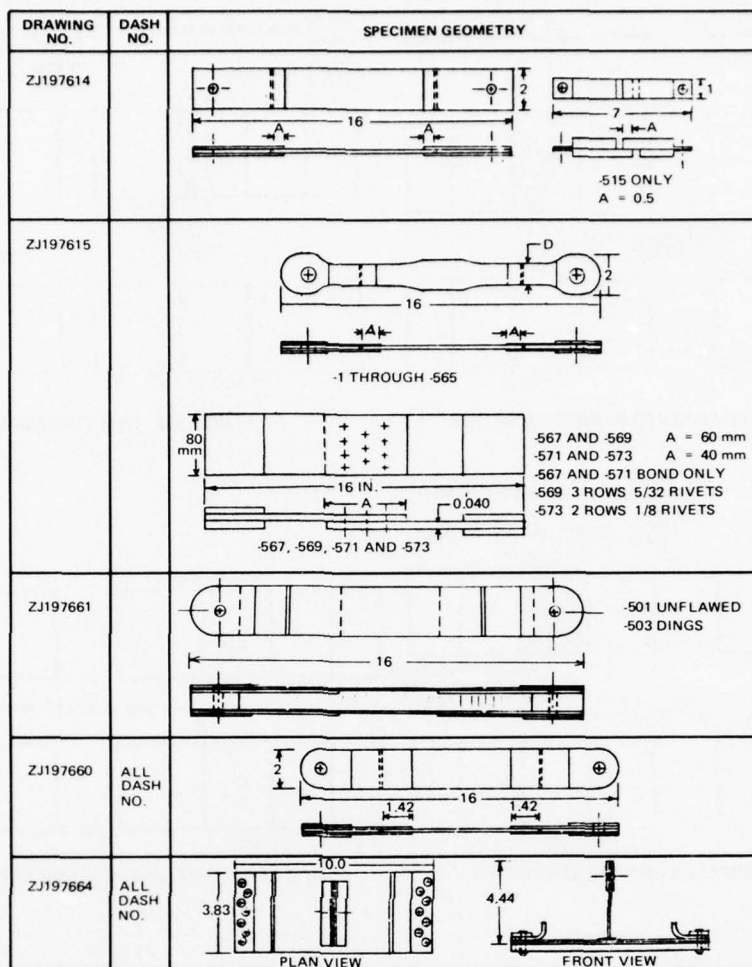


FIGURE 158. EFFECTS OF DEFECTS SPECIMENS

TABLE 11  
METAL FAILURES, 3000-LB LOAD

SPECIMEN	METAL STRESS (KSI)	CYCLES TO FAILURE	AVERAGE CYCLES TO FAILURE
ZJ197614-513 NO. 3	19	18,194	20,793
ZJ197615-515 NO. 3	19	26,638	
ZJ197615-553 NO. 2	19	17,546	
ZJ197615-521 NO. 2	22.5	23,889	23,889
ZJ197615-501 NO. 1	45	4,962	
ZJ197615-501 NO. 3	45	12,039 12,279	
ZJ197615-517 NO. 2	45	10,195 10,301	9,507
ZJ197615-519 NO. 1	45	6,480	
ZJ197615-521 NO. 1	45	10,276 12,728	

TABLE 12  
EFFECT OF DEFECTS FLAW GROWTH AND FAILURES

ADHESIVE	TOTAL NO. OF SPECIMENS	TYPE OF SPECIMEN	SPECIMEN WITH FLAW GROWTH		FAILED SPECIMENS		CYCLES AT FAILURE
			NO.	FLAW TYPE	NO.	FLAW TYPE	
FM 73	19	SPLICE	1	FRACTURED BONDLINE	1	VOID	6,305
			1	VERY LOW BOND STRENGTH	0	3000-LB LOAD BOEING CYCLE	
EAS909	3	SPLICE	0		0		4,012 4,444 8,424 16,086
			1	EXCESSIVE TIME BETWEEN MIXING AND APPLICATION	1	FRACTURED BONDLINE	
			1	CONTAMINATION - BARE HAND WIPE BONDING SURFACE	1	CONTAMINATION - BARE HAND WIPE BONDING SURFACE	
			1	EXCESSIVE TIME BETWEEN MIXING AND APPLICATION	1	EXCESSIVE TIME BETWEEN MIXING AND APPLICATION	
PL729	4	SPLICE	1	FRACTURED BONDLINE	1	FRACTURED BONDLINE	11,545
AF55	3	SPLICE	0		1	POROSITY	18,079
			0		1	LOW BOND STRENGTH	17,187
M1133	5	SPLICE	0		1	VOID	13,361
			0		1	LOW BOND STRENGTH	15,929 20,091



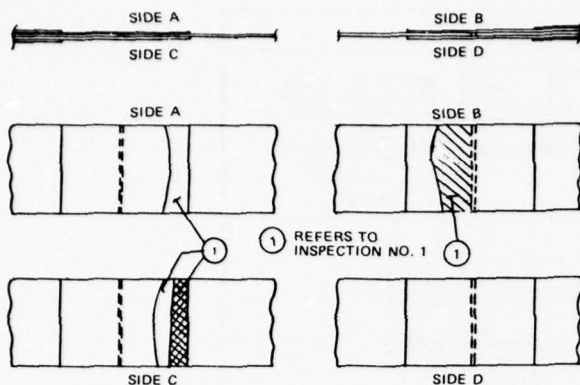


FIGURE 159. POROSITY ACHIEVED BY FOREIGN OBJECT

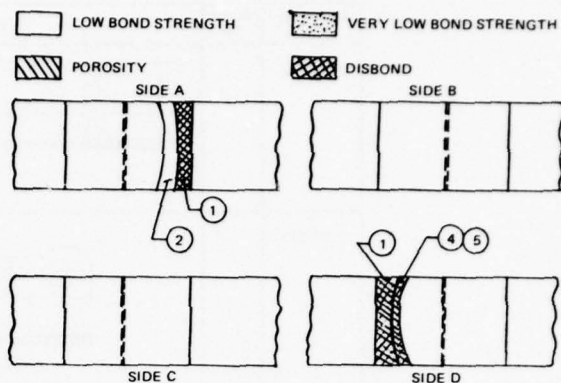


FIGURE 160. FRACTURED BONDLINE

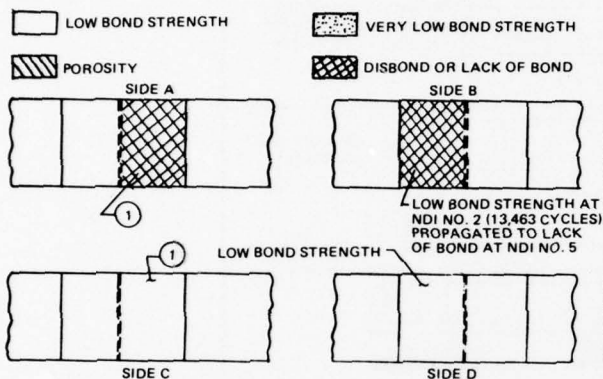


FIGURE 161. VOID AND LOW BOND STRENGTH

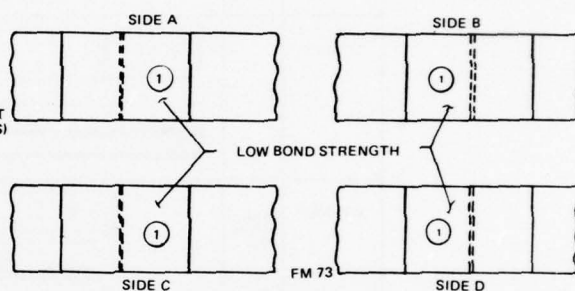


FIGURE 162. SPECIMEN WITH LOW BOND STRENGTH

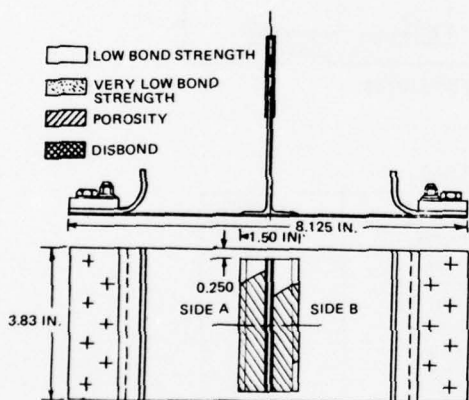


FIGURE 163. FRAME "T" SPECIMEN WITH POROSITY

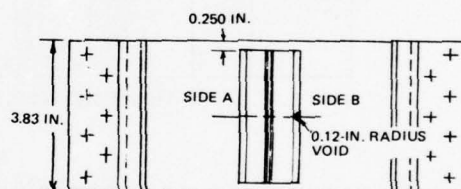


FIGURE 164. FRAME "T" SPECIMEN WITH 0.12-IN.-RADIUS VOID

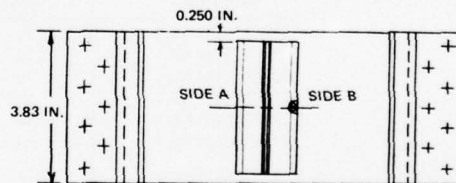


FIGURE 166. 0.25-INCH-RADIUS VOID

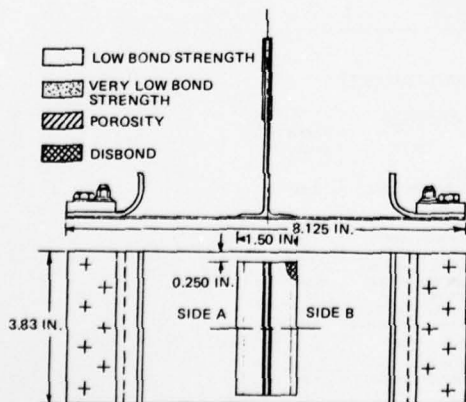


FIGURE 165. CORNER FRACTURED BONDLINE

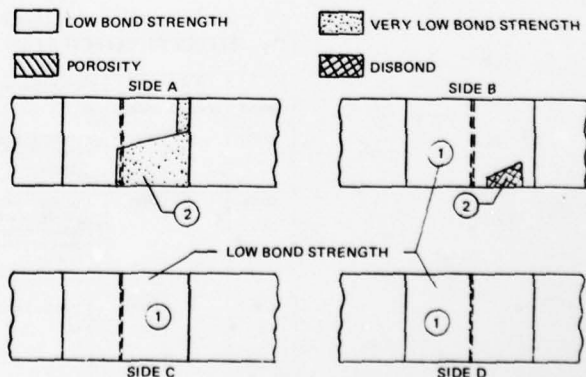


FIGURE 167. LOW BOND STRENGTH ON INITIAL INSPECTION

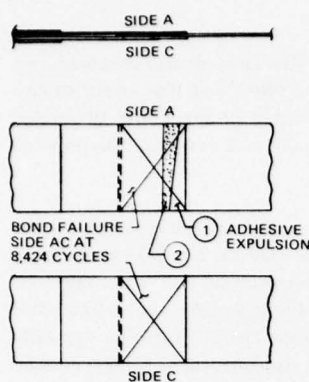


FIGURE 168. CONTAMINATED SPECIMEN (BARE-HAND)

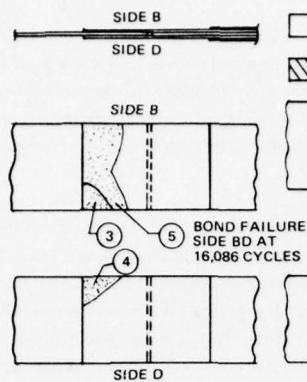


FIGURE 169. FRACTURED BONDLINE SPECIMEN

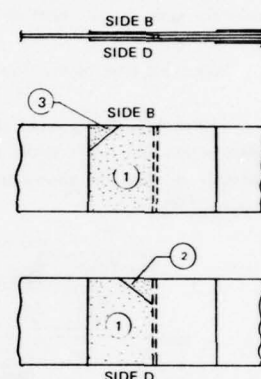
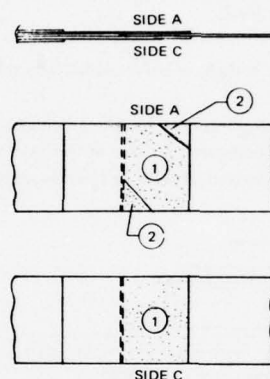
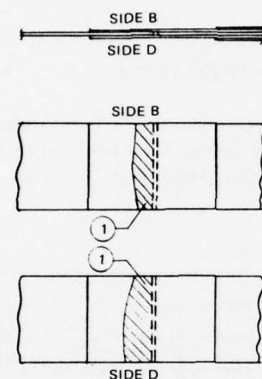
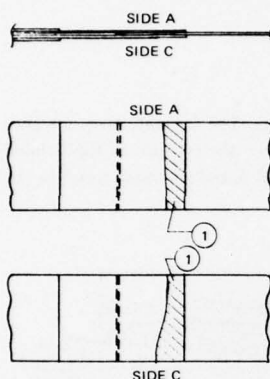
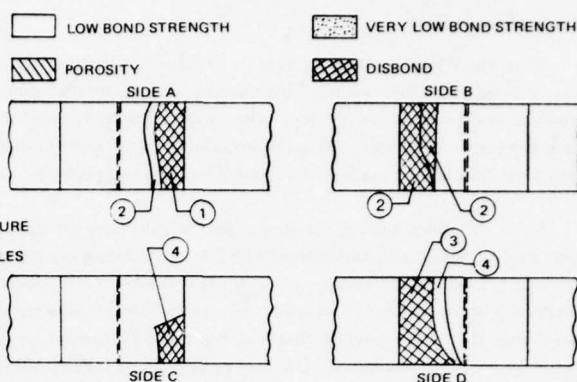


FIGURE 171. VERY LOW BOND STRENGTH



FIGURE 170. POROSITY ACHIEVED BY FOREIGN OBJECT

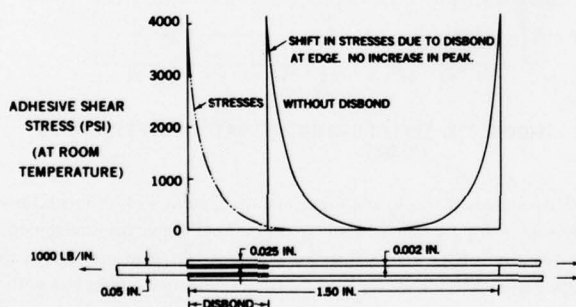


FIGURE 172. ADHESIVE SHEAR STRESSES IN EDGE FLAWED BONDED JOINTS

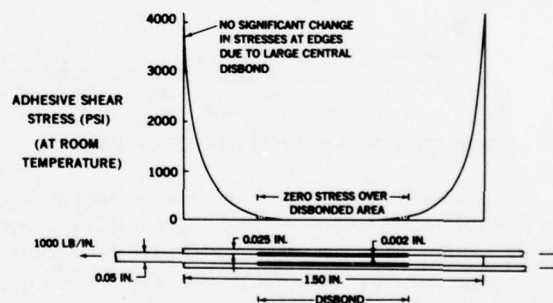


FIGURE 173. ADHESIVE SHEAR STRESSES IN CENTER FLAWED BONDED JOINTS

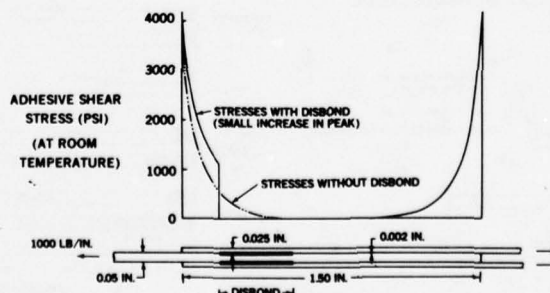


FIGURE 174. ADHESIVE SHEAR STRESSES IN FLAWED BONDED JOINTS

### Effects of Cycle Rate

When the PABST program started in 1975, one of the first questions asked was how good is an adhesive joint under cyclic loads. Six thick-adherend (0.5 inch with 0.5-inch overlap) lap-shear specimens were bonded and then placed in a 140°F and 100-percent relative humidity environment for 69 days. They were then cycle-tested at 30 Hz at room temperature. No failure occurred after  $10^6$  cycles, when the test was stopped. The peak stress level was 30 percent of static strength tested at a stress ratio of +0.2 and -0.2. This provided confidence that fatigue loading of a bonded joint was no problem.

Some data from Boeing obtained a few months later are shown in Figure 175. The 30-Hz (1800-cpm) data given in the table in the figure are the same as in the initial PABST test. The alarming thing was the greatly reduced cycle life when the test had a cycle rate of one hour loaded and 15 minutes at no load. This slow-cycled specimen was exposed to the same environment and loads as the fast-cycle specimen, but the endurance was only 797 cycles. These results are all averages for five specimens. The loading cycle is also realistic when considering the YC-15 aircraft that was the PABST program baseline. The fuselage under study in the PABST program is cyclically loaded by cabin pressurization. The average flight time for the AMST is one hour. For one lifetime the structure will see 19,000 pressure cycles. Therefore, the 797 cycles to which the test specimen was subjected at the one-hour cycle rate is 20 times too short as a minimum, and should probably be 50 times greater. The table also shows that specimens loaded with a constant load will not fail before 3000 hours under the same environment and load level.

Since that time, many slow-cycle tests have been conducted on the PABST program.

Figure 176 shows shear stress-strain curves for thick-adherend specimens run at three loading rates. The fast rate gives a higher failing stress and lower strain when compared to the slower-rate test specimens. It is important to know the end use of the bonded assembly so that test allowables are arrived at with suitable loading rates. Althof made a similar test and noted the same trend in the answers.<sup>(7)</sup>

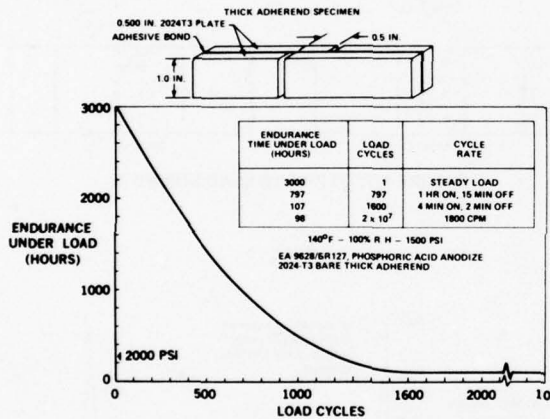


FIGURE 175. EFFECT OF CYCLE RATE ON ENDURANCE

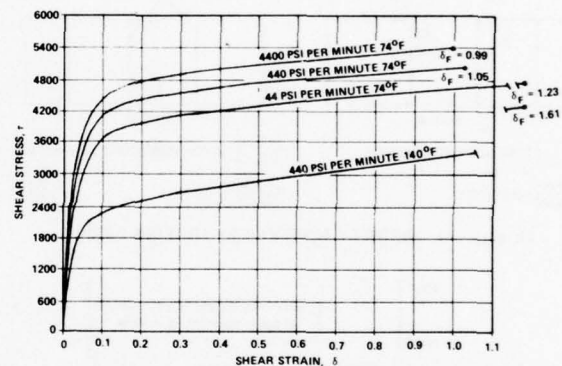


FIGURE 176. EFFECT OF LOADING RATE ON STRESS-STRAIN VALUES

In the course of evaluating different adhesives used in the PABST program, it was found that the normal static environmental tests did not discriminate between the various types at all. The slow-cycle tests using the RAAB specimen in a hot, wet environment sorted out the best or most durable adhesive. Figure 177 shows test results for a set of specimens used for examining differences between the woven versus mat carrier adhesive, all bonded on a primer EC-3950. Figure 178 shows the same series of slow-cycle tests but with a different primer, BR-127, being used.

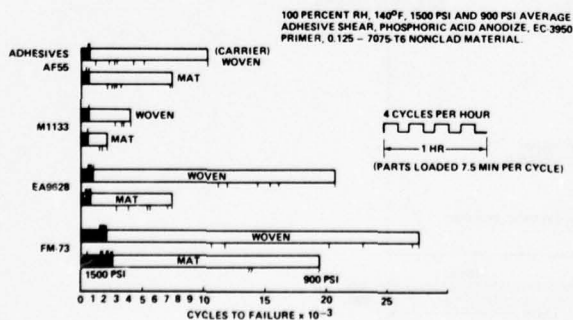


FIGURE 177. RAAB SPECIMENS, FOUR ADHESIVES, EC-3950 PRIMER

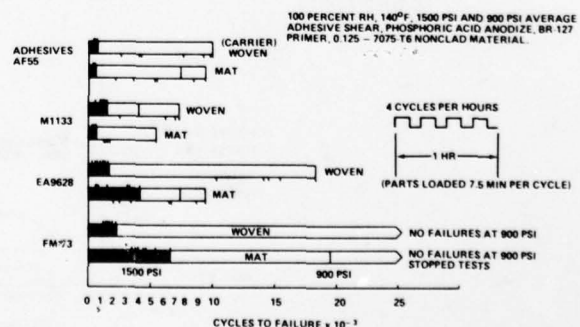


FIGURE 178. RAAB SPECIMENS, FOUR ADHESIVES, BR-127 PRIMER

Another interesting effect of slow-cycling is shown in Figure 179. A set of single-lap shear specimens was tested. The baseline specimens were tested as received and gave the highest shear value. The fast-cycled specimens had reduced static strength and the slow-cycle test parts (four cycles per hour) had the least static strength.



RAAB specimens with cycling environment and cycling load are also being tested in the PABST program. The specimen is hot and wet (140°F, 100-percent relative humidity) without a load and while cooling down, at 40°F the load representing cabin pressure is applied and held as the temperature is reduced to -70°F. Figure 180 shows the results of these tests for four different adhesives. A parallel test was run where the environment had the same cycle as the preceding test but the specimen load was constant at 30 percent of the ultimate strength at 140°F. The results are shown in Figure 181. The tension tee specimens have also been tested with the cycling environment and the cycling load. These results are shown in Figure 182. Two sets of comparative tests were conducted to investigate the cyclic life of a 250°F cure versus a 350°F cure epoxy. Figure 183 shows the comparative life of the specimens tested in the as-received condition while Figure 184 shows the effect of preconditioning for 15 days at 140°F and 92- to 100-percent relative humidity prior to cycling. The cycle life of PL-729 adhesive was greatly affected by the preconditioning.

#### SINGLE-STRAP SPECIMENS 090/080

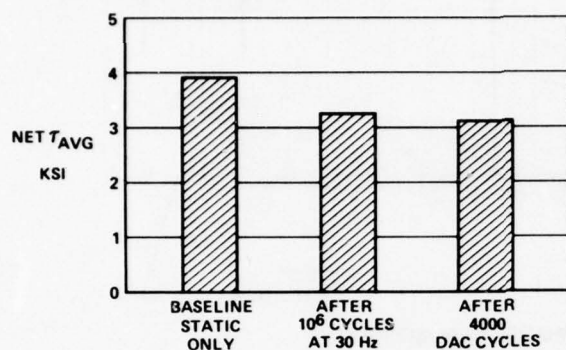


FIGURE 179. EFFECT OF CYCLE RATE ON RESIDUAL STRENGTH

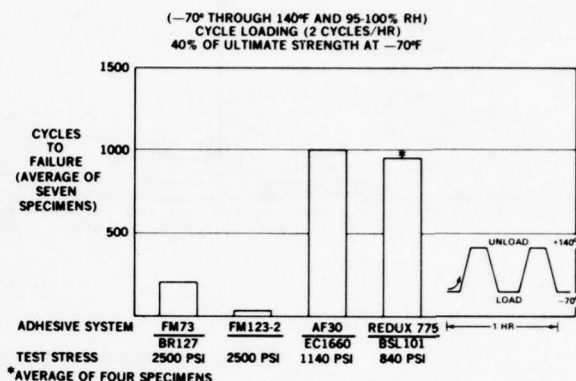


FIGURE 180. RAAB SPECIMENS, CYCLE ENVIRONMENT AND LOAD

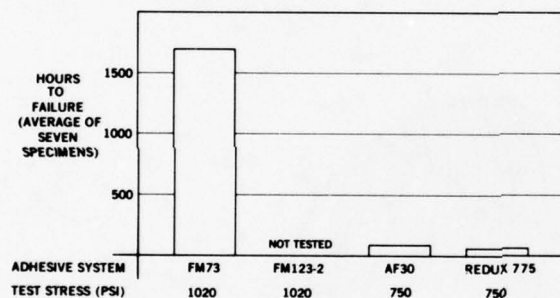


FIGURE 181. RAAB SPECIMENS, CYCLE ENVIRONMENT, CONSTANT LOAD

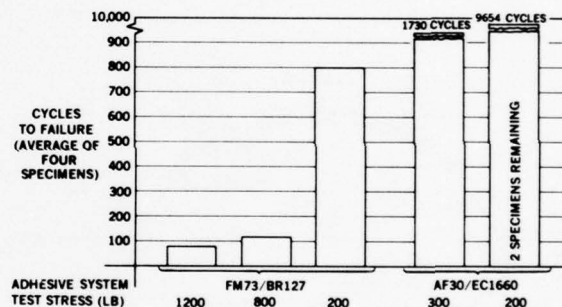


FIGURE 182. TENSION TEE, CYCLE ENVIRONMENT AND LOAD

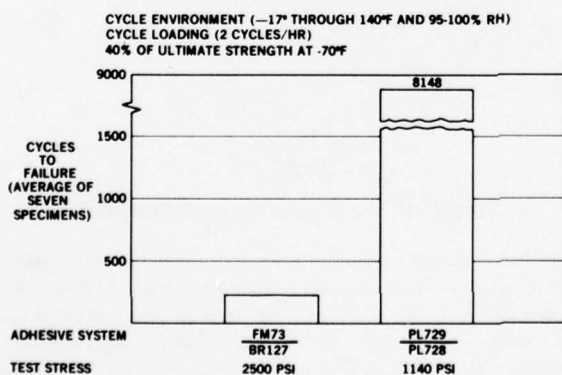


FIGURE 183. RAAB SPECIMENS, 250°F VERSUS 350°F CURE ADHESIVE

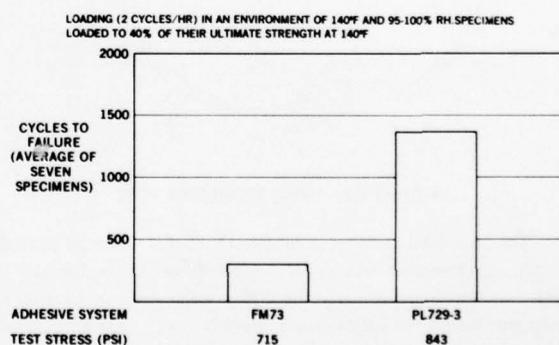


FIGURE 184. RAAB SPECIMENS, 250°F VERSUS 350°F CURE ADHESIVE, PRECONDITIONED

#### THE FULL-SCALE TEST PROGRAM

##### The Test Article Design

The main structural component that was intended to validate adhesive bonding for primary structure was a large, full-size section of the AMST fuselage. As noted previously, this was a representation of the YC-15 airplane fuselage. The final section built was 42 feet long and extended from the forward part of the cargo compartment to a station 24 inches aft of the main fuselage frame which supports the landing gear and the wing rear spar. Figure 185 is a side view of this test component and Figure 186 is a cross section. Figure 187 shows the structural arrangements.

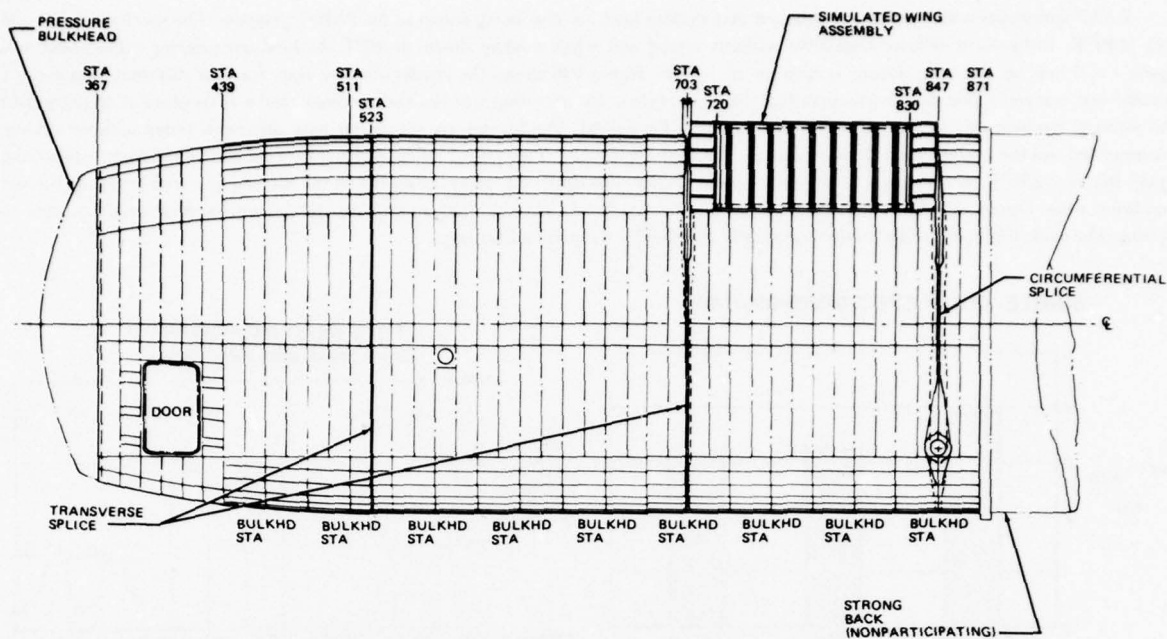


FIGURE 185. FULL-SCALE DEMONSTRATION COMPONENT (FSDC)

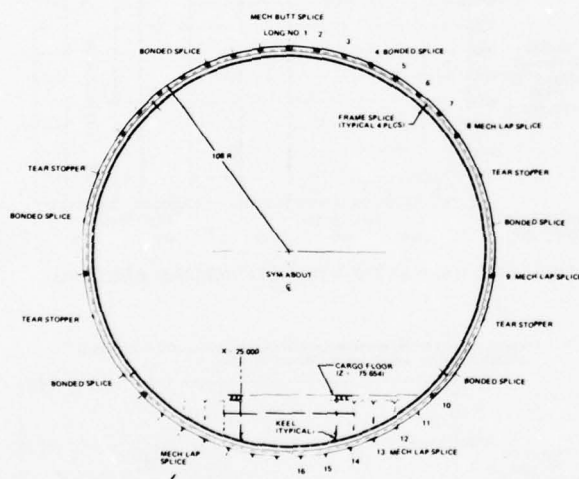


FIGURE 186. CROSS SECTION OF FSDC

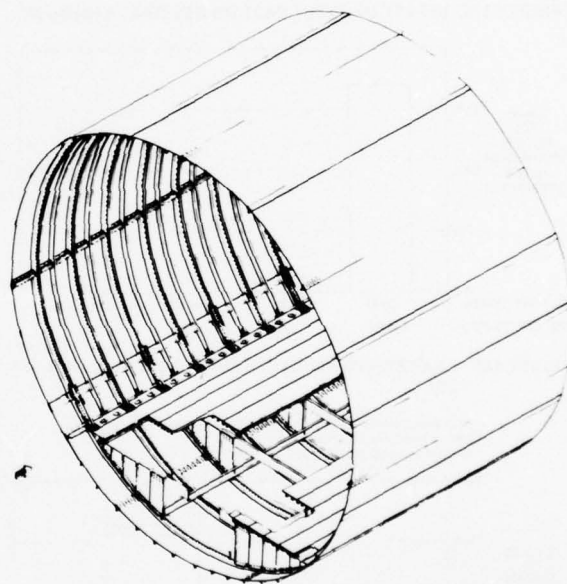


FIGURE 187. FSDC STRUCTURAL ARRANGEMENT

The structural members and assemblies that make up the full-scale demonstration component were designed to the static, fatigue, and damage tolerance criteria established during the preliminary design phase. Since minimum cost was a PABST goal, the frames and longerons were sized to carry the design loads with the least number of different extrusion shapes. Mechanical fastening was kept to a minimum within the limitations of manufacturing capability and the availability of sheet stock. The mechanical splices were designed for four lives of fatigue and met the damage tolerance criteria of MIL-A-83444. The strength criteria and the ease of assembly determined the type of splice selected. Intercostals were added to stabilize all frames and to provide axial load capability to the nose section.

**Skin Splices** — The full-scale demonstration component has both mechanical and bonded skin splices in the longitudinal and circumferential directions. The splices were designed to meet the static ultimate loads and the fatigue and damage tolerance criteria described elsewhere in this paper.

All fasteners that penetrated an adhesive bondline on an exterior skin were installed with wet sealant and the faying surfaces sealed with MIL-S-81733 sealant. This procedure ensured a pressure seal and protected the joint from moisture intrusion.

The bonded panel assemblies were sized to minimize the number of mechanical splices. The primary constraint was the maximum circumferential panel assembly dimension that could be bonded in the PABST autoclave. In addition to the facility limitations, the consideration of manufacturing "breaks" for a production fuselage was included.

As a cost reduction measure, the longitudinal skin splices were all single-overlap designs except for the top centerline splice at longeron 1 that was a symmetrical double-lap butt configuration. The butt splice selection was based primarily on reducing cost by providing a panel assembly that was symmetrical about the full-scale demonstration component centerline.

Designs were evaluated to determine the most efficient longitudinal mechanical splice configuration. The factors considered were cost, structural efficiency, inspectability, and ease of assembly. All of the mechanical splices in the full-scale demonstration component had a combination of 0.188-inch-diameter mechanical fasteners and MIL-S-81733 Type IV-12 (PR 1431G) sealant on the faying surface of the skins to prevent moisture entrapment and corrosion as well as for pressure sealing.

For the longitudinal splices between bonded subassemblies, possible configurations included (1) conventional symmetrical multirow double-strap mechanical butt splices, (2) single-lap purely mechanical splices, (3) single-lap splices with fasteners and hot-bonded doublers for reinforcing the most highly loaded rivet holes, and (4) variations of these cases. These options were reduced to a single-lap unsymmetrical mechanical splice and a symmetrical double-strap splice for the full-scale demonstration component.

Typical single-lap mechanical splice designs for the full-scale demonstration component are shown in Figure 188. One key feature of this configuration was the two full rows of huck bolts in the middle of the overlap passing through (1) the outer bonded doubler, (2) the outer skin, (3) the inner skin, and (4) the hot-bonded inner longeron. The outer doubler never extended to the end of the skin. The outer riveted rows contained only half as many fasteners as the inner bolted rows to maximize the net section and to more equally share the fastener shear loads, which would otherwise concentrate in the outer row if it were full. One row of fasteners was countersunk into the outer skin where the net section stress was lowest. The fastener load was thus shared more evenly. Reinforcing the skin at this point would, of course, attract more load to that last row of fasteners. The end hole through the more highly stressed inner skin was not countersunk. Countersinking the outer row of fasteners on the other end of the lap would represent the weakest loadpath since the highest bearing stresses combine with the highest bending stresses in this location.

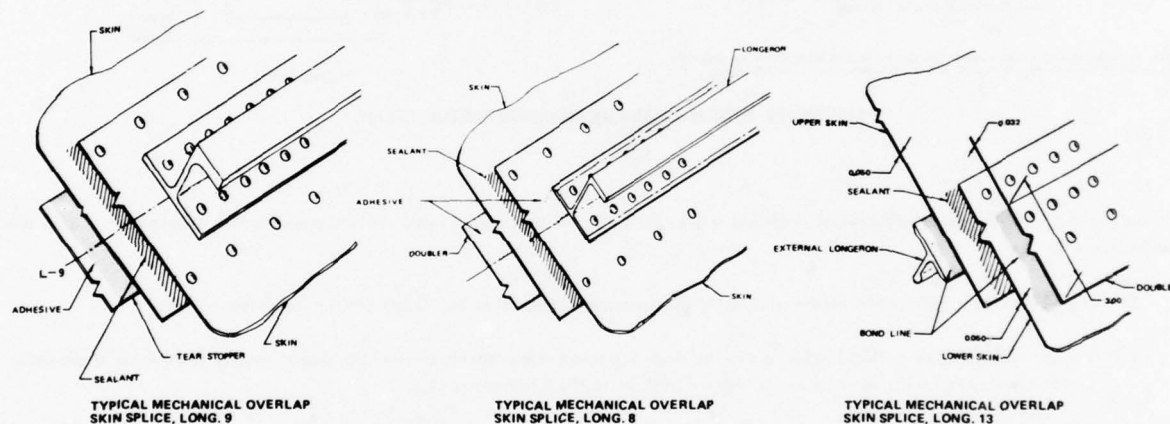


FIGURE 188. FSDC MECHANICAL LAP SPLICES

The basic single-lap mechanical splice was therefore improved by a hot-bonded external strap to eliminate countersinking and associated high bearing stresses at the highest net section stress. This hot-bonded strap also served to reduce the stress level in the outer skin. The inner skin was not correspondingly reinforced because the fasteners were not countersunk on that side. The hot-bonded doublers were either on the inside or the outside of the splice, so the skins made direct contact with each other to minimize loadpath eccentricity. The methods of minimizing the induced bending stresses due to loadpath eccentricity are discussed in the section on adhesive bonded joint analyses. Usually, the hot-bonded longeron was located at the middle of the splice, if on the inner skin. Sometimes, as with the external longeron, it was displaced sideways to reinforce the first row of fasteners at the highest net section stress. This could have been done on the inside also, for a modest increase in life span. However, the life of the current joint was more than adequate.

The double-strap butt splice is shown in Figure 189. A 0.040- by 4.00-inch doubler of 2024-T3 was installed on the inside surface of the upper skin where the two full rows of attachments were located in order to increase the skin bearing allowable. The doubler also acted as a reinforcing member for the skin where the shear tees stopped short of the longeron and created stress risers locally in the skin. The splice consisted of four full rows of steel huck bolts and two half-rows of rivets with the manufactured head on the inboard side of the skins and an 82-degree countersink on the exterior surface of the skins.

For an efficient double-strap joint, the protruding head fasteners in each strap should have half the extensional stiffness of the skins being joined. However, this was incompatible with the need to avoid knife-edging the fastener holes in the outer strap for flush fasteners. Therefore, the load between the fastener rows was shared unequally by thickening the outer strap for countersinking.

The circumferential skin splices were designed to provide a flush exterior for aerodynamic considerations, as shown in Figure 190. An 0.016-inch-thick 2024-T3 doubler was bonded to the inside of the 0.050-inch-thick skin to permit flush fasteners above the cargo floor. Two full rows of lock bolts on each side of the butt splice passed through an 0.071-inch-thick splice plate, an 0.032-inch-thick splice plate, and the outer skin. The inner row of lock bolts also attaches the circumferential frame and provides additional transition of



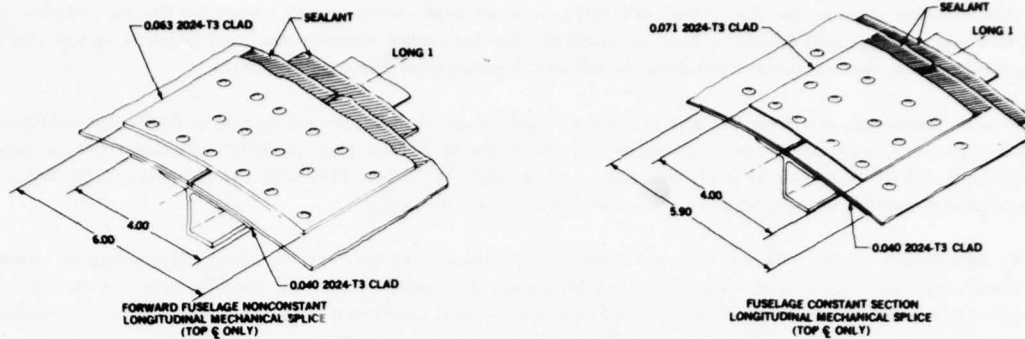


FIGURE 189. FSDC MECHANICAL BUTT SPLICES

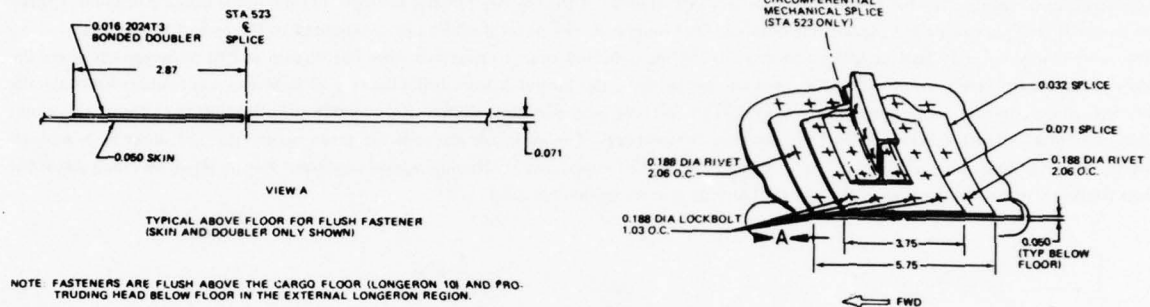


FIGURE 190. FSDC MECHANICAL CIRCUMFERENTIAL SPLICE

the butt splice load. Like the longitudinal single-lap splice, the outer riveted row of fasteners contains only half as many rivets as in the inner rows.

The single-lap splice was found to be superior to the symmetrical double-strap butt splice for the following reasons:

1. For the static load case, the attachments in the single-lap splice were capable of carrying approximately 3500 lb/in. while those in the double-strap splice were good for only 1800 lb/in. in the 0.050-gauge skin.
2. For the fatigue loads, a single-lap test specimen, representative of a current Douglas commercial airplane, lasted 500,000 cycles at 14,000 psi skin stress.
3. Only half as many fasteners were needed since the connection was direct instead of through intermediate members.
4. The single-lap splice was much easier to assemble and did not need as many straps.
5. The single overlap eliminated the need for trimming on assembly which was required by the butting of the skins in the double-strap splice. This resulted in the removal of the protective anodize and primer on the skins in the double-strap configuration.
6. The single-lap splice permitted easier countersinking of the flush fasteners.
7. The single-lap splice was easier to inspect than the double-strap splice.

The only disadvantage of the single-lap splice was the loadpath eccentricity. A generous overlap distance of 4.25 inches (85 times the skin thickness being joined) was used for the 0.050-inch-thick skin to minimize the problem. Consequently, the single-overlap splice was slightly heavier than a double strap joint of equivalent life.

In summary, the single-lap splice employed at the circumferential manufacturing break of the PABST full-scale demonstration component was less expensive than the conventional symmetrical double-strap butt splice with two rows and two half-rows of fasteners instead of four and four half-rows. It was also more resistant to corrosion since all faying surfaces were sealed with hot bond or PR1431G sealant. No anodized or primed areas were trimmed in assembly. In addition, this design had a more than adequate life.

A conventional symmetrical double-strap butt splice was used at the top center of the fuselage to make the design symmetric. There was no need for breaking the protective BR127 primer for this particular splice by trimming in assembly since the tolerances could be absorbed at the adjacent single-lap splices in the full-scale demonstration component.

The PABST design employed one or more bonded splices in each subassembly, the number and location depending on the availability of the skin stock. As stated previously, the skin was broken up into the minimum number of segments compatible with the size of the autoclave.

The bonded splices included double-strap longitudinal butt splices (inner and outer straps) and flush single-strap circumferential butt splices with laminated inner straps only (see Figure 191). The designs were based on both elastic-plastic analysis and on test data.

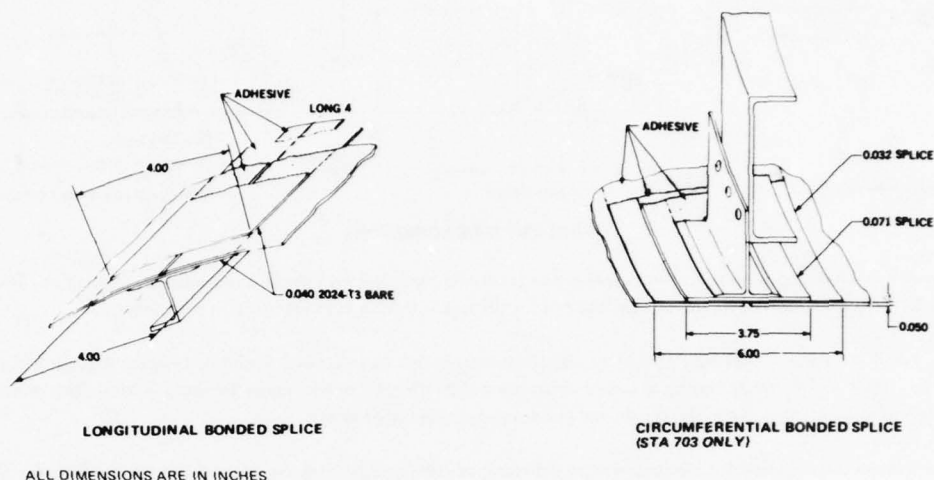


FIGURE 191. FSDC BONDED BUTT SPLICES

To obtain maximum bond strength of the double-strap butt splice, the inner and outer straps should be half the skin thickness of the panels being joined. The mechanical testing of such splices in the PABST program confirmed there would not be any bond failures for environmentally resistant adhesives; e.g., FM-73 and Redux 775. However, the splice strap failed consistently by metal fatigue, although the skin and strap membrane stresses were nominally the same. To improve splice efficiency for the skin gauges of interest (i.e., less than 0.1 inch thick) splice straps were thickened by one gauge above the ideal half-skin-thickness value. The overlap was designed to provide sufficient plastic zones in the adhesive at the overlap ends to utilize the full metal strength to transfer the load. The middle elastic trough inherent in the adhesive bonded joint was designed to be long enough to ensure that this middle section of the adhesive would resist creep by remaining unloaded. The total overlap distance was then set as the sum of the two plastic end zones and the elastic trough in the middle.

The analysis capability for a typical bonded circumferential splice is not as comprehensive as for the longitudinal splices due to the nonlinearities induced by loadpath eccentricity. However, the available analyses satisfactorily predicted the bending stresses in the strap where the skins butt together and in the skins where the splice ends. The associated adhesive peel stresses at the same locations were also obtained. The analyses showed that these splices were very sensitive to the length-to-thickness ( $l/t$ ) ratio. A spliced panel was tested having the same  $l/t$  ratio of 33 to 1 as for an equivalent mechanical splice. The test confirmed the high induced bending stresses predicted by analysis. The high stress was the result of the splice being forced to bend sharply where the skins were butted together. It should be noted that in an equivalent mechanical splice, the splice can deflect smoothly over the gap between the inner row of fasteners, thus reducing the bending.

The test panel sustained the loads for the required life, but the failure was catastrophic and without warning. The splice plate fractured where the skins butted together and the two longerons disbonded. Failure initiated at an 0.4-inch-long fatigue crack on the visible side of the splice and at an 0.7-inch crack on the opposite side under the adhesive. As a result of this test, the PABST  $l/t$  ratio was increased to 50 to 1 in order to reduce the bending stresses. In addition, the splice plate was laminated instead of being tapered from thicker stock. Aerodynamic drag considerations precluded use of the stronger double-strap joint with a transverse external strap. The basic problem with a flush joint is that increased reinforcement also causes greater loadpath eccentricity.

Coupon testing during the PABST development phase showed that adhesive bonds fail progressively if the attached metal is maintained at or in excess of the yield stress. It should be noted that this is a sustained load problem. The same joint could withstand loads up to the metal's ultimate strength if the load is applied rapidly. This phenomenon must be accounted for in the design of bonded splices for production aircraft by using the metal yield strength as the design allowable strength.

**Longerons** — Two basic longeron cross sections were used for the full-scale demonstration component. The internal longeron shape is a J-section and the external longeron shape is a bulb tee.

The J-section was selected in preference to the Z-section, which is more efficient in compression, since it was better suited for the bonding process adopted for the PABST program. The bonding pressure applied to the outstanding flange of the J-section produces a more uniform bonding surface pressure when the flange against the skin is symmetrical with respect to the upstanding web. See Figure 192 for the detailed cross-sectional shape. In addition, the symmetrical constant-thickness flange with a chamfered edge provides the necessary flexibility at the edge to minimize peel action while providing the right-angle intersection of the upstanding leg and flange.

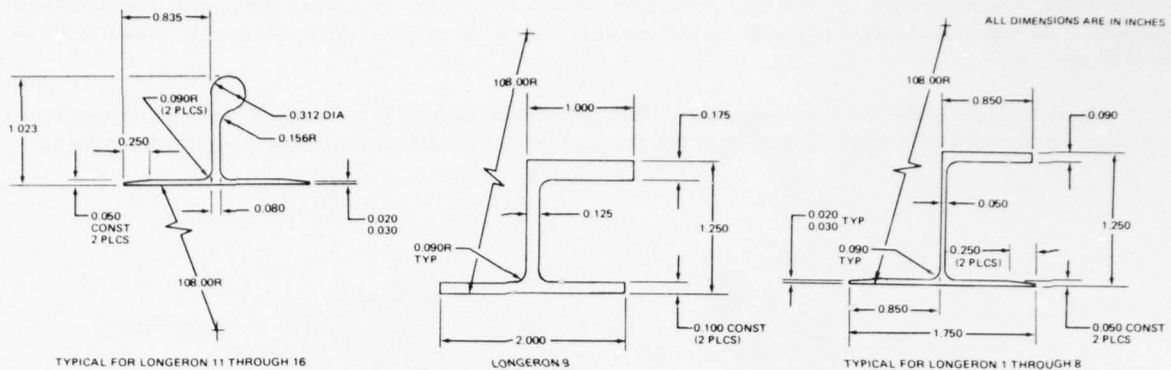


FIGURE 192. FSDC LONGERONS

for the mechanical splice of the longeron. The constant thickness was preferred for ease of nondestructive inspection. The height of the longeron was selected on the basis of the minimum required for the splice and for adequate section properties.

The bulb T-section was selected over the other candidate shapes for the external longeron because it possessed more desirable features than the other shapes while having a compression allowable strength nearly equal to the J-section. The cross sections were evaluated for ease of manufacture, assembly, repair, inspection, and simplicity of design.

**Frames** — Frames are required for circumferential stiffening of the fuselage shell. Spacing of the standard frames for the PABST full-scale demonstration component is 24 inches. This was the spacing used for the baseline fuselage design. It did not appear possible to obtain a single optimum frame spacing for both the wide-spaced and the close-spaced longeron regions. The intermediate frames on the side panels are located midway between the standard frames; i.e., 12 inches.

The typical frame cross section for the full-scale demonstration component, shown in Figure 193, was tailored to provide an acceptable structural section at minimum cost. The preliminary loads which were available at the beginning of the detail design phase indicated that an overall frame height (skin inner surface to inner cap of the frame) could be 4.95 inches. However, the use of a new sheet-metal frame cross section would have meant new stretch form dies with attendant high tooling costs and delays. The frame selected for the full-scale demonstration component measures 5.78 inches in overall height. This dimension was chosen so that existing tooling used to stretch-form sheet aluminum frame details for the YC-15 fuselage could be utilized.

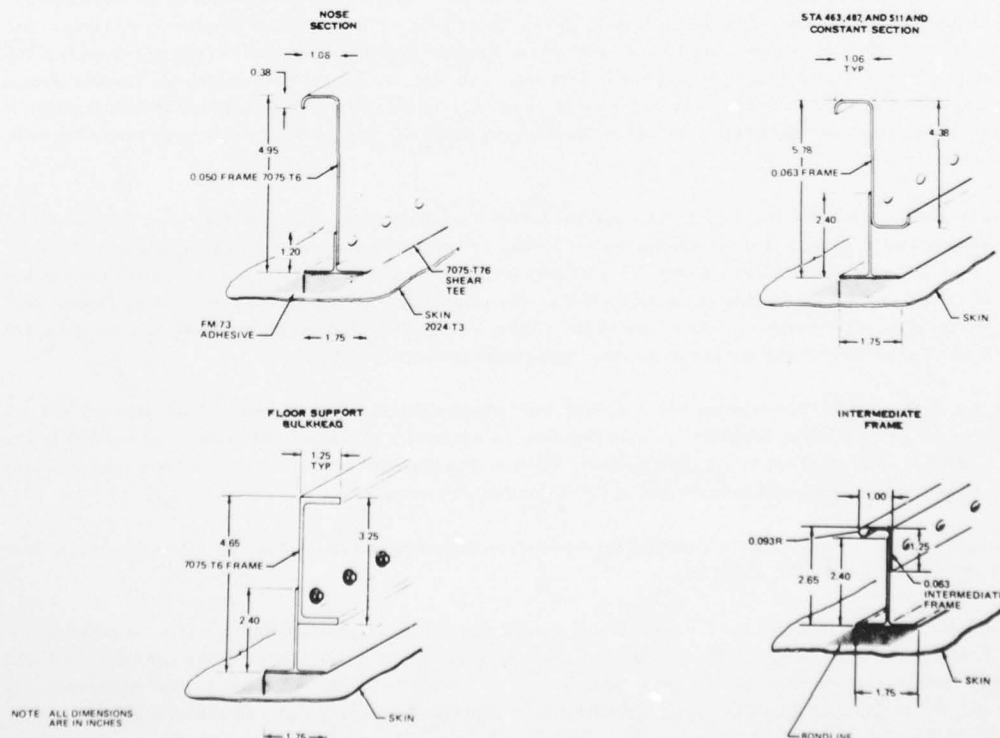


FIGURE 193. FSDC FRAME ARRANGEMENTS



AD-A068 806

ADVISORY GROUP FOR AEROSPACE RESEARCH AND DEVELOPMENT--ETC F/G 13/5  
BONDED JOINTS AND PREPARATION FOR BONDING.(U)  
MAR 79

UNCLASSIFIED

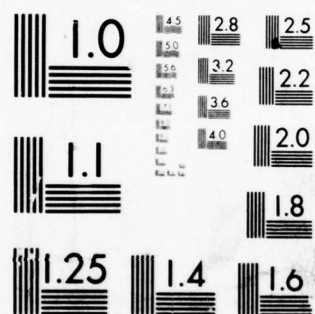
AGARD-LS-102

NL

3 of 4

AD  
A068806





MICROCOPY RESOLUTION TEST CHART  
NATIONAL BUREAU OF STANDARDS-1963-A

A frame tee with cutouts to provide longeron continuity is bonded to the skin. A Z-section frame is attached to this shear tee by means of 0.188-inch-diameter rivets spaced about 1 inch on center. Mechanical splices for the frames are staggered with respect to skin splices, as shown in Figure 186. Frame/shear tee height is 4.95 inches in the nose section and 5.78 inches in the cargo compartment section, as shown in Figure 193. The frame thickness is 0.050 inch in the nose section and 0.063 inch in the cargo compartment except under the wing, where it is 0.080 inch. The frames are rolled 7075-T6 material. The floor-support bulkhead frames are extruded 7075-T6 channel sections. The frame shear tees are 7075-T6 extruded T-sections.

The fuselage frames at station 703 and station 847 are integrally stiffened and numerically machined. They are shown in Figure 194. These 7075-T411 frames are milled from 8.50- by 60- by 200-inch aluminum hand forgings and subsequently heat-treated to a 7075-T73 condition.

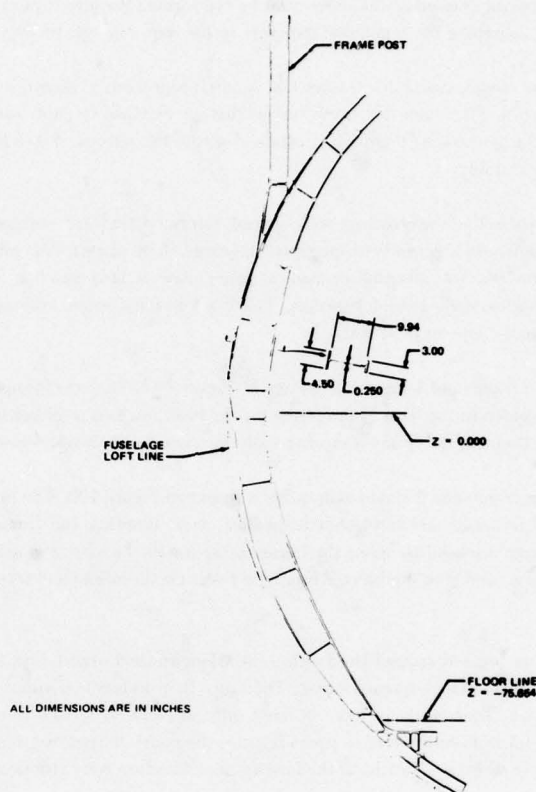


FIGURE 194. FSDC FRONT SPAR FRAME

Vertical loads from the wing front and rear spars were introduced into these frames and eventually sheared out into the fuselage side panels. On the full-scale demonstration component, a vertical load simulating the wing aerodynamic lifting reaction was applied directly to the frame post at station 703. This procedure greatly simplified the design and construction of the wing assembly without adding extra design requirements to the frame.

**Frame and Longeron Intersections** — PABST panel tests demonstrated that the design of the frame-longeron intersections is of major importance for all load conditions. The most critical full-scale demonstration component design problem is where the frame shear tees are notched to permit the internal longerons to pass through uninterrupted.

Two notched shear tee designs for the internal longeron region were fatigue-tested using stiffened flat panels, discussed earlier in this paper under Structural Justification Tests. One design had the interrupted shear clips terminating on the skin. Fatigue cracks initiated at each frame-longeron intersection grew together rapidly, and failed the panel. An artificially induced crack next to the longeron and halfway between the frames grew slowly by comparison and did not attain critical length. The second design had the shear tee notches terminating on a splice doubler instead of the skin alone. No fatigue cracks initiated.

The frame-bending test panel, also discussed earlier under Structural Justification Tests, developed adequate strength but failed by crippling the outer frame flange over the longeron as soon as the skin-to-shear clip bond had begun to fail. A much lighter panel could have been made to withstand those same loads by improving the continuity of loadpath at that intersection.

Significantly higher shear and compression allowables were developed in test panels with external longerons (i.e., unnotched shear tees) than for internal longeron-reinforced panels. The shear panel test results show that for the same skin thickness, the shear allowable was 18 percent higher for the external longeron. The allowable shear stresses for the external and internal longeron stiffened panels were 30,700 psi and 25,300 psi, respectively.



The detail design of a notched frame shear tee should therefore minimize crippling of the unreinforced outer flange of the frame at the intersection and the transfer of tensile load from the notched shear clip into the skin to prevent fatigue-cracking next to the longeron. In addition, the cross-sectional area of the interrupted stiffener must be accounted for in determining the required bond width to preclude disbonding. In short, the panel strength of a bonded, stiffened panel is even more critically dependent upon the details of the stiffener intersections than is the case for riveted construction.

The notched shear tees of the full-scale demonstration component were designed with bonded doublers under the internal longerons or bonded doublers on the exterior of the skin to minimize skin cracking. However, the frame outer flanges were not reinforced. The PABST design philosophy includes minimum reinforcement of known deficiencies only.

The weight of the fuselage shell structure design could be reduced by reinforcing the interrupted stiffeners to be equal in strength to the unnotched basic structure and then lightening the remaining structure to the requirements of the next lower failure mode.

A typical intersection in the cargo compartment for frames and internal longerons is shown in Figure 195. A 2024-T3 aluminum tear stopper is bonded under the longeron. The frame tee is cut out at this intersection to allow for the longeron. It is joggled to fit on top of the tear stopper to ensure that a continuous loadpath is attained across the cutout. A mechanically fastened shear tee ties the longeron to the frame to provide rolling stability.

On the sides of the fuselage shell where the longerons are wide-spaced, intermediate frames are provided between the 24-inch spaced frames. These intermediate frames run from longeron 8 to longeron 10 (cargo floor plane). A typical intersection for an intermediate frame at longeron 8 is shown in Figure 196. The internal mechanical splice plate at longeron 8 is cut out to fit over the intermediate frame tee when the skin panels are mechanically joined together. Two back-to-back splice angles tie the intermediate frame and the longeron 8 flange together with 0.188-inch-diameter lock bolts.

A typical intersection for the nose frame and longeron is shown in Figure 197. The tear stopper ends at the base of the frame tee and the longeron extends over and is bonded to the base of the frame tee. In addition, two steel bolts fasten the longeron, frame tee, and skin together. After the assembly is hot-bonded, the frame is mechanically fastened to the frame tee with aluminum rivets.

A typical intersection for the nose frame and bonded skin splice is shown in Figure 198. The nose frame tee stops short of the skin doublers. The skin, skin doublers, and frame tee are hot-bonded together. After bonding, the frame is installed with aluminum rivets. Two back-to-back angles and a filler plate are used to splice the frame tee across the bonded skin splice. Flush 0.188-inch-diameter lock bolts tie the angles to the frame tee, skin, and skin doublers. Aluminum rivets tie the angles and filler plate to the vertical frame tee and frame web.

**Tear Stoppers** — Tear stoppers were located around the fuselage in a longitudinal orientation to satisfy the slow crack growth and residual strength requirements per MIL-A-83444, Airplane Damage Tolerance Requirements. Fail-safe capability is equivalent to Douglas commercial airplanes currently in service. Tear stoppers were utilized only in the wide-spaced longeron side panels. The close-spaced longeron upper and lower skin panels did not require tear stoppers because the panel dimensions were such that the criteria flaw did not attain critical dimensions in the transverse direction. Cracks in the longitudinal direction were stopped by the bonded frame shear tees.

Three 7475-T761 bonded longitudinal tear stoppers, 0.071 inch by 3 inches, are provided externally on the side where the longerons are wide-spaced in the forward fuselage, as shown in Figure 199. Two tear stoppers, spaced approximately 27 inches apart, are located between longerons 8 and 9. The panel assembly between longerons 9 and 10 has one tear stopper approximately 30 inches below longeron 9, and a bonded longitudinal splice which functions as a tear stopper located close to longeron 10. The constant section of the fuselage has two 7475-T761 bonded tear stoppers located on the wide-spaced side panels. The panel assembly between longerons 8 and 9 has one tear stopper plus a bonded longitudinal skin splice which functions as a tear stopper. The panel assembly between longerons 9 and 10 is similar to the previously described panel between longerons 8 and 9.

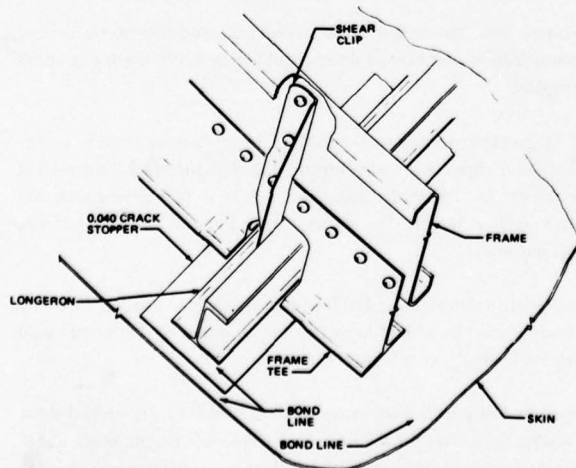


FIGURE 195. FSDC FRAME-LONGERON INTERSECTION

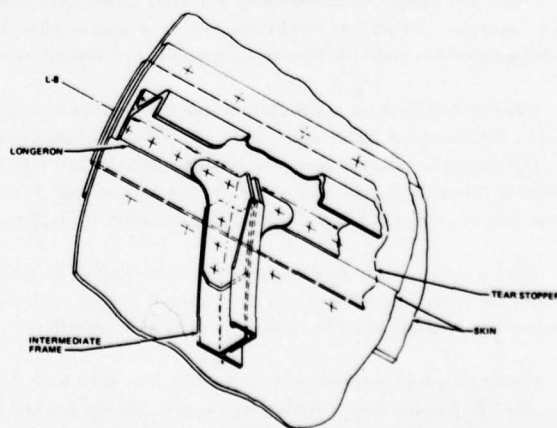


FIGURE 196. FSDC FRAME-LONGERON INTERSECTION

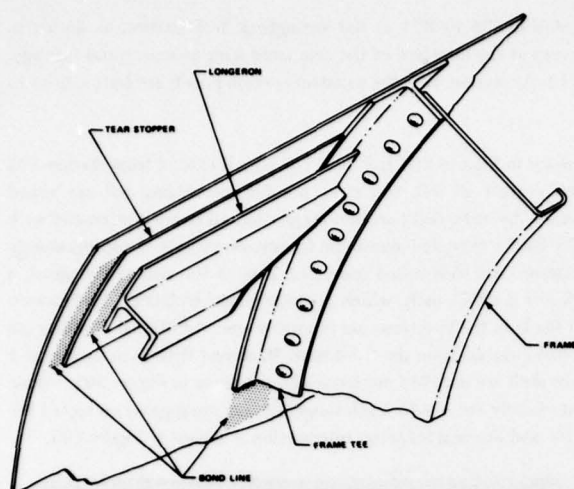


FIGURE 197. FSDC NOSE FRAME-LONGERON INTERSECTION

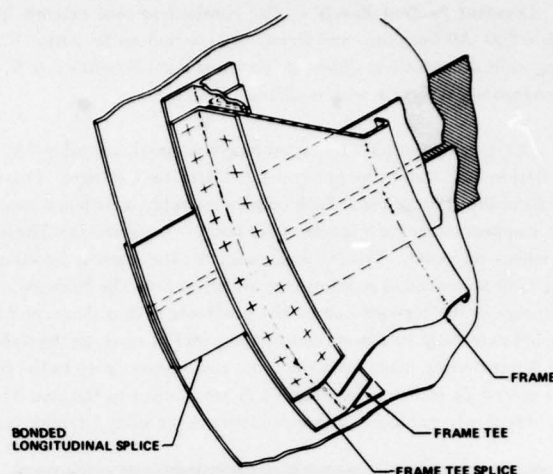
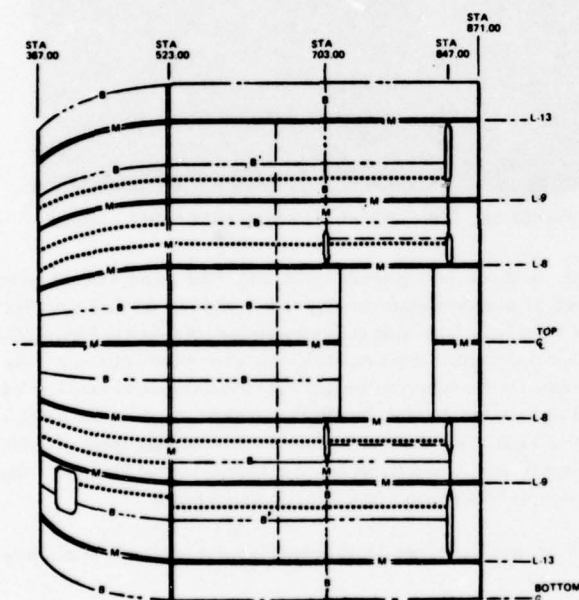


FIGURE 198. FSDC NOSE FRAME/SKIN SPLICE JOINT

**Panel Design** — There are three different types of skin panel designs on the full-scale demonstration component. These are the internal close-spaced longeron panels located in the upper half of the fuselage, the external close-spaced longeron panels located in the lower section of the fuselage, and the wide-spaced longeron panel located at the fuselage sides. Figure 200 shows the locations of all panel boundaries as well as their relationship with one another.



NOTE .... DENOTES 0.071 x 3 x 7475-1781 TEAR STOPPER

FIGURE 199. FSDC BONDED TEAR STOPPERS

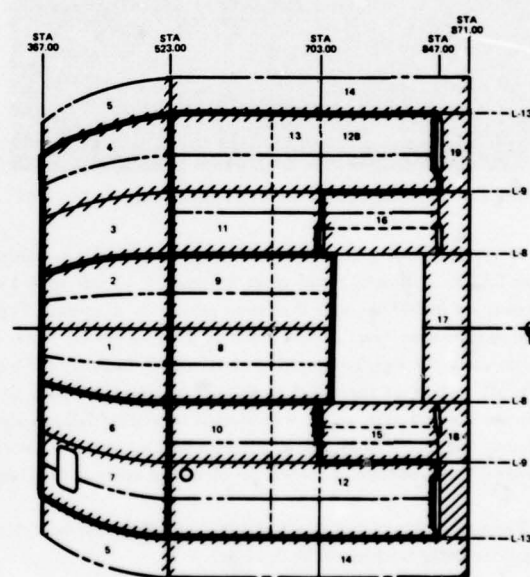


FIGURE 200. FSDC BONDED PANELS

Panel boundaries were situated at the maximum dimensions based on manufacturing and tooling constraints, existing autoclave size limiting panel arc length to 113 inches, the fuselage configuration requirements, and vendor manufacturing constraints based on the skin width of 94 inches for 0.050-inch-thick skin. These limitations are best represented by the following panels. Panel 5A and 14A, the first panels installed in the fuselage assembly fixture, were designed to be cradled in this fixture, thus eliminating the bottom centerline splice and therefore simplifying tooling. The panel width constraint was thus based on the maximum skin width of 94 inches. Due to autoclave width limitations and a natural manufacturing break at longeron 8, panels 1A, 1B, 9A, and 9B were butt-spliced at the top centerline of the fuselage. Panel 3A had special constraints imposed on it. Besides limiting its size to the autoclave dimensions, a large door was designed in this panel to allow for the passage of an integrally bonded upper jamb header. A circumferential mechanical splice was provided at the boundary between the constant section and the double-contoured nonconstant section to simplify tooling as well as to simulate an actual manufacturing break that normally would be required for a production fuselage. Due to the massive loads introduced from the wing and main landing gear, it was necessary to allow for the continuation of the one-piece, hand-forged frame segments to pass through the fuselage skin panels. Therefore, a panel boundary was designed at stations 703 and 847.

The minimum skin thickness over the entire fuselage was set at 0.050 inch based on foreign object damage criteria. To satisfy fatigue criteria for the full-scale demonstration component, 2024-T3 bare aluminum alloy was chosen for all skins and doublers. The skin thickness ranges from a minimum of 0.050 inch in the area forward of the wing to a maximum of 0.10 inch near the rear spar frame where shears are high due to the landing loads induced by the main landing gear and the flight loads induced by the wing.

**Constant Section Panels** — The constant section extends from station 523 to 871 at the strongback test fixture, as shown in Figure 200. All longerons and frames are continuous to station 871 except at the interface of the simulated wing assembly and fuselage. Longitudinal mechanical splices are positioned at longerons 1, 8, 9, and 13. At station 523, the constant-section panels are butt-spliced to the nonconstant section with mechanical fasteners.

A typical close-spaced internal longeron panel, assembly 9A, is shown in Figures 201 and 202. The panels extend from station 523 to station 720 and from longerons L-8 left to L-8 right. The panels consist of left and right bonded assemblies and are joined mechanically at longeron 1. Each bonded assembly is stiffened longitudinally by extruded J-section longerons and bonded internally with tear stoppers under each longeron for fail-safe requirements. These 7075-T6511 extruded aluminum longerons are spaced approximately 15 inches on center. Typical dimensions for the internal J-section longerons are shown in Figure 192. Due to the size of the panel, a longitudinal bonded skin splice is provided at L-4. The basic skin thickness is 0.071 inch, which is chem-milled to 0.060 inch between longerons in the forward half of the panel where skin shears and axial loads in the longerons are relatively low. Additional doublers are bonded externally to the aft end of the panel to carry the high shear load induced from the front spar. Machined fittings in longerons 1 and 4 transferring loads from the links across wing cavity to the fuselage shell are installed mechanically, as shown in Figure 201. Frame tees spaced 24 inches from station 535 are bonded to the skin. They are locally cut out for each longeron, and are joggled on top of the tear stoppers to minimize fatigue problems in the skin. A typical frame tee and internal longeron intersection is shown in Figure 195.



FIGURE 201. UPPER INTERNALLY STIFFENED PANEL — OUTSIDE



FIGURE 202. UPPER INTERNALLY STIFFENED PANEL — INSIDE

A typical close-spaced external longeron panel, assembly 14A, is shown in Figures 203 and 204. This panel extends from station 523 to station 871 and from longeron L-13 left to L-13 right. It measures approximately 8 feet wide by 29 feet long. The longerons are bulb T-sections that were previously discussed. Typical dimensions for a basic external longeron are shown in Figure 192. The longerons were spaced approximately 13.5 inches on center except that additional external longerons were added at the end of the panel to carry the high compressive axial loads induced by the test external load conditions. Internal and external doublers were bonded to the aft section of the panel to provide an interface with the strongback test fixture. Due to the excessive length of the panel, a transverse bonded skin splice was located at station 703, as shown in Figure 191. The longitudinal mechanical skin splice at L-13, previously discussed, is shown in Figure 188. Cutouts are not required in the bonded frame tees due to the external location of the longerons. This eliminates a chronic problem that arises at the frame-longeron intersection with internal longeron panels.

The external longeron panel also has an 0.375-inch-diameter hole in every bay to provide drainage for water or bilge fluid that may accumulate in the bottom of the fuselage.

A typical side panel with wide-spaced longerons is shown in Figures 205 and 206. All the side panels are similar in their structural arrangement. Longerons are wide-spaced from L-8 to L-9 and from L-9 to L-10. In the longitudinal bonded skin splice, the external splice doubler is uninterrupted over the entire length of the panel while internal splice doublers are interrupted and joggled on top of frame

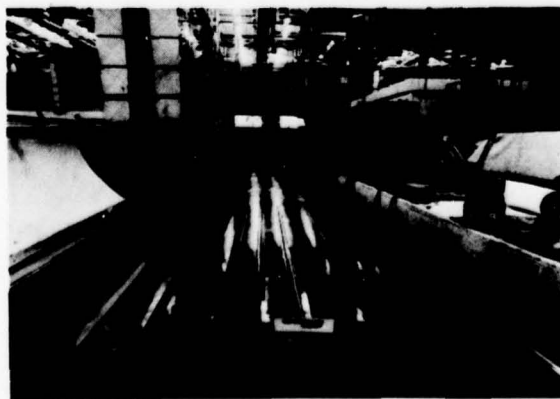


FIGURE 203. EXTERNALLY STIFFENED PANEL — OUTSIDE

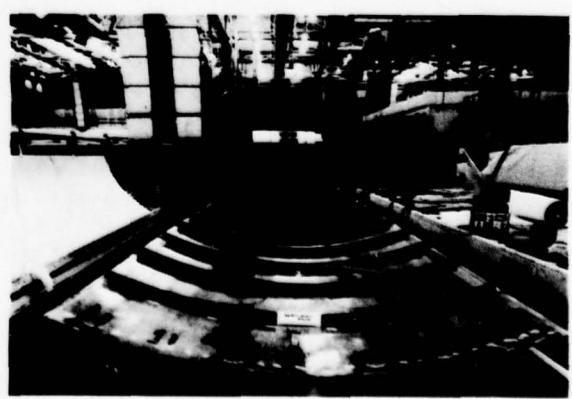


FIGURE 204. EXTERNALLY STIFFENED PANEL — INSIDE





FIGURE 205. WIDE-SPACED LONGERONS PANEL - OUTSIDE



FIGURE 206. WIDE-SPACED LONGERONS PANEL - INSIDE

tees. 7475-T761 external tear stoppers, 0.071- by 3.00-inches wide, are bonded longitudinally to provide added fail-safe capability in these panels. Additional frame tees and light frames between full-depth frames are also provided to increase the initial buckling strength of the skin. Intercoastals and straps are located between longerons to stabilize each frame.

**Nonconstant Section Panels** - All longerons and frames aft of and including station 439 are identical or similar to the constant-section panels. All the longerons end at station 439. Forward of station 439 at longerons 1, 4, 8, and 9, full-depth intercoastals provide axial load capability for the panel (see Figure 199). The frames aft of station 439 are similar to the constant-section frames in size and spacing. The frames at station 439 and forward are full-depth and are spaced at 12-inch intervals.

A typical close-spaced internal longeron panel assembly is shown in Figures 207 and 208. The bonded assembly shown and its opposite assembly are joined mechanically at longeron 1. This assembled internal longeron panel section extends from station 523 forward to station 367 and from L-8 left to L-8 right. The bonded skin splice at L-4 forward of station 439 contains a continuous 2024-T3 external splice, 0.050 by 3.50 inches, and a discontinuous internal splice of the same dimensions. The internal splice is located between the frame tees and is also used as a filler, as shown in Figure 207, for the intercostal tee that is bonded across the frame tees. The mechanical splice at L-1 forward of station 439 is shown in Figure 189.



FIGURE 207. INTERNALLY STIFFENED NONCONSTANT PANEL - INSIDE



FIGURE 208. INTERNALLY STIFFENED NONCONSTANT PANEL - OUTSIDE

A typical external longeron panel assembly is shown in Figures 209 and 210. This panel extends from stations 367 to 523 and from L-13 left to L-13 right. It is similar to the upper panel except that the longerons are bonded on the outside surface of the skin. The longerons are bulb T-sections identical in cross section to the external longerons used in the constant section. The frame shear tees are continuous without interruption. This panel has 0.375-inch-diameter holes near the bottom centerline in every bay to provide drainage for water or bilge fluid that may accumulate in the bottom of the fuselage.

A typical side panel with wide-spaced longerons is shown in Figures 211 and 212. This panel extends from stations 523 to 367 and from bonded longeron 8 to mechanically fastened longeron 9. The one-piece skin is 0.050-inch-thick 2024-T3 bare aluminum alloy. The two 7475-T761 tear stoppers shown in Figure 212 are 0.071 inch thick by 3 inches wide. Intercoastals are located at tear stopper No. 2 in every other bay in order to stabilize the frames. Doublers, 0.016 inch thick, have been added near station 523 to increase the skin thickness to 0.066 inch where countersunk fasteners are to be installed.

The wide-spaced longeron left-side panel with simulated crew entrance door, 3A, shown in Figures 213 and 214, is located between stations 523 and 367 from longeron L-9 to L-13. It contains a 32-inch by 60-inch cutout for the entrance door. The 2024-T3 skins are chem-milled to provide an 0.050-inch-thick skin aft of station 439 and an 0.125-inch-thick skin around the door corners. All chem-milled steps are external as shown in Figure 213. The door corner doublers, shown in Figure 213, are also chem-milled and bonded to the skin. There are two bonded longitudinal skin splices on the panel. One is at mid-door level and the other is at longeron 12. The



FIGURE 209. EXTERNALLY STIFFENED NONCONSTANT PANEL - INSIDE

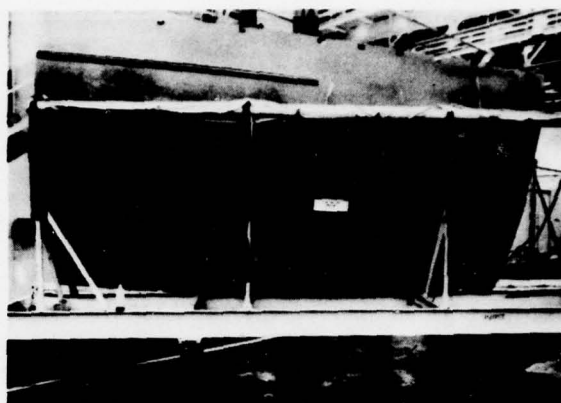


FIGURE 210. EXTERNALLY STIFFENED NONCONSTANT PANEL - OUTSIDE



FIGURE 211. WIDE-SPACED LONGERONS NONCONSTANT PANEL - INSIDE



FIGURE 212. WIDE-SPACED LONGERONS NONCONSTANT PANEL - OUTSIDE

0.050-inch-thick skins are spliced with an inner and outer bonded splice member, as shown in Figure 191. Where the thicker skins are spliced, the double-lap bonded splice has been modified in order to reduce the shear stress in the adhesive. The thick skins are chem-milled at the splice and a third splice member is added between the skin and outer splice. Bonded straps are added to protect the skin from cracking adjacent to the end of the longeron. The door jamb frames, at stations 427 and 391, are 0.090 inch thick. Sheet metal intercostals are added mechanically to form the door jamb structure, as shown in Figure 214. On the fuselage skin side the intercostal picks up a tee that is bonded to the skin.



FIGURE 213. DOOR JAMB PANEL - OUTSIDE

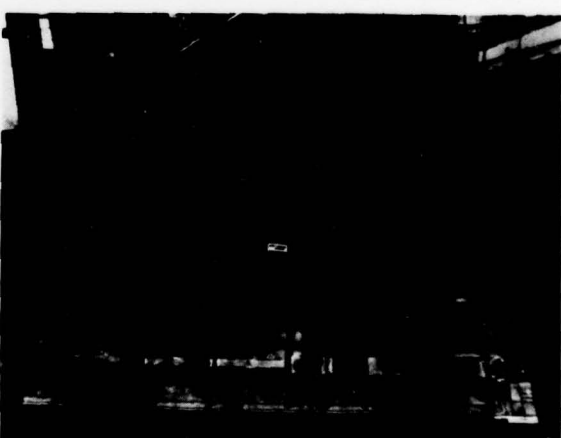


FIGURE 214. DOOR JAMB PANEL - INSIDE

## THE MANUFACTURE

The Manufacturing section that was designated to bond the 19 panels used to build the complete FSDC improved their existing bonding technology by bonding the smaller test panels. These specimens that were fabricated ranged in size from small 2-inch-wide coupons to large 9- by 12-foot panels. Nearly 600 bonded assemblies and 94 mechanical assemblies were fabricated before assembly was started on the FSDC panels. From their experience, it was determined that the female tool was marginal in obtaining a good end product and that the modified male tool, which used a vacuum bag on both sides of the part, yielded the best bonding of the end product. Three basic tools were used for the FSDC. A 10-foot-wide by 30-foot-long female bonding tool was built with a base plate of 1/4-inch-thick aluminum skin formed to a 108.25-inch radius and it was attached to an aluminum egg-crate structure. Studs were welded on the aluminum face sheet and this provided the means to adjust the face sheet radius and longitudinal straight line elements. A 10- by 30-foot male tool was built which consisted of a square tube frame that surrounded the area. A number of contour boards spanned the 10-foot dimension and were located at each frame station. Figure 215 shows the male tool on the left and the female tool on the right. The third tool was also a modified male tool which was made to bond the forward nonconstant section panels. The basic design was the same idea used in the other male tool. It was smaller and the contour boards were arranged to allow for the compound curvature. All frame planes are parallel. In order to bond an assembly the following steps were taken.

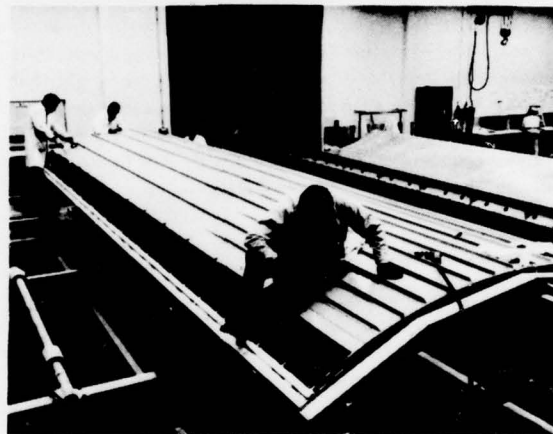


FIGURE 215. MALE AND FEMALE BONDING TOOLS

### Metal Fit Check

All the parts for a panel to be bonded are assembled and laid in the tool in the same order as would be intended for the bond assembly. In Figure 215 the bottom centerline panel is being assembled for a metal fit check. A limited number of screws, in loose-fitting holes, are used to secure the parts together or to the tool. The holes are located where subsequent fasteners will be used to join this panel to an adjacent panel or another riveted assembly. The frame shear tees are fastened to the contour boards with loose-fitting bolts. The part tolerances are checked to be certain that no gaps exist between mating parts. Nominal thumb pressure is used to push things together and represents the position of parts during the pressurized autoclave operation. When it is ascertained that the proper fit exists between all parts, the assembly is broken down and verifilm added between all joints subsequently to be bonded. The complete assembly is again fitted into the bonding tool and after all of the verifilm is installed, the part is encased in a plastic bag and sealed so that no pressure will exist between mating parts. The panel is processed through the autoclave in the same manner as it will be during the final adhesive cure cycle. After a cure cycle of 20 minutes at 250°F, the assembly is cooled down, removed from autoclave, and the vacuum bag is taken off the assembly. The panel is disassembled to allow removal of the verifilm which is checked for thickness variations. The verifilm is actually read with a micrometer for thickness and the values are noted on the film. Where excessive thickness or lack of pressure is found, the part shape is examined and corrected if possible, or the mating parts are adjusted in the tool for better fit. If a sufficient number of excessive or variable glue-line thicknesses are seen, it may be necessary to rerun the verifilm check with the modified parts. An extra layer of adhesive will be added during the final bond cycle to the areas which indicate that a thick glue line will exist in the final product.

### Anodize and Prime

After the verifilm check, the parts are sent to the shop where the anodizing operation takes place. The parts are carefully hung on a large open metal picture frame. Since electrical contact between the frame and the part is essential, Douglas designed a number of titanium springs that greatly reduced the racking time of the parts and provided a positive electrical contact. The rack with the parts is cycled in and out of a number of tanks as noted below:

1. Alkaline wash, 150°F, 10 to 15 minutes;
2. Spray rinse, tap water, 2 minutes;
3. Tap water rinse, 140°F, 5+ minutes;
4. AMCHEM 6-16 etch, ambient, 10 to 15 minutes;
5. Tap water rinse, ambient, 5+ minutes;
6. Spray rinse, cold, deionized water, 2 minutes; spray rinse, tap water, 2 minutes;



7. Phosphoric acid anodize, approximately 25 minutes;
8. Tap water rinse, ambient, 10 to 15 minutes;
9. Spray rinse, cold deionized water, 2 minutes;
10. Oven dry at 170°F maximum.

Note: No more than 2 minutes elapsed time between steps 7 and 8.

The parts are transported from tank to tank on an overhead monorail. This permits the parts to be taken from the drying oven to an inspection area where a visual check is made to determine that all details were anodized. The parts are then taken into the paint spray booth on the monorail and the thin coat (0.0001 to 0.0003 inch thick) of BR-127 primer is applied to all anodized surfaces. Parts are then moved by monorail to the drying oven where the primer is cured at 250°F. It should be noted that the parts are not touched in any way from the start of the anodizing process until the primer cure cycle is complete. This prevents contamination of the anodized surface.

### Bonding

The parts are removed from the anodized frame by people using clean white gloves and making every effort to minimize contact with the panels. The parts are stacked on clean Kraft paper and delivered to the metal bond area. Here, the parts are reassembled on the bonding jig and the adhesive film is added to the faying surfaces. Figure 216 shows the anodized panel being assembled in the male bonding tool. After all the external parts have been secured and the separator films, bleeder cloth, flash-breaker tape, thermocouple, and vacuum bag are installed, the details are secured so that a wood support cradle can be placed in position for turning the bonding tool upside down (see Figure 217). Figure 218 shows the male tool inverted. While it is in this inverted position, the remaining doublers or stiffeners are assembled with adhesive film, this side of the tool is covered with separator films, etc., and finally the vacuum bag is installed and a vacuum applied. The tool is then rotated to its upright position with vacuum applied to the bags. It must be determined that no leaks exist. Figure 219 shows the bond assembly being loaded into the autoclave. Figure 220 shows the female tool with its parts being assembled for bonding. This assembly is the top internal stiffened panel. The following sequence is followed in laying up the parts in the female tool. A layer of release film is placed over the tool and the assembled parts. Next, a silicone rubber blanket and a layer of bleeder cloth fabric are placed over the parts. To reduce the perturbations for the vacuum bag, the space between the contour boards is filled with 0.25-inch-diameter hollow aluminum spheres. Approximately 2 inches of these spheres are used to smooth out the assembly. Two layers of bleeder fabric are then placed over the spheres and the vacuum bag installed and sealed to the edge of the 1/4-inch aluminum sheet of bond tool. A vacuum is applied slowly and the spheres spread evenly over the assembly. The spheres are very effective in transmitting the autoclave pressure to the details beneath. The tool is placed in the autoclave and the temperature and pressure are slowly increased to their limits of 250°F and 40 psi, respectively. These final conditions are held for 90 minutes to cure the FM-73 adhesive.

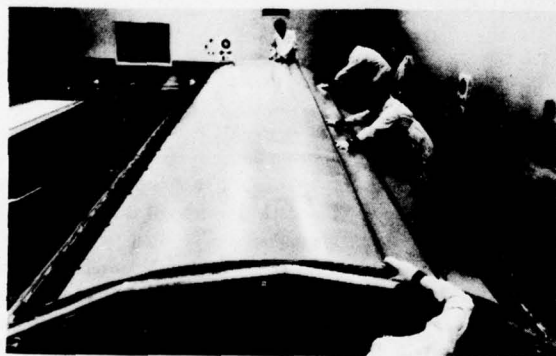


FIGURE 216. ADHESIVE LAYUP OPERATION

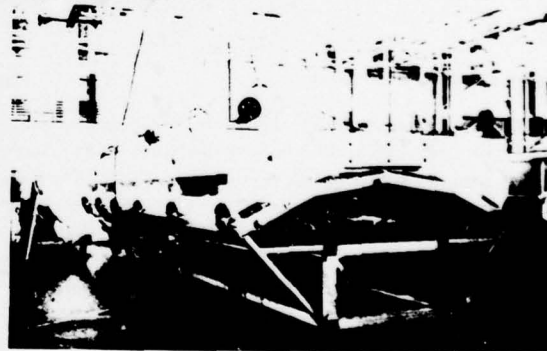


FIGURE 217. SUPPORT TOOL IN POSITION



FIGURE 218. MALE TOOL INVERTED



FIGURE 219. MALE TOOL BEING PLACED IN AUTOCLAVE

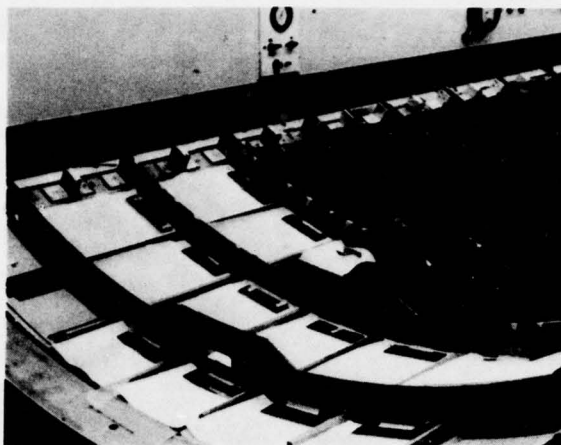


FIGURE 220. FEMALE TOOL DURING LAYUP

When the panel is removed from the bonding tool it must undergo nondestructive testing. However, the FM-73 adhesive flows easily, and no amount of taping will keep it off the surfaces which need to be clean for use of the Fokker Bondtester. Figure 221 shows men using grinding wheels to remove excess adhesive. Figure 222 shows a closeup of the problem, and Figure 223 shows the details cleaned up.

#### Nondestructive Inspection

Figure 224 shows two operators inspecting with Fokker Model 70 Bondtester. This instrument is excellent for detecting voids, porosity, and thick glue lines in bonded laminates. Correlations of the Fokker readings and cohesive bond strength have been made. The pattern on the Bondtester cathode ray tube shifts from center to right or left as the glue line thickness and porosity change. Figure 225 shows the bond joint strength versus left or right shift of Bondtester readout. Figure 226 shows lap shear strength versus adhesive thickness.



FIGURE 221. ADHESIVE CLEANUP OF BONDED PANEL

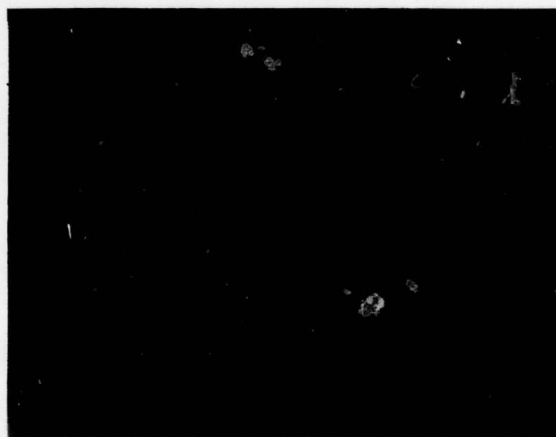


FIGURE 222. ADHESIVE FLASH ON DETAILS

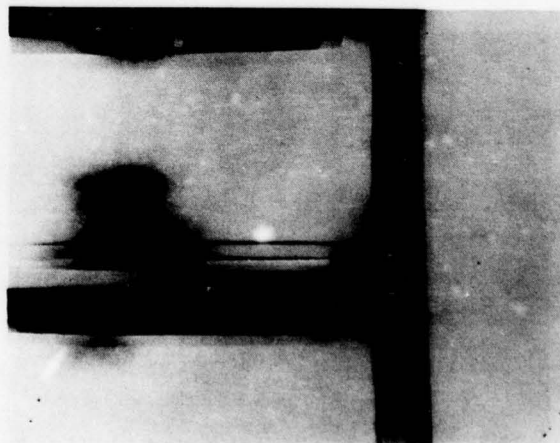


FIGURE 223. ADHESIVE FLASH AFTER CLEANUP



FIGURE 224. NONDESTRUCTIVE INSPECTION

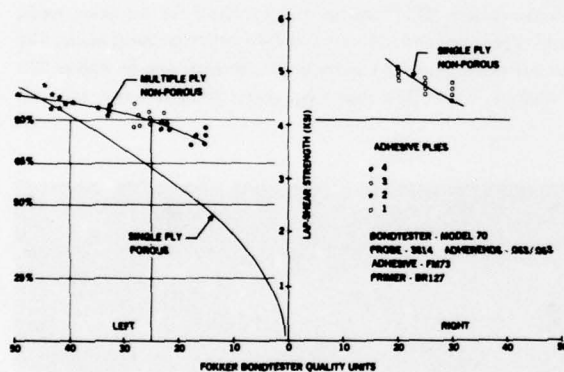


FIGURE 225. FOKKER BONDTESTER CALIBRATION VERSUS SHEAR STRENGTH

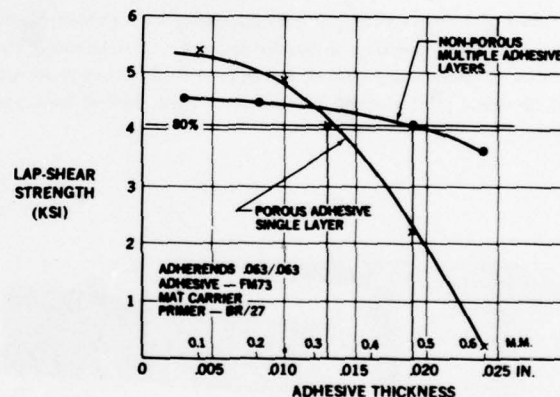


FIGURE 226. EFFECT OF ADHESIVE THICKNESS ON STRENGTH

#### Panel Subassembly

After inspection (NDI) the panel must be assembled to the sheet metal zee-section frames, which are connected to the bonded shear tees with rivets. Figure 227 shows the bottom center panel, constant section, in the assembly jig. The frame members are located by the contour boards shown or angle on the frame members. Frame members exceed the width of the bonded panel. This keeps the frame splice away from the panel splices. Figure 228 shows a nonconstant section assembly tool with panel. Sometimes two bonded panels are joined in the jigs.

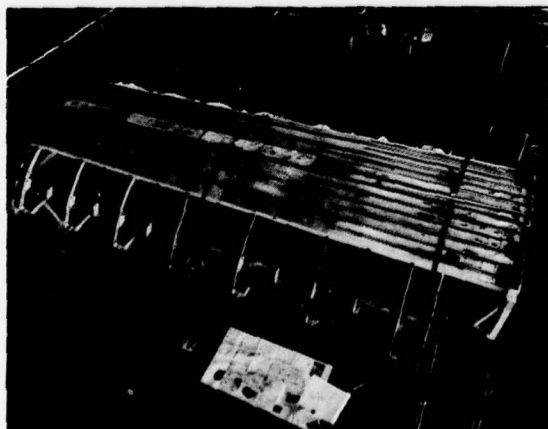


FIGURE 227. BONDED PANEL IN ASSEMBLY JIG

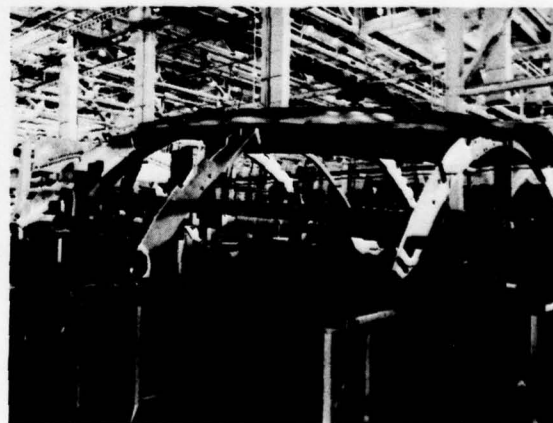


FIGURE 228. NONCONSTANT SECTION ASSEMBLY TOOL



## FINAL ASSEMBLY

The bonded subassemblies are taken to final assembly where the test support jig is used as the final assembly jig. Figure 229 is a schematic drawing of the test setup. The next series of photographs shows the various stages of structural buildup of the Full-Scale Demonstration Component (FSDC). Figure 230 shows the test support fixture and its relation to the forward steel pressure bulkhead. Figure 231 shows the forward pressure bulkhead and its supports. This dome was secured and lined up with the aft support fixture so it would act as an assembly jig. Figure 232 shows the cradles that position the bottom bonded panel for assembly. It also shows the floor support beams and the frame extensions associated with the bottom panel. In Figure 233 the constant-section side panels are shown assembled to the bottom panel and joined to the bottom of the dummy wing and the aft barrel section. It can also be seen that the floor extends forward to the pressure dome in front. The next two figures, Figure 234 and Figure 235, show the test component almost completely built up, lacking only the three nonconstant section panels. The internal jig fixture which mounts on the FSDC cargo floor has an upper working platform that can be seen in these views. Figure 236 shows the completed article with all the bonded panels installed. The lower supporting contour boards have been removed and the temporary support on the nose pressure bulkhead is still in place. Figure 237 is a good view of the dummy wing and the wing load jacks being installed.

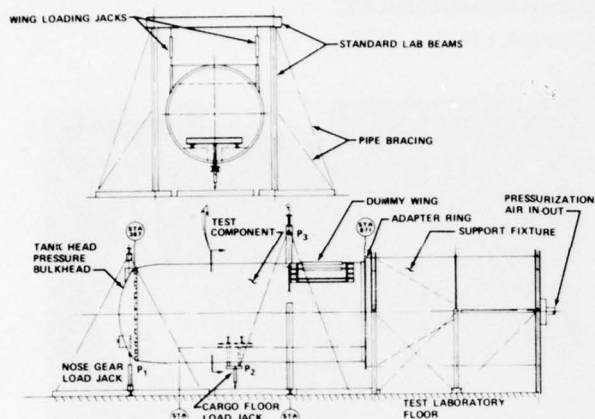


FIGURE 229. FSDC TEST SETUP

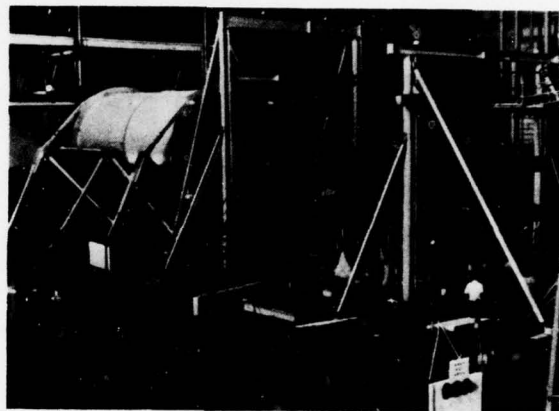


FIGURE 230. TEST SUPPORT FIXTURE

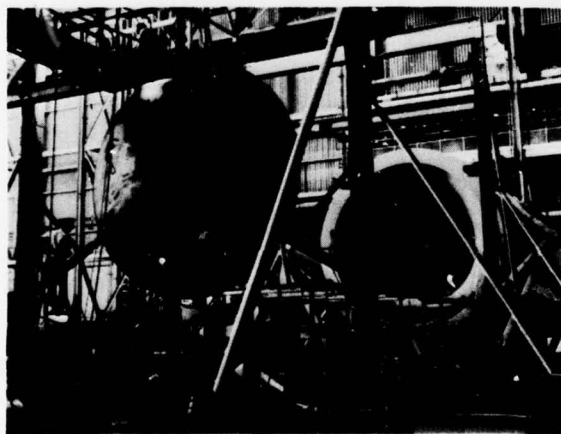


FIGURE 231. FORWARD PRESSURE BULKHEAD



FIGURE 232. FLOOR SUPPORT BEAMS AND BOTTOM PANEL



FIGURE 233. SIDE PANEL ASSEMBLED

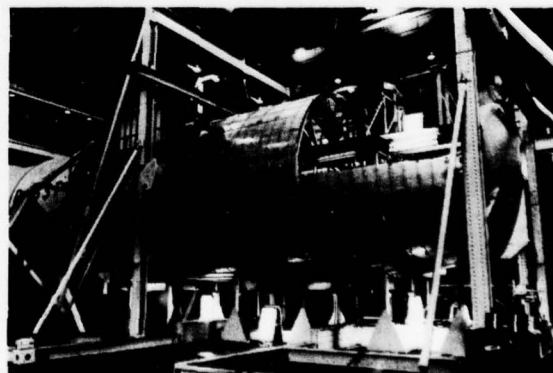


FIGURE 234. FINAL ASSEMBLY MINUS THREE PANELS, LOWER VIEW



FIGURE 235. FINAL ASSEMBLY MINUS THREE PANELS, UPPER VIEW

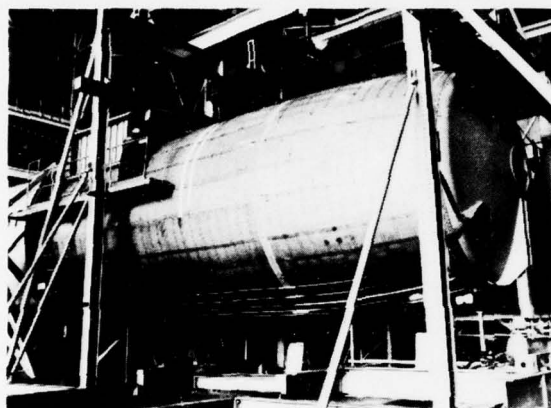


FIGURE 236. COMPLETED ASSEMBLY

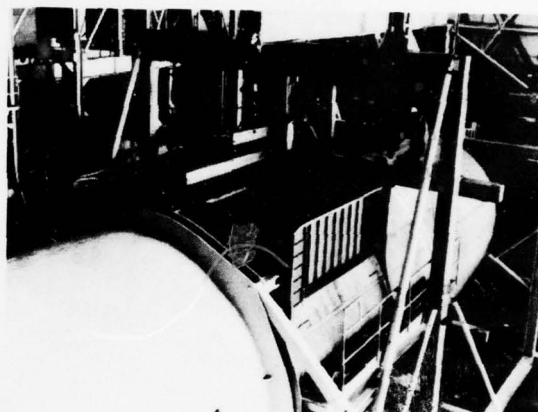


FIGURE 237. DUMMY WING INSTALLATION

### THE TEST

The variable stress spectra were based on the military requirements for atmospheric turbulence, flight maneuvers, ground taxi, and landing impact. They are used to establish a test load profile for the test spectrum that would give equivalent damage. The flight profile distribution was based on a projected YC-15 utilization that requires 19,014 pressurizations per lifetime. Figure 238 shows the four load spectra required for the loading cylinders and cabin pressure for each flight. The figure shows 26 seconds required to apply one flight but actual test limitations have increased this cycle time to 36 seconds per flight. As of November 1, the fuselage had been pressure-cycled 56,350 times. At that date no bond flaws had increased to cause failures, and only one bad rivet had initiated a failure in the structure. Figures 239, 240, and 241 show the extent of the fatigue crack when discovered, a view of the rivet which caused the failure, and a closeup of the poorly bucked rivet. Figure 242 is a comparative presentation showing the number of failures which occurred on a mechanically fastened fuselage test component which was tested in a manner similar to the testing of the PABST F54C. The figure also shows the large number of fatigue failures that occurred on the mechanically joined article through 68,000 cycles. The PABST bonded structure has had one failure at 36,811 cycles out of the total of 56,350 to date. Figure 243 shows the test control center where the load history on each cylinder is recorded on a strip chart. The strain gages are read out on the high-speed printer at the right. The test has been conducted efficiently. First cycles were applied in the first part of July and cycling was accomplished in two shifts, 5 days a week. Saturdays were used for a thorough inspection which included NDI of bond flaws and suspect areas. Test was suspended for 30 test days because of test fixture failures and test article modifications such as adding long skin cracks for failsafe tests.

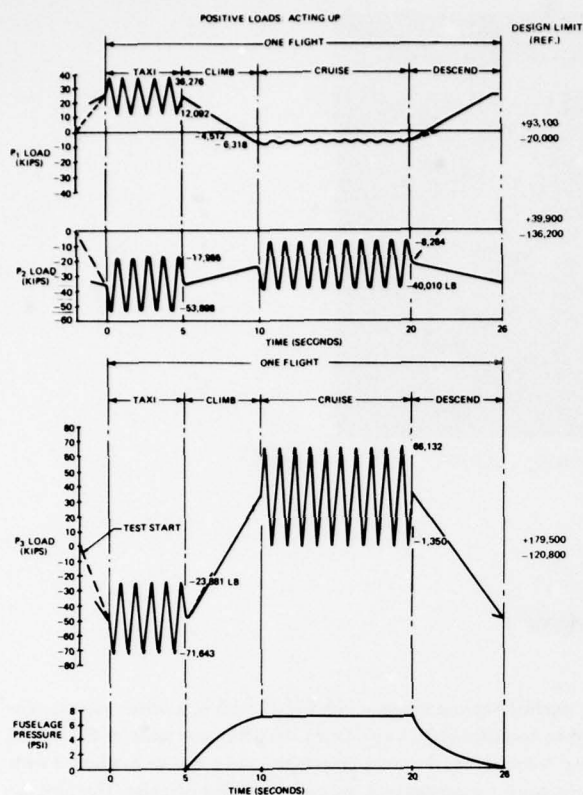


FIGURE 238. FSDC TEST SPECTRUM

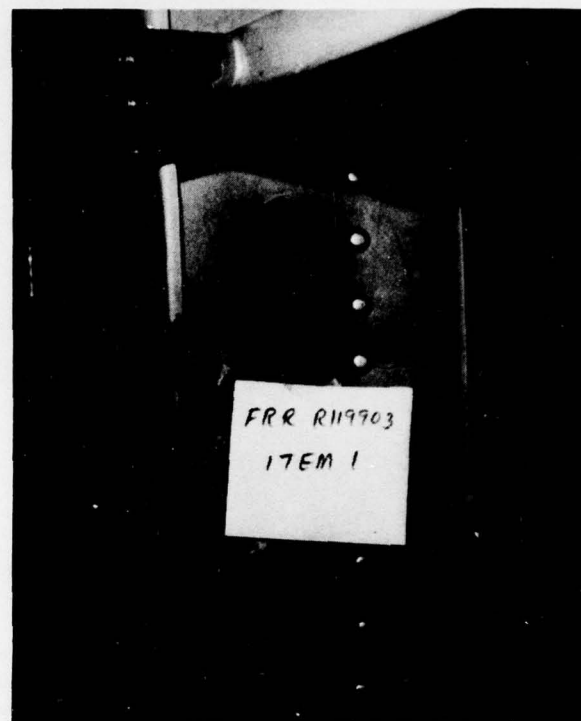


FIGURE 239. FRAME FATIGUE CRACK

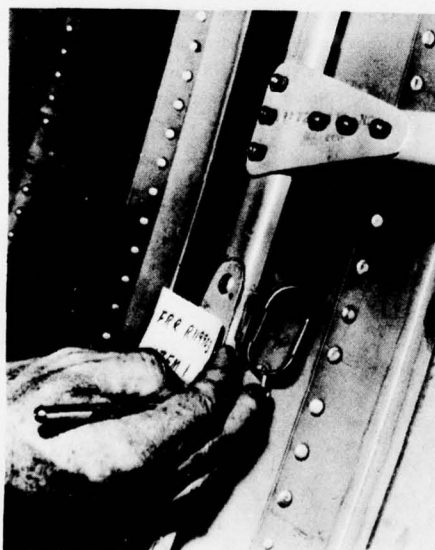


FIGURE 240. RIVET WHICH CAUSED CRACK



FIGURE 241. RIVET DETAIL

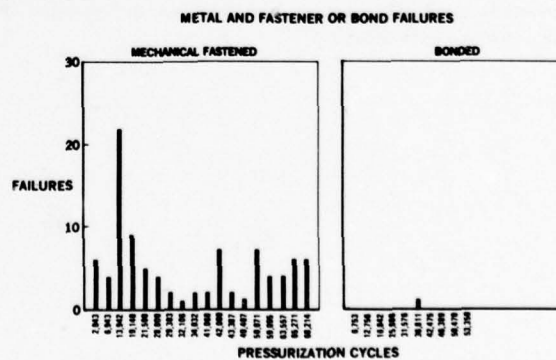


FIGURE 242. FULL SCALE FUSELAGE TEST RESULTS



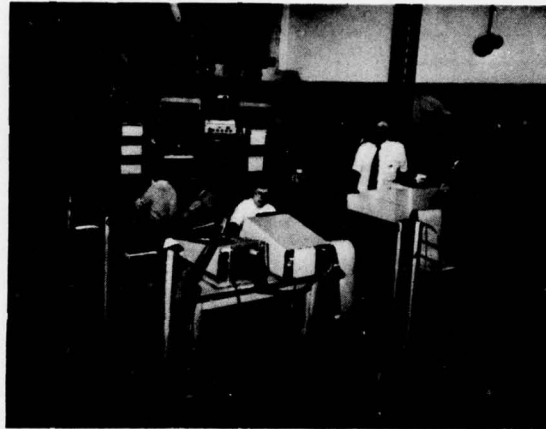


FIGURE 243. TEST CONTROL CENTER

### CONCLUSIONS

The PABST program has clearly shown that the new 250°F cure modified-epoxy adhesive film FM-73 with mat carrier can transfer loads between parts for the full range of static and cyclic loads required by specifications. A significant discovery was made in the area of crack growth. If the panel being tested is subjected to pressure-loading in actual use, the crack-growth test must also be conducted with pressure. The manner of crack arrest differs completely in a panel undergoing nonpressurized test and one under pressure. The fuselage panel cracks are completely stopped by the presence of a bonded stiffener (longeron or frame). This allows bonded fuselage skin panels to be operated safely at higher stress levels than are possible for the riveted counterpart.

Environmental structural tests have not shown any degradation of the bondline strength. These environmental tests on specimens with flaws also show no tendency for the flaw to increase in size. Environmental testing has shown the need for testing specimens at a very slow cycle rate such as one to four cycles per hour. High cycle rate (30 Hz) tests give a false life-cycle count.

Consideration of the adhesive as an elastic-plastic material, in conjunction with linear elastic fracture mechanics for sheet cracks, has led to a series of simple analyses for the effects of cracks and discontinuities in bonded stiffened structures. The methods are slightly lacking in rigor (because the distributed bond loads are reduced to line loads rather than area loads) but account approximately for the known major effects in problems in which the bond can become critical. Excellent agreement with the test results has been shown for a one-bay crack, lending confidence to the methods. Further comparisons of this theory with experiment should be made, to establish any limitations on applicability because of the approximations.

The examples considered reveal that cracks in the metal structural elements can often induce finite disbonds. However, few cases can be anticipated in which the bond failure will immediately induce catastrophic structural failure. Usually, after the initial disbond has been arrested, an increase in load is needed to propagate the disbond.

The full-scale demonstration component has provided proof that fuselage sections with compound curvature can be bonded successfully, good NDI equipment can determine the condition of cured adhesive, and bond flaws will not propagate under cyclic load with or without environment.

## REFERENCES

1. Summary of Air Force/Industry Manufacturing Cost Reduction Study. AFML-TM-LT-73-1, 28 August through 1 September 1972.
2. Summary Report on the Low-Cost Manufacturing/Design Seminar. AFML-TM-LT-74-3, 22-24 May 1973.
3. A. W. Bethune, Durability of Bonded Aluminum Structure, SAMPE Journal, Vol. 11, No. 3, July-September 1975.
4. D. P. Wilhem, Fracture Mechanics Guidelines for Aircraft Structural Applications. Air Force Flight Dynamics Laboratory Technical Report AFFDL-TR-69-111, February 1970.
5. A. F. Liu, Stress Intensity Factor for a Corner Flaw. Engineering Fracture Mechanics 1972, Vol. 4 pp. 175-179, Pergamon Press.
6. A. S. Kobayashi, et al, Approximate Stress Intensity for an Embedded Elliptical Crack Near a Free Surface. International Journal of Fracture Mechanics, June 1965.
7. T. Swift, The Effect of Fastener Flexibility and Stiffener Geometry on the Stress Intensity and Stiffened Cracked Sheet, in Prospects of Fracture Mechanics, edited by G. C. Sih, H. C. Van Elst, and D. Broek. Noordhoff International Publishing, Leyden, 1974, pp. 419-436.
8. P. Kuhn, Notch Effects on Fatigue and Static Strength, published in the Proceedings of the Symposium held in Rome in April, 1963 on Current Aeronautical Fatigue Problems, Pergamon Press.
9. J. D. Willenborg, R. M. Engle, and H. A. Wood, A Crack Retardation Model Using an Effective Stress Concept. AFFDL-TM-FBR-71-1, January 1971, Air Force Flight Dynamics Laboratory.
10. E. J. Hughes, J. L. Rutherford, and F. C. Bossler, Capacitance Methods for Measuring Properties of Adhesives in Bonded Joints. Rev. Sci. Inst., Vol. 39, No. 5, May 1968.
11. F. C. Bossler, M. C. Franzblau, and J. L. Rutherford, Torsion Apparatus for Measuring Shear Properties of Adhesive Bonded Joints. Brit. J. Sci. Inst. (J. of Phys. E.) Series 2, Vol. 1, 1968.
12. J. L. Rutherford, F. C. Bossler, and E. J. Hughes, On Measuring the Properties of Adhesives in Bonded Joints. 14th National Symposium, Society Aerospace and Material Process Engineers, Nov. 1968.
13. Walter Althof, u.a., Environmental Effects on the Elastic-Plastic Properties of Adhesives in Metal Bonded Joints. Deutsche Luft- und Raumfahrt, Forschungsbericht 77-63, Institut für Strukturmechanik der DFVLR, Braunschweig, 1977.
14. W. Cleven, Continuous Determination of the Shear Modulus G, Report Nr. R-2045. Netherlands Aircraft Factories, Fokker-VFW, published Aug. 30, 1976.
15. L. J. Hart-Smith, Analysis and Design of Advanced Composite Bonded Joints, Douglas Aircraft Company, McDonnell Douglas Corporation, NASA Langley Research Center Contract Report, NASA CR-2218, January 1973.
16. L. J. Hart-Smith, Adhesive-Bonded Double-Lap Joints, Douglas Aircraft Company, McDonnell Douglas Corporation, NASA Langley Contract Report, NASA CR-112235, January 1973.
17. L. J. Hart-Smith, Adhesive Bond Stresses and Strains at Discontinuities and Cracks in Bonded Structures. Douglas Aircraft Company, Report No. MDC-J6068, September 1976.
18. T. Swift, The Effects of Adhesive and Stiffener Yielding on the Fracture Strength of Adhesive Bonded Cracked Panels. Douglas Aircraft Company, McDonnell Douglas Corporation, IRAD Technical Report MDC-J7233, May 1976.

## ACKNOWLEDGMENT

This work was sponsored by the Air Force Flight Dynamics Laboratory (AFFDL) under joint management and technical direction of AFFDL and the Air Force Materials Laboratory (AFML), Wright-Patterson Air Force Base, Ohio. This contract is administered as part of the Advanced Metallic Structures, Advanced Development Programs (ASM ADP), Program Element No. 63211F, Project 486U. William R. Johnson is the Acting Program Manager and Jamie M. Florence is the Project Engineer (AFFDL/FBA) for the PABST program. The author wishes to express his appreciation to Dr. L. J. Hart-Smith for his work presented under the Analysis Methods section, and to Tilak Lall, who prepared the section on Damage Tolerance Analysis.

# THE NATURE OF ADHESION MECHANISMS AND THE INFLUENCE OF SURFACE TREATMENTS ON THE BEHAVIOUR OF BONDED JOINTS

by Dr.-Ing. Walter Brockmann,  
Institut für angewandte Materialforschung,  
Lesumer Heerstraße 36, 2820 Bremen 77, Germany

## 1. INTRODUCTION

Strong adhesion between organic substances like adhesives and metal surfaces is needed in bonded aircraft structures. Its origin can base on three mechanisms:

- Physical bond,
- Chemical bond,
- Mechanical anchoring.

Today it is well known, that the strength of physical bonds between the adhesive molecules and the metal surface, according to van-der-Waal's-forces, is not high enough to produce a strong, temperature resistant adhesion stable over a long time. Therefore many attempts for calculating the adhesional strength on hand of surface- and boundary-energies were not successful. For example it is not always correct, that the higher the surface energy of the metal and the lower the surface energy of the adhesive layer the better the adhesion between both substances must be [1,7].

Today, even without an exact knowledge of the surface structures it can be shown that between structural adhesives and most metal surfaces chemical reactions occur which are desirable from the point of view of strong adhesion, because the enthalpy of reaction of chemical bonds ranges from 250 to 600 kJ/mole, while the energy of van-der-Waal's-forces is in this range from 4 to 40 kJ/mole [2,3,7]. After wetting of the pretreated metal surface the adhesive in its low molecular and reactive form builds up chemical bonds with the oxides and hydroxides on the metal. Phenolates in the case of phenolic resin and perhaps alcoholates in the case of epoxide resins result. Beside these chemical bonds it can be shown, that a high number of bridge bonded hydrogen also are present in the boundary layer. The fact of chemical bonds can be demonstrated on hand of the results of adsorption and desorption tests carried out on aluminium surfaces. In Fig. 1 are plotted the amounts of adsorbed phenolic resin on pure aluminium, which was etched in chromic sulphuric acid under different temperatures. Also plotted are those amounts of resin remaining on the surface after a 24-hour period of desorption in pure solvent. In case of only physical bonds between the sorbate and the metal surface the whole adsorbed amount has to disappear after a 24-hour period of desorption. But on the real aluminium surface approximately 20 to 50 percent of the total adsorbed resin still remains on the metal. This leads to the conclusion, that the adsorption of phenolic resin on metals is a largely irreversible process, due to the action of chemical bonds between resin and metal surface. Of further interest is, that the peel strength of thin aluminium sheets treated in the same manner against phenolic resin, which is also plotted in Fig. 1, shows the same characteristics in dependence on etching temperature like the adsorption and chemisorption curves. Similar results are obtained on other metals with other resins like epoxides or polyesters. So the conclusion can be made, that chemical bonds between adhesive and metal surfaces play an important role in the adhesion zone.

Equal results are obtained if, instead in changing the etching temperature, the surface treatment is changed, Fig. 2. Here are only plotted the resin amounts measured after an adsorption process in a resin solution with a concentration of 10 g/l and an adsorption time of 10 minutes. Further are plotted the remaining resin amounts on the aluminium specimens after desorption for 24 hours in the solvent used in the adsorption process. Afterwards the specimens were stored for different times in other organic solvents of higher polarity, such as ethylacetate, tetrahydrofuran, ethylmethylketone and dimethylformamide. In all cases more than a half of the first adsorbed resin amount still remains on the metal surface. Remarkable are the differences in amounts adsorbed in dependence on the surface treatment. Of special interest is the fact, that on chromic acid anodized surfaces adsorbes  $125 \cdot 10^{-4}$  mg/cm<sup>2</sup> resin compared with  $31,5 \cdot 10^{-4}$  mg/cm<sup>2</sup> and  $9 \cdot 10^{-4}$  mg/cm<sup>2</sup> after chemical pretreatment or etching in chromic sulphuric acid. The higher amounts in the anodized surface are probably due to the higher real surface area, obtained by anodizing process, producing surface layers of a high submicroscopical roughness.

Of a special interest with regard to the aging behaviour of boundary layers is beside the fact, that chemical bonds occur, the question in which way the adsorbed and chemisorbed resin layers react under the aggression of water. Using pure water for desorption after the adsorption process instead of organic solvents, about 25 % of the adsorbed resin are dissolved from the aluminium surface. This is plotted in the right side of the diagram, Fig. 2. A following desorption from the water-stored specimens in dimethylformamide reduced the amount of about 10 % again in case of chemoxal and chromic acid anodized treated specimens. Nearly the same results are obtained in the case of epoxide resin and also, of the resin layers are cured before the desorption process in a organic solvent or water. It could be concluded, that the sorptive bonds between structural adhesives and metal surfaces are of chemical nature, but not absolutely water-stable. That is to understand, if one remembers that bonds between organic adhesives and metal



surfaces occur in form of phenolates or alcoholates or hydrogen bonds. All of them, as a result of hydrolysis, deteriorate in the presence of water.

The water-stability of adhesional forces can also be demonstrated on hand of special strength tests, Fig. 3. Plotted in this diagram is the relative peel strength in dependence on storage time in water-vapour of 133 °C and at a pressure of 2 bars. Peel specimen in these investigations was a thin aluminium foil of 0,15 mm thickness, bonded with phenolic resin on a polyamide plate of a thickness of 3 mm and peeled away with a degree of 180° after the different storage times. In these specimens humidity diffuses over the whole bonded area through the polyamide 6,6 and the adhesive into the boundary layer and weakens there the adhesional forces. This peel test is the only investigation method to obtain adhesional failures between the adhesive and the metal foil in all cases, e.g. in the unaged and the aged state, using all known surface treatments [4,7].

The results show clearly, that compared with an etching of the aluminium foil before bonding in chromic sulphuric acid at 60 °C over a time of 30 minutes followed by a chromic acid anodize process increased the stability markedly. Furthermore an only etching of aluminium surfaces in chromic sulphuric acid of 50 °C over a time of 10 minutes, which is like as the well-known FPL-etching, leads to an adhesion of much lower stability.

The results plotted in Fig. 3 show clearly the superiority of chromic acid anodizing over all other treatment methods. This supports the statements by R. Schliekelmann [5,7], that chromic acid anodize after etching in chromic sulphuric acid for 30 minutes at 60 °C leads to the highest quality in aircraft bonding processes. Equal results can be obtained by using modern epoxide nitrilic resin with corrosion inhibitor primers. The question remains, in which way or by which mechanisms the anodizing processes increase the water-stability of adhesion. Comparing the results of adsorption and desorption tests with phenolic resin on chromic acid anodized aluminium with the results of chromic sulphuric acid etched or chemoxal-treated aluminium, Fig. 2, the relative stability of the adsorbed resin against organic solvents and water is the same as on other treated surfaces. Only the amount of adsorbed resins is about 4 times higher, so it might be possible that only the greater number of adhesional bonds, in case of anodize are due to the better aging behaviour. On the other hand it may be that on anodized surfaces besides chemical reaction another adhesion mechanism is formed, which is due to the higher water resistance. Anodizing processes produce aluminium oxide layers with submicroscopic pores, which are schematically shown in Fig. 4. In these submicroscopic pores of the oxide layer on aluminium, especially produced by anodizing processes, a mechanical linking between a low molecular adhesive and a metal surface is possible. This fact very probably demonstrate the experiments, made by Hartmann [7] many years ago. He pretreated aluminium surfaces with different techniques like chromic sulphuric acid etching and etching with a following anodization in chromic acid. Then he applied on these surfaces a phenolic resin, cured it and removed in a following process the aluminium by etching in alkaline solution. After these processes he investigated the surface structures of the adhesive using an electron microscope. He found that, compared with an adhesive cured on a chromic sulphuric etched aluminium, Fig. 5, the surface on an adhesive cured on etched and anodized surface, Fig. 6, show the greater roughening. In the case of etching and anodizing little knobs in the magnitude of the holes produced by anodizing process in the aluminium surface are clearly to be seen. These results are supported by the investigations of Bijlmer [8,7], who in many cases could demonstrate very clearly a direct connection between the micro-topography of treated metal surfaces and their adhesive properties. This shows very impressive Fig. 7, in which are plotted the peel strength of aluminium phenolic bonds in dependence on etching temperature and the electron micrographs of the metal surfaces etched under different temperatures.

Beside chemical reactions in the interface with no question the micromechanic adhesion plays an important role for water-stable adhesion. Good adhesion is in the extreme case also obtainable, if a metal surface of high submicroscopical roughness like an anodized has no chemical reactivity. Such a surface may be produced by anodizing aluminium in sulphuric acid and then, prior to bonding, adsorbing 5,8-dihydroxy-6-(dodecylaminomethyl) naphthoquinone (1,4) (DDNA), Fig. 8, which reacts with aluminium ions, giving metal complexes of high stability. This gives the anodized metal surface a characteristic violet colour. This compound was chosen, because its aliphatic chain gives it aliphatic properties and due to its molecular weight of 387 it is comparable with resins, e.g. not cross linked resins.

It is known that an anodized aluminium surface is completely wettable for example by water, which has higher surface energy than adhesives. But if on such a surface is before water application adsorbed DDNA, the surface energy of the aluminium becomes nearly the same like that of aliphatic substances, which is to be seen by the water drop, which does not spread on such a surface. In this case the chemical reactivity is saturated by DDNA on a so prepared surface. But if we bond such surfaces for example with an epoxide adhesive in a form of shear specimens, we will find out, that the shear strength of the bonds is the same as for specimens, produced with only anodized aluminium with high chemical reactivity and also a good wettability.

## 2. SURFACE TREATMENT AND BONDING DURABILITY

Without doubt the most important property of a bonded metal joint is today not the initial strength, which is obtained with a special combination of an adhesive, a metal and a surface treatment. Of more importance is the long term behaviour of the bond, especially under hostile environmental conditions, for example artificial or natural climate of high humidity.

As discussed in other lectures, usually the strength of metal bonds decreases in dependence of time as shown in Fig. 9 on hand of the shear strength of aluminium bonds, produced with a simple room-temperature curing 2-component epoxide resin. After storing of the bonded specimens in an artificial climate with changing temperatures and 95 % humidity over a time of 6 of 12 months without mechanical loading the strength decreases about 20 to 50 %. Pickling, which means in Europe an etching process in chromic sulphuric acid over a time of 30 minutes under a temperature of 60 °C, Chemoxal and 2K are different surface treatments. The important aging processes, which decrease the strength, are already completed after 6 months. This may be concluded from the small differences in strength values after 6 and 12 months storage. Additional shear stress involved in epoxide or more drastically in polyurethane resin bonded joints in an alternating climate have a more detrimental effect on these joints. This is of importance not in regard to the residual strength, but in particular to the general loading capacity of bonded parts under action of detrimental environmental influences. The load applied to the specimens during the aging process was only 0.07 kp/mm<sup>2</sup>, but also under this small loading in the case of Chemoxal and 2K-treated metals some specimens failed after 170 or 120 days during the aging process.

Apart from the pure load bearing capacity in alternating climate there are only slight differences between the chromic sulphuric acid etched and the Chemoxal treated bonds.

The load bearing capacity is not in all cases as low as shown here on hand of the adhesive Araldit 106. Using modern aircraft adhesives, better results are to be obtained as shown in Fig. 10 for aluminium bonds produced with the modern 1-component epoxide resin FM 123/5. Nearly equal results are to be obtained using phenolic or polyimide adhesive, for example FM 34 from Bloomingdale Corp. All these adhesives are not destroyed in the natural or artificial climate under the additional dynamic load of 0.07 kp/mm<sup>2</sup>, which was applied with a frequency of 40 load cycles per minute. A difference between the residual strength after aging the specimens without load and under load is not clearly to be seen. Both surface treatments, in this case the chromic sulphuric acid etching with following during current anodizing in sulphuric acid and Chemoxal process give nearly the same results in the aging behaviour. With exception of the polyimide resin FM 34 the fracture surfaces of nearly all specimens show, like to be seen in Fig. 11, an increasing part of adhesional failure up to 20 % and more of the whole bonded area after one year in natural or artificial climate. This fact leads to the conclusion, that not the aging processes in the glue line itself, but the changing of the adhesional forces between adhesives and metal surfaces is the most dangerous aging process in metal bonds. The glue line aging is dependent upon the area of the bonded joints and comes after a half or one year to an equilibrium using this shear specimens, leading to a decreasing of the residual strength of the bonded joints of about 20, 30, or in the case of the 2-component epoxide resin, 50 %. The weakening of adhesional bonds by diffusing water or other processes does not come to an equilibrium and decreases the bonded joint strength continuously in dependence upon the time and, what is very important to note, with higher speed when the joints are unloaded under environmental conditions.

This effect may not easily to be seen in aluminium bonds which are aged only over a time of a half or one year, but is drastically demonstrated, for example, on mild steel bondings, produced with an 1-component epoxide resin FM 123/5, Fig. 12. If the surfaces of the bonded mild steel before adhesive application were sand-blasted, the strength of the joints decreases about 30 %. This process is quicker, if the specimens are dynamically loaded. If the metal surfaces before adhesive application are only degreased in organic solvents, the steel bonds will be destroyed totally after 6 months without load and under load they break down after a time of 60 days under natural climate. Also in artificial climates the strength decreases after 6 months to about 50 %, and under load the bondings break down after 120 days, which shows, too, that the aging process under load is quicker than without load. In Fig. 13 the fracture surfaces of such bonds on the left side show, that the corrosion totally had destroyed the adhesion, on the right side that the corrosion of the sand-blasted steel from the sides of the bonding area run slowly and to the adhesive area deteriorating the strength. Equal results can be obtained for example using phenolic resins.

These results are important in considering, that corrosion behaviour of sand-blasted steel is not so good than that of an only degreased steel surface. Electrochemical measurements of the potential of the steel surfaces in sea-water against a Kalomel-electrode show at degreased surfaces a potential of -450 mV<sub>H</sub> and after sand-blasting a potential of -500 mV<sub>H</sub>. On the other hand, the reaction between the adsorbed phenolic molecules and the metal surfaces will not produce a higher passivating effect on sand-blasted steel, too. Because it is also well known, that the stability of the chemical bonds between adhesive and metal surface in the case of sand-blasting is not higher than in the case of degreasing, the better long term behaviour of the metal bonds after sand-blasting can be only explained by mechanical anchoring of the adhesive in the roughened surface produced by the sand-blasting process.



These results lead to the conclusion, that there are three ways for a systematic optimization of the durability of metal joints. The first is, to produce by special surface treatments, surfaces of a high submicroscopical roughness, like in the case of aluminium by etching in chromic sulphuric acid and a following anodizing process. Then the adhesive is anchored mechanically. Results of such tests are shown in Fig. 14, in which are plotted the strength values of unaged and aged shear specimens produced with the adhesives FM 123/5 and FM 73. The aging was made by storing the specimens over a time of 720 hours in climate of 65 °C and 95 % relative humidity without load. Compared in this diagram are the surface treatments: FPL-etch, phosphoric acid anodize, the in Europe used chromic sulphuric acid etch (pickling) over a time of 30 minutes under 60 °C, chromic acid anodizing (after CSA-etching) and the sulphuric acid anodize.

At first it is to be seen, that the aging behaviour of the FM 73 bonded joints is better than that of joints bonded with FM 123/5. Especially in the case of FM 73 it is also to be seen, that the FPL-etching leads to the lowest strength values. More stability is obtained by using the European chromic sulphuric acid etch-process. Differences between phosphoric acid anodize, which is new developed in the United States, and the chromic acid anodize used since more than 20 years by European aircraft manufacturers, are not to be seen. Also the sulphuric acid anodizing leads to good results in these investigations. Its disadvantage is the effect of high hardness of the surface layers produced by this process, which leads under higher deformations to micro cracks and the danger of corrosion.

A second way of systematic optimization of the long term behaviour of metal bonds is replacing the not water-stable chemical bonds between adhesives and metal surfaces by water-stable bonds. This is for example possible by coating the aluminium surface prior to adhesive application with organic substances, which can react with the aluminium oxides and hydroxides in form of water-stable metal complex bonds and with the adhesive in form of water-stable covalent-bonds. As an example in Fig. 3 are plotted the results obtained with 5.7.2.4-Tetrahydroxylavonene (Morin), a heterocyclic substance, reacting with aluminium oxide in form of water-stable metal complexes, which fluoresces. The results shown in Fig. 3 are only first steps and further research work must be done in this field.

The third way of increasing the durability of metal bonds is to reduce the diffusion velocity of water in the adhesive layer by using silanes as additives. During the first step of investigation in this direction the opinion was, that silanes used as primers react with SiO-bonds with the metal oxides and for example with their epoxide groups with the adhesive monomers. But during further work it was found, that the increasing of the durability of the bonds was better mixing the silane, for example epoxi- or amino-silanes (ca. 5 % of the adhesive weight) into the adhesive prior to its application on the metal surface. Some results are plotted in Fig. 15, which shows the shear strength of metal-wood-bonds in unaged and aged state in dependence on surface treatments of the metal, in this special case grinding and sand-blasting, and using a silane-additive in a room-temperature curing 2-component epoxide adhesive. Aging process in this case was storing the specimens in water with 0.5 % tensile at a temperature of 40 °C for one week. The high grade of decreasing of shear strength is due to the fact, that in case of metal-wood-bonding the water can diffuse very quickly through the wood and the glue line in the whole bonding area. The fact that silane reduces the velocity of water diffusion in the glue line can be demonstrated by using special substances mixed into the adhesive, which's colour, for example in the case of dihydroxynaphtoquinone violet, disappears, when water comes into the adhesive layer. The dihydroxynaphtoquinone changes perhaps into its colourless leuco-compound. Also this new way in systematically optimizing the long term behaviour not by increasing the stability of adhesion against water but by inhibiting the water diffusion into the glue line, is not completely developed and further work must be done.

### 3. TEST TECHNIQUES FOR SURFACE PROPERTIES

All results discussed here demonstrate clearly, that the state of surfaces to be bonded is beside the kind of the used adhesive the most important factor for the strength and durability of metal bonds. To test the initial strength of bonded joints in dependence on surface treatment and the durability in long time aging tests on unloaded or loaded joints, the tensile shear test with single overlapped joints and an optical analysis of the fracture surfaces under the aspect of cohesive or adhesional failures is successful to use. If only a short time is available to check for example the water stability of adhesion in metal bonds during the production in the aircraft industry or also in the research laboratory, the tensile test specimen is not usable, because after aging times of for example some hours or days in a humid climate or in a salt-spray test only cohesive failure occur in the bond line. Therefore conclusions on the adhesional stability on hand of the test results are not possible.

So in the most cases as a control method for the quality of the surface treatment process different peel tests like T-peel, CIBA-peel, Bell-peel, or climbing-drum-peel tests are carried out. If in testing with these test methods the peel strength of a metal-bond adhesional failure occurs it is correct to conclude, that the surface treatment was insufficient. The same is possible after long time aging of a peel specimen. In case of short time aging of the specimens for example in humid climate of 60 °C and 95 % relative humidity the peel strength of conventional specimens and also the mode of failure doesn't change. Therefore especially in the United States a new test method, the so-called "wedge-test" was developed, in which in a bonded specimen in an unaged state by departing



the joined metal plates by a steel wedge a crack in the bond line will be produced. With the steel wedge between the joined parts, that means with high stresses on the top of the crack, the specimens are stored for example over a time of some hours or days in humid climate or a salt-spray chamber. In the case of insufficient surface preparation the crack changes from the glue line into the boundary layer between adhesive or primer and metal surface and propagates here the quicker the lower the adhesion stability against water is. So the wedge-test, which is a simplified or modified fracture toughness test method, seems to be usable for a short-time testing of the long-time behaviour of metal bonds in dependence upon surface treatments [6,7]. Following the literature this is true for comparing the adhesion stability produced in metal bonds by using the FPL-etch method and the phosphoric acid anodize as a new surface treatment. On the other hand our investigations lead to the result, that neither in the case of European CSA-etching nor in the case of chromic acid anodizing in wedge specimens which are shown schematically in Fig. 16, adhesion failures occur during aging the specimens for example over a time of 144 hours in a artificial climate of 60 °C and 95 % rel. humidity or over a time of 6 months in the natural climate of northern Germany. Fig. 17 shows the results of these investigations in which the surface treatment in a production line of a German aircraft factory over a time of a half year, in which was used the same etch-solution, and European chromic sulphuric acid process was used. In the upper part of Fig. 15 are plotted the concentrations of sodiumdichromate and sulphuric acid, which changed in dependence upon the time the etching solution was used. Following the measured concentrations before etching the surfaces, at the time E 4 sulphuric acid and sodiumdichromate were added to the solution. The same may be possible at state E 6 and E 8. The properties of metal bonds with aluminium 2024 clad and the adhesive FM 123/5 with pretreated metal parts etched in the solution of the aircraft industry directly in the production line are shown in the lower part of Fig. 17. Crack growth in wedge specimens after aging process of 144 hours in humid climate shows no differences in the adhesion stability. In all cases the crack propagates in the glue line and not in or near the surface of the metal. The strength of adhesion and also its stability in all cases was better than the cohesion strength of the adhesive, so that the test results allow no conclusion on the adhesion stability in dependence on surface treatment. As a control method for the surface preparation during the production a wedge-test compared with a conventional peel-test gives no advantage.

In testing the real adhesion conditions in unaged and aged metal bonds produced after advanced pretreatments like European CSA-etching or anodizing processes remains only the 180° peel-test, which is described before and schematically shown in Fig. 18. The test involves peeling off the thin foil in a small testing machine with a peel angle of 180° with a velocity of 15 mm per minute, which comes to a peel rate of 7,5 mm per minute. The small peel radius of the thin foil associated with a peel angle of 180° is desirable, since in all cases the failure occurs as a result of an adhesion failure between the metal foil and the adhesive. To facilitate a uniform invasion of water in the bonding area during a short time of aging, for example in water vapour at 133 °C the rigid plate may be made from polyamide 6.6. Especially at higher temperatures, water diffusion occurs through this material very quickly. Before application of the adhesive of the adhesive the polyamide is sand-blasted in the area to be bonded, so that the adhesive strength between structure adhesives and the polyamide is sufficiently high to withstand the peel-test. Results obtained by using this test method in controlling aircraft industry etch processes are also plotted in Fig. 17. In an unaged state the peel strength and in this case the adhesion show without exception no differences of the etch state. Differences occur in the stability of the adhesion, which is to be seen on hand of the peel strength, after aging the specimens over a time of 10 hours in water vapour of two bars pressure, which corresponds to a temperature of 133 °C. In today's state of knowledge such a peeling method is the only practicable method to investigate the adhesion stability in metal bonds within a short time.

To control exactly the effect of surface treatments especially in the production line the test of specimens prepared together with the original parts is, as well known, very insufficient. For a better quality control of the bonding process for example in the aircraft industry, nondestructive testing methods are needed, which allow to measure on the surface of real parts and not only small specimens. They have to measure important properties for a good adhesion, which are the chemical behaviour and the topographic properties. Grease, for example, has to be absent and chemical reactive compounds, like oxides, have to form the upper layer of the metal. For laboratory purposes a number of methods like SIMS, ESCA, AES, etc. have been developed. Most of them are only working in vacuum or high vacuum, which can change the surface properties before measuring compared with those to be bonded. Each of these analyzing methods lasts a rather long time, costs a lot of money and is not usable directly in the bonding shop as a quality control for pretreated parts to be bonded. So they hardly can be used for routine tests in a production line.

Beside these methods today only two really simple tests for the detection of contaminants and control of pretreatment in bonding or plating processes are used. One is measuring the contact angle or the wettability, the other one is the determination of the exoelectron emission by measuring the contact potential difference against a standard material. A rather new method for this purpose is the remission photometry, from which some results will be discussed.

Checking the wettability of metal surfaces after pretreatment processes is the oldest known test method. A drop of liquid, mostly water, is applied to the surface, and with a lamp and a lens the drop is projected to a scale for measuring the contact angle between which and the surface tension and the surface energy is a well known dependence [9,7].

Theoretically good adhesion will occur, when the surface energy of the metal is higher or equal to the surface energy of the liquid. In this case the contact angle becomes small or even zero and the liquid or adhesive spreads. This rule - small contact angle equal to good adhesion - is fulfilled on metal surfaces in most cases. A few exceptions are known, but today they seem to have no significance for industrial bonding [10,11]. But the surface tension is a matter of change if we use big polar molecules, like adhesive oligomers. They can adsorb either with aliphatic parts or with heteroatomic groups. This complicates the calculations, because the surface tension must be splitted into terms, which can not be measured in a simple way.

In the most cases the contact angle can not be measured with the adhesive itself, because of its high viscosity. Therefore a liquid of known surface tension is used instead of the adhesive and the required optimum contact angle must be taken from empirical developed equations [9]. Further the wettability is not really a nondestructive test. The liquid will affect the surface for example by adsorption. Another disadvantage is, that the wettability is measurable only in small test spots and not over the whole area of prepared and correctly dried surface. Considering these facts, the contact angle measurement may be a helpful method for testing quickly simple pretreatments of metal surfaces in practice. Doing this, many uncertainties still remain, because a low contact angle must not indicate good adhesion, and vice versa.

The second method for measuring properties of metal surfaces in dependence on pretreatment is the investigation of the electron emission on hand of the contact potential against a standard material. The first investigator of the contact potential was Count Alessandro Volta in 1802, who hold an experimental lecture at the Academie Francaise about this phenomenon. The effect he showed was later named "Volta potential" or "exoelectronemission". It was published again by Lord Kelvin in 1896 [12]. He used a new measuring device which is used in modern form even today containing a capacitor with one plate oscillating. Through the oscillating a voltage is induced, if different metals are taken as plates of the capacitor. Measurements are made by compensation method. Later it was found out, that this method can be used as a real nondestructive system for measuring of surface properties [13].

The electron emission of a metal depends markedly on the manner of surface treatment and on the time between treatment and measuring [14]. Using these facts the Dutch aircraft builder Fokker developed a device for measuring this effect automatically [15]. It is shown in Fig. 19. In this system the surface to be bonded is compared with a gold surface as a standard which means that the measurement give no absolute values, but the contact potential difference between the both metals. The gold surface is said to be constant, which could be verified very well in a lot of experiments. So properties measured on one a surface can be compared with such of another surface, for example after another treatment. On a first glance this system seems to be ideal, because the only thing to do is to set the capacitor shown in the Fig. 19 on the metal surface to be investigated and read the value of the potential on the display after some seconds. The surface will not be affected by the measurement, because only a small metal ring touches it, which gives the optimum distance for the capacitor plates and closes the electric circuit. Using this device smallest differences in the surface state produced for example by variation of etching time or etching temperature, which influence the adhesional properties, too, are detectable. Although this is well known since more than 100 years surprisingly it was found again a fourth time and the results were published recently [16].

The volta potential of the metal surface is, without explaining the theory of this phenomenon, defined as the difference between the work function of the two contacting metals. As the surface activity increases, the work function is lowered and higher volta potentials are the result. As the surface activity decreases, the work function is increased and lower volta potentials are the result. Real volta potentials are difficult to measure, because of influences of the environment. So it is better to use the term surface potential. This value, measurable under normal environmental conditions, for example, between aluminium and a reference of gold is considered as constant is than a function only for the surface state of aluminium, i.e. its effective work function. This increases, if negative potential exists near the surface or vice versa. It decreases after application of an increasing external potential. Due to thermal expansion the work function depends on the temperature, what is also demonstrated in [14]. A very important factor is, that the work function depends on the crystallographic orientation, which also influences the structure of oxide layers. Further adsorbed contamination layers influence the work function.

After this, it is easy to understand, that a defined connection between the measured values in dependence on surface treatment or its parameters and the strength of metal bonds to be reached after the same pretreatments doesn't exist. This is for example to be seen in Fig. 20, in which is plotted the peel strength and the volta potential, measured in aluminium, bonded with phenolic resin in dependence on the temperature of the European CSA etching prior to the bonding. Also under variation of other parameters like etching and measuring no connections between the characteristic of the contact potential difference and the peel strength or sheat strength is to be obtained. So the only thing which can be said is, that at a certain value of the potential may be expect an optimum of adhesion. Is such a value not measurable on a pretreated surface, it can not be stated that the adhesion may be better or poorer, but only that the pretreatment was not absolutely correct. So the method with its high sensivity allows to find nearly all mistakes made during the pretreatment or induced by different surface properties of the metal prior to treatment, but it gives not directly hints to the surface's capability



to produce a good and stable adhesion against organic substances.

But in their very important scientific work about measuring the surface potential differences Bijlmer and Schliekelmann [15,17] could demonstrate some interesting connections between the morphology of especially aluminium surfaces after pretreatment and their bondability and also connections between the morphology investigated by electron microscope and the easily measurable contact potential against gold. With help of an electron microscope they found out, that the well known chromic sulphuric acid etching on aluminium surfaces can produce different surface configurations as also shown in Fig. 7. In Fig. 21 four typical surface structures are to be seen. The oxide layer, called type I, is found on aluminium after a short etching at low temperatures containing residual oxides from the original surface. The bondability of this layer measured on its initial strength can vary in wide ranges and has no importance in practice. The smoother surface, called type II, with only macroscopic large etch pits is typical for poor bondability and for example formed in exhausted bath solutions. In type III filiform like preferential etching is evident. This may be local galvanic cells with anodic potential, moving on the surface, forming a string of anodic oxides. This network becomes finer and finer until a critical dimension is reached and the cathodic area starts to fall up with anodic sites in a pit-like form, which is to be seen in Fig. 22. Type IV is a fully developed etch-pit configuration, which is typical for optimal bondability. In this case, high peel strength values are found on this type of surface with low scattering in strength. Bijlmer and Schliekelmann further could demonstrate on hand of electron micrographs, that the surface morphology by reacting process still exists on top of the anodic layers, produced for example after the CSA-etching by a chromic acid anodizing process. This seems logical, because the formation of the anodic layer takes place below the surface by oxidation of the aluminium. In the small pores initiated by the etching process and deepened by the anodic treatment with high probability the adhesive invades in a monomeric state and cures there. This leads, as shown earlier, to a micromechanical anchoring of the adhesive layer, which may be due for the high water stability of the adhesional zone.

Bijlmer and Schliekelmann could show in their work, that the typical oxide types which its clear correlation to bondability are measurable not only by using an electron microscope, but also on hand of the surface potential using statistical methods. They could show, that type IV with good bondability produces potentials between 750 and 950 mV, whilst for example type I and type II produce lower potentials, and type III such of more than 960 or 1000 mV.

In this way the contact potential difference measuring method can be used in special cases for controlling the bondability of metal surfaces in dependence on its treatment or also on particular parameters of the treatment like degreasing, deoxidizing, etching, anodizing process and also the concentrations and temperatures of the solution to be used and the treatment times. Further it is controllable, in which way the treated surface will be contaminated before the adhesive application for example by grease, impure water or finger prints, which all change the surface contact potential. Though this measurement method doesn't solve all problems in quality control by measuring surface properties, it will be a good help in producing metal bonds of good quality.

The third method for a simple surface test depends on the optical behaviour of metal surfaces. It uses two effects: The good reflexion of light by metals and the absorption of light by oxides and contaminants. Reflexion is highly affected by the roughness of a technical metal surface. Measurements with integrating sphere can suppress this, because nearly all the back scattered light reaches the detector. Fig. 23 shows the principle of the sphere, which is mounted in a common double beam photometer. Measurements with this device can be made in the region from 200 to 800 nm, in which nearly all organic compounds and many oxides absorb light. Like in most photometric methods it is only possible to determine the difference between the sample and a standard. Some first results may demonstrate that using this system on technical surfaces three phenomena of high importance for bondability are measurable: the growth of an oxide layer, the efficiency of pretreatments and the presence of non metallic layers like contaminants or adhesives and their chemical reactions with the oxides or hydroxides.

That sometimes the oxidation is good controllable shows Fig. 24, in which is plotted the absorbance of light at a wave length of 500 nm by a copper surface in dependence on time after grinding. In this case the standard was magnesium oxide. In this special case at a wave length of 500 nm copper oxides have nearly a maximum of light absorption, while copper itself absorbs not very strong. The curve follows a root function, which is also known from other measurements for the oxidation of this material [19].

The second example describes the efficiency of a surface treatment of steel and the following oxidation after an etching process, Fig. 25 [18]. In this experiment the steel surface was ground, etched with diluted hydrochloric acid for 2 minutes, rinsed with water and methanol and dried in warm air. The reference specimen was steel, which was only ground in the same manner as the sample. After grinding both surfaces were compared, and even then they show differences. Directly after etching the sample then absorbs at 350 nm less than the not etched reference. This result shows that the surface becomes cleaner by the etching, because the absorption of light at this wave length is due to oxidation products. After this measurement both surfaces, only ground and ground and etched, were stored in normal climate and after three and seven days compared again in the photometer. It is clearly to be seen, that after a week the etched surface absorbs more light in the 350 nm range than the reference surface due to more contamination by oxidation or corrosion products. This leads to the conclusion, that the che-



mical reactivity of a ground and etched surface must be higher than that of an only ground surface.

In the next experiment tracer labelled phenolic resin was adsorbed on a CSA-etched aluminium surface, and at first on hand of the radioactivity the adsorbed amount was determined to 0.5 mg/cm<sup>2</sup>. In a following test the aluminium surface with the phenolic layer was compared in the photometer with an equal pretreated aluminium surface without phenolic layer. Fig. 26 shows the results of the remission photometric measurements. There is a small maximum at 280 nm. In curve 2 the existence of the organic layer is to be seen, because the organic molecules absorb light at this wave length. Also plotted in Fig. 26 are curves received with an sulphuric acid anodized aluminium surface with the same test technique. It is clearly to be seen on hand of the absorbance at about 250 nm, that the absorbed amount is extremely high compared with this on only CSA-etched specimens. Together with measurements on other surfaces it was found out, that the absorbance follows the Lambert-Beer's-law, so that it is possible to make with remission photometry quantitative determination of compounds on metal surfaces. This may be of importance, too, in carrying out tests on surfaces after adhesion failures of bonded joints. Further changes the wave length of the maximum of light absorption on the anodized surface compared with the CSA-etched indicating in case of anodizing chemical reactions between the phenolic resin and the metal surface. So it is not only possible to determine adsorbates, but also detect chemical reactions, from which it is possible to make conclusions to the chemical reactivity and adhesional properties of the oxide layers, produced on the metal by surface treatments. For these measurements of the chemical reactivity of the surface it will also be possible to use special substances which give a higher sensitivity of the remission photometric system than phenolic resin. Such substances may be also applied in practice during surface control by photometry, because it is possible to give them a chemical structure, which will not reduce the adhesional capacity of the surface. On the other hand it is possible to measure directly for example the reactions between primer layers and the pretreated metal surface as a simple control for a good adhesion and perhaps thickness of the primer.

The results presented here are first steps in using the photometric device for measuring the adhesional properties of metal surfaces. The measuring device can be simplified so that it is usable in a bonding shop. Probably it will be in addition to the measuring of the surface contact potential a further simple and nondestructive system for measuring the reactivity, the oxidation, and the possible contamination of technical metal surfaces.

#### REFERENCES

- [1\_] Mittal, K.L.: The Role of the Interface in Adhesion Phenomena. Polymer Eng. a. Science 17 (1977) H. 7
- [2\_] Lewis, A.F. and L.J. Forrestal: Chemical Nature of Polymer to Metal Adhesion, in: Adhesion, Spec. Techn. Publ. ASTM Philadelphia 1964
- [3\_] Brockmann, W.: Nondestructive Testing of Adhesive Properties of Metal Surfaces, in: Aerospace Adhesives and Elastomers, SAMPE Conference Rep. 1970
- [4\_] Brockmann, W.: Interface Reactions and their Influence on the long term Properties of Metal Bonds; Adhesive Age 20 (1977) No. 7, p. 30/34
- [5\_] Schliekelmann, R.J.: Adhesive Bonding in the Fokker-VFW F 28 "Fellowship"; Rep. Fa. Fokker VFW Shipol, 1973
- [6\_] Bethune, A.W.: Improvements in Environmental Stability of Bonded Aircraft Structure; Lecture on the 19th SAMPE-Symposium Buena Park, Cal., 23.-25.4.1974
- [7\_] Hartmann, A.: An Investigation on the Effect of the Pretreatment of the Metal and the Strength and Adhesion of Adhesive Bonded Joints making Use of Electron Microscopy; National Luchtvaart Laboratorium, Amsterdam July 1961
- [8\_] Bijlmer, P.F.A.: Potentiostatical Pickling as an Alternative for Sulfo-Chromic pickling prior to Adhesive Bonding; Congress Report of "interfinish 76", Amsterdam 1976
- [9\_] Houwink, R. and G. Salomon, Ed.: Adhesion and Adhesives, Vol. 1. p. 29/52
- [10\_] Brockmann, W. and H. Kollek: Possibilities of Increasing the Stability of Adhesion in Metal Bonds. Paper presented on 23rd SAMPE Conf. May 2.-4. 1978, Anaheim, Cal.
- [11\_] Mittal, K.L.: The Role of the Interface in Adhesion Phenomena; Polymer Eng. a. Science (1977), H. 7
- [12\_] Lord Kelvin: Contact Electricity of Metals. Philosophical Magazine and J. of Science 46 (1898) 82/120
- [13\_] Kramer, J.: Oberflächenuntersuchung an Metallen mit Exo- und Photoelektronen. Z. Physik 133 (1952) 629
- [14\_] Brockmann, W.: Die Exoelektronen-emission als Maß für die Adhäsionseigenschaften metallischer Oberflächen; Adhäsion (1973) H. 8, p. 276/87
- [15\_] Bijlmer, P.F.A. and R.J. Schliekelmann: Fokker Contamination Tester. Fokker-VFW-Report No. R-1810, December 1975

[16] Kim, D.H. a. E.F. Sutliff: The Contact Potential Difference (CPD) Measurement Method for Prebond Non-destructive Surface Inspection. SAMPE - Vol. 23, p. 243/52, SAMPE, Azusa 1978

[17] Bijlmer, P.F.A.: Characterization of the Surface Quality by Means of Surface Potential Difference in: 4th Intern. Symposium on Contamination Control. ICCCS, Washington, 1978, p. 247/58

[18] Kollek, H. a. W. Brockmann: Detection of Surface Contaminations in Metal Bonding by Simple Methods; in: 4th Intern. Symposium on Contamination Control. ICCCS, Washington 1978, p. 298/300

[19] Hauffe, K.: Reaktionen in und an festen Stoffen; Berlin-Heidelberg, New York 1966.

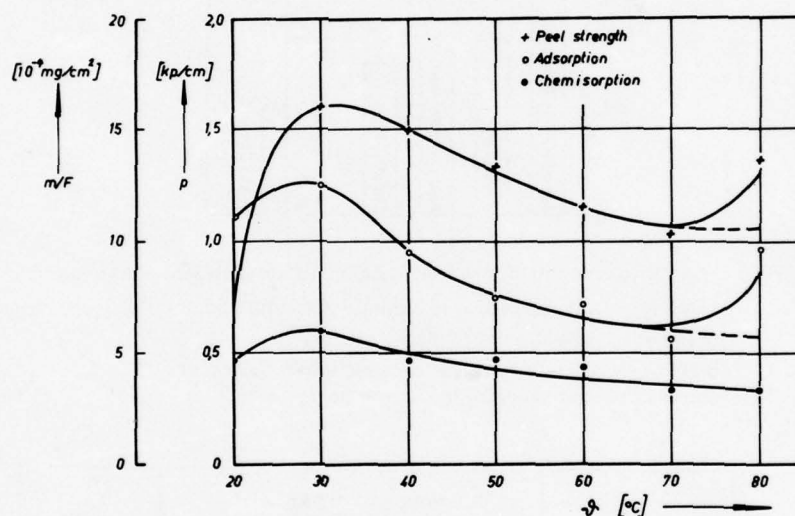


Fig.1 Adsorbed and chemisorbed phenolic resin and peel strength in dependence on temperature of chromic sulphuric acid etching of aluminium (etching time 30 min)

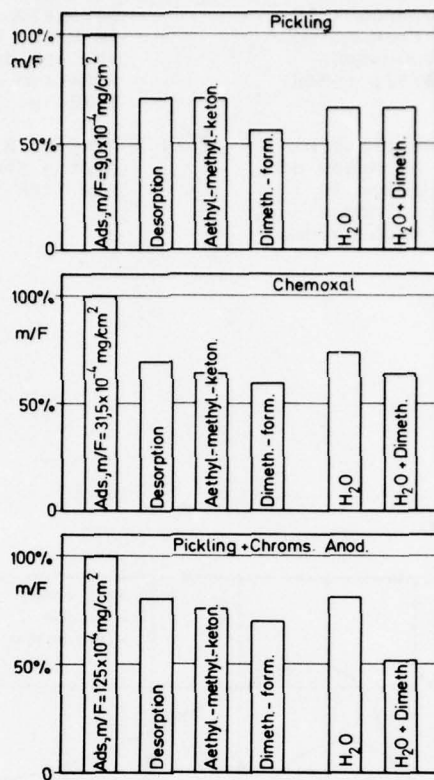


Fig.2 Adsorbed amounts of phenolic resin on different treated aluminium  
 pickling: 30 min etched in chromic sulphuric acid at 60°C  
 chemoxal: new developed alcalic process  
 pickling + 30 min etched in chromic sulphuric acid at 60°C  
 chroms.: and anodized in chromic acid

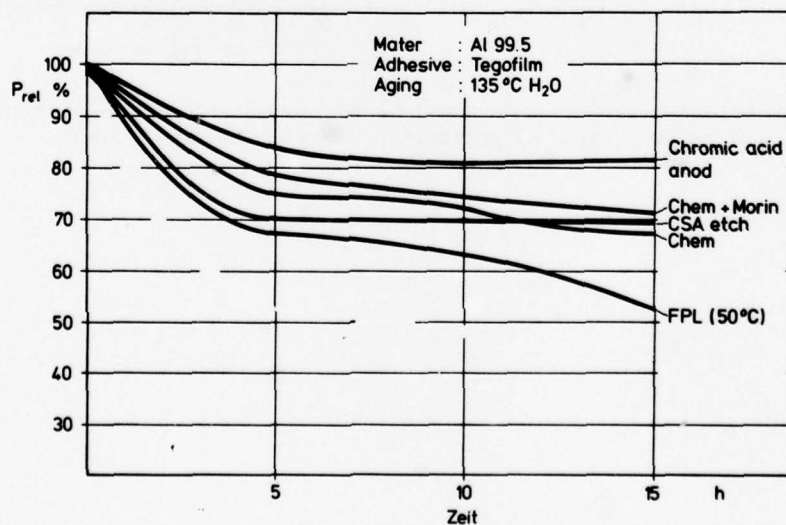


Fig.3 Relative peel strength of aluminium-polyamid bonds in dependence on storing time in water vapour



# OXIDE CHARACTERIZATION

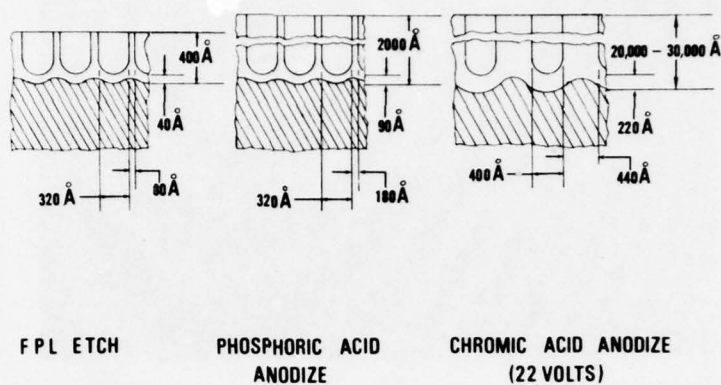
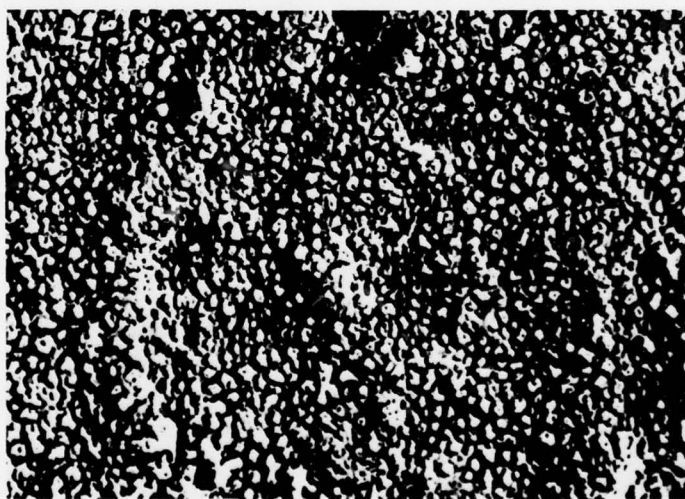


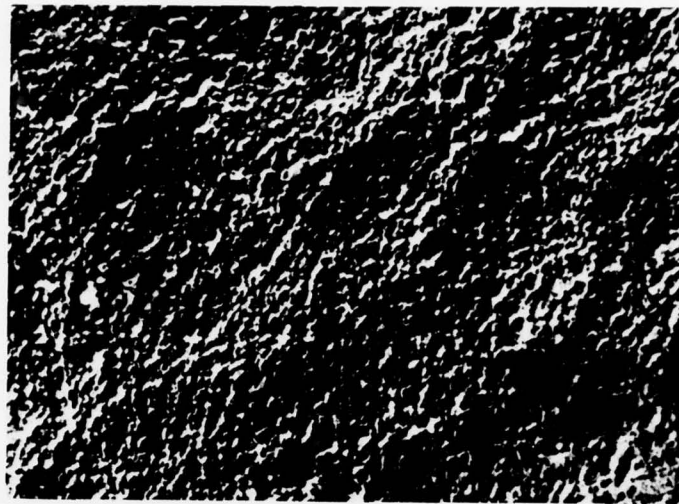
Fig.4 Oxide characterisation



Nach A. Hartman

0,5 μm

Fig.5 Adhesive surface after curing on CSA etched aluminium [7]



Nach A. Hartman

0.5  $\mu\text{m}$ 

Fig.6 Adhesive surface after curing on CSA etched and chromic acid anodized aluminium [7]

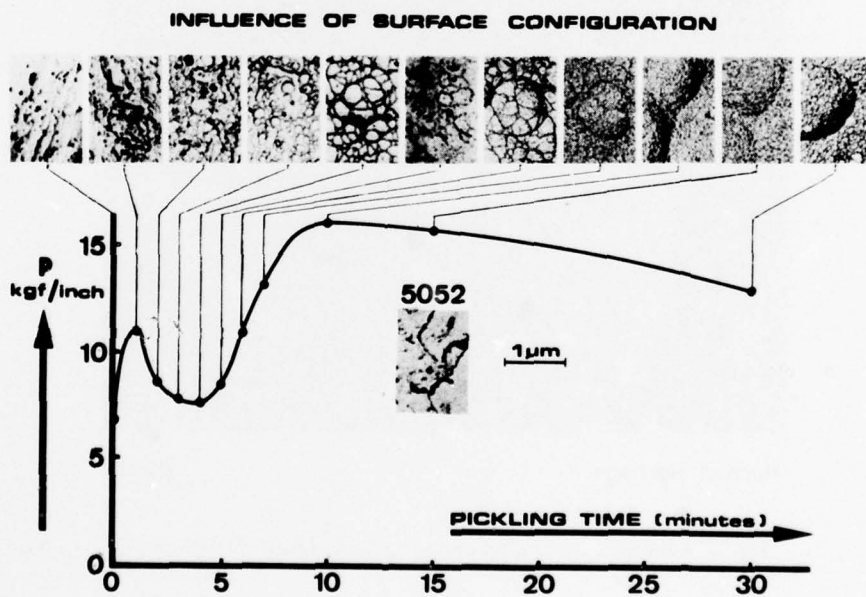


Fig.7 Surface topography and peel-strength in dependence on etching time material: Hydronalium 5052

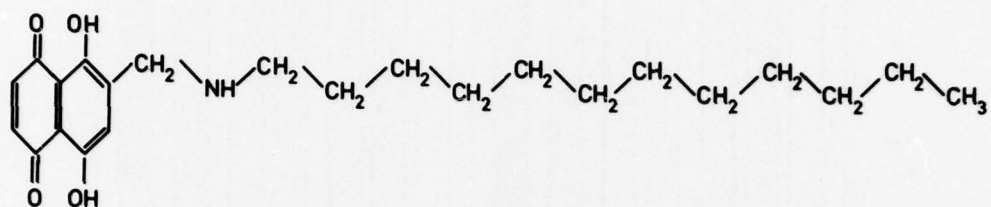


Fig.8 5,8-Dihydroxy-6-(dodecylaminomethyl)-naphthoquinone (1,4)

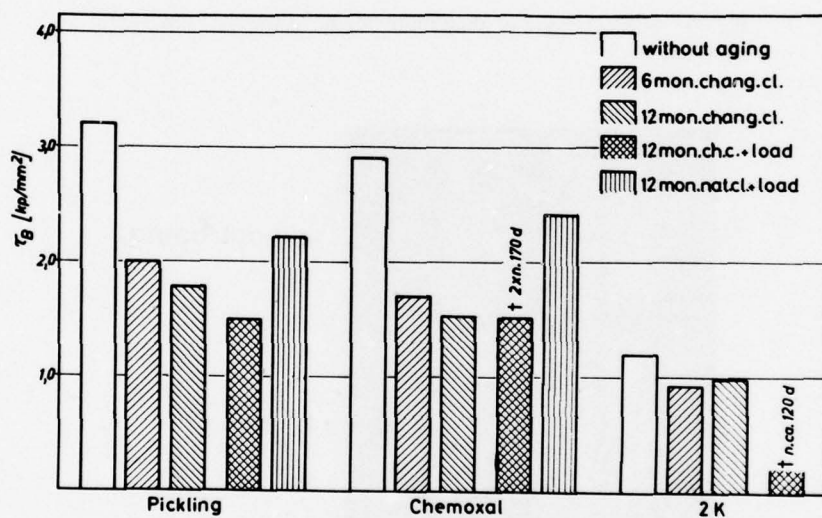


Fig.9 Shear strength of aluminium-bonds. Adhesive: Araldit 106



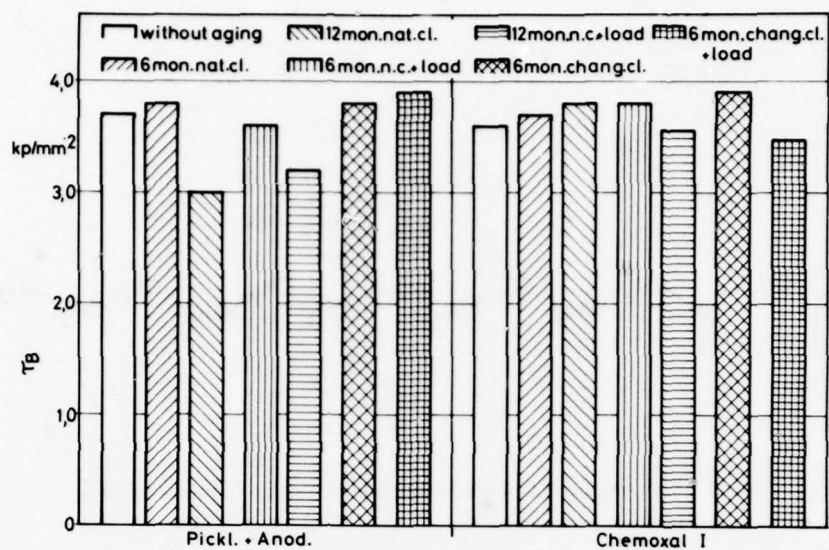


Fig.10 Shear strength of aluminium-bonds. Adhesive: FM 123/5

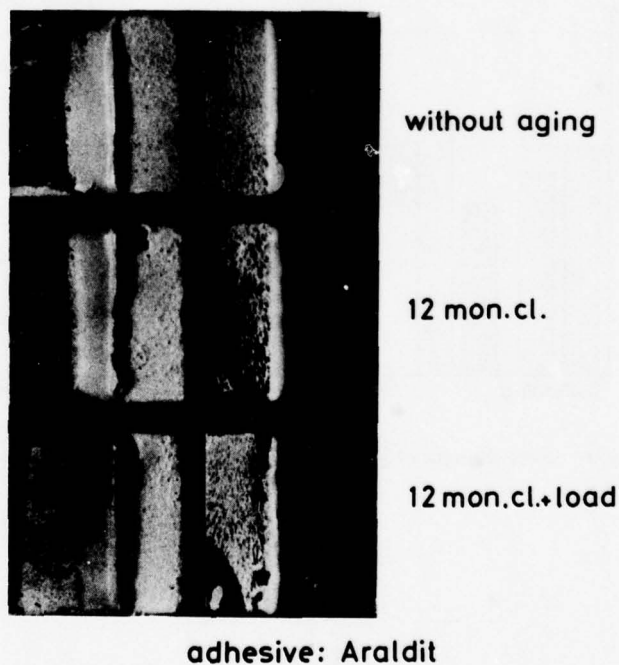


Fig.11 Shear strength of steel-bonds. Adhesive: FM 123/5

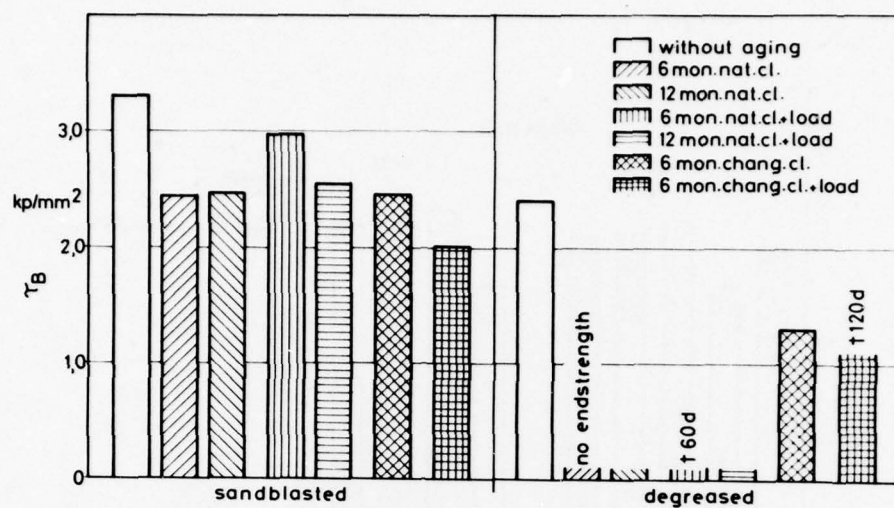


Fig.12 Shear strength of steel-bonds. Adhesive: FM 123/5

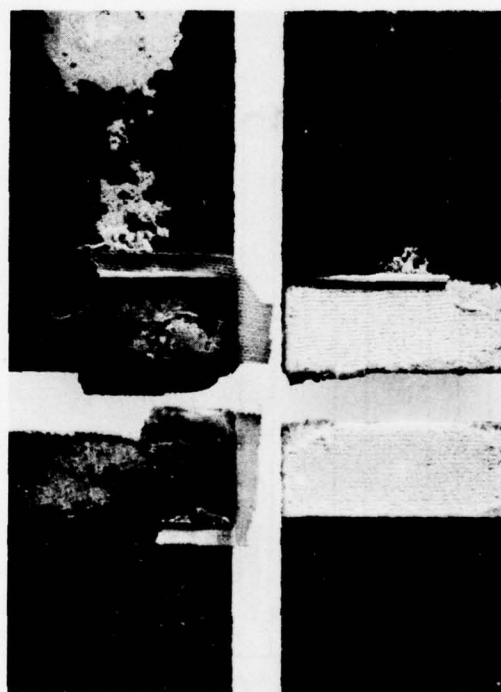


Fig.13 Fracture surfaces of mild-steel-bonds after aging in humid climate.  
left: degreased, right: sand-blasted. Adhesive: FM 123/5

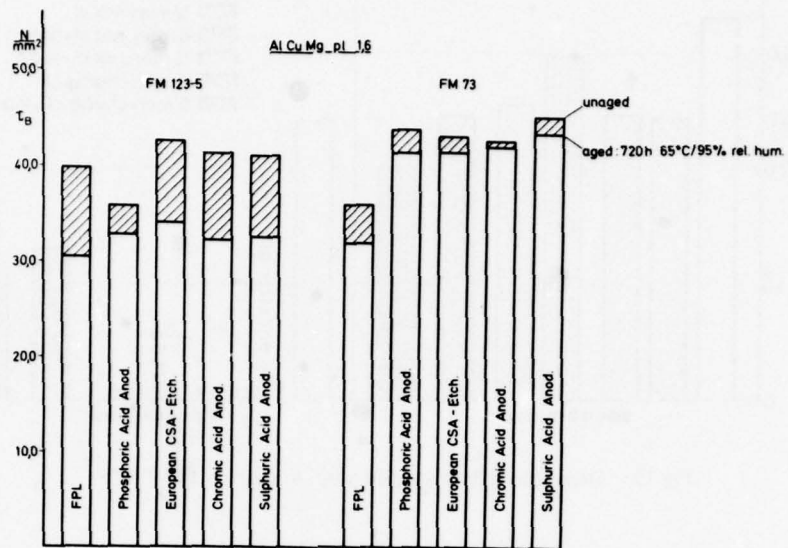


Fig.14 Shear strength of aluminium-bonds. Aluminium alloy 2024 clad

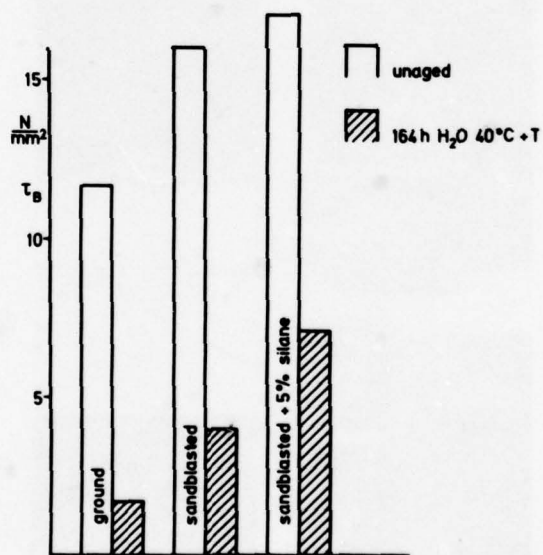


Fig.15 Shear strength of aluminium-wood-bonds



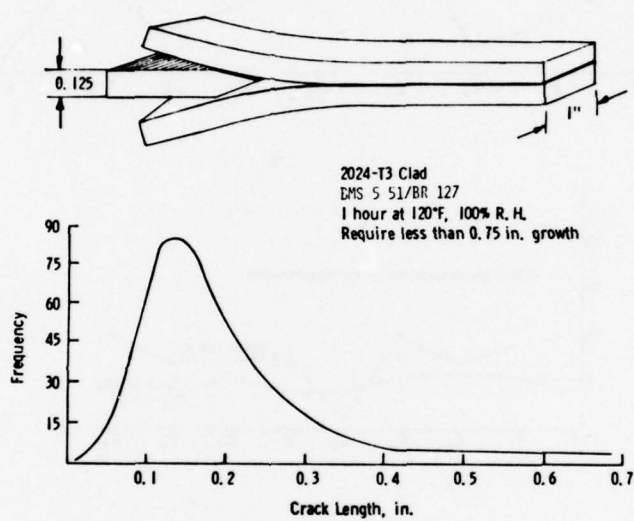


Fig.16 Wedge specimen

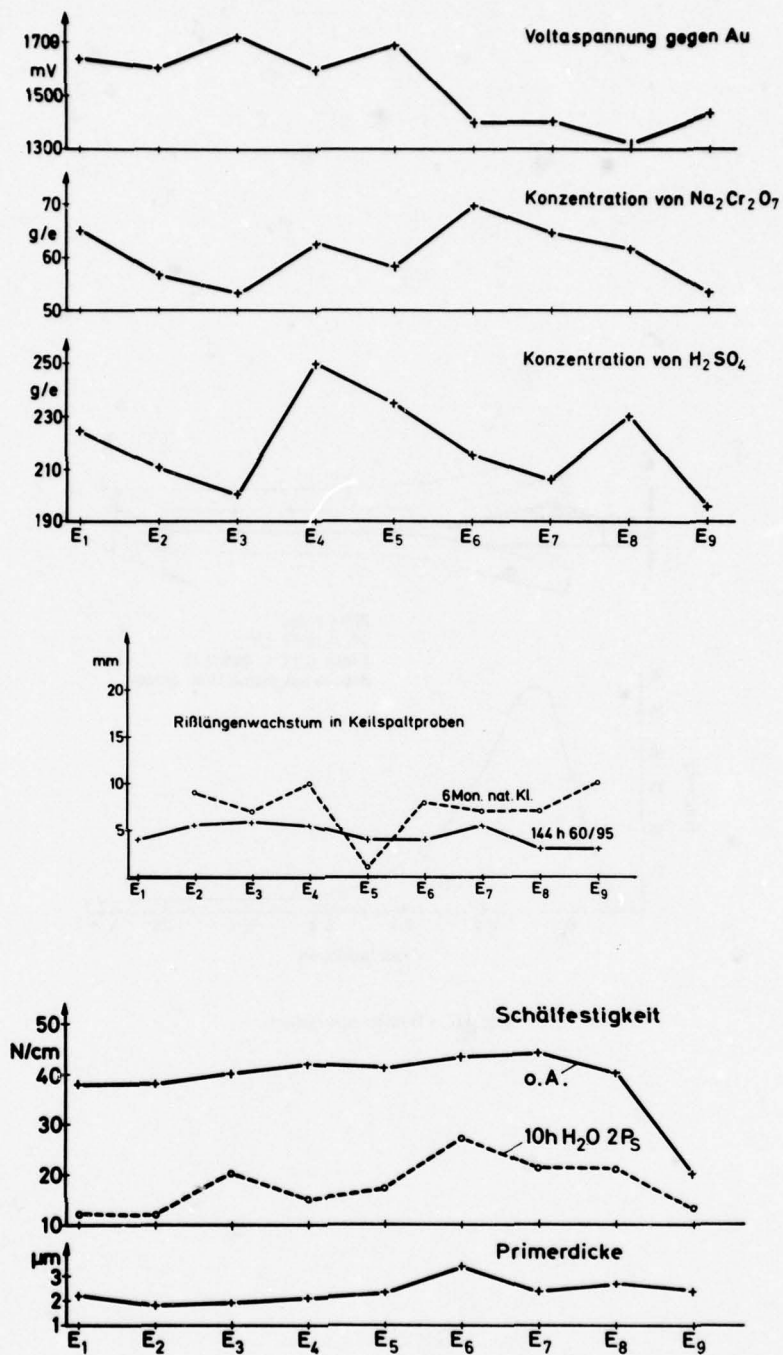


Fig.17 Surface treatment and it's influence on bond properties

Material: Aluminium 2024 clad in wedge-test

Aluminium in clad quality in peel-test

Adhesive: FM 123/5

Primer: BR 127

Surface treatment: European chromic sulphuric acid etch

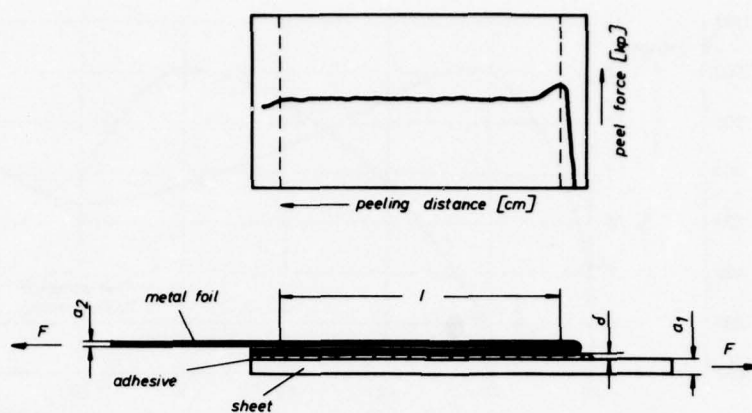


Fig.18 180° Peel-test

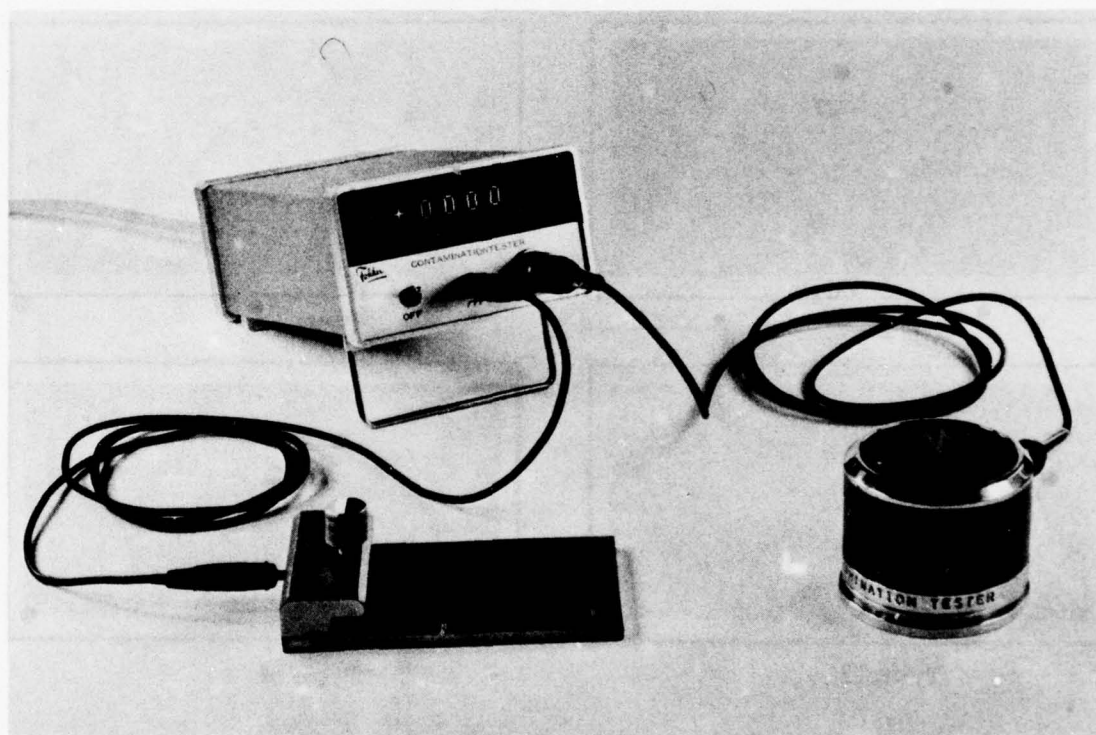


Fig.19 Fokker-contamination-tester



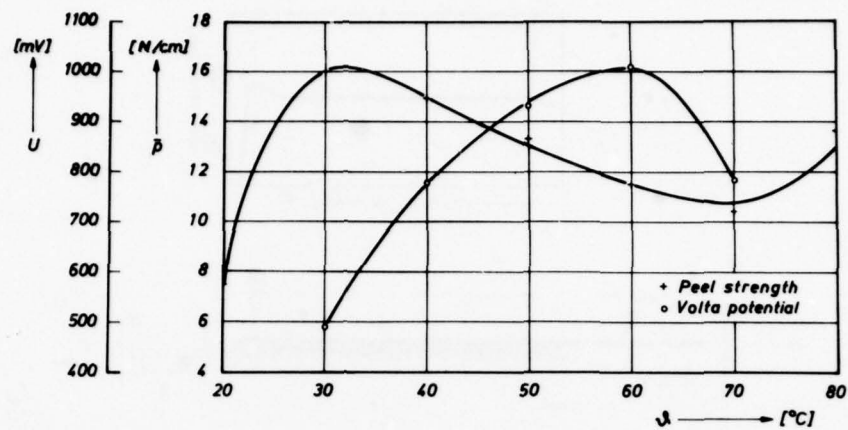


Fig.20 Peel strength and volta-potential in dependence upon CSA-etching temperature

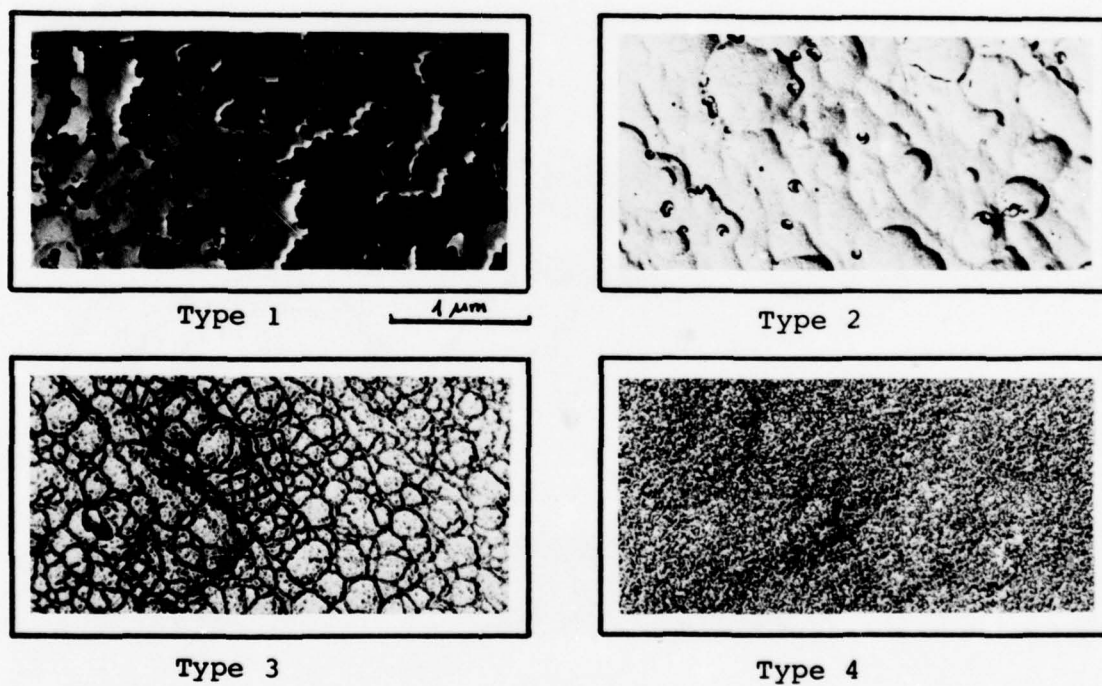


Fig.21 Surface morphology after  $\text{CrO}_3 - \text{H}_2\text{SO}_4$  etching



Fig.22 Transition morphology from Type III to Type IV

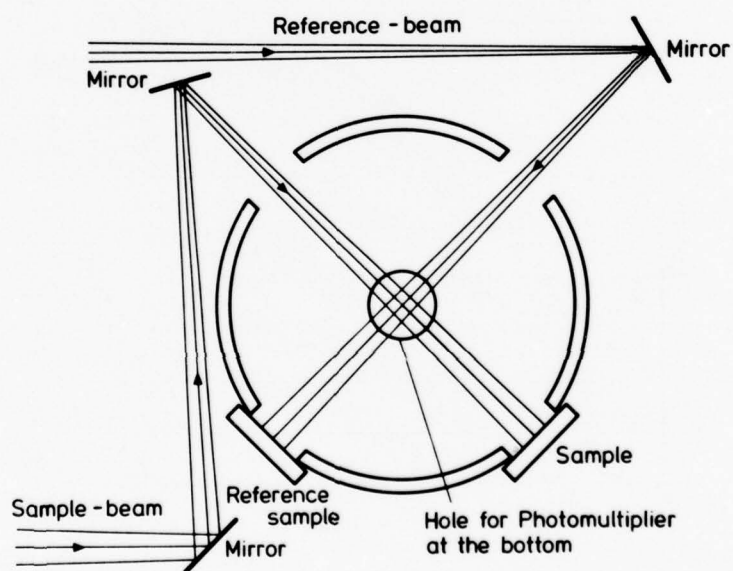


Fig.23 Principle of the integrating sphere

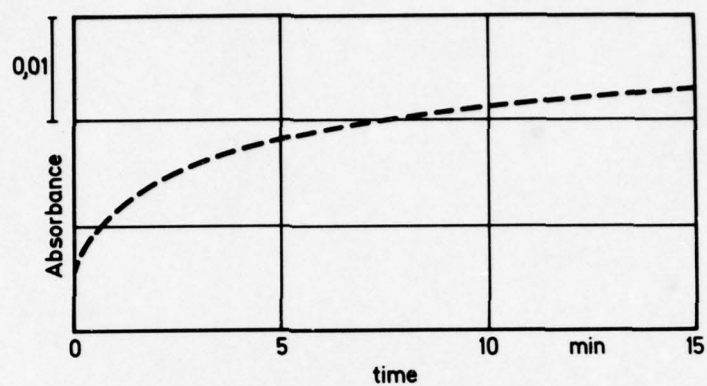


Fig.24 Oxidation of copper at room-temperature, measured by remission photometr

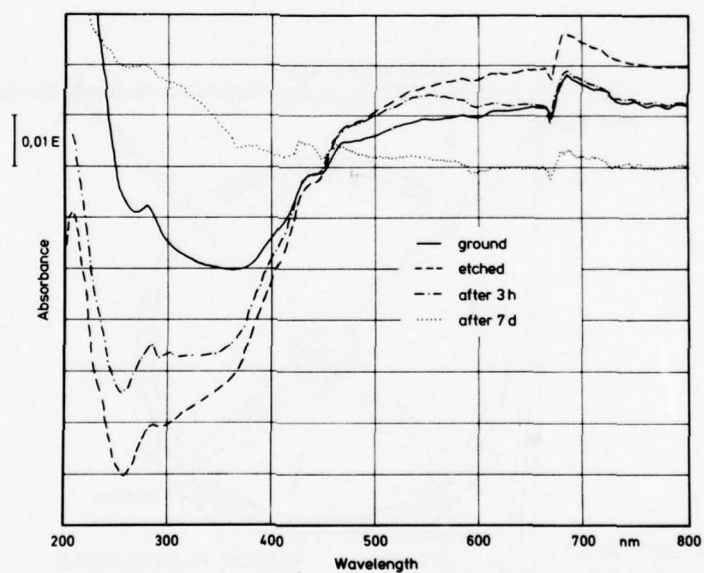


Fig.25 Efficiency of etching (by hydrochloric acid) and following oxidation of the pretreated surface



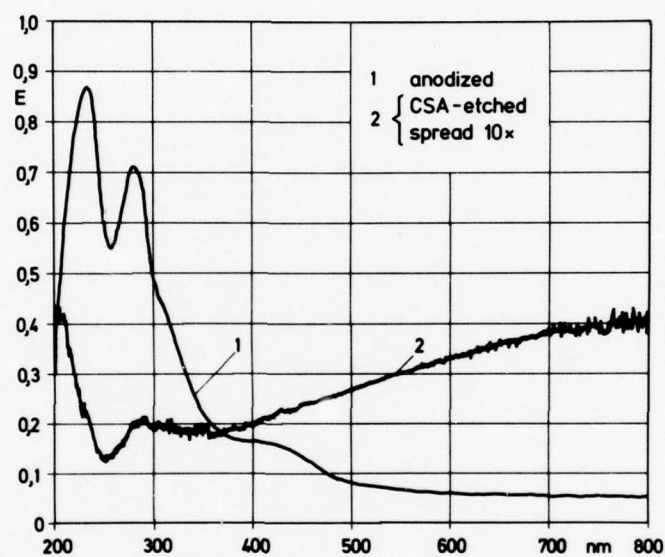


Fig.26 Determination of phenolic resin on aluminium (curve 2 shows the amount of  $0.5 \mu\text{g}/\text{cm}^2$  adsorbed resin)

## SURFACE PREPARATION--THE KEY TO BONDMENT DURABILITY

by

J. Corey McMillan  
 Chief, Chemical Technology  
 Boeing Commercial Airplane Company  
 P.O. Box 3707  
 Seattle, Washington 98124  
 USA

## SUMMARY

A correlation between the variable service performance of bondments employing the 120°C curing modified epoxy adhesives and the variability of production acid etch surface preparation processes is developed using stressed environmental durability test methods. This variability requires special procedures for control in the acid etch processing, but may be precluded by incorporation of phosphoric acid anodizing into the processing sequence. Phosphoric acid anodizing is shown to produce consistent, environmentally durable bondments. A test program comparing the environmental durability of the acid etch with the phosphoric acid anodize surface preparation process under various exposure and loading conditions is reviewed.

## SPECIAL NOTATIONS

Old technology adhesive examples:

FM 123	American Cyanamid Company
AF 126	3M Company

New technology adhesive examples:

FM 73	American Cyanamid Company
EA 9628	Hysol Division of The Dexter Corporation
Metal Bond 1133	Narmco Materials, Inc.

CIAP - Corrosion Inhibiting Adhesive Primer examples:

BR 127	American Cyanamid Company
EC 3950	3M Company

Corrosion resistant honeycomb core examples:

Dura-Core I and II	American Cyanamid Company
CR III, CR/Al	Hexcel Corporation

## 1. INTRODUCTION

Adhesive bonding of high-strength aluminum alloys for aerospace applications offers structural efficiency and manufacturing cost advantages over conventional mechanically fastened structure. However, bonded structure service experience, especially with bondments using 120°C curing modified epoxies, has been varied. Some bondments performed satisfactorily in service for 14 years, while similar or identical bondments experienced disbond and bondline corrosion after service lives of a very few years.

It has been found that service performance is often determined by the surface pretreatment, and that adhesive bonding of high-strength aluminum alloys requires exacting chemical pretreatments to guarantee the necessary mechanical strength and environmental durability.

This paper discusses the effects of production surface preparation processes on environmental durability. Emphasis is on bonding of high-strength aluminum alloys using 120°C curing modified epoxy adhesive systems and evolution of the surface preparation process, from the acid "etches" to the phosphoric acid anodize process, as practiced at the Boeing Commercial Airplane Company.

## 2. SERVICE EXPERIENCE

During the course of Boeing research into the causes and cures of in-service disbond and bondline corrosion, a comprehensive review of service disbands was conducted. This work led to the development and compilation of an actual service experience record versus the materials and processes employed, including surface preparation, and the categorization of disbond modes.

The service experience as it relates to three surface preparation processes is summarized in Table I. The three processes are discussed in later sections. Most

bondments performed satisfactorily in extended service. When disbonds occurred, they commonly were discovered within the first 4 to 7 years of service life, often at the first major overhaul. Certain environmental exposures were more conducive to the occurrence of disbond and corrosion; e.g., bilge areas more than warm engine areas. The categories of environmental disbond are summarized in Table II, with photos of selected examples shown in Figure 1.

The most significant aspect of in-service metal-to-metal disbonds is that the majority result from delamination of the joint at the adhesive/adherend interface. This also is true of honeycomb structure, where adhesive failure to the core (core pullout) also occurs. Very rarely is there a failure of the adhesive itself (i.e., a cohesive failure of the adhesive with adhesive adhering to both adherend surfaces) except as an after-effect where the remaining bond is incapable of sustaining the applied load. Thus, even though there are disbond causes not related to surface preparation, surface preparation is a primary or secondary cause in most cases examined.

Figure 2 illustrates the classic characteristics (Reference 1) of environmental disbond resulting from inadequate surface preparation for a partially disbonded fuselage doubler. These characteristics are:

- Adhesive (or interfacial) failure--between the adhesive/primer and the adherend
- Environmental access--moisture entered around fasteners
- Progressive disbond growth without corrosion--disbond is defined by the successive moisture stain rings; extensive corrosion has not yet occurred but would have followed in time
- Low bondline stress--disbond occurred in a region of low shear and peel stress between fasteners instead of at the doubler edge where internal pressurization produced substantially higher stresses

As a result of these in-service disbond studies, it was concluded that, in the majority of cases, disbond occurred first by mechanical fracture of the environmentally weakened (perhaps through hydration) oxide. Fracture then was followed by corrosion of the exposed metal surface. Additionally, it was concluded that the variable behavior in service was the result of the variability in the oxides produced by the surface preparation steps; therefore, control of the surface preparation was the key to enhanced in-service environmental durability.

### 3. EVALUATION OF ENVIRONMENTAL DURABILITY

Traditional methods of evaluating adhesives and adhesive bondments generally encompass three areas: (1) lap shear testing as a function of temperature, (2) peel testing as a function of temperature, and (3) lap shear residual strength testing after exposure of unstressed specimens to various environments. Examination of fractured specimens from these tests does not show the fracture appearances characteristic of the in-service disbonds.

Fractures exhibit many of the characteristics of in-service failures only when the test specimens while under stress are exposed to aqueous environments for prolonged periods. A comparison of the residual lap shear strengths after prolonged environmental exposure with and without loads is shown in Figure 3. The unstressed specimens typically retain a large percentage of their initial lap shear strength, while stressed specimens fail early or show major residual strength reductions even at relatively low applied stress levels. Equally significant are the fracture characteristics where the unstressed exposure specimens invariably present a 100% cohesive fracture, while the specimens failing during stressed exposure show some degree of the adhesive failure typical of that experienced in service.

In any structural joint, there are three basic modes (Figure 4) by which load can be transferred between members: Mode I--cleavage, Mode II--forward shear, or Mode III--sidewise shear. In adhesive bondments, load transfer is normally designed to be accomplished by Mode II shear, but because of eccentricity of loading, some Mode I cleavage loading always results, particularly at bondline edges.

Our early research work with stressed exposure of lap shear specimens, where the primary loading mode was Mode II shear with secondary Mode I loading at the lap joint edge, showed that the fracture features characteristic of in-service disbond were always most pronounced in the bondline-edge region where the Mode I loading was important. This observation prompted an interest in testing bondments where the primary loading mode was Mode I cleavage and led to a series of programs evaluating several specimen configurations based upon the double cantilever beam (DCB) concepts employed by Mostovoy et al. (Reference 2).

Preliminary studies using the DCB specimens showed that environmental exposure of Mode I loaded specimens duplicated all of the characteristics of in-service failures, including the variability in behavior where some specimens fail early and others are satisfactory after prolonged exposure. In conjunction with this work, a simplified, qualitative, significantly less expensive specimen configuration evolved (Figure 5).



In the configuration generally employed by Boeing, two 6 x 6-inch, 0.125-inch-gage, 2024-T3 clad adherends are bonded. The 6 x 6-inch laminate then is saw cut to form five 1 x 6-inch test specimens. A 0.125-inch-thick wedge is driven or pressed into the bond-line, creating a self-stressed test specimen ready for environmental exposure testing. In the wedge test, the adhesive at the crack tip is stressed to just below its cohesive fracture strength. Because the displacement is fixed by the wedge thickness, if the crack propagates, the load on the adhesive decreases with increasing crack length.

Prior to testing, the original crack length is scribed on the specimen edge. Test performance is evaluated on two bases. Crack extension as a function of time is determined and, following testing, the specimen is opened to evaluate the nature of the crack propagation. Typical results comparing good with poor durability performance are shown in Figure 5. Good durability performance is characterized by very limited amounts of crack extension where the fracture mode is always cohesive, while poor durability is characterized by progressive crack propagation in an adhesive or mixed adhesive/cohesive mode.

#### 4. SERVICE CORRELATION

The inability to evaluate or predict in-service performance was a limitation of past laboratory test techniques. To validate laboratory test results, it was imperative that a laboratory test/in-service performance correlation be developed. To develop this correlation, a number of experiments were conducted using components that had been removed from service (Reference 3). In some cases, the components had been removed because of disbond, while in others, the components were available as the result of structural modification.

A synopsis of this test and evaluation program is presented in Figure 6. All test specimens were fabricated from the still bonded (i.e., no disbond or corrosion) areas of service components and tested in various ways, including lap shear, peel, and under environmental exposure conditions using the wedge test. Failure load, amount of crack extension, and the mode of crack propagation or failure were examined during assessment.

Neither lap shear nor standard peel tests showed any correlation with actual in-service performance. The environmental exposure with peel specimens, and especially with the wedge specimens, did show an excellent correlation with service. In each case where the component had experienced some degree of in-service disbond, crack propagation was in the adhesive mode in the wedge test. The summary of crack extension data (Figure 6) shows that the majority of components experiencing disbond in service will produce adhesive crack extension in excess of 1 inch in 1 hour at 49°C and 100% relative humidity, and that all panels that disbanded in service produced test crack lengths greater than 0.3 inch.

As a result of this test program, we were convinced that a test technique was available that would allow bonding materials and process improvements to be developed. In addition, this specimen/test concept, the Boeing wedge test (Reference 4), appeared well suited for use as a in-process control. For control purposes, it was apparent that a control limit between 0.5 and 1.0 inch would eliminate the majority of in-service disbands and a 0.75-inch control limit was arbitrarily established for 1 hour exposure at 49°C and 100% relative humidity.

#### 5. TEST SPECIMEN CONFIGURATIONS AND TEST CONDITIONS

Subsequent test and evaluation programs examined the environmental durability of aluminum bondments. A variety of test specimens and loading configurations in addition to the wedge test were used; a number of these are shown in Figure 7. Test results using these specimen configurations are included in a later section. Many other specimen configurations have been employed in various studies, a variety of which are described and advantages and disadvantages discussed by Marceau (Reference 5).

The double cantilever beam (DCB) specimen and the thick adherend lap shear specimen were used for controlled Mode I and combined Mode I and Mode II loading, respectively. Data from DCB testing are often presented in terms of the strain energy release rate parameter  $G$  as discussed by Mostovoy (Reference 2).

The single cantilever beam (SCB) specimen was specifically designed for test and evaluation of the materials and processes incorporated in honeycomb sandwich construction. It is especially well suited to the evaluation of core surface preparation quality tested under environmental exposure conditions.

The square edge honeycomb bonded panels (so called because the core edge is left square, without crushed or closed-out edges) were used to evaluate the specific level of durability improvement achievable with improved materials and processes. These panels (shown in Figure 7 in static and cyclic load fixtures) are representative of actual structural designs and were tested under conditions defined by expected operating stresses and environments.

One objective of the Boeing test programs was to establish a prediction of in-service environmental durability. To accomplish this, the various specimen configurations were tested under three conditions (no load on the specimen, static loads imposed, and under cyclic stress) and then compared. Environmental exposure was accomplished under

controlled humidity (dry to saturated at several test temperatures; in natural outdoor exposures such as industrial or semi-tropical; in highly aggressive salt spray; and in the complex temperature, humidity, and pressure conditions representing the actual flight regime (ground-air-ground cycle). In addition, identified components incorporating improved materials and processes have been introduced into actual service and are being traced and periodically examined to increase our understanding of the laboratory test/in-service correlation. This in-service evaluation was initiated in 1973, with additional test components incorporated into the program in 1974 and 1975.

## 6. SURFACE PREPARATION

Even though the specific nature of the adhesion mechanism (whether mechanical keying, chemical adhesion, or some combination of the two) has not been completely defined, it has long been recognized that surface preparation prior to bonding is of critical importance to bond strength. Early surface preparation studies evaluated only the mechanical strength aspects of the bondment, and surface preparation generally was concerned with the removal of oils, mill scale, moisture, fingerprints, etc. Simple mechanical or chemical means such as mechanical abrasion and solvent cleaning often sufficed. Acid etching (Reference 6) and chromic acid anodizing processes were further developments based, at least in part, upon enhancement of mechanical bond strength and an improvement in the bond strength test result consistency.

The basic steps of production etch and anodize processes are shown in Figure 8. The initial vapor degrease step removes the gross organic contaminants, and is optional if the organic contaminant level is low. This is followed by alkaline cleaning, which is the primary cleaning method for removal of organic oils and greases.

Acid etching, or as it is sometimes known, the deoxidizing step, is used to chemically dissolve the existing gross oxide layers and to establish a consistent, thin oxide on the surface. This thin oxide serves as either the bonding surface or as the basis for the development of an anodize oxide and, therefore, its quality is very important to the bondability and long-term durability of the bond (Reference 7). The purpose of the subsequent anodize step is to build an increased thickness of oxide having the special properties required for bonding.

The rinse steps are required to stop chemical action and to prevent solution carry-over from one bath to the next. In production, the achievement of a water-break-free surface upon removal from the rinse tank long was considered evidence of satisfactory cleaning. However, the water-break-free surface, while required to define satisfactory cleaning, is not adequate to guarantee bondability. Upon completion of these processes, the parts are dried, usually in warm air driers.

The objective of all aluminum bonding surface preparation is to develop a consistent, uniform oxide film on the metal surface that is: (1) adhesively strong in attachment of the oxide to the base metal, (2) cohesively strong but not brittle, (3) wettable by the adhesive, (4) active in terms of mechanical keying and/or the formation of chemical bonds, and (5) environmentally stable.

Service disbond analyses, which concluded that variability in surface preparation was responsible for the variability in service performance, resulted in surface preparation research and development being concentrated in two areas: improvement of environmental durability and, especially, an increase in the consistency of bondment in-service performance. One facet of the program was to define and control the optimum operating parameters for the conventional etch process, while a second explored a wide variety of alternate surface-preparation processes.

### 6.1 Optimized FPL Etch

Many conventional production acid etch processes use the aqueous sulfuric-acid sodium-dichromate solution developed by the Forest Products Laboratory (Reference 6), a process commonly referred to in the United States of America as the FPL etch. A systematic examination of the process variables incorporated in the FPL etch was conducted at Boeing, using the wedge test to determine the effect of each variable on environmental durability. Several process parameters proved to be particularly important in controlling bondment environmental durability. Contamination, bath chemistry, immersion time/temperature relationships, and rinse delay effects are compared in Figure 9.

It has been shown that contamination of the bath or the rinse water can result in surfaces with inherent low bondment durability. Fluoride contamination at the 200-ppm level in an otherwise satisfactory solution will result in extremely rapid interfacial crack propagation in the wedge test. It also has been reported that fluoride concentrations in rinse waters significantly lower than 200 ppm, such as that in some municipal water supplies, may reduce durability (Reference 8). Gross contamination normally can be detected through standard chemical analysis. In actual practice, analysis for contaminants usually is not conducted; instead, good housekeeping practices are employed to preclude contamination.

The first specimens etched in a virgin FPL etch solution proved to have very poor environmental durability; as processing continued, the durability improved. This effect, as sometimes evidenced by low peel test values, was known to some experienced production operators, leading them to "sweeten" the bath by dissolving aluminum even though this was



not a specification requirement. Our experiments verified the necessity for "sweetening" or "aging" the bath prior to beginning production as a condition for achieving satisfactory bondment durability.

In the actual tests, it was demonstrated that the copper-bearing aluminum alloys such as 2024 were more effective in conditioning the bath than was pure aluminum. Smith (Reference 9) has shown that the FPL etch develops a porous surface oxide as the result of anodic polarization and that the presence of  $\text{Cu}^{++}$  enhances the cathodic current, thus increasing the mixed potential and the anodic voltage. This "self-anodization" is critically dependent upon the exact chemistry of the etching solution. However, we have been unsuccessful in precise chemical definition of the bath chemistry required to produce environmentally durable bonds. Thus, empirical methods have been used to define the bath requirements.

The time-temperature relationship of immersion also was evaluated. The consistency of the thin oxide formed in the FPL etch is controlled by this relationship. The barrier layer/porous layer (Reference 10) relationship is a constant at equilibrium where dissolution is offset by oxide formation. Thus, if short times and low etch temperatures are employed, the near equilibrium conditions are not always achieved and low durability may result. This is particularly true during production where parts of widely differing surface area-to-mass ratios are processed together. For satisfactory durability of production parts, it, therefore, is mandatory that higher temperatures and intermediate times be employed, or that time at lower temperature be markedly extended.

The time between removal of a part from the etching solution until the residual solution is rinsed from the surface is another parameter shown to have a major effect upon bondment environmental durability. Within a matter of minutes, the chemistry and etching conditions of solution retained on surfaces change to a degree that can completely destroy the environmental durability of the bondment.

These studies and observations led to the definition of a substantially more restrictive process specification for the conventional FPL etch process which is now commonly known as the "optimized" FPL etch. A comparison of the process parameters for the FPL etch, the optimized FPL etch, and the to be discussed phosphoric acid anodize is shown in Table III. Based upon our service experience and laboratory test results, we consider the optimized FPL etch parameters to be the minimum standard mandatory for production of 120°C curing modified epoxy bondments with satisfactory durability for aircraft structural usage.

In the optimized FPL etch process, wedge-test coupons are used as process control specimens. These coupons are processed with each load of production parts and provide an empirical verification of the bath capability of producing environmentally durable bonds. In production, the trends in crack propagation are reviewed and when erratic behavior or consistently increasing crack lengths occur, corrective action is initiated. This normally consists of recharging the etch tank. Once a previously satisfactory bath begins to produce low durability bondments, regeneration methods have been unsuccessful.

Since the optimized FPL etch was incorporated at Boeing in 1973, we and our subcontractors have tested several million wedge test coupons. Figure 10 shows the distribution band of wedge test crack lengths for a large number of tests conducted at several production facilities. To generate these data, all wedge test results from a given facility and for a specific period of time were analyzed. This normally was a period of 30 days or longer and included several hundred to several thousand individual tests. Each data set produced an "exceedances" line. The band encompasses the "exceedance" lines for approximately 50 separate analyses. Superimposed on this plot are the specification control crack length and the in-service correlation data, as discussed in a previous section.

The significance of these test results is that even while operating under the stringent conditions of the optimized FPL etch, a number of test specimens showed crack extensions in the crack length range where failures had been experienced in service. Because the test coupon only measures ability of the bath to produce durable bonds, it must be assumed that the actual production parts will have the same durability distribution. All efforts to eliminate the low durability end in the data have been unsuccessful, leading to the conclusion that this variability is inherent in the optimized FPL etch process.

The variability of performance is a statistical certainty even though the probability is small. This creates a testing problem; that is, the variability is not likely to be observed when limited numbers of specimens are employed, giving rise to a false sense of confidence in the consistency of the total bonding system. The test results for the optimized FPL etch presented in following sections are representative of the better quality bondments achievable, not of the low durability end of the scatter band.

Changing the specification limit will not change the quality of the production parts without concurrent process changes. An assessment of this information led to the conclusion that the optimized FPL etch, while satisfactory for secondary structure, was not adequate for primary structural applications.



## 6.2 Phosphoric Acid Anodizing

Concurrent with the development of the optimized FPL etch, an improved process for the surface preparation of aluminum was developed. The following criteria were established for selection of the process:

1. Hydration-Resistant Oxide. Durability testing clearly showed that water was one necessary element in causing adhesive bondline failures. It has been postulated that this may be the result of mechanical weakening of the oxide due to hydration, permitting fracture of the oxide at low stresses (Reference 1). Phosphoric acid anodizing was of immediate interest because of its known resistance to sealing; i.e., hydration of the oxide (Reference 7).
2. Environmental Durability. Using the fracture-mechanics-type durability testing, the criteria for toughness and durability were established based upon the performance characteristics of a nitrile-phenolic adhesive system that had provided many years of excellent service--even when applied over poorly prepared surfaces. Unfortunately, this adhesive does not lend itself to the bonding of modern, complex aircraft structure.
3. Anodic Process. The applied external voltage of an anodic process was required to provide a sufficient driving force to produce a consistent, uniform oxide.

Secondary considerations included a simple chemistry bath to avoid any critical dependency upon complex solution chemistries, room-temperature operation to minimize energy and containment requirements, and chemistries capable of being handled in compliance with environmental protection laws.

A systematic Boeing program started in the late 1960s led to establishment of the phosphoric acid anodize process currently used in the aerospace industry. The specific process parameters are shown in Table III.

A key portion of the phosphoric acid anodizing process development was the extensive use of stressed durability testing to ensure that the process met the necessary environmental durability criteria. The distribution of wedge test data for phosphoric acid anodize is compared to that of the optimized FPL etch in Figure 11. The optimized etch specification requirement and the service correlation information discussed earlier are superimposed on the figure.

The phosphoric acid anodize developed an exceptionally tight population, all in the range where no service disbands have been observed. The optimized FPL etch also had the bulk of its test data in the satisfactory range; however, some specimens exhibited more extensive crack extension. The consistent, tight population for the phosphoric acid anodize was demonstrated in repeated tests at a number of different facilities. This consistency has given us confidence that the variability inherent in the FPL etch process does not occur in phosphoric acid anodized parts and, therefore, this process is satisfactory for primary structural bondments.

The excellent adhesion characteristics of phosphoric acid surface preparation are easily demonstrated. For example, the results from an evaluation of the effectiveness of paint strippers are shown in Figure 12. These aluminum panels were prepared using optimized FPL etch and phosphoric anodize and primed with corrosion-inhibiting adhesive primer. For the FPL etch, the primer is easily removed, normally in a matter of minutes. By contrast, even though the primer is softened, it is essentially impossible to strip the primer from the phosphoric acid anodized surfaces, even after exposures of 24 hours. Whether the difference in adhesion characteristics is a mechanical keying or chemical effect is unclear. However, the marked difficulty in stripping or removing the organic coating by chemical means has been shown to directly relate to environmental durability. Thus, this stripping procedure provides a referee method when a question exists as to whether primed parts have been correctly processed.

As a result of a thorough evaluation and extensive laboratory testing, phosphoric acid anodizing was placed in production in 1974. It is now the standard for Boeing production, with additional incorporation of this process accomplished or planned at a number of production plants throughout the world.

## 6.3 Comparison of the Surfaces

A thin porous oxide film is a characteristic of production surface preparation processes that have satisfactory environmental durability. Theoretical treatments of formation characteristics and dimensional aspects have been available for many years. The idealized model of the porous oxide consists of a very thin continuous barrier layer with a thicker superimposed hexagonal or cylindrical cell structure (Reference 11). This hexagonal or cylindrical cell has an approximately hemispherical end and a central cylindrical pore. The dimensional aspects are a function of the electrolyte, operating temperature, and applied electrical field.

A synopsis of some of the calculated oxide structural dimensions versus observed measurements is shown in Figure 13. Where data exist, the correlations are generally good; however, the lack of data is significant, both in the fact that the theory does not

provide a completely satisfactory model and that the actual structure is far from idealized. Figure 14 compares the surfaces of phosphoric acid anodized 2024-T3 clad with 7075-T6 bare, both of which produce environmentally durable bondments. There are many similarities in oxide morphology, but there are also striking differences. The 2024-T3 clad specimen exhibits the expected columnar, porous appearance with the aluminum subgrain structure "telegraphed" into the oxide. The 7075-T6 bare oxide structure appears much more amorphous, but the openness of the substructural detail is clearly evident. In neither case is the idealized hexagonal porous structure well defined.

It appears that the techniques and resolution available with conventional scanning electron microscopy (SEM) are not capable of identifying the fine structure surface details responsible for adhesion and durability. More recent developments in analytical techniques have allowed a much more detailed examination of oxide morphology. Some of the more subtle aspects of the detailed structure and local chemical composition are only now beginning to be identified and understood.

Venables et al. (Reference 14) have reported the presence of a whisker-like or filamentary set of protrusions extending outward from the oxide surface of both FPL etched and phosphoric acid anodized surfaces. This concept for phosphoric acid anodize is shown schematically in Figure 15. The phosphoric acid anodized oxide was described as considerably thicker, with a better developed hollow hexagonal cell structure and longer whisker-like protrusions when compared to the FPL etch oxide. It also appeared that the density of whiskers was substantially greater for the phosphoric acid anodized than for the FPL etched surface. The concept of a "fiber-reinforced interface" as an important aspect of bondability was introduced, a concept that correlates well with the practical observation that bondability of the phosphoric acid anodized surface (or FPL etch surface) can be greatly reduced by a very light rubbing of the surface (Reference 15). This may be visualized using the representation in Figure 15 if it is assumed that the tendrils are fragile or brittle under the bending loads caused by rubbing. Due to the small tendril size, the damage would not be apparent with visual observation.

The specific chemistry of the oxide also is a subject for considerable study and speculation. In the past, most analytical tools lacked the resolution required to examine the subtle chemical variations that may exist in the oxide. Recently, Thompson et al. (Reference 16) examined the cell structure of some phosphoric acid anodized porous oxide films and detected a phosphorus concentration gradient with more phosphorus adjacent to the pore than that contained in the interior of the oxide structure. The practical implications of these concentration gradients are yet to be defined.

Light reflection and refraction properties are other characteristics of the oxide formed by phosphoric acid anodizing. With low-angle incident light refraction, complementary colors are observed with a polarized filter in the 0° and 90° positions. This polarized light technique is used in production as an inspection tool to ensure that the part has been electrically connected within the system.

The presence of color is necessary and guarantees the part was anodized, while the absence of color shows improper processing. Color alone, however, does not guarantee bondability, as there are several ways that color (proper oxide thickness for refraction) can be achieved outside of the processing specification controlling parameters. Examples are improper bath temperature, rubbing, physical damage, and improper voltage settings. In addition to the color check, in-process controls are required to ensure bondability.

## 7. ENVIRONMENTAL DURABILITY TESTING

Boeing studies have assessed the effect of the surface preparation and other variables on environmental durability. The variables considered included: (1) loading conditions--no load, static load, or cyclic load, (2) loading mode--Mode I, Mode II, or combined Modes I and II, (3) environment--dry, salt spray, ground-air-ground cycling, or natural outdoor exposure, (4) alloy--2024 bare and clad and 7075 bare and clad, and (5) adhesive system. Data were not available for all variable combinations, but there were sufficient data to establish definite durability trends.

### 7.1 No-Load Testing

The susceptibility of bonded structure to general corrosion has been evaluated using standard unstressed corrosion test specimens. In addition, the unstressed portions of stressed specimens have been examined to quantify the extent of corrosion. In long-term exposures to condensing humidity environments at 60°C, the unstressed portion of DCB specimens experience crevice cell corrosion from the edges when the edges are unprotected. In Figure 16, the extent of crevice cell corrosion may be compared as a function of surface preparation, alloy, adhesive, and primer.

The most pronounced effect is the influence of the adhesive system where the new-technology, high-durability adhesives are very effective in precluding crevice cell corrosion for the three surface preparations and four alloys considered. In contrast, the old-technology adhesive systems allowed extensive crevice corrosion development after approximately 80 weeks exposure. The reason that the adhesive, rather than the primer, controls the occurrence of crevice cell corrosion is unknown, but the trend was consistent throughout many tests.



If crevice cell corrosion does occur, it is most likely to occur and to be more extensive on 7075-T6 clad, with occurrences on 7075-T6 bare being the least likely and least extensive. The differences between 2024-T3 bare and 2024-T3 clad are not as pronounced, but the tendency is for 2024-T3 bare to be less susceptible than the clad alloy. The propensity for clad dissolution crevice cell corrosion that had been documented previously (References 17, 18) led to the general conclusion that "clad is bad" (Reference 19). These results verify the susceptibility of clad, but also show that bare alloys are susceptible as well, emphasizing the need for bondline edge protection.

The influence of surface preparation is more subtle, but both phosphoric and chromic acid anodize processes are superior to the FPL etch in limiting crevice cell corrosion. Of the two tested, the phosphoric acid anodize consistently allowed less extensive corrosion development. This effect was evident independent of alloy, adhesive, or primer system. The primer system comparison is also shown in Figure 16 where the beneficial effects of corrosion-inhibiting adhesive primer (CIAP) are evident. The effect of primer appears to be much less important, however, than the choice of adhesive.

Another form of environmental degradation is filiform corrosion, which occurs on the aluminum surfaces under paint films. This effect is important to bonded structure, since the bonding surface preparation often is used as the surface preparation for the decorative paint on bonded components. Filiform corrosion test results, comparing the corrosion resistance of the phosphoric acid anodize surface preparation with the optimized FPL etch under identical overcoat paint films, are shown in Figure 17. The resistance to filiform corrosion is defined by the extent and distance of the progression of the worm-like corrosion tracks from the X scribed on the sample. The photographs show that the phosphoric acid anodize surface preparation allows measurably less corrosion progression than does an optimized FPL etched surface. This trend is independent of the specific overcoat system employed and has been repeated in numerous tests. Both surface treatments are superior to the standard preparation for painting, which calls for mechanical abrasion followed by chemical conversion coating and priming. This again emphasizes the importance of surface preparation (adhesion) in limiting corrosion.

The effect of the complex temperature-pressure-moisture cycling representing the aircraft ground-air-ground (GAG) cycle has been evaluated using a square-edge honeycomb panel configuration (Figure 7). The moisture pumping and environmental aspects of the GAG cycle have been determined as a function of bonding technology evolution and loading conditions, Table IV. The older technology bonding used 7075-T6 clad face sheets, original FPL etch, and standard core bonded with non-CIAP primer and old-technology adhesives. Under no-load conditions, this system is clearly incapable of precluding water ingestion with prolonged cycling. Bonding technology evolution, which incorporated phosphoric acid anodized 7075-T6 bare face sheets and corrosion-resistant cores bonded by CIAP primers and new-technology, high-durability adhesives, totally precluded water ingestion for twice the cyclic life. These no-load tests are continuing; a several-order-of-magnitude performance improvement is expected.

## 7.2 Static Load Testing

While it is clearly evident that environmental degradation may occur with unstressed bondlines, it has been demonstrated that load application to the bondline during exposure is required to truly define the degradation resistance of bondments. To evaluate the influence of loading, static load tests have been conducted evaluating the specific loading mode and test conditions on various bonding systems. The effect of combined Mode I and Mode II loading as produced in thick adherend lap shear specimens is summarized in Table V. Loading was imposed at two stress levels and, as would be expected, failure was more likely at the higher stress level. This test method is discriminating with respect to primer/adhesive systems and is capable of rating their stressed durability performance. The new-technology adhesive system experienced substantially fewer test failures than the old-technology adhesives at the 1500-psi stress level and had no failures at the 900-psi stress level. At the lower stress level, a number of failures did occur with the old-technology system.

No alloy trends were clearly evident during these 140-day tests. Surface preparation did appear to have at least a minor effect, with the phosphoric acid anodize evidencing fewer failures. If failure occurred with phosphoric acid anodize specimens, it might not have been at a longer test time. For example, the 7075-T6 bare results for both adhesive systems for the phosphoric acid anodize and the FPL etch at the 1500-psi stress level produced equal numbers of failures; however, the average life of the FPL etched specimens was greater than that of the phosphoric acid anodized specimens. The reasons for this anomaly are not understood. The fracture mode in these tests tends to be cohesive, leading to the expectation of a minor effect of surface preparation on test results.

The DCB specimen (Mode I loading) test results for prolonged elevated temperature/condensing humidity exposure are presented in Figure 18. A large number of tests were run comparing surface preparation, alloy, and adhesive system. No definite trends could be established, and it appears that all data fall into a fairly broad, but generally applicable scatter band. Previous work with the original FPL etch has shown a much broader scatter band, with some specimens experiencing extremely rapid adhesive crack propagation. Mode I loading is very effective in demonstrating inadequate surface preparation, but in this environment does not show significant differences between the optimized FPL etch, chromic acid anodize, and phosphoric acid anodize surface preparations.



Examination of opened bondlines does demonstrate that some differences exist (Figure 19). The amount of adhesive bond failure in the test zone varies as a function of alloy, the clad specimens being more susceptible, and the FPL etch is more likely and phosphoric acid anodize least likely to present adhesive failure in the test zone. This factor probably relates to the resistance to crevice cell corrosion described earlier, which is evident in the uncracked portions of these test specimens.

The results of 48 months natural environment exposure (South Florida test site) of Mode I loaded DCB specimens are presented in the Figure 20 photograph. These particular specimens compare the optimized FPL etch with the phosphoric acid anodize surface preparation and are representative of the most durable systems we have been able to produce. Environmental protection included complete painting of the specimen prior to introducing the bondline crack.

The significant finding of these tests is that environmental degradation in a semi-tropical environment can be totally precluded through use of phosphoric acid anodize surface preparation, the new-technology adhesive system, and edge protection of the bondline. This observation is valid even for clad alloys, which verifies the position that, in mildly aggressive environments, clad in the bondline is not detrimental if bondline edge protection is maintained.

The results of DCB testing in the highly aggressive 5% salt spray environment are presented in Figures 21 and 22. In the case of 2024-T3 bare and clad tests (Figure 21), 90-day exposure was insufficient to establish definite trends. It is significant, however, that some crack extension occurred on each specimen and that bondline edge protection with the paint system was unable to completely protect the bondline. No clear-cut superiority of bare over clad is evident. In the FPL etch case, the bare specimens actually experienced more crack extension than the clad alloy. These exposure tests are continuing.

The extended duration tests with 7075 alloy (Figure 22) do show definite trends. In all specimens, crack propagation occurred. The phosphoric acid anodize surface treatment is clearly superior to the optimized FPL etch for both the bare and clad alloys. In the clad case, the FPL etched specimen was unable to resist the aggressive salt spray environment, even when the bondline edges were protected with overcoat paint systems. Protecting the bondline edge did produce a noticeable beneficial effect on the phosphoric acid anodized 7075-T6 clad specimen. It is apparent that in highly aggressive environments, extraordinary measures may be required to guarantee the bondline integrity of clad alloys.

An important question in laboratory testing is the relationship of the test environment to actual service-encountered environments. Our assessment is that the South Florida exposure is slightly less severe, and the salt spray considerably more severe, than the severe commercial aircraft operating environment. Many airlines operate in mild environments that are less damaging than the South Florida exposures.

The effect of honeycomb core surface treatment on environmental durability was assessed in a series of tests using the single cantilever beam (SCB) test specimen (Figure 7). Three core surface treatments were compared: (1) standard core, which is foil with a light FPL type etch surface treatment; (2) corrosion-resistant core, which incorporates proprietary surface treatments of the conversion-coating type; and (3) phosphoric acid anodized foil surface treatment covered by Boeing patents. The comparisons are presented in Figure 23.

The stressed durability SCB tests showed an increasing resistance to crack propagation from standard core to corrosion-resistant core to phosphoric acid anodized core. In addition to the crack length trends, the fracture mode also varied systematically in the same order from 100% adhesive failure (i.e., core pullout) through mixed 50% adhesive/50% cohesive crack propagation to 100% cohesive cracking through the adhesive fillet for the phosphoric acid anodized core. The fracture mode trends are shown in Figure 24.

The load transfer in honeycomb structure is by shear (Mode II) through the adhesive. The capability to transfer load is a function of the adhesive and of the adhesive geometry as it adheres to the core. Effective wetting and development of generous fillets at the adhesive core joint enhance both strength and durability of the joint. Bonds with standard core show wide variation in wetting and filleting, while the corrosion-resistant cores are a marked improvement. However, for total consistency, the phosphoric acid anodized core is unsurpassed. Presently, the phosphoric acid anodized core process is not used in production. Its incorporation would remove a possible durability weak link in honeycomb applications.

The effect of static stress on honeycomb panels subjected to the simulated ground-air-ground environment is shown in Figure 25 and Table IV. As was the case with the unstressed panels, the old-technology bonding system is incapable of preventing water ingestion and migration that fill a number of honeycomb cells, many of which are remote from the exposed honeycomb edge. The effect of stress is to accelerate the rate of water ingestion as compared to the unstressed case, and the higher stress level increases the number of water-filled cells for the same exposure time.

At both static stress levels, cracking of the skin-to-core bonds was observed after very few ground-air-ground cycles for the old-technology test specimens. Continued

cycling resulted in delamination of the panels, the total life being limited to hundreds of cycles.

By way of contrast, the new-technology panels have completed in excess of 9000 cycles with no evidence of water ingestion or core-to-skin cracking. An order-of-magnitude improvement in performance was considered a minimum test goal. The logic for establishment of this goal was as follows. In service, the general occurrence of service disbands is from 2 to 7 years (Table I). Assuming a direct correlation between laboratory test and service, an order-of-magnitude improvement should produce satisfactory service lives in excess of 20 years. This test improvement has been exceeded and testing is continuing.

### 7.3 Cyclic Load Testing

Cyclic load, environmental exposure life data from thick adherend lap shear tests are presented in terms of cycles and hours in Figure 26. The three cyclic rates tested each define a separate test result population.

The slowest cyclic rate, 0.8 cph (1 hour at maximum load, 1/4 hour at minimum load), was more damaging in terms of damage per stress cycle than either the intermediate rate, 10 cph (4 minutes at maximum load, 2 minutes at minimum load), or the 1800 cpm sinusoidal loading. The intermediate cyclic rate also is intermediate in inducing damage per cycle, while the higher cyclic rate requires higher stress levels and more cycles to failure.

Plotting the results as a function of test hours was an attempt to normalize the curves in terms of test time. Even though sufficient data are not available for a complete assessment, it is apparent that this simplistic approach is not adequate to resolve the curves, because a complex interaction of fatigue crack growth, creep rupture, and adhesive at-rest relaxation must be occurring. It is clear, however, that at lower stress levels, the slow cycle tests are significantly more damaging than sustained stress or higher cyclic rates in terms of hours of endurance and, in the cyclic load cases, cycles to failure.

An examination of the fracture mode showed that for the slower cyclic rates, 10 cph and 0.8 cph, the crack propagation path was consistently cohesive, progressing down the centerline of the adhesive (Figure 27). Thus, crack propagation and life are primarily affected by the properties of the adhesive. No effect of surface preparation would be expected, and none was observed. For higher cyclic rates, a well-defined fatigue crack growth zone was observed (Figure 27). Characteristically, this zone is very near the oxide surface and appears to be at the primer/adhesive interface; again, no particular effect of surface preparation was evident.

In certain high-cyclic-rate cases, a surface preparation anomaly was observed. Under certain test conditions (Figure 28), the chromic acid anodized panels showed a significant life reduction. Examination of the fracture faces revealed that a portion of the fatigue crack propagation zone was interfacial between the oxide and the primer, or perhaps intraoxide. This brittle fracture mode is defined within the diamond-shaped pattern of the woven adhesive skrim cloth, which shows a strong influence of the local strain conditions. This effect was systematically observed in the high humidity testing, with only occasional specimens showing the effect in dry air testing.

DCB specimens were tested to examine the cyclic loading effects under Mode I loading conditions and to determine whether a threshold (or no crack propagation) condition existed. Data from one of these test series are shown in Figure 29. Three cyclic rates of 1800 cpm, 10 cpm, and 0.8 cph were examined, but due to the extremely long test time required, the slower rate testing was not carried to the threshold conditions.

In this loading mode, the crack growth per cycle is essentially independent of rate, environment, and surface preparation. If differences exist, it is with the slowest cyclic rate where a tendency to faster propagation is indicated.

These tests also indicated that there is a threshold cyclic strain energy introduction ( $G_{I\text{TH}}$ ) below which growth does not occur. This is analogous to the crack propagation in metals where the cyclic threshold has been well documented.

One anomaly was observed in this test series where a chromic acid anodized specimen experienced a significant crack extension or jump after the apparent threshold level had been reached. The crack fracture face of that specimen is compared to a phosphoric acid anodize specimen in Figure 29. The crack extension regions for both specimens are completely cohesive except for the area of the crack jump where an oxide failure appears to have occurred. Based upon this test and random similar occurrences in the lap shear tests previously mentioned and in concurrent wedge tests, it appears that the chromic acid anodize is susceptible (either through random processing variables or due to complex interactions of applied stress and environmental conditions) to cohesive fracture of the oxide very near the primer/oxide interface. The practical significance, if any, of this weak or brittle oxide condition is unclear.

The results of cyclic stress testing of honeycomb panels in the 60°C/condensing humidity and ground-air-ground environments are summarized in Table IV. In both environments, the cyclic stress application resulted in very early panel failures for the



old-technology panels. Failure occurred at such an early time that none of the scheduled inspections for water ingestion or crack initiation had been performed.

In contrast, the new-technology panels have completed 8000 cycles at 60°C/condensing humidity and 4000 ground-air-ground cycles with no water ingestion or core-to-face sheet crack initiation. An order-of-magnitude improvement in performance considered a minimum test goal has been exceeded and testing is continuing.

## 8. CONCLUSIONS

Conclusions relative to the effect of surface preparation on environmental durability are:

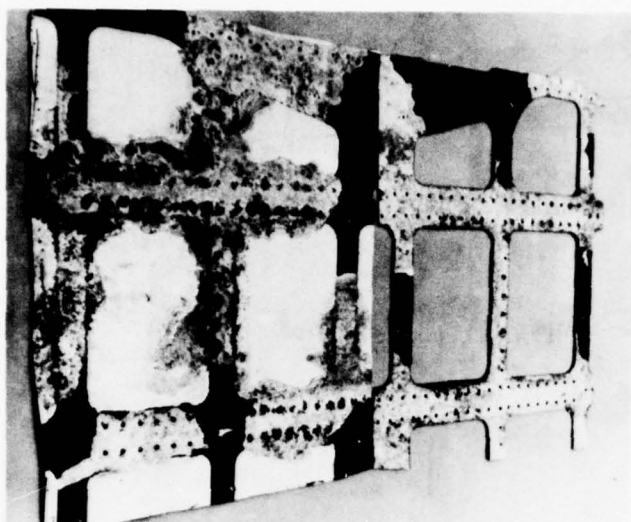
- o The variable service durability of 120°C curing modified epoxy bondments correlates directly with the variability inherent in the production surface preparation processes. Carefully controlled surface preparation is the key to enhanced environmental durability.
- o Stressed environmental durability testing in aqueous environments is required to duplicate the characteristics of in-service failures. Wedge test (Mode I loading) results correlate directly with in-service performance. This technique provides an in-process test capable of demonstrating the capability of a surface preparation process to produce satisfactory bondments.
- o The originally developed FPL etch production process must be operated under tight restrictions to meet the minimum requirements for satisfactory bond durability including: (1) contamination control, (2) higher temperature bath operation with immersion for longer times, (3) limitations on the time from removal of parts from the bath until rinsing, (4) chemical (2024 aluminum alloy) addition to the bath to establish initial bath effectiveness, and (5) wedge test in-process control.
- o Optimized FPL minimizes but does not eliminate the bond durability variability inherent in the FPL etch production process.
- o The phosphoric acid anodize surface preparation production process eliminates the surface preparation variability, consistently producing environmentally durable bondments, and provides an outstanding substrate for adhesion.
- o The anodize surface preparations are superior to the FPL etch in overall resistance to delamination and bondline corrosion. In the milder environments such as 60°C condensing humidity, most optimized FPL etched specimens perform as well as the phosphoric acid anodize. In severe environments; e.g., 5% salt spray; the superiority of the phosphoric acid anodize is clearly established.
- o The order of environmental exposure severity is: mild service, < South Florida semi-tropical, < severe service, << salt spray.
- o The most significant effect of surface preparation is observed under static stress, Mode I loading conditions. No-load environmental exposure tests show a lesser effect of surface preparation and, as long as surface quality equal to or better than typical optimized FLP etch is used, surface preparation does not appear to affect cyclic load environmental test results.
- o Testing of bonding systems where new technology, including the phosphoric acid anodize surface preparation, is compared to the older technology shows that major system durability improvements have been achieved.

## 9. REFERENCES

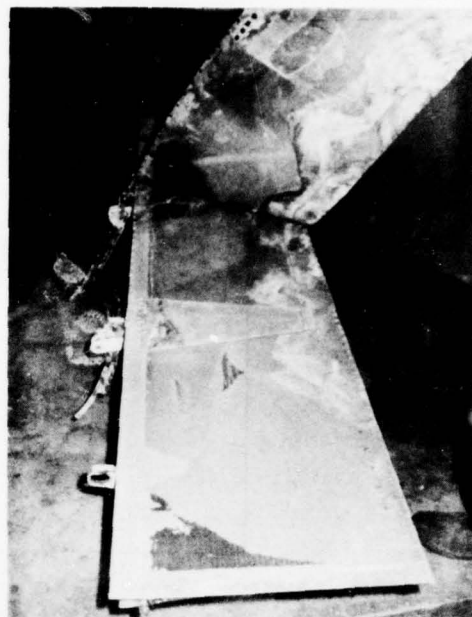
1. A. W. Bethune, "Durability of Bonded Aluminum Structure," SAMPE Journal, vol. 11, no. 3, Jul./Aug./Sept. 1975, pp. 4-10.
2. S. Mostovoy, P. B. Crosley, and E. J. Ripling, "Use of Crack-Line-Loaded Specimens for Measuring Plane-Strain Fracture Toughness," J. Materials, vol. 2, no. 3, 1967.
3. J. A. Marceau and J. C. McMillan, "Exploratory Development on Durability of Adhesive Bonded Joints," 1976, AFML-TR-76-173.
4. J. A. Marceau, Y. Moji, and J. C. McMillan, "A Wedge Test for Evaluating Adhesive-Bonded Surface Durability," Adhesives Age, October 1977, pp. 28-34.
5. J. A. Marceau and W. Scardino, "Durability of Adhesive Bonded Joints," 1975, AFML-TR-75-3.
6. H. W. Eickner and N. E. Schowalter, "A Study of Methods for Preparing Clad 24S-T3 Aluminum Alloy Sheet Surfaces for Adhesive Bonding," Forest Product Laboratory Report No. 1813, May 1950.
7. P. F. A. Bijlmer, "Adhesive Bonding on Anodized Aluminum," Metal Finishing, April 1972, pp. 30-40.



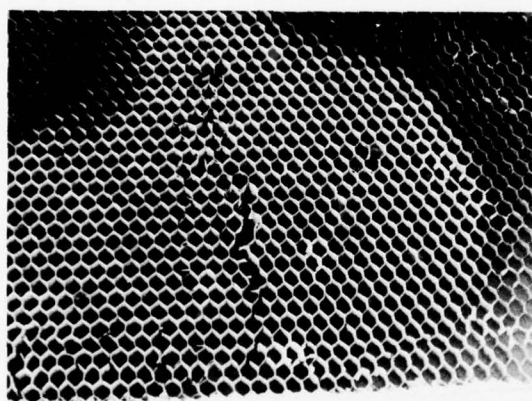
8. J. M. Chen, T. S. Sun, J. D. Venables, and R. Hopping, "Effects of Fluorine Contamination on the Microstructure and Bondability of Aluminum Surfaces," SAMPE Journal, Jul./Aug. 1978.
9. A. W. Smith, "Surface Oxide on Etched Aluminum," J. Electrochem. Soc.: Solid-State Sci. and Tech., Nov. 1973.
10. S. Wernick and R. Pinner, The Surface Treatment and Finishing of Aluminum and Its Alloys, 4th edition, volume 1, Teddington, Robert Draper Ltd., 1972.
11. F. Keller, M. S. Hunter, and D. L. Robinson, J. Electrochem. Soc., vol. 100, no. 9, 1953, pp. 444-19.
12. J. W. Diggle, T. C. Downie, and C. W. Goulding, "Anodic Oxide Films on Aluminum," Chem. Rev., vol. 69, 1969, pp. 365-405.
13. J. O. O'Sullivan and G. C. Wood, "The Morphology and Mechanism of Formation of Porous Anodic Films on Aluminum," Proc. Roy. Soc. Lond. A., 317, 1970, pp. 511-543.
14. J. D. Venables, D. K. McNamara, J. M. Chen, T. S. Sun, and R. Hopping, "Oxide Morphologies on Aluminum Prepared for Adhesive Bonded Aircraft Structures," to be published in Applications of Surface Science.
15. Douglas Aircraft Company, "Primary Adhesively Bonded Structure Technology (PABST), Phase Ib: Preliminary Design," 1976, AFFDL-TR-76-141.
16. G. E. Thompson, R. C. Furneaux, G. C. Wood, and R. Hutchings, "STEM/EDAX Analysis of the Cell Walls in Porous Anodic Films Formed on Aluminum," J. Electrochem. Soc.: Electrochem. Sci. and Tech., Sep. 1978, pp. 1480-1482.
17. F. J. Riel, "Corrosive Delaminations," SAMPE Journal, vol. 7, no. 5, Aug./Sep. 1971.
18. N. Rogers, "Corrosion of Adhesive Bonded Clad Aluminum," presented at the SAE National Business Aircraft Meeting, Wichita, Kansas, Mar. 15-17, 1972.
19. W. Scardino, "Comparative Stressed Durability of Adhesive Bonded Aluminum Alloy Joints," presented at Symposium on Durability of Adhesive Bonded Structured sponsored by U.S. Armament Research and Development Command, Dover, N. J., October 27-29, 1976.



METAL TO METAL DELAMINATION



METAL TO HONEYCOMB DELAMINATION

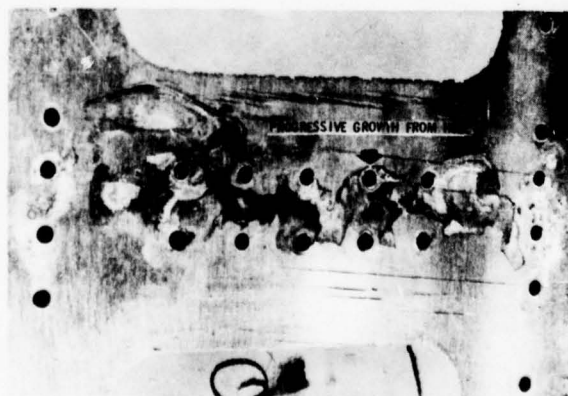


ADHESIVE CORE PULLOUT



CLAD DISSOLUTION CORROSION

*Figure 1. Service Failures Due to Environmental Degradation*



- ADHESIVE
- MOISTURE ACCESS
- PROGRESSIVE
- LOW STRESS

*Figure 2. Characteristics of Service Disbonds*

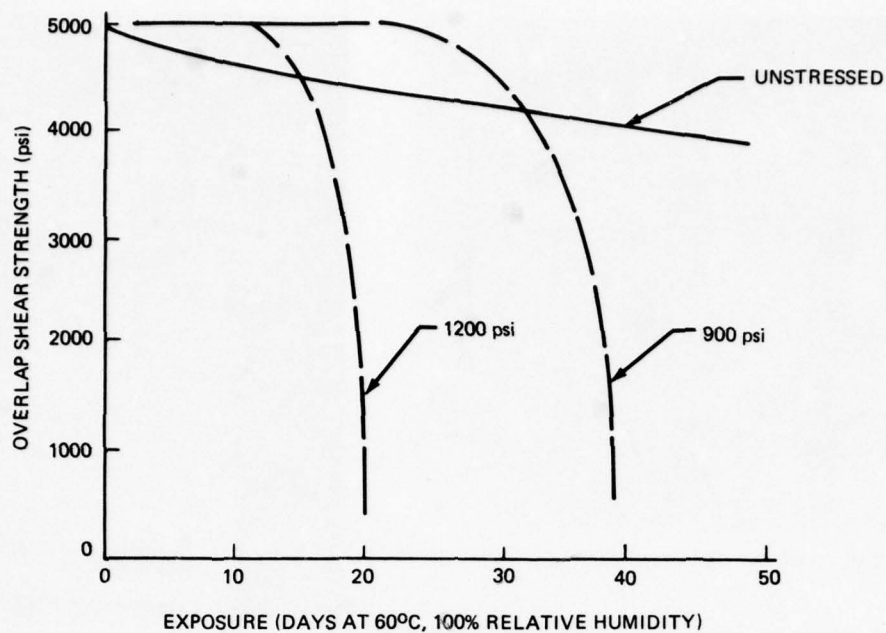


Figure 3. Residual Strength After Environmental Exposure

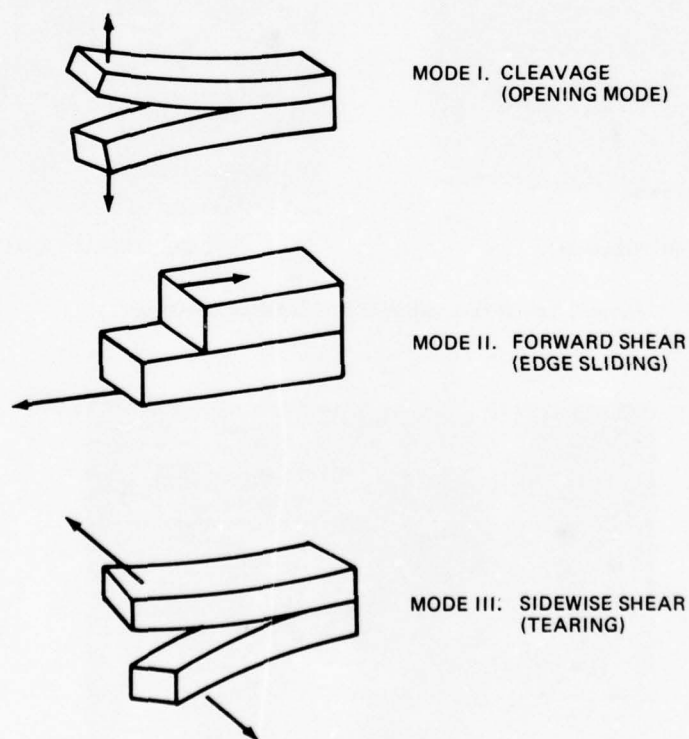


Figure 4. Basic Loading Modes



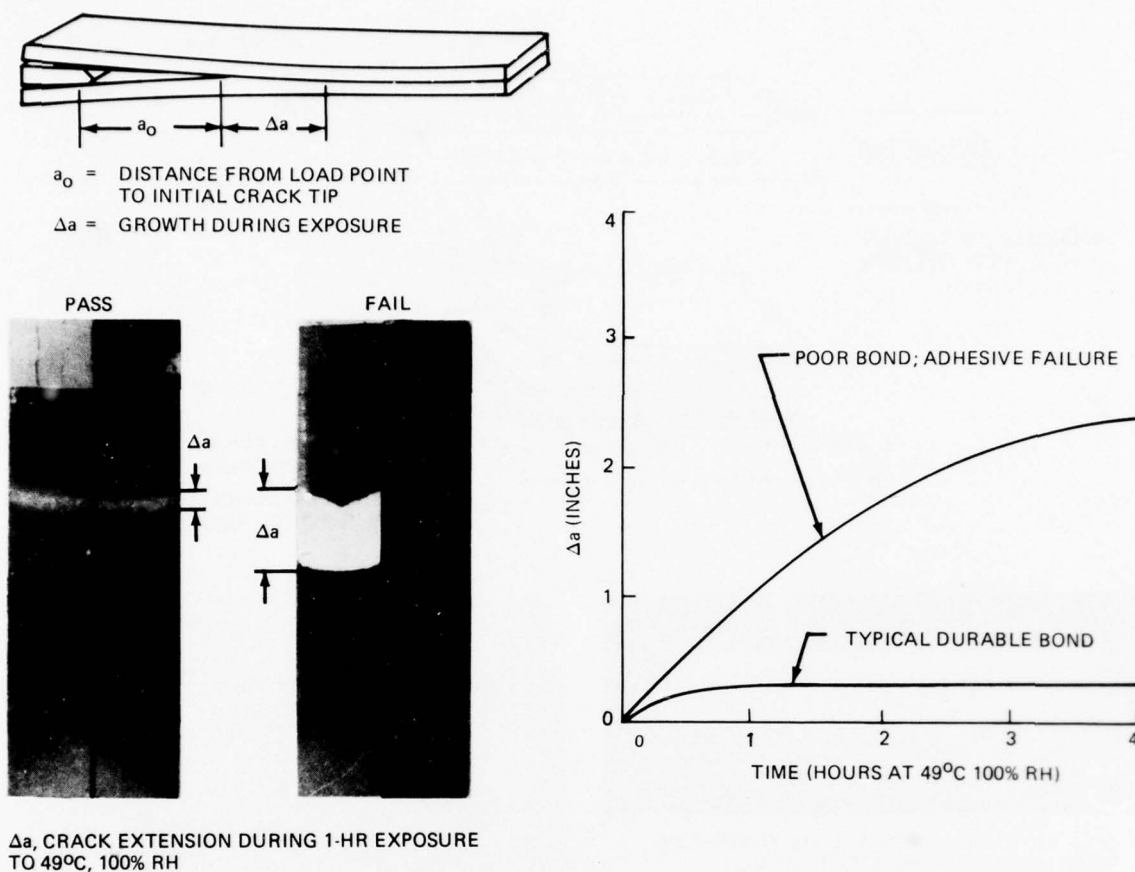


Figure 5. Boeing Wedge Test

BONDLINE TESTED	ASSEMBLY	SERVICE DISBOND	LAP-SHEAR AVG (psi)	PORTA SHEAR AVG (psi)	MODIFIED WEDGE TEST	
					$a_0$	$\Delta a^*$
SKIN/DOUBLER	A	YES	4,828†	4,198†	1.66†	1.84‡
	B	YES	4,795†	4,428†	1.10†	1.16‡
	C	NO	4,415†	4,118†	0.48§	0
	D	NO	4,425†	4,762†	0.33§	0
DOUBLER/TRIPLER	A	YES	4,734†	4,872†	1.53†	2.44‡
	B	YES	4,790†	4,880†	0.93§	1.04‡

\* 1-hr EXPOSURE AT 60°C, 100% RH.  
 † MIXED ADHESIVE-COHESIVE FAILURE MODES.  
 ‡ 100% ADHESIVE FAILURE MODE.  
 § 100% COHESIVE FAILURE MODE.

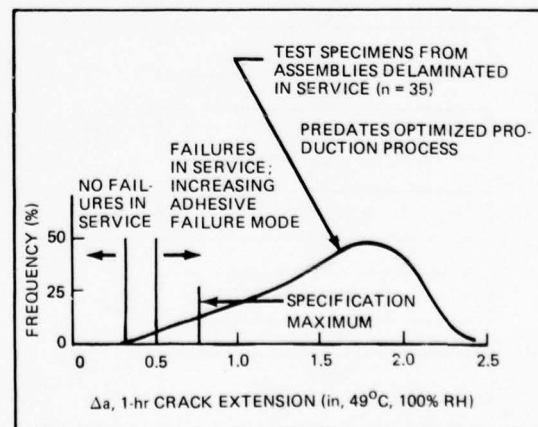
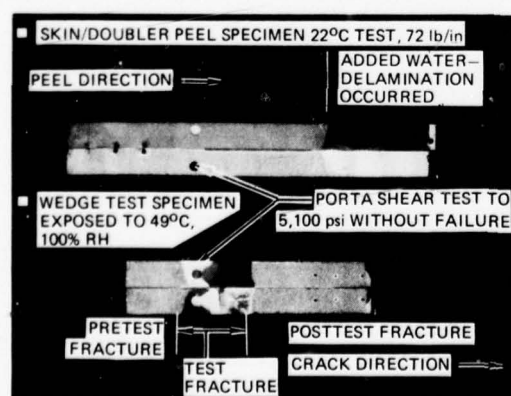


Figure 6. Correlation of Laboratory Testing With Inservice Performance

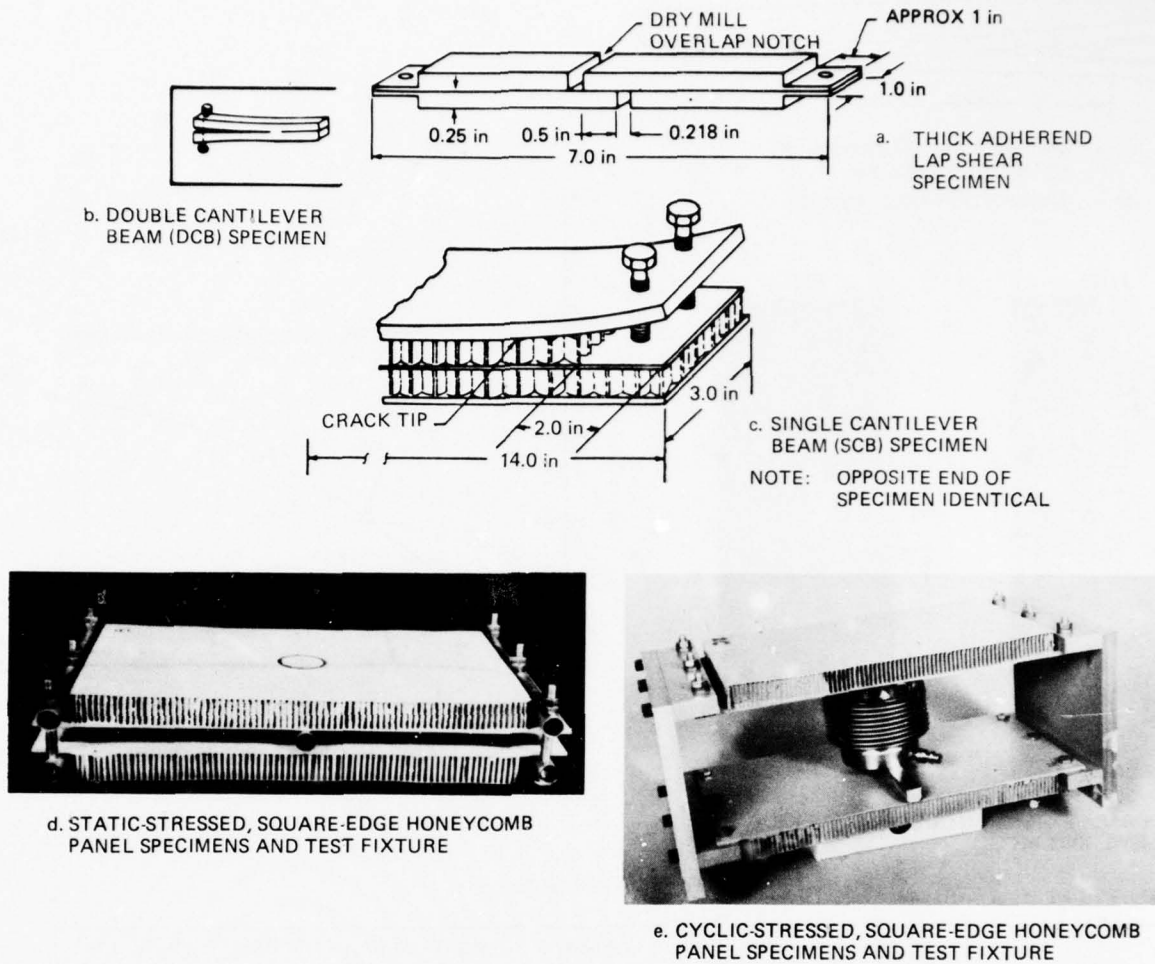


Figure 7. Environmental Durability Test Specimens

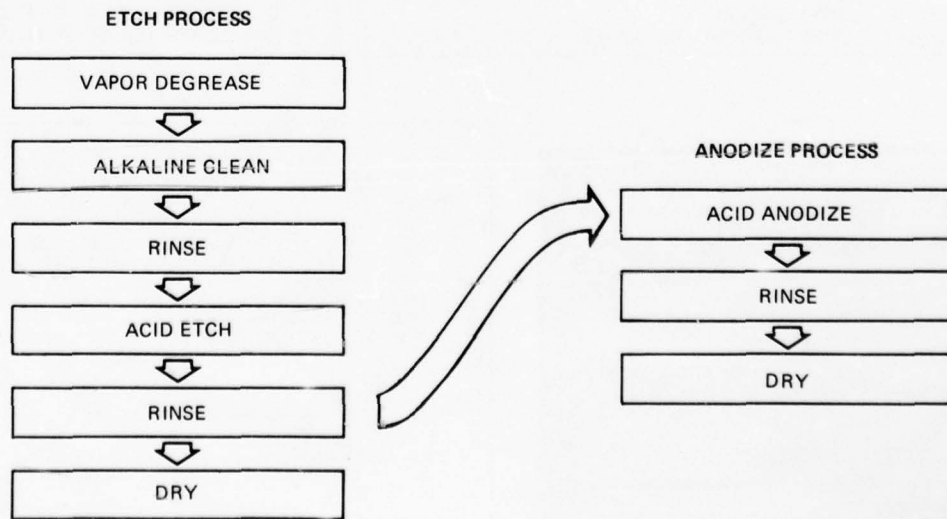


Figure 8. Surface Preparation Steps

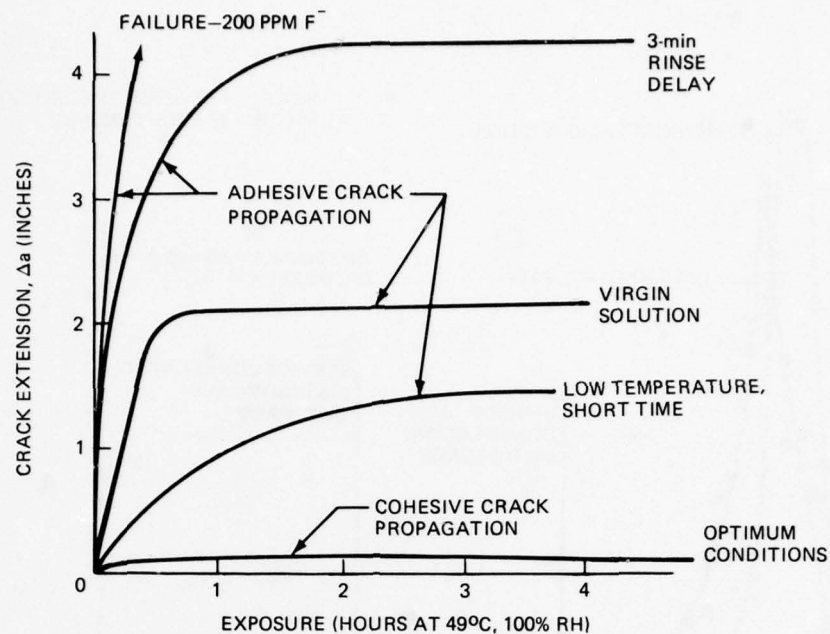


Figure 9. Effect of Process Variables on Crack Propagation

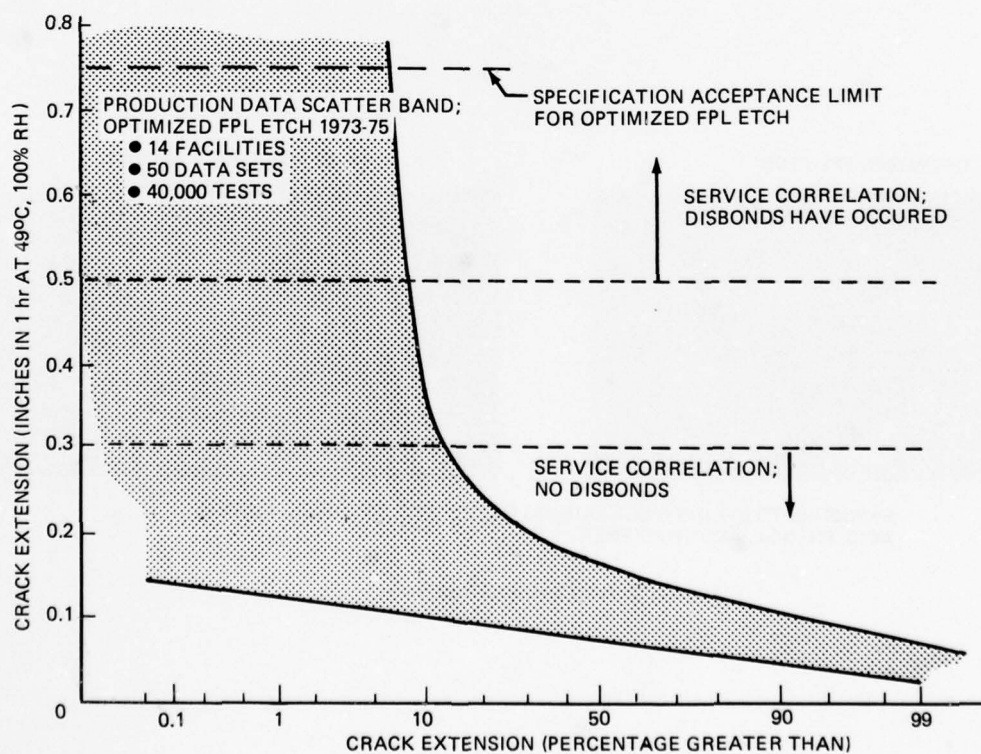


Figure 10. Distribution of Production Process Control Wedge Test Crack Extensions



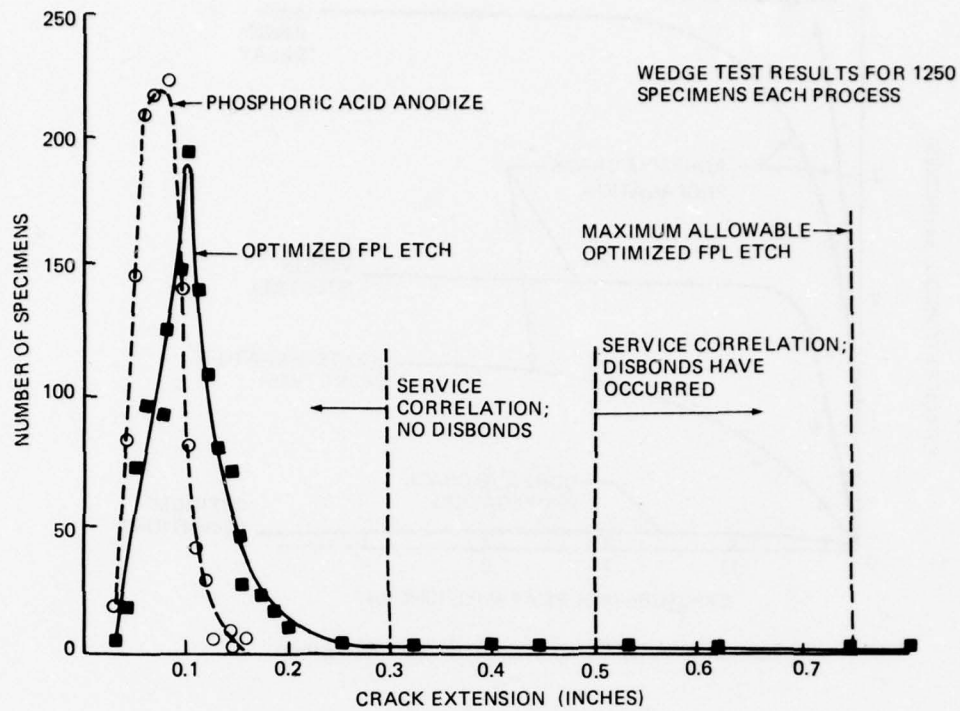


Figure 11. Wedge Test Result Comparison

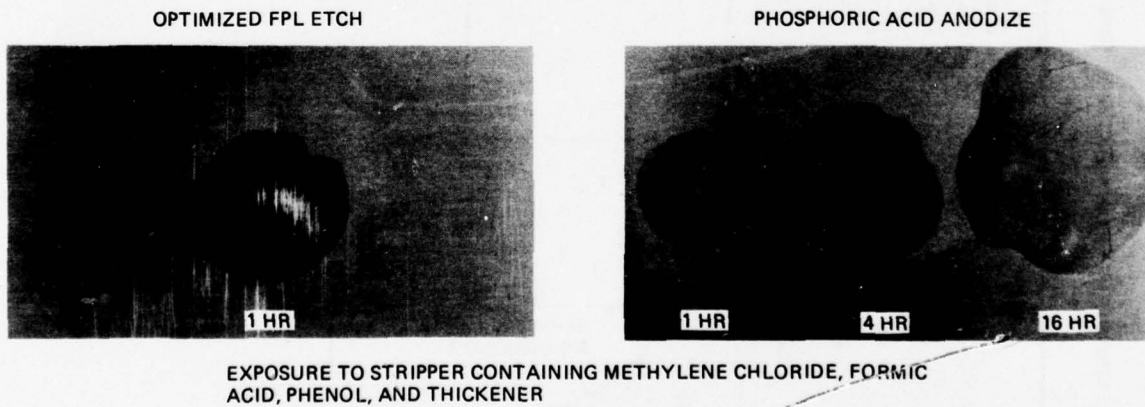
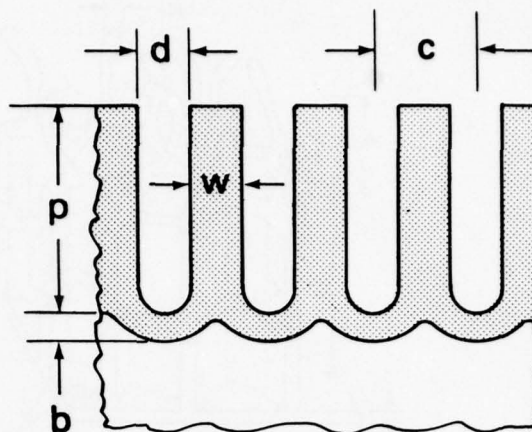


Figure 12. Paint Stripper Effectiveness

b = BARRIER-LAYER THICKNESS  
 p = POROUS-LAYER THICKNESS  
 c = CELL DIAMETER  
 d = PORE DIAMETER  
 w = 2 x CELL WALL THICKNESS



OXIDE FORMATION PROCESS <sup>a</sup>	THEORETICAL, Å					MEASURED, Å				
	b	p	c	d	w	b	p	c	d	w
PHOSPHORIC ACID ANODIZE, 10 VOLT	110 <sup>b</sup> 104 <sup>c</sup>	—	—	> 330 > 275 <sup>c</sup>	220 <sup>b</sup>	~ 100	3000 TO 8000	800 TO 1300	500 TO 1000	300 TO 800
CHROMIC ACID ANODIZE, 40 VOLT	436 <sup>b</sup>	—	1308	—	872	—	—	—	—	—
CHROMIC ACID ANODIZE, 22 VOLT	240 <sup>b</sup>	—	—	—	400	—	5000 TO 30000	—	480	—
FPL ETCH	40 <sup>d</sup> 50 <sup>e</sup>	—	—	—	80 <sup>d</sup>	40 <sup>d</sup>	400 <sup>d</sup> 400 <sup>f</sup>	400 <sup>d</sup> 400 <sup>f</sup>	480 <sup>d</sup>	80 <sup>d</sup>

a. FOR RELATIVELY PURE ALUMINUM; e.g., THE CLADDING ON 2024 ALLOY

b. REFERENCE 12

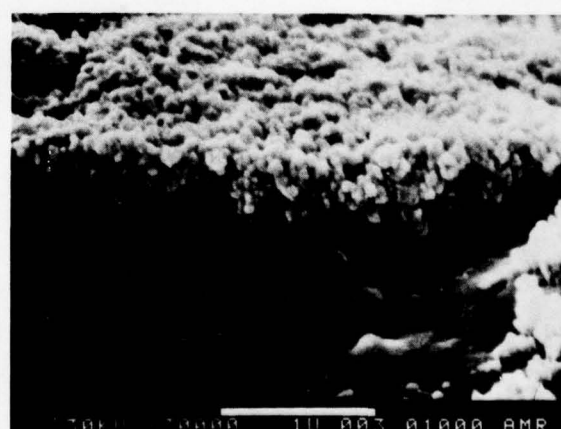
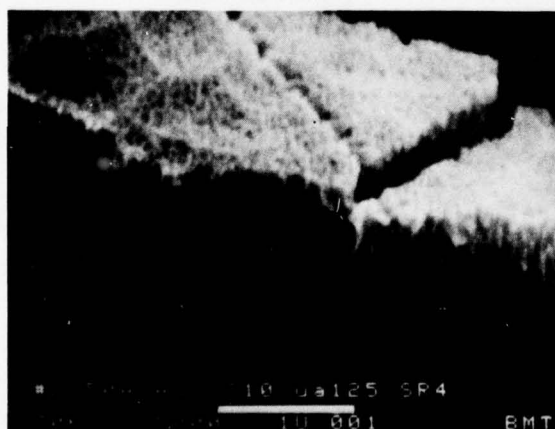
d. REFERENCE 10

f. REFERENCE 8

c. REFERENCE 13

e. REFERENCE 9

Figure 13. Oxide Characteristics



PHOSPHORIC ACID ANODIZE, 10V, 22°C, 10% H<sub>3</sub>PO<sub>4</sub>

ALLOY: 2024-T3 CLAD  
OXIDE THICKNESS (p + b) ~ 7500 Å

ALLOY: 7075-T6 BARE  
OXIDE THICKNESS (p + b) ~ 5000 Å

Figure 14. Characteristic Oxide Morphology

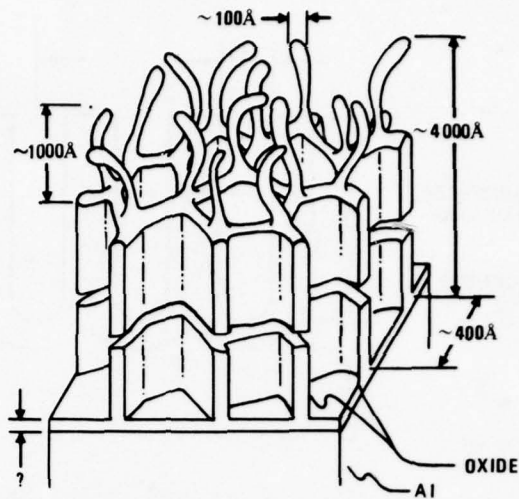
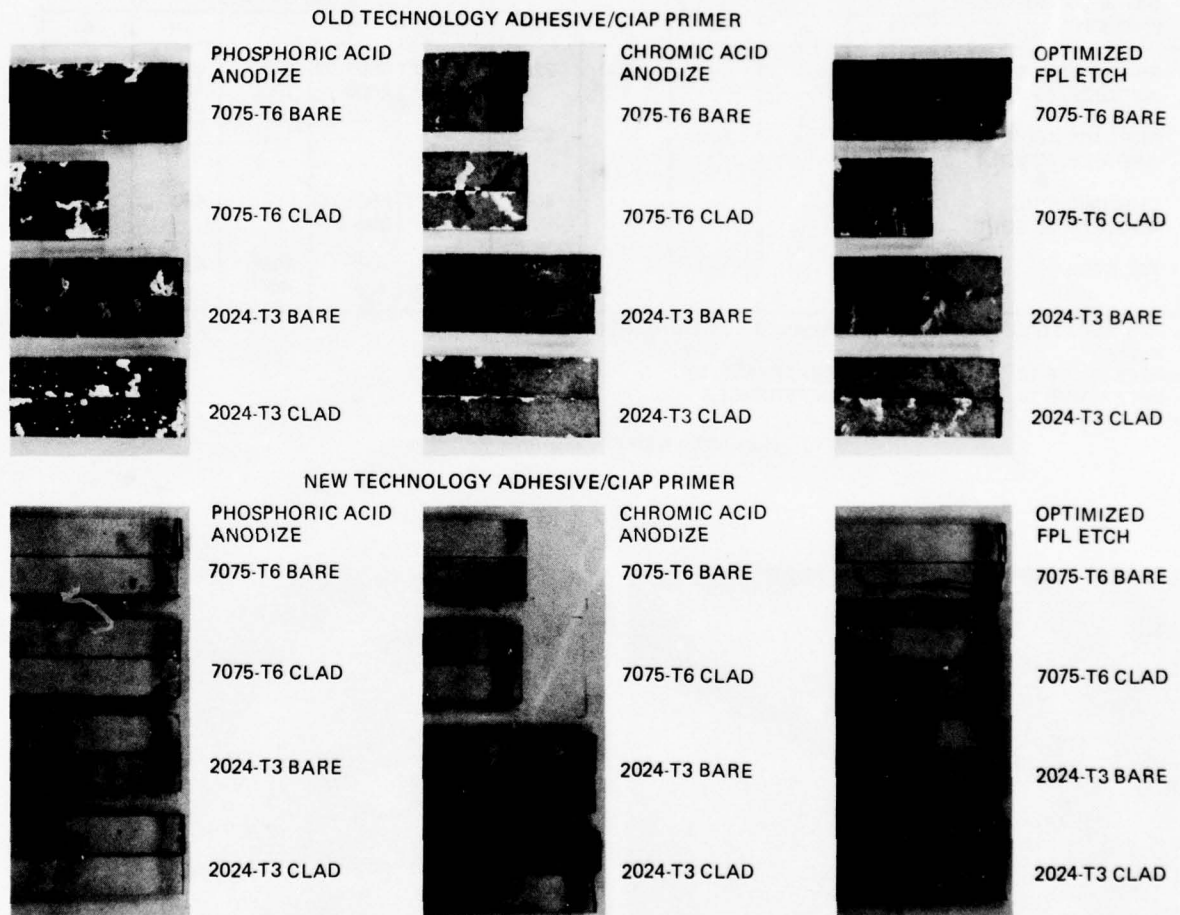


Figure 15. Schematic Representation of Phosphoric Acid Anodized Surface Oxide by Venables, et al. (Reference 14)



a. EFFECT OF ALLOY, SURFACE PREPARATION, AND ADHESIVE (ABOUT 80 WEEKS' EXPOSURE)

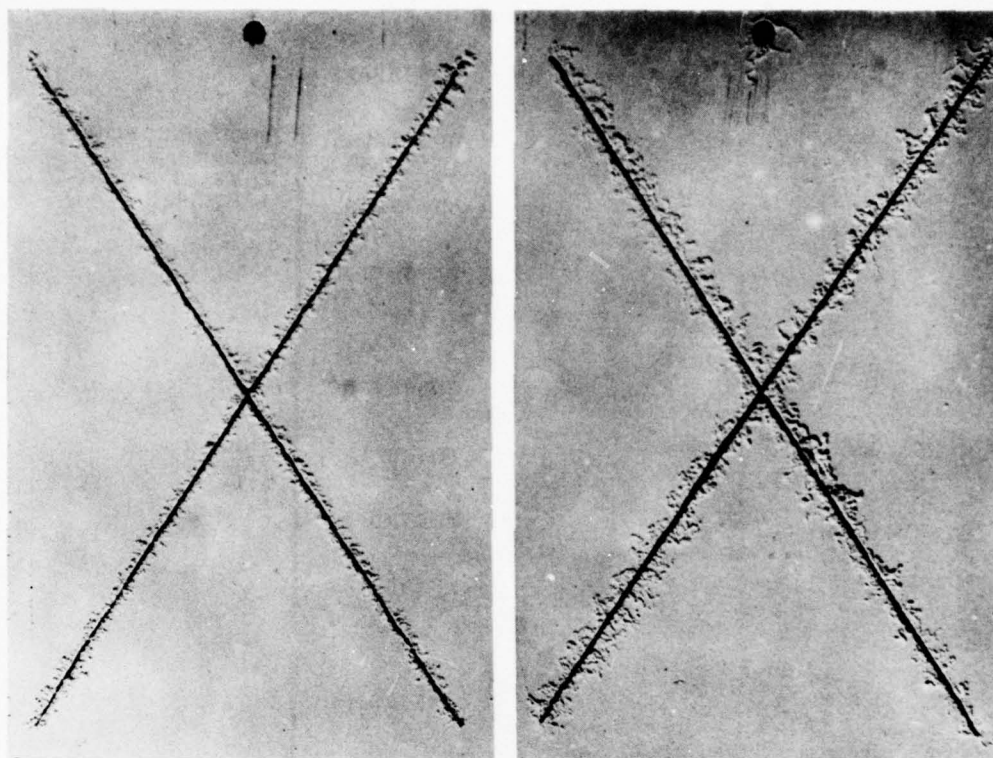


OLD TECHNOLOGY ADHESIVE, 2024-T3 CLAD

b. EFFECT OF SURFACE PREPARATION AND ADHESIVE PRIMER (ABOUT 80 WEEKS' EXPOSURE)

Figure 16. Crevice Cell Corrosion After Long-Term Exposure to 60°C and Condensing Humidity





PHOSPHORIC ACID ANODIZE

OPTIMIZED FPL ETCH

90-DAY TEST; CIAP PRIMER PLUS POLYURETHANE PRIMER PLUS  
POLYURETHANE ENAMEL

Figure 17. Effect of Surface Preparation on Filiform Corrosion Resistance

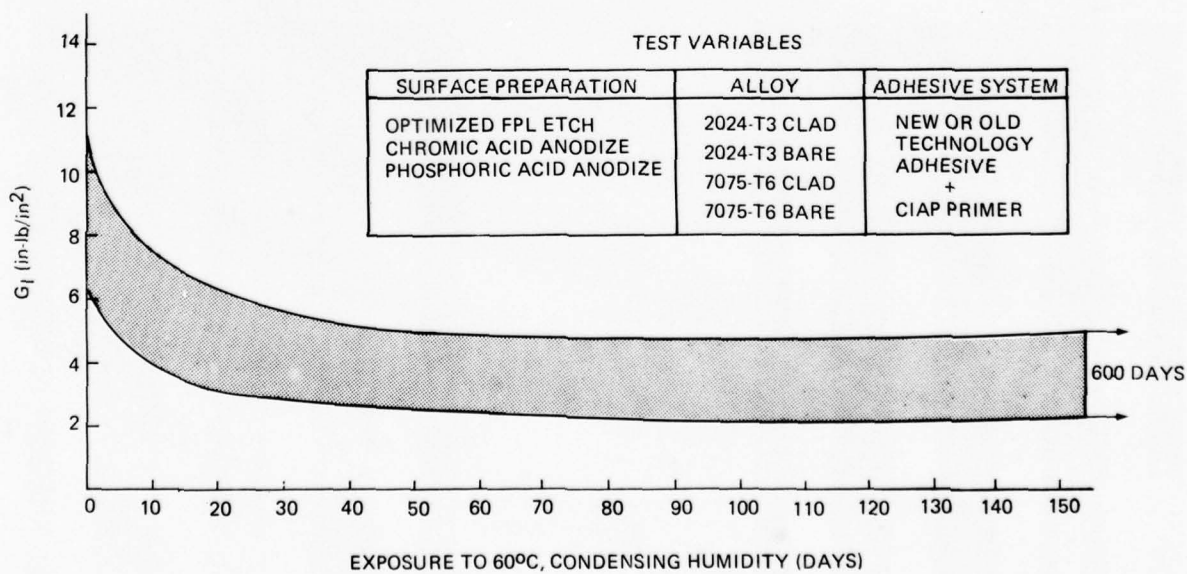


Figure 18. Double Cantilever Beam Specimen Exposure Results

## OLD TECHNOLOGY ADHESIVE/CIAP PRIMER

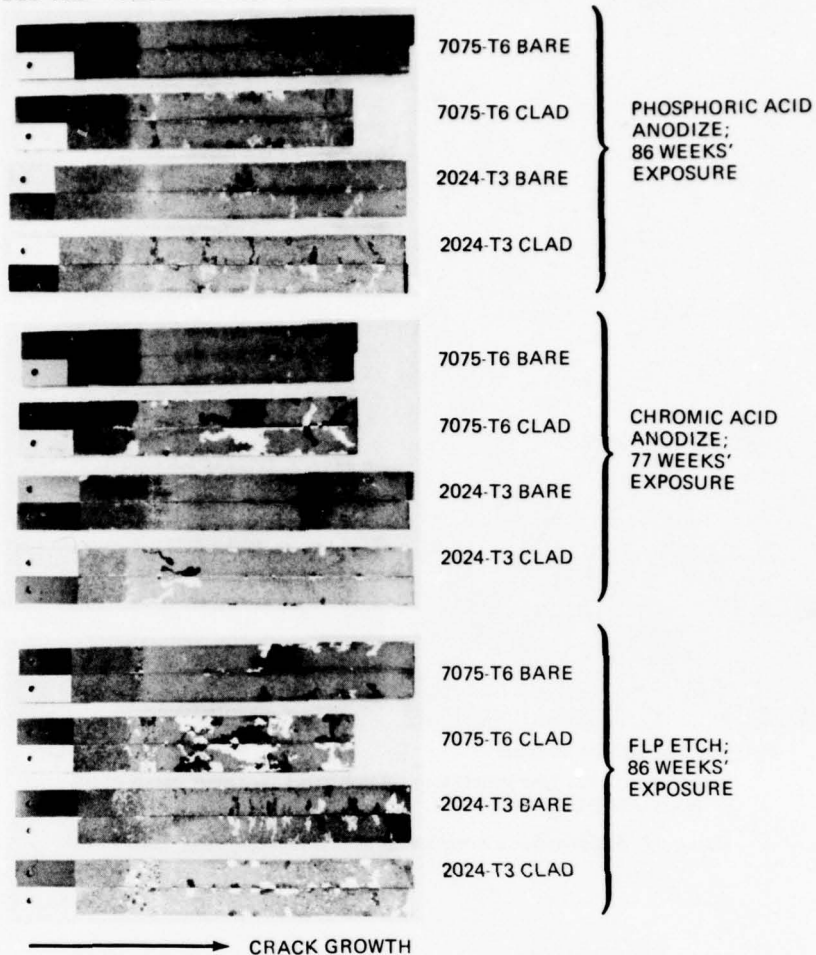
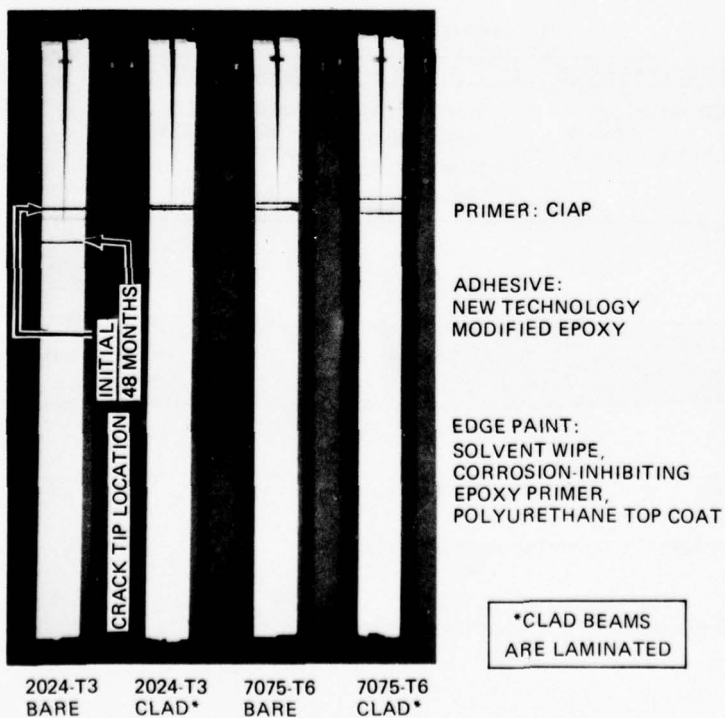


Figure 19. Opened DCB Specimens After Extended Exposure to 60°C and Condensing Humidity

## OPTIMIZED FPL ETCH



## PHOSPHORIC ACID ANODIZE

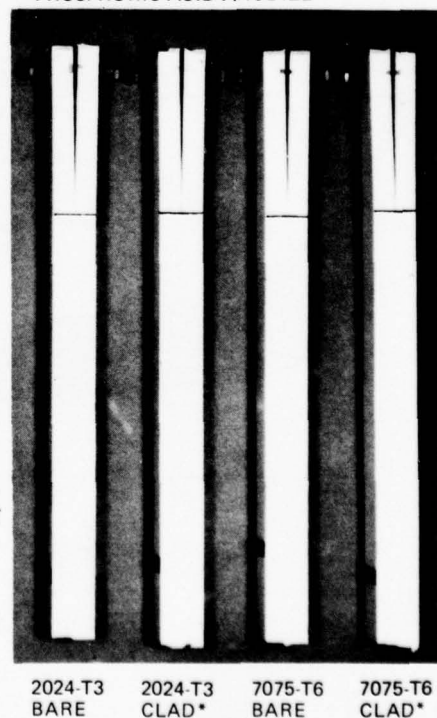
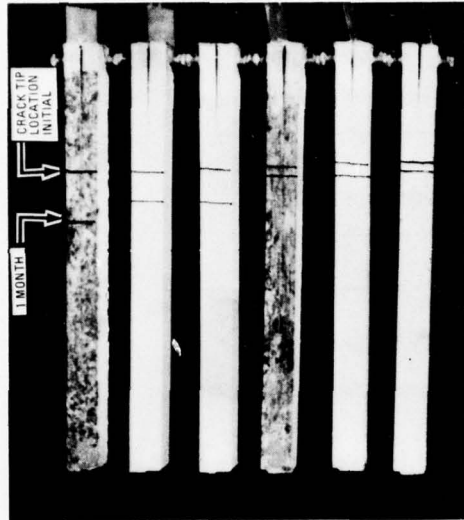


Figure 20. Double Cantilever Beam Specimens, 48-month South Florida Exposure

- ADHESIVE: NEW TECHNOLOGY
- PRIMER: CIAP

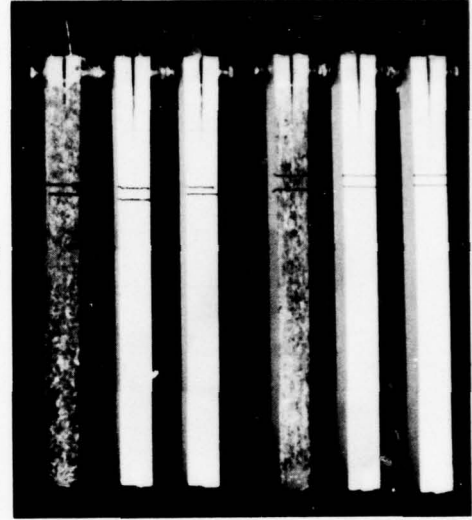
- EDGE TREATMENT: 1-BARE  
2-SOLVENT WIPE PLUS POLYURETHANE PRIMER PLUS POLYURETHANE TOP COAT  
3-PHOSPHORIC ACID ANODIZE PLUS CIAP PRIMER PLUS POLYURETHANE PRIMER AND TOP COAT

## OPTIMIZED FPL ETCH



1 2 3 1 2 3  
2024-T3 BARE 2024-T3 CLAD\*

## PHOSPHORIC ACID ANODIZE



1 2 3 1 2 3  
2024-T3 BARE 2024-T3 CLAD\*

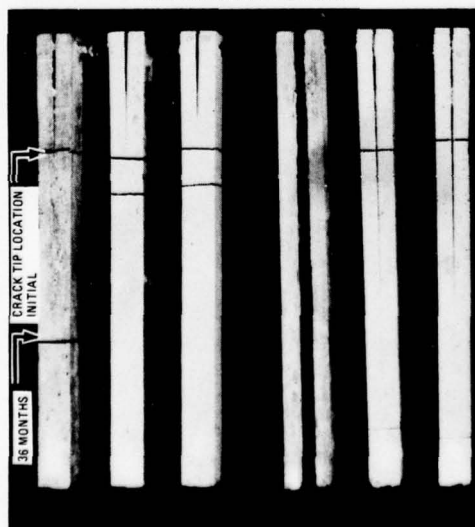
\*CLAD BEAMS ARE LAMINATED

Figure 21. Double Cantilever Beam Specimens, 90-Day 5% Salt Spray Exposure

- ADHESIVE: NEW TECHNOLOGY
- PRIMER: CIAP

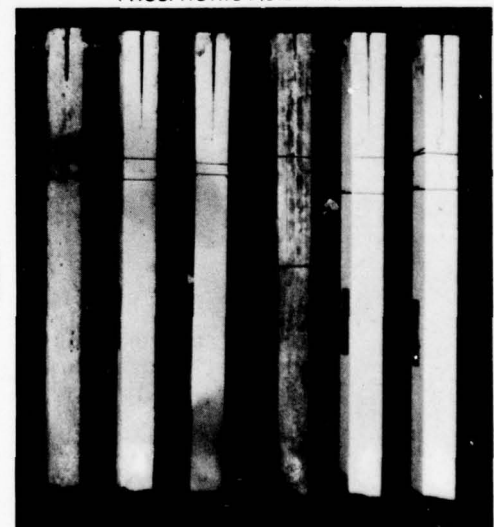
- EDGE TREATMENT: 1-BARE  
2-SOLVENT WIPE PLUS POLYURETHANE PRIMER PLUS POLYURETHANE TOP COAT  
3-PHOSPHORIC ACID ANODIZE PLUS CIAP PRIMER PLUS POLYURETHANE PRIMER AND TOP COAT

## OPTIMIZED FPL ETCH



1 2 3 1 2 3  
7075-T6 BARE 7075-T6 CLAD\*

## PHOSPHORIC ACID ANODIZE



1 2 3 1 2 3  
7075-T6 BARE 7075-T6 CLAD\*

\*CLAD BEAMS ARE LAMINATED

Figure 22. Double Cantilever Beam Specimens, 36-Month 5% Salt Spray Exposure



SUSTAINED STRESS TESTING  
SCB SPECIMENS  
NEW TECHNOLOGY ADHESIVE SYSTEM

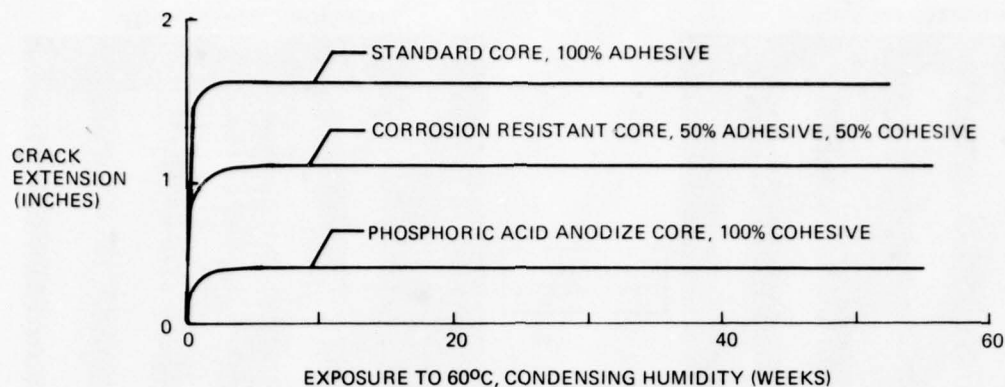


Figure 23. Effect of Core Surface Treatment on Honeycomb Sandwich Durability

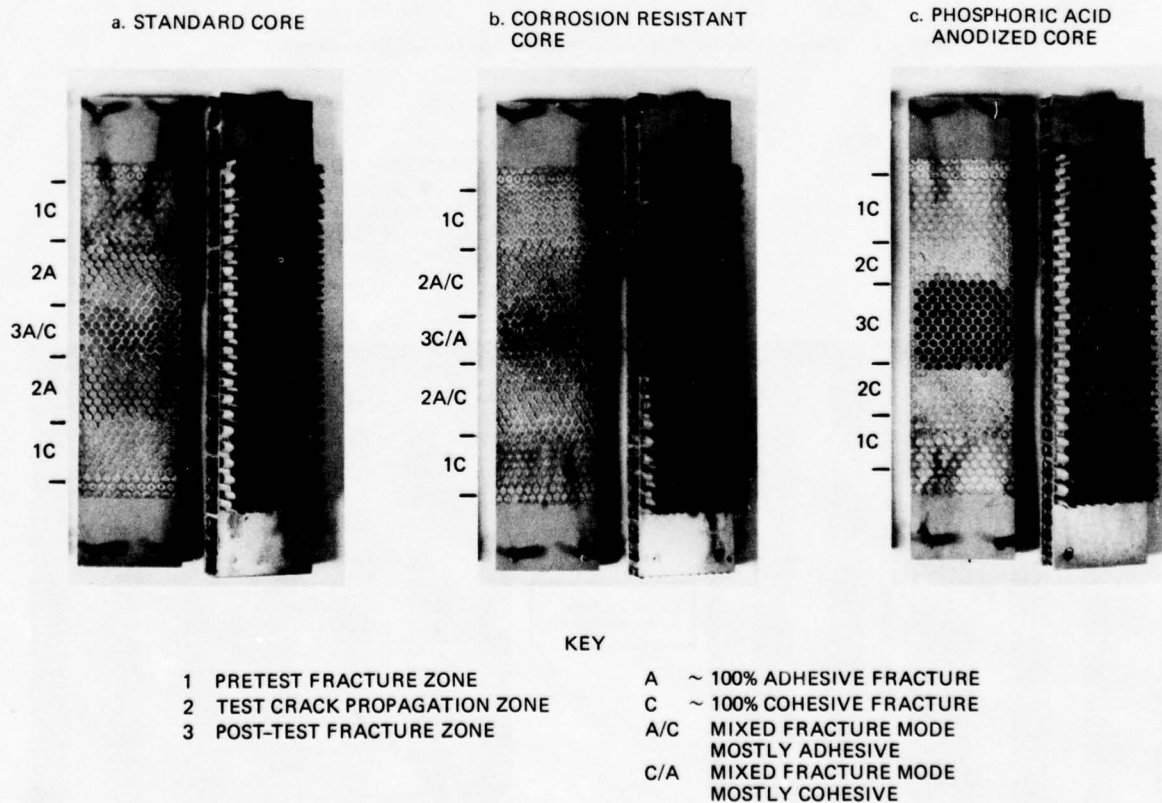


Figure 24. Opened SCB Specimens After Extended Exposure to 60°C and Condensing Humidity

## DELAMINATED PANEL AFTER 400 CYCLES

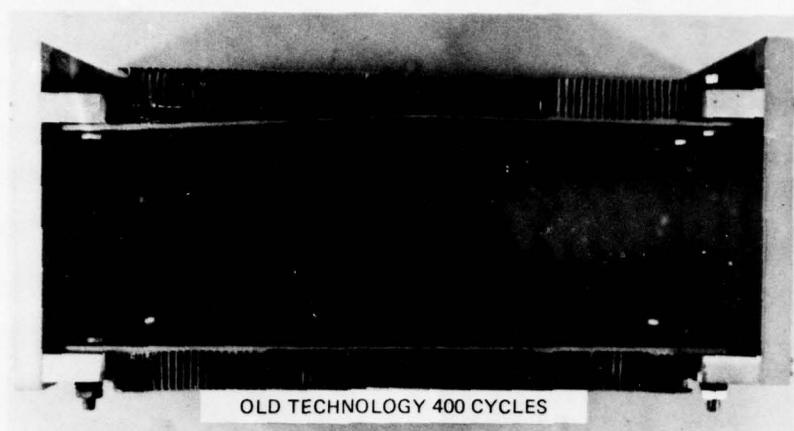


Figure 25. Static-Loaded Honeycomb Panels, GAG Cycling

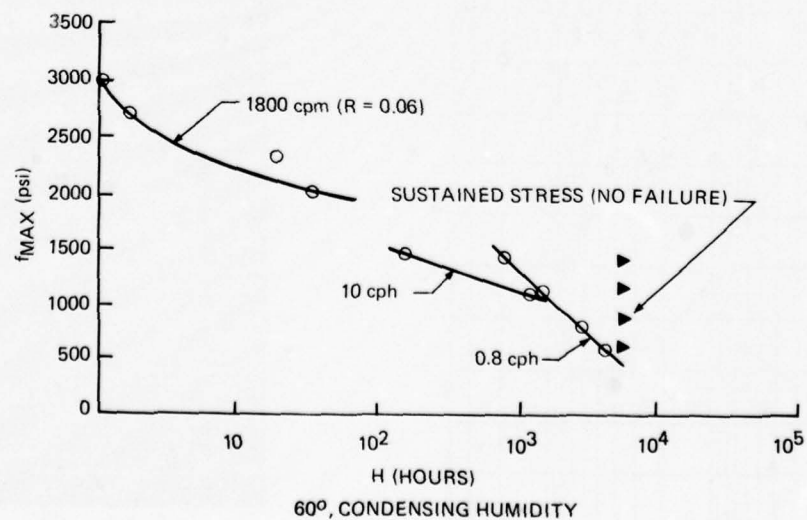
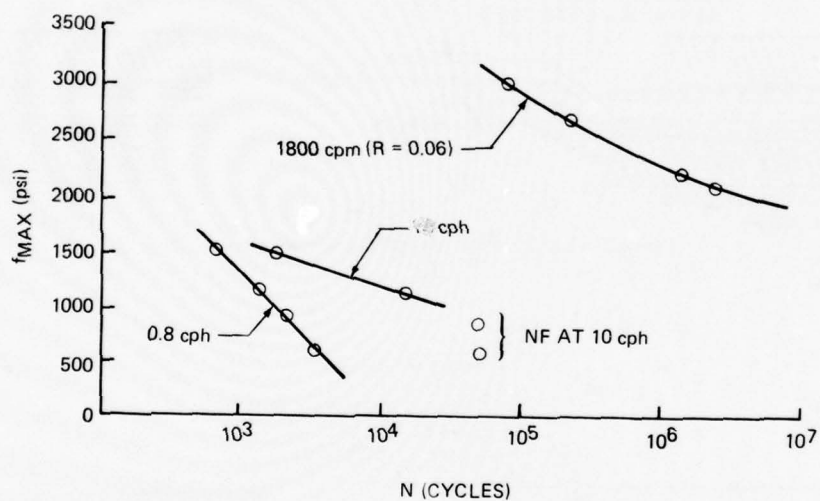


Figure 26. Thick Adherend Specimens, Fatigue Test Results

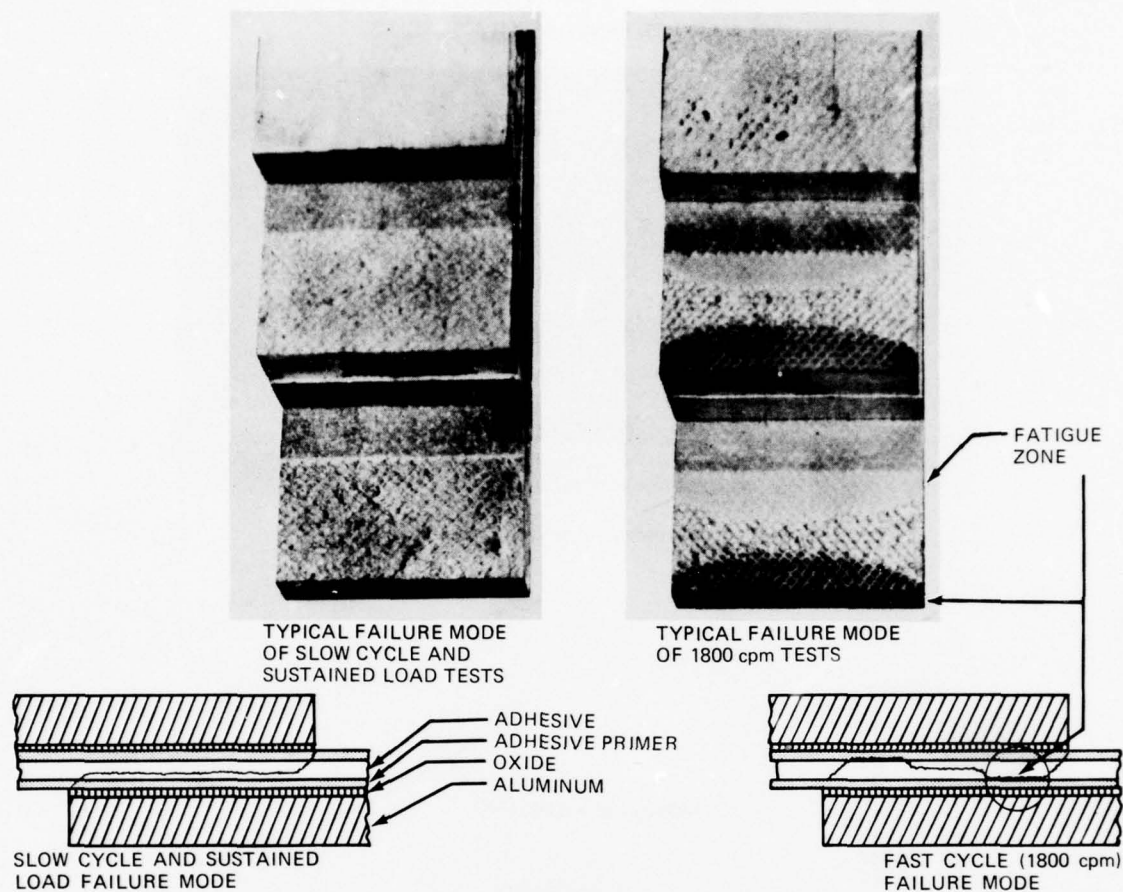


Figure 27. Lap Shear Fatigue Test Crack Propagation Modes

R = 0.06 at 1800 cpm  
60°C/100% RH  
ADHESIVE: NEW TECHNOLOGY  
ADHESIVE/CIAP  
ALLOY: 7075-T6 BARE

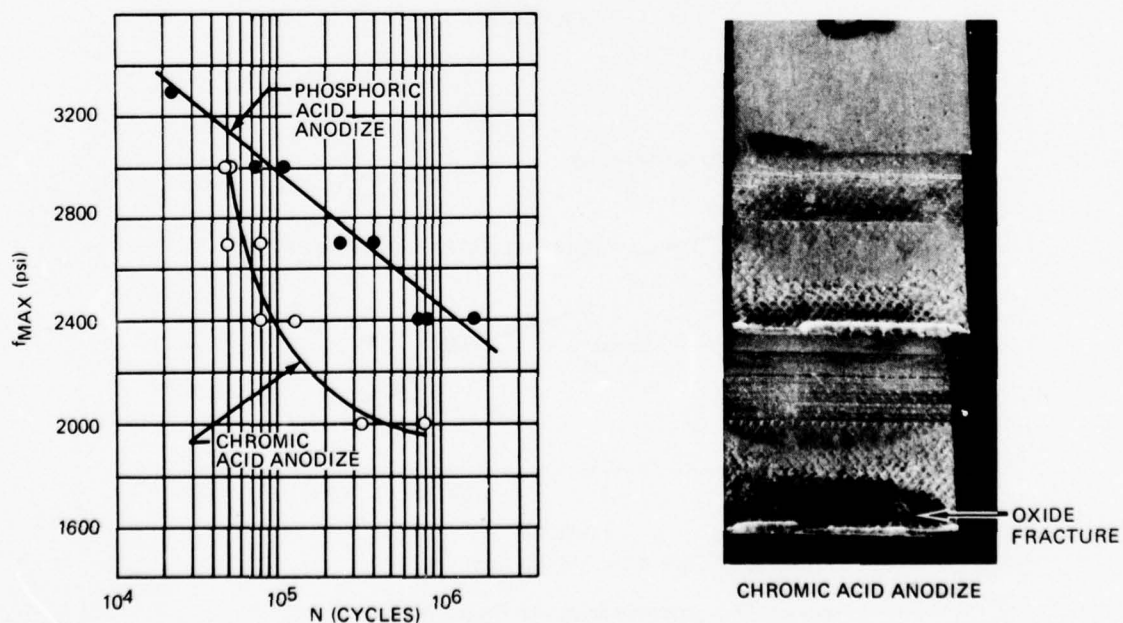
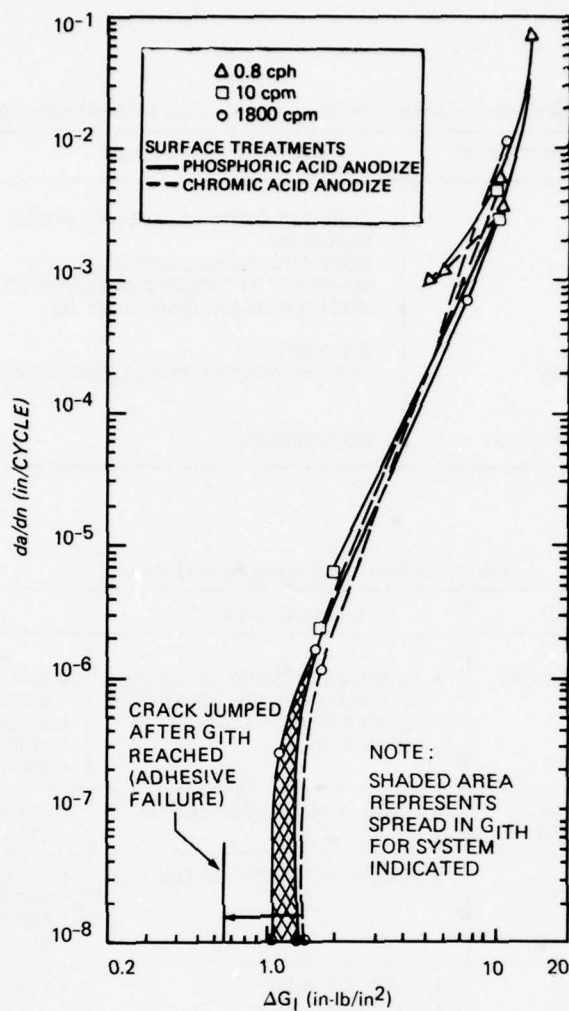


Figure 28. Effect of Surface Preparation on Lap Shear Fatigue Test Results





SPECIMENS TESTED AT ROOM TEMPERATURE, HUMIDITY < 50%,  
NEW TECHNOLOGY ADHESIVE/CIAP PRIMER, 2024-T3 BARE

Figure 29. DCB Fatigue Test Results

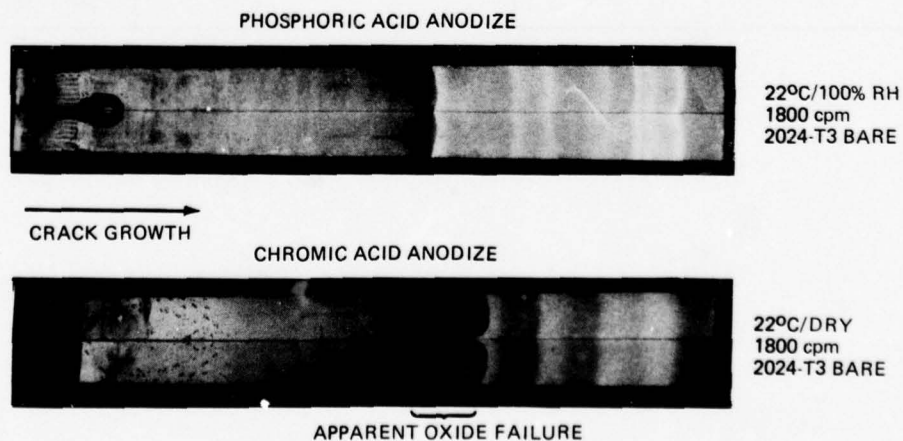


Figure 30. Opened DCB Fatigue Test Specimens

Table I. Commercial Aircraft Service Experience—120°C Curing Modified Epoxy Adhesives

SURFACE PREPARATION TREATMENT	SERVICE EXPERIENCE	YEARS
1965–1973 ORIGINAL FPL ETCH PROCESS	EARLIEST DISBONDS—VERY LIMITED NUMBERS SOME ADDITIONAL DISBONDS MAJORITY OF DISBOND OCCURRENCES MOST BONDS SATISFACTORY TO	0.5 2–3 4–7 14
1973–1978 "OPTIMIZED" FPL ETCH PROCESS	NO DISBONDS ONE INCIDENT OF CLAD DISSOLUTION	6 3
1975–1978 PHOSPHORIC ACID ANODIZE PROCESS	NO DISBONDS	4

Table II. Categories of Environmental Disbond

FORM	MODE	CHARACTERISTICS	CAUSE
METAL-TO-METAL BONDMENT	DELAMINATION	• ADHESIVE DISBOND AT METAL INTERFACE—SUBSEQUENT MILD TO SEVERE EXFOLIATION CORROSION	• ENVIRONMENTALLY INDUCED DISBOND • INADEQUATE SURFACE PREPARATION • CREVICE CELL ESTABLISHED
	CREVICE CELL CORROSION	• LOCAL, LIMITED CORROSION	• LOCAL CREVICE CORROSION CELL ESTABLISHED
	CLAD DISSOLUTION	• CLAD IN BONDLINE DISSOLVED	• POTENTIAL DIFFERENCE BETWEEN CLADDING AND BASE METAL PLUS CREVICE CELL CORROSION
METAL-TO-METAL HONEYCOMB BONDMENT	WATER INGESTION	• CORE CORROSION • CORE FRACTURE • COHESIVE DISBOND OF FACE SHEETS	• CONTINUOUS MOISTURE PATHS
	ADHESIVE CORE PULLOUT	• CORE PULLOUT WITH ADHESIVE ON FACE SHEETS • CORE CORROSION	• INADEQUATE CORE SURFACE PREPARATION OR INADEQUATE ADHESIVE FLOW
	DELAMINATION	• DISBOND WITH ADHESIVE ON CORE	• ENVIRONMENTALLY INDUCED DISBOND • INADEQUATE FACE SHEET SURFACE PREPARATION

Table III. Comparison of Surface Preparation Methods—Boeing Practice

	ORIGINAL FPL ETCH	OPTIMIZED FPL ETCH	PHOSPHORIC ACID ANODIZING
CHEMISTRY	*****COMPLEX*****		SIMPLE
ANODIZE VOLTAGE	"SELF-ANODIZE" MIXED POTENTIAL, ELECTROCHEMICAL EQUIVALENT TO 2 TO 3 VOLTS		EXTERNAL APPLIED 10 OR 15 VOLTS
SOLUTION COMPOSITION SULPHURIC ACID, OZ/GAL SODIUM DICHROMATE, OZ/GAL "SEEDING" OR "AGING"	38.5–41.5  4.1–4.9 NONE REQUIRED BY SPECIFICATION	38.5–41.5  4.1–12.0 0.2 OZ/GAL 2024 ALUMINUM PLUS COPPER SULFATE AS REQUIRED UP TO 400 ppm COPPER	NONE REQUIRED
PHOSPHORIC ACID	—	—	13–16 OZ/GAL
EFFECT OF SOLUTION CONTAMINANTS	*****LOW TOLERANCE*****		MODERATE TOLERANCE
SOLUTION LIFE	NOT DEFINED	1 TO 2 YEARS	NO KNOWN LIMIT
SOLUTION TEMPERATURE	144–160°F 60–71.1°C	150–160°F 65.5–71.1°C	67–77°F 19.4–25°C
PROCESSING TIME	8–10 MINUTES	12–15 MINUTES	20–25 MINUTES
RINSING REQUIREMENTS	CONVENTIONAL IMMERSION OR SPRAY	RINSE AS REMOVED FROM SOLUTION (ZERO RINSE DELAY)	CONVENTIONAL IMMERSION OR SPRAY. 2.5-MINUTE RINSE DELAY TOLERABLE
PROCESS CONTROL REQUIREMENTS	IN-PROCESS CONTROL LAP SHEARS ON A PART-BY-PART BASIS; PEEL TEST ON EACH LOAD	IN-PROCESS CONTROL, WEDGE TESTS FOR EACH LOAD	IN-PROCESS CONTROL, POLARIZED LIGHT, INTERFERENCE COLOR CHANGE ON EACH PART
RESISTANCE OF PREPARED SURFACE TO HUMIDITY	MODERATELY REACTIVE, PRIME WITHIN 16 HOURS		QUITE RESISTANT, PRIME WITHIN 72 HOURS
SENSITIVITY OF PREPARED SURFACE TO ABRASION DAMAGE IN HANDLING	*****QUITE SENSITIVE, NEED TO AVOID OR MINIMIZE*****		
ENVIRONMENTAL DURABILITY	GOOD TO POOR	MOSTLY GOOD, SMALL PERCENTAGE MARGINAL TO POOR	CONSISTENTLY GOOD



Table IV. Square Edge Honeycomb Tests

TECHNOLOGY	GROUND-AIR-GROUND CYCLING				60°C/100% RH
	NO STRESS	23 lb/LINEAR in., STATIC	42 lb/LINEAR in., STATIC	23 lb/LINEAR in., CYCLIC	23 lb/LINEAR in., CYCLIC
OLD TECHNOLOGY 7075-T6 CLAD FACE SHEETS, ORIGINAL FPL ETCH, STAND- ARD CORE, NON- CIAP PRIMER, OLD GENERATION ADHESIVES	<ul style="list-style-type: none"> <li>9000 CYCLES ACCUMULATED (NOV. 78)</li> <li>100 CELLS WATER 4000 CYCLES</li> <li>NO SKIN-CORE CRACKS</li> <li>NO FAILURE</li> <li>TEST CONTINUING</li> </ul>	<ul style="list-style-type: none"> <li>PANEL FAILED 1024 CYCLES</li> <li>10-20 CELLS WATER 496 CYCLES</li> <li>INITIAL SKIN-CORE CRACK 153 CYCLES</li> </ul>	<ul style="list-style-type: none"> <li>PANEL FAILED 768 CYCLES</li> <li>60 CELLS WATER 768 CYCLES</li> <li>INITIAL SKIN-CORE CRACK 66 CYCLES</li> </ul>	<ul style="list-style-type: none"> <li>PANEL FAILED 260 CYCLES</li> <li>100 CELLS WATER</li> <li>SKIN-CORE DISBONDED</li> </ul>	<ul style="list-style-type: none"> <li>PANEL FAILED 168 CYCLES</li> </ul>
NEW TECHNOLOGY 7075-T6 BARE FACE SHEETS, PHOS- PHORIC ACID ANODIZE, CORRO- SION-RESISTANT CORE, CIAP PRIMER, NEW TECHNOLOGY ADHESIVES	<ul style="list-style-type: none"> <li>9000 CYCLES ACCUMULATED (NOV. 78)</li> <li>NO WATER INGESTION</li> <li>NO SKIN-CORE CRACKS</li> <li>NO FAILURE</li> <li>TEST CONTINUING</li> </ul>	<ul style="list-style-type: none"> <li>9000 CYCLES ACCUMULATED (NOV. 78)</li> <li>NO WATER INGESTION</li> <li>NO SKIN-CORE CRACKS</li> <li>NO FAILURE</li> <li>TEST CONTINUING</li> </ul>	<ul style="list-style-type: none"> <li>9000 CYCLES ACCUMULATED (NOV. 78)</li> <li>NO WATER INGESTION</li> <li>NO SKIN-CORE CRACKS</li> <li>NO FAILURE</li> <li>TEST CONTINUING</li> </ul>	<ul style="list-style-type: none"> <li>4000 CYCLES ACCUMULATED (NOV. 78)</li> <li>NO WATER INGESTION</li> <li>NO SKIN-CORE CRACKS</li> <li>NO FAILURE</li> <li>TEST CONTINUING</li> </ul>	<ul style="list-style-type: none"> <li>8000 CYCLES ACCUMULATED (NOV. 78)</li> <li>NO WATER INGESTION</li> <li>NO SKIN-CORE CRACKS</li> <li>NO FAILURE</li> <li>TEST CONTINUING</li> </ul>

Table V. Sustained Stress Test Results—Average Values, Thick Adherend Lap Shear Specimens

		PHOSPHORIC ACID ANODIZE		CHROMIC ACID ANODIZE		OPTIMIZED FPL ETCH	
ALLOY	RESIDUAL STRESS, psi	DAYS TO FAILURE	RESIDUAL STRENGTH, psi <sup>a</sup>	DAYS TO FAILURE	RESIDUAL STRENGTH, psi	DAYS TO FAILURE	RESIDUAL STRENGTH, psi
OLD TECHNOLOGY ADHESIVE/CIAP PRIMER							
2024-T3 CLAD	1500 900	31.0 —	— 4753	25.7 104 (1)	— 4750 (2)	70.7 —	— 4853
2024-T3 BARE	1500 900	35.7 —	— 5486	38.7 (2) 70 (2)	— 4280 (1)	34.0 91.5 (2)	— 5200 (1)
7075-T6 CLAD	1500 900	28.0 35 (1)	— 4220 (2)	30.0 50 (1)	— 4620 (2)	41.0 102	— —
7075-T6 BARE	1500 900	39.7 —	— 5326	34.0 35 (1)	— 5430 (2)	51.0 36 (1)	— 4690 (2)
NEW TECHNOLOGY ADHESIVE/CIAP PRIMER							
2024-T3 CLAD	1500 900	— —	4993 5600	121 (1) —	4045 (2) 5173	— —	5506 5600
2024-T3 BARE	1500 900	— —	5473 6146	34 (1) —	4430 (2) 6073	67.0 (2) —	4900 (1) 6066
7075-T6 CLAD	1500 900	— —	5830 5700	76 (1) —	3620 (2) 5533	76 (2) —	3760 (1) 5833
7075-T6 BARE	1500 900	34.6 (1) —	5910 (2) 6426	34 (2) —	5240 (1) 6206	93 (1) —	5730 (2) 6266

( ) REPRESENTS NUMBER OF SPECIMENS IF OTHER THAN 3

<sup>a</sup> TESTED AFTER 140 DAYS AT 60°C/ 100% RH

## NON-DESTRUCTIVE TESTING OF ADHESIVE BONDED JOINTS

Rob. J. Schliekelmann  
Fokker-VFW  
Technological Centre  
Schiphol-Oost  
The Netherlands

## SUMMARY

With the increased interest in the use of adhesive bonded joints in structural applications the importance of a reliable non-destructive evaluation is growing. In this lecture requirements for application of non-destructive testing of bonded joints are discussed. Available methods are presented with their capabilities and limitations.

## 1 INTRODUCTION

The introduction of adhesive bonding as a means for attaching metal components, introduced a quite new aspect to the technology of fastening. Rivets and bolts had been used for a considerable number of years during which extensive experience had been accumulated about the strength of riveted and bolted joints. By taking a statistically significant number of samples out of a production batch of these fasteners the installed strength could be predicted with an acceptable accuracy. The use of structural adhesives, instead of fasteners, has introduced new factors of process variability and process-control into the fastening field.

The manufacturer using a certain adhesive knows that, if he carries out a quite complicated process according to certain rules, he will obtain a bonded joint meeting a given set of requirements. Besides careful control of the process concerned he has no way of verification of bond-quality other than testing to destruction. Due to the large variety of applications bonding has in airframe structures, universal N.D.T. methods are a basic requirement for large scale production of these joints in critical applications.

Adhesive bonding in the aerospace industry includes both metal-to-metal and metal-to-core sandwich joints. Metal-to-metal joints are found in local reinforcements of sheets, in areas of concentrated loads and in panels having adhesive bonded stiffeners or stringers. Very often a combination of both types of joints is present in one component, having a multi-layer skin, bonded reinforcement doublers and stringers. In sandwich structures both skin-to-core joints as well as attachments with edge-member profiles, doublers and inserts are bonded joints of great importance.

Adhesive bonded joints have offered an efficient alternative to mechanical fasteners in many applications. It has also opened the road for completely novel structures that improve the fatigue characteristics and mode of failure of important aerospace structures today and of other structures in the future. The honeycomb sandwich structure could not exist without bonding.

The laminated metal structures replace components machined from solid, because of their good fracture-toughness characteristics and low fatigue crack propagation rate. Metal bonded doublers are loaded primarily in shear. Bonded stiffeners on skin panels can be loaded in shear as well as in peel because the bonded area must prevent buckling of the skin. Investigations of bond strength, to ensure that the bonded stringer-flange fulfils its function as a stabilizing member, have shown that even quite low-strength bonds give sufficient performance during static loading tests. However, in cases where the adhesive bond is used as the last joining element of a heavily loaded, but cracked, structure a bond quality of the highest order is required.

## 2 QUALITY OF ADHESIVE BONDED JOINTS

In general, for the development of N.D.T. methods, measurable parameters must be found that have a close correlation with the mechanical properties to be determined. These properties are measurable only in a destructive way. Unique conditions apply in the case of bonded metal-to-metal joints which makes a solution of this task rather complex.

There are two completely different quality problems in the case of adhesive bonded joints: of adhesion quality and of cohesion quality. Adhesion quality control requires the non-destructive evaluation of interface phenomena between the adherend surface and the cured adhesive layer, after the bond has been created. This is similar to the non-destructive determination of intermolecular forces within one material. Excluding the case when these forces are zero no successful and truly non-destructive solution is known for this problem to-day. None of the N.D.T. methods described in the following report, therefore, can give a reliable non-destructive indication of the adhesion strength of the bonded joints after the joint has been created. All claims that a method would do this must be viewed critically.

Fortunately, however, controllable suitable surface treatment processes are available that promote adhesion between the adherend surface and the adhesive considerably stronger than intermolecular forces within the cured adhesive layer. As long as the adhesive layer forms the weakest link, non-destructive evaluation of the cured adhesive layer is able to characterize the quality of the total adhesive bonded joint.

The control of the adhesion quality must, therefore, be carried out during, or immediately after, the surface treatment of the surfaces to be bonded. Some of the quality control methods applied at this stage of the bonding process can be qualified as non-destructive and are consequently discussed in the following.

In recent years it has become clear that some cases originally thought to have poor adhesion quality, in that failure took place at the interface and not in the adhesive layer, really had insufficient cohesive strength in the oxide layer formed during treatment of the adherend surface. Since such a weak link in the adhesive bonded joint as a whole must be discovered in time, non-destructive means have been developed to guarantee that the adherend surface is suitable for bonding.

### 3 ADHEREND SURFACE INSPECTION

Without re-opening the discussion about the validity of the various adhesion theories, it can be stated that a minimum condition for the establishment of adhesion between the adherend surface and the adhesive is that the surface is entirely free from contamination. Such contamination may prevent the molecules, on either sides of the interface, from coming within each others spheres of attraction. Furthermore it has been proven repeatedly that porous or loose oxide layers have to be removed to eliminate the possibility that a weak link may be left at the innerface.

In the case of bonding aluminium alloys, there is a considerable amount of evidence that the surface texture at the moment of adhesive application is of prime importance, most probably because of enlargement of the effective adhesion area. During the pickling process, using either chromic-acid or sodium-dichromate both mixed with sulphuric acid, the aluminium surface passes through four significantly different configurations. During the first stage the old oxide layer is removed. Under an electron microscope the residual oxides then can be seen quite clearly (Fig. 1). Gradually the surface becomes smooth showing only rather large but shallow etchpits. Then the new oxide layer starts to grow along the grain-boundaries and finally the whole surface is covered with numerous and evenly distributed, very small etchpits superimposed on the earlier large etchpits. /1/

There are clear indications that the configuration with the small etchpits is the most favourable for adhesive bonding. This must be related to the type of oxide but the increase of the effective surface area is also regarded as of great importance. Quality control activities must in view of the above be directed to:

- ensuring a complete absence of contamination of this ideal oxide layer;
- ensuring the presence of the desired kind of oxide layer;
- ensuring the correct kind of surface texture or morphology of this surface.

#### 3.1 Contact angle measurement

Perhaps the oldest way to determine whether a surface is free of contamination is to study its wettability with liquids by means of contact angle measurements. The contact angle of a liquid drop on a surface is the result of the interaction between the free energy on the liquid/vapour interface, the surface energy on the bond-surface/vapour interface and the surface energy on the bond-surface/liquid interface (Fig. 2). The adhesion energy liberated when one unit area of free liquid surface is brought into contact with one unit area of free bonding surface, is optimum when the contact angle is minimum. The liquid must spread easily over the surface. The requirement of optimum wetting is that the contact angle must be practically equal to zero. Because of this it is difficult to use this test for routine quality control activities; variations in quality between optimum and marginal may show over a contact angle range of only a few degrees. The method developed by Cools was an attempt to overcome this drawback; it measures the spread of a liquid drop of a constant volume with the help of transparent gauge placed over the drop. The dependence of peel strength on drop-surface area is shown in Fig. 3. In spite of this improvement the contact angle measurement has not seen wide acceptance in industry. The wettability is, however, qualitatively checked during the production process by watching the retreating pickling- or rinsing-liquid when the components to be bonded are removed from the treatment tanks. Local insufficient wettability can be clearly seen by discontinuities in the liquid film. /2/

#### 3.2 Surface potential difference measurement

Adsorption of the activated surface by water vapour, hydro-carbons or other contaminants from the environment is the greatest potential danger to the adhesion quality of a bonding surface. Such adsorbed layers can be detected by measurement of the energy required for an electron to leave the metal surface. Adsorbed gasses, water vapour, hydrocarbons or other contaminants, that form electrical double layers on the surface, give a considerable change in that electron emission energy compared to a surface in optimal adhesion condition.

Practical measurements of the electron emission energy, volta potential, or surface potential difference are carried out with the help of Kelvin's dynamic condensor method. A golden reference plate, insulated from environmental influence, is placed close to and in electrical contact, via a resistor, with the surface. An electrical field is created in the air gap between the reference plate and the surface. If the reference plate is moved relative to the treated surface a charge will be displaced through the resistor. If the displacement of the reference plate is sinusoidal the signal can be shown on an oscilloscope. A compensator circuit is made in such a way that this signal can be reduced



to zero by adjusting the charge on the reference plate to a sufficient magnitude. This compensating charge is called the Volta-potential and is used as a quantitative parameter for checking the adsorption status of a treated surface. Since the method is extremely sensitive to electrical disturbance from foreign sources, screening the circuits and the test specimens is of great importance. The phenomena typical for the optimum oxide configuration for bonding are responsible for distinctly recognizable potential values. (Fig. 4). /3, 4/

The method is also able to detect residues from alkaline cleaning operations and absorption of water-vapour after pickling. The Fokker Contamination Tester (Fig. 5) has been useful in the optimization of various surface treatment processes, and offers a good capability for routine quality control activities. The hand-held probe, containing the vibrating reference electrode is the result of many years of development work. Fig. 6 shows a typical correlation between surface potential and surface treatment before bonding.

### 3.3 Surface impedance measurements

As shown in Fig. 1, the oxide configuration plays an important role in the adhesion between adhesive and chromic-sulphuric acid pickled aluminium alloy adherend.

In view of this, the surface impedance measurement principle, used in the quality control of anodization, has been adopted also for the very thin oxide layers of pickled surfaces. Instruments like the Twin City Industries Corp Z-Scope are used for inspection of the anodization layer for sufficient sealing quality.

The instruments used to test the thick anodization layers were not sensitive enough to measure the impedance of the very thin oxide layers resulting from chromic-sulphuric acid pickling during the bonding pretreatment. For this reason Fokker developed a much more sensitive surface impedance measuring system (Fig. 7).

A rubber ring with a well defined surface area is pressed onto the surface to be tested. A sodium chloride solution is introduced into the cavity formed. An electrode is placed in contact with the solution and another electrode is pressed into the base metal of the sheet through the oxide layer by means of a sharp point. The impedance is measured in the circuit so formed. In some cases also the loss tangent is measured.

The impedance measurement does not help only to distinguish the desired from the undesired oxide configurations after pickling. Its extreme sensitivity allows also control of the effectiveness of the alkaline cleaning prior to pickling, etc. Fig. 8 shows the relationship between impedance and degreasing time for two different alkaline cleaning solutions. The right hand curve is for a mild cleaner, having hardly any effect on the oxide layer; the left-hand curve shows clearly the effect of aggressive components in another alkaline cleaning solution that effectively attacks the oxide layer during the cleaning operation. It has been demonstrated that the type of alkaline cleaner solution used prior to the pickling solution may have an important influence on the pickling process. The impedance measurement method offers a good means of accurately controlling the alkaline cleaning, pickling and anodization processes as far as their influence on the oxide layers is concerned.

## 4 COHESION TESTING

The problem with development of non-destructive testing methods for a new material is to find material properties that can be measured without damage to the material but having a close relationship to its strength properties. The adhesive layer of a bonded joint is the result of the polymerization of a monomeric material initiated and accelerated by additives or heat or both. The objective of N.D.T. development for bonded joints therefore must be to find those related non-destructive parameters of this thin, cured layer of resin between two adherends.

Quality variations in the adhesive layer occur as a result of variations in the polymerization process parameters of temperature and time. Such variations can have an effect on the properties of the resin in the cured state. These parameters, however, are quite easy to control with modern recording equipment. The most recent of this is the method of cure monitoring by means of measurement of the dielectric properties of an adhesive sample during the cure cycle (Fig. 9). Another, even more important parameter, is the pressure during the curing process. This pressure cannot be measured because the overall pressure of a press platen of an autoclave very often is not equally distributed over the bond area. This is because of bad fit of component parts or tools, as well as human error during the assembly prior to curing. The results of bond pressure variations show up as unequal resin distribution and subsequent local, thick glue layers, porosity and voids. The voids arise from the amount of volatile by-products that are formed during the curing process and air enclosures.

Summarizing it can be stated that cohesion quality variations can be of the following nature:

- (a) undercure; resulting in low resin-stiffness, -strength and -durability;
- (b) overcure, resulting in a degradation of the resin and leading to loss of stiffness and strength because of part or complete carbonization of the adhesive;

- (c) insufficient curing pressure; resulting in either thick but solid or thick but porous or void-rich glue layers; thick solid resin layers have no loss of strength or stiffness in the resin but have a lower stiffness in the joint as a whole because of the greater thickness.

The porous or voided layers have a lower stiffness and strength because of the smaller effective material cross-section or density. Moreover, the greater thickness also results in a lower joint stiffness.

An N.D.T. method for cohesion quality, therefore, must be based on non-destructive parameters related to:

- . the Young's modulus of the cured resin;
- . the thickness of the glue layer;
- . the density of the glue layer.

The stiffness of the complete joint is also important. An analysis showed that as a result of the worst deviations in the practical production process the cured resin modulus varies from 80 to 100% of the desired quality. The density varies between 0 (for a complete void) to 100% and the thickness of the glue layer will vary from 50 to 400% of the ideal figure. From this it follows that the best method for the control of quality of cohesion would be a method related to the density and thickness of the glue layer.

#### 4.1 Capacitance measurement

Capacitance is a function of dielectric constant, the density of the insulating material the surface area and the distance between the plates.

Before introduction of cure monitoring, capacitance measurements have been carried out on small bonded areas with some success since the early days of metal bonding. The method, however, appears to be most sensitive to variations in the thickness of the glue layer. Moreover, little discrimination is possible between solid and porous, thick glue layers. A solid, thick glue layer could still have acceptable strength. For larger bond areas this method is not very effective as it gives only an indication of the capacity of the total bond area and does not show local areas of different capacity within the large bonded joint. Also, the test suffers from electrical short circuiting between the top and bottom sheet. Adhesives containing metallic fillers are impossible to test in this way in any case. The method has seen very limited application on small bonded joints. The cure monitoring method, however, is very promising. (Fig. 9) /5, 6/

#### 4.2 Thermal inspection methods

Inspection methods for bonded joints may be based on variations in thermal conductivity, thermal emissivity or thermal capacity. All of these thermal properties are related to the thickness of the glue layer and its density. Variation in cohesion quality may be detected from differences in temperature during heating or cooling of the bonded component.

- One method is to heat the entire bonded assembly and to detect the differences in heat dissipation. Areas of void in the bonded sheet will cool more rapidly than well bonded areas where the adhesive acts as a heat-sink and a more gradual heat dissipation takes place.
- Another method is to heat a panel from the rear and to observe the differences in temperature of the frontside during heating. Heating by means of radio frequency techniques is also feasible if no short circuits exist between metal components. Thermal methods are less effective for aluminium alloy metal-to-metal laminates because of the good thermal conductivity of these light alloys; a rapid levelling of temperature differences results. They are most effective on bonds between metals and non-metallic materials and honeycomb sandwich structures.
- Mesophase materials are crystalline over a certain well defined temperature range. The crystalline phase has a considerable difference in colour compared to the non-crystalline phase. Certain cholesterol materials are used for this purpose. The colour may p.e. change from transparent to red or from green to blue. A disadvantage is that the surface has to be painted black for optimum temperature-pattern definition. /7/  
A maximum face sheet thickness of 1.5 mm may be tested, when aluminium alloys are used. Voids of 25 x 25 mm can be detected under a 0.5 mm face sheet. Liquid crystals are more effective on titanium than on aluminium alloy components.  
This method seems too time consuming for economical inspection for large scale applications. Developments in the use of black pvc film stuck firmly to the face surface by means of vacuum or liquid crystal material as a film may lead to wider application.
- A method similar to the liquid crystal system is the use of thermographic indicators. These are surface coatings with a sharp melting point, that change colour above their melting point. When using these coatings the bonded component is preferably heated from the rear, so that the observer can see the areas with highest temperatures which indicate high cohesion. In a similar way thermoluminescent coatings are used, that change in fluorescence under U.V. light with changing temperature. /8/



- Temperatures can be detected with an accuracy of in the order 0.1 degree centigrade with modern infra-red (I.R.) equipment. The temperature patterns from panels can be recorded either by making an I.R. photograph of the heated panel or by scanning with a spot-heat source and immediately measuring the resultant face temperature or heat radiation at that location. These infra-red photographs are not based on the use of I.R. sensitive photographic film, but are pictures of the CRT attached to the radiometer apparatus. /9, 10/

The CFR records the temperature pattern during the scanning operation of the radiometer, which may be in a zig-zag or in a spiral motion. The detection level can be adjusted so that an optimum difference between low and high cohesion quality can be observed during the heating period. The recordings were made with help of a Thomson-CSF IR camera installation. Fig. 10 shows a picture of a production panel with a bonded doubler reinforcement around a large cut-out in the skin; variations in black and white show the cohesion strength differences. In this picture the component has cooled so far that the void areas remained the warmer ones and show up as white areas. The interpretation requires considerable experience and must take into account the heating condition of the component. Difficulties also arise from the extruded adhesive and adhesive stains. The stains, in particular, make quality assessment very difficult with complicated and multi-layer bonded components.

- At the periphery of the non-destructive testing field there is an interesting method that has been developed by the Aeronautical Quality Control Directorate laboratories at Harefield in England. This method uses heat to create local thermal expansion of the top sheet of a bonded structure and measures the deformation of the top sheet under the thermal load. /11/

The method is unique in its ability to detect adhesion quality defects in that areas of both low adhesive strength and low cohesive strength may fail under the thermal stresses. Strictly speaking, however, it is not a non-destructive test because it may cause bond failures during testing.

The principle of the system is straightforward. The area to be tested is heated either by focussed heat lamps or with the help of a high frequency heating coil. The deformation in the centre of the heated area is measured by means of an air-jet that is adjusted to an exactly known distance from the surface of the cold top sheet. The test area is heated rapidly.

The temperature rise is strongly influenced by the dissipation of heat in the direction of the adhesive layer. Even if there is only an airbubble underneath the top sheet the temperature will rise in a matter of a few seconds and a clearly measurable deformation will be immediately indicated by the gauge. The increase of temperature on a well bonded area will be much slower and the deformation will be hardly measurable. Low adhesion quality bond areas will fail in the early stages of the heating cycle. Porous areas and areas of low cohesion will allow a certain movement of the top sheet towards the heating source and will give a measurable amount of deformation.

The practical application of this method, initially, has been on helicopter-tail rotor blades. The method has not yet seen a large scale application, most probably because of the limited testing speed. Ten to fifteen seconds of heating time may be required for each test area. Another disadvantage is that the large measuring head can only be used on easily accessible parts.

## 5 ACOUSTIC EMISSION

All migrations of dislocations, precipitations and elastic movements of atoms create sound at sonic and ultrasonic frequencies which can be detected with modern highly sensitive transducers, amplifiers and recorders. During recent years techniques have been developed of recording the pressure waves emitted in a material, during loading or deformation. Predictions of stress at failure for some materials have been made by observing the stress associated with certain, typical, acoustic emissions. These observations are compared with destructive tests on the same material where the relationship of stress to high-frequency emission has been recorded. (Fig. 11, 12)

It is interesting that this method has also been applied to adhesive bonded metal joints; it will also detect low adhesion quality areas. Whether or not it is a true non-destructive test is doubtful as the acoustic emissions recorded are indications of local failure of the material or the bond. The accuracy of the prediction of the failing stress increases with the percentage of the normal failing stress reached during preloading. The error in the prediction is reported as being 31% for eight trials at 30% of the failing stress. This error is only 13% when the load is increased to 90% of the normal failing load. /12, 13/

It is easy to see that the acoustic-emission method suffers from a number of problems of practical application at present. For a complete bonded component the question arises of how the preloading stress is to be applied. An apparatus could be developed that exerts a calibrated force on a well defined area of the bond and records the acoustic emission during the loading cycle, in order to guarantee a certain bond quality. The level of loading must be chosen such that a certain amount of emitted energy must not be exceeded. By placing microphones at strategic positions on the component the location of the emissions can be plotted.



## 6 RADIOGRAPHY

Radiography can generally detect density variations by means of attenuation of rays passing through the material. When using X-rays the attenuation is determined largely by the density of the material. However, in metal-to-metal bonded joints the material in which density variations are to be detected, the adhesive layer, has a density which is considerably lower than that of the bonded metals. Thus the adhesive cannot normally be seen on X-radiographs unless the adhesive contains metallic fillers. These fillers allow estimation of the density and thickness of the adhesive layer from variations in shading in the bond area. Filler can also be used to indicate the flow of the adhesive during the curing cycle; very thin fibres of metallic or other heavy materials are suitable for this purpose. However, X-radiography has found little use for metal-to-metal joints in contrast to its use on honeycomb structures, where it is used for inspection of the core on position and defects. (Fig. 13) Neutrons are either absorbed or scattered, in particular by hydrogenous materials, like hydrocarbons. Therefore Neutron radiography is an ideal method for visualization of density variations in cured adhesive layers. (Fig. 14) For the time being, however, the sources of neutrons are rather limited. Neutrons are produced from sources such as accelerators, radio isotopes or reactors. For practical applications Californium 252 mobile sources look promising. /14/

## 7 ACOUSTIC INSPECTION

Tapping with a hard object is probably the oldest N.D.T. method there is; every inspector of bonded structures has his favourite device to enable him to distinguish between the clear sound from solid bonds and the dull sound from voided bonds. The relatively good initial success of this method can be explained by the fact that the acoustic properties of the bonded joints are closely related to the non-destructive parameters: modulus of elasticity  $E$  and density  $\rho$ . Both parameters are related to important acoustic material properties:

$$\text{velocity of sound } c = \left( \frac{E}{\rho} \right)^{\frac{1}{2}} \quad \text{and} \\ \text{acoustic impedance } Z = (E \cdot \rho)^{\frac{1}{2}}$$

Unfortunately the sonic tapping method is very subjective and gives no information about the bond quality other than the opinion of a more or less experienced man.

Many attempts have been made to develop and use more objective methods based on the principle that the acoustic properties of the cured adhesive layer are closely related to the cohesion quality of the bond. The acoustic inspection methods in widest use, at present are ultrasonic pulse and resonance testing.

As quality control method the determination of the velocity of sound is of little practical use for adhesive bonds, because of their very thinness. The impedance of sound waves in various materials, however, has proved to be of great value. The impedance plays a particularly important role at the interface between the metal surface and the adhesive layer. The reflection of sound by the interface of two materials that are in firm contact with each other, is governed by the respective acoustic impedances of these materials  $Z_I$  and  $Z_{II}$ . The coefficient of reflection  $R$  being the ratio of the amplitude of the reflected and the incident sound waves, can be expressed as follows:

$$R = \frac{Z_I - Z_{II}}{Z_I + Z_{II}}$$

Where the sound passes through a metal sheet and hits the interface with an attached adhesive layer, the reflected wave may vary considerably in amplitude for various values of  $Z_{II}$ . Information can be deducted about the quality of the bond from comparison of the amplitudes of the received and transmitted signal. Where an air bubble or void is present in the adhesive layer,  $Z_{II}$  will approach zero and nearly full reflection will be obtained. For impedance values  $Z_{II}$  of respectively 25 and 50% of  $Z_I$  the reflection coefficient  $R$  will be 0.6 and 0.33. The higher the adhesive impedance, the smaller will be the reflection and the higher the sound energy that passes through the bonded joint.

## 8 SONIC TESTING

Originally, bonded joints were tested with techniques based on the tapping method and ultrasonic techniques were not yet popular. Mechanical tapping was used with limited success. Some systems used microphones or other listening devices. The Fokker Bond Tester Type I (the fore-runner of the Fokker Bond Tester Type II) was related to these methods. That instrument was based on resonance principles. From the following it will appear that there are several different methods of resonance testing. Such as the resonance of the bonded panel as a whole, resonance of unbonded areas and resonance of the glue layer itself.

The Fokker Bond Tester Type I used two probes: a transmitter and a receiver. The transmitter introduces vibrations, known as white noise, into the bonded topsheet. The lower and upper frequencies and amplitude of the noise can be adjusted: the lower frequency between 0.5 and 5 kHz and the upper frequency between 1 and 10 kHz (Fig. 15). The meter on the instrument indicates the ratio between the transmitted and received energy. The instrument can detect those areas having resonance frequencies within its frequency band. The limits of the transmitted frequency may be adjusted to give the greatest difference in the indication on the meter between well bonded and partly

bonded areas. The transmitter and the receiver probe can be moved independently to make a full investigation of the bonded joint. Geometry and edge-effects play an important rôle because of the low frequencies used. For this reason Fokker continued development of a system working with higher frequencies.

The recently introduced Sondicator probably works on a similar principle to the Fokker Bond Tester Type I. It also uses separate contact probes, but the energy is transmitted in pulses and in a frequency range of 20-40 kHz. Not only is the received amplitude measured but also the phase is indicated by a special instrument or on a CRT which allows a more complete analysis of the received signal. Reports show that the Sondicator is also suitable for void detection but suffers from the same limitations as the other low frequency resonance systems.

A more sophisticated method uses the same principle but with a single probe and excites the upper sheet of the bonded laminate by induced eddy currents and measures the response with detection devices within the eddy-current coil. The latest of such instruments is the Harmonic Bond Tester, developed by the Boeing Company but produced by Shurtronics Corporation. The probe contains an electromagnetic coil which maintains an oscillating field which induces eddy currents in the conductive upper sheet. The interaction of the original and the induced fields causes the sheet to be driven at a frequency double the coil frequency. The Harmonic Bond Tester uses an oscillator of 14-15 kHz. The response of the laminate is detected by a wide band microphone suitable for frequencies upto 28-30 kHz. /15/

The serious limitation in the detection of small voids by these low-frequency resonance systems can be easily shown by calculation. If we assume that the voids are square and that the bond provides clamped edges of the sheet element at the location of the void then the basic resonances for different thickness of sheet are as given in Table 16.

If we assume 30 kHz to be the highest frequency detectable for an upper sheet 0.4 mm thick, the void size must be in the order of 7 x 7 mm to be detectable.

For a sheet thickness of 1.2 mm, which is still thin for modern aircraft structures, a detectable void size of about 12 x 12 mm must be expected. In many cases this is not an acceptable figure; and it is even greater for thicker sheets. Therefore, in order to have a wider scope of application and also to include detection of quality of the cured adhesive layer and not just of voids, the use of resonance techniques has to follow different lines.

## 9 ULTRA SONIC INSPECTION

The ultra sonic equipment used for inspection of bonded joints is similar to that used for inspection of solid metal. There are two distinctly different methods used on bonded joints: through transmission, pulse-echo and the ultrasonic resonance method. /16/

### 9.1 Ultra sonic through transmission

Through transmission uses a separate transmitter and receiver on either side of the bonded joint. In most cases piezoelectric transducers are used for both the transmitter and the receiver; these transform electrical into mechanical vibrations and vice versa. The simplest equipment uses probes that are in direct contact with the opposite surfaces of the bonded component (Fig. 17). Extreme care has to be taken to ensure that both transducers are exactly in line with each other, so that the ultrasound from the transmitter can reach the receiver if the bond is complete. An oil of low viscosity or water must be used as a couplant between the probe and the component to ensure acoustic contact. The direct contact method has the disadvantage that during movement from one area to the other the probes have to remain aligned exactly, while the probes have to slide over the surface of the component.

If the received energy is very small compared to the transmitted energy, it must be concluded that most energy has been reflected; that is the impedance of the adhesive layer is low. In this way complete voids and porous areas can be detected; further assessment of cohesion quality can be done by analysis of the amplitudes of the received signal. The contact through-transmission technique has found little practical use because of the difficulty of probe alignment and the requirement for good contact on both sides of the component. A considerable improvement came with the introduction of the immersion technique in which the bonded assembly and both transducers are submerged in water which acts as a couplant (Fig. 18). A variation of this technique is the water-jet technique which uses a water-jet as a pathway for the ultrasound. (Fig. 19)

With the immersion technique the component is stationary under water; both probes can be moved together along the component by means of a simple, but accurate, guide-rail system. The instrumentation can be arranged such that a signalling device is triggered when the received signals are at various levels. Thus using a x-y recorder operating simultaneously with the probe-mounts, it is possible to make a complete facsimile recording or C-scan of the component that indicates all those bond areas yielding reception signals below the previously arranged minima.

Another development of through-transmission uses a search wheel (Fig. 20). Each of the two transducers is mounted in the hub of a wheel with a rubber tyre filled with water or some other liquid couplant. The transducer is so mounted that the emitted sound strikes the point of contact of the tyre with the surface to be inspected. When water is sprayed into



this point of contact, sound is transmitted into the component as before. Thus through-transmission can be achieved using a yoke mounting with a rotating probe held by springs on either side of the component and a water-jet system to ensure acoustic contact between tyre and metal surfaces. The method is limited to products with rather flat surfaces on both sides. The disadvantage of all through-transmission methods is the problem of identifying the particular faulty bond line in multiple laminates and the technical difficulties in the use of transducers on opposite sides of the component.

## 9.2 Pulse-echo technique

The technical difficulties presented by the probe system required for through transmission can be avoided by using an echo technique in which the same transducer is used as transmitter and receiver. In this method an echo is received from the bond interface. If ultrasound were transmitted as a continuous signal the reflected signal would interfere with the transmitted signal; for this reason pulsed ultrasound has to be used to allow reception of energy in the dead periods between short pulses of transmitted energy. There are several pulse-echo techniques in use for adhesive bonded metal-to-metal joints.

Where the thickness is large enough compared to the pulse length it is possible to distinguish the reflected signals from each interface (Fig. 21) The amplitudes of the echoes from the metal/adhesive interfaces, in particular those from the lower surfaces, are quality parameters of interest. Where echoes from the lower interfaces are missing it can be taken for granted that no firm bond has been formed with the lower sheet. If the sheets are thin there may still be interference between the reflected and transmitted pulse. Probes have been developed with frequencies upto 10 MHz and very short pulses to test bonded joints of very thin sheets. A reverberation of signals within the top sheet may occur; this is sometimes known as ringing. The difference in impedance at each interface dictates the amount of reflected energy; hence conclusions about the cohesive properties of the cured adhesive layer may be drawn from observation of the ringing pattern on the CRT. The higher the adhesive quality the smaller will be the number and amplitudes of the reflected signals. Single probes with separate and insulated transmitter and receiver transducers, built together more or less compact, can be used as a compromise between through-transmission and pulse echo (Fig. 22). This method takes advantage of the fact that the pulses reflect several times from the metal adhesive interface over the full distance between both transducers. This results in an amplification of any large difficulty of interference of the transmitted and received pulses when testing thin sheets. The optimum pulse path may be obtained by placing a wedge prism of carefully selected angle between the transducer and the metal surface.

The pulse-echo technique can be adapted for immersion testing in a water tank. An electronic system, incorporating a gate, can be arranged to indicate areas giving less damping than a prearranged level. The output signal can then be used to supply a C-scan recorder to show those areas below chosen standards of quality. A variant of this principle is the reflector plate technique where the sound pulse after passing through the bonded component bounces back from a glass or metal plate behind or below that and passes again through the component and is received by the same transducer that transmitted the pulse (Fig. 23).

## 9.3 Practical applications of ultrasonics

The ultrasonic pulse-echo technique has seen in recent years many developments aiming towards improvement of the efficiency of the non-destructive testing operation itself. Semi automatic systems for the inspection of such bonded structures as helicopter- rotorblades, space missile components, etc. have been developed applying the immersion; water-jet or search-wheel pulse-echo principles. /17/

Much sophistication has been shown in the recording methods. Initially the recording was limited to the indication whether or not the received signal had an amplitude higher than a previously specified level. A stylus moving synchronously with the probe would or would not write a line on a facsimile drawing of the component to be tested. Bond areas of unacceptable level then show up as white areas (Fig. 24). Demands for somewhat more qualitative indication were fulfilled by various recording methods. Fig. 25 shows how the amplitude of the received signal is shown as a deviation perpendicular to the written line on the recording. An anomaly in the bond quality is then showing up as strong deviations of the lines from the general path. This method is used in conjunction with a double search wheel installation as used by the Swedish SAAB-SCANIA Company (Fig. 26). Another method is to separate the received signal levels in preadjusted increments. Signals received in each increment are then written in a particular colour or in various grey tones. This is achieved by using an electrostatically sensitive recording paper and a stylus on which the voltage varies with the increment of the received signal. This results in C-scan recordings in a variation of grey tones showing the density variations of the glue-line. An example is given in Fig. 27.

It will be well understood that in this way the U.S. pulse method is able to give a nearly quantitative indication of the glue-line quality. However, as soon as multiple bonded joints in honeycomb sandwich or multilaminated structures have to be inspected things become more complicated. It would then be possible to reserve each reception energy increment for an acceptance level of each individual glue-line. In that case problems like signal damping by different metal thicknesses have to be taken into account.



An example of the complexity of the problem is given by the installation that has been developed by the Boeing Commercial Airplane Company (Fig. 28). The through-transmission scanner uses six pairs of horizontally opposed water-jet coupled 1 or 5 MHz pulse-transducers mounted in a large joke structure enclosing the part to be inspected on both sides. The part is moved through the joke opening with increments of p.e. 60 cm. At each increment the joke scans the bonded component vertically with small increments. The whole system is hooked to a computer system that has the ability to store the received data and to correct these in view of the number of gluelines and sheetthicknesses involved at the particular location of the structure. The plotting of the data is carried out by an electrostatic printer/plotter separating the received signal into 13 increments of 6 dB wide, each of which is indicated by a single character. An asterisk corresponds to the maximum received signal and the numbers 0 through 9 denote progressively smaller signals. Reversed field 0 and 1 are used for the two lowest reception levels. The optical contrast between the chosen characters indicating the higher levels of reception and those indicating the lower ones creates in addition to the numerical quality indication also a dark grey tone indication for the lower quality levels on the plot (Fig. 29). The wide dynamic range of the detection electronics enables the system to prepare plots of parts differing greatly in complexity. The main problem, even with such rather sophisticated systems, remains the inability to distinguish for multiple bonded structures the gluelines that cause the excessive damping out of the total available gluelines at the particular location. Other, most probably, contact methods will have to be used to give the complete answer. /18/

#### 9.4 Ultrasonic resonance testing

An analysis of the characteristics of the thickness resonance of a bonded laminate of two sheets with an adhesive layer in between, shows us that there are three distinct modes of resonance for such a mass-spring system (Fig. 30). /19, 20, 21/

- Mode 1: The sheets behave as rigid bodies and the resin layer acts as an almost massless spring.
- Mode 2: The sheets vibrate in their natural frequencies but in opposite phase (assuming both sheets have equal thickness) without deformation of the adhesive layer that behaves as a rigid body.
- Mode 3: The sheets vibrate in their natural frequencies but in the same phase so that the adhesive layer is compressed and elongated.

The first type of resonance is similar to the one used for determination of the dynamic modulus  $E$  of adhesive layers between end-to-end bonded cylinders. Experiments with this method were first used to test cement layers between pieces of marble by Bordoni (Fig. 31). Such experiments showed that the resonance frequency of such specimens could be fairly well correlated with the tensile strength of the adhesive layers of such specimens. For this reason this first mode of resonance formed the subject of considerable study in the Netherlands. From the simple formula for this mode the influence of the various parameters can be seen.

$$f = \frac{1}{2\pi} \left( \frac{2E_1}{\rho \delta t} \right)^{\frac{1}{2}}$$

- $f$  = resonance frequency  
 $\delta$  = thickness of adhesive layer  
 $t$  = sheet metal thickness  
 $E_1$  = modified modulus of the adhesive layer (restrained condition)  
 $\rho$  = density of the metal

The modulus  $E_1$  for unmodified epoxy and phenol/vinyl adhesives ranges from  $9,0 \cdot 10^9$  to  $7,0 \cdot 10^9$  GNm<sup>-2</sup>. Modern nitrile-modified epoxy<sub>2</sub> resins have somewhat lower values of around  $5,6 \cdot 10^9$  GNm<sup>-2</sup> and for nylon epoxies around  $3,2 \cdot 10^9$  GNm<sup>-2</sup>. The lowest values are as low as  $20 \cdot 10^6$  MNm<sup>-2</sup> for phenolformaldehyde/nitrile-rubber adhesives. Thus the first resonance frequency for good quality adhesive layers of the lowest moduli between sheets 1 mm thick, is about 50 kHz and it goes up to about 1800 kHz for the rigid adhesives between sheets  $\frac{1}{2}$  mm thick. Less dense and thicker adhesive layers (lower cohesion quality) may reduce the resonance frequency by about 30%. This means that the first resonance mode is considerably influenced by the following:

- adhesive type whether rigid or not;
- thickness of the sheet;
- thickness of the adhesive cohesion quality.

The measurement of the cohesion of the adhesive layer boils down to an accurate resonance analysis of the bonded joint. Experiments with a modified ultrasonic thickness tester the Vidi-Gauge Model 21 confirmed these theories very well. From a practical point of view the situation is difficult because the sheet thickness within one component may vary considerably. This, combined with the strong influence of the cohesion quality of the adhesive layer, results in a very wide range of frequencies. These problems, in particular that of the wide frequency range, at which resonance can occur, have been resolved by the design principle of the Fokker Bond Tester Type II. /22/

The solution used at Fokker was to couple the system of sheets and adhesive layers of a bonded joint to a body of well defined resonance characteristics. This led to a limitation of the range that the system could resonate in. Subsequently the testing system was developed as an accurate analyser of the resonance characteristics of the calibrated body coupled to the bonded laminate.

An important feature of the instrument is that the calibrated body is in fact a transducer that can be driven at different frequencies. The dimensions of the transducer are chosen in relation to the total thickness of metal sheet to be tested and to the required mode of resonance. Within certain limits pure thickness-resonance modes are not used; instead modes are selected that have proved to give the most reliable correlation with the adhesive layer.

The resonance characteristics of the bonded joint together with those of the transducer are analysed by sweeping the driving frequency through the band in which the resonance mode can be expected. The response of the total system, as shown by the impedance curve over the swept frequency band, is displayed on a CRT display (A-scale) and the peak-to-peak amplitude of the curve is shown by a micro-ammeter, (B-scale). The A-scale display incorporates a calibration system to facilitate reading of the resonance frequency changes on the horizontal axis.

The probe containing the calibrated body is placed on top of a piece of sheet material with the same thickness as the upper sheet of the bonded laminate. The central frequency of the oscillator is selected such that the lowest point of the impedance curve is in the centre of the A-scale; at the same time the B-scale is adjusted to 100. The frequency calibration of the A-scale has then to be carried out. With the Model 67 and earlier models this has to be done with help of a calibration signal that gives a set of vertical peaks on the A-scale at an interval of 10 kHz. The divisions of the A-scale can be given a certain frequency shift value by adjusting the sweep width. (Fig. 32)

If for example, two peaks are separated by two scale divisions then one scale division is equal to a frequency shift of 5 kHz. In the Model 70 Fokker Bond Tester (Fig. 33) the A-scale calibration is much simpler and is done with a calibration selector switch using pre-set values of frequency shift for each scale division. Calibration of the instrument on a non-bonded sheet ensures that in all cases of a complete void the peak position will return to the centre of the A-scale and to a B-scale indication of 100. Another calibration, although not strictly mandatory, is to place the probe on a piece of solid metal sheet of the same thickness as all the metal sheet in the subject bonded laminate. The peak thus obtained is the resonance frequency to be expected of an ideally bonded laminate containing that thickness of metal.

The quality of cohesion from any test may be accurately determined by comparing the instrument reading with established correlation curves. In practice the acceptance limits are decided for the particular requirements of the various categories of joints. The correlation curves for the Fokker Bond Tester have some remarkable features resulting from the typical resonance behaviour of bonded joints. /23, 24/

If, after calibration, the probe is placed on a well-bonded joint the resonance frequency will be lower than the central frequency and the impedance minimum will move slightly to the right on the A-scale. Lower cohesion yields a peak even more to the right and finally the peak will move off the A-scale; simultaneously the B-scale indicator will show a very low value. At even lower cohesion the peak will return on the left of the A-scale and as the cohesion approaches zero the peak will move towards the centre of the A-scale; the deflection of the B-scale indicator moves towards a maximum. This phenomenon results in the typical, double, correlation curve (Fig. 34). The quality of cohesion for this right-to-left transition is related to the ratio of the thickness of the bonded sheets and to the type of adhesive. The accuracy of the prediction of quality depends mostly on the accuracy of manufacture of the correlation specimen and that of the non-destructive and destructive tests.

#### 9.5 Ultrasonic spectral analysis

In the previous paragraph it was mentioned that in early days of low frequency resonance testing the response of a total bonded structure on the excitation with low frequency "white noise" was analysed. The same can be done in the ultrasonic frequency range. Broadband ultrasound of a frequency between 0,5-12 MHz is injected into the bonded panel as very short pulses. This is done not perpendicularly to the top sheet but under an angle smaller than 90°. This allows to analyse in particular the reflections from those energy pulses that have passed through the gluelayer twice or more. By analyzing the impedance of the glueline over the applied frequency range much can be learned of the acoustic properties of the gluelayer. Phenomena such as moisture absorption can be detected. (Fig. 35). The method is for the time being not yet applied in practical production inspection, but may have promises for the future. However, many problems have to be solved in particular its application on multiple bonded joints. /25/

## 10 HOLOGRAPHIC INTERFERENCE

In a survey of non-destructive bond inspection, the holographic method offers some difficulties. Holography is a method of recording the geometry of an object at a certain moment in time. With help of holographic interference two geometric recordings of the same object, but at two different moments are compared by interference of these images. These differences in geometry may be the result of external static loading, thermal stresses or vibration. Irregularities in the deformed geometry show up as irregularities in the interference pattern. Such deformations, to be seen, must be in the direction of the observer and in an order of magnitude of a quarter of the wave length of the light used ( $\frac{1}{4} \times 632.8 \text{ nm}$ ).

This means that deformation differences of the bonded joints in the direction of vision must be at least approximately 160 nm ( $0.16 \mu\text{m}$ ). It is obvious that deformations of this order are generally much more difficult to obtain for metal-to-metal joints than for light-weight sandwich structures that have thin upper sheets.

Extensive studies in the Netherlands showed that thermal deformation was difficult to use for metal-to-metal structures. So much thermal deformation of the component took place that reconstruction of the hologram was not possible. The use of fringe control gave some improvement but no satisfactory solution (Fig. 36, 37, 38, 39).

The beam of coherent light from the laser is split by a semi-transparent mirror. One beam is directed by mirrors and a spatial filter arrangement onto a photographic plate. The other beam is directed by a similar arrangement to illuminate the object. The hologram is made by interference of the reference beam and the reflected light from the object. The movement of the panel after this first hologram has been taken can be compensated for by movement of a lense system placed between the spatial filter and the mirror in the illuminating beam. The correction obtained in this way is not enough because the heating needed to give movement of the upper sheet in the direction of vision in the order  $0.16 \mu\text{m}$  generally gives too large a general deformation of the bonded panel.

These difficulties led workers in the Netherlands to concentrate on vibration testing because of the relation between resonance properties and the quality of cohesion. The aim of the programme was to develop a method that would make visible, over the whole area of the bond surface, that which Fokker Bond Tester could measure only locally.

It early became apparent that a very high driving energy is necessary, even with efficient transducers, to show up low cohesion when vibrating in the first thickness mode; and even then only a limited area may be covered. Detection of voids by a holographic interference technique with vibration deformation appears to be possible within the same limits of void dimensions as by membrane resonance. Voids in the skin bonds of a stringer flange may be detected by extension of the membrane-resonance pattern into the area of the bonded joint (Fig.40). The higher the frequency, the smaller will be the smallest void detectable.

Two methods of assessment of cohesion by resonance testing using interference holography have been developed in the Netherlands.

The first used the membrane resonance of the bonded laminate as a whole. The wavelength at which resonance of the bonded laminate takes place must be regarded as a parameter for bond-quality. The stiffness of the adhesive layer, and thus the flexural stiffness, dictate the resonance frequency of the entire bonded laminate. As the amplitude of the resonance of the bond is of a much lower magnitude than that of the single vibrating skin alone the areas of maximum deformation show as black spots in the bond line. However, these spots are much larger than in the single unbonded skin. The distance between the areas of maximum amplitude indicate the half wavelength of the laminate in resonance. Correlation between the half wavelength and the bond quality seems possible.

Another interesting feature of bond quality is the influence of the clamping stiffness on the sheet membrane adjacent to the bond. This is of particular importance for panels with bonded stiffener flanges.

Well bonded flange joints clamp the membrane between the joints much stiffer than poorly bonded joints. When brought into resonance there will be a distinct difference in resonance characteristics between the two membranes. The frequency at which a certain mode of membrane resonance occurs is higher for well-bonded components than for poor bonding. This means that at a given frequency it is possible that the well bonded component has a lower mode of resonance than the poor bonded component (Fig. 41). Fig.42 shows the relationship between field resonance frequency and the number of half wavelengths in the length direction of the membrane ( $m = 2 \frac{L}{\lambda}$ ) and those in the width direction ( $n = 2 \frac{b}{\lambda}$ ), for two different qualities of edge bond. Testing of quality seems to be possible using vibration of the component at frequencies which are just in the transition zones from resonance with mode 1 or 2 into mode 2 or 3 respectively. It will take, however, considerable time to develop a universal system of quality testing based on interference holography.



## 11 NON-DESTRUCTIVE ACCEPTANCE TESTING

The objective of N.D.T. of adhesive bonded joints is to determine whether the joints are acceptable for use in the structure concerned under the specified operation conditions. In metal-to-metal bonded joints this is a particularly serious problem; even when this determination of quality is carried out by testing to destruction. The main reason for this problem is that the strength of a bonded joint is dictated not only by the strength of the cured adhesive layer and its adhesion to the surfaces to be joined but also by the geometry of the joint and the stiffness of the adherends. These two parameters are responsible for the stress distribution in the joint. The joint will fail when the load relating to the highest stress peak reaches the failing stress of the adhesive. Consequently a joint that will yield at an average shear stress on a half-inch standard lap-joint of  $20.6 \text{ N mm}^{-2}$  when tested to destruction, may show an entirely different failing stress for a joint of different geometry. This phenomenon must be taken into account when judging the value of N.D.T. methods as means of predicting the strength of metal-to-metal bonded joints.

Fig. 43 shows the dependence of the average shear strength of bonded lap-joints on the parameter  $t/l$ . In which  $t$  stands for sheet thickness and  $l$  for overlap length. Low values of the  $t/l$  ratio result in high stress-concentrations at the overlap ends and consequently at low average shear stress at failure; and a high  $t/l$  values, high average failing shear stresses. Consequently bonded joints with identical cohesive quality will still yield different average shear stresses at failure, when different joint geometries are involved. This effect must be considered when destructive test results are used to judge non-destructive inspection methods on their performance in estimating joint quality. Joints with identical quality give identical results when non-destructively tested. For many people it is hard to believe that sometimes the non-destructive method is the only method indicating the true bond quality and all destructive results are misleading.

Destructive test results must be always corrected for geometry, using a diagram like Fig. 43. Specifications of acceptance limits must take the  $t/l$  ratio into account. The cohesion quality is expressed as percentage of the best possible cohesion strength of the adhesive.

It is not enough to specify only acceptance limits on the required room-temperature static strength of the joint. A designer selecting a certain structural adhesive for an application makes his choice after studying quite a range of mechanical properties. One of these properties is the shear strength at room temperature and furthermore he must judge whether reduction of that figure during and after exposure to various environmental conditions is acceptable. Unfortunately it is not generally understood that these reduction figures, after exposure, are valid only for specimens of ideal quality and made under laboratory conditions.

When the initial quality of shear strength is not 100% then many of these reduction factors may have to be increased considerably. For this reason quality requirements for bonded joints have to be specified at such a high level that it seems excessive in many cases in view of the function of the structure concerned in order to ensure sufficient durability of the joint.

These considerations apply to adhesives which give a complete range of cohesion qualities. This range is due to production process variables of which the curing pressure is the most important. There are many other adhesive types, however, that under low curing pressure will form a thick, but solid, glue layer as long as sufficient adhesive is available to fill the gap between the adherends. The quality of the cured adhesive, regardless of the thickness, is then excellent. Voids will be formed only in the areas where the adhesive quantity is insufficient to fill the available cavity. The shear strength reduction due to this kind of low quality will not only be related to the size of the voids but also to the position of the voids relative to the boundaries of the bond areas. The acceptance limits for these adhesives must therefore include limits for void size and location.

Again, correlation with destructive testing creates problems since in the narrow half-inch overlap joints the void size or position plays a completely different role, than in the adhesive bonded structure itself. Even small voids at the edge of the overlap can be disastrous for the shear strength of such specimens; when located more in the middle of the overlap their presence will be hardly noticeable. As N.D.T. is not so influenced the correlation may suffer from considerable scatter. In the correlation between destructive and non-destructive tests of adhesive bonded joints this sometimes must be taken into account when setting N.D.T. acceptance limits.

## 12 COMPARISON OF N.D.T. METHODS

When comparing non-destructive testing methods many aspects other than the correlation with the cohesive quality of the glue layer come into consideration. The ideal non-destructive testing instrument would be a robot telling the detailed story of the particular bonded component, listing all deviations that were made from the ideal bonding process. Indeed, methods that, in addition to variations in the cohesive quality, record anomalies resulting from human error are extremely important. A typical example in this respect is the detection of the adhesive manufacturer's separator sheet that erroneously may be left in a bonded joint, causing practically entire loss of bond strength. An excellent example of evaluation of N.D.T. methods can be found in the publications of Hagemaier

of Douglas Aircraft Company. The comparative evaluation-results of a number of N.D.T. methods for adhesive bonded structures are given in Fig. 44 for metal-to-metal and in Fig. 45 for honeycomb sandwich structures bonded with a modified epoxy adhesive film. /26/ It must be stated clearly, however, that it is dangerous to make general statements. The effectivity of the various methods may differ for different configurations of bonded structures, adhesives and applied manufacturing processes.

### 13 CONCLUSION

The given survey of non-destructive testing methods for adhesive bonded structures is certainly not complete. Even more different methods could have been discussed, but were left out for reasons of space. It may be clear, however, that non-destructive testing is an indispensable means for the realization of reliable and durable adhesive bonded structures.

### 14 REFERENCES

- /1/ Bijlmer, P.F.A. and Schliekelmann, R.J. "The Relation of surface condition after pretreatment to bondability of aluminium alloys", SAMPE Quarterly, October 1973, p. 13.
- /2/ Cools, J.J. "Inleidend onderzoek naar een methode ter bepaling van de adhesiesterkte van metaallijmvlakken", Fokker Aircraft Company, Report R-237.
- /3/ Bijlmer, P.F.A. "Characterization of the surface quality by means of the surface potential difference" Proceedings ICAS Conference, Lisbon, August 1978, p. 247.
- /4/ Kim, D.H. and Sutliff, E.F. "The contact potential difference (C.P.D.) measurement method for prebond non-destructive surface inspection", SAMPE Quarterly, July 1978, p. 59.
- /5/ Allen, J.D. "In-process diëlectric monitoring of polymeric resin cure", SAMPE (1977).
- /6/ Hudson, D. "The use of automatic diëlectrometry of autoclave molding of low void composites", COMPOSITES, Vol. 4, May (1974), p. 247.
- /7/ Woodmansee, W.E. "Cholesteric liquid crystals and their application to thermal N.D.T.", Materials Evaluation, Oct. (1966), p. 564.
- /8/ N.N. "Detecto Temp." brochure W.H. Brady Co., 727, W. Glendale Ave, Milwaukee, Wisc. U.S.A.
- /9/ Vettito, P.R. "A thermal I.R. inspection technique for bond flaw inspection", Appl. Polymer Symp. No. 3, p. 435 Interscience Publ., New York, 1966.
- /10/ Steffens, H.D. "Advanced Manufacturing Techniques in Joining of Aerospace Materials" AGARD-LS-91 (1977) p. 7-25.
- /11/ Thompson, W. and Senior, H.A. "A non-destructive test for adhesive bonded, fibre-glass-aluminium alloy joints", Ministry of Aviation (U.K.) N.D.T., p. 56.
- /12/ Pollock, A.A. "Stress wave emission in N.D.T." Non Destructive Testing 2 (1969) 3 p. 178.
- /13/ Brockmann, W. "Acoustic emission - a testmethod for metal adhesive bonded joints" Materialprüfung 19 (1977) 10 October, p. 430.
- /14/ N.N. "Californium 252 Progress", VW Atomic Energy Commission, P.O. Box A, Aiken, South Carolina, 29801.
- /15/ Botsco, R. "The Eddy-sonic test method. Materials Evaluation, Vol. 26, February (1968), p. 21.
- /16/ Curtis, G.J. "Bonded Structure Testing", U.K. Atomic Energy Authority Report (1968) AERE R-6098, 3.
- /17/ Hagemaiier, D. "Sonic and ultra sonic testing applications in the aerospace industry" ASNT Sonics Handbook Section VIII.
- /18/ Buffum, H.E. and Whealy, R.D. "Thru-transmission ultrasonic inspection system", Report Boeing Commercial Airplane Company, Renton, Wash. U.S.A.
- /19/ Nolle, A.W. and Westervelt, P. "Testing adhesive properties with the resonant bar technique", Journal of Appl. Physics 21 (4) (1959) 304.
- /20/ Dietz, A.G.H., Proceedings ASTM, 50 (1950) 17.
- /21/ Fukada, E and Kanamaru, K. "The non-destructive testing of the strength of adhesive bonds", Third Conference on Non-destructive testing, Japan, March 15-21, 1960.

- /22/ Schijve, J. "Investigation on the ultrasonic testing of glued metal joints",  
Neth. Nat. Aerospace Lab. N.L.R. Report M-1995 (1955).  
Also Aircr. Engin. 30 (1958) 355, 269.
- /23/ Clemens, R.E. "Application of N.D.T. on adhesive bonded structures for Northrop  
Aircraft Div. F5 and T-38 aircraft", SAMPE Quarterly, Jan. (1970) 170.
- /24/ Gonzalez, R.M. and Merschel, R.P. "Ultrasonic inspection of Saturn II tankinsulation"  
Nat. Conf. of N.D.T., Los Angeles, 1964.
- /25/ Lloyd, E.A. and Brown, A.F. "Testing of adhesive bonded joints by broadband ultra-  
sound" "Adhesion" 12, Applied Science Publishers, 1978.
- /26/ Hagemaiier, D. and Fassbender, R. "Non-Destructive Inspection", Primary Adhesively  
Bonded Structure Technology, Industry Review, 14-16/9/1977, Book 2, p. 233.

15 ACKNOWLEDGEMENTS

The information given in this presentation is based on the extensive data accumulated by the Non-destructive Testing Group of the Technological Centre of Fokker-VFW under Mr. K.J. Rienks, who has been pioneering in this field from the early days of adhesive bonding. Mrs. I. Höhle-Meijer is thanked for her efforts in preparing this manuscript.



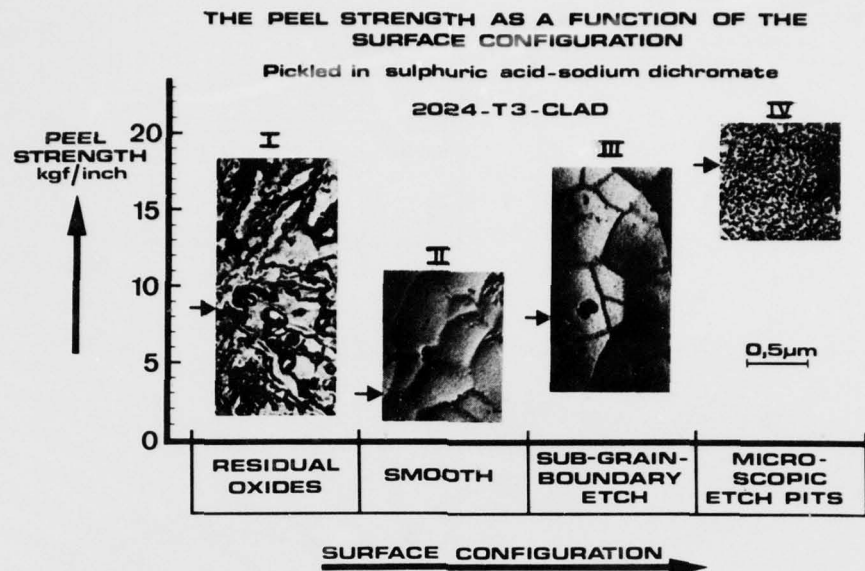


Fig. 1 The relation between the four configurations the aluminium surface oxide passes through during the sulphuric acid/sodium dichromate etching process and the peel-strength of a bonded joint. The arrows indicate the average peel-strength values and the vertical dimension of each picture indicates the magnitude of the scatter band. The configuration (IV) with the micro-etch pits gives the highest average and the smallest scatter.

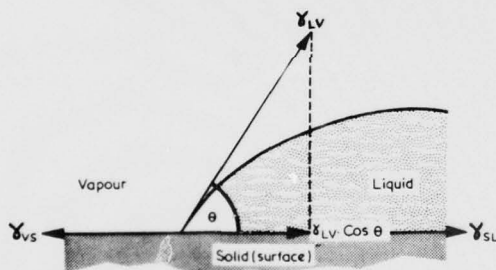


Fig. 2 The contact angle  $\theta$  between a liquid drop and a surface. The surface energies at the different interfaces are: liquid/vapour  $\gamma_{LV}$ ; vapour/solid  $\gamma_{VS}$ ; solid/liquid  $\gamma_{SL}$ .

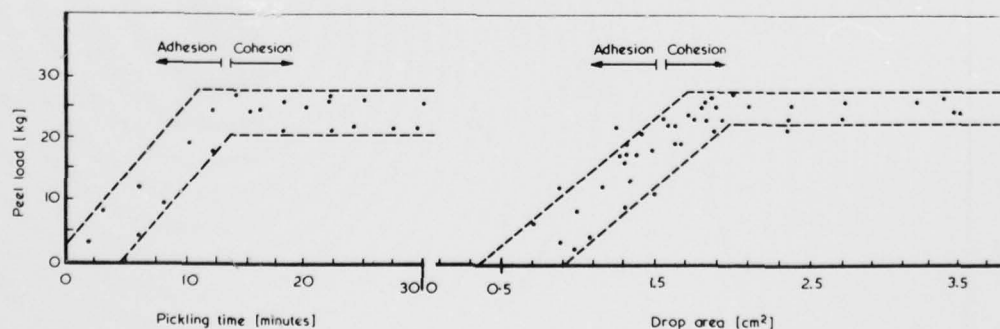


Fig. 3 The relationship between peel-load to drop-area is shown in the righthand diagram. A similar relationship exists between the peel-load and the time the aluminium surfaces were in the chromic/sulphuric pickling bath, as shown in the lefthand diagram.

Fig. 4 Schematic diagram of the measurement of the Voltapotential or Contact Potential Difference by means of the dynamic condenser principle of Kelvin.

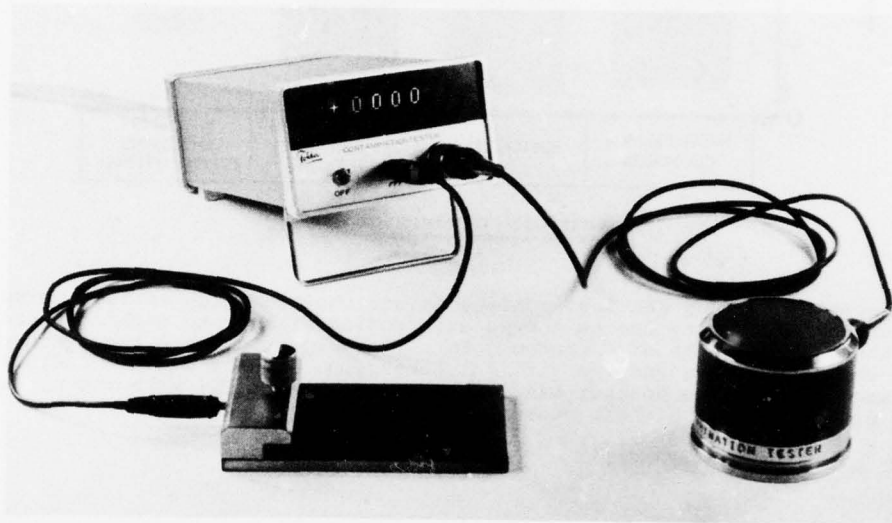
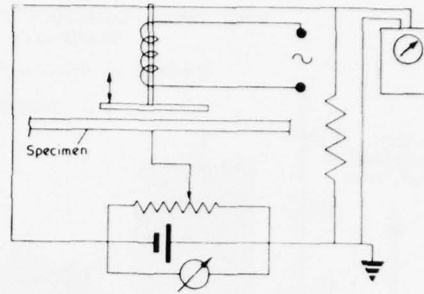


Fig. 5 The Fokker Contamination Tester for non-destructive testing of surfaces after surface treatment such as for adhesive bonding.

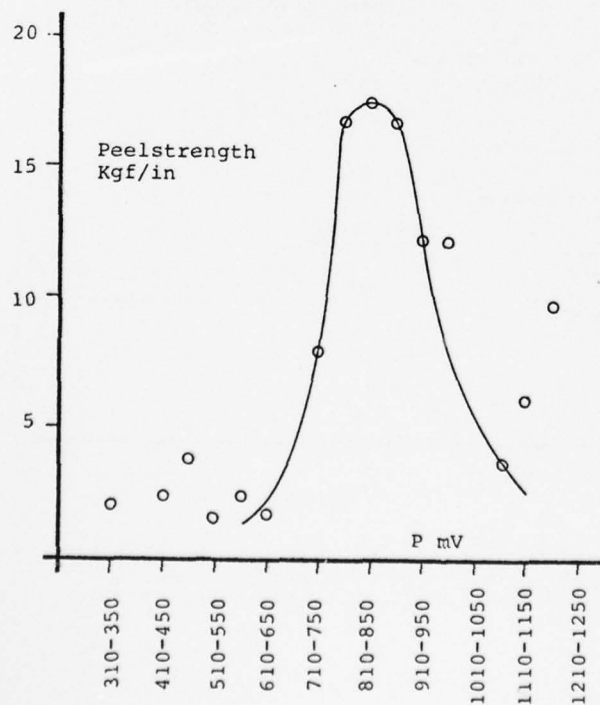


Fig. 6 Relation between Fokker Contamination Tester readings and peel-strengths resulting from prebond etching in chromic-sulphuric acid of various levels of effectivity.



Fig. 7 Prototype of the Fokker Impedance Tester that can be used for both analysis of metal surface-oxide and for cure-monitoring of structural adhesive and laminating resins.

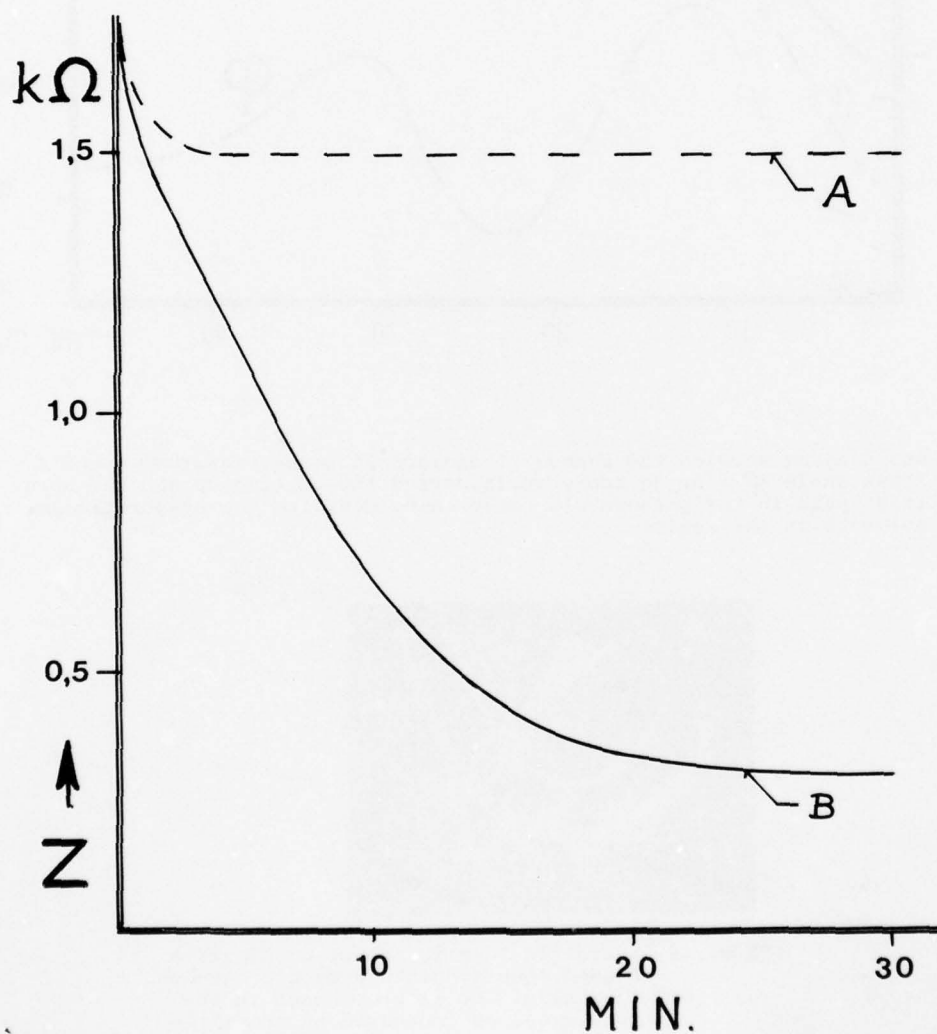


Fig. 8 Relation between surface impedance with degreasing time in minutes for a mild cleaner (A) and an aggressive cleaner (B). The surface area was constant 0.02 square inch<sup>2</sup> (0,13 cm<sup>2</sup>).



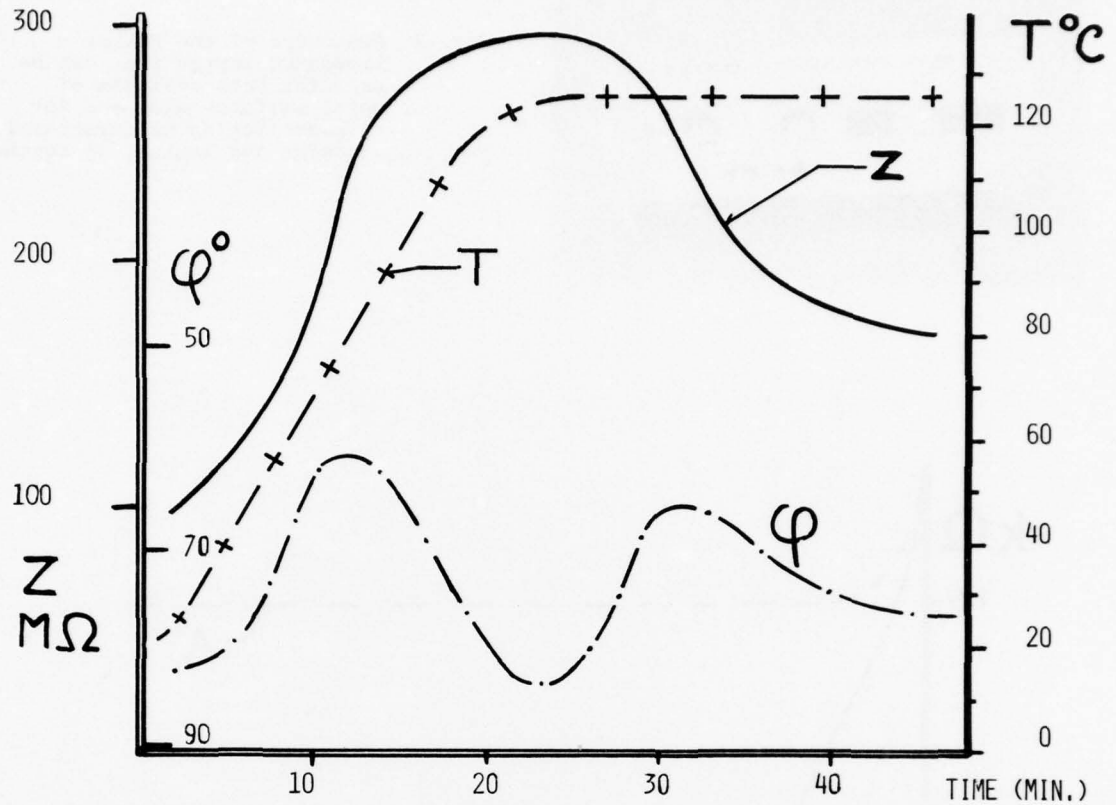


Fig. 9 Typical diagram showing the change of dielectric properties (Impedance  $Z$  and Phase angle  $\phi$ ) of an epoxy resin during the heating-up and the cure. The first peak in the phase-angle curve coincides with the evaporation of the solvents in the resin.



Fig. 10 Infra-red thermograph of an adhesive bonded doubler plate around a cut-out in a skin. The light patches in the bond area, as indicated by the white arrow, are voids in the adhesive layer.

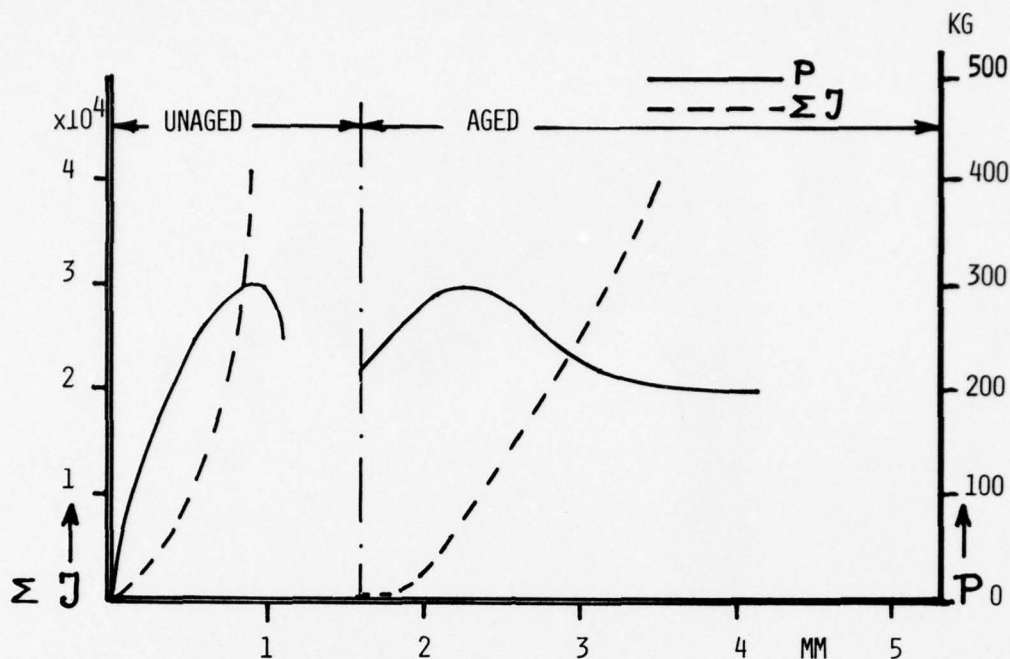


Fig. 11 Curves for impulse sum  $\Sigma J$  and crack opening force  $P$  for phenolic/vinyl adhesive. Both lefthand curves are for the adhesive at roomtemperature in the unaged condition. Both curves on the righthand side have been taken after the specimen had been exposed 40 hours to an environment of  $40^\circ\text{C}$  and 95% R.H.

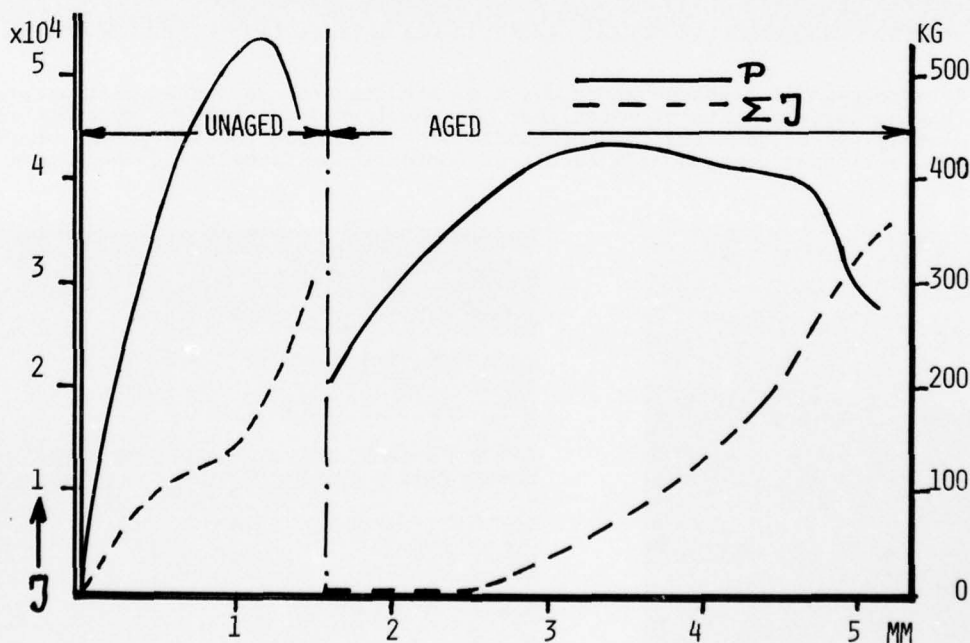


Fig. 12 Same curves as shown in figure 11, but now for a nylon-epoxy adhesive. Note the small amount of energy recorded during the opening in the aged condition. The high humidity sensitivity of this adhesive allows a much more plastic deformation in the aged condition. (Ref. Brockmann).

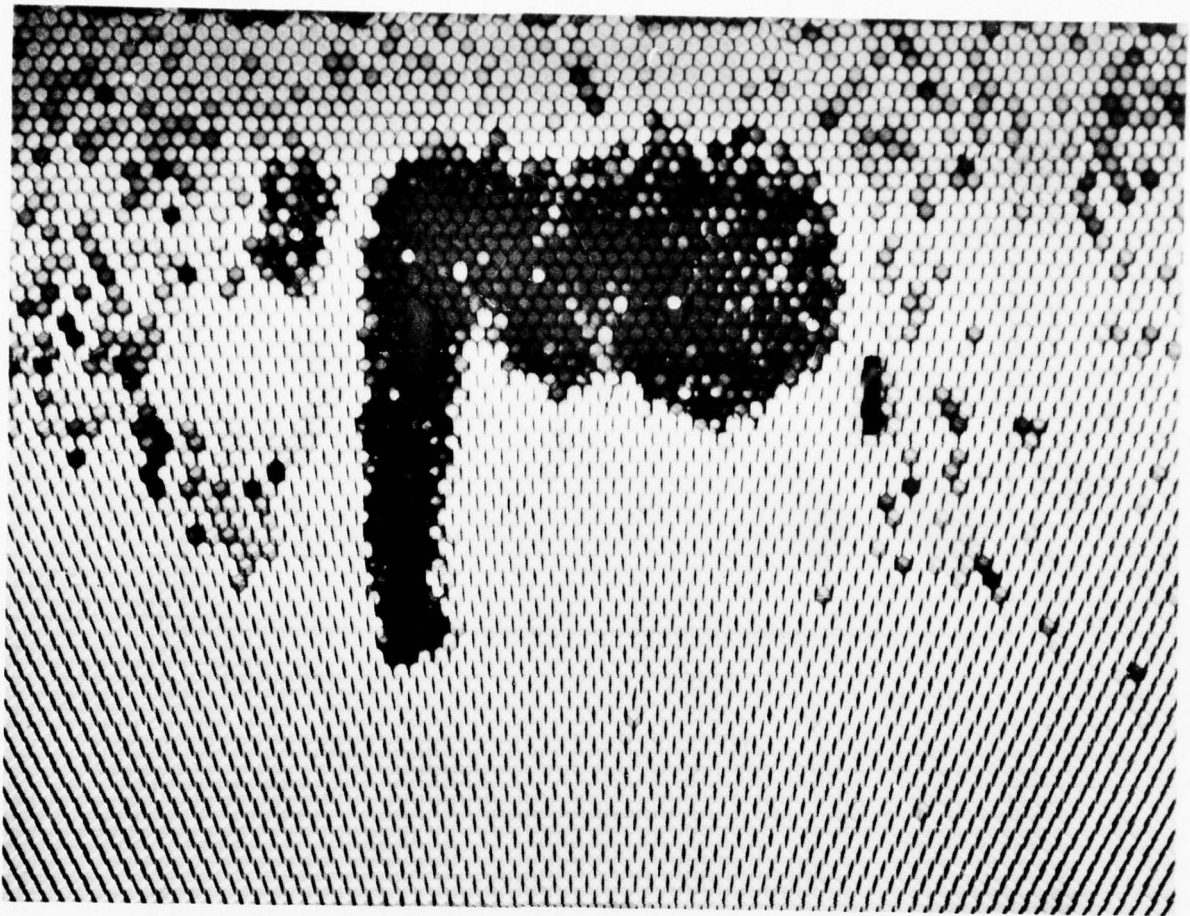


Fig. 13 X-radiograph of a honeycomb sandwich construction of an operational airplane, showing large amounts of water, that has penetrated into the honeycomb core. Clearly can be seen that in the middle of the picture the honeycomb core has been seriously damaged as a result of corrosion or freezing of the water.

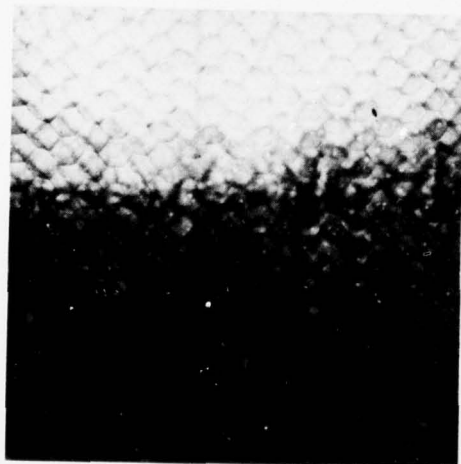


Fig. 14 a Neutrographic picture of a honeycomb sandwich panel. Note the airbubbles in each individual cell area, that can be clearly seen in the adhesive layer.

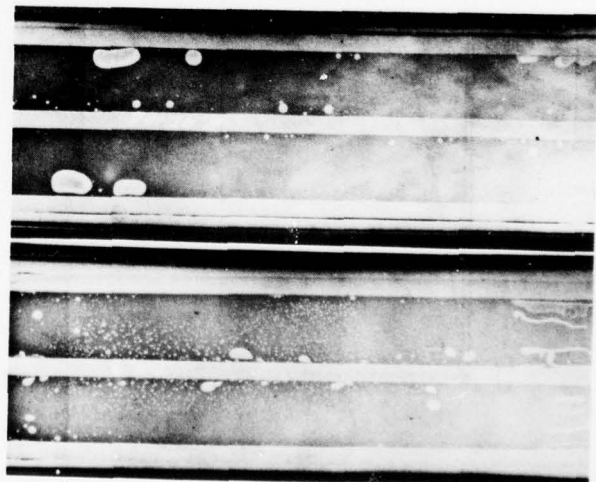


Fig. 14 b Neutrographic picture of metal-to-metal adhesive bonded joint showing clearly density variations, porosities and voids in the adhesive layer.



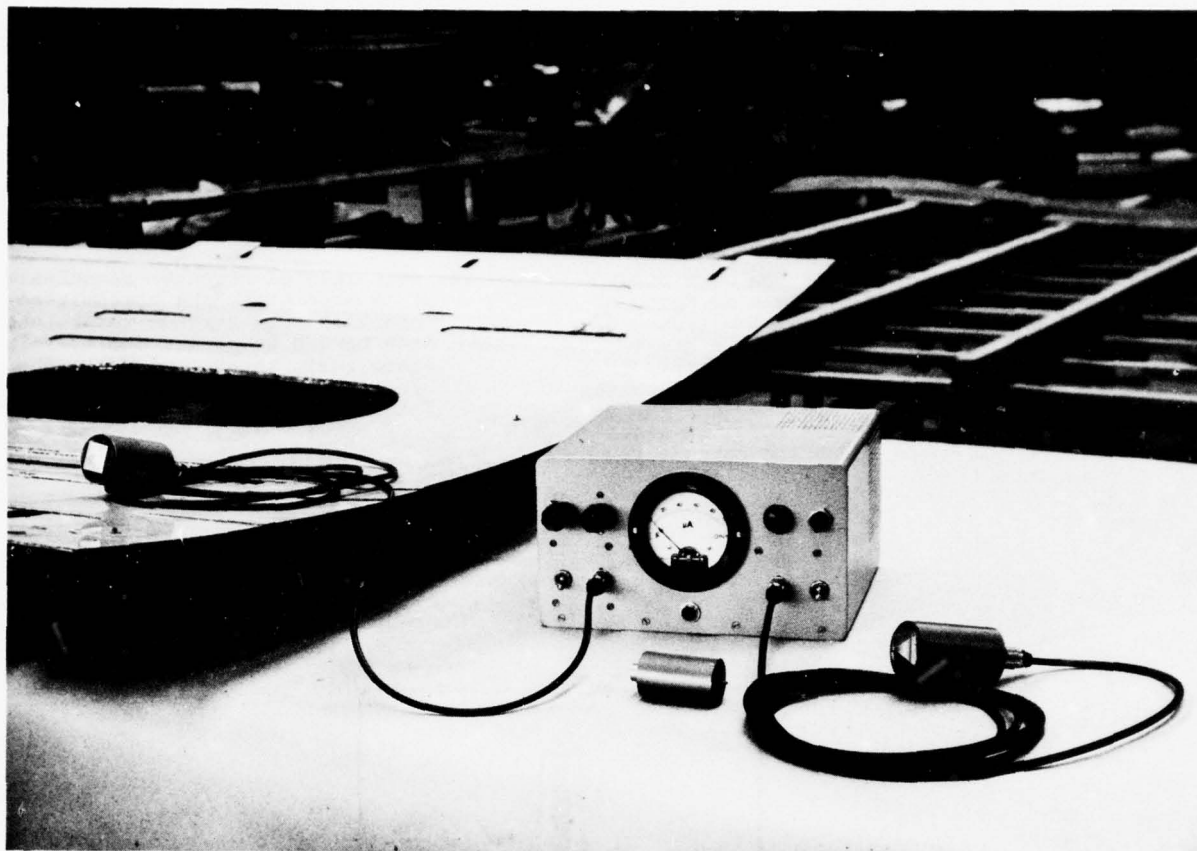


Fig. 15 Fokker Bond Tester Type I working at sonic frequencies. The probe at the lefthand side is the transmitter that feeds random frequency noise, with adjustable lower and upper frequency limits, into the panel. The righthand probe is the receiver, the energy of which can also be limited by adjustments of the lower and upper frequencies.

VOID SIZE (MM)	3 x 3	5 x 5	8 x 8	10 x 10	15 x 15	20 x 20	25 x 25
SHEET THICKNESS (MM)	FREQUENCY KHZ						
0,4	153	55	21	14	6,2	3,4	2,2
0,8	306	110	43	28	12,4	6,8	4,4
1,0	382	138	53	35	15,4	8,6	5,5
1,2	459	165	64	41	18,5	10,3	6,6

Table 16 Resonance frequencies of square unbonded sheet elements.

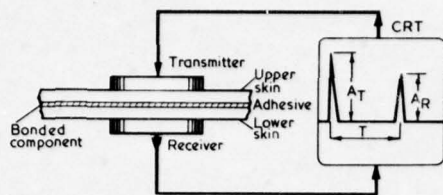


Fig. 17 Principle of inspection of a bonded metal-to-metal laminate by means of through-transmission of ultrasound. The ultrasonic signal is sent from the transmitter-transducer through the bonded component to the receiver-transducer. The amplitudes of the transmitted and the received signal can be compared at the cathode ray tube (resp.  $A_T$ ,  $A_R$ ).

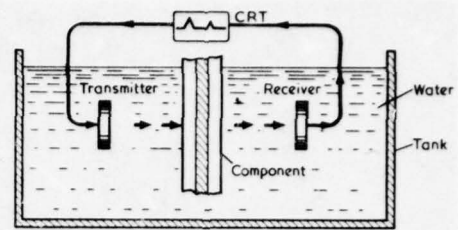


Fig. 18 Principle of through-transmission in a watertank. The transmitted signal passes through water into the bonded component and travels then again through water to the receiver transducer.

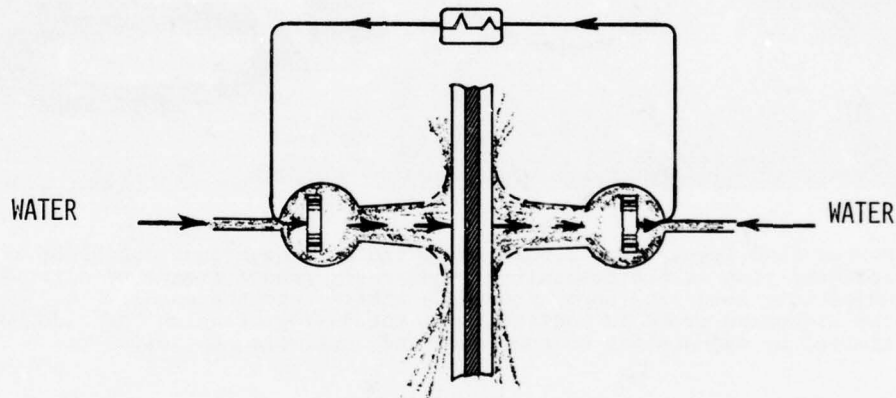


Fig. 19 Principle of through-transmission inspection with help of waterjets.

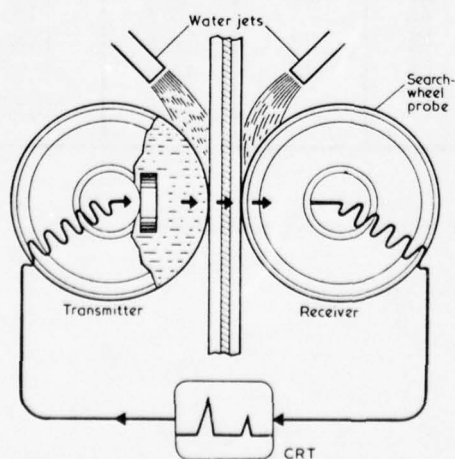


Fig. 20 Principle of through-transmission by means of rotating search-wheels that are coupled to the components by means of waterjets. The transducers of the transmitter, respectively the receiver, are both within a wheel that is filled with a liquid.

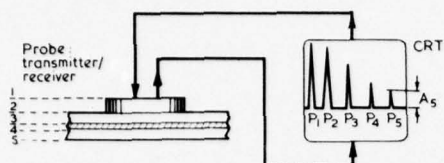


Fig. 21 Principle of the pulse-echo technique using a single transducer for transmission and reception. The ultrasonic pulse is transmitted into the bonded structure and is received by the same transducer at different time delays after being reflected from the various interfaces as indicated by 1, 2, 3, 4, 5.

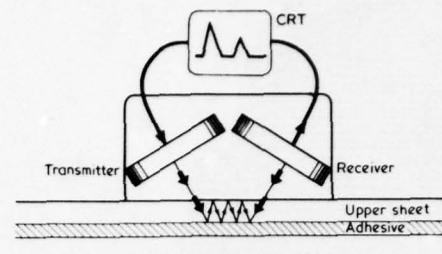


Fig. 22 Single probe in which two transducers respectively for transmission and reception are mounted. Depending from the way the transducers are mounted in the probe the signal is reflecting within the layers over a given distance; in this way the attenuation of the signal is enhanced.

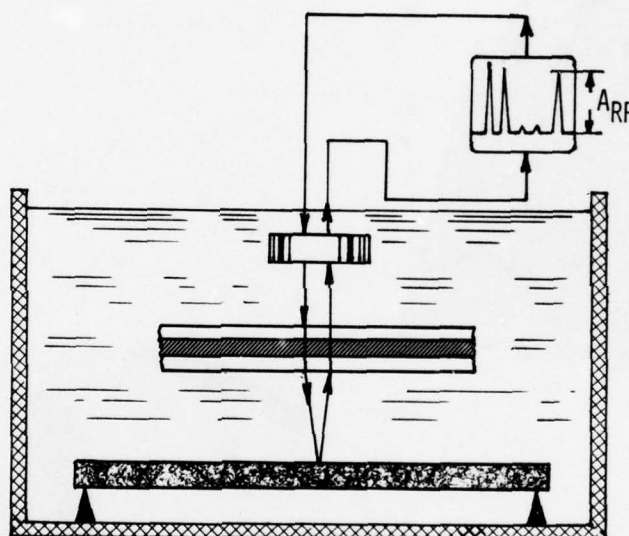


Fig. 23 Principle of the use of a combined transmitter-reception transducer used in a watertank applying the reflector-plate technique. The quality of the bonded joint is primarily observed by the amplitude of the signal that is reflected from the reflector plate ( $A_{RP}$ ).

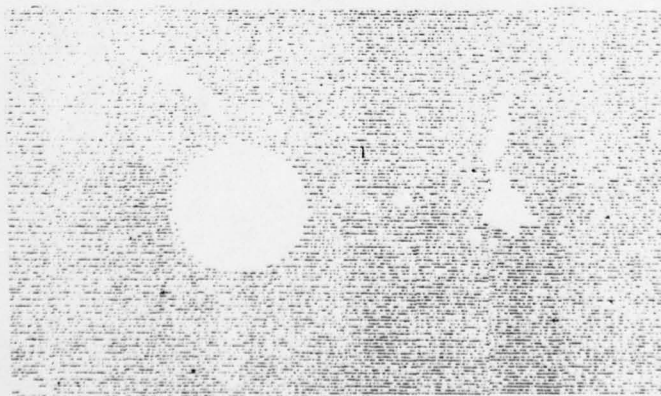


Fig. 24 Example of a C-scan recording based on the acceptance amplitude of the received signal of a prior set level. All amplitudes below this level do not show up as a black line and mark the void areas as white spots on the recording. (Ref. Hagemaijer).



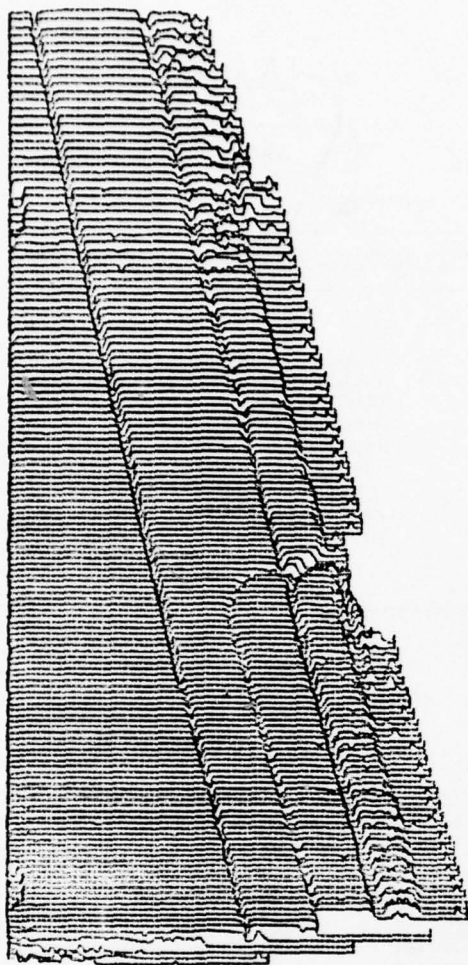
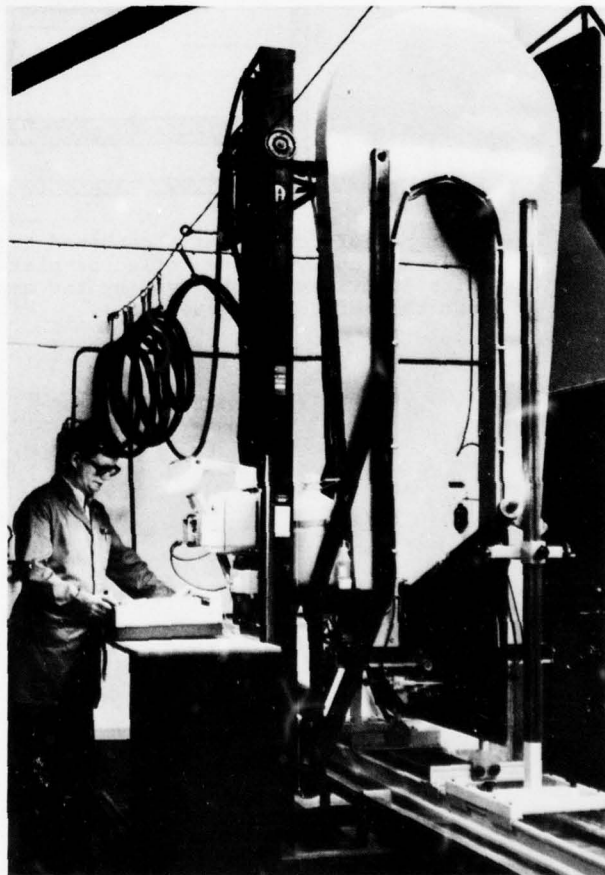


Fig. 25 C-scan showing the variation in the received signal amplitude as a vertical deviation from the horizontal line. The location of the change in amplitude is so clearly marked on a scaled-down picture of the component. (Ref. SAAB-SCANIA Company).

Fig. 26 a C-scan installation such as in use by the SAAB-SCANIA Company. The installation uses a pair of search-wheels moving up and down in a joke-type of construction. The C-scan is recorded on a X-Y recorder shown on the lefthand side.



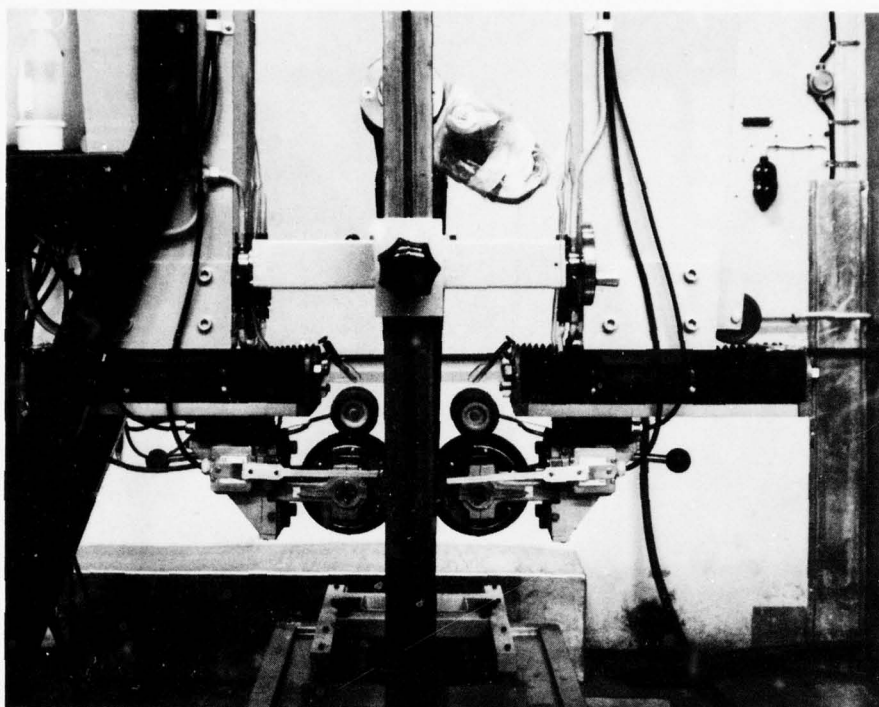


Fig. 26 b Close-up of the search-wheel configuration as used in the SAAB-SCANIA C-scan installation.



Fig. 27 C-scan in various grey tones. Each tone is indicating a certain preset level of amplitude. (Ref. Fokker-VFW Technological Centre).

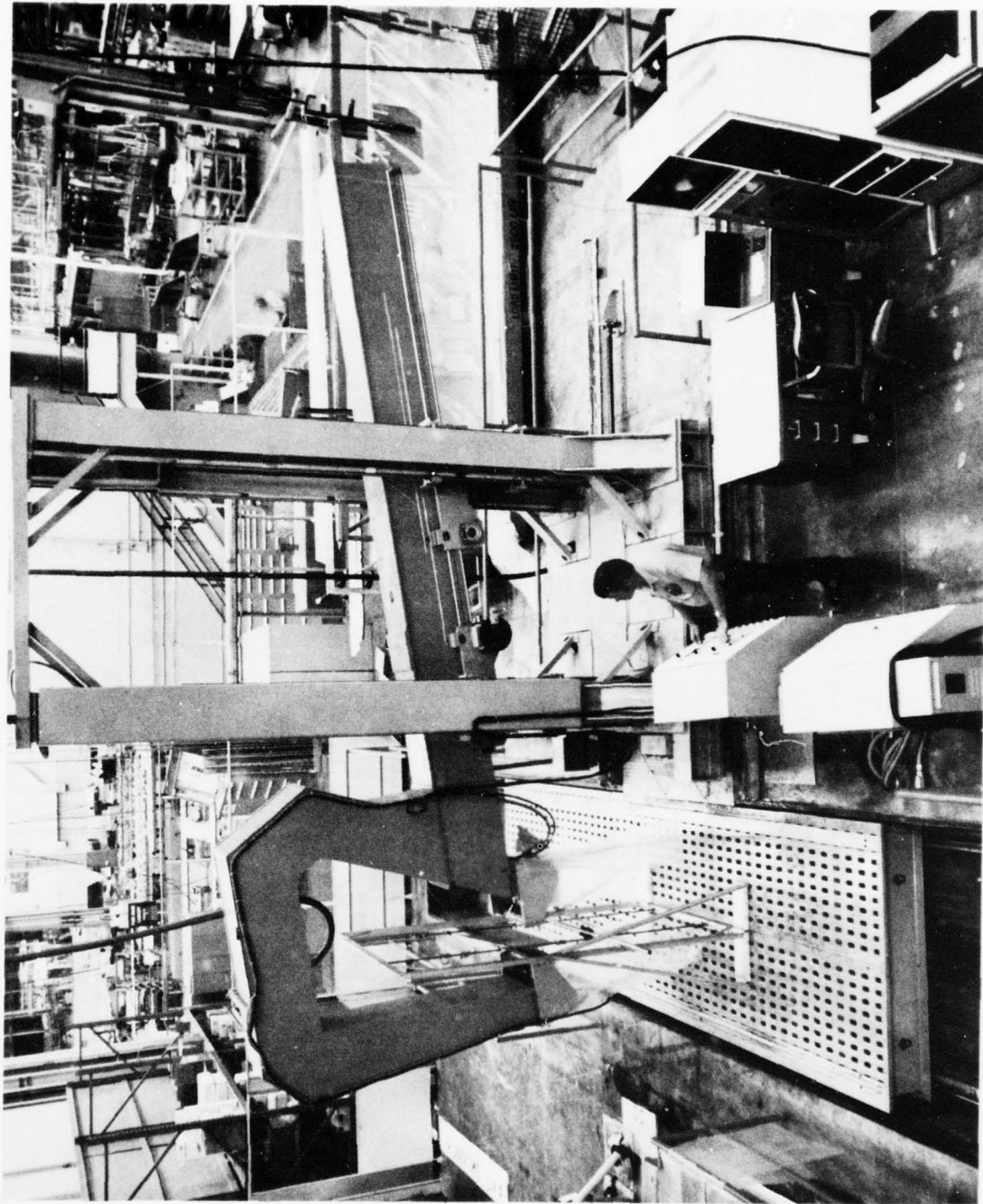


Fig. 28 Waterjet C-scan installation such as in use by the Boeing Commercial Airplane Company. 6 pairs of horizontally opposed waterjet-coupled pulse-transducers are mounted in the large joke-structure that is moved up and down. The component to be tested is moved horizontally through the joke. All data received are stored and corrected by means of the computer installation shown on the lower righthand side.



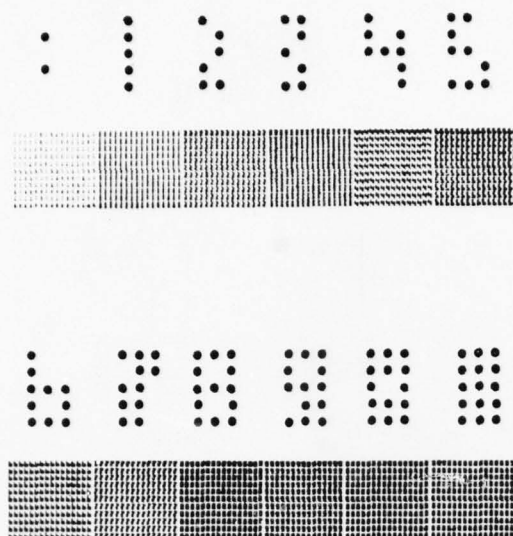
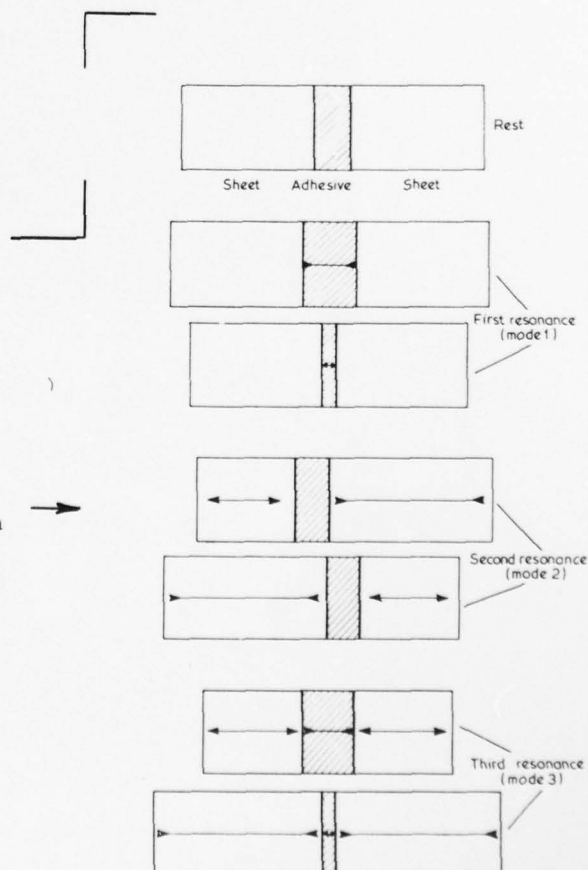


Fig. 29 a Symbol system used in the Boeing installation as shown in fig. 28, dividing the received signal into the 13 increments of 6 dB. The maximum received signal is indicated by an asterisk, that is not shown on this diagram and further symbols 0, 1, 2, 3, 4, 5, 6, 7, 8, 9 and so-called reversed-field 0 and 1.

The characters have been chosen such that when printed in the scaled-down picture of the component to be tested the lower quality levels are shown as a dark grey tone. This is indicated by each square shown under the particular character.

Fig. 30 The three modes of resonance of a bonded laminate of two sheets with an adhesive layer in between according to Schijve.



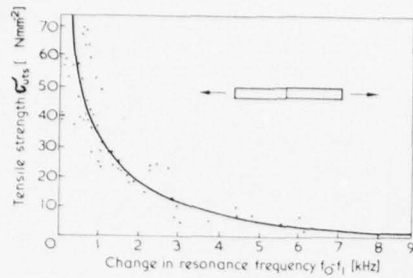


Fig. 31 Results of resonance tests according to Bordonni on adhesive bonded aluminium bars using a phenolic/vinylic adhesive. The tensile stress at failure is correlated with the difference in resonance frequency of a solid bar of the same length as the bonded one, and the frequency of the latter

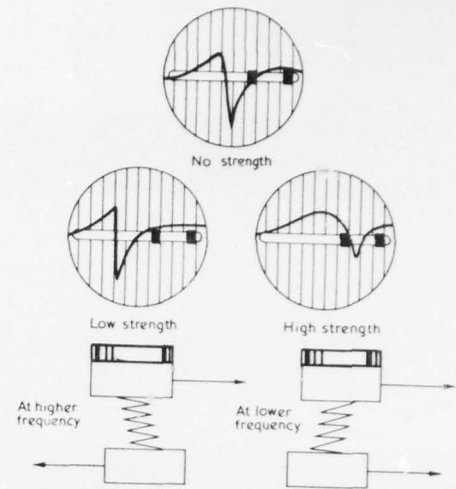


Fig. 32 The three basic positions of the resonance peak on the A (frequency)-scale; the two positions for bonded joints correspond to different modes of resonance such as for a low strength (low stiffness) adhesive at a high frequency, and a high strength (high stiffness) adhesive at a low frequency.

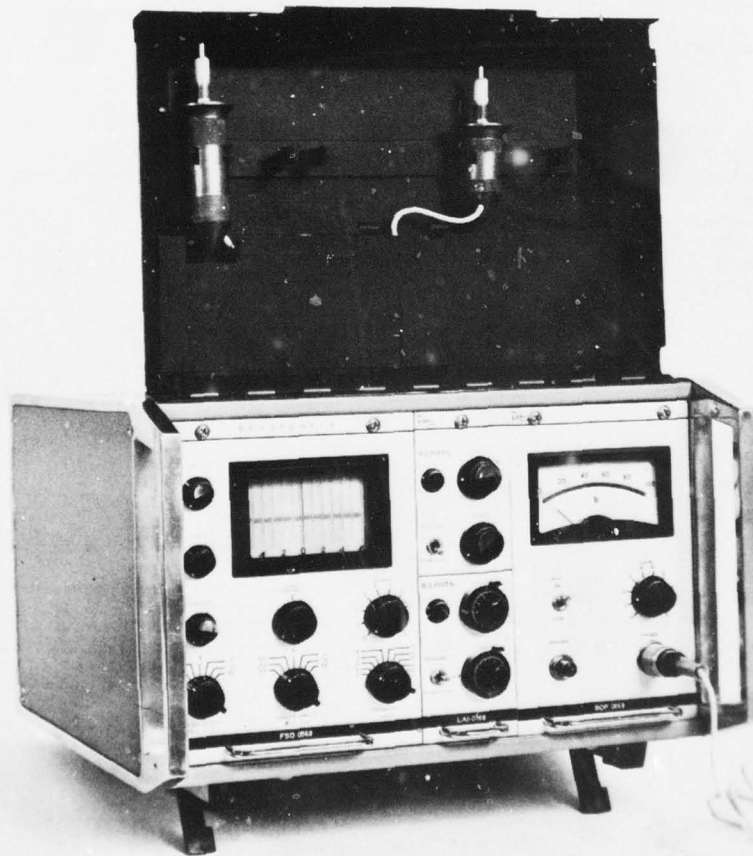


Fig. 33 The Fokker Bond Tester model 70.

AD-A068 806

ADVISORY GROUP FOR AEROSPACE RESEARCH AND DEVELOPMENT--ETC F/G 13/5  
BONDED JOINTS AND PREPARATION FOR BONDING.(U)  
MAR 79

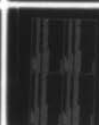
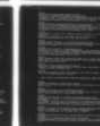
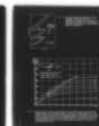
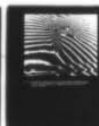
UNCLASSIFIED

AGARD-LS-102

NL

4 of 4

AD  
AO 68806



END  
DATE  
FILMED

6 --79

DDC





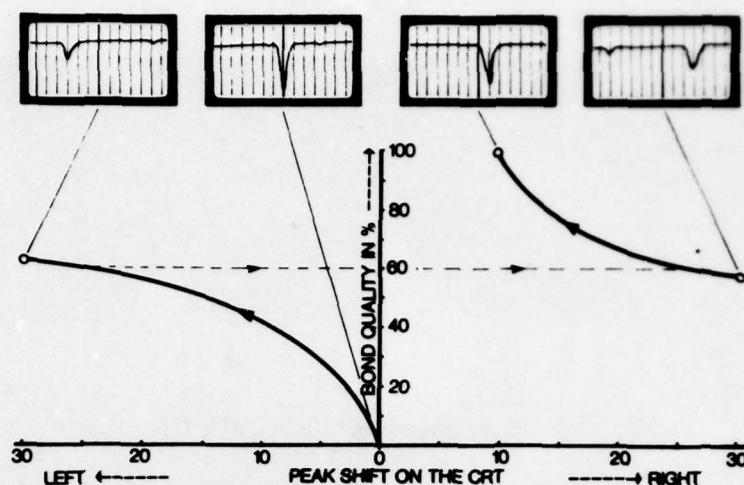


Fig. 34 Typical relation between lap-shear strength and response on the Fokker Bond Tester A-scale. With strengths increasing from 0 upto about 50%, the resonance peak moves to the left; further increase of quality brings the peak back to the far righthand side of the scope. The peak moves now further to the left with continued increase of strength to the maximum value. The peak position moves so far to the centre of the diagram that the location is reached which would have been obtained when the probe would have been placed on a piece of solid material of the same thickness as the total metal involved in the adhesive bonded laminate.

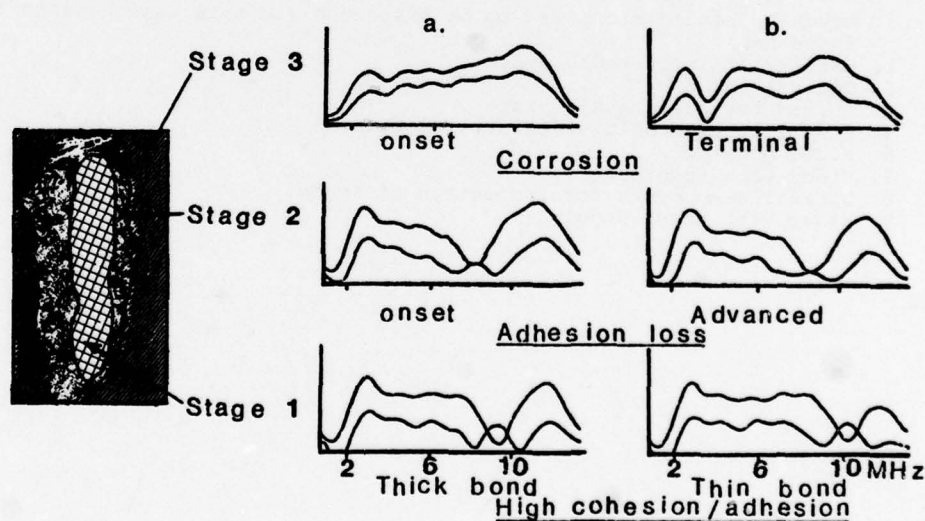


Fig. 35 Examples of differential spectral analysis of degradation of a nylon-epoxy adhesive-bonded specimen. The specimen is exposed to an environment of high humidity and temperature. The area which is indicated by stage 1 is the adhesive layer in its original state. The testing method differentiates between a thick and a thin bond. In stage 2 the effect of moisture penetration causing desorption and subsequent loss of adhesion is shown in changes of the spectrum. In stage 3 is shown how the subsequent corrosion can be determined by changes in the spectrum (Ref. Brown of the City University London).

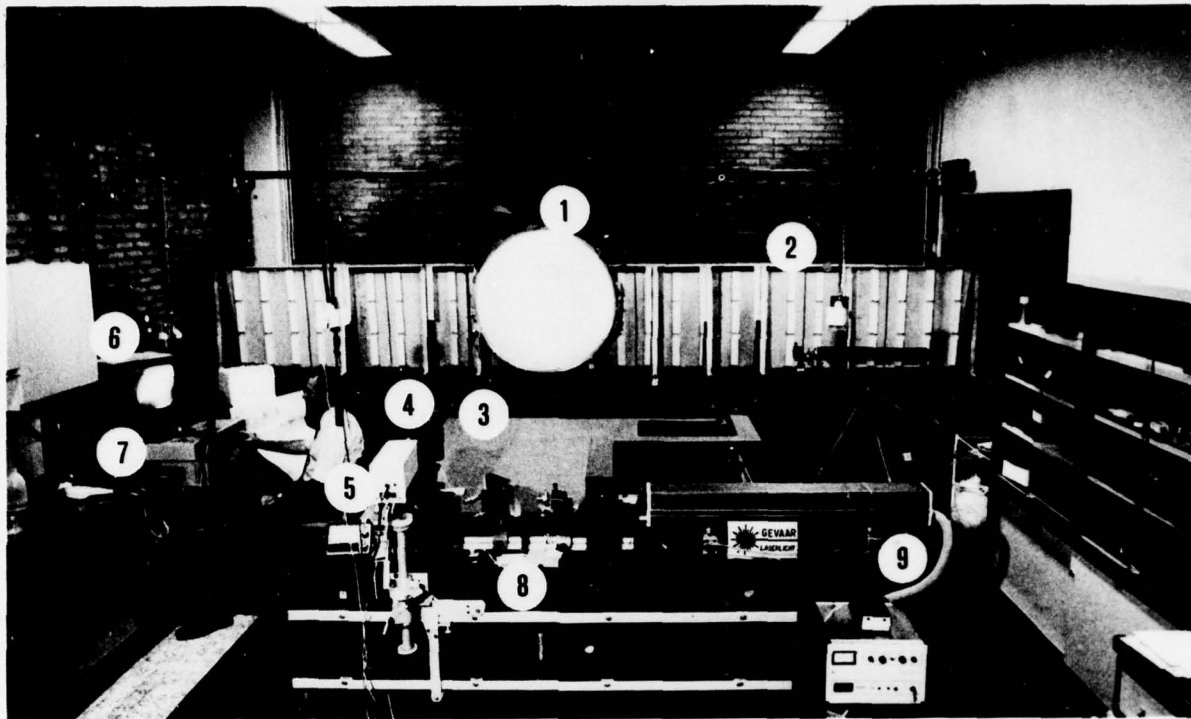


Fig. 37 Fokker Holographic Bond Tester installation

1. Adhesive bonded structure to be inspected (in this case a hatch for Space Lab)
2. Battery of infra-red heaters
3. Optical table
4. Holder for holographic plate
5. Highly light-sensitive television camera
6. Video monitor
7. Video tape recorder
8. Optical components for inspection of object
9. Laser with power supply



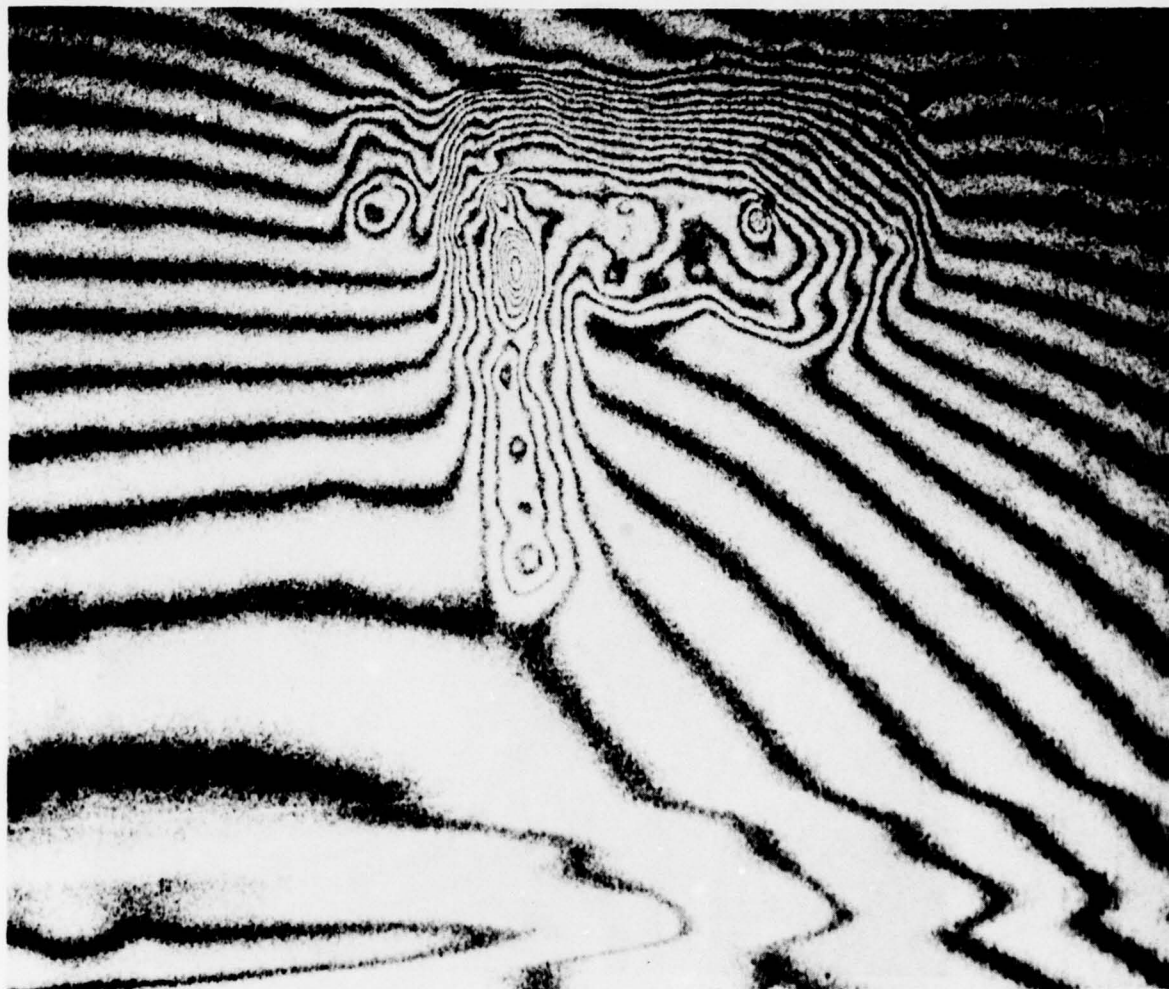


Fig. 38 Holographic inspection pattern of the same damaged honeycomb sandwich panel of which in figure 13 a radiographic picture is shown. The area in which the honeycomb core is damaged by water and corrosion is clearly indicated.



Fig. 39 Holographic inspection result of an adhesive bonded control surface of honeycomb sandwich configuration. The arrows indicate defects in the joints between honeycomb core sections among themselves and with edge members.



Fig. 40 Holographic interference pattern obtained from a resonating adhesive bonded skin to tophat stringer panel. The white non-vibrating horizontal areas are the adhesive bond regions. In between the resonating skin membranes are visible. In areas such as indicated by the arrows the resonance patterns extend into the bond area, indicating low cohesion strength of the adhesive layer.

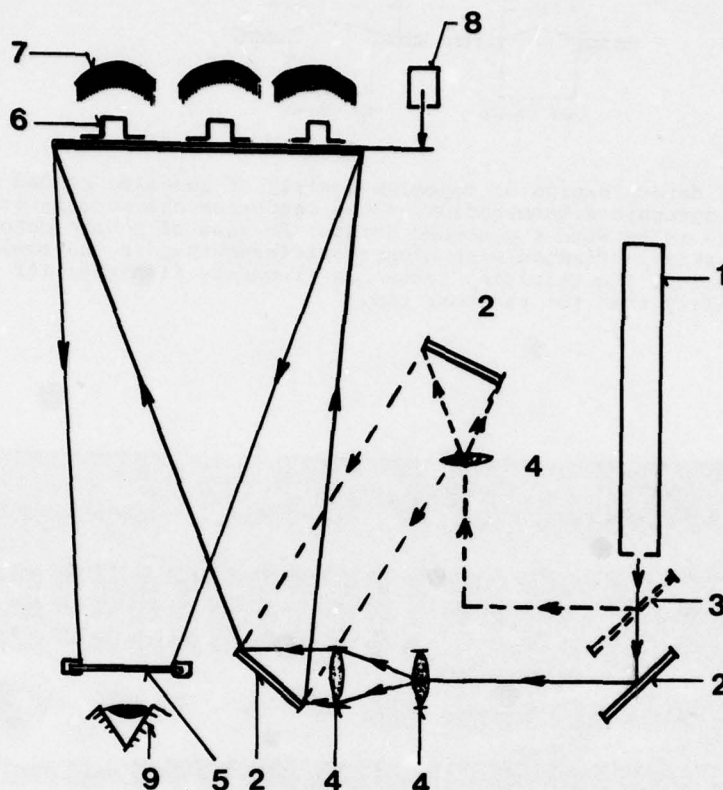


Fig. 36 Schematic arrangement for holographic-interference inspection of adhesive bonded joints, incorporating compensation for deformation of the object during the inspection.

1. Laser
2. Fully reflecting mirror
3. Half transparent mirror
4. Expanding lens
5. Holographic plate
6. Object to be inspected
7. Infra-red heating elements
8. Excitation device
9. Observer



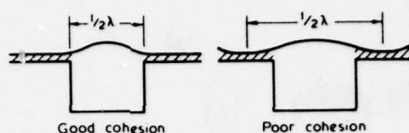


Fig. 41 a Principle of determination of cohesion quality of adhesive bonded joints by means of holographic determination of the resonance characteristics of the skin membrane in between the bonded joints. In case of a high cohesion quality the skin is clamped with higher stiffness than in the case of a poor cohesion quality. The resulting resonance frequency is higher for the good cohesion quality than for the poor one.

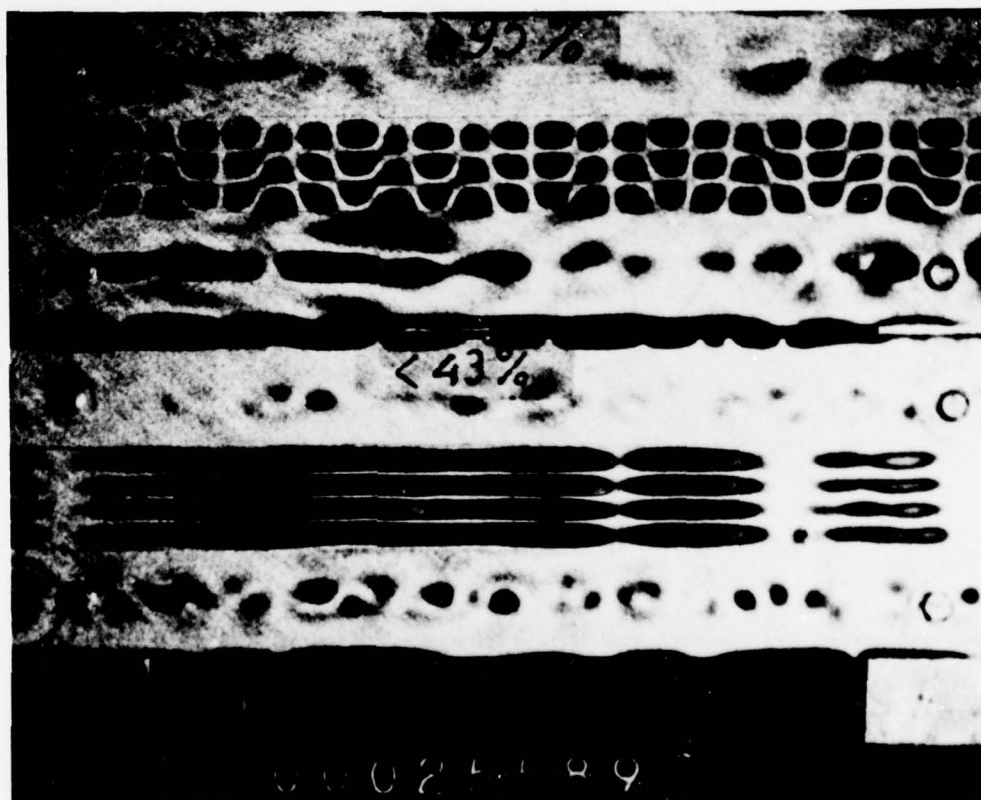


Fig. 41 b Example of cohesion quality determination by means of resonance measurements. Two sheets have been bonded on edge profiles. The top sheet has been bonded with the highest possible bonding quality, indicating by a quality better than 95% of ideal. The lower skin panel has been bonded with a quality which is lower than 43%. At the indicated frequency of 25,6 kHz the upper panel vibrates in a pattern that shows in vertical direction 3 half wave lengths and a short wave length horizontally. The lower panel however, vibrates at this frequency with 4 half wave lengths in vertical direction and a long wave length horizontally. In this way the lower clamping effect of the low quality bond is demonstrated.

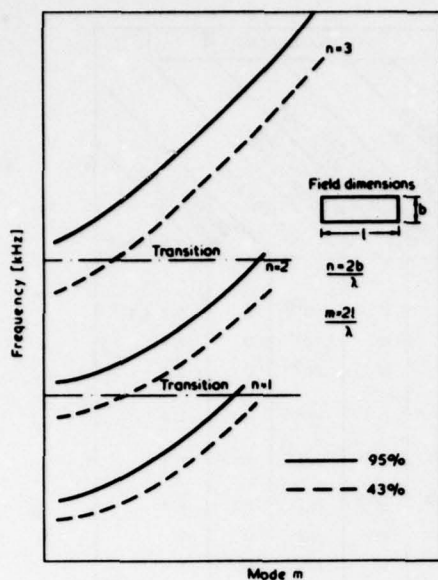


Fig. 42 Relation between the membrane resonance frequency and the mode for two different qualities (95% and 43%) of edge bond. It appears that significantly different modes occur for the different qualities in particular in the indicated zones of transition.

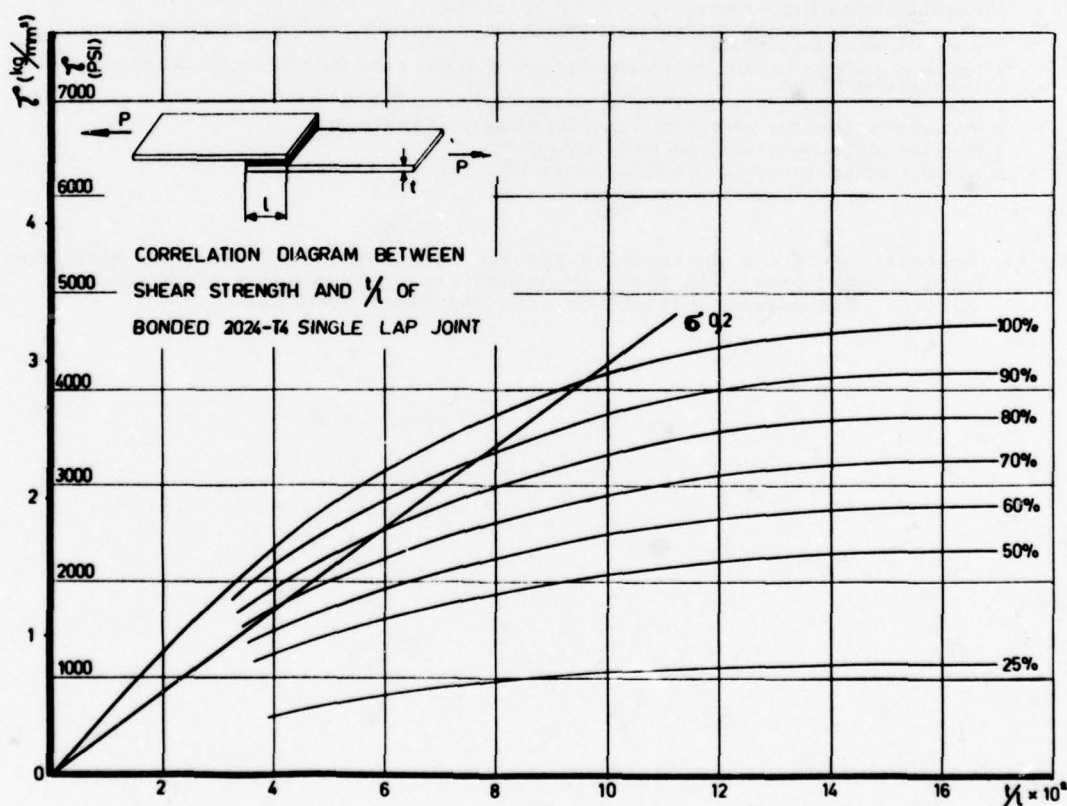


Fig. 43 Typical relation between the geometry of the bonded joint (sheet thickness/overlap-length) and the average shear strength of a bonded lap joint. The diagram shows how the cohesion quality expressed in percentages of the ideal quality (100%) influences the average shear strength. The latter figure does not change proportional with the cohesion quality. The straight line in the diagram indicates the line of the yield strength of the metal. The area of the diagram left of this line indicates that the stresses in the metal are above the yield stress.

LAMINATE DEFECTS	ULTRASONIC (5)													REMARKS
	NOE METHODS	LOW KV X-RAY	FOKKER BONDTESTER	SONDICATION	HARMONIC BONDTESTER	210 SONIC BONDTESTER	CONTACT PULSE ECHO	CONTACT THROUGH TRANSMISSION PULSE ECHO	IMMERSION C-SCAN	IMMERSION C-SCAN THROUGH TRANSMISSION	IMMERSION C-SCAN REFLECTOR PLATE	COIN TAP TEST	NEUTRON RADIOGRAPHY	
1. VOID	(1)	D	D	D	D	D	D	D <sup>(2)</sup>	D	D	PD <sup>(4)</sup>	D		1, 2, 4, 6
2. VOID (C-14 REPAIR)	(1)	D	D	D	D	D	D	D <sup>(2)</sup>	D	D	PD <sup>(4)</sup>	D		2, 4
3. VOID (9309 REPAIR)	(1)	D	D	D	D	D	D	D <sup>(2)</sup>	D	D	PD <sup>(4)</sup>	D		2, 4
4. LACK OF BOND (SKIN TO ADHESIVE)	(1)	D	D	D	D	D	D	D <sup>(2)</sup>	D	D	PD <sup>(4)</sup>	ND		2, 4
5. MFGR'S SEPARATOR SHEET (FM123-41)	(1)	D	D	ND	PD	ND	PD	D <sup>(2)</sup>	D <sup>(3)</sup>	D <sup>(3)</sup>	ND	PD <sup>(3)</sup>		2, 3
6. THICK ADHESIVE (1, 2, 3 PLY)	(1)	D	ND	ND	D	ND	ND	ND <sup>(4)</sup>	PD <sup>(2)</sup>	D <sup>(2)</sup>	ND	ND		2, 4
7. POROUS ADHESIVE	(1)	D	ND	ND	D	D	D	D	D	D	ND	D		1
8. BURNED ADHESIVE	(1)	D	ND	ND	D	D	D	PD	D	D	ND	ND		7
9. CORRODED JOINT	D	D	PD	PD	D	D	D	PD	D	D	PD	D		8

ND - NOT DETECTED

PD - PARTIAL DETECTION

D - DETECTED

- PANELS WERE MADE USING FM-73 WHICH IS NOT X-RAY OPAQUE. WITH X-RAY OPAQUE ADHESIVE, DEFECTS 1, 2, 3, 5, 6, 7, ARE DETECTED
- METHOD SUFFERS FROM ULTRASONIC WAVE INTERFERENCE EFFECTS CAUSED BY TAPED METAL DOUBLES OR VARIATIONS IN ADHESIVE THICKNESS.
- MANUFACTURER'S SEPARATOR SHEET NOT DETECTABLE BUT DEVELOPED POROSITY AND AN EDGE UNBOND DURING CURE CYCLE WHICH WAS DETECTABLE.
- MIL-C-88286 (WHITE) EXTERNAL TOPCOAT AND PR14326 (GREEN) PLUS MIL-C-83019 (CLEAR) BILGE TOPCOAT DAMPENED THE PULSE-ECHO RESPONSE.
- CONTACT SURFACE WAVE WAS TRIED BUT DID NOT DETECT ANY BUILT-IN DEFECTS.
- MINIMUM DETECTABLE SIZE APPROXIMATELY EQUAL TO SIZE OF PROBE BEING USED.
- CAUSED BY DRILLING HOLES OR BAND SAWING BONDED JOINTS
- MOISTURE IN BOND JOINT (ARMCO 252 ADHESIVE, FPL ETCH)

Table 44 Correlation of non-destructive results with built-in defects in metal-to-metal bonded panels as found by Hagemaiier and Fassbender of Douglas Aircraft Company in conjunction with the PABST program.



HONEYCOMB DEFECTS	NDE METHODS	LOW K <sub>α</sub> X-RAY	FOKKER BONDTESTER	SONDicator	HARMONIC BONDTESTER	210 BONDTESTER	CONTACT PULSE ECHO	CONTACT THROUGH TRANSMISSION	CONTACT SHEAR WAVE	ULTRASONIC			COIN TAP TEST	NEUTRON RADIOGRAPHY	REMARKS
										IMMERSION C-SCAN	IMMERSION C-SCAN THROUGH TRANSMISSION	IMMERSION C-SCAN			
11. VOID (ADHESIVE TO SKIN)	ND <sup>(1)</sup>	D	D	D	D	D	D	ND	D	D	D	D	D		REPLACEMENT STANDARD
12. VOID (ADHESIVE TO SKIN) REPAIR WITH C-14															NO VOID IMPROPERLY MADE
13. VOID (ADHESIVE TO SKIN) REPAIR WITH 9309															NO VOID IMPROPERLY MADE
14. VOID (ADHESIVE TO CORE)	ND	D	-	D	D	ND	D	ND	D	D	D	D	D		REPLACEMENT STANDARD
15. WATER INTRUSION	D	ND	ND	ND	ND	ND	D	ND	ND	D	D	D	D		
16. CRUSHED CORE (AFTER BONDING)	D <sup>(2)</sup>	PD <sup>(4)</sup>	ND	PD <sup>(4)</sup>	ND	ND	PD <sup>(4)</sup>	ND	PD <sup>(4)</sup>	PD <sup>(4)</sup>	D	PD			2, 4
17. MFGRS SEPARATOR SHEET (SKIN TO ADHESIVE)	ND <sup>(3)</sup>	ND	ND	PD	ND	PD	D	ND	D	D	PD	D	D		3
18. MFGRS SEPARATOR SHEET (ADHESIVE TO CORE)	ND <sup>(3)</sup>	ND	ND	ND	ND	D	ND	ND	D	PD	D	D	D		3
19. VOID (FOAM TO CLOSURE)	D	D	D	D	D	D	D	ND	D	D	D	D	D		
20. INADEQUATE TIE-IN OF FOAM TO CORE	D	D	D	D	D	ND	D	ND	D	ND	D	D	D		
21. INADEQUATE DEPTH OF FOAM AT CLOSURE	D	D	D	ND	PD <sup>(5)</sup>	ND	ND	ND	ND	ND	PD	D	D		5
22. CHEM-MILL STEP VOID	ND <sup>(3)</sup>	ND	ND	ND	ND	ND	ND	ND	ND	ND	ND	ND	D		3

ND - NOT DETECTED

PD - PARTIAL DETECTION

D - DETECTED

- PANELS WERE MADE USING FM-73 WHICH IS NOT X-RAY OPAQUE.
- THE 0.005- AND 0.010-INCH CRUSHED CORE DETECTED BY STRAIGHT AND BETTER BY ANGLE SHOT.
- HAS BEEN DETECTED BY X-RAY WHEN ADHESIVE WAS X-RAY OPAQUE (FM-400).
- DETECTS 0.010 CRUSH CORE.
- DISCLOSES DEFECT AT A VERY HIGH SENSITIVITY.

Table 45 Similar correlation as shown in table 44, but now for honeycomb sandwich panels, also established by Hagemaiier and Fassbender of Douglas Aircraft Company.

## SELECTIVE BIBLIOGRAPHY

The Bibliography which follows has been prepared by the AGARD Technical Information Panel and is a compilation of references selected specially to suit this particular Lecture Series; it is not intended to be comprehensive. It is regretted that AGARD cannot undertake to provide copies of the documents listed. These should be sought from the organizations which published them.

	Page
A: INTERFACE PHENOMENA	B-1
B: SURFACE TREATMENT, BONDING PROCESSES AND DURABILITY ASPECTS	B-1
C: STRESS ANALYSIS STRENGTH AND FRACTURE MECHANICS OF BONDED JOINTS	B-5
D: MECHANICAL PROPERTIES OF ADHESIVE BONDED STRUCTURES	B-11
E: QUALITY CONTROL AND NON-DESTRUCTIVE INSPECTION TECHNIQUES FOR BONDED JOINTS	B-12

## A INTERFACE PHENOMENA

77A42403

The role of the interface in adhesion phenomena.

A/Mittal, K.L., A/(IBM Corp., Poughkeepsie, N.Y.)

Polymer Engineering and Science, vol. 17, July 1977, p. 467-473.

77A41354

Interlaminar behaviour of bonded bimaterial systems.

A/Peretz, D.A., A/(Technion - Israel Institute of Technology, Haifa, Israel)

Composites, vol. 8, July 1977, p. 153-156.

77A27478

Interface reactions and their influence on the long term properties of metal bonds.

A/Brockmann, W., A/(Fraunhofer-Gesellschaft, Institut fuer angewandte Materialforschung, Bremen, West Germany).

In: Bicentennial of materials progress; Proceedings of the Twenty-first National Symposium and Exhibition, Los Angeles, Calif., April 6-8, 1976 (A77-27451 11-23) Azusa, Calif., Society for the Advancement of Material and Process Engineering, 1976, p. 383-397.

76A15152

Surface energetics criteria for bonding and fracture.

A/Kaelble, D.H., A/(Rockwell International Science Center, Thousand Oaks, Calif.).

In: Materials review '75; Proceedings of the Seventh National Technical Conference, Albuquerque, N. Mex., October 14-16, 1975, (A76-15151 04-27) Azusa, Calif., Society for the Advancement of Material and Process Engineering, 1975, p. 1-9.

75A34737

Apparent interfacial failure in mixed-mode adhesive fracture.

A/Bascom, W.D.; B/Timmons, C.O.; C/Jones, R.L., C/(U.S. Navy, Naval Research Laboratory, Washington D.C.).

Journal of Materials Science, vol. 10, June 1975, p. 1037-1048.

75A14889

An adhesion science viewpoint.

A/Dukes, W.A.; B/Kinloch, A.J., B/(Explosives Research and Development Establishment, Waltham Abbey, Essex, England).

Non-Destructive Testing, vol. 7, Dec. 1974, p. 324-326.

76N16184

Investigations into adhesion interactions between resins and metals.

A/Brockmann, W.

Royal Aircraft Establishment, Farnborough (England).

Transl. into English from Adhaesion (Berlin), v. 19, no. 2, 1975, p. 34-39.

75N30577

Mechanisms of adhesion failure between polymers and metallic substrates: Aluminium 2024-T3 and Titanium 6Al-4V with HT 424 adhesive, Final Report, 1 Jun. 1972 - 1 Feb. 1974.

A/Smith, T.; B/Kaelble, D.H.

Rockwell International Corp., Thousand Oaks, Calif. (Science Center).

## B SURFACE TREATMENT, BONDING PROCESSES AND DURABILITY ASPECTS

78A45936

A round robin evaluation of adhesive bonding processes.

A/Levi, D.W.; B/Wegman, R.F., B/(U.S. Army, Armament Research and Development Command, Dover, N.J.)

SAMPE Quarterly, vol. 9, July 1978, p. 28-35.

78A30569

A practical approach to the environmental testing of coatings and adhesives as used in aircraft manufacture.

A/Albericci, P., A/(British Aerospace, Weybridge, Surrey, England).

Society of Environmental Engineers, Journal vol. 17-1, Mar. 1978, p. 13-17.

78A29292

Effects of chemical and thermal treatments on the composition of 2024 aluminium adherend surfaces.

A/Sun, T.S.; B/Chen, J.M.; C/Venables, J.D.; D/Hopping, R. D/(Martin Marietta Aerospace, Baltimore, Md.).

Applications of surface science, vol. 1, Jan. 1978, p. 202-214.

78A26116

A new technique for assessing the durability of structural adhesives.

A/Wegman, R.F.; B/Bodnar, M.J.; C/Ross, M.C., C/(U.S. Army, Large Caliber Weapon Systems Laboratory, Dover, N.J.).

SAMPE Journal vol. 14, Jan. - Feb. 1978, p. 20-23.



7816916

Durability of structural adhesive bonds /A review/

A/DeLollis, N.J., A/(Sandia Laboratories, Albuquerque, N. Mex.).

In: Diversity - Technology explosion; Proceedings of the Twenty-second National Symposium and Exhibition, San Diego, Calif., April 26-28, 1977 (A78-16870 04-23), Azusa, Calif., Society for the Advancement of Material and Process Engineering, 1977, p. 536-554.  
USAF-sponsored research.

78A16899

Cure monitoring techniques for adhesive bonding processes ---- by examining dielectric properties.

A/Fritzen, J.S.; B/Wereka, A., jr.; C/Arvay, E.A., B/(Lockheed Missiles and Space Co., Inc., Sunnyvale, Calif.); C/(USAF, Materials Laboratory, Wright-Patterson AFB, Ohio).

In: Diversity - Technology explosion; Proceedings of the Twenty-second National Symposium and Exhibition, San Diego, Calif., April 26-28, 1977 (A78-16870 04-23) Azusa, Calif., Society for the Advancement of Material and Process Engineering, 1977, p. 430-434.

78A16881

Effects of moisture upon mean strength of composite-to-metal adhesively bonded joint elements.

A/Wolff, R.V., A/(General Dynamics Corp., Materials Engineering Group, Fort Worth, Texas).

In: Diversity - Technology explosion; Proceedings of the Twenty-second National Symposium and Exhibition, San Diego, Calif., April 26-28, 1977. (A78-16870 04-23) Azusa, Calif., Society for the Advancement of Material and Process Engineering, 1977, 183-194.

78A16872

Alternative cleaning methods for aluminium honeycomb core.

A/Carrillo, G., A/(Rohr Industries, Inc., Riverside, Calif.).

In: Diversity - Technology explosion; Proceedings of the Twenty-second National Symposium and Exhibition, San Diego, Calif., April 26-28, 1977. (A78-16870 04-23) Azusa, Calif., Society for the Advancement of Material and Process Engineering, 1977, p. 47-58.

77A36674

Automated application of structural adhesive forms.

A/Wilson, P.H., A/(Boeing Commercial Airplane Co., Renton, Wash.).

In: Bicentennial of materials; Proceedings of the Eight National Technical Conference, Seattle, Wash., October 12-14, 1976. (A77-36669 16-23) Azusa, Calif., Society for the Advancement of Material and Process Engineering, 1976, p. 52-58.

77A29903

Effects of adherend surface treatment on stressed durability of adhesive bonded aluminium alloys.

A/Schwartz H.S., A/(USAF, Materials Laboratory, Wright-Patterson AFB, Ohio).

SAMPE Journal, vol. 13, Mar. - Apr. 1977, p. 2-13.

77A27519

PABST surface treatment and adhesive selection ---- Primary Adhesively Bonded Structure Technology for aircraft structures.

A/Thrall, E.; B/Shannon, R., B/(Douglas Aircraft Co., Long Beach, Calif.).

In: Bicentennial of materials progress; Proceedings of the Twenty-first National Symposium and Exhibition, Los Angeles, Calif., April 6-8, 1976 (A77-27451 11-23) Azusa, Calif., Society for the Advancement of Material and Process Engineering, 1976, p. 1004-1014.

77A27488

New test methods for the prediction of environmental resistance of adhesive bonded joints.  
A/Althof, W.; B/Brockmann, W., A/(Deutsche Forschungs- und Versuchsanstalt fuer Luft- und Raumfahrt, Braunschweig, West Germany); B/Fraunhofer-Gesellschaft, Institut fuer angewandte Materialforschung, Bremen, West Germany).

In: Bicentennial of materials progress; Proceedings of the Twenty-first National Symposium and Exhibition, Los Angeles, Calif., April 6-8, 1976 (A77-27451 11-23) Azusa, Calif., Society for the Advancement of Material and Process Engineering, 1976, p. 581-591.

77A27119

The effect of surface pretreatment on the properties of metal adhesive bonded joints.

A/Brockmann, W., A/(Institut fuer angewandte Materialforschung, Bremen-Lesum, West Germany)  
Metall, vol. 31, Mar. 1977, p. 245-251. In German.

77A24924

Aerospace adhesive bonding.

A/Reynolds, B.L., A/(Boeing Commercial Airplane Co., Seattle, Wash.).

In: Advances in joining technology; Proceedings of the Fourth Army Materials Technology Conference, Boston, Mass., September 16-19, 1975. (A77-24901 10-31) Chestnut Hill, Mass., Brook Hill Publishing Co., 1976, p. 605-614.

77A13744

Strength of joints to selected corrosion resistant finishes.

A/Ross, M.C.; B/Wegman, R.F.; C/Bodnar, M.J.; D/Tanner, W.C., C/(U.S. Army, Materials Engineering Laboratory, Picatinny Arsenal, Dover, N.J.).

SAMPE Journal, vol. 12, Sept. - Oct. 1976, p. 4-6.

77A13741

Effect of surface exposure time on bonding of engineering thermoplastics.

A/Ross, M.C.; B/McAbee, E.; C/Bodnar, K.J.

SAMPE Journal, vol. 12, May-June 1976, p. 15-18.

77A13737

Effect of surface exposure time on bonding of 6 aluminium - 4 vanadium titanium alloy

A/Ross, M.C.; B/Wegman, R.F.; C/Bodnar, M.J.; D/Tanner, W.C.

SAMPE Journal, vol. 12, Jan. - Febr. 1976, p. 12, 13.

77A13735

Effect of surface exposure time on bonding of commercially pure titanium alloy.

A/Ross, M.C.; B/Wegman, R.F.; C/Bodnar, M.J.; D/Tanner, W.C.

SAMPE Journal, vol. 11, Oct. - Dec. 1975, p. 4-6.

77A13734

Effect of surface exposure time on bonding of ferrous metals.

A/Ross, M.C.; B/Wegman, R.F.; C/Bodnar, M.J.; D/Tanner, W.C.

SAMPE Journal, vol. 11, July - Sept. 1975, p. 20-23.

76A39731

Structural adhesives with emphasis on aerospace applications.

Research supported by the U.S. Department of Defense; New York, Marcel Dekker, Inc.

(Treatise on Adhesion and Adhesives, Vol. 4), 1976, 258 p.

76A36323

Surface analysis of 2024 aluminium after treatment with sulphuric achromic acid solutions.

A/McDevitt, N.T.; B/Baun, W.L.; C/Solomon, J.S., B/(USAF, Materials Laboratory, Wright-Patterson AFB, Ohio); C/(Dayton, University, Dayton, Ohio).

Electrochemical Society, Journal, vol. 123, July 1976, p. 1058-1061.

76A34808

A study of the FPL etching process used for preparing aluminium surfaces for adhesive bonding.

A/Russell, W.J.; B/Garnis, E.A., B/(U.S. Army, Materials Engineering Laboratory, Picatinny Arsenal, Dover, N.J.).

SAMPE Quarterly vol. 7, Apr. 1976, p. 5-12.

76A34807

Use of hot water aging for estimating lifetimes of adhesive bonds to aluminium.

A/Levi, D.W.; B/Wegman, R.F.; C/Ross, M.C.; D/Garnis, E.A., D/(U.S. Army, Materials Engineering Laboratory, Picatinny Arsenal, Dover, N.J.).

SAMPE Quarterly, vol. 7, Apr. 1976, p. 1-4.

76A16556

Evaluation of an accelerated characterization technique for reliability assessment of adhesive joints.

A/Berens, A.P.; B/West, B.D., B/(Dayton, University, Dayton, Ohio).

In: Composite reliability; Proceedings of the Symposium, Las Vegas, Nev., April 15, 16, 1974 (A76-16551 05-24).

Philadelphia, Pa., American Society for Testing and Materials, 1975, p. 90-101.

76A15187

Non-tank phosphoric acid anodize method of surface preparation of aluminium for repair bonding.

A/Locke, M.C.; B/Scardino, W.; C/Croop, H., A/(Boeing Co., Seattle, Wash.); B/(USAF, Materials Laboratory, Wright-Patterson AFB, Ohio); C/(USAF, Flight Dynamics Laboratory, Wright-Patterson AFB, Ohio).

In: Materials review '75; Proceedings of the Seventh National Technical Conference, Albuquerque, N. Mex., Society for the Advancement of Material and Process Engineering, 1975, p. 488-504.

76A15160

Advancements in applications of adhesive to core cell edge and flat sheet material.

A/Green, G.M., A/(Hexcel Corp., Dublin, Calif.).

In: Materials review '75; Proceedings of the Seventh National Technical Conference, Albuquerque, N. Mex., Society for the Advancement of Material and Process Engineering, 1975, p. 118-125.

76A15158

Controlled flow structural adhesives for film reticulation.

A/Weber, C.D.; B/Gross, M.E.; C/Austin, H.J., C/(B.F. Goodrich Co., Breckville, Ohio).

In: Materials review '75; Proceedings of the Seventh National Technical Conference, Albuquerque, N. Mex., October 14-16, 1975. (A76-15151 04-27) Azusa, Calif. Society for the Advancement of Material and Process Engineering, 1975, p. 83-97.

75A40992

Preproduction evaluation of an improved titanium surface prebonding process.

A/Wegman, R.F.; B/Bodnar, M.J., B/(U.S. Army, Materials Engineering Div., Picatinny Arsenal, Dover, N.J.).

In: Technology in transition; Proceedings of the Twentieth National Symposium and Exhibition, San Diego, Calif., April 29 - May 1, 1975. (A75-40955 2023-) Azusa, Calif., Society for the Advancement of Material and Process Engineering, 1975, p. 533-545.

78N33235

A technique for assessing the durability of structural adhesives.

A/Wegman, R.F.; B/Ross, M.C.; C/Garnis, E.A.; D/Santa, S.A.

Army Armament Research and Development Command, Dover, N.J. (Large Caliber Weapon Systems Lab.).

78N32270

Adhesive bonded aerospace structures standardized repair handbook, Final Report, 1 Oct. 1973 - 30 Sept. 1977.

A/Horton, R.F.; B/McCarty, J.E., Boeing Commercial Airplane Co., Seattle, Wash.

78N18199

Characterization of chromic-acid anodized 2024-T3 aluminium adherends.

A/Russell, W.J.; B/Westerdahl, C.A.L., Army Armament Research and Development Command, Dover, N.J. (Large Caliber Weapons Systems Lab.).

78N15292

Durability of structural adhesive bonds (A review)

A/Delollis, N.J.

Sandia Lab., Albuquerque, N. Mex., presented at the 22nd National SAMPE Symposium/Exhibition, San Diego, Calif. 26 Apr. 1977.

78N14144

Evaluation of the quality of pickling as a surface pretreatment in aluminium bonding.

A/Peterka, J., Royal Aircraft Establishment, Farnborough (England).

Transl. into English from Adhaesion (West Berlin) v. 20, no. 1, 1976, p. 3-7.

78N11000

Adhesive bonded aerospace structures standardized repair handbook, Final Report, 1 Oct. 1975 - 31 Mar. 1976.

A/McCarty, J.E.; B/Horton, R.F.; C/Locke, M.C.; D/Satterthwait, M.L.; E/Parashar, B.D., Boeing Commercial Airplane Co., Seattle, Wash.

77N30249

Exploratory of development on durability of adhesive bonded joints, Final Report, 1 Febr. 1974 - Oct. 1976.

A/Marceau

77N29282

Fundamental investigation of anodic oxide films on aluminium alloys as a surface preparation for adhesive bonding, Final Report, 1 Apr. 1975 - 30 Jun. 1976.

A/Herfert, R.E., Northrop Corp., Hawthorne, Calif. (Aircraft Div.), Wright-Patterson AFB, Ohio, AFML.

77N28279

Adhesion promoters for bonding titanium, Interim Report.

A/Schrader, M.E.; B/Cardamone, J.A.

Naval Ship Research and Development Center, Annapolis, Md (Materials Dept.).

77N21231

Surface characterization of titanium and titanium alloys, Part 3: Effect of Ti (c.p.) and Ti-8Mn of laboratory chemical treatments, Interim Report, Jul. 1975 - Apr. 1976.

A/Baun, W.L.; B/McDevitt, N.T.; C/Solomon, J.S.

Air Force Materials Lab., Wright-Patterson AFB, Ohio.

7719245

Some observations of the relation between chemical surface treatments and the growth of anodic barrier layer films, Final Report, Jun. - Dec. 1975.

A/McDevitt, N.T.; B/Baun, W.L., Air Force Materials Lab., Wright-Patterson AFB, Ohio.

77N19241

Two techniques for characterizing surfaces for adhesive bonding.

A/Jennings, C.W., Sandia Labs., Albuquerque, N. Mex. (Passive Components Div.).

77N16157

A chromate-free process for preparing aluminium substrates for adhesive bonding: A preliminary study.

A/Russell, W.J., Picatinny Arsenal, Dover, N.J.

77N13124

Corrosion of aluminium alloys and joints in marine atmosphere --- after 3-year exposure. A/La Crois, A.H., Royal Netherlands Aircraft Factories Fokker, Schiphol-Oost.



77N12200

Surface analysis of 6061 and 7050 aluminium alloys after conditioning by chemical treatment, Final Report, Jan. - Aug. 1975.

A/McDevitt, N.T.; B/Baun, W.L.; C/Solomon, J.S., C/(Dayton University, Research Inst.)  
Air Force Materials Lab., Wright-Patterson AFB, Ohio.

77N11405

Research on adhesive bonding and surface characteristics of metals at Fokker-VFW.  
A/Schliekelmann, R.J., Royal Netherlands Aircraft Factories, Fokker, Schiphol-Oost.

76N27431

Long-term artificial ageing tests on structural adhesive REDUX 775 liquid powder --- tensile shear tests on lap joints.

A/Koetsier, J., Royal Netherlands Aircraft Factories, Fokker, Schiphol-Oost.

76N27414

The influence of rinsing and drying procedures on the surface quality of  $\text{CrO}_3\text{-H}_2\text{SO}_4$  pickled Alclad 2024-T3 material.

A/Kwakernaak, A., Royal Netherlands Aircraft Factories Fokker, Schiphol-Oost.

76N24410

Adhesion of the room temperature curing adhesives EC 2216 B/A and AV 123 B on the cured adhesive primer BR 227.

A/Koetsier, J., Royal Netherlands Aircraft Factories Fokker, Schiphol-Oost.

76N14266

Effect of polymer properties and adherend surfaces on adhesion --- titanium, aluminium, Final Report, Dec. 1974 - Nov. 1975.

A/Dwight, D.W.; B/Counts, M.E.; C/Wightman, J.P., Virginia Polytechnic Inst. and State Univ., Blacksburg (Chemistry Dept.).

75N16673

Environmental failure of structural adhesive joints: A literature survey.

A/Kinloch, A.J., Explosives Research and Development Establishment, Waltham Abbey (England).

#### C STRESS ANALYSIS STRENGTH AND FRACTURE MECHANICS OF BONDED JOINTS

78A45934

Fracture analysis of adhesive-bonded joints.

A/Russell, W., A/(U.S. Army, Picatinny Arsenal, Dover, N.J.).  
SAMPE Quarterly, vol. 9, July 1978, p. 1-7.

78A42569

The effect of strain rate on mechanical properties of adhesive and adhesive bonded joints.  
A/Amijima, S.; B/Fujii, T., B/(Doshisha University, Kyoto, Japan).

In: International Conference on Fracture Mechanics and Technology, Hong Kong, March 21-25, 1977, Proceedings.

Volume 1 (A78-42551 18-29) Alphen aan de Rijn, Netherlands, Sijthoff and Noordhoff International Publishers, 1977, p. 363-372.

78A42434

Effect of bond angle on mixed-mode adhesive fracture specimens --- Double Cantilever Beam.

A/Wang, S.S.; B/Mandell, J.F.; C/McGarry, F.J., A/(Illinois, University, Urbana, Ill.); C/(MIT, Cambridge, Mass.).

International Journal of Fracture, vol. 14, Febr. 1978, p. 39-58, Research supported by the American Cyanamid Co.

78A40314

Crack stability in epoxy-bonded aluminium component.

A/Chow, C.L.; B/Sykes, J.L., B/(University of Hong Kong, Hong Kong).

In: Recent advances in engineering science; Proceedings of the Fourteenth Annual Meeting, Bethlehem, Pa., November 14-16, 1977. (A78-40301 17-31) Bethlehem, Pa., Lehigh University, 1977, p. 307-316. Research supported by the University of Hong Kong.

78A40305

Studies of adhesive fracture in mixed-mode loading.

A/Bascom, W.D., A/(U.S. Navy, Naval Research Laboratory, Washington D.C.).

In: Recent advances in engineering science; Proceedings of the Fourteenth Annual Meeting, Bethlehem, Pa., November 14-16, 1977. (A78-40301 17-31) Bethlehem, Pa., Lehigh University, 1977, p. 195-205.

78A33780

Fracture resistance of adhesively-bonded 7076-T6 aluminium alloy laminates.

A/Alic, J.A., A/(Wichita State University, Wichita, Kan.).

In: Advances in research on the strength and fracture of materials; Proceedings of the Fourth International Conference on Fracture, Waterloo, Ontario, Canada, June 19-24, 1977, Volume 3B (A78-33601 13-23) New York, Pergamon Press, 1978, p. 1031-1037.

78A32147

Influence of adhesive non-linearities on the performance and optimal length of adhesive bonded joint.

A/Ramamurthy, T.S.; B/Rao, A.K., B/(Indian Institute of Science, Bangalore, India). Mechanics Research Communications, vol. 5, no. 1, 1979, p. 9-14.

78A31261

Investigation of the stress-distribution non-uniformity in an adhesive joint subjected to the combined effect of normal and shear stresses.

A/Aleksyuk, M.M.; B/Petrenko, A.I., B/(Akademiia Nauk Ukrainskoi SSR, Institut Problem Prochnosti, Kiev, Ukrainian SSR).

Problemy Prochnosti, Feb. 1978, p. 71-73. In Russian.

78A29812

Stress analysis of typical flaws in aerospace structural components using 3-D hybrid displacement finite element method.

A/Atluri, S.N.; B/Kathiresan, K., A/(Georgia Institute of Technology, Atlanta, Ga.).

In: Structures, Structural Dynamics and Materials Conference, 19th Bethesda, Md., April 3-5, 1978. Technical Papers (A78-29776 11-39), New York, American Institute of Aeronautics and Astronautics, Inc. 1978, p. 340-350.

Research supported by the Georgia Institute of Technology.

78A29790

Analysis of cracked, adhesively bonded structures.

A/Ratwani, M.M., A/(Northrop Cor., Hawthorne, Calif.).

In: Structures, Structural Dynamics and Materials Conference, 19th, Bethesda, Md., April 3-5, 1978. Technical papers (A78-29776 11-39), New York, American Institute of Aeronautics and Astronautics, Inc., 1978, p. 155-163.

78A27872

Analysis and testing of adhesive bonds --- Book.

A/Anderson, G.P.; B/Bennett, S.J.; C/De Vries, K.L., B/(Thiokol Corp., Brigham City, Utah); C/Utha, University, Salt Lake City, Utah), Thiokol Chemical Corp., Brigham City, Utah, Utah Univ., Salt Lake City.

78A26832

Fracture of laminates combining 2024-T3 and 7075-T6 aluminium alloys.

A/Alic, J.A.; B/Danesh, A., B/(Wichita State University, Wichita, Kan.).

Engineering Fracture Mechanics, vol. 10, no. 2, 1978, p. 177-181, 183-186.

78A26338

Crack arrest in duplex specimens.

A/Dally, J.W.; B/Kobayashi, T., B/(Maryland University, College Park, Md.).

International Journal of Solids and Structures, vol. 14, no. 2, 1978, p. 121-129, Research supported by the Nuclear Regulatory Commission.

78A25186

Strength of bonded aluminium-CFRP single lap joints.

A/Ishai, O.; B/Girshengorn, T., B/(Technion - Israel Institute of Technology, Haifa, Israel).

In: Materials and Processes - In service performance; Proceedings of the Ninth National Technical Conference, Atlanta, Ga., October 4-6, 1977 (A78-25276 09-23) Azusa, Calif., Society for the Advancement of Material and Process Engineering, 1977, p. 100-110.

78A23373

Development of random fatigue data for adhesively bonded and weldbonded structures subjected to dynamic excitation --- aircraft structures.

A/Wentz, K.R.; B/Wolfe, H.F., B/(USAF, Flight Dynamics Laboratory, Wright-Patterson AFB, Ohio). (American Society of Mechanical Engineers, Winter Annual Meeting, Atlanta, Ga., Nov. 27 - Dec. 1, 1977) ASME, Transactions, Journal of Engineering Materials and Technology, vol. 100, Jan. 1978, p. 70-76.

78A23372

Spectrum crack growth in adhesively bonded structure.

A/Johnson, W.S.; B/Rister, W.C.; C/Spamer, T., C/(General Dynamics Corp., Fort Worth, Tex.). (American Society of Mechanical Engineers, Winter Annual Meeting, Atlanta, Ga., Nov. 27 - Dec. 2, 1977, ASME, Transactions, Journal of Engineering Materials and Technology,

vol. 100, Jan. 1978, p. 57-63.

78A23371

Growth characteristics of a fatigue crack approaching and growing beneath an adhesively bonded doubler.

A/Anderson, J.M.; B/Chu, C.S.; C/McGee, W.M., A/(Georgia Institute of Technology Atlanta, Ga.); C/(Lockheed-Georgia Co., Marietta, Ca.). (American Society of Mechanical Engineers, Winter Annual Meeting, Atlanta, Ca., Nov. 27 - Dec. 2, 1977) ASME, Transactions, Journal of Engineering Materials and Technology, vol. 100, Jan. 1978, p. 52-56.

78A23370

A parametric study of fatigue crack growth behavior in adhesively bonded metallic structures.

A/Ratwani, M.M., A/(Northrop Corp., Hawthorne, Calif.) (American Society of Mechanical Engineers, Winter Annual Meeting, Atlanta, Ga., Nov. 27 - Dec. 2, 1977) ASME, Transactions, Journal of Engineering Materials and Technology, vol. 100, Jan. 1978, p. 46-51.

78A23369

Fatigue crack growth of bondline cracks in structural bonded joints.  
A/Brussat, T.R.; B/Chiu, S.T., B/(Lockheed California Co., Burbank, Calif.)  
ASME, Transactions, Journal of Engineering Materials and Technology, vol. 100, Jan. 1978,  
p. 39-45.

7823368

Fatigue crack propagation in 8- and 22-layer 7075-T6 aluminium alloy laminates.  
A/Pfeiffer, N.J.; B/Alic, J.A., B/(Wichita State University, Wichita, Kan.).  
(American Society of Mechanical Engineers, Winter Annual Meeting, Atlanta, Ga., Nov. 27 -  
Dec. 2, 1977) ASME, Transactions, Journal of Engineering Materials and Technology, vol. 100,  
Jan. 1978, p. 32-38.

78A23367

Developing failure criteria for adhesive joints under complex loading.  
A/Mulville, D.R.; B/Hunston, D.L.; C/Mast, P.W., C/(U.S. Navy, Naval Research Laboratory,  
Washington, D.C.) (American Society of Mechanical Engineers, Winter Annual Meeting, Atlanta,  
Ga., Nov. 27 - Dec. 1977) ASME, Transactions, Journal of Engineering Materials and Technology,  
vol. 100, Jan. 1978, p. 25-31. Navy supported research.

78A23073

On stress singularities and interfaces in linear elastic fracture mechanics.  
A/Atkinson, C., A/(Imperial College of Science and Technology, London, England)  
International Journal of Fracture, vol. 13, Dec. 1977, p. 807-820.

78A23068

Stress-free end problem in layered materials.  
A/Erdogan, F.; B/Bakiloglu, M., B/(Lehigh University, Bethlehem, Pa.) Lehigh Univ. Bethlehem,  
Pa., International Journal of Fracture, vol. 13, Dec. 1977, p. 738-749.

78A19173

A theory for elastic stresses in adhesive bonded lap joints.  
A/Allman, D.J., A/(Royal Aircraft Establishment, Farnborough, Hants, England)  
Quarterly Journal of Mechanics and Applied Mathematics, vol. 30, Nov. 1977, p. 415-436.

78A17788

Stresses in adhesive joints due to moisture and temperature ---- analysis based on  
variational principles.  
A/Weitsman, Y., A/(USAF, Materials Laboratory, Wright-Patterson AFB, Ohio; Texas A & M  
University, College Station, Tex.)  
Journal of Composite Materials, vol. 11, Oct. 1977, p. 378-394.

78A16921

Progress in structural bonding through effective bondline stress analysis.  
A/Althof, W., A/(Deutsche Forschungs- und Versuchsanstalt fuer Luft- und Raumfahrt, Insti-  
tut fuer Strukturmechanik, Braunschweig, West Germany)  
In: Diversity - Technology explosion; Proceedings of the Twenty-second National Symposium  
and Exhibition, San Diego, Calif., April 26-28, 1977. (A78-16870 04-23) Azusa, Calif.,  
Society for the Advancement of Material and Process Engineering, 1977, p. 784-795.

78A15853

Mechanical behavior of cast adhesive film.  
A/Schjelderup, H.C.; B/Jones, W.B., jr., B/(Douglas Aircraft Co., Long Beach, Calif.)  
SAMPE Quarterly, vol. 9, Oct. 1977, p. 17-21

77A44561

Bond thickness effects upon stresses in single lap adhesive joints.  
A/Ojalvo, I.U.; B/Eidinoff, H.L., B/(Grumman Aerospace Corp., Bethpage N.Y.)  
Society of Automotive Engineers, International Automotive Engineering Congress and Expo-  
sition, Detroit, Mich., Feb. 28 - Mar. 4, 1977, 11 p.

77A42402

Peel mechanics of adhesive joints.  
A/Gent, A.N.; B/Hamed, G.R., B/(Akron, University, Akron, Ohio).  
Polymer Engineering and Science, vol. 17, July 1977, p. 462-466. NSF supported research.

77A39296

The role of the adhesive layer in a double cantilever joint.  
A/Farhad, F.; B/Muki, R.; C/Westmann, R.A., A/(Gruen Associates, Los Angeles, Calif.);  
C/(California University, Los Angeles, Calif.).  
International Journal of Solids and Structures, vol. 13, no. 6, 1977, p. 561-570.

77A39113

Direct determination of interlaminar stresses in polymeric adhesive layer.  
A/Ishai, O.; B/Peretz, D.; C/Gali, S., C/(Technion - Israel Institute of Technology,  
Haifa, Israel).  
Experimental Mechanics, vol. 17, July 1977, p. 265-270.



77A38687

Effective remote stresses and stress intensity factors for an adhesive bonded multi-ply laminate.

A/Johnson, W.S.; B/Stratton, J.M., B/(General Dynamics Corp., Fort Worth, Texas).  
Engineering Fracture Mechanics, vol. 9, no. 2, 1977, p. 411-421.

77A24912

Design parameter considerations for composite sandwich bonding.

A/Brentjes, J., A/(Hexcel Corp., Dublin, Calif.)

In: Advances in joining technology; Proceedings of the Fourth Army Materials Technology Conference, Boston, Mass., September 16-19, 1975. (A77-24901 10-31) Chestnut Hill, Mass., Brook Hill Publishing Co., 1976, p. 339-353.

77A24910

On improvement in structural efficiency of single-lap bonded joints.

A/Renton, W.J.; B/Pajerowski, J.; C/Vinson, J.R., A/(Advanced Technology Center, Inc., Dallas, Tex.); C/(Delaware, University, Newark, Del.).

In: Advances in joining technology; Proceedings of the Fourth Army Materials Technology Conference, Boston, Mass., September 16-19, 1975. (A77-24901 10-31) Chestnut Hill, Mass., Brook Hill Publishing Co., 1976, p. 305-316.

77A24488

Note on the dependence of crack velocity on driving force for an epoxy adhesive.

A/Mostovoy, S.; B/Crosley, P.B.; C/Ripling, E.J., C/(Materials Research Laboratory, Inc., Glenwood, Ill.)

In: Cracks and fracture: Proceedings of the Ninth National Symposium on Fracture Mechanics, Pittsburgh, Pa., August 25-27, 1975. (A77-24476 09-39) Philadelphia, Pa., American Society for Testing and Materials, 1976, p. 234-244.

77A20988

Effect of adhesive layer elasticity on the fracture mechanics of a blister test specimen.

A/Updikte, D.P., A/(Lehigh University, Bethlehem, Pa.).

International Journal of Fracture, vol. 12, Dec. 1976, p. 815-827.

77A19397

Fracture analysis of adhesively bonded sheets.

A/Keer, L.M.; B/Mura, T.; C/Lin, C.T., B/(Northwestern University, Evanston, Ill.);

C/(Northwestern University, Evanston; Arthur G. McKee and Co., Chicago, Ill.).

(American Society of Mechanical Engineers, Winter Annual Meeting, New York, N.Y., Dec. 5-10, 1976) ASME, Transactions, Series E - Journal of Applied Mechanics, vol. 43, Dec. 1976, p. 652-656.

76A35843

Measurement of the elastic moduli of structural adhesives by a resonant bar technique.

A/Adams, R.D.; B/Coppendale, J., A/(Bristol, University, Bristol, England).

Journal of Mechanical Engineering Science, vol. 18, June 1976, p. 149-158.

76A35794

Plane stress analysis of a scarf joint.

A/Wah, T., A/(Texas A & I University, Kingsville, Tex.)

International Journal of Solids and Structures, vol. 12, no. 7, 1976, p. 491-500.

76A22604

Characterization of crack growth in bonded structures ---- metal laminates.

A/Anderson, J.M.; B/Hsu, T.M.; C/McGee, W.M., A/(Georgia Institute of Technology, Atlanta, Ga.); C/(Lockheed-Georgia Co., Marietta, Ga.)

In: Society of Engineering Science, Annual Meeting, 12th, Austin, Tex., October 20-22, 1975, Proceedings. (A76-22551 09-31) Austin, University of Texas, 1975, p. 1283-1292.

76A22558

Adhesive fracture, evaluation and engineering.

A/De Vries, K.L., A/(Utah, University, Salt Lake City, Utah).

In: Society of Engineering Science, Annual Meeting, 12th, Austin, Tex., October 20-22, 1975, Proceedings. (A76-22551 09-31) Austin, University of Texas, 1975, p. 197-207.

76A16822

Rate and time dependent failure of structural adhesives.

A/Brinson, H.F.; B/Renieri, M.P.; C/Herakovich, C.T., C/(Virginia Polytechnic Institute and State University, Blacksburg, Va.)

Virginia Polytechnic Inst. and State Univ., Blacksburg.

In: Fracture mechanics of composites; Proceedings of the Symposium, Gaithersburg, Md., September 25, 1974, (A76-16813 05-39) Philadelphia, Pa., American Society for Testing and Materials, 1975, p. 177-199.

76A13835

Double cantilever beam models in adhesive mechanics.

A/Chang, D.J.; B/Muki, R.; C/Westmann, R.A., A/(Aerospace Corp., El Segundo, Calif.);

C/(California, University, Los Angeles, Calif.).

International Journal of Solids and Structures, vol. 12, no. 1, 1976, p. 13-26.

76A10680

Quasi-static adhesive fracture.

A/Mai, Y.W., A/(Michigan, University, Ann Arbor, Mich.).  
Journal of Adhesion, vol. 7, July 1975, p. 141-153.

76A10678

Stresses in adhesive between dissimilar adherends.

A/Williams, J.H., Jr., A/(MIT, Cambridge, Mass.)  
Journal of Adhesion, vol. 7, July 1975, p. 97-107.

75A41261

Stable crack growth in adhesively bonded aluminium alloy laminates.

A/Alic, J.A., A/(Wichita State University, Wichita, Kan.)

International Journal of Fracture, vol. 11, Aug. 1975, p. 701-704.

Research supported by the Wichita State University.

75A40996

New concepts in fatigue resistant adhesives.

A/Kuhbender, R.J.; B/Aponyi, T.J., A/(Dayton, University, Dayton, Ohio); B/USAF, Materials Laboratory, Wright-Patterson AFB, Ohio).

In: Technology in transition; Proceedings of the Twentieth National Symposium and Exhibition San Diego, Calif., April 29 - May 1, 1975. (A75-40955 2023) Azusa, Calif., Society for the Advancement of Material and Process Engineering, 1975, p. 589-605.

75A40995

Improved fatigue life through high modulus-fiber reinforcement of adhesives.

A/Klapprott, D.K.; B/Mahoney, C.L.; C/Mika, T.F.; D/Stifel, P.M.; E/Aponyi, T.J.,  
C/(Dexter Corp., Pittsburg, Calif.); D/(McDonnell Aircraft Co., St. Louis, Mo.);  
E/(USAF, Materials Laboratory, Wright-Patterson AFB, Ohio)

In: Technology in transition; Proceedings of the Twentieth National Symposium and Exhibition, San Diego, Calif., April 29 - May 1, 1975. (A75-40955 20-23) Azusa, Calif., Society for the Advancement of Material and Process Engineering, 1975, p. 563-581.

75A40993

The mechanical behavior of adhesive materials.

A/May, L.C.; B/Adsit, N.R., B/(General Dynamics Corp., Convair Div., San Diego, Calif.)

In: Technology in transition; Proceedings of the Twentieth National Symposium and Exhibition, San Diego, Calif., April 29 - May 1, 1975. (A75-40955 20-23) Azusa, Calif., Society for the Advancement of Material and Process Engineering, 1975, p. 546-553.

75A40991

Adhesive bonding failure mechanics and their cure.

A/Vaughan, R.E., A/(Martin Marietta Aerospace, Orlando, Fla.)

In: Technology in transition; Proceedings of the Twentieth National Symposium and Exhibition, San Diego, Calif., April 29 - May 1, 1975. (A75-40955 20-23) Azusa, Calif., Society for the Advancement of Material and Process Engineering, 1975, p. 503-512.

75A36654

Comparison of fracture and fatigue properties of clad 7075-T6 aluminium in monolithic and laminated forms.

A/Alic, J.A.; B/Archang, H., B/(Wichita State University, Wichita, Kan.)

Society of Automotive Engineers, Business Aircraft Meeting, Wichita, Kan., Apr. 8-11, 1975, 12 p., Research supported by the Wichita State University.

75A35107

Stress analysis of a double lapjoint.

A/Keer, L.M.; B/Chantaramungkorn, K., A/(Northwestern University, Evanston, Ill.).

(American Society of Mechanical Engineers, Applied Mechanics Summer Conference, Rensselaer Polytechnic Institute, Troy, N.Y., June 23-25, 1975).

ASME, Transactions, Series E - Journal of Applied Mechanics, vol. 42, June 1975, p. 353-357, Research supported by the John Simon Guggenheim Foundation.

75A32678

The efficient design of adhesive bonded joints.

A/Renton, W.J.; B/Vinson, J.R., B/(Delaware, University, Newark, Del.).

AIAA, ASME and SAE, Structures, Structural Dynamics and Materials Conference, 16th, Denver, Colo., May 27-29, 1975, AIAA, 9 p.

75A29109

The plane solution for joined dissimilar elastic semistrips under tension.

A/Bogy, D.B., A/(California, University, Berkeley, Calif.)

American Society of Mechanical Engineers, Applied Mechanics Western Conference, University of Hawaii, Honolulu, Hawaii, Mar. 25-27, 1975, 6 p. Research supported by the University of California.

75A24791

Geometrical effects in adhesive joints.

A/Westmann, R.A., A/(California, University, Los Angeles, Calif.).

International Journal of Engineering Science, vol. 13, Apr. 1975, p. 369-391.

75A19536

Control of cracks by interfaces in composites.

A/Kendall, K., A/(Monash University, Clayton, Victoria, Australia).

Royal Society (London), Proceedings, Series A, vol. 341, no. 1627, Jan. 14, 1975, p. 409-428.

75A17319

Metal joining with adhesives.

A/Cotter, J.L.; B/Hockney, M.G.D., B/(Royal Aircraft Establishment, Farnborough, Hants., England)

International Metallurgical Reviews, vol. 19, Sept. 1974, p. 103-115.

75A14985

Experimental problems in adhesive joints.

A/Quozzo, G.; B/Grillo, F., B/(Roma, Università, Rome, Italy). (Associazione Italiana di Aeronautica ed Astronautica, Congresso Nazionale, 2nd, Pisa, Italy, Sept. 1973)

L'Aerotecnica - Missili e Spazio, vol. 53, Aug. 1974, p. 277-290. In Italian.

75A10374

Stress analysis for bonded layers.

A/Keer, L.M., A/(Northwestern University, Evanston, Ill.). (American Society of Mechanical Engineers, 1974) ASME, Transactions, Series E - Journal of Applied Mechanics, vol. 41,

Sept. 1974, p. 679-683.

78N29509

Fracture mechanics for structural adhesive bonds, Final Report, 15 June 1975 - 15 July 1977.

A/Brussat, T.R.; B/Chiu, S.T.; C/Mostovoy, S., Lockheed-California Co., Burbank.

78N23491

Shear fatigue tests with aluminium alloy joints bonded with SAAB adhesive 9313-2 (BSL 308A)

A/Larsson, N., Aeronautical Research Inst. of Sweden, Stockholm. (Structures Dept.)

78N21271

Fatigue in adhesively bonded laminates --- aluminium alloy laminates, Final Technical Report, Mar. 1976 - Sept. 1977.

A/Alic, J.A., Wichita State Univ., Kans. (Dept. of Mechanical Engineering)

78N14433

Stress analysis of double-lap joints bonded with a viscoelastic adhesive Ph.D. Thesis

A/Sen, J.K., Southern Methodist Univ., Dallas, Tex.

77N29547

Linear elastic and elasto-plastic stress analysis for adhesive lap joints Ph.D. Thesis

A/Liu, A.T., Illinois Univ., Urbana-Champaign.

77N25601

Fracturing characteristics of adhesive joints, Final Report, 16 Jan. 1975 - 16 Jan. 1976

A/Mostovoy, S.; B/Ripling, E.J., Materials Research Lab., Inc., Glenwood, Ill.

77N23547

A failure criterion for the fracture of structural adhesive joints

A/Gledhill, R.A.; B/Kinloch, A.J., Explosives Research and Development Establishment, Waltham Abbey (England).

77N12132

The effect of adhesive layer on crack propagation in laminates Ph.D. Thesis.

A/Gecit, M.R., Lehigh Univ., Bethlehem, Pa.,

77N11112

Rate and time dependent behavior of structural adhesives Ph.D. Thesis.

A/Renieri, M.P., Virginia Polytechnic Inst., Blacksburg.

76N24407

Rate and time dependent behavior of structural adhesives Ph.D. Thesis.

A/Renieri, M.P.; B/Herakovich, C.T.; C/Brinson, H.F., Virginia Polytechnic Inst. and State Univ., Blacksburg. (Coll. of Engineering).

76N22589

Effects of viscoelasticity on adhesive joints.

A/Glahn, M., Technische Univ., Berlin (West Germany). Inst. fuer Luft- und Raumfahrt).

76N19501

Crack resistance of some structural adhesives determined on adhesive bonded TDCB-specimens.

A/Hartman, A., National Aerospace Lab., Amsterdam (Netherlands). (Div. Structures and Materials).



76N13226

Mechanical behavior of multimaterial composite systems. Interlaminar behavior, Final Technical Report, Dec. 1974.  
A/Ishai, O.; B/Peretz, D.; C/Galili, N., Technion - Israel Inst. of Techn. Haifa. (Dept. of Mechanics).

75N31535

The role of transient spectrum and damping analysis in assessing the strength of polymeric adhesive metal bonding, Final Scientific Report, 1 July - 30 June 1974.  
A/Curtis, G.J.; B/Johnson, A.B.; C/Lloyd, P.A., Atomic Energy Research Establishment, Harwell (England). (Non-Destructive Testing Centre).

75N25213

The effect of bending on the stresses in adhesive joints.  
A/Yuceoglu, U.; B/Updike, D.P., Lehigh Univ., Bethlehem, Pa. (Inst. of Fracture and Solid Mechanics).

75N22791

Mechanics of adhesive joints with a thin adhesive layer Ph.D. Thesis.  
A/Farhad, B., California Univ., Los Angeles.

75N21673

Analysis of bonded joints ---- shear stress and stress-strain diagrams.  
A/Srinivas, S., National Aeronautics and Space Administration, Langley Research Centre, Hampton, Va.

75N19725

Stress analyses for layered media Ph.D. Thesis.  
A/Chantaramungkorn, K., Northwestern Univ., Evanston, Ill.

75N18604

Experimental evaluation of a reliability assessment model for adhesively bonded joints, Final Report, Oct. 1972 - Apr. 1974.  
A/Berens, A.P.; B/Johnson, P.E.; C/West, B.S., Dayton Univ. Research Inst. Ohio.

75N14895

Fatigue behavior of metal laminates.  
A/Throop, J.F.; B/Miller, J.J., Watervliet Arsenal, N.Y. (Benet Weapons Lab.)

#### D MECHANICAL PROPERTIES OF ADHESIVE BONDED STRUCTURES

78A44739

Beryllium satellite thrust cone design, manufacture and test.  
A/Schneider, H.; B/Chandler, D., B/(Contraves, A.G., Zurich, Switzerland).  
In: Beryllium 1977; International Conference, 4th, London, England, October 4-7, 1977, Conference Preprints (A78-44706) London, Metals Society, 1977, p. 59/1-59/11.

78A28375

Repaired damaged aluminium honeycomb panels.  
A/Kesler, R.D., A/(General Dynamics Corp., Convair Div., San Diego, Calif.).  
Metal Progress, vol. 113, Mar. 1978, p. 79-82.

78A23365

Fracture analysis of adhesively bonded cracked panels.  
A/Swift, T., A/(Douglas Aircraft Co., Long Beach, Calif.). (American Society of Mechanical Engineers, Winter Annual Meeting, Atlanta, Ga., Nov. 27 - Dec. 2, 1977) ASME, Transactions, Journal of Engineering Materials and Technology, vol. 100, Jan. 1978, p. 10-15.

78A23364

The effect of adhesive layers on the fracture of laminated structures.  
A/Gecit, M.R.; B/Erdogan, F., B/(Lehigh University, Bethlehem, Pa.). Lehigh Univ. Bethlehem, Pa. (American Society of Mechanical Engineers, Winter Annual Meeting, Atlanta, Ga., Nov. 27 - Dec. 2, 1977) ASME, Transactions, Journal of Engineering Materials and Technology, vol. 100, Jan. 1978, p. 2-9.

77A28505

Analysis of adhesively bonded joints between panels of composite materials.  
A/Renton, W.J.; B/Vinson, J.R., A/(Advanced Technology Center, Dallas, Tex.).  
B/(Delaware, University, Newark, Del.). (American Society of Mechanical Engineers, Applied Mechanics/Bioengineering/Fluids Engineering Summer Conference, Yale University, New Haven, Conn., June 15-17, 1977) ASME, Transactions, Series E - Journal of Applied Mechanics, vol. 44, Mar. 1977, p. 101-106.

76A15161

Metal-to-metal adhesive bonded aircraft structures.

A/Koetsier, J., A/(Fokker-VFW, Schiphol-Oost, Netherlands)

In: Materials review '75; Proceedings of the Seventh National Technical Conference, Albuquerque, N. Mex., October 14-16, 1975. (76-15151 04-27) Azusa, Calif., Society for the Advancement of Material and Process Engineering, 1975, p. 126-140.

76A15159

Bonding development of improved adhesives for acoustic structures --- jet engine liners.

A/Arnold, D.B., A/(Boeing Commercial Airplane Co., Seattle, Wash.)

In: Materials review '75; Proceedings of the Seventh National Technical Conference, Albuquerque, N. Mex., October 14-16, 1975 (A76-15151 04-27) Azusa, Calif., Society for the Advancement of Material and Process Engineering 1975, p. 98-117.

75A29962

On the behavior of bonded joints in composite material structures --- for aerospace engineering.

A/Renton, J.W.; B/Winson, J.R., B/(Delaware, University, Newark, Del.)

Engineering Fracture Mechanics, vol. 7, Mar. 1975, p. 41-60.

75A16221

Aerospace sandwich materials. II --- fabrication, properties, tests.

A/Dzalba-Lydis, F., A/(Societe Nationale Industrielle Aerospatiale, Paris, France)

Materiaux et Techniques, vol. 62, Oct. 1974, p. 405-415. In French.

75A13046

Laminated metallic structure - Advanced applications.

A/McClaren, S.W.; B/Ellis, J.R., B/(LTV Aerospace Corp., Vought Systems Div., Dallas, Tex.).

In: Materials on the move; Proceedings of the Sixth National Technical Conference, Dayton, Ohio, October 8-10, 1974. (A75-02-24) Azusa, Calif., Society for the Advancement of Material and Process Engineering, 1974, p. 345-351.

78N33095

Primary Adhesively Bonded Structure Technology (PABST) Phase 1: Detail design, Final Report, Sept. 1976 - Dec. 1977. Douglas Aircraft Co., Inc., Long Beach, Calif.

Wright-Patterson AFB, Ohio, AFFDL

76N24411

Metal-to-metal adhesive bonded aircraft structures.

A/Koetsier, J., Royal Netherlands Aircraft Factories Fokker, Schiphol-Oost. (Manufacturing Research and Product Development Dept.)

75N25998

Space Shuttle structural integrity and assessment study, Executive Summary, Jun. 1972

- Jul. 1974. Lockheed-Georgia Co., Marietta.

## E QUALITY CONTROL AND NON-DESTRUCTIVE INSPECTION TECHNIQUES FOR BONDED JOINTS

78A36802

Ultrasonic spectroscopy in non-destructive testing.

A/Brown, A.F., A/(City University, London, England), Science Progress, vol. 65, Spring 1978, p. 51-74.

78A28372

Materials and processes for the Tomahawk cruise missile.

A/Torgerson, R.T.; B/Christion, J.L., B/(General Dynamics Corp., Convair Div., San Diego, Calif.), Metal Progress, vol. 113, Mar. 1978, p. 52-58.

78A16888

Acoustic emission analysis as a method of testing adhesive metal joints.

A/Brockmann, W.; B/Fischer, T., B/(Institute for Applied Materials Research, Bremen, West Germany).

In: Diversity - Technology explosion; Proceedings of the Twenty-second National Symposium and Exhibition, San Diego, Calif., April 26-28, 1977. (A78-16870 04-23) Azusa, Calif., Society for the Advancement of Material and Process Engineering, 1977, p. 277-300.

77A49610

Ultrasonic attenuation effects associated with the physical modeling of adhesive bonds.

A/Meyer, P.A.; B/Rose, J.L., B/(Drexel University, Philadelphia, Pa.).

Journal of Applied Physics, vol. 48, Sept. 1977, p. 3705-3712.

77A30135

Holographic non-destructive testing of advanced composite materials in aerospace constructions.

A/Querido, R.J., A/(Fokker-VFW, Schiphol Airport, Netherlands).

In: World Conference on Non-destructive Testing, 8th Cannes, France, September 6-11, 1976. Proceedings, (A77-30101 13-38) Paris, Institute de Soudure, 1976, Section 3A, Paper 3A-6. 8 p.

77A29390

Ultrasonic techniques for measuring the strength of adhesive bonds.  
A/Alers, G.A.; B/Flynn, P.L.; C/Buckley, M.J., A/(Rockwell International Science Center, Thousand Oaks, Calif.); B/(General Dynamics Corp., Fort Worth, Tex.)  
Materials Evaluation, vol. 35, Apr. 1977, p. 77-84.

77A28754

The use of acoustic emission for characterising adhesive joint failure.  
A/Hill, R., A/(Robert Gordon's Institute of Technology, Aberdeen, Scotland).  
NDT International, vol. 10, Apr. 1977, p. 63-72. Research supported by the Ministry of Technology.

77A25777

Primary adhesively bonded structures technology /PABST/ - A technology analogous to advanced composites.  
A/Schjelderup, H.C.; B/Shannon, R.W., B/(Douglas Aircraft Co., Long Beach, Calif.).  
In: Structures, Structural Dynamics and Materials Conference, 18th, March 21-23, 1977, and Aircraft Composites: The Emerging Methodology for Structural Assurance, San Diego, Calif., March 24, 25, 1977. Technical Papers, Volume A. (A77-25726 10-39) New York, American Institute of Aeronautics and Astronautics, Inc., 1977, p. 450-457.

77A24922

Detection of adhesive bond-line flaws by neutron radiography.  
A/Petersen, D.H.; B/Dance, W.E., B/(Advanced Technology Center, Inc., Dallas, Tex.).  
In: Advances in joining technology; Proceedings of the Fourth Army Materials Technology Conference, Boston, Mass., September 16-19, 1975. (A77-24901 10-31) Chestnut Hill, Mass., Brook Hill Publishing Co., 1976, p. 583-591.

77A20648

A new penetrant for composite and adhesively bonded structures.  
A/Crane, R.L., A/(USAF, Materials Laboratory, Wright-Patterson AFB, Ohio).  
Materials Evaluation, vol. 35, Feb. 1977, p. 54, 55.

76A41835

Detection of delaminations by ultrasonic spectroscopy.  
A/Gericke, O.R.; B/Monagle, B.L., B/(U.S. Army, Army Materials and Mechanics Research Center, Watertown, Mass.).  
IEEE Transactions on Sonics and Ultrasonics, vol. SU-23, Sept. 1976, p. 399-345.

76A41834

Principles and application of ultrasonic spectroscopy in NDE of adhesive bonds.  
A/Chang, F.H.; B/Flynn, P.L.; C/Gordon, D.E.; D/Bell, J.R., D/(General Dynamics Materials Research Laboratory, Fort Worth, Tex.)  
IEEE Transactions on Sonics and Ultrasonics, vol. SU-23, Sept. 1976, p. 334-338.

76A32146

Correlation of NDE parameters with adhesive bond strength in multi-layered structures --- Non-Destructive Evaluation.  
A/Chang, F.H.; B/Couchman, J.C.; C/Bell, J.R.; D/Gordon, D.E., D/(General Dynamics Materials Research Laboratory, Fort Worth, Tex.)  
In: Symposium on Non-Destructive Evaluation, 10th, San Antonio, Tex., April 23-25, 1975, Proceedings. (A76-32126 15-38) San Antonio, Tex., Southwest Research Institute, 1975, p. 266-273.

76A19721

Ultrasonic maintenance inspection of aircraft structures.  
A/Hagemaier, D., A/(Douglas Aircraft Corp., Long Beach, Calif.).  
Materials Evaluation, vol. 34, Jan. 1976, p. 9-19.

75A46633

Advanced NDE techniques --- ultrasonic spectroscopy and acoustic emission.  
A/Thompson, D.O., A/(Rockwell International Science Center, Thousand Oaks, Calif.)  
In: Prevention of structural failure: The role of quantitative non-destructive evaluation; Proceedings of the Second Materials/Design Forum, Port St. Lucie, Fla., April 9-11, 1974. (A75-46626 24-38) Metals Park, Ohio, American Society for Metals, 1975, p. 114-145.

75A46566

Acoustic emission energy relates to bond strength.  
A/Curtis, G.J., A/(Atomic Energy Research Establishment, Non-Destructive Testing Centre, Harwell, Oxon., England). (Institute of Physics, Meeting on Problems in Non-Destructively Testing Adhesively Bonded Joints, City University, London, England, Apr. 8, 1974)  
Non-Destructive Testing, vol. 8, Oct. 1975, p. 249-257. Research supported by the Ministry of Defence (Procurement Executive).

75A34203

The effect of water path variations on ultrasonic through-transmission sensitivity ---- for adhesively bonded aircraft honeycomb structures.  
A/Palmer, C.J., A/(McDonnell Aircraft Co., St. Louis, Mo.). (American Society for Non-Destructive Testing, National Fall Conference, Detroit, Mich., Oct. 21-24, 1974).  
Materials Evaluation, vol. 33, June 1975, p. 128-132, 134.



75A31675

NDT techniques for the prediction of adhesive failure loci prior to bonding.  
A/Smith, T., A/(Rockwell International Science Center, Thousand Oaks, Calif.)  
Materials Evaluation, vol. 33, May 1975, p. 101-106.  
Independent Research and Development Interdivisional Technology Program.

75A26829

Non-destructive testing of bonded joints - Recent developments in testing systems.  
A/Schliekelmann, R.J., A/(Fokker-VFW, Schiphol-Oost, Netherlands).  
Non-Destructive Testing, vol. 8, Apr. 1975, p. 100-103.

75A25950

Requirements for and advances in non-destructive evaluation.  
A/Thompson, D.O., A/(Rockwell International Science Center, Thousand Oaks, Calif.)  
In: Ultrasonics Symposium, Milwaukee, Wis., November 11-14, 1974, Proceedings. (A75-25931  
10-33) New York, Institute of Electrical and Electronics Engineers, Inc., 1974, p. 642-652.

75A16898

Ultrasonic applications in the aerospace industry.  
A/Hagemmaier, D., A/(McDonnell Douglas Corp., St. Louis, Mo.)  
Society of Automotive Engineers, National Aerospace Engineering and Manufacturing Meeting,  
San Diego, Calif., Oct. 1-3, 1974, 31 p.

75A14982

The control of adhesive bonding in the production of primary aircraft structures.  
A/Norris, T.H., A/(Hawker Siddeley Aviation, Ltd., Chester, England).  
Non-Destructive Testing, vol. 7, Dec. 1974, p. 335-339.

75A14891

A case for testing laminated structures by wide-band ultrasound.  
A/Lloyd, E.A., A/(City University, London, England)  
Non-Destructive Testing, vol. 7, Dec. 1974, p. 331-334.

78N33468

Exploratory development of nondestructive evaluation techniques, Final report,  
15 Mar. 1976 - 15 Nov. 1977.  
A/Moyzis, J.A.; B/Raney, J.M., Systems Research Labs., Inc., Dayton, Ohio (Research  
Applications Div.)

78N31245

Feasibility of using fluorescent materials in product assurance applications and for  
locating adhesive bond fractures.  
A/Westerdahl, C.A.L.; B/Hall, J.R., Army Armament Research and Development Command, Dover,  
N.J. (Large Caliber Weapon Systems Lab.)

78N27445

Ultrasonic procedures for the determination of bond strength, Final Report,  
1 Jan. 1973 - 1 Jan. 1978.  
A/Rose, J.L.; B/Thomas, G.H., Drexel Univ., Philadelphia, Pa. (Dept. of Mechanical  
Engineering and Mechanics.)

78N12200

Nondestructive inspection of phosphoric acid anodized aluminium panels for contamination,  
Final Report, 15 Mar. 1975 - 15 Dec. 1976.  
A/Smith, T., Rockwell International Corp., Thousand Oaks, Calif. (Science Center).

77N18226

Ultrasonic spectrum analysis for NDT of layered composite materials, Final Report.  
A/Scott, W.R., Naval Air Development Center, Warminster, Pa. (Air Vehicle Technology Dept.)

77N14502

Ultrasonic procedures for the determination of bond strength, Interim Report.  
A/Rose, J.L., Drexel Univ., Philadelphia, Pa. (Dept. of Mechanical Engineering and  
Mechanics)

76N25393

Surface analysis of 2024 and 7075 aluminium alloys after conditioning by chemical treat-  
ments, Final Report, Jan. 1974 - Jan. 1975.  
A/McDevitt, N.L.; B/Baun, W.L.; C/Solomon, J.S., Air Force Materials Lab., Wright-  
Patterson AFB, Ohio; Dayton Univ., Ohio..

76N24536

Interference holography: A means for non-destructive testing.  
A/Schliekelmann, R.J., Royal Netherlands Aircraft Factories Fokker, Schiphol-Oost.

76N16480

NDI of bonded structures

A/Treca, M., Societe National Industrielle Aerospatiale, Suresnes (France).

In: AGARD Non-Destructive Inspection Practices p. 529-577 (SEE N76-16477 07-38)

75N31459

Modelling concepts for evaluating selected aspects of ultrasonic wave interaction with an adhesive bond Ph.D. Thesis.

A/Meyer, P.A., Drexel Unvi., Philadelphia, Pa.

75N23946

Nondestructive holographic techniques for structures inspection, Final Report,

1 Jul. 1971 - 30 Apr. 1974.

A/Erf, R.K.; B/Gagosz, R.M.; C/Waters, J.P.; D/Stetson, K.A.; E/Aas, H.G., United Aircraft Corp., East Hartford, Conn. (Research Labs.)

75N17423

Initial feasibility study employing holographic vibrational analysis to locate non-bonds in thick ceramic to fiberglass composite.

A/Barabaris, M.J.; B/Chisolm, B.R., Picatinny Arsenal, Dover, N.J.

# REPORT DOCUMENTATION PAGE

<b>1. Recipient's Reference</b>	<b>2. Originator's Reference</b>	<b>3. Further Reference</b>	<b>4. Security Classification of Document</b>								
	AGARD-LS-102	ISBN 92-835-1313-4	UNCLASSIFIED								
<b>5. Originator</b>	Advisory Group for Aerospace Research and Development North Atlantic Treaty Organization 7 rue Ancelle, 92200 Neuilly sur Seine, France										
<b>6. Title</b>	BONDED JOINTS AND PREPARATION FOR BONDING										
<b>7. Presented</b>	on 2-3 April 1979, Oslo, Norway and 5-6 April 1979 in The Hague, The Netherlands.										
<b>8. Author(s)/Editor(s).</b>	Various		<b>9. Date</b> March 1979								
<b>10. Author's/Editor's Address</b>	Various		<b>11. Pages</b> 320 including Bibliography of 183 items								
<b>12. Distribution Statement</b>	This document is distributed in accordance with AGARD policies and regulations, which are outlined on the Outside Back Cover of all AGARD publications.										
<b>13. Keywords/Descriptors</b>	<table border="0"> <tr> <td>Bonded joints</td> <td>Composite materials</td> </tr> <tr> <td>Bonding</td> <td>Mechanical properties</td> </tr> <tr> <td>Construction materials</td> <td>Durability</td> </tr> <tr> <td>Structural design</td> <td>Metals</td> </tr> </table>			Bonded joints	Composite materials	Bonding	Mechanical properties	Construction materials	Durability	Structural design	Metals
Bonded joints	Composite materials										
Bonding	Mechanical properties										
Construction materials	Durability										
Structural design	Metals										
<b>14. Abstract</b>	<p>After more than thirty years of application in aircraft construction in roles with various degrees of structural importance, adhesive bonded joints are expected to see an increased use in more primary structural applications, both in conjunction with metals as well as with advanced composites.</p> <p>The basis for such advanced applications of bonded joints, however, must be ample knowledge on:</p> <ul style="list-style-type: none"> <li>- structural design aspects</li> <li>- durability aspects</li> </ul> <p>of bonded joints in order to provide the required static and dynamic strength of the bonded structure during its operational life time. It is with these demands in mind that the lectures have been planned.</p> <p>The material in this publication was assembled to support a Lecture Series under the sponsorship of the Structures and Materials Panel and the Consultant and Exchange Programme of AGARD.</p>										



<p>AGARD Lecture Series No.102 Advisory Group for Aerospace Research and Development, NATO <b>BONDED JOINTS AND PREPARATION FOR BONDING</b> Published March 1979 320 pages including Bibliography of 183 items</p> <p>After more than thirty years of application in aircraft construction in roles with various degrees of structural importance, adhesive bonded joints are expected to see an increased use in more primary structural applications, both in conjunction with metals as well as with advanced composites.</p> <p>The basis for such advanced applications of bonded joints, however, must be ample knowledge on:</p> <p>P.T.O.</p>	<p>AGARD-LS-102</p> <p>Bonded joints Bonding Construction materials Structural design Composite materials Mechanical properties Durability Metals</p>	<p>AGARD Lecture Series No.102 Advisory Group for Aerospace Research and Development, NATO <b>BONDED JOINTS AND PREPARATION FOR BONDING</b> Published March 1979 320 pages including Bibliography of 183 items</p> <p>After more than thirty years of application in aircraft construction in roles with various degrees of structural importance, adhesive bonded joints are expected to see an increased use in more primary structural applications, both in conjunction with metals as well as with advanced composites.</p> <p>The basis for such advanced applications of bonded joints, however, must be ample knowledge on:</p> <p>P.T.O.</p>	<p>AGARD-LS-102</p> <p>Bonded joints Bonding Construction materials Structural design Composite materials Mechanical properties Durability Metals</p>
<p>AGARD Lecture Series No.102 Advisory Group for Aerospace Research and Development, NATO <b>BONDED JOINTS AND PREPARATION FOR BONDING</b> Published March 1979 320 pages including Bibliography of 183 items</p> <p>After more than thirty years of application in aircraft construction in roles with various degrees of structural importance, adhesive bonded joints are expected to see an increased use in more primary structural applications, both in conjunction with metals as well as with advanced composites.</p> <p>The basis for such advanced applications of bonded joints, however, must be ample knowledge on:</p> <p>P.T.O.</p>	<p>AGARD-LS-102</p> <p>Bonded joints Bonding Construction materials Structural design Composite materials Mechanical properties Durability Metals</p>	<p>AGARD Lecture Series No.102 Advisory Group for Aerospace Research and Development, NATO <b>BONDED JOINTS AND PREPARATION FOR BONDING</b> Published March 1979 320 pages including Bibliography of 183 items</p> <p>After more than thirty years of application in aircraft construction in roles with various degrees of structural importance, adhesive bonded joints are expected to see an increased use in more primary structural applications, both in conjunction with metals as well as with advanced composites.</p> <p>The basis for such advanced applications of bonded joints, however, must be ample knowledge on:</p> <p>P.T.O.</p>	<p>AGARD-LS-102</p> <p>Bonded joints Bonding Construction materials Structural design Composite materials Mechanical properties Durability Metals</p>

<ul style="list-style-type: none"> <li>- structural design aspects</li> <li>- durability aspects</li> </ul> <p>of bonded joints in order to provide the required static and dynamic strength of the bonded structure during its operational life time. It is with these demands in mind that the lectures have been planned.</p> <p>The material in this publication was assembled to support a Lecture Series under the sponsorship of the Structures and Materials Panel and the Consultant and Exchange Programme of AGARD, presented on 2-3 April 1979 in Oslo, Norway and 5-6 April 1979 in The Hague, The Netherlands.</p> <p>ISBN 92-835-1313-4</p>	<ul style="list-style-type: none"> <li>- structural design aspects</li> <li>- durability aspects</li> </ul> <p>of bonded joints in order to provide the required static and dynamic strength of the bonded structure during its operational life time. It is with these demands in mind that the lectures have been planned.</p> <p>The material in this publication was assembled to support a Lecture Series under the sponsorship of the Structures and Materials Panel and the Consultant and Exchange Programme of AGARD, presented on 2-3 April 1979 in Oslo, Norway and 5-6 April 1979 in The Hague, The Netherlands.</p> <p>ISBN 92-835-1313-4</p>
<ul style="list-style-type: none"> <li>- structural design aspects</li> <li>- durability aspects</li> </ul> <p>of bonded joints in order to provide the required static and dynamic strength of the bonded structure during its operational life time. It is with these demands in mind that the lectures have been planned.</p> <p>The material in this publication was assembled to support a Lecture Series under the sponsorship of the Structures and Materials Panel and the Consultant and Exchange Programme of AGARD, presented on 2-3 April 1979 in Oslo, Norway and 5-6 April 1979 in The Hague, The Netherlands.</p> <p>ISBN 92-835-1313-4</p>	<ul style="list-style-type: none"> <li>- structural design aspects</li> <li>- durability aspects</li> </ul> <p>of bonded joints in order to provide the required static and dynamic strength of the bonded structure during its operational life time. It is with these demands in mind that the lectures have been planned.</p> <p>The material in this publication was assembled to support a Lecture Series under the sponsorship of the Structures and Materials Panel and the Consultant and Exchange Programme of AGARD, presented on 2-3 April 1979 in Oslo, Norway and 5-6 April 1979 in The Hague, The Netherlands.</p> <p>ISBN 92-835-1313-4</p>

4

AGARD

NATO OTAN

7 RUE ANCELLE · 92200 NEUILLY-SUR-SEINE  
FRANCE

Telephone 745.08.10 · Telex 610176

DISTRIBUTION OF UNCLASSIFIED  
AGARD PUBLICATIONS

AGARD does NOT hold stocks of AGARD publications at the above address for general distribution. Initial distribution of AGARD publications is made to AGARD Member Nations through the following National Distribution Centres. Further copies are sometimes available from these Centres, but if not may be purchased in Microfiche or Photocopy form from the Purchase Agencies listed below.

NATIONAL DISTRIBUTION CENTRES

**BELGIUM**

Coordonnateur AGARD - VSL  
Etat-Major de la Force Aérienne  
Quartier Reine Elisabeth  
Rue d'Evere, 1140 Bruxelles

**CANADA**

Defence Scientific Information Service  
Department of National Defence  
Ottawa, Ontario K1A 0Z2

**DENMARK**

Danish Defence Research Board  
Østerbrogades Kaserne  
Copenhagen Ø

**FRANCE**

O.N.E.R.A. (Direction)  
29 Avenue de la Division Leclerc  
92 Châtillon sous Bagneux

**GERMANY**

Zentralstelle für Luft- und Raumfahrt-  
dokumentation und -information  
c/o Fachinformationszentrum Energie,  
Physik, Mathematik GmbH  
Kernforschungszentrum  
7514 Eggenstein-Leopoldshafen 2

**GREECE**

Hellenic Air Force General Staff  
Research and Development Directorate  
Holargos, Athens, Greece

**ICELAND**

Director of Aviation  
c/o Flugrad  
Reykjavik

**ITALY**

Aeronautica Militare  
Ufficio del Delegato Nazionale all'AGARD  
3, Piazzale Adenauer  
Roma/EUR

**LUXEMBOURG**

See Belgium

**NETHERLANDS**

Netherlands Delegation to AGARD  
National Aerospace Laboratory, NLR  
P.O. Box 126  
Delft

**NORWAY**

Norwegian Defence Research Establishment  
Main Library  
P.O. Box 25  
N-2007 Kjeller

**PORTUGAL**

Direcção do Serviço de Material  
da Força Aérea  
Rua da Escola Politécnica 42  
Lisboa  
Attn: AGARD National Delegate

**TURKEY**

Department of Research and Development (ARGE)  
Ministry of National Defence, Ankara

**UNITED KINGDOM**

Defence Research Information Centre  
Station Square House  
St. Mary Cray  
Orpington, Kent BR5 3RE

**UNITED STATES**

National Aeronautics and Space Administration (NASA)  
Langley Field, Virginia 23365  
Attn: Report Distribution and Storage Unit

THE UNITED STATES NATIONAL DISTRIBUTION CENTRE (NASA) DOES NOT HOLD STOCKS OF AGARD PUBLICATIONS, AND APPLICATIONS FOR COPIES SHOULD BE MADE DIRECT TO THE NATIONAL TECHNICAL INFORMATION SERVICE (NTIS) AT THE ADDRESS BELOW.

PURCHASE AGENCIES

*Microfiche or Photocopy*

National Technical  
Information Service (NTIS)  
5285 Port Royal Road  
Springfield  
Virginia 22161, USA

*Microfiche*

Space Documentation Service  
European Space Agency  
10, rue Mario Nikis  
75015 Paris, France

*Microfiche*

Technology Reports  
Centre (DTI)  
Station Square House  
St. Mary Cray  
Orpington, Kent BR5 3RF  
England

Requests for microfiche or photocopies of AGARD documents should include the AGARD serial number, title, author or editor, and publication date. Requests to NTIS should include the NASA accession report number. Full bibliographical references and abstracts of AGARD publications are given in the following journals:

Scientific and Technical Aerospace Reports (STAR)  
published by NASA Scientific and Technical  
Information Facility  
Post Office Box 8757  
Baltimore/Washington International Airport  
Maryland 21240, USA

Government Reports Announcements (GRA)  
published by the National Technical  
Information Services, Springfield  
Virginia 22161, USA



Printed by Technical Editing and Reproduction Ltd  
Harford House, 7-9 Charlotte St, London W1P 1HD

ISBN 92-835-1313-4